TRANSIENT TWO PHASE FLOWS:
REFILLING AND REWETTING OF A HOT HORIZONTAL TUBE

by

© ALBERT M. C. CHAN, B.ENG., M.ENG.

A Thesis
Submitted to the School of Graduate Studies
in Partial Fulfilment of the Requirements
for the Degree
Doctor of Philosophy

McMaster Univerisity
June , 1980

REFILLING AND REWETTING OF A HOT HORIZONTAL TUBE

DOCTOR OF PHILOSOPHY (1980)
(Nuclear Engineering)

McMASTER UNIVERSITY
Hamilton, Ontario

TITLE: Transient Two Phase Flows: Refilling and Rewetting of a Hot Horizontal Tube

AUTHOR: Albert M. C. Chan, B.Eng. (University of Alberta)
M.Eng. (McMaster University)

SUPERVISOR: Professor S. Banerjee

NUMBER OF PAGES: xxvii, 431

ABSTRACT

The refilling and rewetting of a directly heated horizontal channel has been studied experimentally. The quenching characteristics and rewetting rates were obtained under different well-defined initial and boundary conditions. The parametric effects of initial wall temperature, inlet water flow rate and inlet water subcooling as well as effects of residual power input, tube insulation and dissolved air and ions in the inlet water were investigated.

The results show that, in horizontal channels, the transverse gravity forces significantly affect the hydraulic, and consequently thermal, behavior of the system. The heat transfer mechanisms were found to vary during transients, both axially and circumferentially. This results in large differences in the pre-quench characteristics with regard to the bottom and top of the channel.

A simple physical model which can account for most of the observed characteristics was developed. The model consists of an inclined rewetting front and an entrained "liquid tongue" extending downstream from the rewetting front. The model was also supported by photographic studies.

The propagation of the rewetting front appears to be largely controlled by hydrodynamic mechanisms. It was found that surface quenching can occur at very different wall temperatures along the tube. Thus, there is no well defined rewetting temperature. This is contrary

to the predictions of the generally accepted conduction controlled rewetting model.

Since hydrodynamic mechanisms dominate the thermohydraulic processes in the present flow situation, a simplified two-fluid model was used to analyze the processes. The wall temperature was obtained after the hydraulic equations of the liquid phase were solved. The wall was assumed to be in stable film boiling before quenching.

A quench model based on a critical water level, $(h_L)_{crit}$, determined the transition of heat transfer mode from film boiling to transition boiling and subsequent quenching of the surface. $(h_L)_{crit}$ was obtained using a model based on initiation of a Kelvin-Helmholtz type instability at the vapor film-liquid interface.

The initiation of the interfacial instability is believed to be the governing mechanism that leads to surface rewetting. When the instability starts, local regions of enhanced heat transfer are assumed to form on the heater surface. This provides the necessary conditions for surface rewet. However, if the surface is highly conductive and has a high thermal capacity, these rewet spots may not grow and surface rewet may not occur. Therefore, the sufficient conditions would require that the rewet spots could grow or spread on the heating surface. For thin-walled tubes, because of low thermal capacity, rewet spots may spread once they are formed. Hence, interfacial instability is postulated to be both necessary and sufficient to quench thin-walled systems of the type studied.

The simplified two-fluid model, together with the quench model were found to be quite successful in predicting the rewetting rates and details of the quenching characteristics for the refilling and rewetting experiments.

ACKNOWLEDGEMENT

The author gratefully acknowledges the supervision, encouragement and support of his supervisor, Professor S. Banerjee throughout the investigation. He also wishes to thank M. Vandenbroek for his help in setting up and maintaining the experimental facility, D. Bot and G. Leinweber for setting up the data acquisition system and their help with electronics apparatus, and M. Yu of the McMaster Computer Center with regard to data transfer and storage.

Thanks also go to Canadian General Electric for providing the Zircaloy-2 test section and to the Atomic Power Division of Westinghouse Canada Ltd. for spot welding the thermocouples onto the test section surface.

The work was supported financially by Whiteshell Nuclear Research Establishment, Atomic Energy of Canada Ltd. This is greatly appreciated. Financial support provided by both the National Research Council of Canada and the Ontario Ministry of Education in the form of scholarships is also gratefully acknowledged.

Lastly, the author wants to thank his wife, Cindy, for her understanding and patience during the work.

TABLE OF CONTENTS

Page

ABSTRACT iii

ACKNOWLEDGEMENT vi

TABLE OF CONTENTS vii

LISTS OF TABLES xiv

LISTS OF FIGURES xv

LISTS OF PHOTOGRAPHS xxii

NOMENCLATURE xxiii

CHAPTER 1. INTRODUCTION 1

1.1 Background 1

1.2 Objectives 3

CHAPTER 2. REWETTING IN NUCLEAR REACTOR EMERGENCY CORE COOLING STUDIES 4

2.1 General 4

2.2 Review of Top Spray Cooling and Bottom Reflooding of Vertical System 7

2.2.1 Experimental Work - Rod Bundles 8

2.2.2 Experimental Work - Single Channel 10

2.2.3 Experimental Work - Results and Observations 12

2.2.4 Theoretical Work 15

2.3 Horizontal Channel Rewetting 21

CHAPTER 3. MODELS FOR TRANSIENT SEPARATED FLOW 23

3.1 General 23

Page

3.2 Local Instantaneous Conservation Equations 25

3.3 Averaging Procedures 29

3.4 Averaged Conservation Equations and Jump Conditions 32

3.5 Interphase Transfer Functions and Intraphase Distribution Coefficients 40

3.6 Simplified One-Dimensional Models 43

CHAPTER 4. EXPERIMENTAL FACILITY 49

4.1 Test Loop 49

4.1.1 Test Section 49

4.1.2 Inlet Water Supply 55

4.1.3 Power Supply 55

4.2 Instrumentation 56

4.2.1 Temperature Measurements 56

4.2.2 Pressure Measurements 60

4.2.3 Flow Measurements 60

4.2.4 Power Input 64

4.2.5 Void Fraction Measurements 64

4.3 Automatic Data Acquisition System (ADAS) 65

4.3.1 Low-Level Analog Input System (RTP-model 7471) 67

4.3.2 Computer Control of Analog Input System 67

4.3.3 Signal Conditioning of AIS Inputs 69

CHAPTER 5. VOID FRACTION MEASUREMENTS 73

5.1 General 73

Page

5.2 Fast Neutron Scattering Technique 73

5.3 Gamma Ray Attenuation Technique 82

5.4 Gamma Densitometer Design 84

5.4.1 Test Section 87

5.4.2 Gamma Source 89

5.4.3 Source Strength 91

5.4.4 Scintillator and Counting System 93

5.4.5 Source Container Design 96

5.5 Calibration 101

CHAPTER 6. EXPERIMENTAL PROCEDURE 108

6.1 System Calibration 108

6.2 Experimental Procedure 109

6.3 Matrix of Experiments 111

6.4 Data Reduction 113

CHAPTER 7. CHARACTERISTICS OF HORIZONTAL CHANNEL REWETTING AND REFILLING 115

7.1 Rewetting of a Dry Hot Surface 115

7.2 Leidenfrost Temperature 117

7.3. Refilling and Rewetting of Horizontal Channels 120

7.3.1 Photographic Studies 120

7.3.2 A Physical Model 129

CHAPTER 8. DATA ANALYSES, RESULTS, AND DISCUSSION 135

8.1 Experimental Results 135

Page

8.2 The Rewetting Model 151

8.3 Rewetting Velocities 157

  8.3.1 Local Rewetting Velocities 157

  8.3.2 Average Rewetting Velocities 158

    8.3.2.1 Effect of Initial Wall Temperature 163

    8.3.2.2 Effect of Inlet Flow Rate 178

    8.3.2.3 Effect of Inlet Water Subcooling 180

    8.3.2.4 Effect of Power Input 183

    8.3.2.5 Effect of Flow Boundary Conditions 183

    8.3.2.6 Effect of Insulation 184

    8.3.2.7 Effect of Inlet Water 184

8.4 Void Fraction Profiles 184

  8.4.1 Average Rewetting Velocity 185

  8.4.2 Average Entrained Water Velocity 188

8.5 Stratified Length of the Quench Front 190

8.6 Heat Transfer Mechanisms and Coefficients 193

CHAPTER 9. SIMPLIFIED TWO FLUID MODEL
(I) REFILLING OF DRY HORIZONTAL CHANNEL WITH NO HEAT TRANSFER 207

9.1 Simplified Two Fluid Model 207

9.2 Mathematical Formulation 207

9.3 Refilling of a Dry Horizontal Channel With No Heat Transfer 214

9.4 Numerical Solution - The Method of Characteristics 217

Page

9.5 Frictional Resistance in Developing Open Channel Flow 226

9.6 Verification of the Simplified Two-Fluid Model Approach - A Simple Experiment 231

CHAPTER 10. SIMPLIFIED TWO FLUID MODEL (II) REFILLING AND REWETTING OF HOT HORIZONTAL CHANNEL 245

10.1 General 245

10.2 Mathematical Formulation 245

10.2.1 Hydraulic Equations 245

10.2.2 Thermal Equations 247

10.3 Numerical Procedures 249

10.3.1 System and Nodalization 251

10.3.2 Initial and Boundary Conditions 251

10.3.3 Local Heat Transfer Coefficient 254

10.3.4 Wall Temperature 260

10.3.5 Liquid Temperature 266

10.3.6 Output of the Dependent Variables 268

10.3.7 Time Step Size 269

10.3.8 Interfacial Transfer Terms 269

10.3.8.1 Interfacial Mass Transfer 271

10.3.8.2 Wall Shear - Liquid Phase 271

10.3.8.3 Wall Shear - Vapor Phase 272

10.3.8.4 Interfacial Shear 273

10.3.8.5 Vapor Inertia 273

10.3.8.6 Momentum Transfer due to Mass Transfer 274

Page

10.3.9 Hydraulic Equations 274

10.4 Surface Rewetting 275

10.4.1 Necessary and Sufficient Conditions for Surface Rewetting 275

10.4.2 Instability in Film Boiling 278

10.4.3 Vapor Flow in Film Boiling 279

10.4.4 Onset of Instability 286

10.5 The Quench Model 295

10.5.1 Critical Water Level 298

10.6 Numerical Results 301

10.6.1 Constitutive Models 301

10.6.2 Quenching Characteristics 307

10.6.2.1 Transient Wall Temperatures 307

10.6.2.2 Average Rewetting Velocities 314

10.6.2.3 Refilling and Rewetting Fronts 318

10.7 Numerical Tests 323

10.7.1 Convergence Studies 323

10.7.2 Sensitivity to Constitutive Models 324

10.8 Usefulness and Limitations of the Simplified Two-Fluid Model Approach 325

CHAPTER 11. CONCLUSIONS AND RECOMMENDATIONS 332

11.1 Concluding Remarks 332

11.1.1 Experimental Work 332

11.1.2 Theoretical Work 335

11.1.3 Two Phase Flow Instrumentation 337

Page

11.2 Recommendations for Future Work 338

11.2.1 Experimental Work 338

11.2.2 Code Development 340

REFERENCES 341

APPENDIX I

(A) Numerical Calculation of Average Void Fraction in a Circular Duct Using a Single-Beam Gamma-Densitometer 351

A.1 Stratified Flow 351

A.2 Annular Flow 354

A.3 Core Flow 356

A.4 Transmission of a Circular Beam Through an Empty Duct With Wall Thickness t 356

(B) Calculation of Dose Rate for a 50 mCi Sealed Co-57 Source with Shielding Container 359

APPENDIX II TRANSIENT CIRCUMFERENTIAL HEAT CONDUCTION 362

APPENDIX III LIST OF EXPERIMENTAL RUNS AND DATA STORAGE 367

III.1 List of Experimental [illegible]ns 367

III.2 Raw Data Storage and Interpretation 370

APPENDIX IV COMPUTER PROGRAM LISTINGS 393

IV.1 Program STRIP 394

IV.2 Program RWRFPL 397

IV.3 Program REWET 406

List of Tables

Table	Description	Page
3.1	One-Dimensional Two-Phase Flow Models	46
4.1	Physical and Thermal Properties of Zircaloy-2	53
4.2	Sensors and Locations	57
5.1	Void Fraction Measurement Techniques	74
5.2	Nuclear Properties of Isotopes used in Low Energy Photon Sources	90
5.3	Properties of Some Scintillation Crystals	95
5.4	Maximum Permissible Annual Exposures for Radiation Workers	98
7.1	Leidenfrost Temperature of Water	119
9.1	Convergence Studies for Refilling with No Heat Transfer	242
10.1	Constitutive Relations Used in REWET	304
10.2	Convergence Tests --- Computer Code REWET	324
10.3	Sensitivity Studies	326
III.1	Channel to Sensor Correspondence	368
III.2	Calibration Curves for the Sensors	369
III.3	List of Experimental Runs	372
III.4	Procedures Used to Write Data onto Magnetic Tape	388
III.5	Procedures Used to Read Data from Magnetic Tape	390
III.6	Data Storage on Magnetic Tapes	391

LIST OF FIGURES

Figure	Description	Page
1.1	Methodology of Canadian Approach to LOCA Analysis	2
2.1	PWR Primary Coolant System Schematic	5
2.2	CANDU Reactor Simplified Flow Diagram	6
3.1	Transport Theorem With a Singular Surface	28
3.2	Definitions of Symbols and Geometry for the Averaging Process	33
4.1	Schematic Diagram of Rewetting Facility	50
4.2	Test Section and Flanges	54
4.3	Locations of Transducers	59
4.4	Pressure Transducer Calibration Curve	62
4.5	Flowmeter Calibration Curves	63
4.6	Schematic Diagram of Data Acquisition System	66
4.7	RTP7471 Series Analog Input System -- Block Diagram	68
4.8	Flowmeter Electronics	71
4.9	Block Diagram of Gamma Densitometer Electronics	72
5.1	Schematic Plan View of Experimental Setup -- Fast Neutron Scattering Technique	76
5.2	Simulated Flow Patterns	77
5.3	Static Void Fraction Measurements Using Neutron Scattering Method (25.4 mm Specimen)	78
5.4	Static Void Fraction Measurements Using Neutron Scattering Method (50.8 mm Specimen)	79
5.5	Void Fraction Measurements -- Comparison Between Neutron Scattering and Trapping Air-Water Mixture Methods	81

Figure	Description	Page
5.6	Schematic Diagram of a Gamma Densitometer	85
5.7	Transmission of a Circular Gamma Beam Through a Circular Tube	88
5.8	Gamma Densitometer Counting System	97
5.9	Shielding Container Design	99
5.10	Mass Attenuation Coefficient of Water and Lucite	102
5.11	Void Fraction Predicted by Gamma Attenuation Measurements Compared to Actual Void Fraction	103
5.12	Void Fraction Calculated Based on Gamma Attenuation Compared to Actual Void Fraction	106
5.13	Experimentally Measured Mass Absorption Coefficient of Water Using a Co-57 Source	107
7.1	Rewetting of a Hot Surface	116
7.2	Characteristic of Horizontal Channel Rewetting	130
7.3	Quenching Characteristics -- Top and Bottom of Channel	132
7.4	Transient Circumferential Heat Conduction	134
8.1	Inlet Water Flow Rate -- Constant Flow System	136
8.2	Residual Power Input to Test Section	137
8.3	System Inlet Pressure	138
8.4	Local Void Fraction Measurements	139
8.5	Fluid Temperature at Exit of Test Section -- Measured Close to Top of Channel	140
8.6	Fluid Temperature at Exit of Test Section -- Measured Close to Bottom of Channel	141
8.7	Transient Mid-Side Wall Temperature	142
8.8	Transient Top and Bottom Temperatures	143
8.9	Inlet Water Flow Rate -- Constant Pressure System	144
8.10	Exit Fluid Temperature and Local Void Fraction Measurements	147

Figure	Description	Page
8.11	Transient Mid-Side Wall Temperature -- Group III Results	149
8.12	Transient Top and Bottom Wall Temperatures -- Group III Results	150
8.13	Transient Mid-Side Wall Temperature -- Group VI Results	152
8.14	Transient Top and Bottom Wall Temperatures -= Group VI Results	153
8.15	Quenching Characteristics -- Mid-Side Wall Temperature and γD1 (Inlet Flow = 77.0 ml/s)	155
8.16	Quenching Characteristics -- Mid-Side Wall Temperature and γD1 (Inlet Flow = 32.0 ml/s)	156
8.17	Local Rewetting Velocity -- Mid-Side of Test Section	159
8.18	Average Rewetting Velocities vs Inlet Flow Rates (T_w = 600 ^oC)	160
8.19	Average Rewetting Velocities vs Inlet Flow Rates (T_w = 500 ^oC)	161
8.20	Average Rewetting Velocities vs Inlet Flow Rates (T_w = 300 ^oC)	162
8.21	Average Rewetting Velocity ($\bar{V}_S$) vs Inlet Flow Rates for Different Wall Temperatures -- Group I Results	164
8.22	Average Rewetting Velocity ($\bar{V}_B$) vs Inlet Flow Rates for Different Wall Temperatures -- Group I Results	165
8.23	Average Rewetting Velocity ($\bar{V}_T$) vs Inlet Flow Rates for Different Wall Temperatures -- Group I Results	166
8.24	Average Rewetting Velocity ($\bar{V}_S$) vs Inlet Flow Rates for Different Wall Temperatures -- Group II Results	167
8.25	Average Rewetting Velocity ($\bar{V}_B$) vs Inlet Flow Rates for Different Wall Temperatures -- Group II Results	168
8.26	Average Rewetting Velocity ($\bar{V}_T$) vs Inlet Flow Rates for Different Wall Temperatures -- Group II Results	169
8.27	Average Rewetting Velocity ($\bar{V}_S$) vs Inlet Flow Rates for Different Wall Temperatures -- Group III Results	170
8.28	Average Rewetting Velocity ($\bar{V}_S$) vs Inlet Flow Rates for Different Wall Temperatures -- Group IV Results	171

Figure	Description	Page
8.29	Average Rewetting Velocity ($\bar{V}_S$) vs Inlet Flow Rates for Different Wall Temperatures -- Group IV & V Results	172
8.30	Average Rewetting Velocity ($\bar{V}_S$) vs Inlet Flow Rates for Different Wall Temperatures -- Group VI Results	173
8.31	Inverse Rewetting Velocity ($1/\bar{V}_S$) vs Wall Temperature -- Group I Results	175
8.32	Inverse Rewetting Velocity ($1/\bar{V}_S$) vs Wall Temperature -- Group III Results	176
8.33	Inverse Rewetting Velocity ($1/\bar{V}_S$) vs Wall Temperature -- Group IV Results	177
8.34	Inverse Rewetting Velocity ($1/\bar{V}_B$) vs Wall Temperature -- Comparing Group I & II Results	181
8.35	Inverse Rewetting Velocity ($1/\bar{V}_S$) vs Wall Temperature -- Comparing Group I & II Results	182
8.36	Local Void Fraction Measurements -- Average Rewetting and Entrained Water Velocities Determination	186
8.37	Average Rewetting Velocity vs Inlet Flow Rates for Different Wall Temperature -- $\bar{V}_S$ and $\bar{V}_Y$	187
8.38	Average Entrained Water Velocity ($\bar{V}_{ent}$) vs Inlet Flow	189
8.39	$\bar{V}_{ent}/\bar{V}_S$ Ratio vs Inlet Flow Rates	191
8.40	Determination of Stratified Length (ℓ_s) of the Quench Front	192
8.41	Stratified Length of Quench Front at Different Axial Locations	194
8.42	Heat Transfer Characteristics	195
8.43	Coordinate System for Transient Radial Heat Conduction Calculation	199
8.44	Average Heat Transfer Coefficient vs Bulk Liquid Temperature	201
8.45	Effective Heat Transfer Coefficient vs Wall Temperature	202
8.46	Total Power Input and Heat Loss	204

Figure	Description	Page
9.1	Definition of Variables in the Simplified Two Fluid Model Formulation	210
9.2	Finite Fifference Grid Used	220
9.3	Forward and Backward Characteristics	222
9.4	Possible Boundaries	225
9.5	Filling of a Dry Horizontal Tube	229
9.6	Schematic of Refilling Setup With No Heat Transfer	232
9.7	Refilling Characteristic of a Dry Horizontal Tube With No Heat Transfer	234
9.8	Transient Stratified Length -- Refilling With No Heat Transfer	236
9.9	Steady State Friction Factor Multiplier	237
9.10	Refilling Velocities with No Heat Transfer -- Q_{in} = 90.0 ml/s	238
9.11	Refilling Velocities with No Heat Transfer -- Q_{in} = 70.0 ml/s	239
9.12	Refilling Velocities with No Heat Transfer -- Q_{in} = 35.0 ml/s	240
9.13	Propagation of Refilling Front -- Refilling of a Dry Horizontal Channel	244
10.1	Flow Diagram of Computer Code REWET	250
10.2	Schematic of System and Nodalization	252
10.3	Axial Heat Transfer Regions	255
10.4	Boiling Curve	259
10.5	Finite Difference Grid for T_w Computation	261
10.6	Finite Difference Grid for Convective Boundary Condition	263
10.7	Finite Difference Grid Used for Bulk Liquid Temperature Calculation	267
10.8	Film Boiling Model	281
10.9	Vapor Film Thickness at Origin (δ_o) vs Wall Superheat (ΔT_w)	287

Figure	Description	Page
10.10	Vapor Velocity and Vapor Film Thickness	288
10.11	Possible Modes of Oscillation	290
10.12	Critical and Average Vapor Velocities vs Water Level	291
10.13	Comparison of Theoretical and Empirical Critical Water Level for Vapor Film Instability	293
10.14	Quench Model	296
10.15	Transient Circumferential Heat Conduction	297
10.16	Rewetting Velocity ($\bar{V}_B$) vs Critical Water Level $(h_L)_{crit}$	300
10.17	A Simple Model to Determine β	303
10.18	Transient Top and Bottom Wall Temperatures -- Numerical Solutions (Inlet Flow Rate = 84.5 ml/s)	308
10.19	Transient Top and Bottom Wall Temperatures -- Experimental Results (Inlet Flow Rate = 84.5 ml/s)	309
10.20	Transient Top and Bottom Wall Temperatures -- Comparison of Experimental and Numerical Results	310
10.21	Transient Top and Bottom Wall Temperatures -- Experimental Results (Inlet Flow Rate = 47.0 ml/s)	312
10.22	Transient Top and Bottom Wall Temperatures -- Numerical Results (Inlet Flow Rate = 47.0 ml/s)	313
10.23	Average Rewetting Velocity ($\bar{V}_S$) vs Inlet Flow Rate	316
10.24	Average Rewetting Velocity ($\bar{V}_S$) for Different Inlet Water Subcoolings	317
10.25	Propagation of Refilling and Rewetting Fronts -- Numerical Results (T_w = 400 °C)	319
10.26	Propagation of Refilling and Rewetting Fronts -- Numerical Results (T_w = 500 °C)	320
10.27	Propagation of Refilling and Rewetting Fronts -- Numerical Results (T_w = 600 °C)	321

Figure	Description	Page
10.28	Flow Pattern Map for Horizontal Flow	328
10.29	A Modified Quench Model	330
A.1	Gamma Densitometer Calibration -- Horizontal Beam and Stratified Flow	352
A.2	Gamma Densitometer Calibration -- Vertical Beam and Stratified Flow	355
A.3	Gamma Densitometer Calibration -- Annular Flow	357
A.4	Gamma Densitometer Calibration -- Core Flow	358
II.1	Transient Circumferential Heat Conduction	363

LIST OF PHOTOGRAPHS

Plate	Description	Page
4.1	Rewetting Experimental Facility	51
4.2	Spot Welded Surface Thermocouples	51
4.3	Mounting of Micro-Thermocouple and Pressure Transducer in the Feeder	61
5.1	Source Containers and Shaped Lucite Pieces for Densitometer Calibration	100
5.2	Gamma Densitometer Setup	100
7.1	Refilling and Rewetting of a Hot Section of a Duct -- Length of Section Photographed	122
7.2	Refilling and Rewetting Sequence -- Picture Number 1	122
7.3	Refilling and Rewetting Sequence -- Picture Number 2	123
7.4	Refilling and Rewetting Sequence -- Picture Number 3	123
7.5	Refilling and Rewetting Sequence -- Picture Number 4	124
7.6	Refilling and Rewetting Sequence -- Picture Number 5	124
7.7	Refilling and Rewetting Sequence -- Picture Number 6	125
7.8	Refilling and Rewetting Sequence -- Picture Number 7	125
7.9	Refilling and Rewetting Sequence -- Picture Number 8	126
7.10	Refilling and Rewetting Sequence -- Picture Number 9	126
7.11	Refilling and Rewetting Sequence -- Picture Number 10	127
7.12	Refilling and Rewetting Sequence -- Picture Number 11	127
7.13	Refilling and Rewetting Sequence -- Picture Number 12	128
7.14	Refilling and Rewetting Sequence -- Picture Number 13	128

NOMENCLATURE (1)

Independent Variables

r	radial coordinate in cylindrical system
t	time
x	horizontal coordinate
y	vertical coordinate
z, Z	axial coordinate
θ	azimuthal coordinate in cylindrical system

Variables

a	interfacial area
A	flow area, gamma source strength
Bi	Biot number
c	gravity wave velocity
C	heat capacity, Chezy coefficient
D	diameter
d_h	hydraulic diameter
e	internal energy, surface emissivity
E	total energy
f	friction factor
$\vec{F}$	external forces
F_y	total hydrostatic thrust
g	gravitational force

Gr	Grashof number
h	heat transfer coefficient, enthalpy
h_L	liquid level
$(h_L)_{crit}$	critical liquid level
h_q	effective quench level
h_{fg}	heat of evaporation
$\bar{\bar{I}}$	identity matrix
$\vec{j}$	surface flux
k	thermal conductivity
L	width
m	friction force multiplier, wave number
$\dot{m}$	rate of interfacial mass transfer
M	mass
$\hat{n}$	normal unit vector
N	gamma flux
N_o	incident flux
p,P	pressure
P	Peclet number
Pr	Prandtl number
q	surface heat flux
Q	heat generation term, volumetric flow rate
r,R	radius
R_h	hydraulic radius
Re	Reynolds number
$s(t)$	surface of discontinuity
$S(t)$	Surface enclosing material volume $V(t)$

S	gamma beam sensitivity to water content
S_f	friction or energy slope
t	wall thickness
T	temperature
$\overline{\overline{T}}$	stress tensor
T_{CHF}	critical heat flux temperature
T_o	sputtering temperature
T_s	coolant temperature
u,U	velocity, flow velocity in the axial direction
u_r	relative velocity
u_{crit}	critical velocity
$\vec{v}$	velocity vector
$V(t)$	material volume
V	rewetting velocity
y	vertical distance
y_h	hydraulic depth
z	axial distance

Greek

α	void fraction, thermal diffusivity
β	fraction of energy input used for evaporation
γ	slip ratio, weighting factor for the determination of the interface velocity

Γ	vapor generation term
δ	wall thickness
Δt	time step size
Δz	mesh size
ε	wall thickness, statistical error
θ	angular position
ℓ_s	stratified length
λ	wave length
Λ	void propagation velocity
μ	viscosity, mass absorption coefficient
ν	kinematic viscosity
ρ	density
σ	Stefan-Boltzman constant, surface tension
τ	dimensionless time, shear stress
ϕ	two phase friction multiplier, dimensionless temperature
Φ	source term
ψ	local instantaneous variable
ω	Escoffier stage variable
Ω	source term in void propagation equation

Subscripts

a	ambient
B	bottom of channel
f,F	liquid phase
g,G	vapor phase

i	interface
in	inlet
k	phase k
L	liquid phase
S	mid-side of channel
sat,s	saturation
T	top of channel
z	axial direction
w	wall

Notes:

(1) Quantities that are not included in the list are defined where they are used.

1. INTRODUCTION

1.1 Background

To license nuclear power stations in Canada, postulated loss of coolant accidents (LOCA) must be analysed and radioactivity releases shown (by calculation) to be below the maximum levels prescribed by the Atomic Energy Control Board. An empirical basis for analysing LOCA does not exist. Therefore, LOCA analysis must be based on the soundest theory available at any given time, and systematically checked against experiments of increasing complexity and scale.

The Canadian approach to developing the thermohydraulic aspects of LOCA analysis is shown in Figure 1.1. The analysis essentially consists of the system of governing equations (conservation equations, boundary conditions and constitutive relationships) and the solution technique. The solution technique for a set of governing equations can be checked against a reference, but much less computationally efficient solution technique, such as the method of characteristics. Thus computationally efficient solution techniques can be developed independent of experiment for certain forms of the governing equations. Once an accurate solution technique is available the assumptions leading to the governing equations must be checked by comparing predictions with experimental results. Special experiments must also be done to develop constitutive relationships appropriate to the various primary heat transport components and for each phase of the postulated LOCA.

Several benchmark blowdown experiments have been done in simple geometries. These have been used to check the systems of governing equations by Banerjee et al [1]. They have shown that the set of governing equations used in licensing calculations adequately predict experimental results for blowdown.

FIG. 1.1 METHODOLOGY OF CANADIAN APPROACH TO LOCA ANALYSIS

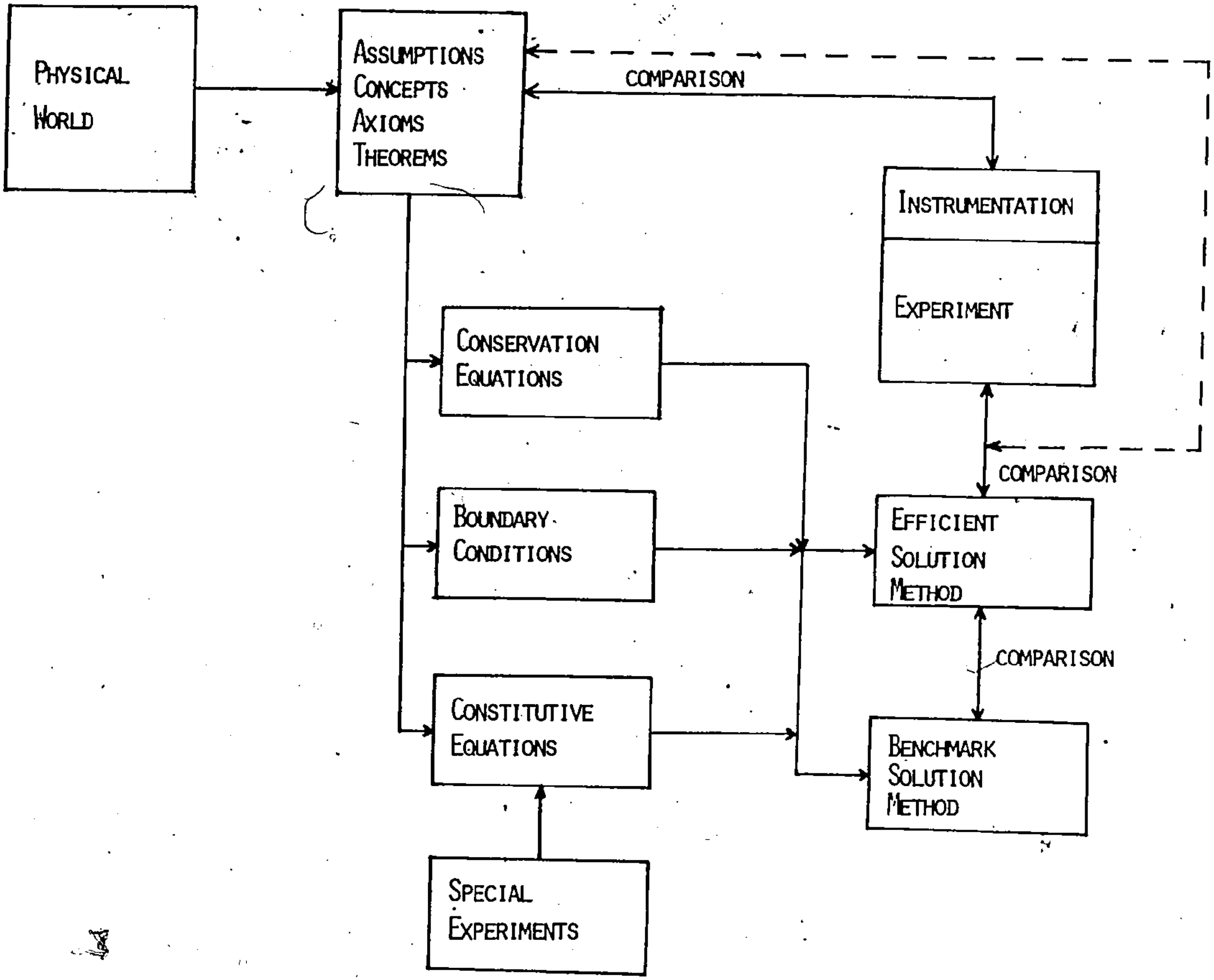

Benchmark experiments do not however, exist for refilling and rewetting of systems for horizontal channels similar to those in CANDU reactor cores. Such experiments are needed so that the form of the conservation equations and constitutive relationships during the emergency core cooling (ECC) phase of a postulated LOCA can be developed. This need leads to the objectives in the next section.

1.2. Objectives

The main objectives of the work are to measure thermohydraulic parameters during transient rewetting and refilling of hot horizontal channels so as to:

(i) identify the dominant phenomena and develop simplified multi-fluid models and

(ii) obtain forms of the interphase heat, mass and momentum transfer relationships in relatively simple flow regimes.

To achieve the second objective it is desirable to measure pressure, wall temperature, liquid and vapor temperature, void fraction, phase distribution, and liquid and vapor mass velocities. However, considerable difficulties are involved in making these measurements. For example, the insertion of pressure or temperature probes into the channel will lead to secondary quench fronts. Therefore, only the inlet and exit pressures and fluid temperatures, outside channel wall temperature, cross-sectional averaged void fraction and inlet water mass velocity could be measured in these experiments. Other parameters are deduced or inferred.

The results of experiments and analysis on the refilling and rewetting processes in hot horizontal systems will be presented in this report.

2. REWETTING IN NUCLEAR REACTOR EMERGENCY CORE COOLING STUDIES

2.1 General

Surface rewetting is of fundamental importance for the re-establishment of normal and safe temperature levels following dryout in a loss of coolant accident (LOCA) in a water cooled nuclear reactor. In the event of a LOCA, fuel temperature rises rapidly due to poor heat transfer resulting from dryout and due to continuing fission product decay heat. To prevent the fuel temperature from rising too high and possibly damaging or melting the fuel rods, it is usually thought desirable to arrest the temperature rise and restore a high heat transfer condition in the core. This is done by injecting emergency cooling water into the reactor core and re-establishing water contact with the hot surfaces.

The techniques used for emergency core cooling vary according to reactor designs. There are basically two design concepts for water cooled nuclear reactors. The first design concept has a reactor core placed in a reactor vessel. The fuel rods in the core are arranged in arrays vertically. Cooling water comes in and out through the reactor vessel. Reactors of this type are being widely used world-wide. The boiling water reactors (BWR) and pressurized water reactors (PWR) fall into this category. A schematic diagram of a PWR primary coolant system is shown in Figure 2.1.

The CANDU pressurized heavy water reactor (PHR) constitutes the other major commercial water cooled reactor design. Instead of a reactor vessel, a calandria is used. The fuel bundles are housed in horizontal channels consisting of pressure and calandria tubes as shown in Figure 2.2.

A very important difference in the two basic designs is the orientation of the fuel elements. In the first case, the fuel rods are in vertical

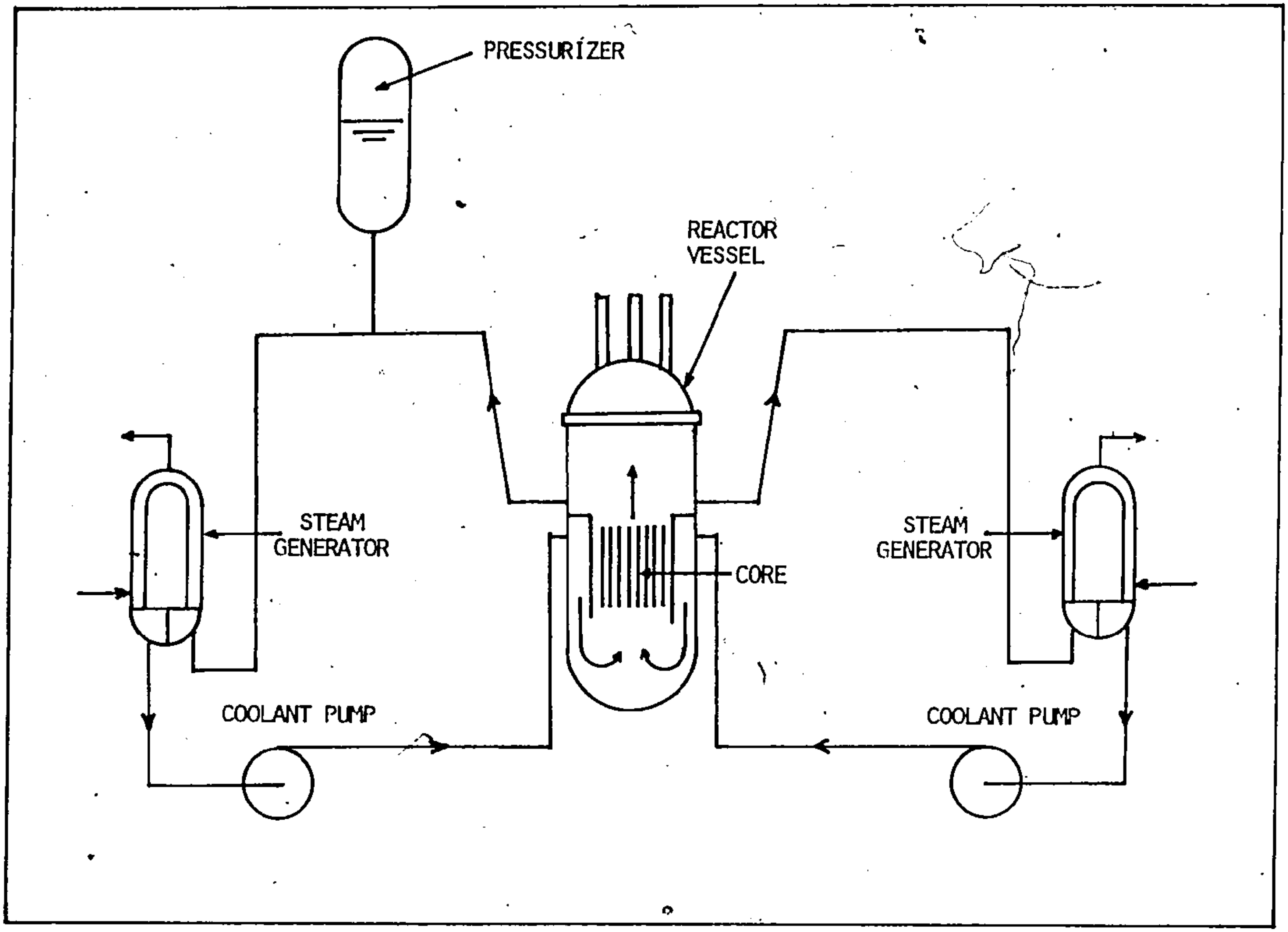

FIG. 2.1 PWR PRIMARY COOLANT SYSTEM SCHEMATIC

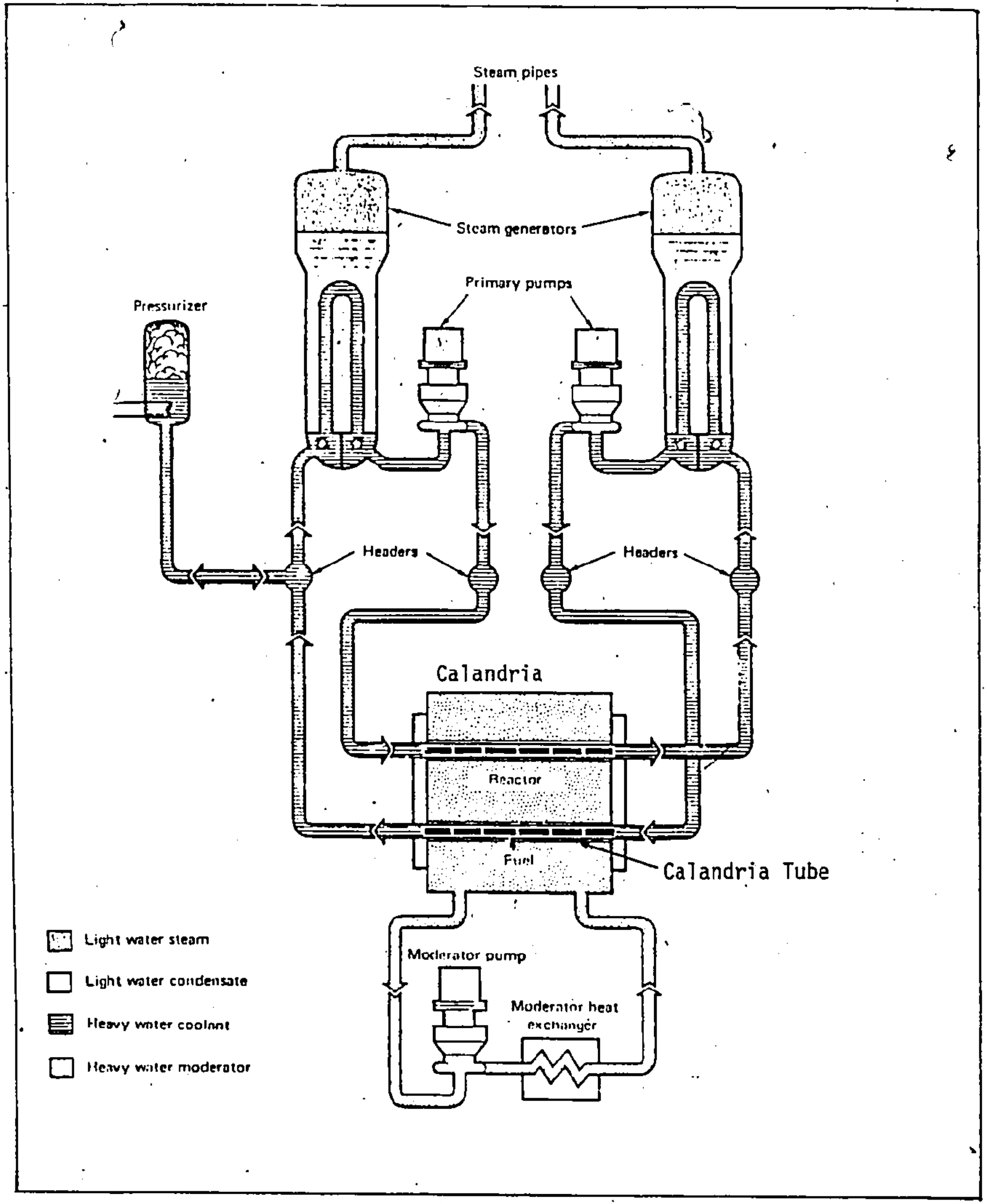

FIG. 2.2 CANDU REACTOR SIMPLIFIED FLOW DIAGRAM

assemblies which make up the reactor core. In the second case, horizontal fuel channels (calandria tubes) are used. The calandria tubes are supported at both ends by the calandria end shields and the interstitial spaces are filled with heavy water which acts as the moderator.

Because of the difference in basic reactor designs, the emergency core cooling systems (ECCS) are also different. For the BWR - and PWR - type reactors, two techniques have been used, namely top spray cooling and bottom reflooding. Following the blowdown phase, the ECCS injects cooling water into the primary system until the core is totally rewetted and refilled with water. In the CANDU PHR-type reactors, emergency cooling water is injected into the headers connected to the individual horizontal channels.

The physical processes involved in the rewetting and refilling of hot vertical systems, have been studied both for falling water drops and films (top spray cooling) and upflow of water (bottom flooding). Considerable experimental and theoretical work on effects of different parameters on the effectiveness of rewetting now exists. The work is reviewed later. For horizontal channel rewetting and refilling, the physical processes are different because of the gravity forces which lead to flow stratification. Very little systematic investigation has been done in simple geometries.

2.2. Review of Top Spray Cooling and Bottom Reflooding of Vertical System

In the past decade, work has been done in many countries (notably in the United States, Canada, Western Europe and Japan) on top spraying and bottom flooding of vertical channels. The effort may be divided into experimental and theoretical. Reviews are given by Yadigaroglu et al [2], Swan and Carbon [3] and Butterworth and Owen [4].

Experiments were performed both with single heated tubes or rods in annuli and with arrays of heated rods simulating fuel bundles. The objectives of the single-channel experiments were to gain a basic understanding of the thermohydraulic phenomena involved in the quench process. The bundle experiments gave the fluid flow and heat transfer information needed for reactor safety analysis.

Transient heat transfer coefficients at different axial positions are of primary interest. Various simple models have been proposed and it is normally calculated using the system saturation temperature as the coolant temperature. The experiments, however, usually lead to data that include the average quench velocity,quench temperatures and times, liquid entrainment, vapor velocity and other parameters depending on individual experimental designs. These results are now being used to develop more sophisticated models.

2.2.1 Experimental Work - Rod Bundles

A number of quenching experiments with full-length and some full-size rod bundles have been performed. The most important investigation of top spray cooling was conducted by the General Electric Company (United States) under the FLECHT (Full Length Emergency Cooling Heat Transfer) program (Duncan and Leonard [5, 6]). The experiments were done with full-size (12 ft or 3.66 m), stainless steel and Zircaloy-clad, 49-rod BWR bundle simulations. The results showed that spray cooling is a suitable standby cooling system to protect the reactor core in case of a LOCA.

Bottom-reflooding experiments with full-length and full-size rod budles were conducted in the United States under the PWR-FLECHT program (Haire and Brockett [7], O'Brien [8], Cermak et al. [9] and Cadek et al

[10, 11]) and its continuation, the FLECHT-SET (Full Length Emergency Cooling Heat Transfer - Systems Effects Tests) program (Cadek et al. [12], Blaisdell et al. [13], Cleary et al. [14] and Waring et al. [15]).
The objectives of the program were to obtain experimental reflooding heat transfer data for PWR LOCA analysis. The experiments were performed by the Westinghouse Electric Corporation using full-scale, electrically heated 49- and 100- rod stainless-steel and zircaloy-clad bundles mounted in square flow housings. The results of the PWR-FLECHT experiments are discussed in detail by Cadek et al [10,11].

Other core reflooding experiments conducted in the United States include the SECHT (Scoping Emergency Cooling Heat Transfer) Series Experiments (Forbes et al. [16], Schlenker et al. [17], Moser and Griebe [18] and Plum [19]) and the FHUST (Fuel Heatup Simulation Tests) Experiments (Curet et al. [20] and Jensen [21]). The objectives of the SECHT series of experiments were to provide an early evaluation of emergency core cooling system effectiveness, identify any unexpected phenomena occuring during reflooding and evaluate the parametric trends. The FHUST experiments were planned to investigate the thermodynamic and mechanical behaviour of PWR fuel pins under simulated LOCA conditions.

Bottom reflooding experiments were also done in Canada, Italy, Japan and Germany.

In Canada, experiments were conducted at Chalk River Nuclear Laboratories using a mockup of the 18-rod CANDU-type fuel bundle. The purpose was to obtain data on the rate of quenching, preferential radial cooling and pre-quenching heat transfer during the early stages of bottom flooding. Details of the experimental design and results are given by Thompson [22].

The Italian effort was conducted by FIAT in cooperation with SORIN (Societa Ricerche Impianti Nucleari). The possibility of cooling a PWR-type rod bundle at a very low reflooding velocity (0.5 to 1.5 cm/s) was investigated (Campanile and Pozzi [23]). The test section consisted of 21 rods in a square pitch. Both transient and steady state experiments were performed. However, the results are not directly applicable to the LOCA of large PWR s because the heated length was short and the axial power distribution was uniform.

In Japan, the work on ECC of BWR's was conducted uder the Hitachi experimental program. A mockup of the entire BWR vessel and core reflooding system was used. The program was similar to the BWR-FLECHT program conducted by the General Electric Company. Details of the program are given by Ogasawara et al [24]. Experiments on top spray cooling in a 36-rod assembly were done by Yamanouchi. The effects of initial wall temperature and water flow rate were investigated (Yamanouchi [25]).

In Germany, Siemens has conducted reflooding experiments with a 340-rod bundle. The purpose of the program was to investigate the performance of the low pressure ECCS's used in Siemen's PWR s and to obtain experimental reflooding data under simulated LOCA conditions. The experiments were reported by Riedle and Winkler [26].

2.2.2 Experimental Work - Single Channel

A considerable amount of work has been done on the quenching of single channels. The purpose of the experiments was to gain a fundamental understanding of the quenching phenomena under well defined and relatively simple conditions. The test sections were either heated tubes or heated rods in annuli. The main advantages of the annular geometry are that a rod closely simulating a fuel rod can be used and flow visualization is possible if the outside surface is made of glass.

Early British work was done at Winfrith by Shires et al. [27]. The mechanism of film flow and heat transfer for vertical rods were investigated. Tests were run both with single heated rods (0.625 in. O.D.) and with a cluster of seven rods. Bennett et al. [28] carried out experiments on rewetting of a vertical stainless steel tube (0.5 in. o.d. by 0.064 in. thick) in a steam environment at pressures ranging from 100 to 1000 psia. Elliot and Rose [29,30] did a series of experiments to measure the quenching rate in a steam environment for a range of water flows and in pressures up to 800 psia. They studied the effects of spraying on the inside of Zircaloy, stainless steel and Inconel tubes. Inside surface quenching was used rather than outside because the fuel elements are better represented as a collection of sub-channels rather than a set of individual rods. Duffey and Porthouse [31] studied the physical mechanism governing the water distribution and cooling capability on surface quenching at atmospheric pressure. Experiments were performed with single rods and tubes as well as a cluster of tubes. Experiments with both top spray and bottom flooding were done at atmospheric pressure by Piggot and Porthouse [32] to study the effects of surface conditions and water subcooling on rewetting rates. White and Duffey [33] performed a series of single-rod reflooding experiments with special emphasis on the unsteady flow and steam binding phenomena. Steam binding was simulated by a variable test-section - outlet orifice. More recently, Pigott and Duffey [34] presented the results of falling film rewetting experiments on two types of irradiated fuel pins and on a complementary range of tubes and heaters. Preliminary measurements of rewetting rates in bottom flooding were also presented. Comparisons were made between falling film and bottom flooding rewetting, including the effects of surface finish.

In France, experiments were carried out in the Heat Transfer Laboratory at Grenoble. Preliminary single-channel, atmospheric-pressure quenching experiments were conducted to investigate parametric trends and the influence of channel lengths, heater thermal capacity and bundle effects. Results are presented and discussed by Andreoni and Courtand [35] and Andreoni et al [36].

In Germany, single-tube, top - and bottom - reflooding experiments were conducted by Schneider and Thomas [37]. These experiments were part of the German ECC research program and preceded the Siemens 340-rod experiments discussed previously.

Thermal transients following bottom-flooding were studied in Italy as part of the CIRENE reactor safety analysis program. Both tubular and externally-heated annular test sections were used. Test conditions, measured quench times and surface temperature traces are reported by Martini and Premoli [38].

In Canada, experimental work on single channel rewetting was reported by Groeneveld and Young [39] and Lee et al [40]. Parametric effects of mass flux, inlet subcooling, wall thickness and power input on quench velocity were discussed. The facility used by Lee et al. allowed experiments to be carried out with test sections at any angle between horizontal and vertical.

2.2.3. Experimental Work - Results and Observations

All transient quenching experiments were conducted in a similar fashion. The rod or tube or cluster of rods are preheated to the desired initial temperature at a relatively low power level. During this time, the test section contains air or saturated steam only. Quenching is initiated by injecting cooling water either from the top (top spray) or from below (bottom flooding). Surface temperatures and pressure drop were recorded during the entire quenching period. For a given test section geometry, the parameters investigated were normally the water flow rate, the inlet subcooling, the initial test section temperature, the system pressure, the power level and the thickness and physical properties of the test section.

Since the physical processes involved in the quenching of hot surfaces are the same for both top spray or bottom flooding (Thompson [22] and Duffey and Porthouse [41]), very similar experimental results were obtained. Some of the more important results and observations are summarized as follows.

(1) As the initial cladding temperature increases, the temperature rise, ΔT_{rise}, defined as the difference between the initial cladding temperature and the peak clad temperature decreases. The turn around time, t_{turn}, which is the time at which maximum clad temperature occurs also decreases (Duncan and Leonard [5,6] and Cadek et al. [10,11]). This implies that the effective heat transfer coefficient increase, with initial clad temperature.

(2) Increasing the water flow rate decreases the clad temperature rise, the turn around time and the quench time (Duncan and Leonard [5,6] and Cadek et al. [10,11]).

(3) The quench velocity decreases with increase of initial clad temperature.

(4) The quench velocity increases with water flow rate when the environment is air at atmospheric pressure (Yamanouchi [25], Shires et al. [27] and Duffey and Porthouse [31]). When the environment is steam and the pressure greater than atmospheric, the quench velocity was found to be independent of water flow rates (Bennett et al. [28] and Elliot and Rose [29,30]). The reason for this discrepancy is not clear and further investigation is needed.

(5) Preferential cooling was observed in both top spray and bottom flooding of rod clusters. At the time of peak clad temperature, the inner rods experienced temperature increases much higher than the outer ones.

(6) The quench front travels down the unheated canister faster than the heated rods and the effective heat transfer coefficient prior to rod quenching increases dramatically (as much as 10 times) at the time of canister wetting.

(7) Increasing pressure above atmospheric pressure improved performance of both top spray and bottom flooding. As the pressure increases, the quench velocity increases, the peak clad temperature decreases and the turn around time decreases. These effects are resulted from an increase in sputtering temperature with pressure.

(8) The quench velocity was nearly constant with time (Yamanouchi [25] and Shires et al. [27]).

(9) Both Zircaloy and stainless steel-clad rods were reported to be quenched at similar rates in spite of their difference in thermal capacities in the BWR-FLECHT program (Duncan and Leonard [5,6]). In single

channel experiments, however, the quench rate of a Zircaloy tube was found to be approximately twice that of stainless steel and Inconel (Elliot and Rose [29, 30] and Piggott and Duffey [34]). The reason for the discrepancy again is not clear. It should be noted that results from the single channel experiments are in agreement with theory as will be shown in next section.

(10) It was observed in all cases that the quench rate increases with inlet water subcooling.

(11) It was also observed that quench rate could be changed by up to a factor of five by changing the surface finish in single channel experiments (Elliot and Rose [29] and Duffey and Porthouse [31]). This is believed to be related to changes in surface nucleation characteristics.

(12) The quench velocity decreases with increases in wall thickness in single channel experiments (Groeneveld and Young [39] and Lee et al. [40]).

2.2.4. Theoretical Work

From the experimental work discussed in the previous sections, it has been shown that the rate at which a hot surface is quenched by either top spray or bottom flooding depends on the initial surface temperature, system pressure, inlet water flow rate and subcooling, volumetric heat capacity, thickness and condition of the surface. A theoretical model is necessary in order to understand and to interpret experimental data obtained and to predict the thermohydraulic behaviour of the primary cooling loop in water-cooled reactors in LOCA analysis.

Unfortunately, such a model does not exist. Part of the reason is because the quenching process is not completely understood at present.

For example, the effect of flow parameters on the physical mechanisms that govern the quench phenomena is not entirely clear, and the physical mechanisms controlling the boiling heat transfer coefficient and the sputtering temperature (the temperature at which the surface first wets) are not well understood. A model that is generally used is the so-called two-region "Conduction Controlled" model. The model assumes that the quench velocity is determined by the rate at which heat can be conducted from the dry hot side through the surface to the wetted side where it is removed by boiling. Although the model can describe a lot of quench data reasonably well, its weakness lies in the fact that its governing equation is just the transient heat conduction equation. The thermohydraulic aspect of the process is ignored. Thus, the effects of system pressure, precursory cooling, inlet water flow rate and subcooling on the quench velocity cannot be determined explicitly. However, the conduction controlled model is useful in understanding the effects of wall temperature, wall thickness and wall physical properties on rewetting. Practically all the theoretical work done to date has attempted to solve this conduction controlled model. A brief review will be given below.

For the case of no heat generation in the wall, the governing equation is the two-dimensional transient conduction equation

$$\frac{\rho C}{k}\frac{\partial T}{\partial t} = \frac{1}{r}\frac{\partial}{\partial r}\left(r\frac{\partial T}{\partial r}\right) + \frac{\partial^2 T}{\partial z^2} \qquad (2.1)$$

The equation is shown in cylindrical coordinate, Where ρ is the density, C is the heat capacity and k is the thermal conductivity of the wall. Since the quench velocity was found to be nearly constant with time, eq. (2.1) can be simplified by performing the transformation

$$Z = z - ut$$

where u is the quench velocity and is assumed to be constant, t is time.

With the transformation, in which the new coordinates move along with the quench front, the transient equation is reduced to a quasi-static one

$$\frac{\rho C u}{k}\frac{\partial T}{\partial Z} + \frac{1}{r}\frac{\partial}{\partial r}\left(r\,\frac{\partial T}{\partial r}\right) + \frac{\partial^2 T}{\partial Z^2} = 0 \qquad (2.2)$$

The problem can be simplified considerably if the wall temperature is assumed to be uniform throughout its thickness (δ). By assuming that the heat transfer coefficient (h) is constant in the quenched region ($Z \leq 0$) and is zero in the dry region ($Z > 0$), and also assuming that the wall temperature at the quench front equals the sputtering temperature, Yamanouchi [25] obtained the one-dimensional analytical solution

$$u^{-1} = \rho C\left(\frac{\delta}{hk}\right)^{\frac{1}{2}}\left(\frac{T_w - T_0}{T_0 - T_s}\right) \qquad (2.3)$$

Where T_w is the initial dry wall temperature, T_s is the coolant temperature and T_0 is the sputtering temperature.

Duffey and Porthouse [41] using the same assumptions but a slightly different approach, obtained an approximate one-dimensional solution

$$u^{-1} = \rho C\left(\frac{\delta}{hk}\right)^{\frac{1}{2}}\frac{(T_w - T_s)^{\frac{1}{2}}(T_w - T_0)^{\frac{1}{2}}}{(T_0 - T_s)} \qquad (2.4)$$

which is the same as that obtained by Semeria and Martinet [42]. For high initial wall temperatures, $T_0 \simeq T_s << T_w$, Eq. (2.4) can be written as

$$u^{-1} = \rho C \left(\frac{\delta}{hk}\right)^{\frac{1}{2}} \left(\frac{T_w - T_0}{T_0 - T_s}\right) \tag{2.5}$$

which is identical to the Yamanouchi equation (Eq. 2.3).

Duncan and Leonard [6] extended the one-dimensional solution given by Eq. (2.3) to include a uniform heat generation term. They obtained the expression

$$u^{-1} = \rho C \left(\frac{\delta}{hk}\right)^{\frac{1}{2}} \left(\frac{T_w - T_0}{T_0 - T_s - q/h}\right) \tag{2.6}$$

where q is the surface heat flux.

Using the two-region conduction model, Yamanouchi [25] obtained unreasonably high heat transfer coefficients (of the order of 10^5 to 10^6 $w/m^2 - {}^oK$) in order to predict quench velocities comparable to the observed values. To relax the constant wet-side heat transfer coefficient assumption (which is essential for analytic solutions), Thompson [43] solved the one-dimensional case numerically assuming a temperature dependent heat transfer coefficient. However an even higher heat transfer coefficient ($\sim 5 \times 10^6$ $w/m^2 - {}^oK$) was obtained at the quench front.

Sun et al [44] proposed an improved analytical model which divides the quenching process into three regions instead of two. A sputtering region was added right behind the wet front. Thus, the surface was divided into three regions; a dry region ahead of the wet front, a sputtering region right behind the wet front, and a region of continuous liquid film further upstream. The length of the sputtering region is quite short, on the order of ten times the wall thickness. Constant heat transfer coefficients were used in the different regions. A one-dimensional analytical solution was obtained. The result reduces to Yamanouchi's equation in the limit when the sputtering region goes to zero. With the three-region model, Sun et al. [44] arrived at a reasonable heat transfer coefficient for the sputtering region. The predicted value of 1.7×10^{4} w/m^{2}-^{0}C compares favourably with the corresponding transition and nucleate pool boiling values.

The one-dimensional solutions have been found to successfully correlate much experimental data (Riedle and Winkler [26], Duffey and Porthouse [41], Semeria and Martinet [42] and Sun et al. [44]). However, the solutions are valid only at very low quench rates and for small Biot numbers or very thin walls. In many practical situations, when the quench velocity is relatively high, a two-dimensional analysis is necessary.

Two-dimensional analyses have been reported by Yoshioka and Hasegawa [45] and Edwards and Mather [46]. The governing equation was solved analytically. However, the models were not entirely satisfactory and the solutions were approximate.

Duffey and Porthouse [41] solved the two-dimensional problem analytically, again assuming a constant wet-side heat transfer coefficient. A first order two-dimensionsal solution was obtained. It was shown that for very small Biot numbers, the solution reduces to the one-dimensional solution as expected. For large Biot numbers, the solution can be written in the first order in approximate form as

$$u^{-1} \simeq \frac{\pi \rho C}{2h} \left(\frac{T_w - T_s}{T_0 - T_s}\right) \qquad (2.7)$$

which is independent of the wall thickness and thermal conductivity.

Instead of truncating an infinite series expansion after the first term to obtain a first-order solution as Duffey and Porthouse [41] did, Blair [47] retained all the terms in the series and derived an accurate asymptotic solution

$$\frac{T_w - T_s}{T_0 - T_s} \simeq 1 + \frac{Bi}{\pi P}\left(2 + \frac{\pi}{2P} + \frac{2}{P^2}\right) + \frac{Bi^2}{2\pi^2 P^2}\left(\frac{8}{3} - \pi^2 - \frac{13\pi}{3P}\right) \qquad (2.8)$$

Where Bi and P are the Biot and Peclet numbers respectively and the solution is valid for $Bi/P > 1$. For high wetting rates or large P, Eq. (2.8) can be reduced to

$$u^{-1} \simeq \frac{\pi \rho C}{2h} \left(\frac{T_w - T_0}{T_0 - T_s}\right) \qquad (2.9)$$

which is very close to (2.7).

Using a different approach (the Wiener - Hopf technique), Tien and Yao [48] solved the two-dimensional problem analytically. Their solution agrees well with numerical results (Anderson and Hansen [49] and Coney [50]) for large Peclet numbers and reduces to the one-dimensional solution for small Peclet numbers. For large Peclet numbers, the functional form of Blair's asymptotic solution (Eq. 2.9) is obtained.

Thompson [43] used a two-dimensional model in which the wet-side heat transfer coefficient was allowed to be temperature dependent. The problem was solved numerically and the heat transfer coefficient in the vicinity of the quench front was evaluated by analyzing the data given by Elliot and Rose [29]. Reasonable values were obtained.

Coney [50] approached the two-dimensional problem in a different way. The energy equation was solved analytically on both the wet- and dry - side. The two solutions were then matched at a large number of points across the quench front. A high degree of accuracy was obtained. However, a computer was necessary to solve the resulting set of simultaneous equations. The functional interdependence of u, h, T_0 and T_w were obtained and plotted. A large quantity of experimental data was analysed using this approach and correlations giving the quench heat transfer coefficient and sputtering temperature were proposed (Yu et al. [51]).

The effect of precursory cooling on the rewetting rate was investigated analytically by Sun et al [52] and Dua and Tien [53]. The energy equation was solved using the Wiener-Hopf technique. It was found that (i) precursory cooling increases the rewetting rate substantially, (ii) precursory cooling is enhanced at high flow rates and (iii) assuming a constant average boiling heat transfer coefficient in the sputtering region with respect to flow rates, the available rewetting data obtained under an atmospheric steam environment with variable flow rates can be successfully correlated by taking precursory cooling into account.

2.3 Horizontal Channel Rewetting

Work on horizontal channel is rare. The obvious reasons are: (i) the problem is much more complicated and (ii) other than CANDU reactor, all other reactor designs have vertical fuel rods or channels.

Work is being done in Canada to study the reflooding of horizontal fuel bundles (Yadigaroglu et al. [2]). Some initial experimental results on the rewetting of very hot horizontal channels by flooding were reported recently by Lee et al [40]. Rewetting times in horizontal tubes were found to be about 20 to 30% higher than the corresponding rewetting times in vertical tubes.

Some qualitative results on the flooding of a hot, horizontal voided system were given by Banerjee and Hancox [54]. The experimental facility closely resembled a CANDU reactor fuel channel. The fuel bundles were simulated by 37 element internal electric heaters. The channel was closed at both ends. Two feeders were connected to the channel from the top near the ends. Cooling water was injected into the system through one feeder and discharged from the other. Attempts were made to model the process using a one-dimensional two-fluid model. However, only illustrative results were presented. Banerjee and Hancox [54] stated that considerable data on rewetting and refilling of 37 rod bundles had been taken and were being analysed before publication.

3. MODELS FOR TRANSIENT SEPARATED FLOW

3.1 General

Rewetting and refilling of a heated tube or heated rod(s) in annuli by flooding is a very complicated thermohydraulic process. To model this process, the two-region or three-region conduction-controlled model is clearly inadequate as discussed in Section 2.2.4. Physically, rewetting is the re-establishment of water contact with a hot surface. In the case of a moving quench front, highly non-equilibrium processes exist. For example, sputtering exists at, and violent boiling exists behind, the quench front. These processes determine the quench rate and cannot be "frozen" as assumed in the conduction-controlled model through the use of the constant quench velocity assumption. Instead they are strongly affected by the flow parameters, such as local pressures, local heat transfer coefficient, local water flow rates and subcoolings. Thus, to better model the situation, a non-equilibrium two-fluid model is necessary. The wall effects and transient wall temperature variations will appear as boundary conditions and through the use of appropriate heat transfer coefficients.

This two-fluid model approach is necessary, especially when a more complicated flow situation is involved, such as stratified flow in horizontal channel rewetting. The approach is, of course, a lot more complicated than the relatively simple conduction-controlled model.

For non-equilibrium two-phase flows, separate treatment of the phases (steam and water) and a detailed treatment of interphase transfer (evaporation, interfacial and wall shears, local heat transfer) are essential. In principle, a minimum of six equations will be required. That is, the mass, momentum and energy conservation equations for each phase. It should be noted here that, the development of multi-fluid models for transient two-phase flow is still at its infant stage, the state of art can be summarized as follows (Agee et al. [55]):

(1) Mathematical difficulties are encountered with solving the full equation sets for unequal phase velocities.

(2) Physical difficulties are common in the inclusion of adequate interphase relations (so called "constitutive relations") to treat mass, momentum and energy transfer.

An essential feature of multiphase flows is the presence of moving internal interfaces. Their shape and kinematics affect the structure of the flow field and may dominate interfacial transfers. In principle, the local instantaneous conservation equations for the phases may be obtained together with appropriate molecular transport properties, boundary and initial conditions. The resulting initial moving boundary value problem is completely intractable. Therefore, simplifications have to be made, leading to a "model" for a set of physical processes (Banerjee and Chan [56]).

Since for most design and analysis procedures, averaged flow quantities appear to be sufficient, one of the main approaches in multiphase flow modelling has been to develop an averaged set of field equations based on the local instantaneous conservation equations (Ishii [57], Hughes et al. [58], Delhaye and Achard [59] and Agee et al. [60]). The resulting set of averaged equations and interfacial jump conditions form a mathematical model that is much simpler than the original local instantaneous formulation. However, information is lost in the averaging process and must now be supplied in the form of constitutive equations (Banerjee and Chan [56]).

The averaging procedures that are of engineering interest are averages in space, time or over an ensemble, or some combination of these. The most general averaged formulation in use is the one-dimensional two-fluid model. It is obtained by volume averaging the local instantaneous equations. The one-dimensional two-fluid equation set, however, is still very general and because of the difficulties in providing the necessary interfacial relationships, further simplification is desirable. Such further simplification must come from physical insight, by identifying the dominant phenomena in a given two-phase flow situation. Terms that are of secondary importance are dropped from the equations. For example, in a well-mixed two-phase flow situation, velocities, temperatures and pressures of the two phases can be assumed equal and the two-fluid model will then reduce to the simple homogeneous model.

In the following sections, the local instantaneous conservation equations and averaging processes will be briefly reviewed. The form of the volume averaged one-dimensional conservation equations and jump conditions will be derived. This will be followed by a discussion of the form of interphase transfer functions and intra-phase distribution coefficients. Finally, some simple models will be discussed in the context of the more general two-fluid model. Part of the discussion will closely follow the work presented by Banerjee and Chan [56].

3.2 Local Instantaneous Conservation Equations

The conservation equations for two-phase flows have been studied in detail by Vernier and Delhaye [61] and Ishii [57], among others. The fundamental conservation laws are expressed by macroscopic balance equations written for a finite volume. They are the balances of mass, momentum and energy. The rate of accumulation of any quantity ψ, a local instantaneous variable in a finite material volume, V(t) is equal to the sum of transfer across the surface S(t) bounded by V(t) and the rate of generation in the volume V(t).

Let $\vec{J}(\psi)$ and $\phi(\psi)$, which are functions of ψ, be the flux and source of ψ respectively, the macroscopic balance equation can then ~~be written in~~ the mathematical form

$$\frac{d}{dt}\int_{V(t)} \rho\psi dt = -\int_{S(t)} \vec{J}(\psi).\hat{n}dS + \int_{V(t)} \rho\phi(\psi)dV \qquad (3.1)$$

where $\rho\psi$ is the quantity being conserved and $\hat{n}$ is the normal unit vector pointing outward from the surface S(t).

Using the Transport Theorem

$$\frac{d}{dt}\int_{V(t)} FdV = \int_{V(t)} \frac{\partial F}{\partial t}.dV + \int_{S(t)} F\vec{v}.\hat{n}\, dS \qquad (3.2)$$

and the Gauss Theorem

$$\int_{V(t)} \nabla.\vec{a}\, dV = \int_{S(t)} \vec{a}.\hat{n}\, dS \qquad (3.3)$$

where $\vec{v}$ is the velocity field of the fluid, eq. (3.1) can be transformed into

$$\int_{V(t)} [\frac{\partial}{\partial t}(\rho\psi) + \nabla.(\rho\psi\vec{v}) + \nabla.\vec{J}(\psi) - \rho\phi(\psi)]dV = 0 \qquad (3.4)$$

Since Eq. (3.4) must be valid for any V(t), the integrand must be zero at any point,

$$\frac{\partial}{\partial t}(\rho\psi) + \nabla.(\rho\psi\vec{v}) + \nabla.\vec{J}(\psi) - \rho\phi(\psi) = 0 \qquad (3.5)$$

This is the generalized local instantaneous conservation equation. It holds in each phase only and is not valid across interfaces. [illegible] make this point more explicit, Eq. (3.5) can be written in terms of variables in phase k

$$\frac{\partial}{\partial t}(\rho_k\psi_k) + \nabla.(\rho_k\psi_k\vec{v}_k) + \nabla.\vec{J}_k(\psi_k) - \rho_k\phi_k(\psi_k) = 0 \qquad (3.6)$$

For a material volume V(t), the expressions of ψ_k, $\vec{J}_k$ and ϕ_k for mass, momentum and energy conservation are given in the following table:

Balance	ψ_k	$\vec{J}_k$	ϕ_k
Mass	1	0	0
Momentum	$\vec{v}_k$	$-\overline{\overline{T}}_k$	$\vec{F}_k$
Energy	$e_k + \frac{v_k^2}{2}$	$\vec{q}_k - \overline{\overline{T}}_k.\vec{v}_k$	$\vec{F}_k.\vec{v}_k + Q_k$

Where $\vec{v}_k$ is the velocity field of the fluid, $\overline{\overline{T}}_k$ is the stress tensor, $\vec{F}_k$ is the external forces, e_k is the internal energy, $\vec{q}_k$ is the heat flux and Q_k is the heat generation term.

If the material volume V(t) contains an interface, that is a surface of discontinuity s(t) as shown in Figure 3.1, Eq. (3.1) can be written as

$$\int_{V(t)} \frac{\partial}{\partial t}(\rho\psi)dV + \int_{S(t)} \rho\psi\vec{v}.\hat{n}\, dS - \int_{s(t)} [\rho\psi]\vec{v}_i.\hat{n}\, dS$$

$$= - \int_{S(t)} \vec{J}(\psi).\hat{n}\, dS + \int_{\hat{V}(t)} \rho\,\phi(\psi)dV \qquad (3.7)$$

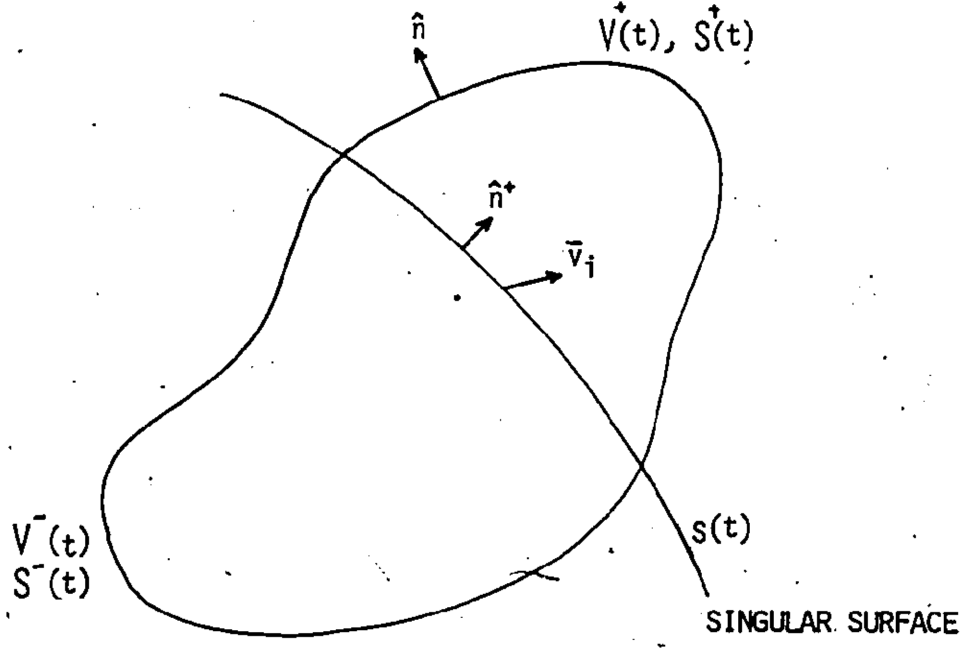

FIG. 3.1 TRANSPORT THEOREM WITH A SINGULAR SURFACE

where $\vec{v}_i$ is the velocity of the interface. [ ] is defined as

$$[F] = F^+ - F^-$$

where F^+ and F^- are quantities in the two regions divided by the interface. For example, $v^+ = v_g$ and $v^- = v_f$ in Figure 3.1.

Now if we allow the volume V(t) to approach zero, that is S^+ and S^- collapse onto s(t), Eq. (3.7) becomes

$$\int_{s(t)} \{[\rho\psi\vec{v}.\hat{n}^+] - [\rho\psi]\vec{v}_i.\hat{n}^+ + [\vec{J}(\psi).\hat{n}^+]\} dS = 0 \tag{3.8}$$

Since Eq. (3.8) must be valid for any s(t), the integrand again must be zero, that is

$$[\rho\psi\vec{v}.\hat{n}^+] - [\rho\psi]\vec{v}_i.\hat{n}^+ + [\vec{J}(\psi).\hat{n}^+] = 0 \tag{3.9}$$

or

$$\sum_{k=1}^{2} \{\rho_k\psi_k(\vec{v}_k - \vec{v}_i) + \vec{J}_k]\cdot\vec{n}_k = 0 \tag{3.10}$$

which is Kotchine's Theorem for jump conditions across an interface.

3.3 Averaging Procedures

Review of averaging operators have been presented by Delhaye and Achard [59]. Ishii [57] and Nigmatulin [62]. The commonly used averaging procedures are:

(i) volume or area averaging, with no averaging in time,
(ii) time averaging, with no averaging in space,
(iii) ensemble averaging, with no averaging in space
(iv) ensemble/space averaging or time/space averaging.

It is important to note that the proper averaging procedure should give flow parameters that are continuous and have continuous first derivatives. The procedure should also separate "signal" from "noise", and result in averaged flow variables that can be measured with practical instrumentation.

If time or cross-sectional area averaging is used alone, difficulties with the continuity of flow parameters and their derivatives may arise. For example, if cross-sectional area averaging is used, the first derivatives of the flow parameters (void fraction, velocity, pressure and enthalpy) will become discontinuous each time an interface becomes tangent to the cross-sectional plane. Similarly, the time derivative of a point void fraction measurement becomes discontinuous, since at any instant the vapor phase is either present or not present at that point.

This problem of discontinuities in the derivative of the area averaged flow parameters disappears if the volume averaging procedure is used. However, if volume averaging is done alone, the volume must be chosen such that the instantaneous value of the fluctuation (or noise) in the flow parameters is small compared to their average. Physically, the averaging volume has to be large compared to the dimensions characterizing the flow regime involved. An acceptable volume depends on the flow structure and how rapidly it is changing and cannot usually be determined a priori. Consider, for example, volume averaged void fractions determined by trapping flow between two quick closing valves. The experiment can be repeated again and again by starting from the same initial conditions and by closing the valves after the same elapsed time. If the void fraction measured remains about the same in successive runs, then the volume between the valves is large enough. Otherwise, it is too small to be used for volume averaging alone.

If the volume is too small for volume averaging alone, a combination of volume and ensemble averaging can be used. The procedure involves the averaging of the measured void fractions over a set of repeated experiments. By considering how much the moving average changes between successive runs one can determine the number of runs necessary to give an acceptable accuracy. This type of averaging is extensively used in practice when calibrating void measurement devices, like gamma or neutron densitometers against quick closing valve measurements (Banerjee et al. [63]).

If ensemble averaging is to be used alone, the experimental volume would have to be a point. This can be realized experimentally by inserting a tiny optical probe into the flow to determine which phase is present at a point at any instant. In this case one could repeat the same experiment and, in principle, determine the likelihood that a particular phase occupies a given point. In general, a very large number of repeated experiments is necessary to get a good average. Thus ensemble averaging alone is not appealing from a practical viewpoint.

Single time, space or ensemble averages can lead to difficulties as discussed. Therefore, combined space/time or space/ensemble averages are normally used. While space/time averages are the simplest to obtain in experiments, difficulties may arise in distinguishing signal from noise in rapid transients. Space/ensemble averages are also straight forward to obtain from a set of repeated experiments. However, for larger experiments, ensemble averages can only be obtained at prohibitive costs. Thus more work still remains to be done on the use of appropriate averaging procedures, especially for rapid transients.

3.4 Averaged Conservation Equations and Jump Conditions

To illustrate the mathematical procedures used in averaging, the volume averaged one-dimensional conservation equations and jump conditions will be derived. Other types of averages can be derived in exactly the same way and will not change the form of the equations. In particular, time or ensemble averaging can be done before or after volume averaging. The averaging operators are commutative (Delhaye and Achard [59]). The mathematical system derived is sometimes called a "multi-fluid model".

Consider the flow situation in Figure 3.2. Let V_k be the volume of phase k enclosed between the walls and the cross-sectional planes spaced a distance Z apart (Z can be arbitrarily small). To derive the volume averaged form of the conservation equations, we will use Gauss' theorem and Leibnitz' rule (Bird et al. [64]). The particular forms applying to Figure 3.2 are given in Eqs. 3.11 and 3.12 respectively.

$$\int_{V_k} \nabla\cdot\vec{a}\, dV = \frac{\partial}{\partial z}\int_{V_k} \hat{n}_z\cdot\vec{a}\, dV + \int_{a_i} \hat{n}_k\cdot\vec{a}\, dS \qquad (3.11)$$

$$\frac{\partial}{\partial t}\int_{V_k} F dV = \int_{V_k} \frac{\partial F}{\partial t} + \int_{a_i} F(\vec{v}_i\cdot\hat{n}_k)dS \qquad (3.12)$$

We will define averages by the following symbols

$$\langle f_k\rangle = \frac{1}{V_k}\int_{V_k} f_k dV \qquad (3.13)$$

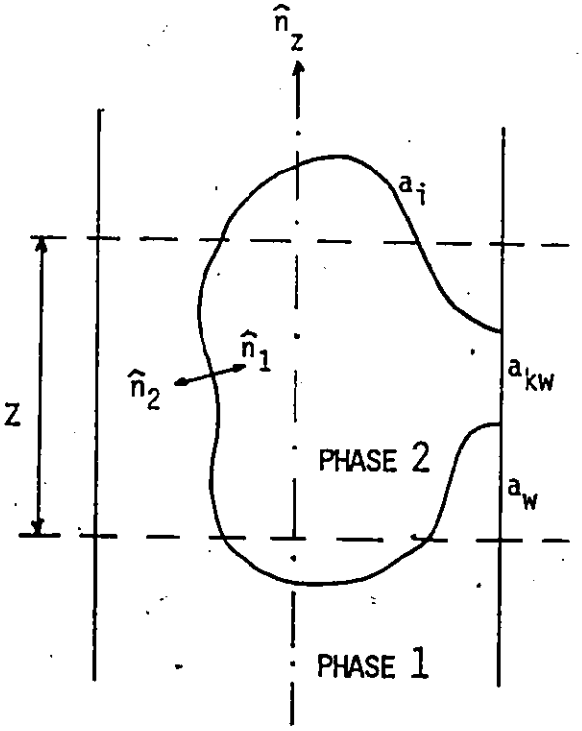

FIG. 3.2 DEFINITIONS OF SYMBOLS AND GEOMETRY FOR THE AVERAGING PROCESS

$$<f_k>_i = \frac{1}{V} \int_{a_i} f_k dS \tag{3.14}$$

where

$$V = \Sigma V_k$$

The generalized local instantaneous conservation equation as derived in Section 3.2 is

$$\frac{\partial}{\partial t} (\rho_k \psi_k) + \nabla . \rho_k \psi_k \vec{v}_k + \nabla \cdot \vec{j}_k - \rho_k \Phi_k = 0 \tag{3.6}$$

This equation may be volumed averaged and by using Gauss' theorem (3.11) and Leibnitz' rule (3.12), it can be reduced to

$$\frac{\partial}{\partial t} \int_{V_k} \rho_k \psi_k \, dV + \frac{\partial}{\partial z} \int_{V_k} \hat{n}_z \cdot (\rho_k \psi_k \vec{v}_k + \vec{j}_k) dV - \int_{V_k} \rho_k \Phi_k \, dV$$

$$= \int_{a_i} \rho_k \psi_k \hat{n}_k \cdot (\vec{v}_i - \vec{v}_k) dS - \int_{a_i + a_{kw}} \hat{n}_{kw} \cdot \vec{j}_k \, dS \tag{3.15}$$

where the assumption that $\vec{v}_k = 0$ at the wall (a_{kw}) has been made.

Defining the phase volume fraction

$$\alpha_k = \frac{V_k}{V}$$

and using Eq. (3.13), Eq. (3.15) can be written as

$$\frac{\partial}{\partial t} \alpha_k <\rho_k \psi_k> + \frac{\partial}{\partial z} \alpha_k < \hat{n}_z \cdot (\rho_k \psi_k \vec{v}_k + \vec{j}_k)> + \alpha_k \; <\rho_k \Phi_k>$$

$$= - \frac{1}{V} \int_{a_i} .(\dot{m}_k \psi_k + \vec{j}_k \cdot \hat{n}_k) dS - \frac{1}{V} \int_{a_w} \hat{n}_{kw} \cdot \vec{j}_k dS \tag{3.16}$$

where $\dot{m}_k$ is the rate of interphase mass transfer

$$\dot{m}_k = \rho_k \hat{n}_k \cdot (\vec{v}_k - \vec{v}_i) \tag{3.17}$$

Eq. (3.16) is the generalized volume averaged one-dimensional conservation. The forms of the mass, momentum and energy conservation equations will now be derived.

Mass Conservation

In this case, $\psi_k = 1$, $\vec{j}_k = 0$ and $\Phi_k = 0$, Eq. (3.16) becomes

$$\frac{\partial}{\partial t} \alpha_k \langle \rho_k \rangle + \frac{\partial}{\partial z} \alpha_k \langle \rho_k u_k \rangle = -\langle \dot{m}_k \rangle_i = \Gamma_{mk} \tag{3.18}$$

In general, the volume averaged interfacial mass transfer rate (Γ_{mk}) is not known "a priori" and a correlation must be supplied.

Momentum Conservation

In this case $\psi_k = \vec{v}_k$, $\vec{j}_k = P_k \overline{\overline{I}} - \overline{\overline{\tau}}_k$ and $\Phi_k = \vec{F}_k$. Taking the dot product of Eq. (3.16) with $\hat{n}_z$, the unit Z direction vector, the z-direction momentum conservation equation is obtained

$$\frac{\partial}{\partial t} \alpha_k \langle \rho_k u_k \rangle + \frac{\partial}{\partial z} \alpha_k \langle \rho_k u_k^2 \rangle + \frac{\partial}{\partial z} \alpha_k \langle P_k \rangle + \frac{\partial}{\partial z} \alpha_k \langle \hat{n}_z \cdot (\overline{\overline{\tau}}_k \cdot \hat{n}_z))$$

$$- \alpha_k \langle \rho_k F_{z,k} \rangle = -\frac{1}{V} \int_{a_i} [\dot{m}_k u_k + \hat{n}_z \cdot \hat{n}_k P_k - \hat{n}_z \cdot (\hat{n}_z \cdot \overline{\overline{\tau}}_k)] dS$$

$$+ \frac{1}{V} \int_{a_{kw}} \hat{n}_z \cdot (\hat{n}_{kw} \cdot \bar{\bar{\tau}}_k) dS \tag{3.19}$$

where the relationship $\hat{n}_{kw} \cdot \hat{n}_z P_k = 0$ has been used, since $\hat{n}_{kw} \cdot \hat{n}_z = 0$ if there is no area change and $u_k = \vec{v}_k \cdot \hat{n}_z$.

The pressure term on the right-hand side can be made more explicit by considering an average and a fluctuating part. The procedure also elucidates the "apparent mass" effect. Consider

$$\int_{a_i} \hat{n}_k \cdot (\hat{n}_z P_k) dS = \int_{a_i} \hat{n}_k \cdot [\hat{n}_z (<P_k> + \Delta P_{ki} + \Delta P'_{ki})] dS$$

where $\Delta P_{ki} = <P_{ki}> - <P_k>$ and $\Delta P'_{ki} = P_{ki} - <P_{ki}>$. If ΔP_{ki} is assumed constant over a_i, then the fluctuating part between the bulk and interfacial pressure $\Delta P'_{ki} = 0$. This is only true in stratified flow with no waves. As soon as waves appear $\Delta P'_{ki} \neq 0$. The difference between bulk and interfacial pressure may arise from a variety of reasons, for example, gravitational forces in stratified flow, flow separation behind bubbles and slugs, rapid bubble growth etc. Using Eq. (3.11)

$$\frac{1}{V} \int_{a_i} \hat{n}_k \cdot (\hat{n}_z P_k) dS = -[<P_k> + \Delta P_{ki}] \frac{\partial \alpha_k}{\partial z} + \frac{1}{V} \int_{a_i} \hat{n}_k \cdot (\hat{n}_z \Delta P'_{ki}) dS \tag{3.20}$$

Substituting into Eq. (3.19), the momentum conservation equation is obtained

$$\frac{\partial}{\partial t} \alpha_k <\rho_k u_k> + \frac{\partial}{\partial z} \alpha_k <\rho_k u_k^2> + \alpha_k \frac{\partial <P_k>}{\partial z} - \frac{\partial}{\partial z} \alpha_k <\tau_{zz,k}>$$
$$- \Delta P_{ki} \frac{\partial \alpha_k}{\partial z} = \alpha_k <\rho_k F_{z,k}> - <\dot{m}_k u_k>_i - <\Delta P'_{ki}>_i$$

$$+ <(\hat{n}_z \cdot \bar{\tau}_z)>_i + <(\hat{n}_{kw} \cdot \bar{\tau}_z)>_w \qquad (3.21)$$

Note that the equation reduces to the usual constant phase pressures form if $\Delta P_{ki} = \Delta P'_{ki} = 0$. $<\Delta P'_{ki}>_i$ is the term that leads to the "apparent mass" effect for inviscid flows. It may be calculated for inviscid flows if the shape of the interface is known a priori. However, this is generally not the case, and semi-empirical expressions are needed.

Energy Conservation

For the energy equation, $\psi_K = e_k + \frac{u_k^2}{2} = E_k$, $\vec{j}_k = \vec{q}_k - (P_k \bar{\bar{I}} - \bar{\bar{\tau}}_k) \cdot \vec{v}_k$ and $\Phi_k = F_k \cdot \vec{v}_k + Q_k$.

Eqn. (3.16) becomes

$$\frac{\partial}{\partial t} \alpha_k <\rho_k E_k> + \frac{\partial}{\partial z} \alpha_k <\rho_k E_k u_k> + \frac{\partial}{\partial z} \alpha_k <q_{z,k}>$$

$$+ \frac{\partial}{\partial z} \alpha_k <\rho_k u_k> - \frac{\partial}{\partial z} \alpha_k <\hat{n}_z \cdot (\bar{\bar{\tau}}_k \cdot v_k)>$$

$$= \alpha_k <\rho_k (\vec{F}_k \cdot \vec{v}_k + Q_k)> - \frac{1}{V} \int_{a_i} [\dot{m}_k E_k + \hat{n}_k \cdot (\vec{q}_k + P_k \vec{v}_k - \bar{\bar{\tau}}_k \cdot \vec{v}_k)] dS$$

$$- \frac{1}{V} \int_{a_{kw}} \hat{n}_{kw} \cdot \vec{q}_k \, dS \qquad (3.22)$$

Now

$$\hat{n}_k \cdot P_k \vec{v}_k = \frac{P_k}{\rho_k} [\hat{n}_k \cdot (\vec{v}_k - \vec{v}_i) \rho_k] + P_k \hat{n}_k \cdot \vec{v}_i$$

$$= \dot{m}_k P_k / \rho_k + P_k \hat{n}_k \cdot \vec{v}_i$$

Therefore

$$- \frac{1}{V} \int_{a_i} (\dot{m}_k E_k + \hat{n}_k \cdot P_k \vec{v}_k) dS$$

$$= - \frac{1}{V} \int_{a_i} [\dot{m}_k (h_k + \frac{u_k^2}{2}) + P_K (\hat{n}_k \cdot \vec{v}_i)] dS \qquad (3.23)$$

Where the relation $E_k = h_k + u_k^2/2 - P_k/\rho_k$ has been used. h_k is the enthalpy of phase k.

To be consistent with the treatment of the pressure term in the momentum equation

$$\frac{1}{V} \int_{a_i} P_K (\hat{n}_k \cdot \vec{v}_i) dS = \frac{1}{V} \int_{a_i} [<P_K> + \Delta P_{Ki} + \Delta P_{Ki}'] (\hat{n}_k \cdot \vec{v}_i) dS$$

ΔP_{Ki} and $\Delta P_{Ki}'$ are defined as before. Using Leibnitz's rule (Eq. 3.12), we may write

$$\frac{1}{V} \int_{a_i} P_i (\hat{n}_k \cdot \vec{v}_i) dS \doteq [<P_k> + \Delta P_{ki}] \frac{\partial \alpha_k}{\partial t} + \frac{1}{V} \int_{a_i} \Delta P_{ki}' (\hat{n}_k \cdot \vec{v}_i) dS \qquad (3.24)$$

Substituting Eq. (3.24) into (3.23) and then (3.23) into (3.22), the energy equation in enthalpy form can be written as

$$\frac{\partial}{\partial t} \alpha_k < \rho_k (h_k + \frac{u_k^2}{2}) > + \frac{\partial}{\partial z} \alpha_k < \rho_k u_k (h_k + \frac{u_k^2}{2}) > - \alpha_k \frac{\partial <P_k>}{\partial t}$$

$$+ \Delta P_{ki} \frac{\partial \alpha_k}{\partial t} + \frac{\partial}{\partial z} \alpha_k < q_{z,k} > - \frac{\partial}{\partial z} \alpha_k < \hat{n}_z \cdot (\bar{\bar{\tau}}_k \cdot \vec{v}_k) >$$

$$= - < [\dot{m}_k (h_k + \frac{u_k^2}{2}) + \hat{n}_k \cdot \vec{v}_i \, \Delta P_{ki}' + \hat{n}_k \cdot \vec{q}_k - \hat{n}_k \cdot \vec{v}_k \cdot \bar{\bar{\tau}}_k] >_i$$

$$- < (\hat{n}_{kw} \cdot \vec{q}_k) >_w + \alpha_k < (\rho_k \vec{v}_k \cdot \vec{F}_k + Q_k) > \qquad (3.25)$$

Interface Jump Conditions

If the interface is treated as a contact discontinuity the local instantaneous form of the generalized conservation equation across the interface is given by Kotchine's theorem (Sect. 3.2)

$$\sum_{k=1}^{2} [\rho_k \, \psi_k (\vec{v}_k - \vec{v}_i) + \vec{j}_k] \cdot \hat{n}_k = 0 \tag{3.10}$$

or

$$\sum_{k=1}^{2} [\dot{m}_k \, \psi_k + \vec{j}_k \cdot \hat{n}_k] = 0 \tag{3.26}$$

The equation can be volume averaged in the same way as for the phase conservation equations. The interfacial mass, momentum and energy jump conditions are derived below with ψ_k and $\vec{j}_k$ as previously given

Interface Mass

$$\sum_{k=1}^{2} \frac{1}{V} \int_{a_i} \dot{m}_k \, dV = 0$$

or

$$\langle \dot{m}_1 \rangle_i = - \langle \dot{m}_2 \rangle_i \tag{3.27}$$

Interface Momentum

$$\sum_{k=1}^{2} \frac{1}{V} \int_{a_i} [\dot{m}_k u_k + \hat{n}_z \cdot (\hat{n}_k P_k) - \hat{n}_z \cdot (\hat{n}_k \cdot \bar{\bar{\tau}}_k)] dS = 0$$

Using Eqs. (3.20) and (3.27), and the identity $\hat{n}_1 = -\hat{n}_2$

$$[\langle P_{1i} \rangle - \langle P_{2i} \rangle] \frac{\partial \alpha}{\partial z} = \langle \dot{m}_i (u_1 - u_2) + (\Delta P'_{1i} - \Delta P'_{2i})$$

$$- \hat{n}_1 \cdot (\bar{\tau}_{1,z} - \bar{\tau}_{2,z}) \rangle_i \tag{3.28}$$

where $\alpha=\alpha_1$ and $\alpha_2=1-\alpha$.

Interface Energy

$$\sum_{k=1}^{2}\int_{a_i}[\dot{m}_k(h_k+\frac{u_k^2}{2})+P_k(\hat{n}_k\cdot\vec{v}_i)+\hat{n}_k\cdot(\vec{q}_k-\bar{\bar{\tau}}_k\cdot\vec{v}_k)]dS=0$$

Using eqs. (3.24) and (3.27), we have

$$[\langle P_{1i}\rangle-\langle P_{2i}\rangle]\frac{\partial\alpha}{\partial t}=\langle\hat{n}_1\cdot[(\vec{v}_1\cdot\bar{\bar{\tau}}_1)-(\vec{v}_2\cdot\bar{\bar{\tau}}_2)]$$

$$-\hat{n}_1\cdot(\vec{q}_1-\vec{q}_2)-\hat{n}_1\cdot\vec{v}_i(\Delta P'_{1i}-\Delta P'_{2i})$$

$$-\dot{m}_1[(h_1+\frac{u_1^2}{2})-(h_2+\frac{u_2^2}{2})]\rangle_i \tag{3.29}$$

To summarize, the one dimensional form of the volume averaged phasic conservation equations are given by Eqs. (3.18), (3.19) or (3.21), (3.22) or (3.25). The jump conditions are given by Eqs. (3.27), (3.28) and (3.29).

It should be noted that all the equations in this section have been derived in instantaneous volume averaged form. They may now be time or ensemble averaged and the form remains exactly the same. Terms like $\frac{\partial}{\partial t}\ \alpha_k\langle\rho_k\ u_k\rangle$ will become $\frac{\partial}{\partial t}\ \overline{\alpha_k\langle\rho_k\ u_k\rangle}$, where the overbar denotes time or ensemble averaging. The averaging operators are commutative.

3.5 Interphase Transfer Functions and Intraphase Distribution Coefficients

In the process of averaging the local instantaneous conservation equations to form a simpler mathematical model, information is lost. This must be supplied in the form of auxiliary relationships - the interfacial transfer relationships and the intraphase distribution coefficients of the dependent variables.

To obtain a model that can be used for predictive purposes, the phasic conservation equations must be supplemented with relationships for the integrals on their right hand sides (Eqs. 3.18, 3.19 and 3.22). The jump conditions impose certain restrictions on their form. These relationships include interfacial and wall mass, momentum and energy transfer, as well as interfacial area per unit volume. An extensive compilation of expressions for these quantities is available in the report by Hughes et al [58]. Though these expressions should not be regarded as definitive, they are a valuable first step in developing constitutive equations for multi-fluid models.

To illustrate the forms of the auxiliary relationships, consider the volume averaged single phase momentum conservation equation (from Eq. 3.21)

$$\frac{\partial}{\partial t} \langle \rho u \rangle + \frac{\partial}{\partial z} \langle \rho u^2 \rangle + \frac{\partial \bar{P}}{\partial z}$$

$$= \langle \rho F_z \rangle + \langle (\hat{n} \cdot \bar{\tau}_z) \rangle_w + \frac{\partial}{\partial z} \langle \tau_{zz} \rangle \qquad (3.30)$$

The symbols have their usual meanings. $\langle \hat{n} \cdot \bar{\tau}_z \rangle_w$ is the component of the averaged wall shear stress in the z direction and is often approximated by the externally supplied steady flow expression

$$\langle \hat{n} \cdot \bar{\tau}_z \rangle_w = - 2 \, f \, \rho \, u^2 / d_h \qquad (3.31)$$

where d_h is the hydraulic diameter and f is the friction factor. Eq. (3.31) is a form of the wall momentum transfer relationship.

It is also desirable to separate the averages of products in Eq. (3.30) into the product of averages of the dependent variables ρ and u.

For this we need relationships between $<\rho u>$ and $<\rho><u>$, and between $<\rho u^2>$ and $<\rho><u>^2$. This is another type of auxiliary relationship, the intra-phase distribution relationship.

To obtain a working set of volume/time or volume/ensemble averaged equations, it is usual to assume that the phase density variations within the averaging volume are small, that is

$$\overline{\alpha_k <\rho_k u_k>} = \overline{\rho_k}\, \overline{\alpha_k <u_k>} \tag{3.32}$$

It is also usual to define average velocities and enthalpies as

$$\overline{<u_k>_k} \triangleq \frac{\overline{\alpha_k <u_k>}}{\overline{\alpha}_k} \tag{3.33}$$

$$\overline{<h_k>_k} \triangleq \frac{\overline{\alpha_k <h_k>}}{\overline{\alpha}_k} \tag{3.34}$$

Definition (3.33) allows the mass conservation equation (3.18) to be written in terms of $\overline{\alpha}_k$, $\overline{\rho}_k$ and $\overline{<u_k>_k}$. At present, very little data on distribution coefficients are available, so they are generally set equal to unity. It is possible to evaluate these coefficients taking power law profiles as suggested by Bankoff [65]. However, the usual approach has been to split a phase into two components if they are known to have very different velocities and enthalpies. Thus, in annular flow the liquid is usually split into a droplet "phase" and a liquid film "phase" (Saito [66]). Instead of writing a set of liquid conservation equations with distribution coefficients, one now writes two sets of equations (one set for the droplets and one set for the liquid film) with distribution coefficients set equal to unity. Similarly, for subcooled boiling, the approach has been to account for this by splitting the vapor generation source term into two components, one for the bulk liquid and one for the wall liquid (Hughes et al [58]).

This approach, of course, merely shifts the problem from one regarding distribution coefficients to one regarding transfer relationships for the new "phase (s)". However, in cases like annular flow and subcooled boiling, it appears easier to determine the transfer relationships for a new "phase" on the basis of the data available. The approach in future will undoubtedly depend on the flow regime being modelled and the type of data that can be taken.

3.6 Simplified One-Dimensional Models

The general transient non-equilibrium one-dimensional two-fluid model has been derived in the last two sections. There are six phasic equations but seven dependent variables. They are α, P_G, P_L, u_G, u_L, h_G and h_L, where subscript G and L denote vapor (or gas) and liquid phase respectively. An additional equation is needed to close the set. Essentially we seek a relationship between the phasic pressures or an explicit transport equation for void fraction. Quite often, the assumption is made that $P_G=P_L$. This is of course equivalent to a statement regarding the calculation of void fraction. Agee et al. [60] obtained a transport equation for void fraction which holds for all cases if the two-phase pressures are not identically equal on each side of the interface.

$$\frac{\partial\alpha}{\partial t} + \Lambda \frac{\partial\alpha}{\partial z} = \Omega \tag{3.38}$$

where Λ is the void propagation velocity and Ω is a source term.

Whether Eq. (3.38) is the right equation to effect the closure or whether it is in its correct form is, however, still in dispute: This coupled with the fact that detailed transfer relationships are still not available, makes the usefulness of the general model limited for the time being. The more physically appealing approach is to derive an explicit relationship between the phasic pressures, using for example, the transverse momentum equation. This procedure has recently been used by Banerjee [67] to show that higher order dispersion terms must be incorporated in multifluid models when studying wave propagation.

In many situations, it is possible and also desirable to reduce the complexity of the problem by making assumptions based on the physical mechanisms perceived to be important. This results in the many different simplified one-dimensional models. It should be noted that any such model, if consistent, should appear as a particular case of the general model. In general the number of conservation equations used in these one-dimensional models varies between 3 (mixture model) and 7 (general model). The larger the number of conservation equations, the more detailed the transfer relationships (between the phases and between each phase and the wall) have to be.

In simplified models, when less than seven equations are used, the "missing" equation (s) is/are replaced by restriction (s) or assumption (s). Since the minimum number of conservation equations used in consistent models is three, the maximum number of assumptions that can be made on the dependent variables is 7 - 3 = 4

Most of the cases met in practice are summarized in Table 3.1 which is an extension of the table given by Boure [68].

With 4 restrictions (Table 3.1), we obtain the widely used "mixture models". This includes the homogeneous, slip and diffusion models. In the mixture models, the individual phases are not accounted for explicitly, the interfaces are ignored and the mixture is considered as a single fluid, having its own properties. The conservation equations obtained are the same as for the single phase flows. There are only three of them, mixture mass, momentum and energy. The use of a mixture model may be justified when one phase is finely dispersed in the other, for example, in bubbly flow and mist flow. However, even in these cases the propagation of distrubances may not be modelled correctly.

The set of conservation equations as deduced from Eqs. (3.18), (3.21) and (3.25) are, for mixture models,

$$\frac{\partial \rho}{\partial t} + \frac{\partial}{\partial z} (\rho u) = 0 \tag{3.39}$$

$$\frac{\partial}{\partial t} (\rho u) + \frac{\partial}{\partial z} (\rho u^2) + \frac{\partial P}{\partial z} = - \tau_w + \rho F \tag{3.40}$$

and

$$\frac{\partial}{\partial t} \rho (h + \frac{u^2}{2}) + \frac{\partial}{\partial z} \rho u (h + \frac{u^2}{2}) - \frac{\partial P}{\partial t} = - q_w + \rho u F + Q \tag{3.41}$$

where ρ, u and h are the mixture density, velocity and enthalpy respectively, τ_w is the wall shear and q_w is the wall heat flux. To close this set of equations (Eq. 3.39 to 3.41), an intrinsic constitutive law (the equation of state of the mixture) and two transfer relationships (τ_w and q_w)

TABLE 3.1

ONE-DIMENSIONAL TWO-PHASE FLOW MODELS

No. of Restrictions	Restrictions in Practice	Dependent Variables	Governing Equations Used
4	$u_G=u_L$; $P_G=P_L$; $\Delta h_G=\Delta h_L=0.$	α,P,u	3 mixture conservation equations.
	$u_G=\gamma u_L$; $P_G=P_L$; $\Delta h_G=\Delta h_L=0.$	α,P,u_L	- id -
3	$P_L=P_G$; $\Delta h_G=\Delta h_L=0.$	α,P,u_G,u_L	3 mixture conservation equations + 1 phasic (momentum) equation
	$u_G=u_L$; $P_G=P_L$; Δh_G(or Δh_L)=0.	$\alpha,P,u,$ Δh_L(or Δh_G)	3 mixture conservation equations + 1 Phasic (energy) equation
	$u_G=\gamma u_L$; $P_G=P_L$; Δh_G(or Δh_L)=0.	$\alpha,P,u_L,$ Δh_L(or Δh_G)	- id -
2	$P_G=P_L$; Δh_G(or Δh_L)=0.	$\alpha,P,u_G,u_L,$ Δh_L(or Δh_G)	3 mixture conservation equations + 1 phasic (momentum) equation + 1 phasic (energy) equation
	$u_G=u_L$; $P_G=P_L$	$\alpha,P,u,$ $\Delta h_L,\Delta h_G$	3 mixture conservation equations + 1 phasic (mass) equation + 1 phasic (energy) equation
	$u_G=\gamma u_L$ $P_G=P_L$	$\alpha,P,u_L,$ $\Delta h_G,\Delta h_L$	- id -
	$u_G=u_L$; Δh_G(or Δh_L)=0.	$\alpha,u,P_L,P_G,$ Δh_L(or Δh_G)	3 mixture conservation equations + 1 phasic (mass) equation + 1 void transport equation (or relation between phasic pressures)
1	$\Delta h_G=0.$ or $\Delta h_L=0.$	$\alpha,P_G,P_L,u_G,$ $u_L,\Delta h_G$(or Δh_L)	3 mixture conservation equations + 1 phasic (momentum) equation + 1 phasic (energy) equation + 1 void transport equation (or relation between phasic pressures)
	$u_G = u_L$	$\alpha,P_G,P_L,u,$ $\Delta h_L,\Delta h_G$	3 mixture conservation equations + 1 phasic (mass) equation + 1 phasic (energy) equation + 1 void transport equation (or relation between phasic pressures
	$u_G = \gamma u_L$	$\alpha,P_G,P_L,u_L,$ $\Delta h_L,\Delta h_G$	- id -
	$P_G= P_L$	$\alpha,P,u_G,u_L,$ $\Delta h_L,\Delta h_G$	6 phasic conservation equations or 3 mixture + 3 phasic equations
0		$\alpha,P_G,P_L,u_G,$ $u_L,\Delta h_L,\Delta h_G$	6 phasic eqns. + 1 void transport eqn. (or phasic pressure relation)

are needed.

As can be seen in Table 3.1, models involving 4, 5 or 6 governing equations (corresponding to 3, 2 or 1 restrictions) are many. These models are in fact two-fluid models in the sense that individual phase exists. The missing equation (s) are replaced by assumptions (or restrictions). These are most often one to three of the following:

(i) equal phase pressure, $P_G = P_L$

(ii) no slip , $u_G = u_L$

(iii) vapor phase at saturation, $h_G = h_G^{sat}$ (P)

(iv) liquid phase at saturation, $h_L = h_L^{sat}$ (P)

For example, if the vapor and liquid phases are at saturation, the fluid is at thermal equilibrium and we will have the UVETUP (Unequal Velocity, Equal Temperature and Unequal Pressure) model. Likewise, the other models such as UVUTEP, EVUTUP, UVETEP etc. can be obtained. To close the set of equations in two-fluid models, nine constitutive equations are necessary assuming no interface material properties. These include two phasic equations of state, two friction factor correlations, two heat transfer relationships and three interfacial transfer functions (mass, momentum and energy).

In conclusion, it should be stressed that it will be advantageous to keep a working model as simple as possible as long as it is consistent with the physical process being studied. This of course requires physical insight and is only really suitable for particular situations. In general calculations where many different processes may occur, e.g. LOCA calculations, it may be necessary to use general models with appropriate constituitive and closure relationships derived from simple "separate effects" experiments. The obvious advantages of having a simple model are

(1) The functional dependence of dependent variables of interest can be investigated systematically.

(2) Computational costs can be reduced if a computer program is used to solve the resulting set of governing equations.

Starting from the general two-fluid model, a simpler model can be obtained by making appropriate assumptions. The procedures will be described and illustrated later in this thesis when a simplified two-fluid model is developed to model the horizontal channel rewetting and refilling process.

4. EXPERIMENTAL FACILITY

4.1 Test Loop

The test loop for the study of the rewetting and refilling process in a horizontal channel is shown schematically in Figure 4.1. It is relatively simple, because the work was done at low pressures.

The test section is direct resistance heated. QAV1 is kept closed and QAV2 kept open, when the test section is being heated up, so that water by-passes the test section via QAV2. When the test section is at the desired temperature, QAV1 will be opened and QAV2 closed at the same time, forcing water into the heated channel. The steam or steam-water mixture is discharged into the condenser which is kept at atmospheric pressure.

A picture of the test loop is shown in Plate 4.1. The major components of the facility can be seen. In the center is the horizontally mounted test section. At the far right is the condenser. The quick acting valves and the water injection piping can be seen at the other end of the test section. On top of the table are the data acquisition system, the power control system and various instrumentation.

4.1.1 Test Section

The basic requirements for the test section are:

(i) low thermal expansion coefficient for high temperature operation,

(ii) relatively high electrical resistivity for direct ohmic heating,

(iii) thin-walls for void measurement using the gamma ray attenuation technique.

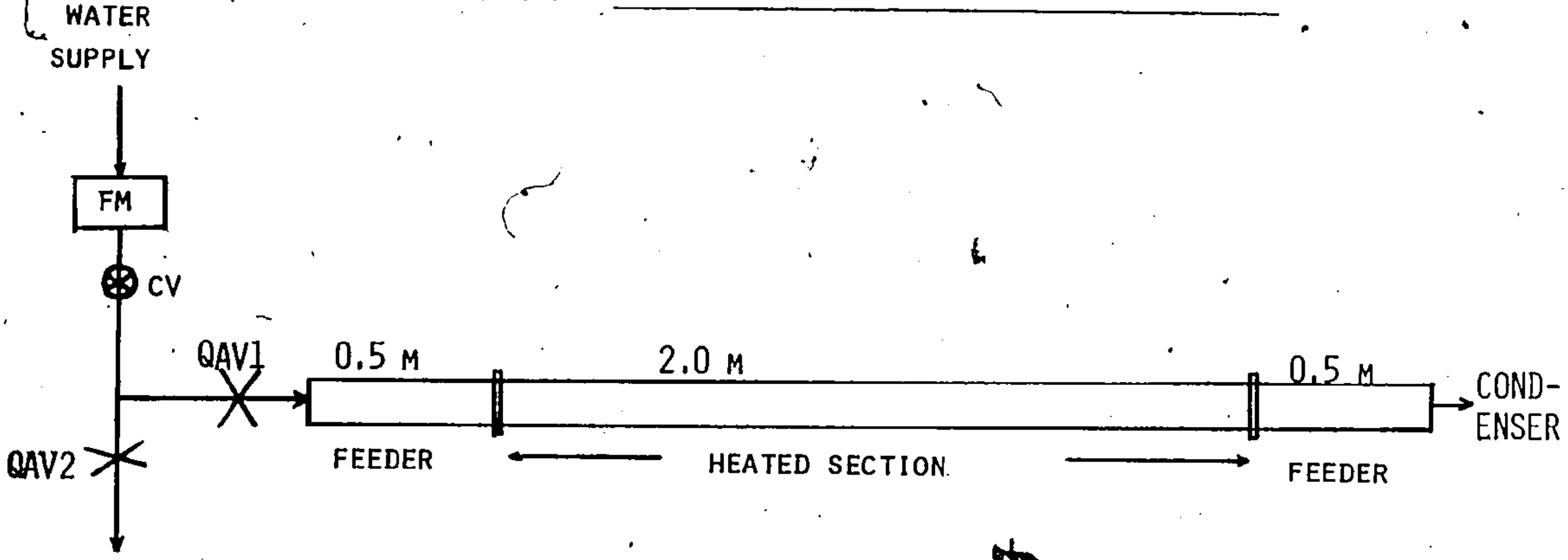

FIG. 4.1. SCHEMATIC DIAGRAM OF REWETTING FACILITY

FM = FLOWMETER
QAV = QUICK ACTING VALVE
CV = CONTROL VALVE

TEST SECTION

ZR - 2
O.D. = 0.0197 M
I.D. = 0.0180 M

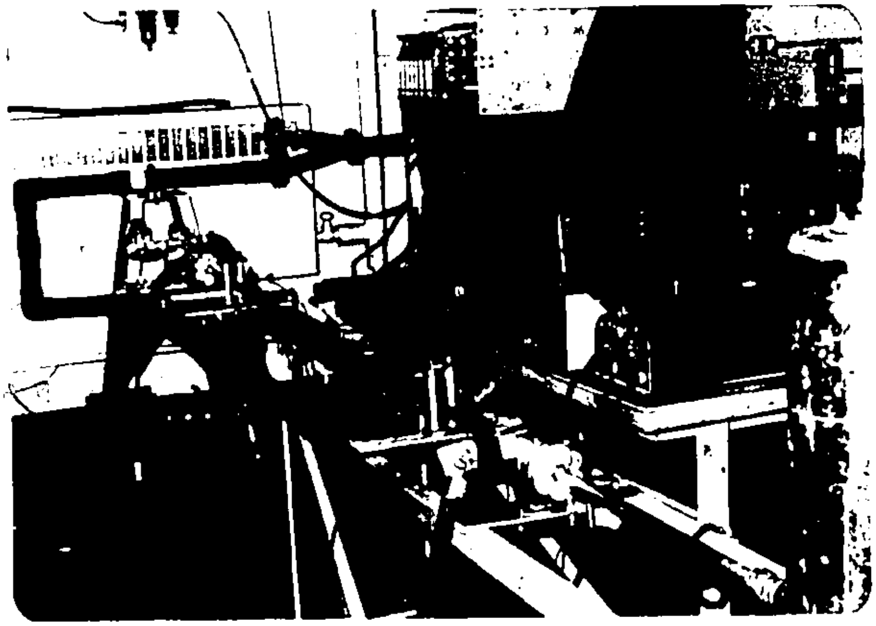

Plate 4.1 REWETTING EXPERIMENTAL FACILITY

Plate 4.2 SPOT WELDED SURFACE THERMOCOUPLES

The first requirement is the most restrictive for horizontal channel rewetting. Because of the stratified nature of the flow, the bottom of the test section will be quenched before the top and large circumferential temperature differences will thus exist. With high thermal expansion coefficients, this differential quenching may result in high local stresses and damage the test section.

The thermal expansion coefficients of Inconel and stainless steel were found to be higher than is desirable. Other alternatives were investigated. For example, the thermal expansion coefficient of Invar is practically zero. However, it is not available in tubes commercially. Zirconium was thus chosen as a compromise because of its relatively good characteristics and commercial availability.

The test section is a 6.56 feet (2 meters) long Zircaloy-2 tube with an outside diameter of 0.77 inch (19.6 mm) and a wall thickness of 0.034 inch (0.86 mm). It was provided by Canadian General Electric at Peterborough, Ontario. Some physical characteristics of Zircaloy-2 are listed in Table 4.1. The tube is electrically heated by attaching power leads to two 4.5 inches (114.3 mm) square, 0.5 inch (12.7 mm) thick end Zirconium flanges. It is electrically insulated from the feeders at both ends with 3 inches (76.2 mm) diameter, 0.25 inch (6.35 mm) thick teflon flanges sandwiched between the square Zirconium end flanges and circular stainless steel flanges of the feeders. The design of the test section and flanges is shown in Figure 4.2. The wall temperature of the tube is measured by glass-wrapped gauge 30 (0.01 inch) wire chromel-alumel thermocouples spot-welded onto the outside surface. No insulation was used in general so that void fraction measurements could be made with gamma

TABLE 4.1

PHYSICAL AND THERMAL PROPERTIES OF ZIRCALOY-2

Atomic Number	40
Atomic Weight	91.2
Melting Point	1852°C
Density	6573 - 0.0763 T kg/m^3
Thermal Conductivity	10.0 + 0.016 T w/m-°C
Heat Capacity	285 + 0.1 T J/kg-°C
Coefficient of Thermal Expansion (25°C - 800°C)	
Longitudinal	4.62 x 10^{-6}/°C
Normal	8.71 x 10^{-6}/°C
Transverse	6.85 x 10^{-6}/°C
Spectral Emisivity (1200°C - 1750°C)	0.44
Electrical Resistivity	74 μΩ-cm

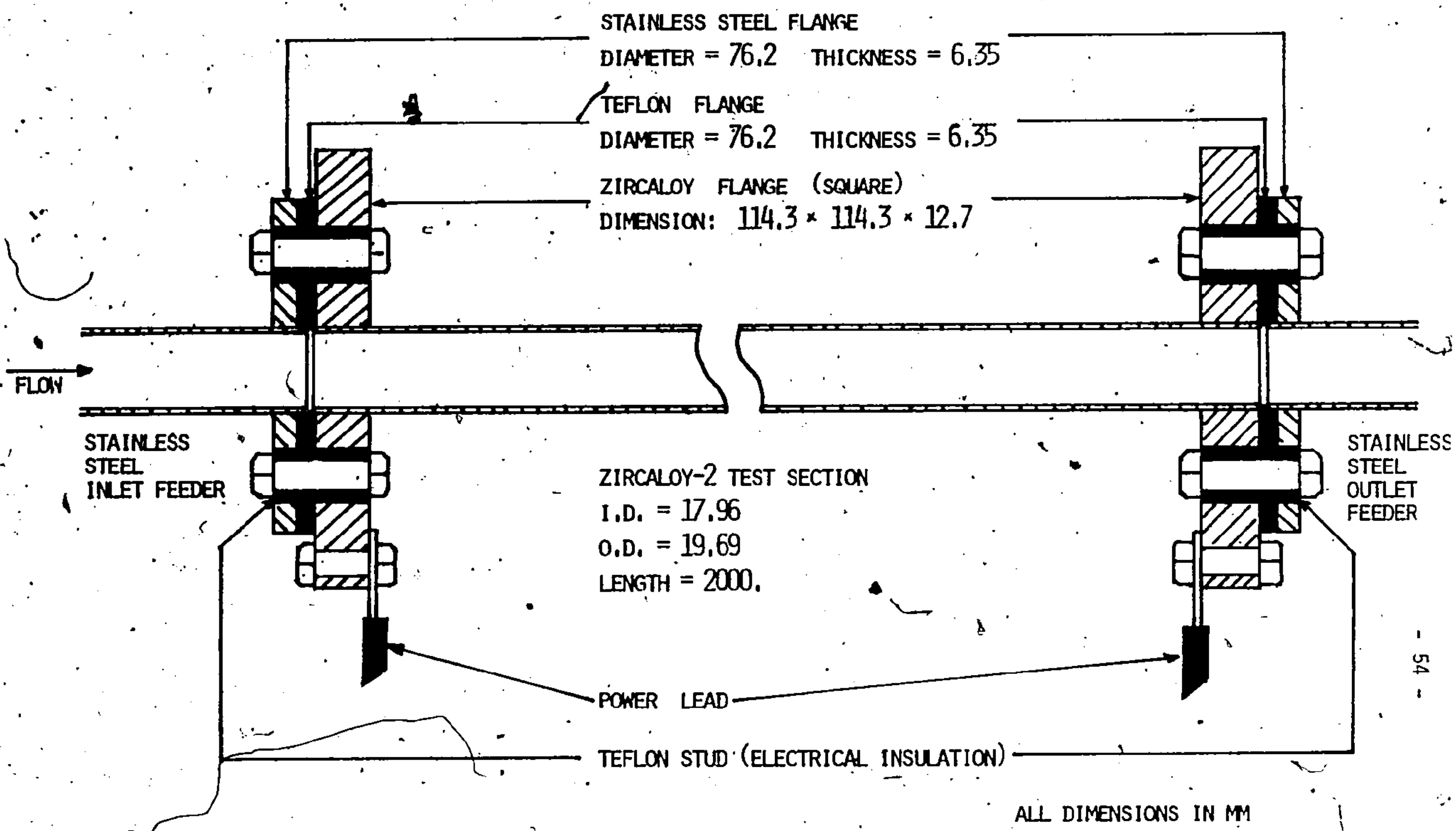

FIG. 4.2 TEST SECTION AND FLANGES

densitometers. However, a few experiments were done with glass-wool insulation wrapped around the tube for comparison purposes.

4.1.2 Inlet Water Supply

Inlet water is supplied either by a building water line or by a constant-water-level head tank. In the first case, a constant flow boundary condition was closely realized because of the large pressure drop across the regulating valve and negligible pressure build-up in the test section during the transients. Inlet water subcooling could be adjusted by adjusting the cold and hot water supplies. We had a constant pressure boundary condition in the second case. Building tap water as well as de-aerated and deionized water were used.

4.1.3 Power Supply

The Zircaloy test section is heated directly (ohmic heating) by using a d.c. motor generator (ANKER ELECTRIC). The unit is capable of delivering a maximum of 35 KVA d.c. power. Its power output can be controlled using a manual variac. At the start of the transients, that is when the rewetting and refilling process was initiated, the power supply is either switched off or cut off using a circuit breaker. In the first case, the power input drops to zero exponentially and in the latter case, it drops instantaneously to zero. The power input during the transients for the exponential decay cases could not be controlled because the total resistance of the test section changes rapidly as the tube is being quenched. However, the instantaneous power level was measured in all cases.

4.2 Instrumentation

The thermohydraulic parameters measured during the transients are:

(i) test section outer surface temperatures, axial and circumferential,
(ii) inlet and exit fluid temperatures,
(iii) inlet and exit differential pressures,
(iv) inlet volumetric flow rates,
(v) local volume averaged void fractions and
(vi) total power input to the test section.

Except for the single-beam gamma densitometers used in void fraction measurements, all other instruments used are fairly standard, commercially available equipment. A list of sensors and locations is summarized in Table 4.2.

4.2.1 Temperature Measurements

All thermocouples used were chromel-alumel, type K.

The wall temperature along the test section was monitored by 28 gauge 30 (0.01" wire) glass-wrapped unsheathed thermocouples. The junctions were attached to the outer surface using a 1045 UNITEK spot welding machine. Thin stainless steel straps (~0.001 inch thick) were used to hold the thermocouple wires and protect the junctions. A picture of the thermocouple junction and steel strap is shown in Plate 4.2.

Table 4.2

INSTRUMENTATION

SENSOR	LOCATION	EXPECTED RANGE	FUNCTION
Test section wall thermocouples (28)*	spot welded on outer wall of test section (see Fig. 4.3)	0-700°C	measure transient axial and circumferential temperature of the test section.
Inlet coolant thermocouple (1)	50.8 mm upstream of heated test section, immersed	0-100°C	measure inlet water temperature.
Outlet fluid thermocouples (2)	50.8 mm downstream of heated test section, immersed	0-700°C	measure exit steam, water or steam-water mixture temperatures
Gamma densitometer (2)	Along the heated test section (see Fig. 4.3)	0-1.0	measure local volume averaged void fractions
Pressure transducers (2)	across the test section. One 50.8 mm. upstream and one 50.8 mm. downstream of test section	0-20 psig	measure the pressure drop across the test section
Turbine flow meter (1)	before the unheated inlet feeder	0-120 ml/s	measure the inlet water flow rate
Voltage divider (1)	across the test section	0-10 volts	measure voltage across the test section
50 mV shunt (1)	in series to test section	0-600 amps	measure the current supplied to test section

*Number in bracket shows the number of sensors used in the experiment.

The location of the test section wall thermocouples is shown in Figure 4.3. They were attached to the mid-side of the channel and placed equal distances apart (166.7 mm) in the axial direction. The circumferential temperature variations are measured at five locations at which temperatures at the top, bottom and mid-sides are obtained.

Because the tube is resistance heated using a direct current, an extraneous voltage will be picked up by the surface thermocouples. When two lead wires are spot welded to form a junction on the surface, sometimes they may not come exactly to a point at the surface but are instead a small distance apart. This again results in an additional emf being picked up by the thermocouples. This problem was studied by Yu et al. [69]. They obtained two sets of thermocouple readings with a constant induced power supply voltage on the tube, one set with a given voltage polarity, the other set with the voltage polarity reversed. Averaging the two readings resulted in the correct thermocouple signal and a correction factor was deduced. They concluded that "the dependence of the correction factor on test section temperature was found to be very small and was ignored". Since Yu's situation and the present situation are identical as far as spot-welding of thermocouples and ohmic heating of the tube are concerned, their conclusion was adopted and no correction factor is used in the present investigation.

A 0.01 inch (0.254 mm) o.d. stainless steel-sheath, ground micro-thermocouple was used to measure the inlet water temperature. It was located 2 inches (50.8 mm) upstream of the test section inlet, in the inlet feeder. The exit fluid temperatures were measured using two 0.01 inch (0.254 mm) o.d. stainless steel-sheath, exposed junction micro-thermocouples. The nominal conductor size of the wire was 0.0015 inch (0.038 mm). The thermocouples

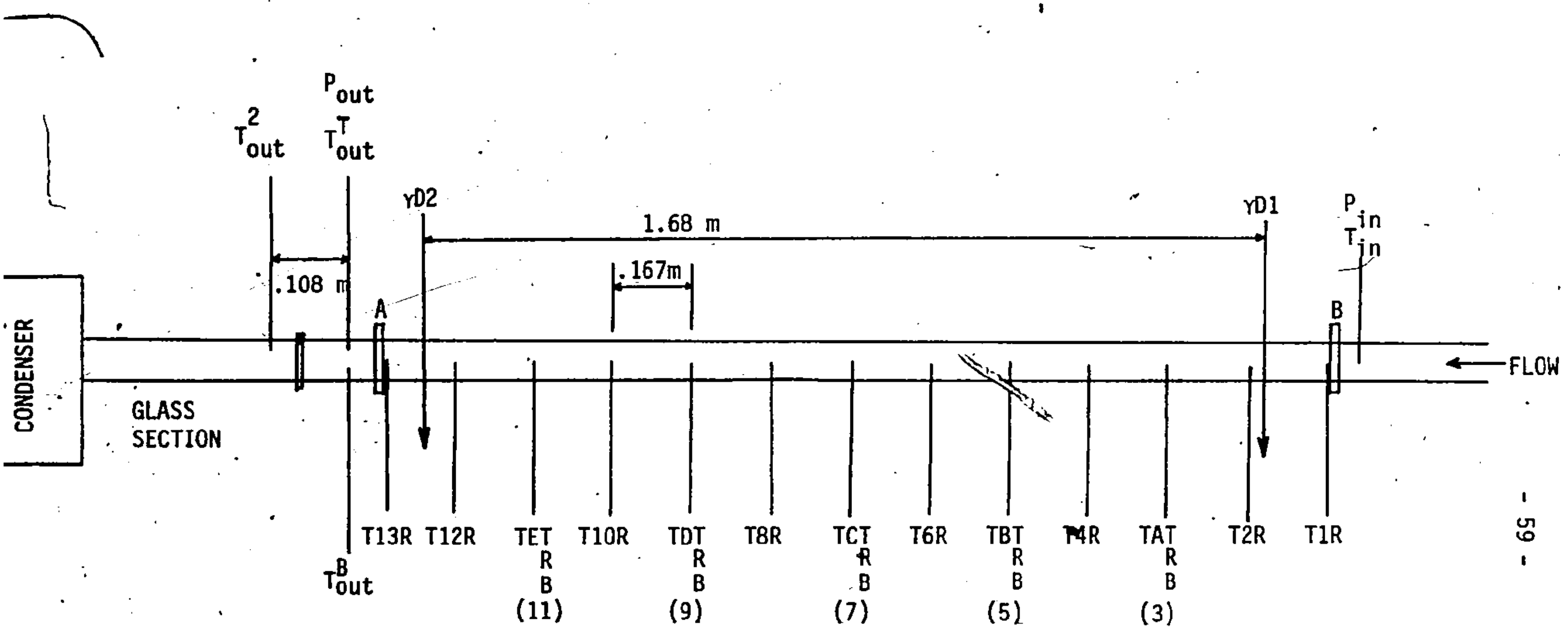

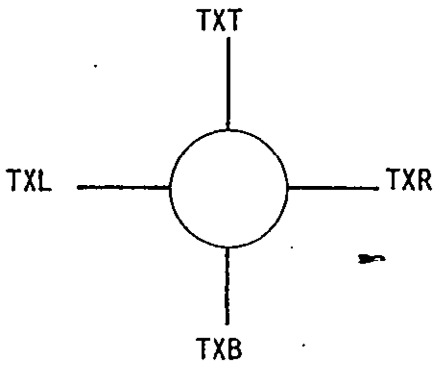

FIG. 4.3 LOCATIONS OF TRANSDUCERS

AB — HEATED TEST SECTION
(L = 2.0 M)

were located 2 inches (50.8 mm) downstream of the test section exit, in the outlet feeder. They were inserted 0.24 inch (6.1 mm) into the feeder, one from the top and the other from below. 0.125 inch (3.175 mm) o.d. stainless steel sleeves were used and soldered to the feeders for structure reinforcement and easier mounting of the micro-thermocouples. They were also used to mount the pressure transducers for differential pressure measurements (Plate 4.3).

4.2.2 Pressure Measurements

Pressure fluctuations during the transients were measured by two VALIDYNE model DP15TL multiple range differential pressure transducers. The range used was 0 to 20 psi. They were situated 2 inches (50.8 mm) upstream and downstream of the test section in the unheated inlet and exit feeder respectively. Thus, the test section inlet and exit differential pressures were obtained. The voltage output of the transducers were calibrated against known system pressures using a pressure gauge. The calibration curve is shown in Figure 4.4.

4.2.3 Flow Measurements

The inlet water flow rate was measured with a WAUGH FL-6SB turbine flowmeter. The volumetric flow rates were directly calibrated by collecting the amount of water discharged from the test section for a given flowmeter setting over a period of time. Two flowmeters of different inner diameters have been used. The calibration curves are shown in Figure 4.5.

PLATE 4.3 MOUNTING OF MICRO-THERMOCOUPLE AND PRESSURE TRANSDUCER IN THE FEEDER

FIG. 4.4. PRESSURE TRANSDUCER CALIBRATION CURVE

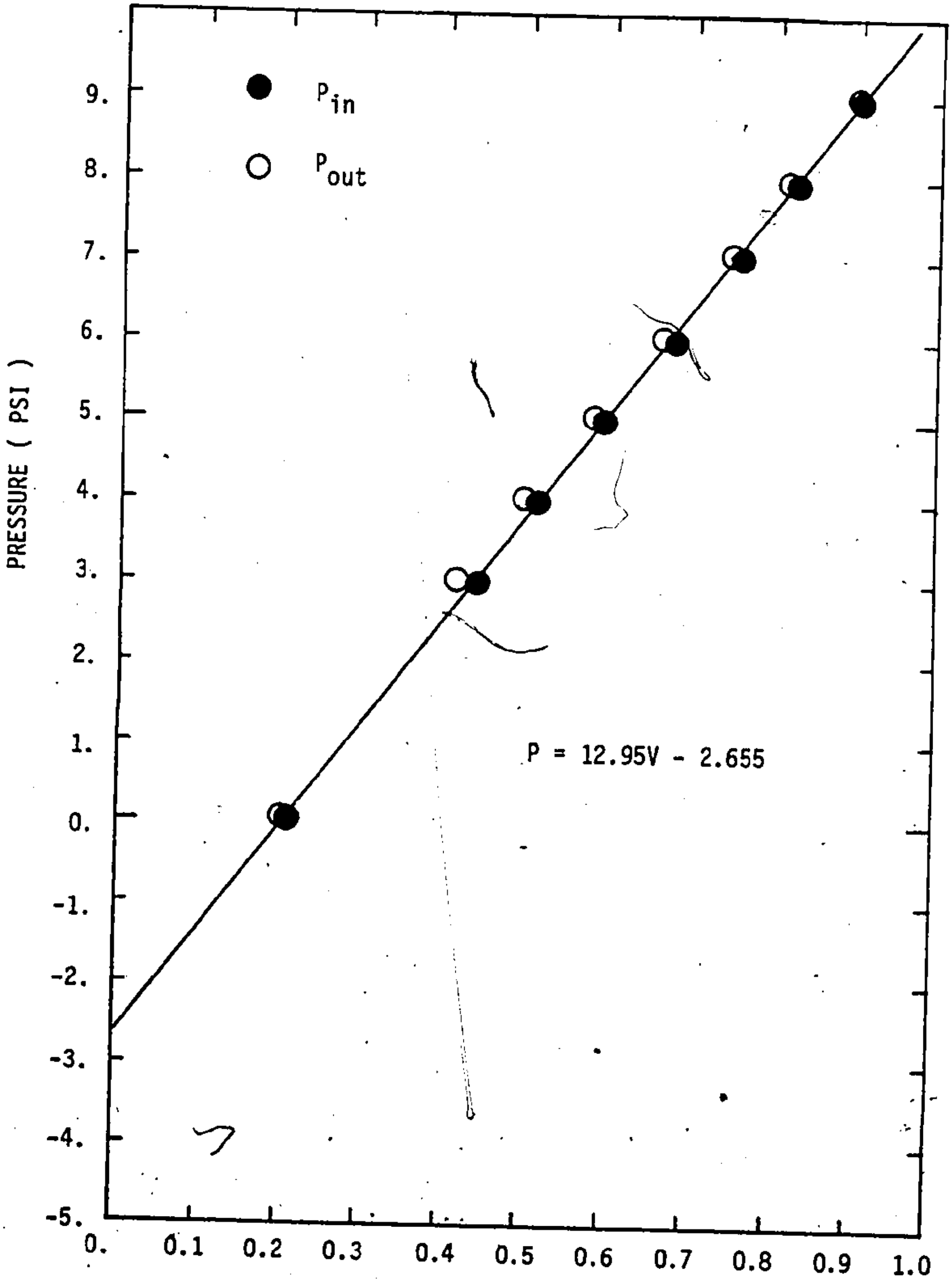

FIG. 4.5 FLOWMETER CALIBRATION CURVES

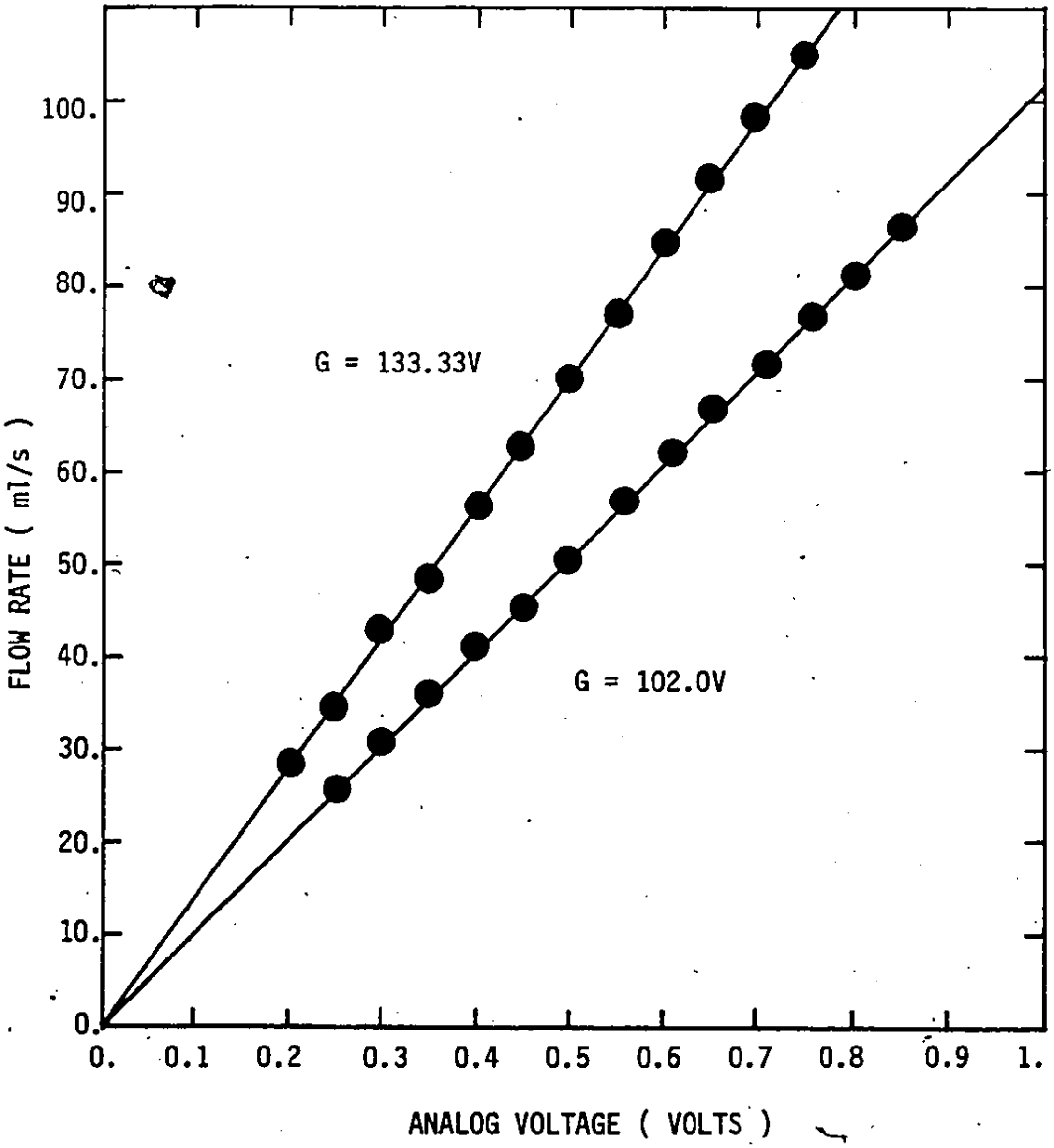

4.2.4 Power Input

The total power input to the test section was obtained from voltage and current measurements. A voltmeter is used to monitor the voltage across the test section. An ammeter, across the shunt (50 mV, 600 A) in series with the test section was used to measure the current. The voltmeter signal went to a voltage dividing circuit and this signal, together with the current signal, were recorded.

4.2.5 Void Fraction Measurements

Volume averaged local void fractions were measured using single-beam gamma densitometers. They were specially designed and constructed for our experiments.

The use of radiation (gamma or X-ray) techniques in void fraction measurements was reported decades ago (Cook [70] and Petrick and Swanson [71]). The techniques have always been regarded as the most reliable method of void measurement. They are frequently used as a standard against which other techniques are compared and calibrated (Lahey [72]). However, the potential of these techniques is still not fully exploited. Most of the existing devices suffer from one or more of the following drawbacks:

(i) too cumbersome to set up and use,
(ii) slow response to changes in void fraction, and
(iii) output signal drift.

Our densitometers are free of most of these shortcomings. They are simple, easy to handle and easy to operate, portable and have a fast response time. A detailed description of our gamma densitometer design is given in Chapter 5 together with a discussion on void measurement techniques.

The gamma densitometers can be mounted either horizontally or vertically with respect to the test section axis. Vertical mounting was used in the present experiments. The reasons are:

(i) During the transients, because of the differential quenching at a given location, the test section will move slightly in the vertical direction. If the densitometer is horizontally mounted, part of the test section may move out of the beam and result in erroneous measurements.

(ii) Because of the gravitational effect, the flow is usually stratified during the transients and a more accurate void measurement can be obtained if the beam is perpendicular to the interface. This will also be discussed in Chapter 5.

4.3 Automatic Data Acquisition System (ADAS)

During the transients, since the system parameters change quite rapidly, an on-line computer is used for data acquisition. The system can scan and process several sensor inputs, namely, thermocouples, pressure transducers, gamma densitometers and turbine flowmeters.

The Data Acquisition System is shown schematically in Figure 4.6. It consists of four parts:

(i) Signal conditioners for sensors

(ii) A Low-Level Analog Input System

(iii) A NOVA-3 Computer

(iv) A magnetic tape drive.

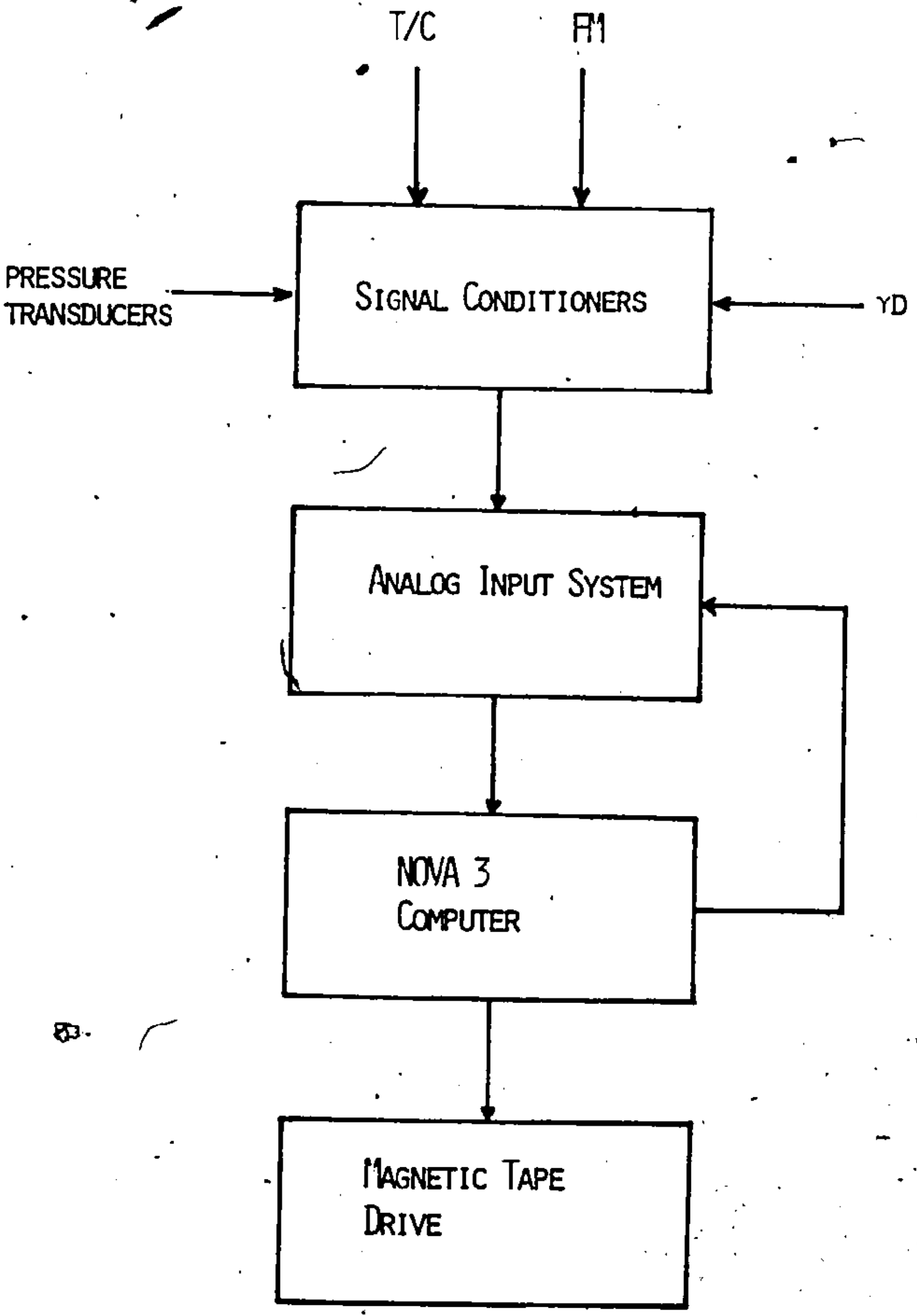

FIG. 4.6 SCHEMATIC DIAGRAM OF DATA ACQUISITION SYSTEM

4.3.1 Low-Level Analog Input System (RTP-model 7471)

The Analog Input System (AIS) is a slave system controlled by a digital computer. The unit provides random access sampling and digitizing of up to 64 low-level analog input signals in eight program selectable full-scale ranges from ± 5.0 millivolts to ± 1.0 volt. Input channels are multiplexed and a particular channel (input) is selected for processing by computer instruction. The processing of a channel involves signal amplification and analog-to-digital conversion. The analog-to-digital converter (ADC) converts the amplified voltage input into a digital number ranging between -2048 and +2047, including zero. The amplifier gain is digitally selectable through a computer command. Depending upon the analog input voltage range or the nature of the voltage excursion of the sensor input, the amplifier gain can be coded into the computer command. The unit can sample at a maximum rate of 8000 channels per second. A block diagram of the AIS unit is shown in Figure 4.7. It is a reprint from the RTP technical manual [73]. Our unit has only 32 channels. That is, only 32 sensor inputs can be logged at the same time during the transients.

4.3.2 Computer Control of Analog Input System

The analog Input System (AIS) can be accessed by the NOVA computer either on interrupt mode or a device checking mode. The present ADAS employs only two peripheral units on line to the computer, namely, a magnetic tape drive and the AIS. The magnetic tape drive is used to store the transient data on magnetic tapes. Hence the interupt mode of the AIS command and data collection is not used. The computer control

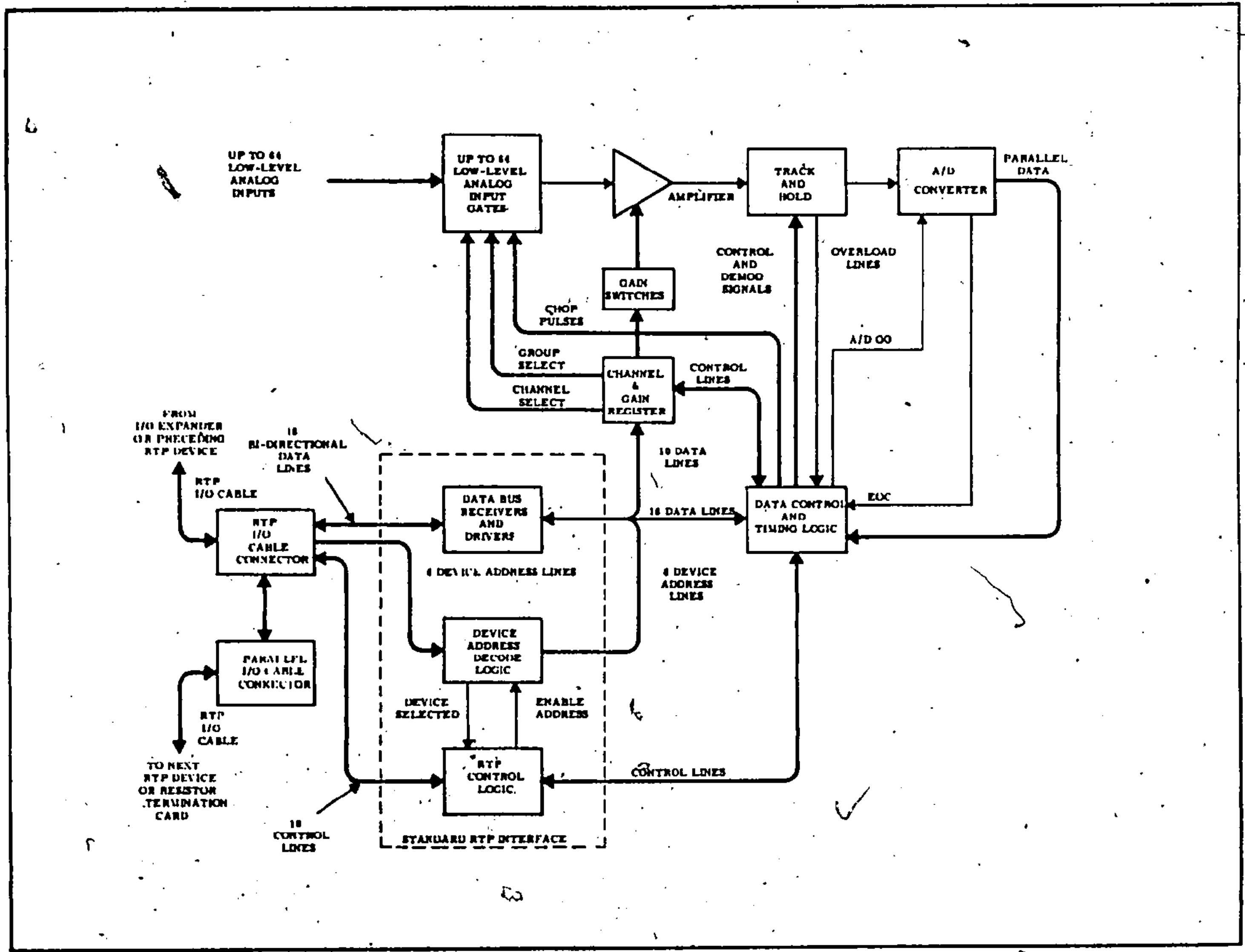

FIG. 4.7 RTP7471 SERIES ANALOG INPUT SYSTEM - BLOCK DIAGRAM

of the AIS is performed through the following steps:

(i) disable interrupts for AIS

(ii) transmittal of a code containing the channel number and gain range information (this sets the AIS on the "busy" mode and AIS returns to "ready mode" after the analog input is digitized).

(iii) Receipt of the digital output from AIS.

These steps are repeated for each channel sampling. The sampling rate can be preset at 8000, 4000, 2000 or 1000 channels per second. The AIS channel counter operates the multiplexer sequentially at the selected sampling rate whenever the computer is not requesting a channel to be sampled.

4.3.3 Signal Conditioning of AIS Inputs

The AIS hardware for differential overload protection, common mode rejection and normal mode rejection seems to be sufficient for thermocouples. Therefore, no signal conditioning is necessary. A carrier-demodulator unit (transduction model no. TR377) is, however, required for every pressure transducer. The output from the demodulator unit is an analog voltage in the range of ± 10 volts. This analog voltage is fed into the AIS input after suitable gain attenuation.

The signal output from a turbine flowmeter is a sine wave with varying amplitude and frequency depending on flow rates. This has to be converted into analog form before it can be accepted by the AIS. The electronics which are necessary to effect this conversion is shown schematically in

Figure 4.8. The same is true for the gamma densitometers. The gamma densitometers operate in the count mode and output logic pulses after energy selection by a single channel analyser (SCA). These pulses have to be converted into an analog voltage proportional to pulse frequency. A block diagram of the circuitry required is shown in Figure 4.9.

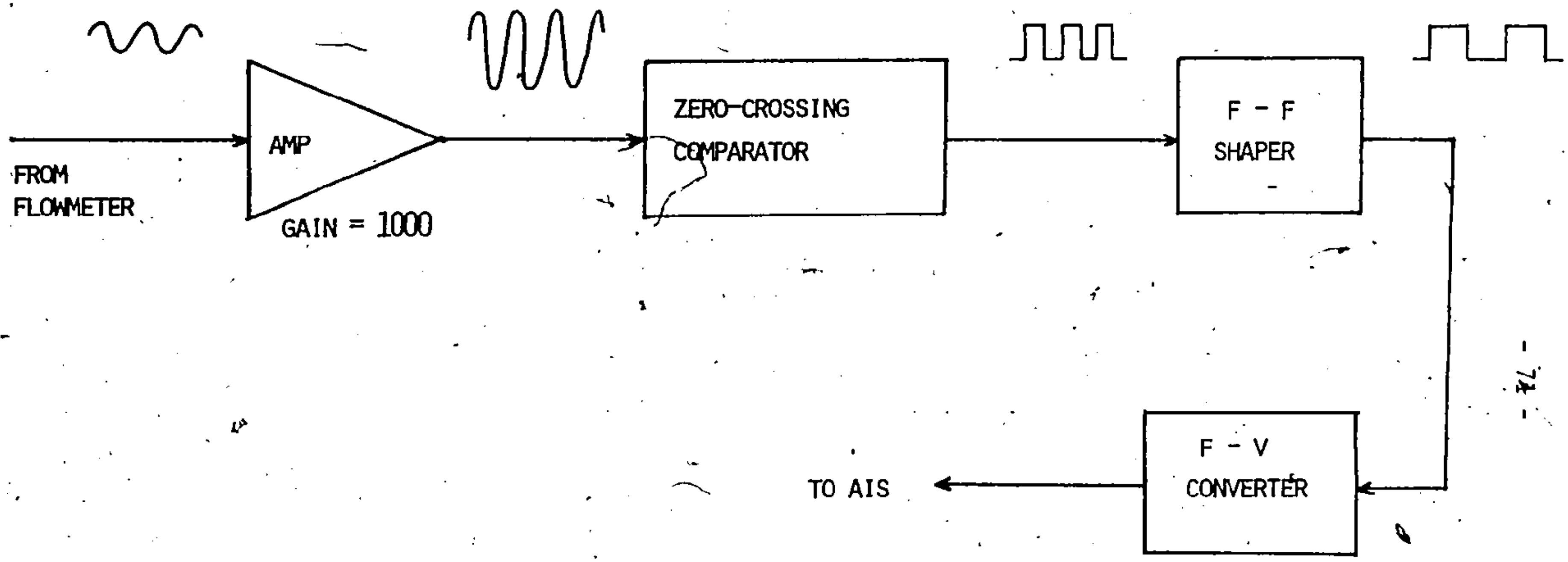

FIG. 4.8 FLOWMETER ELECTRONICS

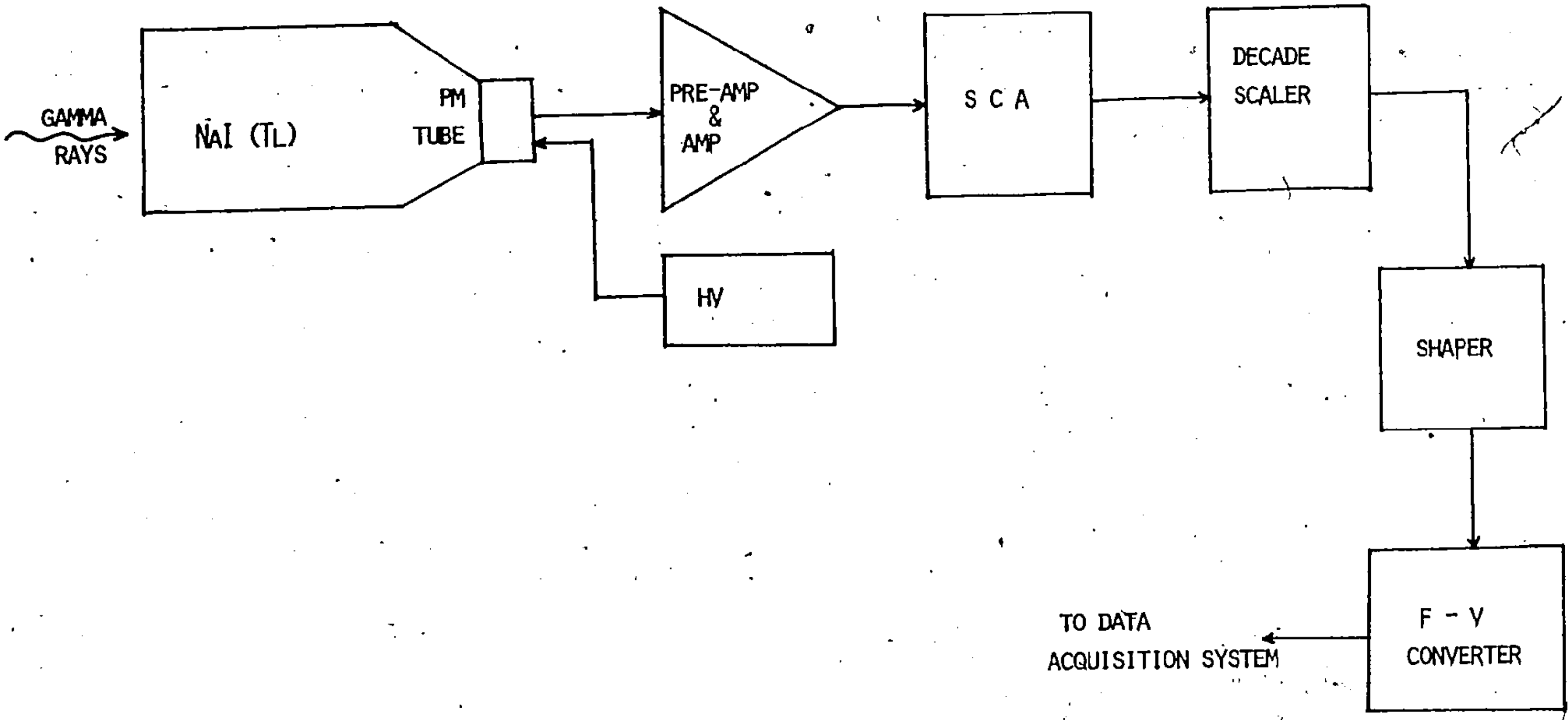

FIG. 4.9 BLOCK DIAGRAM OF GAMMA DENSITOMETER ELECTRONICS

5. VOID FRACTION MEASUREMENTS

5.1 General

Void fraction is one of the most important parameters characterizing vapor-liquid two-phase flow situations. A knowledge of the phase content is of key importance in predicting the performance of many processes and energy transfer systems. For example, it is required in the calculation of the gravitational and accelerational components of pressure drops. It is also important in estimating the behaviour of a nuclear reactor system. In particular, it must be measured in order to interpret blowdown and emergency cooling experiments related to reactor safety assessments.

A large variety of techniques has been proposed for void fraction measurements, reflecting the great importance of this parameter. However, no really adequate technique exists. Excellent reviews on the subject are given by Lahey [72] and Hewitt and Lovegrove [74]. Some of the available techniques are listed in Table 5.1.

5.2. Fast Neutron Scattering Technique

The use of the fast neutron scattering technique in void fraction measurement was studied in the present investigation for the following reasons:

(i) No really adequate techniques for measuring void fraction in vapor-liquid flows are available. The gamma ray attenuation technique is quite reliable; however, its resolution is rather poor in high void dispersed flow regimes, and the results depend somewhat on phase distribution.

(ii) To develop an accurate void fraction measurement technique which can be used as a reference for calibration of other types of void

TABLE 5.1

VOID FRACTION MEASUREMENT TECHNIQUES

I. Electrical Techniques
- (i) Electrical Impedance (Z) technique
  - global Z-probes.
  - local Z-probes
- (ii) Hot Wire and Hot Film Anemometry

II. Optical Techniques
- (i) High Temperature Local Probes
- (ii) Infrared Techniques
- (iii) Photographic Techniques
- (iv) Holographic Techniques
- (v) Light Scattering and Attenuation Techniques

III. Ultrasonic Techniques
- (i) Pulse-Echo Techniques
- (ii) Transmission Techniques
- (iii) Doppler Shift Techniques
- (iv) Shear and Torsional Wave Techniques

IV. Radiation Techniques
- (i) Gamma Ray Attenuation Techniques
- (ii) X-ray Attenuation Techniques
- (iii) Side-Scatter Gamma Ray Techniques
- (iv) Neutron Scattering and Transmission Techniques

meters, such as gamma densitometers.

(iii) To study the possibility of constructing a portable neutron densitometer for use in rewetting and refilling experiments.

Neutrons are fundamentally more attractive than gammas for measuring phase content in steam-water flow situations. This is because neutrons are more sensitive to water content than gamma rays and are less affected by metal walls containing the flow. Preliminary studies using fast neutron beams were discussed by Rousseau et al. [75] and Banerjee [76]. Initial results suggested that the technique was promising for practical application.

The technique consists of counting the scattered neutron flux from a fast/epithermal neutron beam incident on the test section. The beam is in the shape of a slit with the plane of the slit perpendicular to the test section axis. A fast/epithermal neutron beam from the McMaster Research Reactor was used. Details of the experiment are given by Yuen [77] and Banerjee et al. [78]. The experimental arrangement is shown schematically in Figure 5.1.

The first series of experiments was performed with aluminum-water test sections shaped to represent various typical two-phase flow patterns. Aluminium was used to simulate the vapor phase. The flow patterns simulated include stratified, annular and core. They are shown schematically in Figure 5.2.

Experiments were done with containers of 25.4 mm and 50.8 mm inner diameter. Results are shown in Figures 5.3 and 5.4. The predicted values

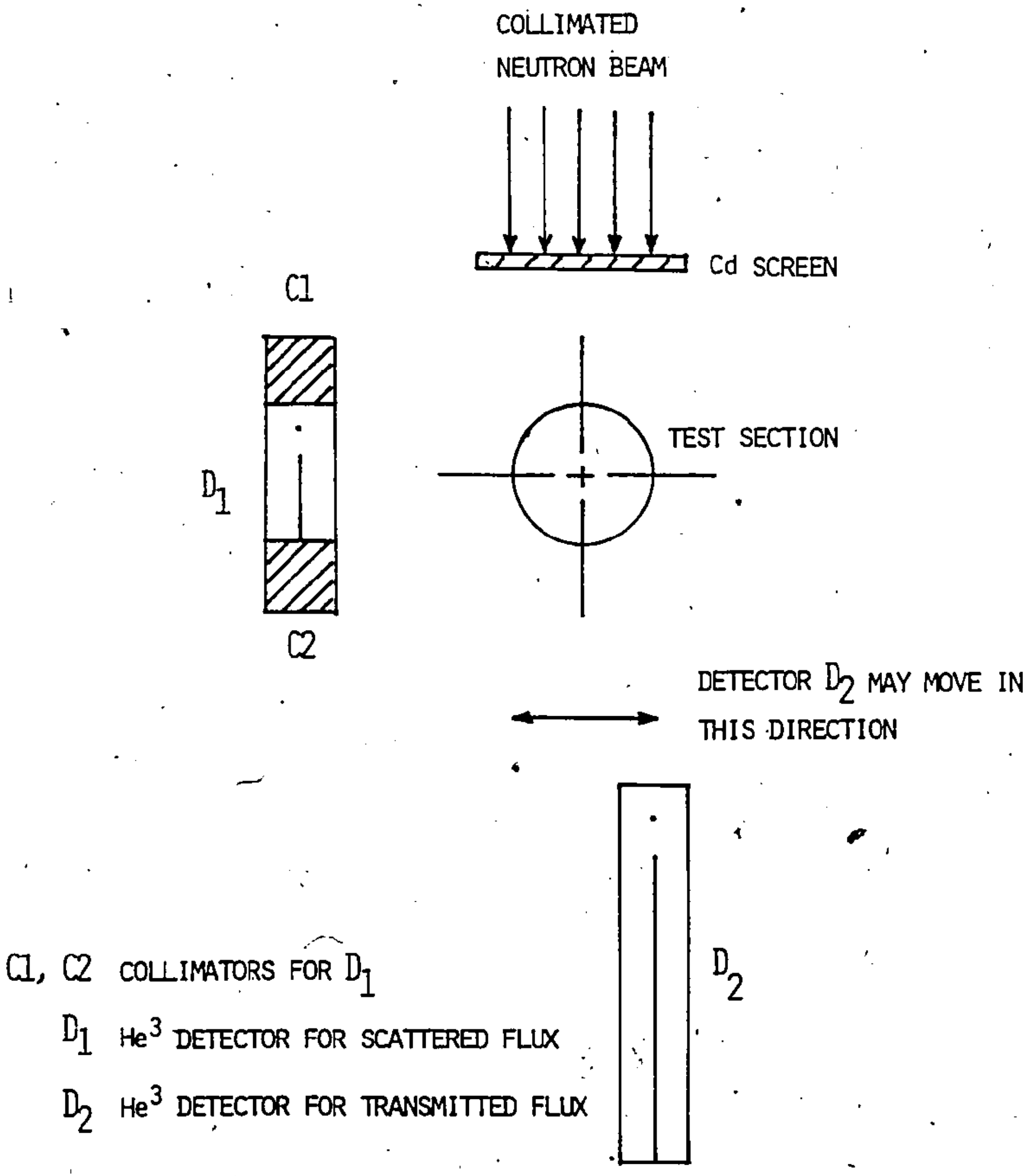

FIG. 5.1 SCHEMATIC PLAN VIEW OF EXPERIMENTAL SETUP

— FAST NEUTRON SCATTERING TECHNIQUE

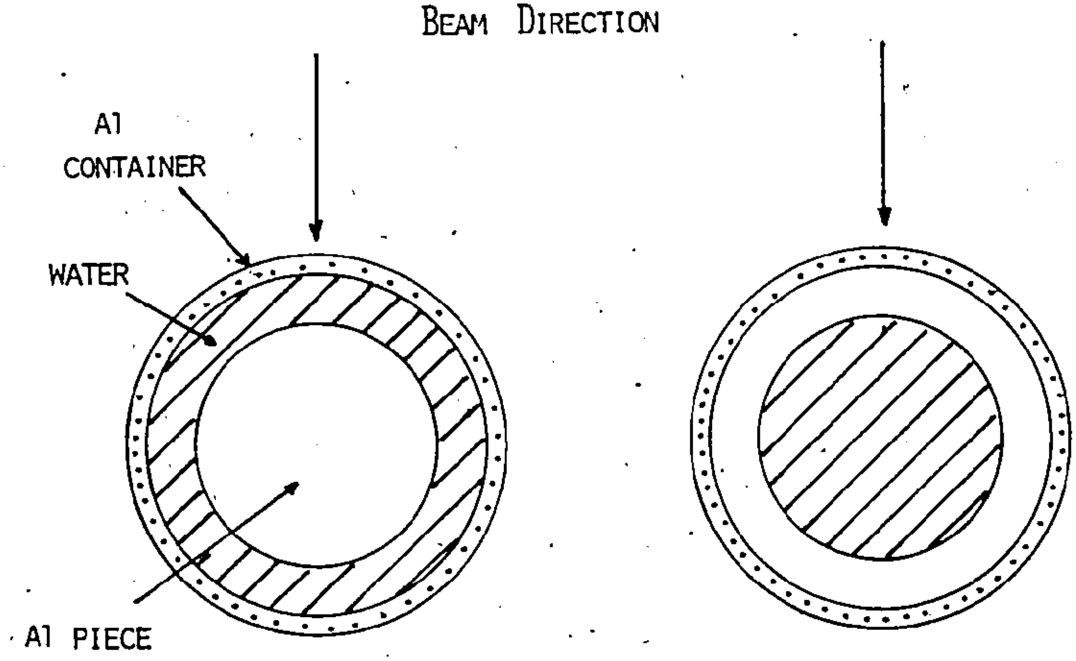

ANNULAR FLOW

CORE FLOW

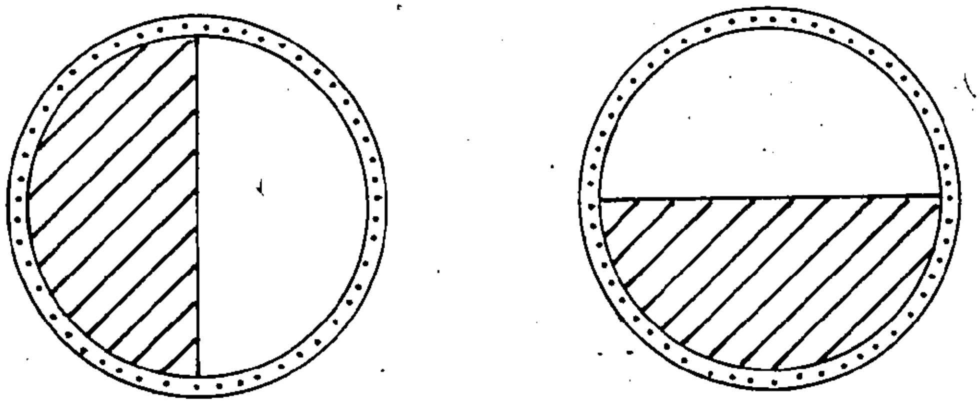

STRATIFIED FLOW
(VOID PARALLEL TO
BEAM PATH)

STRATIFIED FLOW
(VOID PERPENDICULAR
TO BEAM PATH)

FIG. 5.2 SIMULATED FLOW PATTERNS

FIG. 5.3 STATIC VOID FRACTION MEASUREMENTS USING NEUTRON SCATTERING METHOD (1" SPECIMEN)

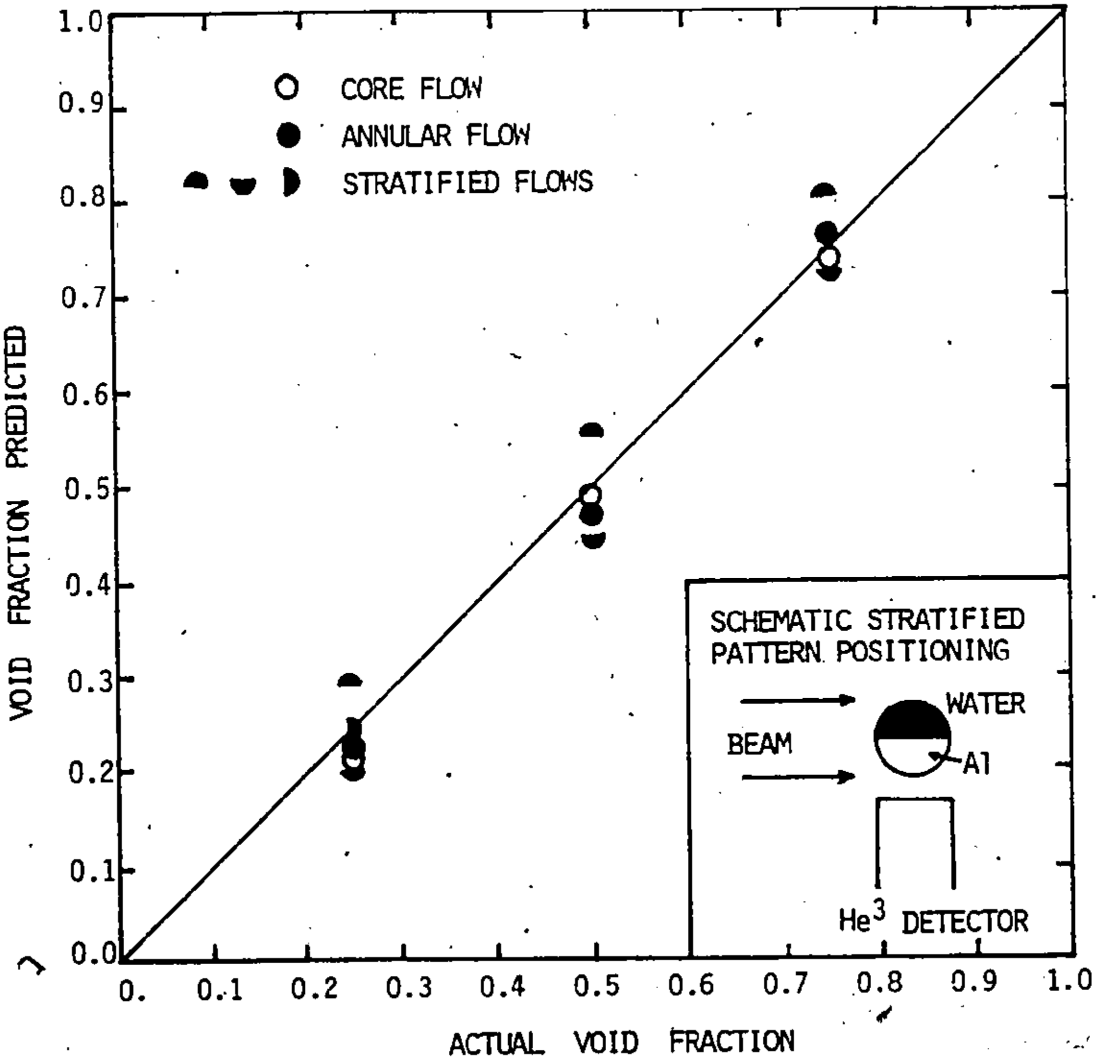

FIG. 5.4 STATIC VOID FRACTION MEASUREMENTS USING NEUTRON SCATTERING METHOD (2" SPECIMEN)

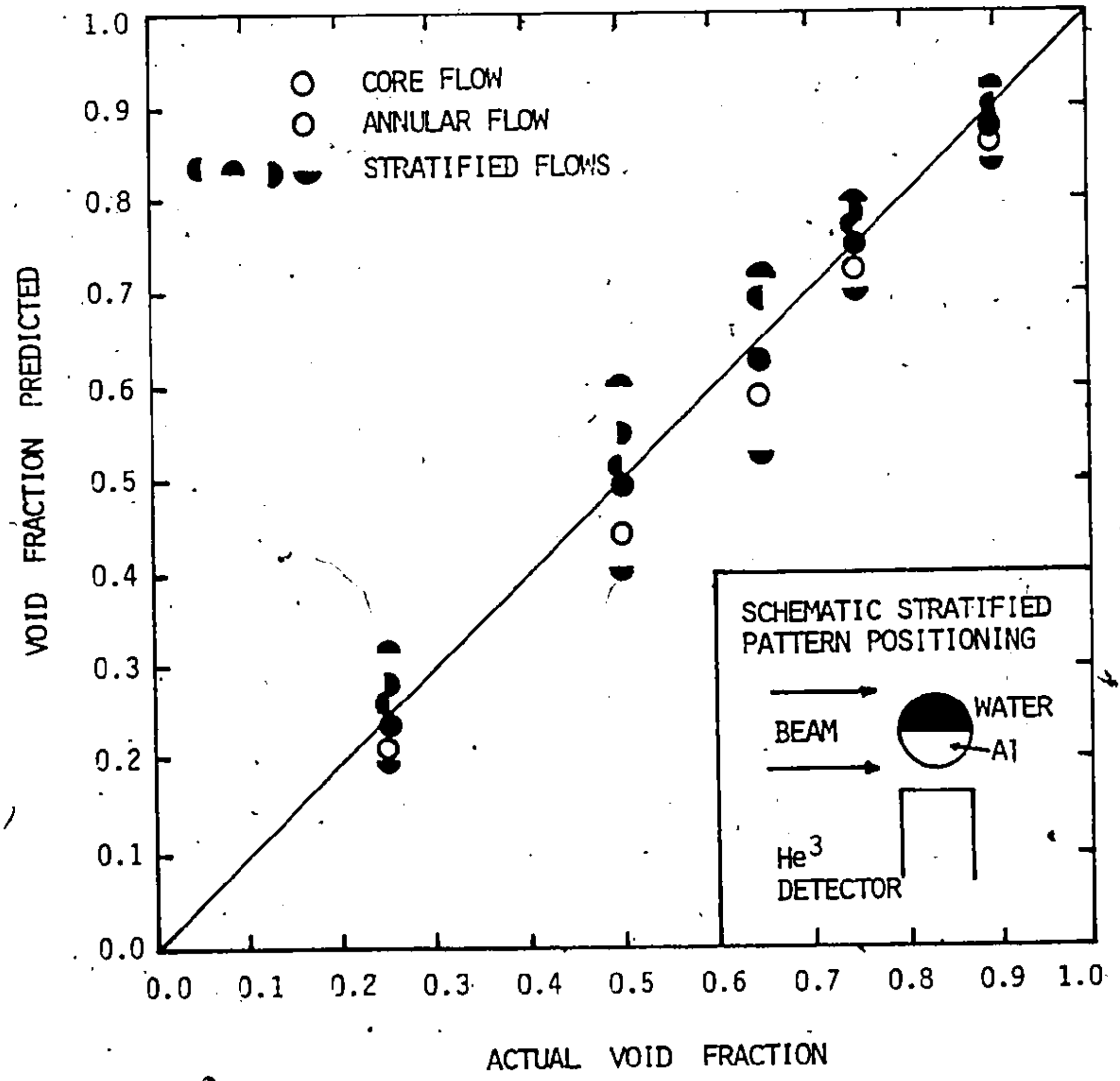

are directly obtained from the neutron flux with a correction for the background. No other correction or adjustment has been made. From the Figures, it is evident that there is a difference between measurement for the stratified patterns. If the aluminium (i.e. the void) is closer to the counter, a higher value of void fraction is predicted than actually present. Conversely if water is closer to the counter, a lower value of void fraction is obtained. This effect can be corrected by positioning two counters opposite each other and averaging the count rate. A second effect is that annular and core patterns in general give predicted void fractions which are slightly lower than the actual values.

The static experiments were followed by a series of quasi-static experiments in which the aluminum-water test sections were replaced by a vertical air-water flow loop. The test section used was an aluminum pipe with 38.1 mm internal diameter. The air and water flow rate, could be varied so that bubbly, slug, slug-annular and annular flows were obtained. The void fractions in the test section were measured both by the neutron scattering technique and by trapping the air-water mixture between two quick closing valves and weighing the content. Results obtained using the two techniques are compared in Figure 5.5. The void fraction obtained by trapping water is an average of a number of measurements. It can be seen that, except for a couple of points, the agreement is very good and the neutron scattering method always predicts a slightly lower void fraction. This is to be expected from the static aluminum-water tests.

From the experimental results obtained, it is clear that neutron scattering is a promising technique to use in predicting volume averaged void fractions. It gives very good results for static and quasi-static

FIG. 5.5 VOID FRACTION MEASUREMENTS — COMPARISON BETWEEN NEUTRON SCATTERING AND TRAPPING AIR - WATER MIXTURE METHODS

(TEST SECTION INTERNAL DIAMETER = 38.1 MM)

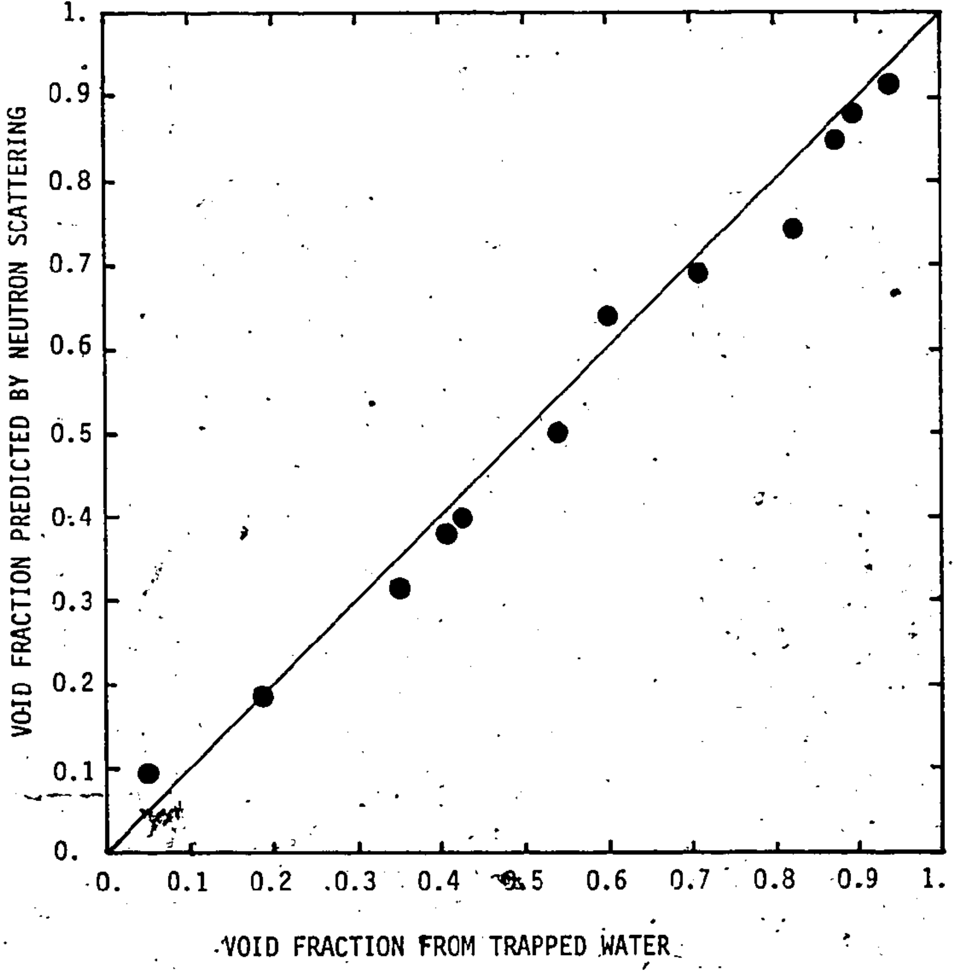

flow situations. However, a long counting period is needed. For the experiments described, a typical single counting time was 100 to 200 seconds in order to get good counting statistics (below 1%). Typical counting rates were about 200 to 400 scattered neutrons per second with a neutron beam strength of $\sim 10^6$ neutrons/cm^2 - s. Therefore, the use of the neutron scattering technique in rapid transient flow situations is not possible unless a very strong neutron source is available.

Work is currently underway at McMaster to make use of the transmitted instead of scattered neutrons to predict the averaged void fraction as well as phase distribution. The neutron transmission technique will give much higher counting rates. Thus, its application to rapid transients may be possible if it is developed and established.

Because of the long counting time required with scattered neutrons and readily available sources, the possibility of constructing neutron densitometers for the rewetting and refilling experiments was considered impractical. It was decided that the gamma ray attenuation technique should be used. The objective was to develop a compact gamma densitometer design for rapid transient operation.

5.3 Gamma Ray Attenuation Technique

The basic principle of the gamma ray attenuation technique is the familiar experimentally observed fact that the intensity of a collimated gamma beam decreases exponentially as it goes through matter. Mathematically, the attenuated flux is given by

$$N = N_0 \, e^{-\mu x} \qquad (5.1)$$

where N_0 is the incident flux, μ is the absorption coefficient of the absorber and x is the absorber thickness. There are three major processes responsible for absorption of gamma rays in matter. They are the photoelectric effect, the Compton effect, and pair production . Enge [79] contains a detailed discussion on the subject.

We can now apply the basic principle to two-phase flow situations. For a well mixed two-phase flow, in a conduit of width L and wall thickness t, eq. (5.1) can be written for the three cases when the conduit is filled with vapor alone, with liquid alone and with a well mixed two-phase mixture:

$$N(\alpha=1) = N_0\, e^{-2\mu_W t}\, e^{-\mu_g L} \tag{5.2}$$

$$N(\alpha=0) = N_0\, e^{-2\mu_W t}\, e^{-\mu_f L} \tag{5.3}$$

$$N(\alpha) = N_0'\, e^{-2\mu_W t}\, e^{-[\alpha\mu_g+(1-\alpha)\mu_f]L} \tag{5.4}$$

where μ_W, μ_f and μ_g are the absorption coefficients of wall, liquid and vapor respectively. α is the void fraction.

Combining (5.2) with (5.3), and (5.2) with (5.4), we have respectively

$$\frac{N(\alpha=0)}{N(\alpha=1)} = e^{-(\mu_f-\mu_g)L} \tag{5.5}$$

and

$$\frac{N(\alpha)}{N(\alpha=1)} = e^{-(1-\alpha)(\mu_f-\mu_g)L}$$

$$=[e^{-(\mu_f-\mu_g)L}]^{(1-\alpha)} \tag{5.6}$$

Substituting (5.5) into (5.6)

$$\frac{N(\alpha)}{N(\alpha=1)} = \left[\frac{N(\alpha=0)}{N(\alpha=1)}\right]^{(1-\alpha)}$$

This is normally written as

$$\alpha = \frac{\ln[N(\alpha=0)/N(\alpha)]}{\ln[N(\alpha=0)/N(\alpha=1)]} \tag{5.7}$$

If $N(\alpha=0)/N(\alpha=1)$ and $N(\alpha)/N(\alpha=1)$ are close to unity, i.e. $(\mu_f-\mu_g)L$ and $(1-\alpha)(\mu_f-\mu_g)L$ are small which is true in most cases, Eq. (5.5) and (5.6) can be approximated by

$$\frac{N(\alpha=0)}{N(\alpha=1)} \simeq 1 - (\mu_f-\mu_g)L \tag{5.8}$$

$$\frac{N(\alpha)}{N(\alpha=1)} \simeq 1 - (1-\alpha)(\mu_f-\mu_g)L \tag{5.9}$$

Dividing (5.9) by (5.8), we obtain

$$\alpha \simeq \frac{N(\alpha) - N(\alpha=0)}{N(\alpha=1) - N(\alpha=0)} \tag{5.10}$$

which is the linear interpolation equation.

5.4 Gamma Densitometer Design

The basic components of a single-beam gamma densitometer for averaged void fraction measurement is shown schematically in Figure 5.6. The device consists of a sealed gamma source, beam collimator, a scintillator and a signal detection system. The signal from the photo-multiplier tube can either be measured as a d c current/voltage output or counted as individual photons. In the first case, the system is said to be operating in the

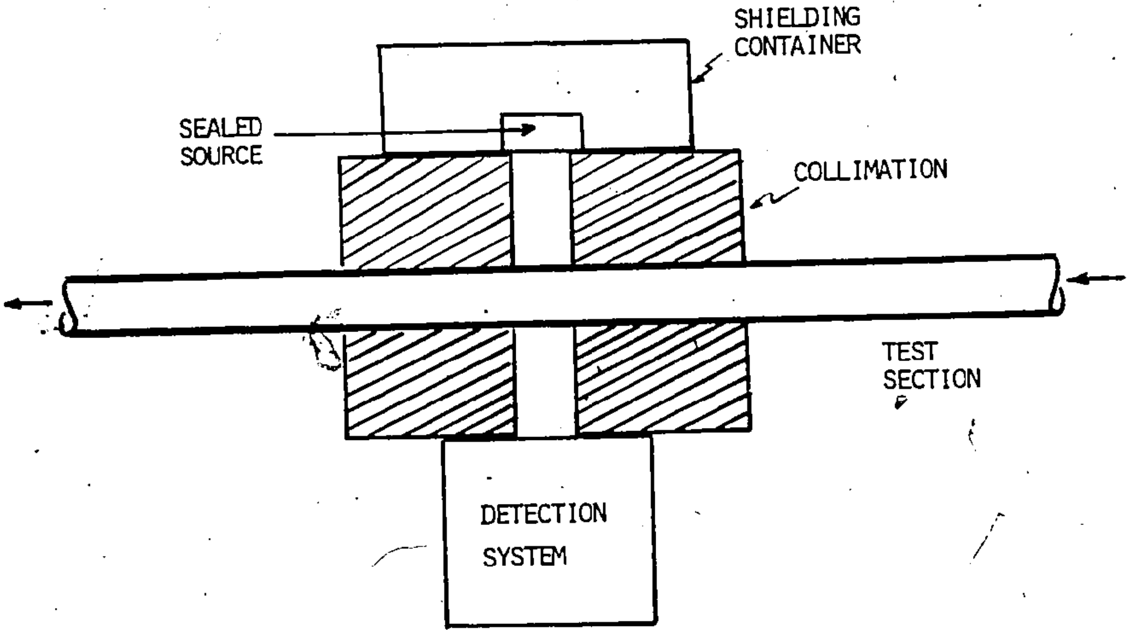

FIG. 5.6 SCHEMATIC DIAGRAM OF A GAMMA DENSITOMETER

current mode and in the latter case in the count mode.

Current mode devices have been widely used. Examples are the LOFT three-beam gamma densitometer (Lassahn [80]) and similar units developed by AECL (Heidrick et al. [81]). The advantages of operating in the current mode are:

(i) They are simple and relatively inexpensive.

(ii) Source intensity may be increased beyond the saturation point of the detector (i.e. the detector can no longer discriminate individual photons). This can result in faster response to density changes and smaller statistical error.

However, current mode devices are generally more prone to drift. This includes detector and scintillation phosphor drifts. An evaluation of the AECL densitometer performance is given by Piggott [82].

The drift problem can be largely eliminated if the count mode is used. In the current mode, the output changes directly as the gain changes, whereas, in the count mode, only the pulse height, not the count rate will be changed. Thus by using a single channel analyser (SCA) to band pass only the pulses in the photopeak, very stable count rates can be obtained. The densitometers used in the present investigation operate in the count mode.

To design the densitometer properly for use in a given experimental situation is quite difficult. Improper design may result in units that are unnecessarily bulky and cumbersome and have poor performance. A step by step design procedure will be given below. The test section used in the rewetting and refilling experiments will be used to illustrate the design procedure. Other geometries and materials can, of course be used, The procedures can be summarized as follows:

(i) specify the test section geometry and material
(ii) choose the radioactive isotope with reference to (i)
(iii) calculate the required source strength
(iv) choose the scintillator and counting system with reference to (iii)

5.4.1. Test Section

For the proper design of a gamma densitometer, the test section dimensions and material must be specified. The test section used determines the choice of photon energy and source strength required. In general, the source should have mono-energetic gammas with an energy which is high enough to penetrate the test section wall with minimal attenuation and at the same time low enough to be still sensitive to the water content. For a given test section, the attenuation of the gamma beam through the wall and the water can be calculated independently. The transmission curves of a circular gamma beam through a circular test section of the same diameter are shown in Figure 5.7. The test section used is the Zr-2 tube with O.D. = 0.775" and I.D. = 0.707". The calculation procedures can be found in Appendix I. It should be noted that the equations derived in Appendix I are for the calculation of averaged void fractions for given water volumes. The water transmission curve is obtained by comparing the transmitted gamma fluxes for the cases with $\alpha=0$ and $\alpha=1$.

From Fig. 5.7 it can be seen that the water transmission curve rises rapidly as the photon energy increases. Thus, as far as the sensitivity of the gamma to the water content is concerned, it is obvious that

Fig. 5.7 TRANSMISSION OF A CIRCULAR GAMMA BEAM THROUGH A CIRCULAR TUBE

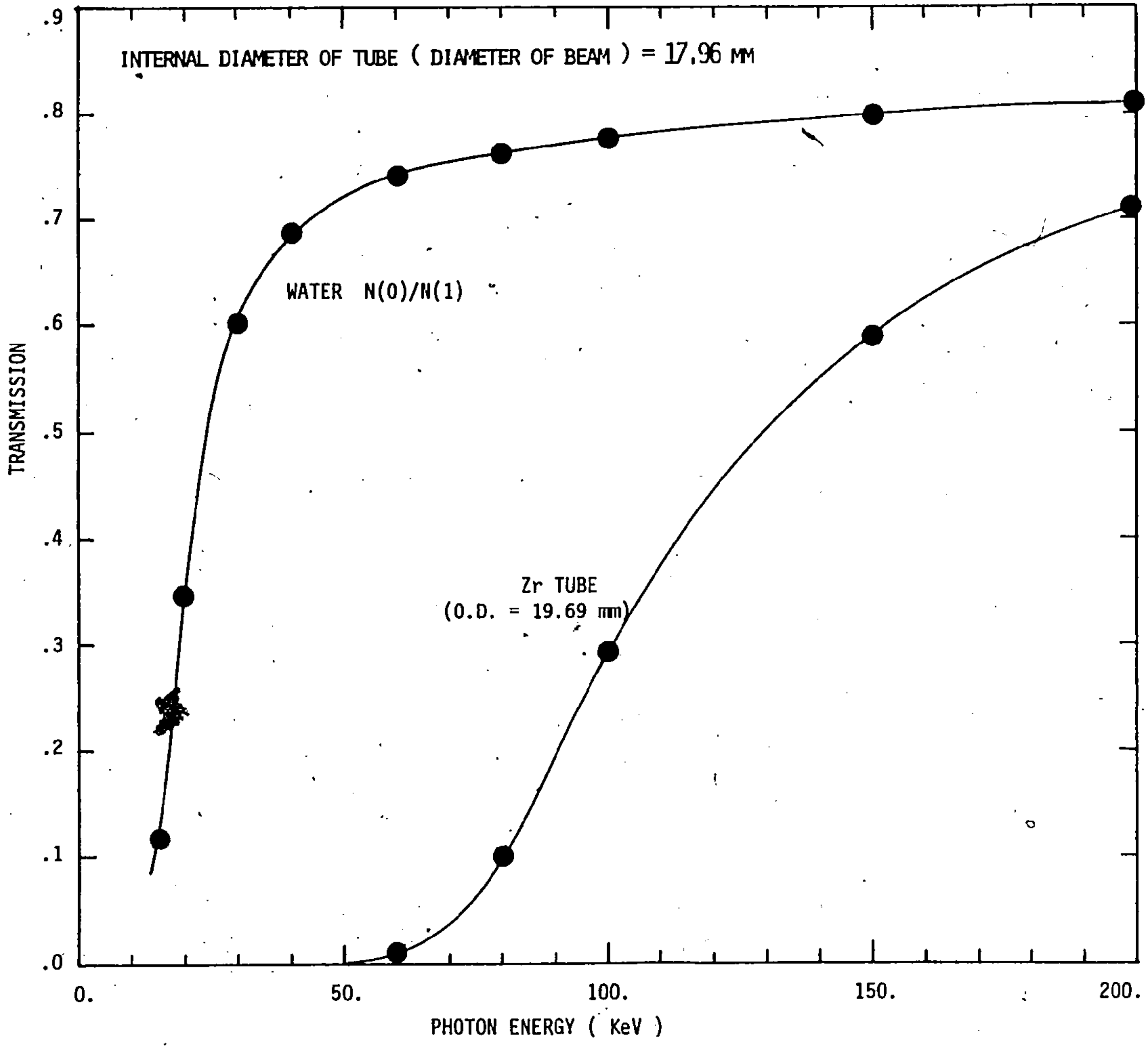

E (KeV)	μ_W (1/cm)	μ_{Zr} (1/cm)
15	1.48	--
20	.711	--
30	.337	--
40	.248	72.1
50	.214	--
60	.197	23.6
80	.179	11.2
100	.168	6.42
150	.149	2.50
200	.136	1.51

lower energy gammas are desirable. However, if the photon energy is too low, the gamma beam will be heavily attenuated by the wall and a very strong source may be necessary to obtain the desired count rates. On the other hand, a high energy gamma ray penetrates the wall with little loss, but it may be very insensitive to the water content. Therefore, a compromise has to be made in choosing the most suitable source.

5.4.2 Gamma Sources

To choose the appropriate source to use in a given situation is important. Transmission through the wall and sensitivity to the water content is of major importance. Other constraints include: (i) half-lives, (ii) conversion ratios of the desired gammas and (iii) availability and costs. A rule of thumb to follow is not to choose a source with gamma energy higher than is necessary. This is to minimize shielding requirements, and keep the unit compact and light.

Using the example in Fig. 5.7, it is clear that the desirable photon energy will be in the range of ∿80 KeV to ∿ 200 KeV. Higher energy gammas can of course be used at the expenses of water sensitivity and unit compactness. A list of commercially available low energy gamma sources is given in Table 5.2 [83]. A number of isotopes can be seen to have gamma energies within the desirable energy range. They are: Cd-109 (88 KeV), Co-57 (122 and 136.5 KeV), Gd-153 (97.4 and 103.2 KeV) Te-123m (159 KeV) and Tm-170 (84.3 KeV). Of these possible candidates, Co-57 is clearly superior to the others in the sense that it has high conversion (or emission) ratios for the desired gammas and relatively long half life. The conversion ratio is defined as the number of gammas of a particular energy emitted per 100 disintegrations of the radio nuclide. The lower the conversion ratio for the desired gammas, the stronger the source has to

TABLE 5.2

NUCLEAR PROPERTIES OF ISOTOPES USED IN LOW ENERGY PHOTON SOURCES

Isotope	Half-life	Principal Photon Energy (KeV)	Emission	Notes
^{241}Am	433 y	(Np L X-rays) 11.9 -22.3	∿40%	Other low abundance high energy γ's present.
		59.5	35.3%	
^{109}Cd	453 d	(Ag K X-rays) 22.1 , 25.0	102.3%	
		(Ag L X-rays) 2.63 - 3.80	∿10%	
		88.0	3.6%	
^{57}Co	270.5 d	(Fe K X-rays) 6.40,7.06	∿55%	γ at 692 KeV (0.16%)
		14.4	9.4%	
		122.0	85.2%	
		136.5	11.1%	
^{244}Cm	17.8 y	(Pu L X-rays) 12.1 - 23.0	∿8%	
^{153}Gd	241.5 d	(Eu K X-rays) 41.3, 47.3	∿110%	
		69.7	2.6%	
		97.4	30%	
		103.2	20%	
^{125}I	60.0 d	(Te K X-rays) 27.4, 31.1	138%	
		35.5	7%	
^{210}Pb	22.3 y	(Bi L X-rays) 9.42 - 16.4	∿21%	
		46.5	∿4%	
		+ Bremsstrahlung extending to 1.16 MeV		
^{238}Pu	87.75 y	(U L X-rays) 11.6 -21.7	∿13%	
^{123m}Te	119.7 d	(Te K X-rays) 27.4,31.1	∿50%	
		159.0	83.5%	
^{170}Tm	128 d	(Yb K X-rays) 52.0, 59.7	∿5%	
		84.3	3.4%	
		+ Bremsstrahlung extending to 968 KeV		

be for a specific gamma flux. This increases cost and shielding requirements.

Once the appropriate source is selected, its required strength can be calculated for particular applications and densitometer designs.

5.4.3. Source Strength

In counting experiments, the statistical error involved for high enough counts (N) is given by

$$\varepsilon = \frac{\sqrt{N}}{N} = \frac{1}{\sqrt{N}} \qquad (5.11)$$

Consider the linear interpolation equation for void fraction measurements

$$\alpha = \frac{N_\alpha - N_0}{N_1 - N_0} \qquad (5.10)$$

If N_1 and N_0 are averaged over a long enough period of time, we can assume that their statistical errors are insignificantly small and we can determine the statistical error in void fraction measurements as

$$\alpha = \frac{(N_\alpha - N_0) \pm \sqrt{N_\alpha}}{N_1 - N_0} = \alpha_0 \pm \varepsilon_\alpha \qquad (5.12)$$

Define the sensitivity (S) of the gamma beam to the water content in the test section to be

$$S = \frac{N_1 - N_0}{(N_1 + N_0)/2} = \frac{N_1 - N_0}{\bar{N}} \qquad (5.13)$$

Substituting into (5.12), we have

$$\varepsilon_\alpha = \pm \frac{\sqrt{N_\alpha}}{S\overline{N}} \qquad (5.14)$$

Since $N_0 \leq N_\alpha \leq N_1$ and N_0/N_1 is close to unity in most cases, we can write to a first approximation

$$N_\alpha \simeq \overline{N}$$

Therefore, eq. (5.14) becomes

$$\varepsilon_\alpha \simeq \pm \frac{1}{S\sqrt{N_\alpha}} \qquad (5.15)$$

That is, the statistical error in void measurement is inversely proportional to the sensitivity. The higher the sensitivity, the smaller the error will be. This is precisely why the use of lower photon energy is desirable.

For the 0.707" I.D. Zr-2 test section, with C_o-57 source (S=0.24), ε_α can be computed as a function of N_α

N_α	ε_α
300	23%
500	18%
1000	13%
5000	5.7%

Depending on how fast the transient is, the counting period can be very short. For example, if a sampling time of 16 ms is used as in the rewetting and refilling experiments, in order to achieve $\varepsilon_\alpha < 5\%$, the integral counting rate has to be $N_R > 0.4$ MHz (4×10^5 counts per second).

The source strength can then be estimated

$$A = N_R/(Gfc) \qquad (5.16)$$

where c = the conversion ratio of the desired gamma

f = the efficiency of the scintillator used

G = TΩ = a geometric factor

T = transmission of gamma beam through window, tube wall, etc.

$\Omega = 1/4\ (d/2D)^2$ = solid angle factor

d = diameter of beam

D = Distance between source and scintillator.

From eq. (5.16), it is clear that the required source activity depends on the design of the voidmeter, the speed of the transient, as well as source and scintillator used. With a counting period of 16 ms, a beam diameter of 1.80 cm, a collimation length of 15.2 cm, a scintillator of efficiency 50% and if Co-57 (c=96%) is used, it can be shown that a source activity of about 40 milli-curie is enough to have ε_α below 5%. Whereas, if Tm-170 (c=3.4%) is used, this will require an activity of about 5 curies.

5.4.4 Scintillator and Counting System

Thallium activated sodium iodide, NaI(Tℓ) crystal has been the most efficient and extensively used scintillator for gamma ray detection. Its high light output yields relatively good energy resolution. Its detection efficiency is close to 100% for low energy gammas (<200 keV). However, an important drawback of NaI(Tℓ) crystals in integral counting experiments is its low intensity acceptance. Its long decay time (230 ns) sets a practical limit of the integral counting rate to about 100 kHz (10^5 counts per second). For higher counting rates, a faster response scintillator has to be used.

Table 5.3 lists the properties of a number of commonly used scintillation crystals [84]. It can be seen that the only crystals that have decay constants significantly less than that of NaI(Tℓ) are CsF and Plastics. However, both of these have very poor efficiency compared to NaI(Tℓ). This means a much stronger source is necessary (Eq. 5.16) if they are to be used. Instead of a 40 milli-curie Co-57 source, a 0.66 curie source will be required, which is prohibitively expensive.

Heavy metal loaded plastic scintillators, on the other hand, have the desired properties for fast counting experiments when a low energy gamma ray is used. By introducing high atomic-number elements into plastic materials, a much higher detection efficiency can be achieved without affecting the short decay time characteristic for energies up to about 150 keV (Eriksson et al. [85] and Cho and Tsai [86]). For a 5% tin loaded plastic scintillator, its detection efficiency for 100 KeV gammas can be as high as 80% relative to that of NaI(Tℓ). Thus counting rates in the MHz region can be handled. 10% lead loaded plastic scintillators were used in our voidmeters and they were found to perform well with the 122 KeV (Co-57) gamma ray.

When higher energy gamma rays are used, e.g. > 200 KeV, no efficient and fast responding scintillator exists for operation in the MHz range. This poses a limitation to the use of the count mode in many practical situations. In these situations, current mode operation would have to be used and extreme care must be taken to minimize drift problems.

The choice of the counting system depends on the count rates. For relatively low count rates (≤ 200 KHz), an ordinary system can be used.

TABLE 5.3

PROPERTIES OF SOME SCINTILLATION CRYSTALS

Material	Wavelength of Maximum Emission (nm)	Dacay Constant (μs)	Index of Refraction	Density (gm/cm^3)	Scintillation Conversion Efficiency (%)*
NaI(Tl)	410	0.23	1.85	3.67	100
CsI(Na)	420	0.63	1.84	4.51	85
CsI(Tl)	565	1.0	1.80	4.51	45
CsF	390	0.005	1.48	4.11	3
CaF_2(Eu)	435	0.9	1.44	3.19	50
$Bi_4Ge_3O_{12}$	480	0.30	2.15	7.13	8
BaF_2	325	0.63	1.49	4.88	10
Kl(Tl)	426	.24/2.5	1.71	3.13	24
$CaWO_4$	430	.5 - 20.	1.92	6.12	50
$CdWO_4$	530	.5 - 20.	2.2	7.9	65
Ps	425	∿ 0.002	1.58	1.05	< 5
Ps(10% Pb)	425	∿ 0.002	1.58		∿ 90 (<100 KeV)

---

* Referred to NaI(Tl) with S-11 photocathode response

For high count rates (> 200 KHz), a fast responding system is necessary. Typical counting systems are shown in Figure 5.8. The "fast" system is capable of handling counting rates of up to 100 MHz.

5.4.5 Source Container Design

The use of radioactive material at McMaster University is supervised by the McMaster Health Physics Advisory Committee (HPAC). It is charged with the authority to ensure the University's compliance with radiation protection regulations promulgated by federal, provincial and local authorities. The maximum permissible annual exposures for radiation workers as set forth by the Atomic Energy Control Board are given in Table 5.4 [87]. The design of the source container is to provide adequate shielding to the experimenter.

The shielding container design for the 50 mCi Co-57 source is shown in Figure 5.9. Steel is used as the shielding material because of the relatively low energy gammas (122 KeV). If the gamma energy is high, lead is normally used. It should be noted that lead is hard to machine and it is advantageous to use steel if possible. Using 1 1/2" (39.1 mm) steel shielding in all directions, it was found that the total exposure that an experimenter would accumulate in a year is less than 0.3 rems. This is well below the maximum permissible exposure given in Table 5.4. Detailed dose rate calculations can be found in Appendix I.

A picture of the source container is shown in Plate 5.1. A 12-inch ruler is also shown. The larger container houses the 50 mCi Co-57 source whereas the smaller container contains a 100 mCi Pu-238 source used in another experiment. The source containers are designed such that the top

FIG. 5.8 GAMMA DENSITOMETER COUNTING SYSTEMS

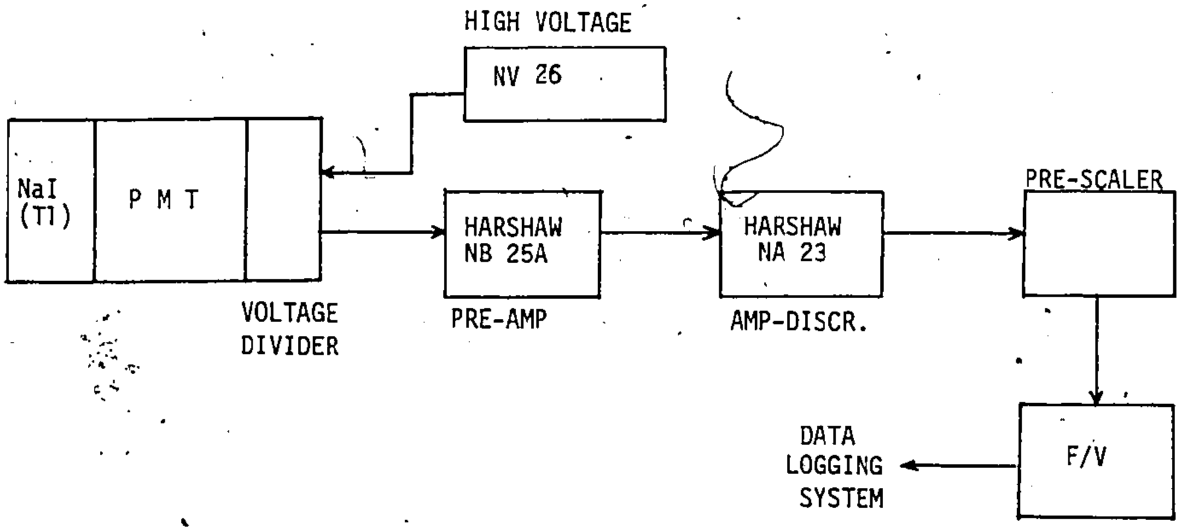

(A) SYSTEM FOR LOW COUNTING RATES (≤ 200 KHZ)

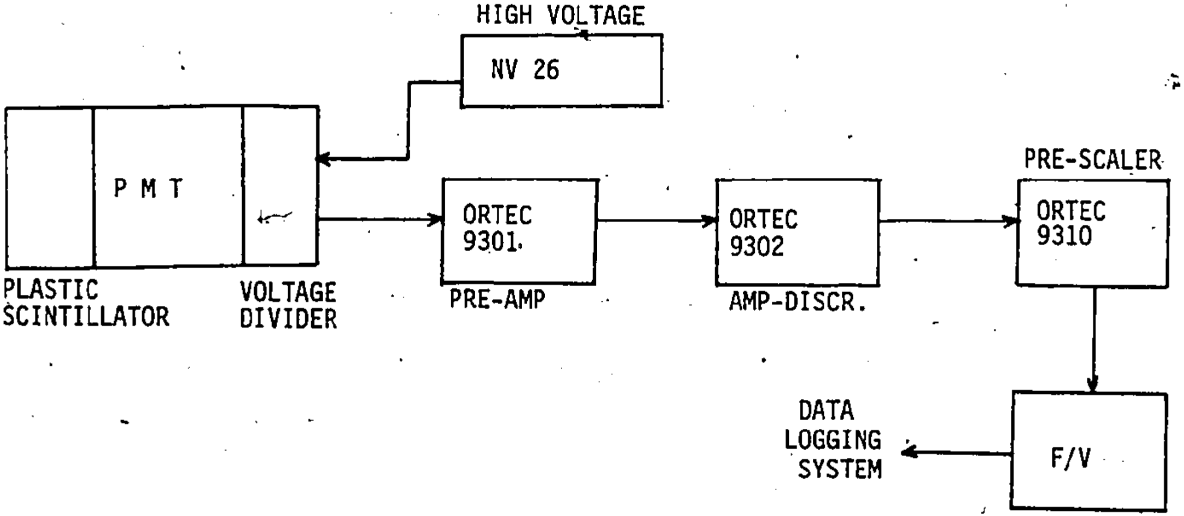

(B) SYSTEM FOR HIGH COUNTING RATES (> 200 KHZ)

TABLE 5.4

MAXIMUM PERMISSIBLE ANNUAL EXPOSURES FOR RADIATION WORKERS

Organ	Quarterly Limit (rem)	Yearly Limit (rem)
1. Whole body, gonads, red bone marrow	3	5
2. Any single organ, excluding the gonads, the red bone marrow, bone, thyroid and skin	8	15
3. Bone, thyroid, skin of the whole body (excluding the skin of the hands, forearms, feet, and ankles)	15	30
4. Hands, forearms, feet and ankles	40	75

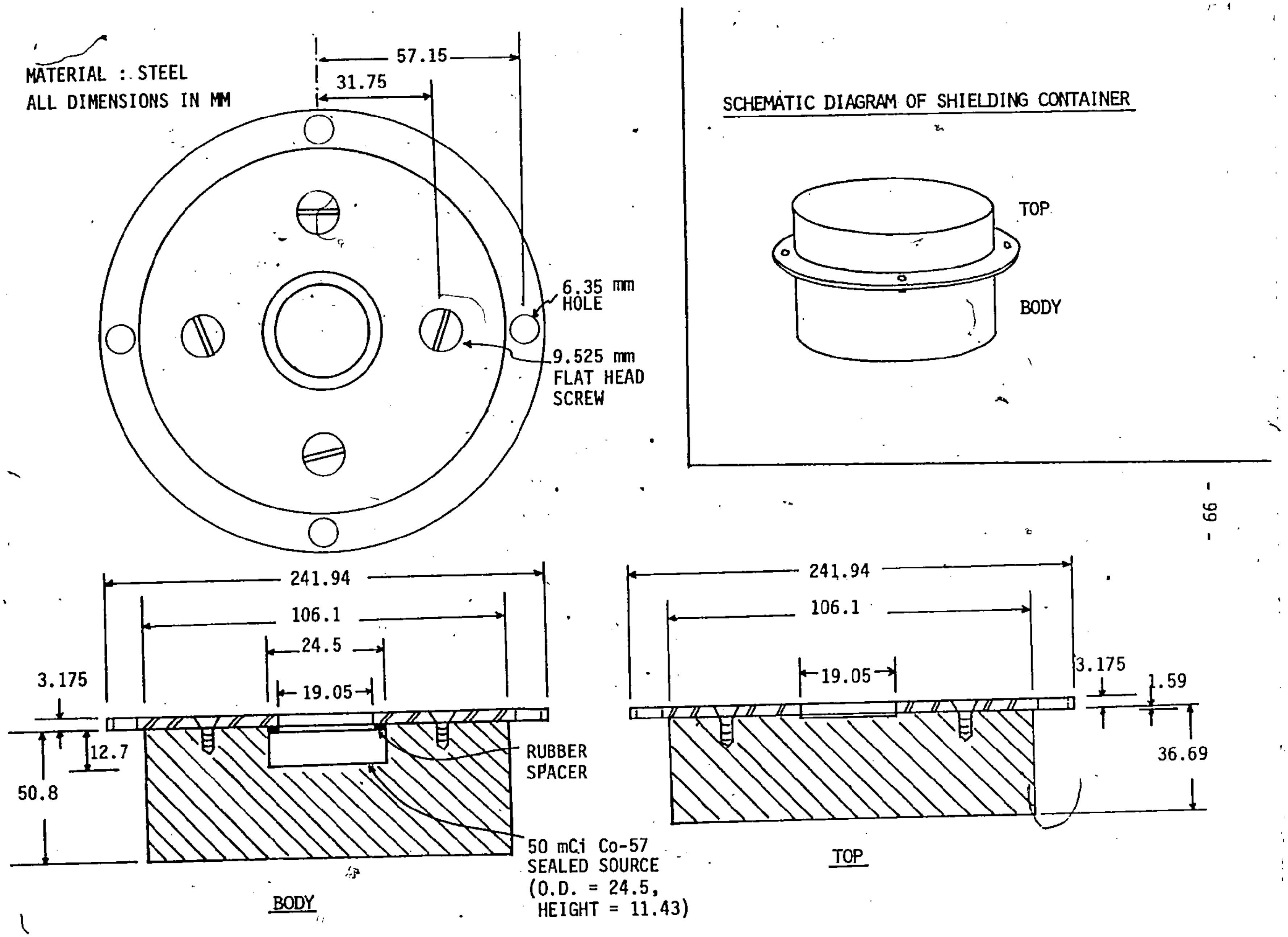

FIG. 5.9 SHIELDING CONTAINER DESIGN

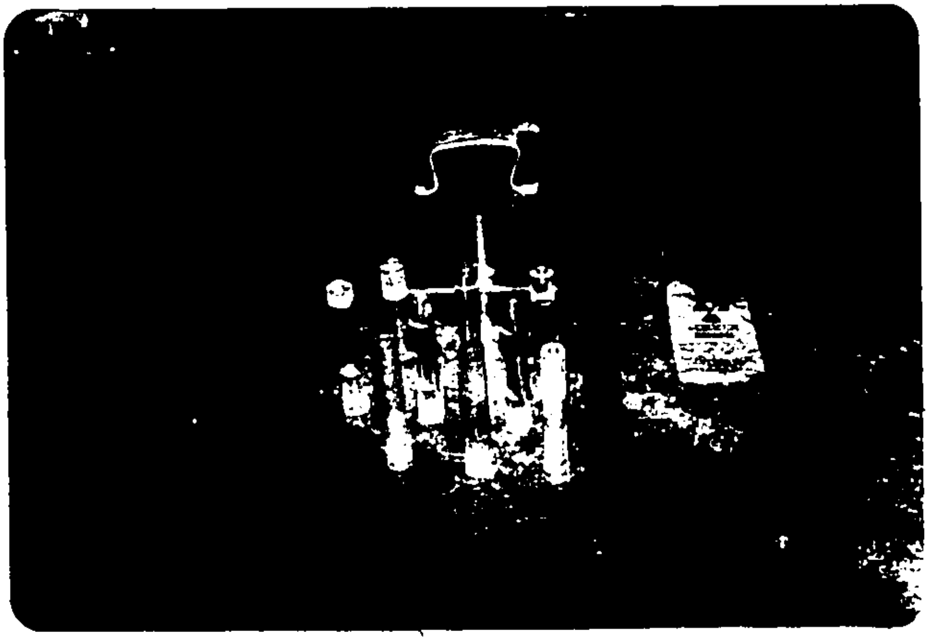

Plate 5.1 SOURCE CONTAINERS AND SHAPED LUCITE PIECES FOR DENSITOMETER CALIBRATION

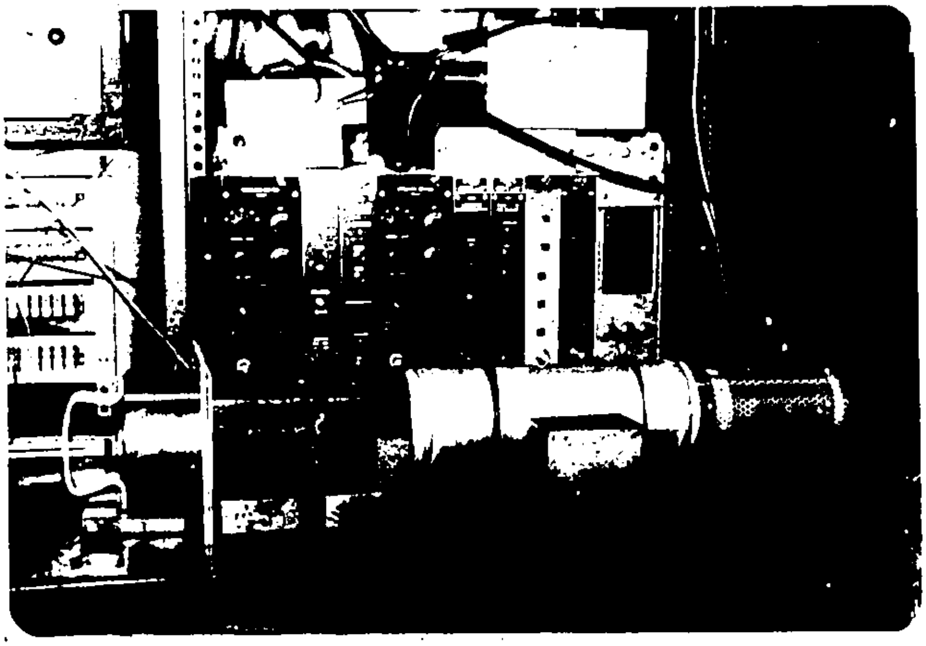

Plate 5.2 GAMMA DENSITOMETER SETUP

can be taken off and the body directly hooked up to the collimator when used.

The shaped pieces shown are made from Lucite and used for calibration purposes. This will be described in the next section.

5.5 Calibration

Shaped Lucite pieces are used to simulate the liquid phase in different flow distributions, namely annular, core and stratified. Lucite is used because its gamma ray absorption coefficient is very close to that of water. A comparison of the mass absorption coefficients for water and Lucite is shown in Figure 5.10. Values for water are taken from Jaeger [88], while those for Lucite are computed using the weighted average equation for the constituent elements,

$$\frac{\mu}{\rho} = \sum_i w_i \left(\frac{\mu}{\rho}\right)_i \tag{5.17}$$

where w_i is the proportion by weight and $(\mu/\rho)_i$ the mass absorption coefficient of the ith constituent respectively. The chemical formula for Lucite (polymethyl-methacrylate) is $[CH_2C(CH_3)(CO_2CH_3)\text{-}]_n$. There are 5 carbon atoms, 8 hydrogen atoms and 2 oxygen atoms in a molecule.

A picture of the densitometer set up for calibration is shown in Plate 5.2. A piece of Zr-2 tube is used as the specimen holder and shaped Lucite pieces simulating different void fractions and flow distributions can be inserted. The measured and actual void fractions are compared in Figure 5.11. It can be seen that the measured void fraction is always lower than the actual value for core flows and higher for annular flows. For stratified flows, if the beam is parallel to the interface. α_{meas} is lower than α_{actual} in low voids and higher in high voids. α_{meas} crosses

FIG. 5.10 MASS ATTENUATION COEFFICIENT OF WATER AND LUCITE

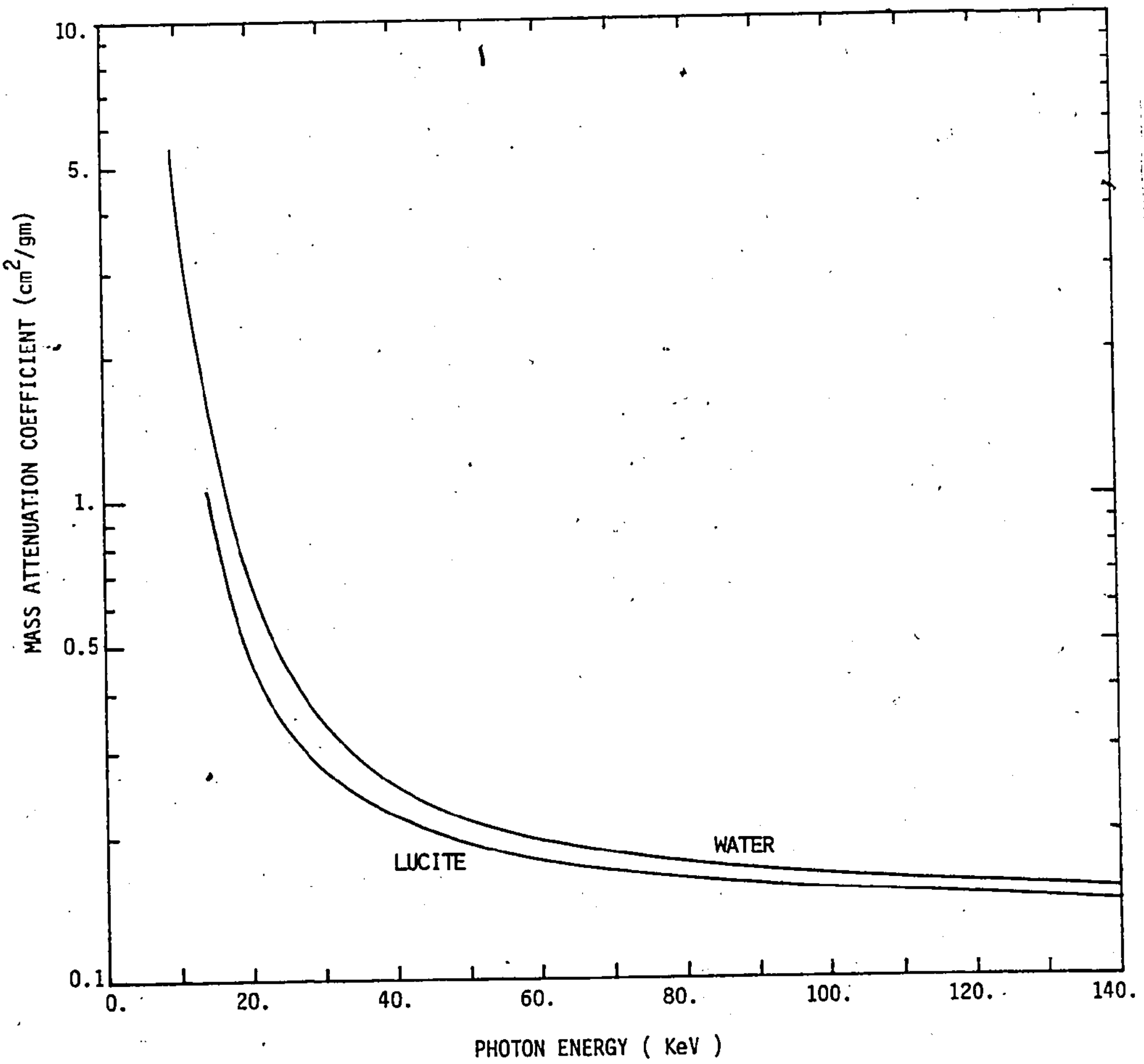

Fig. 5.11 VOID FRACTION PREDICTED BY GAMMA ATTENUATION MEASUREMENTS COMPARED TO ACTUAL VOID FRACTION

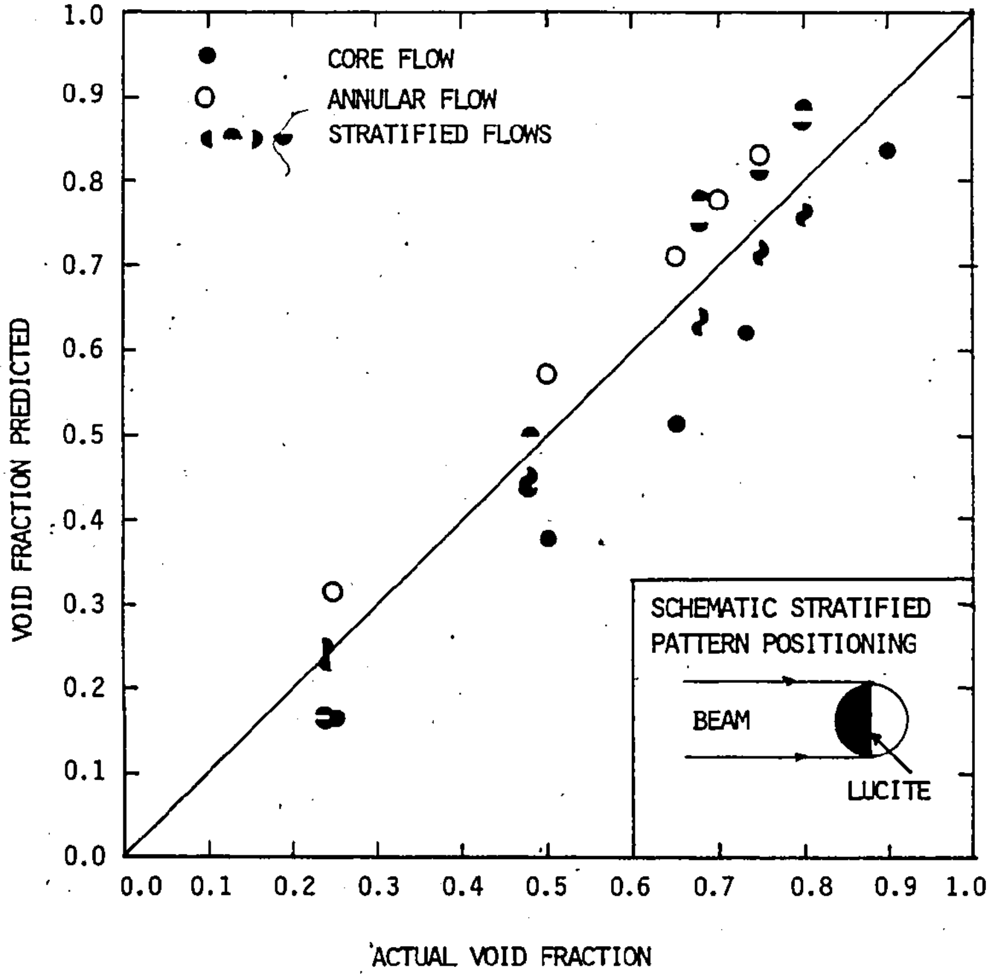

the 45° line at $\alpha = 0.5$. If the beam is perpendicular to the interface, α_{meas} is slightly lower than α_{actual}. In general, the difference between α_{meas} and α_{actual} is less than 15% except for core flows. The deviation is less for stratified flows with the interface perpendicular to the beam. Therefore, it may be concluded that fairly accurate void measurements can be obtained using the present single-beam gamma densitometers, especially when the beam is perpendicular to the interface in stratified flows.

The difference between α_{meas} and α_{actual} as shown in Figure 5.11 can be explained in terms of system geometry and beam profile. When a circular beam crosses a circular test section of the same diameter as the beam, it is obvious that the central region will affect the measurement more. Thus, when water is concentrated at the center of the tube (core flow), the gamma beam will get attenuated more and result in lower α_{meas}. The opposite is true when the central region is filled with vapor or air (annular flow). For stratified flows with the interface parallel to the beam, when α_{actual} is less (or greater) than 0.5, the more heavily weighted central region contains more water (or air) and thus results in lower (or higher) α_{meas}. When the beam is perpendicular to the stratified interface, the differential weighting effect will be minimal and gives α_{meas} values closer to α_{actual}. The shape of the beam will also affect the void measurements. In principle, a flat profile should be used. However, for any disc source the flux at the center tends to have a maximum and drops off as it gets to the edge, this will aggravate the differential weighting effect of the central region.

In order to estimate these two effects separately, the effect of system geometry is obtained by calculating (numerical summation) the void fractions assuming a flat beam profile. Details of the calculation are given in Appendix I. The numerically calculated versus the experimentally measured void fractions are shown in Figure 5.12. It is evident that the trends of α_{calc} for different flow distributions are the same as α_{meas} shown in Figure 5.11. It can also be seen that α_{calc} is very close to α_{actual} even for core flows. This indicates that the geometric effect is not very important. In other words, the beam profile has a much stronger effect on α_{meas} (Figure 5.11). The flatter the beam is, the more accurate α_{meas} will be. Therefore, in the design of gamma densitometers, a flat beam profile should be used. This can be approximated by using a disc source with a diameter larger than the diameter of the beam and taking the beam from the central portion of the source.

The calculated results shown in Figure 5.12 are obtained using an experimentally determined water absorption coefficient for Co-57 gamma rays. Since Co-57 has two important gammas (122 KeV and 136 KeV), the mean absorption coefficient of water has to be determined experimentally. This is shown in Figure 5.13. The result ($\mu = 0.130$ cm^{-1}) is slightly lower than that given in Figure 5.11 ($\mu = 0.155$ cm^{-1}). However, the change in α_{calc} is found to be insignificant when the higher absorption coefficient is used.

Fig. 5.12 VOID FRACTION CALCULATED BASED ON GAMMA ATTENUATION COMPARED TO ACTUAL VOID FRACTION

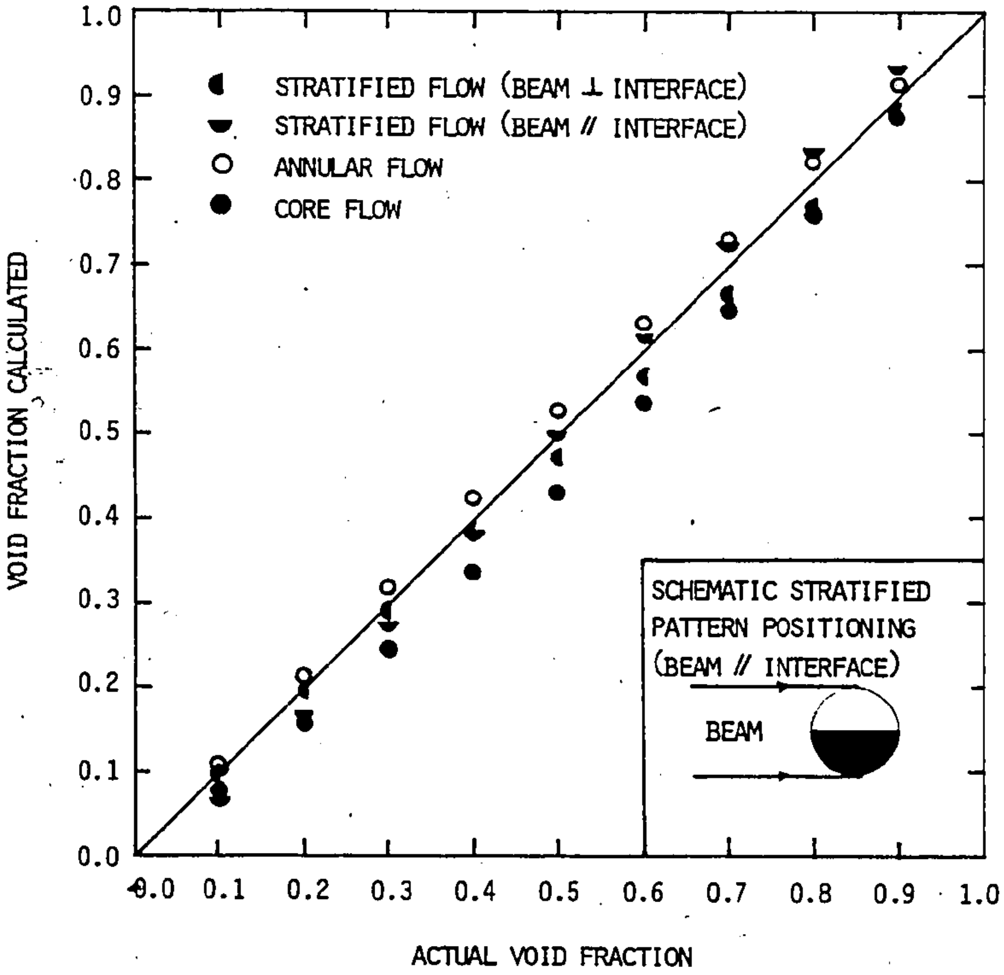

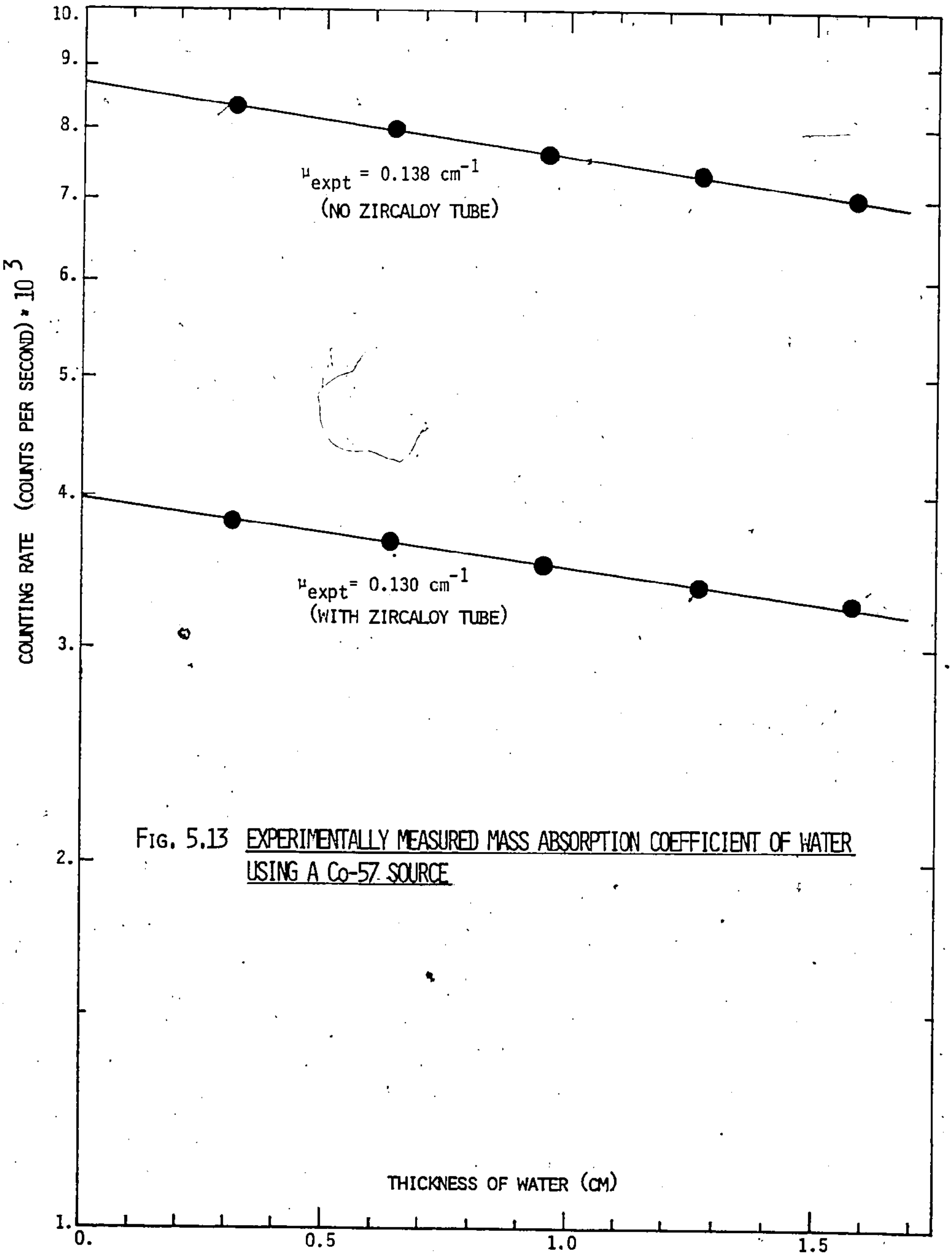

FIG. 5.13 EXPERIMENTALLY MEASURED MASS ABSORPTION COEFFICIENT OF WATER USING A Co-57 SOURCE

6. EXPERIMENTAL PROCEDURE

6.1 System Calibration

The instrumentation used was calibrated and tested on a regular basis. Those most likely to drift were examined most frequently.

The Automatic Data Acquisition System (ADAS) was tested by comparing its output with known voltage inputs to individual channels. All 32 channels were tested. It was found that the ADAS always gave the same output voltages as input.

The flowmeter was calibrated directly by measuring the volumetric flow rate at the exit of the channel using a graduated measuring cylinder and a stop watch. The measurement was repeated five to ten times for a given analog voltage output and the ensemble average was obtained. Two turbine flow meters with different inner diameters have been used. The calibration curves which show the inlet volumetric flow as a function of analog voltage output are shown in Figure 4.5. Water of different subcooling (55°C-95°C) was used and the flowmeters were each re-calibrated three times during the experiments. Identical calibration curves were obtained in each case.

The pressure transducers were calibrated against known pressures. Compressed air was used to pressurize the system with both ends closed. The system pressure was obtained using a pressure gauge. The zero offset and operational range of the analog output could be adjusted by adjusting the trim pots in the carrier demodulator unit (Transduction model no. TR377). The calibration curve is shown in Figure 4.4. It was found that the transducer zero offset can drift significantly in a period of a few hours. No significant change in the operational range was observed due to drift in zero offset. Care was taken to check and readjust the zero offset of the transducers before every experiment. The transducers were calibrated more than five times during the experiments and the same calibration curve (Figure 4.4) was obtained using the identical zero offset and operational range.

The gamma densitometers were calibrated using shaped Lucite pieces as described in Chapter 5. In order to deduce the void fraction during the transients, the empty (α=1) and full (α=0) readings have to be known. These calibration conditions were obtained before and checked after each experiment. The change in the calibration conditions was normally insignificant for a set of experiments done on the same day, for identical operational conditions: that is, the same high voltage supply, same amplifier gain and same SCA settings. However, they did change slightly from day to day due to electronic drifts and reductions in beam intensity because of radioactive decay.

6.2 Experimental Procedure

The experimental procedure can be summarized by the following step by step sequence:

1. Load the computer routine (RTP Data Acquisition Program) into the NOVA3 computer. The routine controls the automatic data acquisition processes through the computer. Individual channel gain (Section 4.3.1) can be changed if necessary. Set up the magnetic tape in the tape drive. Move the program pointer to the start of the routine. The computer is now all set for data acquisition.
2. Check the pressure transducers, adjust the zero offset if necessary.
3. Check the output of all thermocouples to make sure they are functioning properly.

4. Check that the electronics of the gamma densitometers are properly set.
5. Turn on the water supply. Adjust the flow rate to the desired value. For a constant flow system (Section 4.1.2), the inlet water subcooling can be adjusted by controlling the inflow of hot and cold water.
6. Obtain the full tube ($\alpha=0$) calibration condition for the gamma densitometers.
7. Close the inlet valve, QAV 1 and open QAV 2 (Figure 4.1) so that water by-passes the test section. Use compressed air to blow the test section dry.
8. Switch on the power supply. Raise the input power very slowly so that the test section can be heated up uniformly. Monitor the test section temperature constantly by checking the wall thermocouple output.
9. Obtain the empty tube ($\alpha=1$) calibration condition for the gamma densitometers.
10. Adjust the input power until a steady, desired surface temperature is achieved. Check to make sure that the temperature is reasonably uniform both axially and circumferentially. If not, let the test section be heated for a longer time so that conduction can smooth out the temperature gradients.
11. Initiate the refilling and rewetting transient by opening QAV1 and closing QAV2 at the same time, forcing water into the heated test section. The power input can either be switched off (power drops to zero exponentially) or cut off using a circuit breaker (power drops to zero instantaneously) at the start of the transient. The data acquisition system is also activated at the same instant. Data acquistion starts through

the computer system and is stored on magnetic tape.

12. Interrupt and stop data acquisition when the transient is over and the test section is totally quenched.

The test section was cleaned regularly by filling it with an acid solution (5% by weight of HCl) and letting it stand for 4 to 5 hours. This dissolved stains and deposits (mainly $CaCO_3$) on the inner tube surface. It was then rinsed with Na(OH) solution.

6.3 Matrix of Experiments

A total of 200 experimental runs were done for different initial and boundary conditions. The runs can be grouped into six groups. The main parameters varied were the test section initial wall temperature (300-600°C) and the inlet water mass flow (130-410 Kg/m^2-s). The operating conditions for each group are given below.

Group I - Building water supply was used (constant inlet flow system) and input power was switched off at the start of the transient. The test section was not insulated and the inlet water temperature used was about 8° C.

Group II - Same as in Group I, only warmer inlet water was used. $T_{in} \approx 45°C$. The effects of inlet water subcooling were investigated.

Group III - Same as in Group I, only that the input power was cut off instead of switched off at the start of the transient. That is the input power drops instantaneously to zero and there is no residual power input during the transient. This group of experiments was performed to investigage the effects of the residual power input.

Group IV - A constant-water-level head tank (constant inlet pressure system) and building tap water were used. Input power was cut off instantaneously at the start of the transient. The test section was not insulated. Two inlet water temperatures were used: ∿ 7°C and 22°C. This group of experiments was intended to study the effects of constant pressure boundary condition as compared to the constant flow case (Group I).

Group V - Same as in Group IV except that deaerated and deionized water was used this time. $T_{in} \approx 22°C$. The effects of dissolved air and ions in the inlet water were investigated in this group of experiments.

Group VI - Same as in Group IV except that the test section was insulated. $T_{in} \approx 22°C$. Effects of heat losses by natural convection and radiation from the outer tube surface were studied.

In order to obtain qualitative information and to observe the refilling and rewetting process visually, some simple experiments were performed. The experiments were done using a horizontally mounted quartz tube with a short, externally heated section (∿ 30 cm). Large numbers of pictures were taken during the transient. The pictures give valuable information on the shape of the refilling front and the propagation of the rewetting front. Details of the experiment and results are given in Section 7.3.

Experiments were also performed to study the refilling characteristic of a dry horizontal tube with no heat transfer. A pyrex tube was used. The velocities of the refilling front were obtained. These relatively simple experiments provided data for checking and developing models. Details of the experiment and results can be found in Section 9.6.

6.4 Data Reduction

Experimental data were obtained and written on magnetic tape using the NOVA 3 computer and were processed and plotted using the McMaster CDC6400 Computer. Since a NOVA 3 computer uses 16-bit words whereas a CDC-6400 uses 60-bit words, when the NOVA 3 produced data are read into the CDC-6400, three and three-quarter NOVA 16-bit words are read as one 60-bit CDC word. Therefore, the information has to be extracted from the 60-bit CDC words. This was done by the computer program STRIP. A listing of the program can be found in Appendix IV . For a given 60-bit word, STRIP reads the first 16 bits, puts them in the first 16 bits of a new 60-bit word and assigns zeros to all other bits in the new word. The given word is then shifted forward by 16 bits and another word will be obtained using the first 16 bits. This procedure will be repeated until all the data have been converted. The converted data were then stored in permanent files for further processing and subsequently written on magnetic tape again for future use.

To process the raw data and plot system transient behaviour, a computer program named RWRFPL was developed. A listing of the program is given in Appendix IV . RWRFPL reads data from a permanent file or magnetic tape. The data are processed channel by channel according to the channel gain used in acquiring the data (Section 4.3.1) and the nature of the signal. Appropriate calibration curves are used to transform the analog signals back into engineering units. The results are then plotted as a function of time. All 32 channels are processed and plotted.

Plotting is done using the VERSATEC 1200A printer-plotter which is directly connected to the CDC-6400. The VERSATEC 1200A is a standard feature of the McMaster Computing Center. It was obtained from CDC and its software was developed by the Academic Computing Services of McMaster University[89]. Once all the transient results are plotted the data can be analysed in detail and this will be discussed in Chapter 8.

7. CHARACTERISTICS OF HORIZONTAL CHANNEL REWETTING AND REFILLING

7.1 Rewetting of a Dry Hot Surface

The actual process of rewetting is very complicated. It is still not well understood from a microscopic point of view. Macroscopically, rewetting is the re-establishment of continuous water contact with a dry hot surface. It has been found experimentally that rewetting always occurs when the temperature of the hot surface is below a certain value; generally known as the rewetting, sputtering or Leidenfrost temperature. The phenomenon is known as the Leidenfrost pheonomenon. However, for a hot surface with low heat capacity, rewetting can also be initiated by the instability of the vapor film separating the hot surface and the liquid. This will be discussed in section 10.4.

In general, when a droplet impinges onto a hot surface as shown in Figure 7.1, the droplet can stay and wet the surface only if the surface temperature T_W is less than the sputtering temperature, T_O. If T_W is greater than T_o, the droplet will bounce off and the surface remains unwetted.

The mechanisms involved can be summarized macroscopically: when the liquid interface is close enough to the hot surface, evaporation occurs due to radiation heat transfer. Conduction and convection heat transfers are negligible because a continuous vapor film has yet to be established. The rate of evaporation increases as the liquid interface comes closer to the hot surface. The dominant mode of heat transfer changes from radiation to conduction through the thin vapor layer formed between the liquid and the hot surface. This vapor layer thickness decreases as the liquid interface approaches the hot surface and results in higher heat transfer. If the surface temperature is above the Leidenfrost temperature, the evaporation rate will eventually become so great that the vapor thrust force exceeds the

FIG. 7.1 REWETTING OF A HOT SURFACE

(I) DROPLET IMPINGING

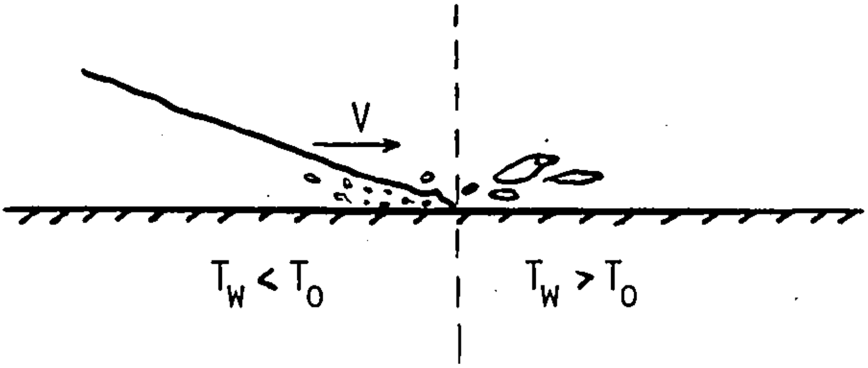

(II) MOVING REWETTING FRONT

liquid inertia forces and the interface will be forced back.

The Leidenfrost Phenomenon (Godleski and Bell [90]) in film boiling of liquid masses on a hot surface is another example. The vapor thrust force exceeds the liquid pressure and prevents the liquid from collapsing onto the surface.

The same happens for a moving quench front (Figure 7.1), the front advances only when the temperature of the surface ahead of it can be cooled to the sputtering temperature. Any excess liquid which is proportional to the difference of flow rate and the rate at which the quench front can propagate, will be sputtered off the surface and appear as entrained liquid in the vapor stream or form a "liquid tongue" if the surface is horizontal. Heat is removed from the dry side by heat transfer to the entrained liquid or liquid tongue and by conduction to the wet side. The velocity of the quench front is determined by the rate at which the surface ahead of it can be cooled.

7.2 Leidenfrost Temperature

Since liquid cannot wet the wall when the surface temperature is above the Leidenfrost temperature, except under special conditions (section 10.4), this parameter is of considerable interest in reactor safety analysis. The main reason is because of the very poor heat transfer associated with film boiling compared to nucleate boiling heat transfer if the surface is wetted. Considerable experimental and theoretical work has been done to determine the Leidenfrost temperature. Some of the results will be discussed below.

The definition of Leidenfrost temperature is not unique. For small droplets in the spheroidal state, the Leidenfrost temperature is commonly defined as the surface temperature corresponding to the maximum evaporation time (Bell [91]). The evaporation time is the time required to totally evaporate the droplet. For extended liquid masses, the Leidenfrost temperature is defined as the minimum surface temperature at which the vapor film which separates the liquid and the hot surface breaks down at least occasionally and the liquid touches the surface (Godleski and Bell [90]). The Leidenfrost temperature can also be determined by a transient plate temperature technique as described by Godleski and Bell [90]. A mass of liquid is placed on a plate with temperature higher than the Leidenfrost temperature. The plate is then cooled while the liquid evaporates. The plate temperature at which the liquid collapses onto the surface is considered as the transient Leidenfrost temperature

Because of the different definitions, it is obvious that the Leidenfrost temperature will depend upon the technique used in its determination. A comparison of the Leidenfrost temperatures of water at atmospheric pressure as determined by a number of investigators is given in Table 7.1. It can be seen that evaporation of droplets gives the highest Leidenfrost temperature whereas the transient plate technique gives the lowest. It was suggested by Godleski and Bell [90] that the experiments with transient plate temperatures represent a state of metastable film boiling where small surface disturbances results in regression to transition boiling. With carefully designed experiments, plate temperatures lower than those reported are attainable. Wachters et al [99] found that under ideal conditions the Leidenfrost temperature can be reduced below the saturation temperature of the liquid. In the case of refilling and rewetting of hot horizontal systems, the Leidenfrost temperature as determined by the transient plate technique appears to be the most appropriate definition to use from a physical viewpoint.

Table 7.1

Leidenfrost Temperatures of Water

(A) Drops (Spheriodal State)	
Godleski and Bell [90]	320°C
Gottfried et al [92]	280°C
Tamura and Tanasawa [93]	302°C
Kenrick et al [94]	270°C
*Groeneveld [95]	273°C
(B) Extended Masses	
Godleski and Bell [90]	264°C
Patel and Bell [96]	300°C
Hosler and Westwater [97]	258°C
*Berenson [98]	177°C
(C) Transient Technique	
Godleski and Bell [90]	161°C

*Theoretical work

In general, the Leidenfrost temperature is not constant even when the same technique is used for its determination. It has been found to depend on the fluid properties, the heated surface properties and roughness, the surrounding atmosphere (pressure, steam or air environment), mass and subcooling of the liquid (Bell [91], Bradfield [100], Baumeister and Simon [101]). For impinging droplets, it also depends on the impact velocity, impact angle and droplet sizes (Kendall [102], Wachters and Westerling [103], Cumo and Pitimada [104]).

7.3 Refilling and Rewetting of Horizontal Channels

The most important characteristic of refilling and rewetting of a hot horizontal system as opposed to vertical channels, is the stratified nature of the refilling water. Because of the transverse gravitational effects, the flow is stratified, thus the channel will be quenched in the sequence of bottom, mid-side and top at a given location. The characteristics were studied photographically and a simple physical model for the process is proposed. These will be discussed below.

7.3.1 Photogrpahic Studies

The refilling and rewetting process is extremely complicated. Valuable qualitative information on the phenomena can be obtained by photographic studies. A simple setup was used to simulate the actual refilling and rewetting experiments. A 4-foot (122 cm) length quartz tube (2.0 cm O.D. and 1.8 cm I.D.) was mounted horizontally. A short length of about 12 inches (30.5 cm) was heated up externally using Bunsen burners. Subcooled water was injected from one end. Photographs were taken at a rate of about 4 pictures per second as the water refilled and rewetted the heated section of the tube. Some typical results are shown in Plates 7.1 - 7.14. The wall temperature was about 550 - 650°C. It was obtained by pressing a sheathed microthermocouple against the external tube wall. It should be pointed out that the section was not very uniformly heated, and therefore, no quantitative information can be deduced from the photographs. The inlet flow velocity used in the sequence of pictures shown was about 20 cm/s.

Plate 7.1 shows the length of the section photographed. The camera was focussed at the middle of the heated section. Plates 7.2 to 7.14 show the refilling and rewetting sequence. The flow was from right to left, except for Plate 7.14, the time difference between individual pictures is about 0.25 seconds.

In Plate 7.2, the bulk of the refilling water is somewhere upstream. However, liquid droplets of different sizes can be seen. The droplets are from the sputtering quench region and are carried downstream by the vapor stream. It should be noted that the droplets are concentrated on the lower portion of the channel. Thus the bottom will be slightly precooled by the impinging droplets.

In Plate 7.3, a "liquid tongue" appears. Since the wall temperature is above the Leidenfrost temperautes, the liquid mass cannot wet the wall. Stable film boiling exists and the "liquid tongue" flows downstream on a vapor cushion (Plate 7.4).

The advance of the leading edge of the quench front is shown in Plates 7.5 to 7.13. The violent boiling, sputtering quench region can be seen moving downstream. This region corresponds to the quench of the lower portion of the channel. The side of the channel is quenched at a later time. Since the surface of contact is small, the quench of the side is not as violent.

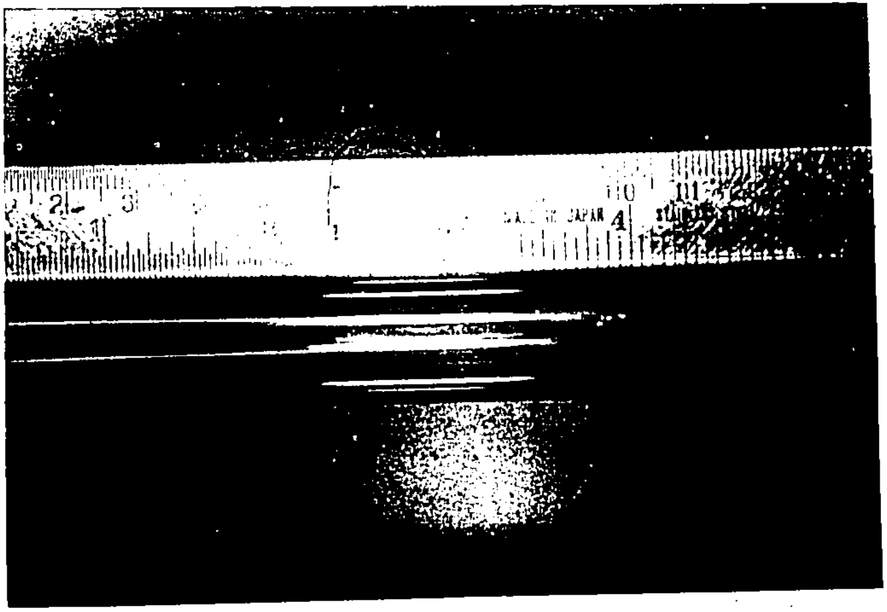

PLATE 7.1 REFILLING AND REWETTING OF A HOT SECTION OF A DUCT -- LENGTH OF SECTION PHOTOGRAPHED

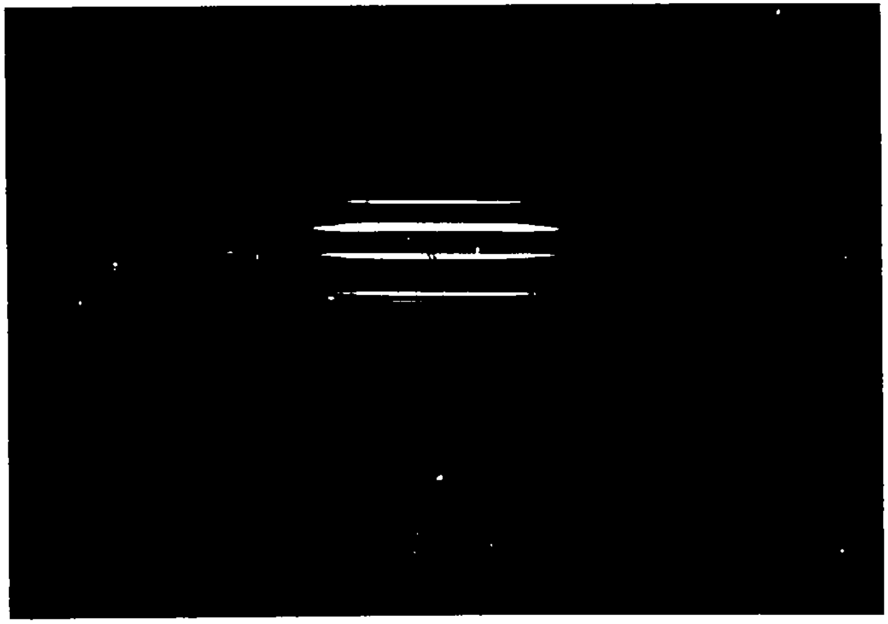

PLATE 7.2 REFILLING AND REWETTING SEQUENCE -- PICTURE NUMBER 1

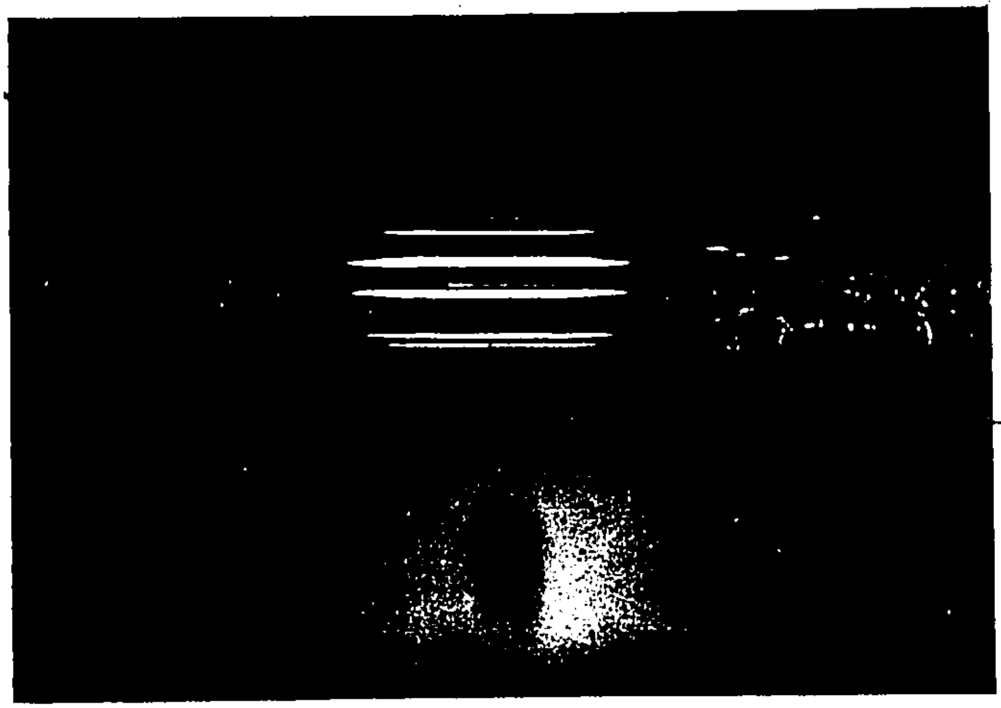

PLATE 7.3 REFILLING AND REWETTING SEQUENCE -- PICTURE NUMBER 2

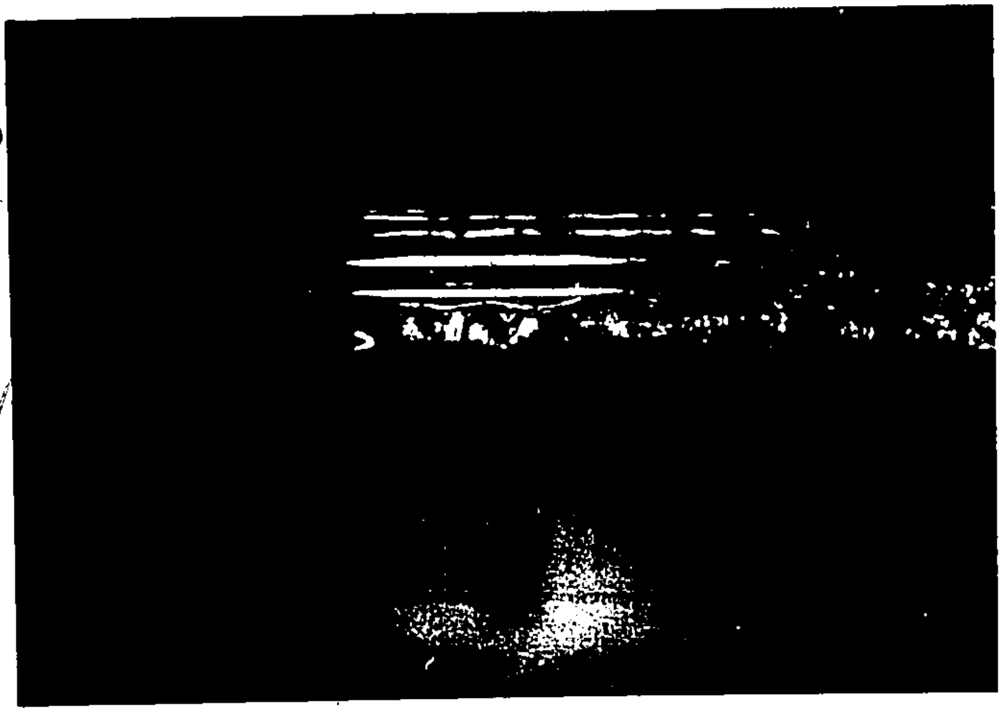

PLATE 7.4 REFILLING AND REWETTING SEQUENCE -- PICTURE NUMBER 3

Plate 7.5 REFILLING AND REWETTING SEQUENCE -- PICTURE NUMBER 4

Plate 7.6 REFILLING AND REWETTING SEQUENCE -- PICTURE NUMBER 5

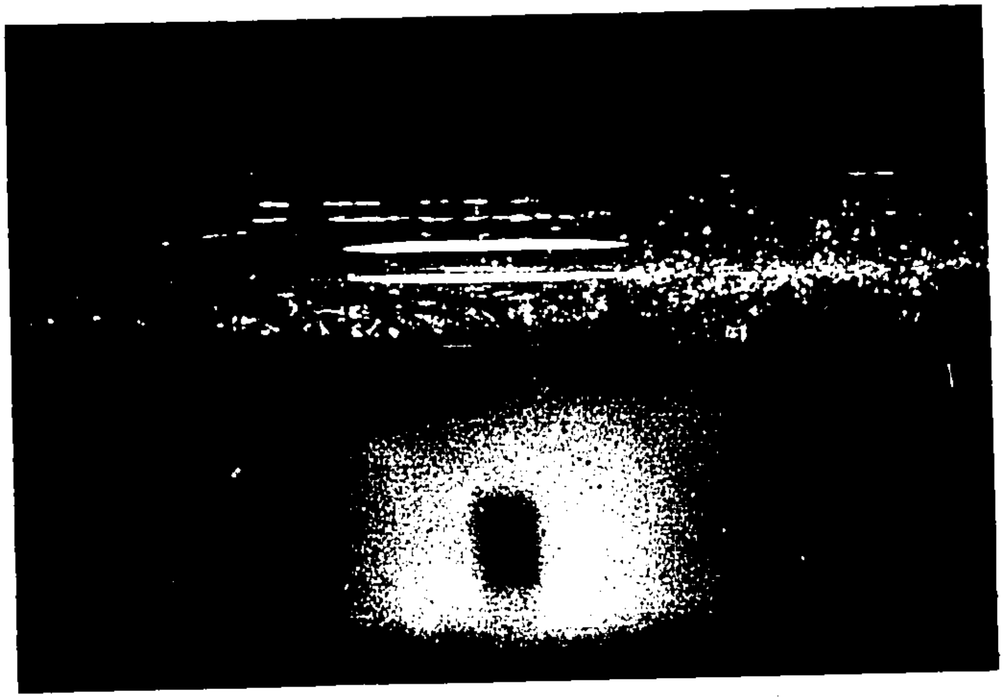

Plate 7.7 REFILLING AND REWETTING SEQUENCE -- PICTURE NUMBER 6

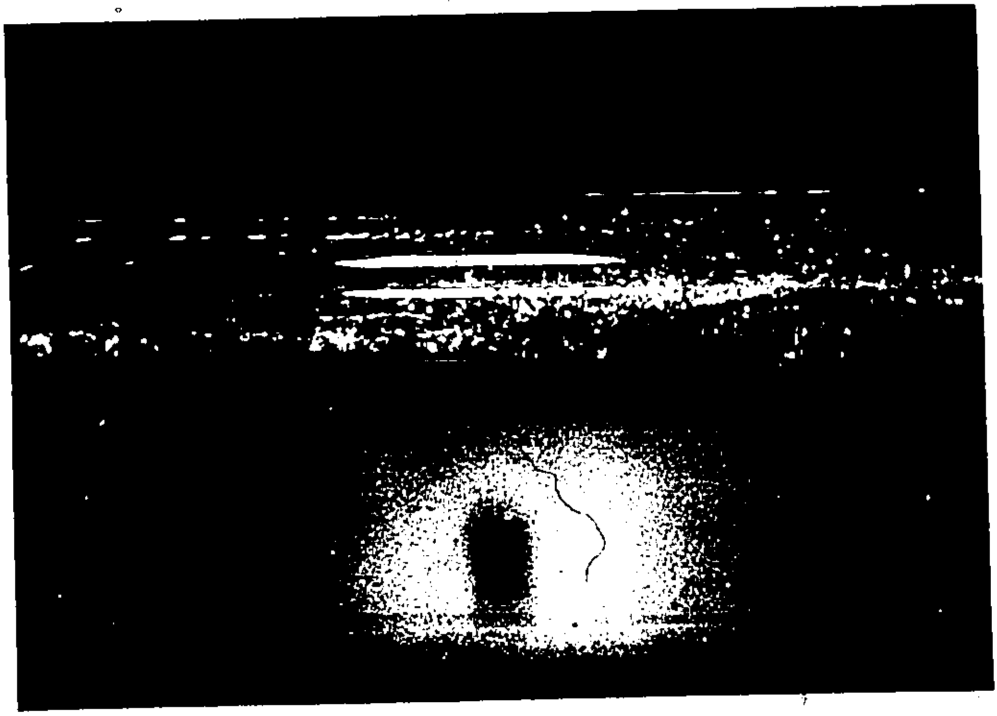

Plate 7.8 REFILLING AND REWETTING SEQUENCE -- PICTURE NUMBER 7

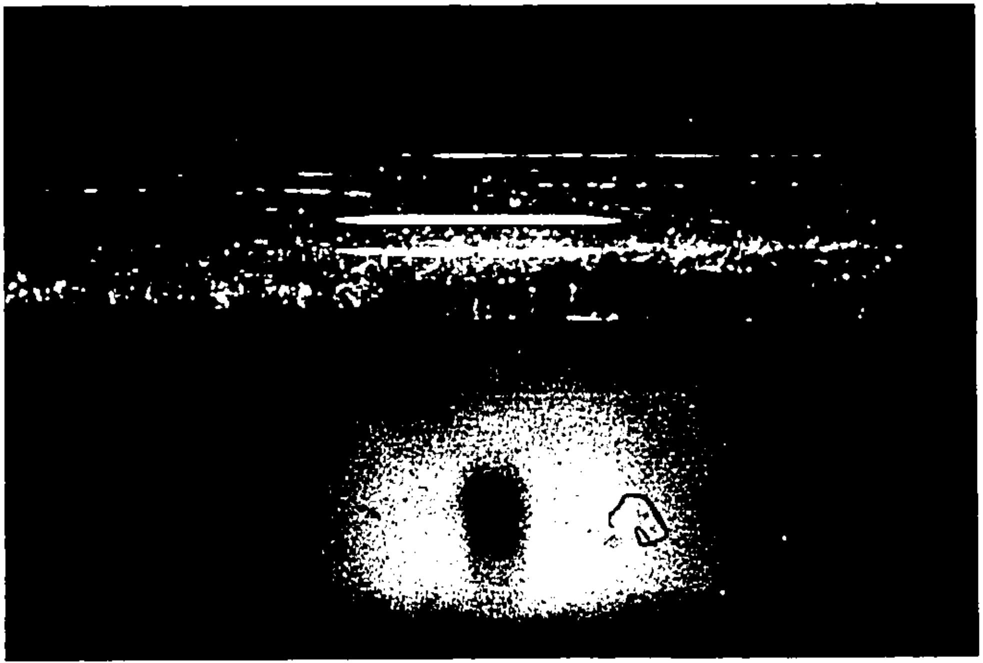

PLATE 7.9 REFILLING AND REWETTING SEQUENCE -- PICTURE NUMBER 8

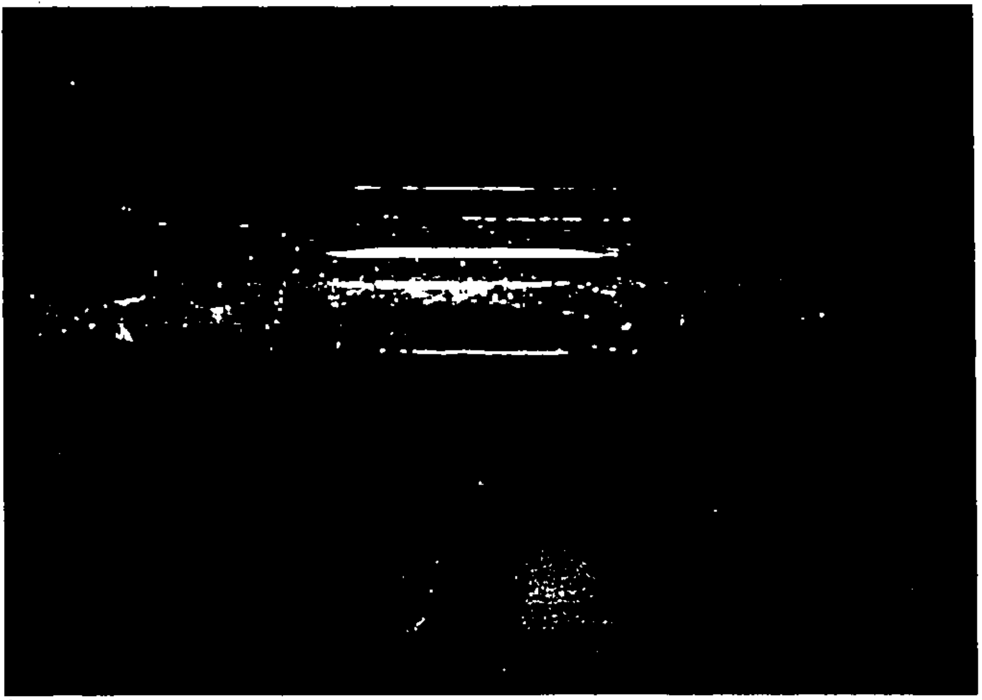

PLATE 7.10 REFILLING AND REWETTING SEQUENCE -- PICTURE NUMBER 9

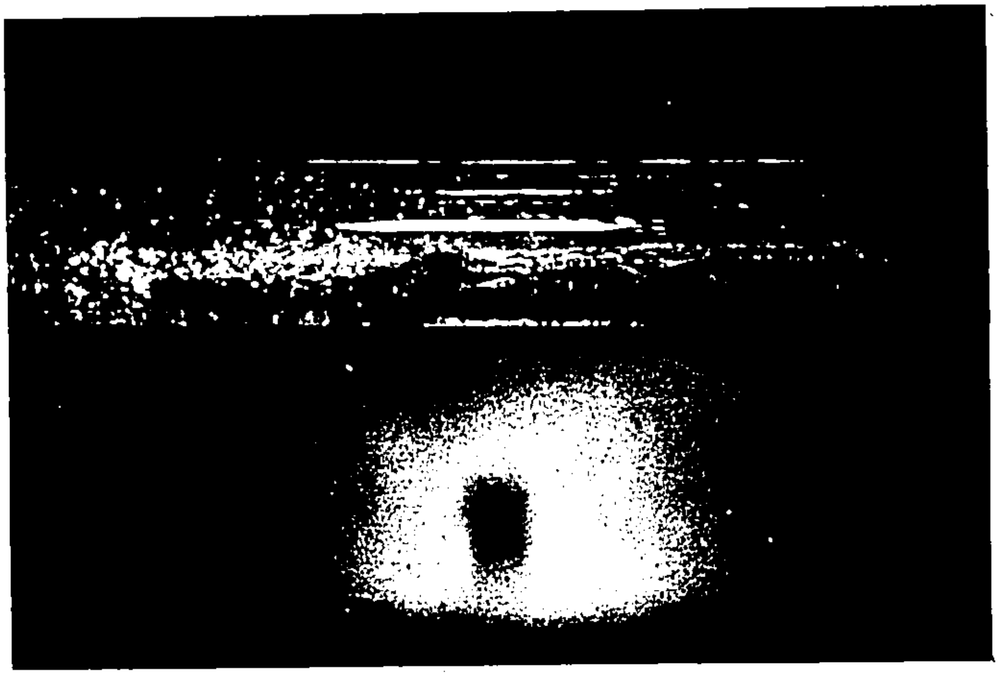

PLATE 7.11 REFILLING AND REWETTING SEQUENCE
-- PICTURE NUMBER 10

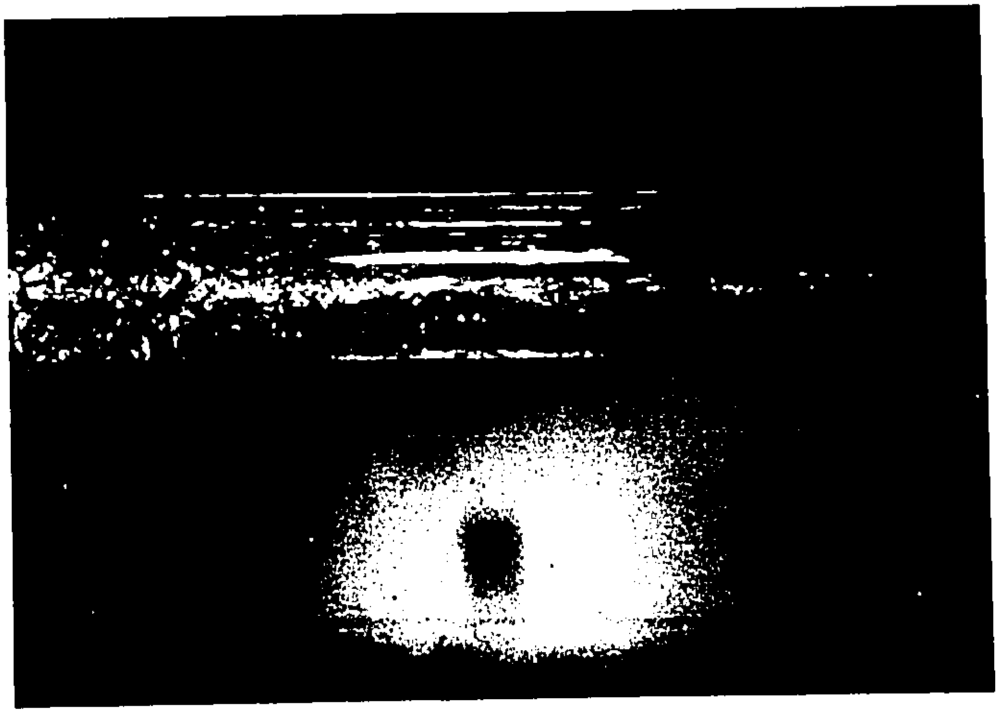

PLATE 7.12 REFILLING AND REWETTING SEQUENCE
-- PICTURE NUMBER 11

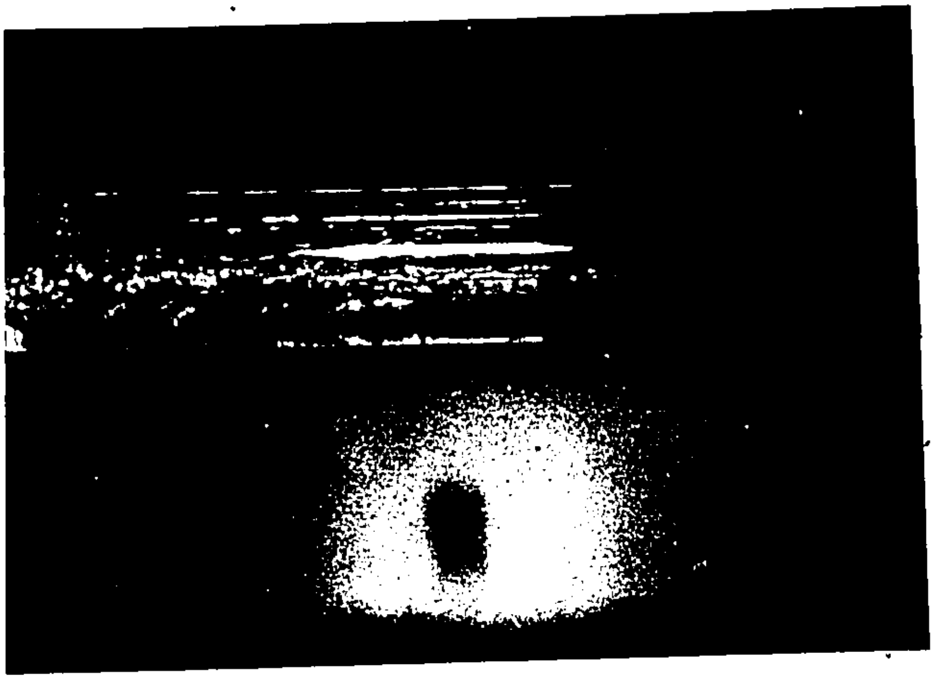

Plate 7.13 REFILLING AND REWETTING SEQUENCE -- PICTURE NUMBER 12

Plate 7.14 REFILLING AND REWETTING SEQUENCE -- PICTURE NUMBER 13

Plate 7.14 was taken at a considerably later time when the channel is beginning to fill up and the top is being quenched.

7.3.2 A Physical Model

From the photographic studies and experimental evidence (which will be discussed in Chapter 8), the refilling and rewetting process in a horizontal channel can be visualized as sketched in Fig. 7.2. This is, of course, a highly simplified picture of a very complicated process. However, it does contain all the important phenomena.

The quench front (Q_T-Q_B) is inclined. The angle of inclination depends on the quench velocity, the effective friction factor and the radius of the channel. It is not a constant. It changes as the flow develops and the channel fills up. For low inlet mass flows, the leading edge (Q_B) can be more than 0.5 meter ahead of Q_T, the trailing dege.

Behind the trailing edge (Q_T), the channel is totally quenched (A-A'). The flow is single-phase liquid with bubbles near the top (Plate 7.14). The normal single-phase pipe flow equations apply in this region and the heat transfer mechanism will be single phase forced convection heat transfer.

In the quenching region (Q_T-Q_B), the channel is partially quenched as can be seen (B-B'). Since the bottom is quenched before the top for a given location, a large circumferential temperature gradient exists. Thus circumferential heat conduction may be important and has to be examined. Violent boiling exists as the quench front advances and the hot surface in front of it is being quenched.

Downstream of the quench front, the excess water appears as a "liquid tongue" (Plate 7.2). This liquid mass is prevented from wetting the wall by a thin film of vapor resulting in stable film boiling. As

FIG. 7.2 CHARACTERISTIC OF HORIZONTAL CHANNEL REWETTING

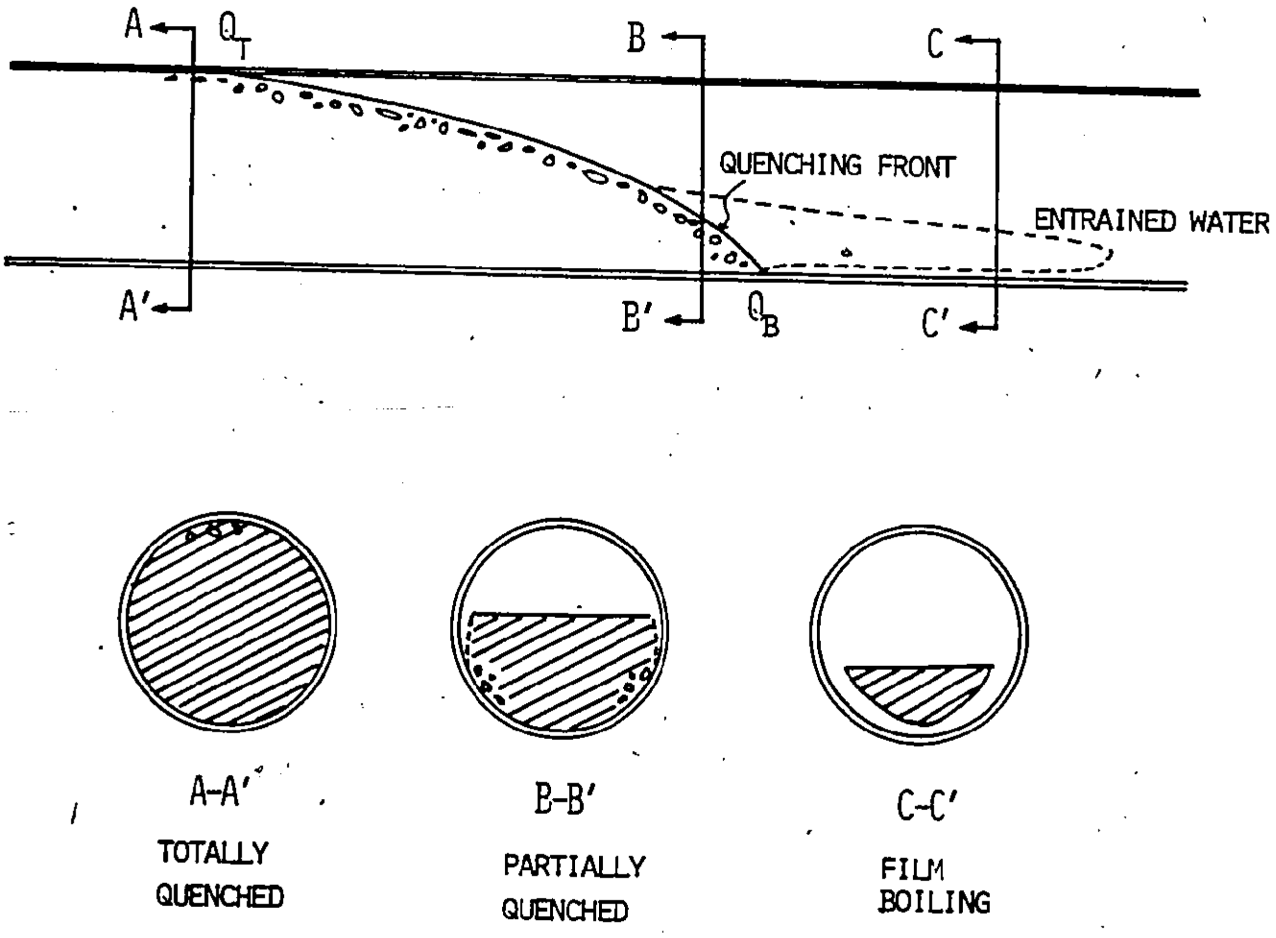

the local level of the "liquid tongue" rises, the vapor film can become unstable and water can momentarily touch the surface, creating rewet spots. The mode of heat transfer thus changes from stable film boiling to transition boiling. Quenching occurs when the rewet spots grow and expand to cover the surface. This is possible if the surface temperature is below the Leidenfrost temperature or the wall heat capacity is low. Details of the quenching mechanism will be discussed in section 10.4.

Because of the existence of film boiling in this region, the bottom region of the channel will be precooled significantly before the arrival of the quench front. On the other hand, the top of the channel will be affected to a much smaller extent. This precooling characteristic is shown clearly in Figure 7.3.

Figure 7.3 shows the quenching of the top (T) and bottom (B) of the channel for a typical run. The location of the thermocouples are as shown. It can be seen that the temperatures at the bottom drop significantly before being quenched, especially at the exit end. The temperatures at the top, however, do not show a significant precooling effect.

In the figure, it can also be seen that the bottom always rewets before the top and the temperature difference between the top and bottom can be as much as 400°C for an initial dry wall temperature of 500°C. This corresponds to the inclinded quench region (Q_T-Q_B) in the previous figure. Because of the large circumferential temperature difference, rewetting at the top may occur due to circumferential heat conduction resulting from the quench of the bottom and sides. However, no significant precooling of the top is observed. The circumferential heat conduction is relatively slow except in the immediate vicinity of the quench front. Therefore no significant precooling of the top due to circumferential conduction is observed when

FIG. 7.3 QUENCHING CHARACTERISTICS -- TOP AND BOTTOM OF CHANNEL

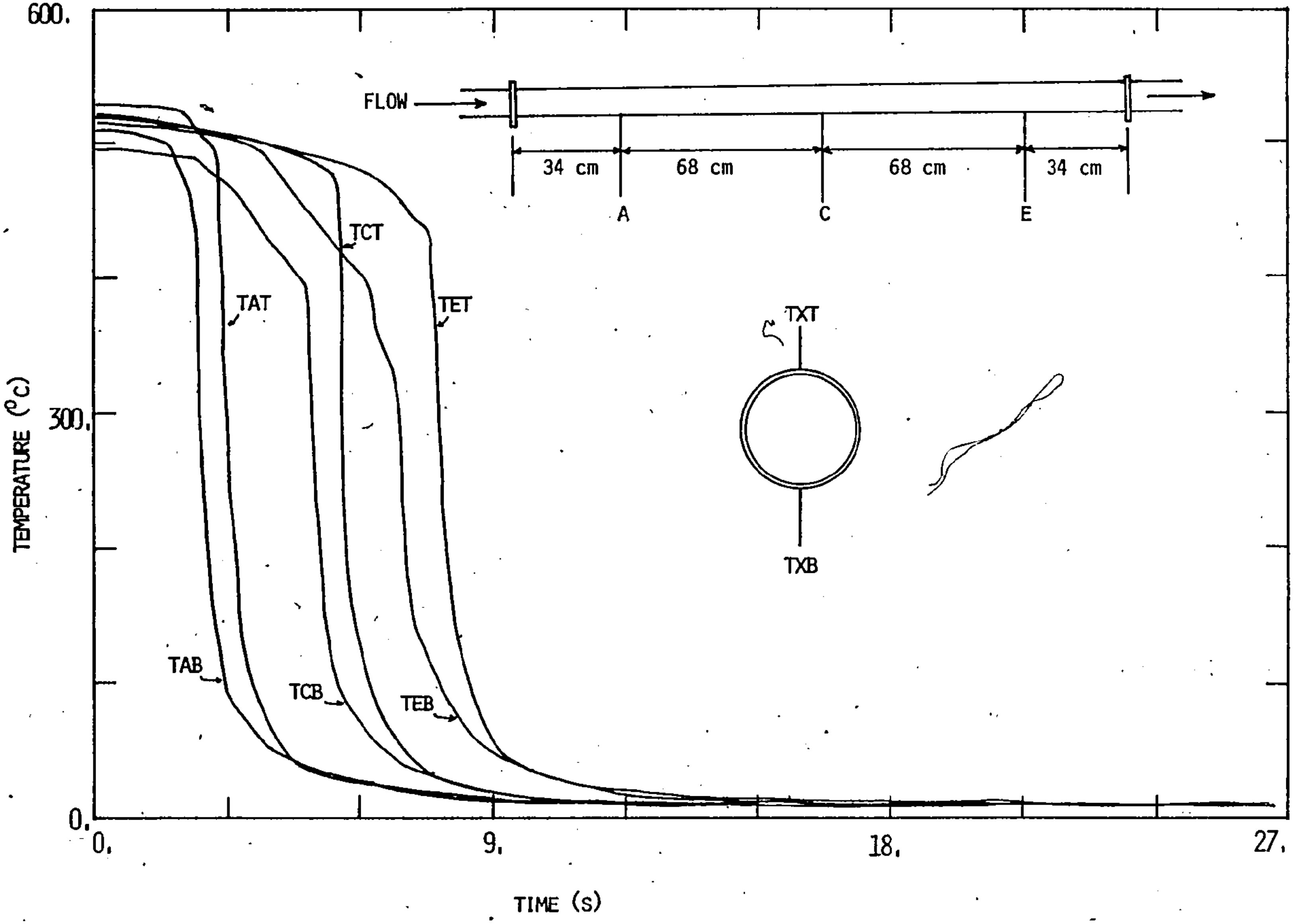

the difference in quench time for bottom and top is short. For example, it is less than one second in the figure shown.

The effect of circumferential heat conduction may be studied by solving the transient problem in a thin walled tube. An analytical solution has been obtained. Details of the analysis can be found in Appendix II . The wall temperature is assumed to vary circumferentially but not radially, thus simplifying the analysis considerably. This is usually a reasonable assumption for thin walled tubes. The lower portion of the tube, defined by the azimuthal angle θ_0 is assumed to be quenched and the wall is assumed to be at the saturation temperature of the fluid.

Results for θ_0 equal to $3\pi/4$ is plotted in Figure 7.4. It can be seen that a relatively long time is required to cool the top significantly by circumferential conduction. For example it takes more than 6 seconds to lower the temperature at the top by 20°C. Compared to the quench time of less than one second between bottom and top shown in Figure 7.3, it is obvious that circumferential conduction is of secondary importance as far as pre-cooling of the top is concerned in the refilling and rewetting process. Near the quench front, however, the conduction effect can be important as apparent from the rapid change in the temperature gradient in this region.

FIG. 7.4 TRANSIENT CIRCUMFERENTIAL HEAT CONDUCTION

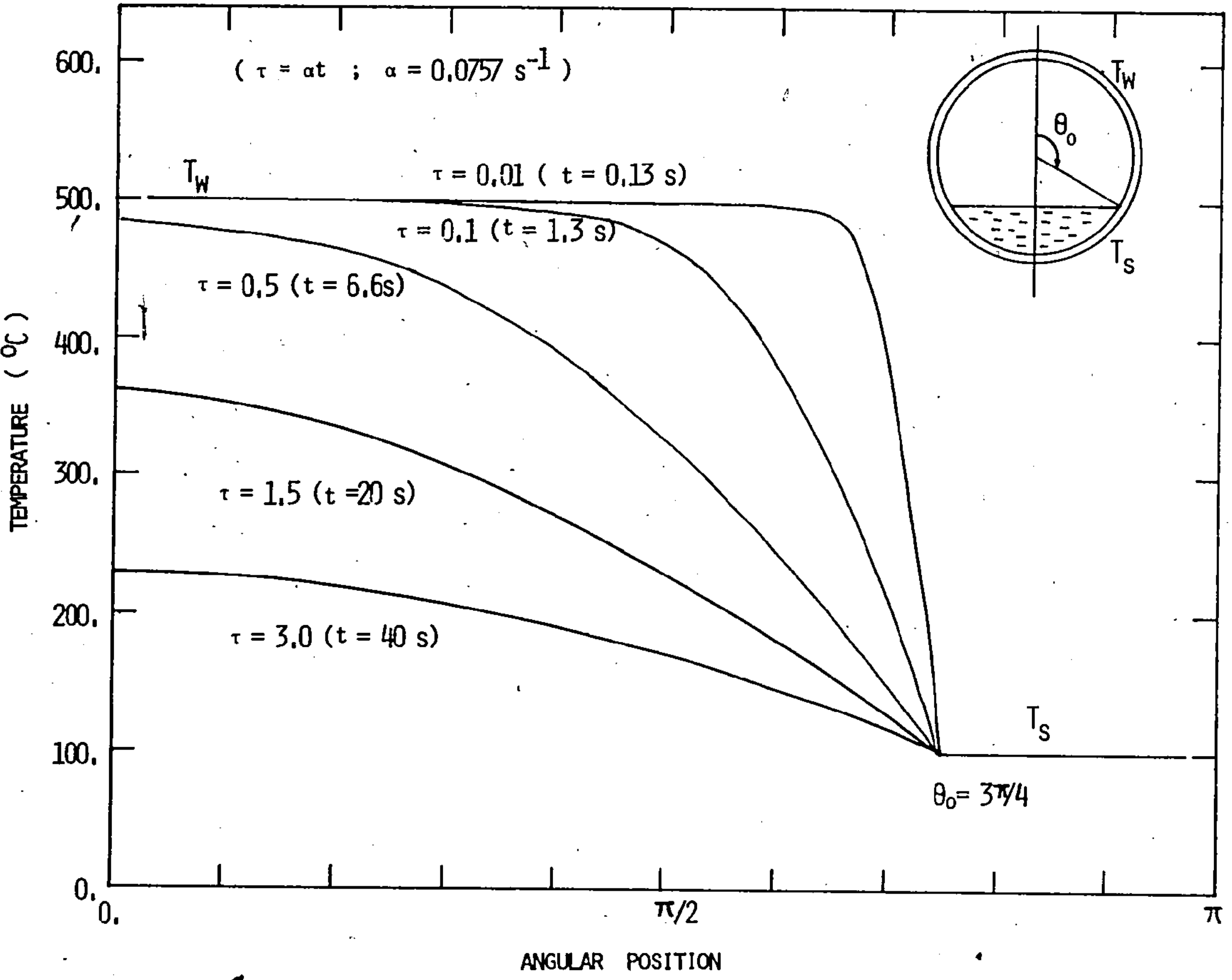

8. DATA ANALYSES, RESULTS, AND DISCUSSION

8.1 Experimental Results

A total of 200 runs have been done in six groups. The matrix of the experiments performed is given in Section 6.3. Some typical results will will be described below. Details of the experimental runs and raw data storage can be found in Appendix III.

A set of Group I data is shown in Figure 8.1 through 8.8. Results were obtained by scanning the low-level Analog Input System at a frequency of 62.5 Hz per channel. This corresponds to a time difference of 16 milliseconds between individual data points for a given channel. The results are typical in the sense that the type of general system behaviour is observed for all the experiments. Therefore, some general observations and conclusions can be drawn by studying the set of data shown.

Figure 8.1 shows the inlet flow rate. It is fairly constant and the boundary condition is close to a constant flow one. The low frequency fluctuations are water supply line fluctuations and the amplitude is relatively small. In comparison when a constant inlet pressure is impressed by using a constant water-level-head-tank, a typical transient inlet flow curve is as shown in Figure 8.9. It can be seen that the flow is very steady except for some high frequency, large amplitude, fluctuations which correspond to system pressure fluctuations. The same system pressure fluctuations are present in the first case (Figure 8.1), however, because of the large pressure drop across the regulating valve when the building water supply is used, the inlet flow fluctuations due to system pressure changes is negligible. In Figure 8.9, the inlet flow fluctuations can also be neglected to a first approximation because they appear in high frequency packets of short duration. In other words a constant flow boundary condition is approximated in both situations.

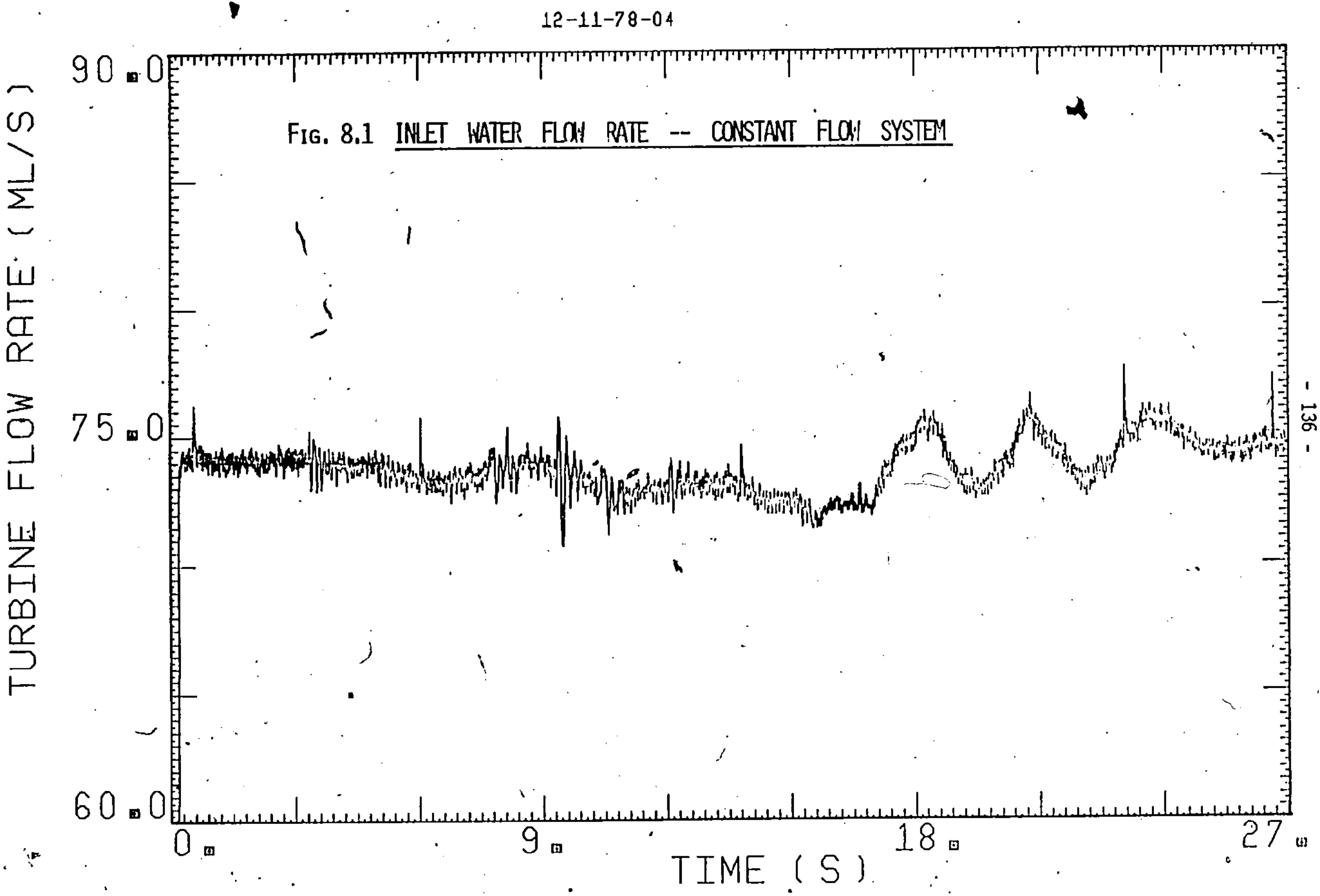

FIG. 8.1 INLET WATER FLOW RATE -- CONSTANT FLOW SYSTEM

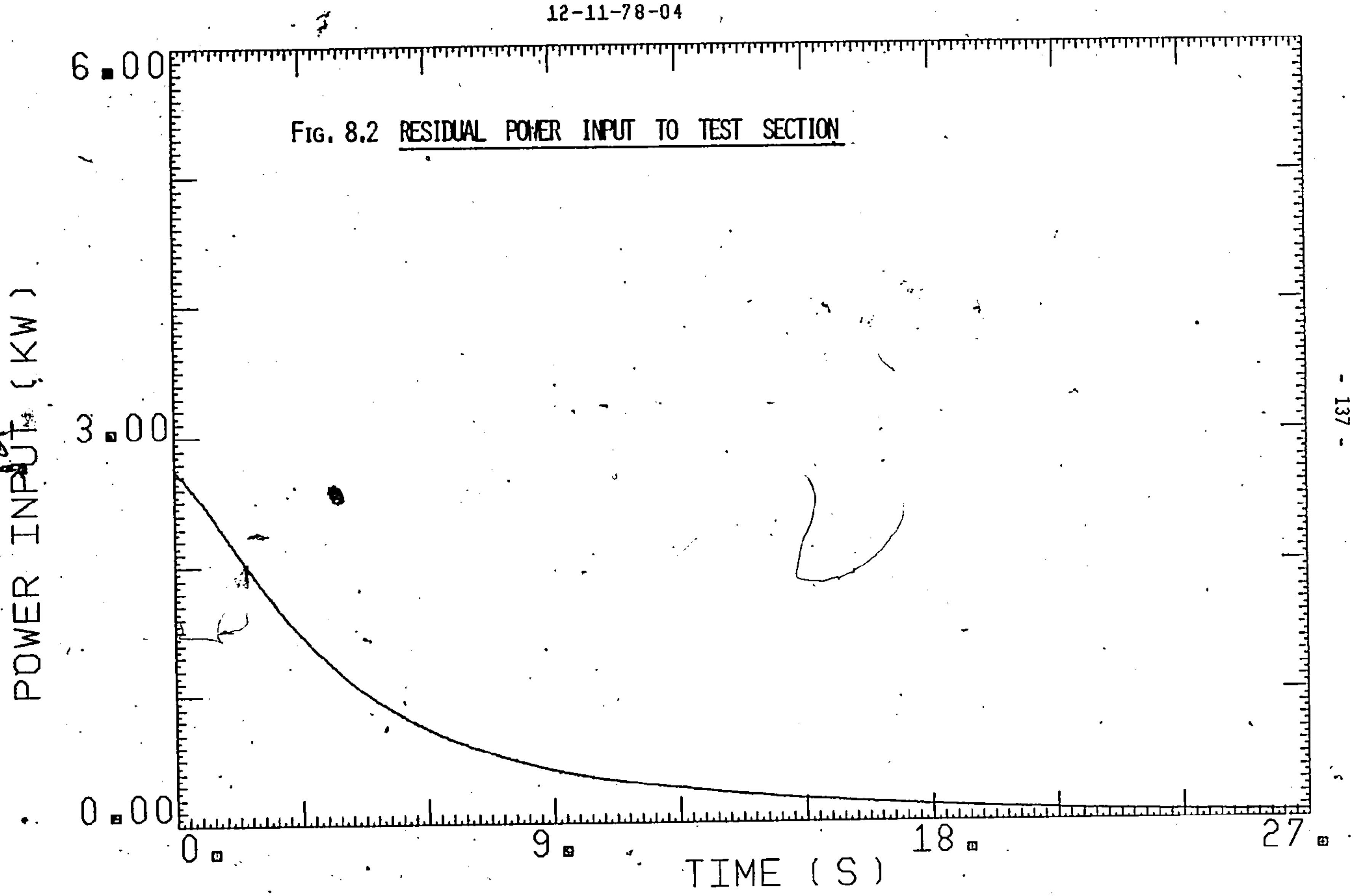

Fig. 8.2 RESIDUAL POWER INPUT TO TEST SECTION

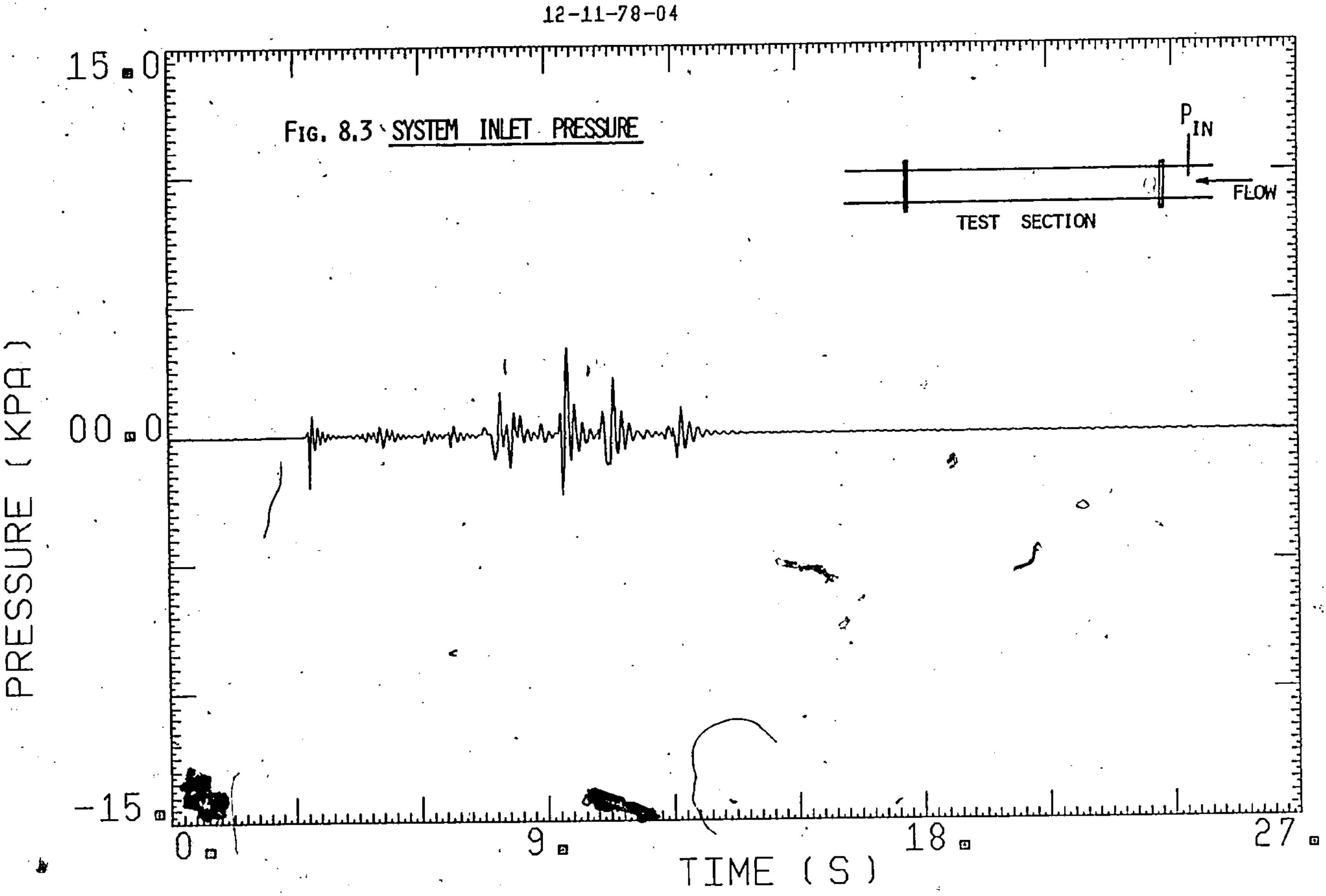

Fig. 8.3 SYSTEM INLET PRESSURE

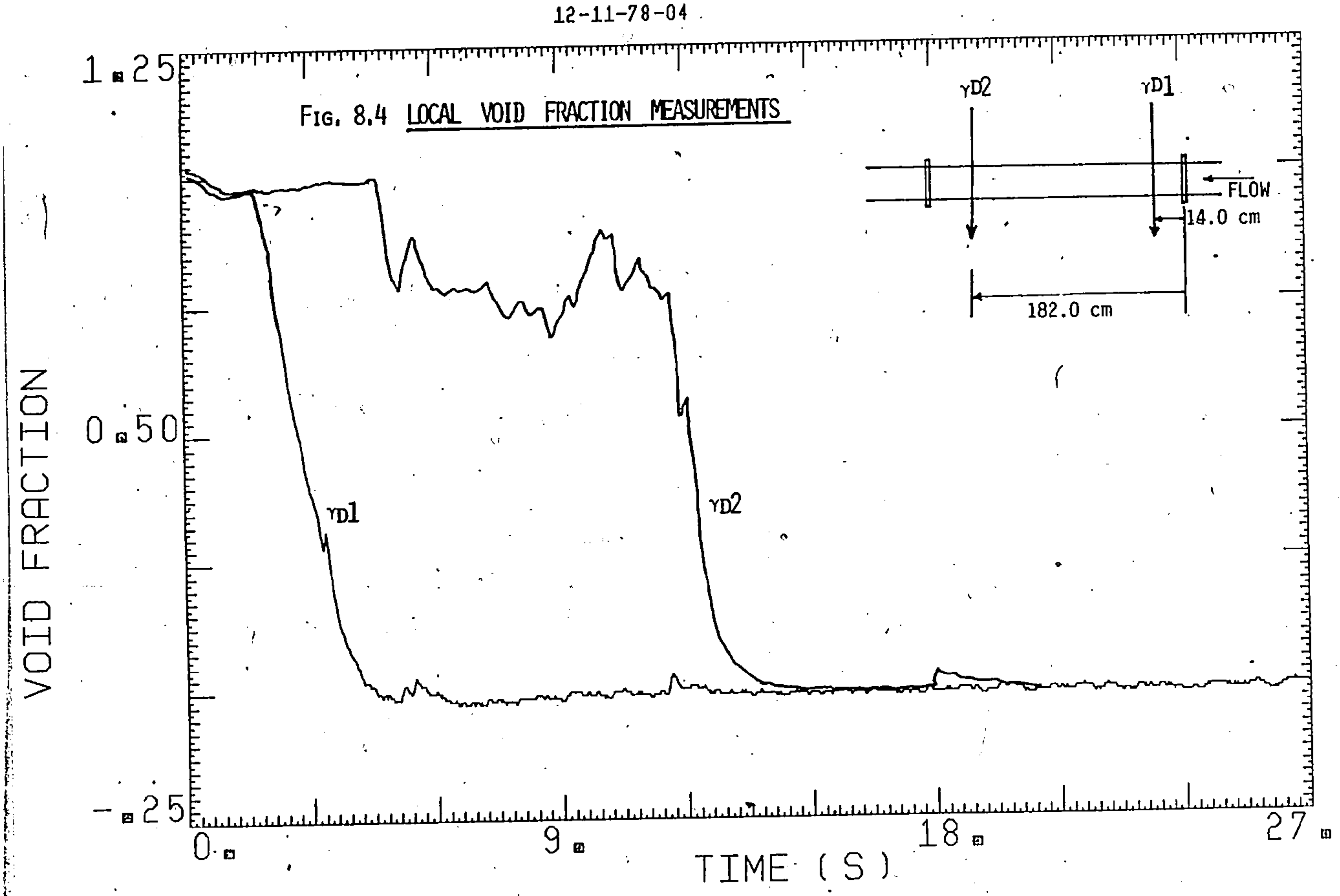

FIG. 8.4 LOCAL VOID FRACTION MEASUREMENTS

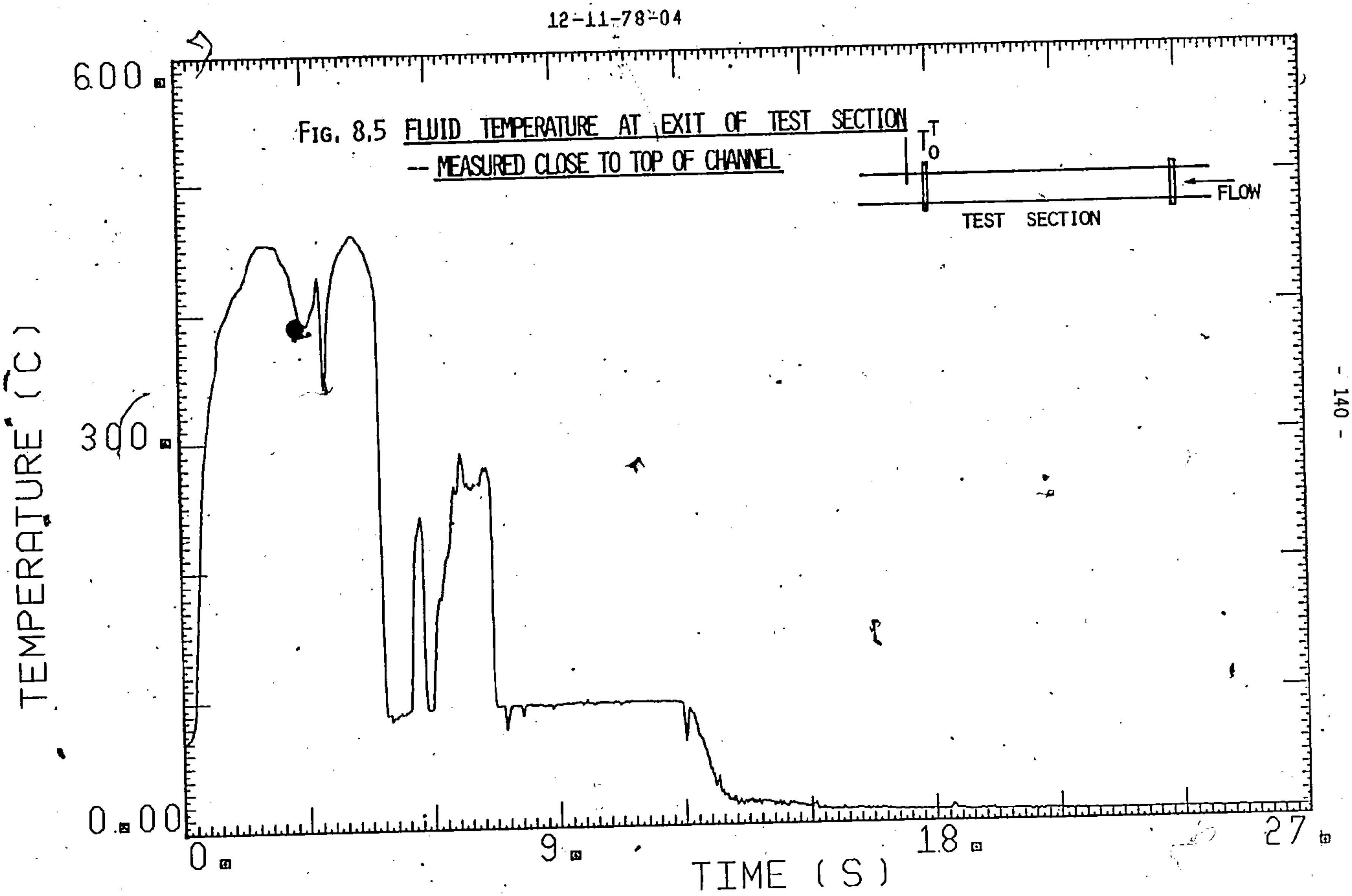

FIG. 8.5 FLUID TEMPERATURE AT EXIT OF TEST SECTION -- MEASURED CLOSE TO TOP OF CHANNEL

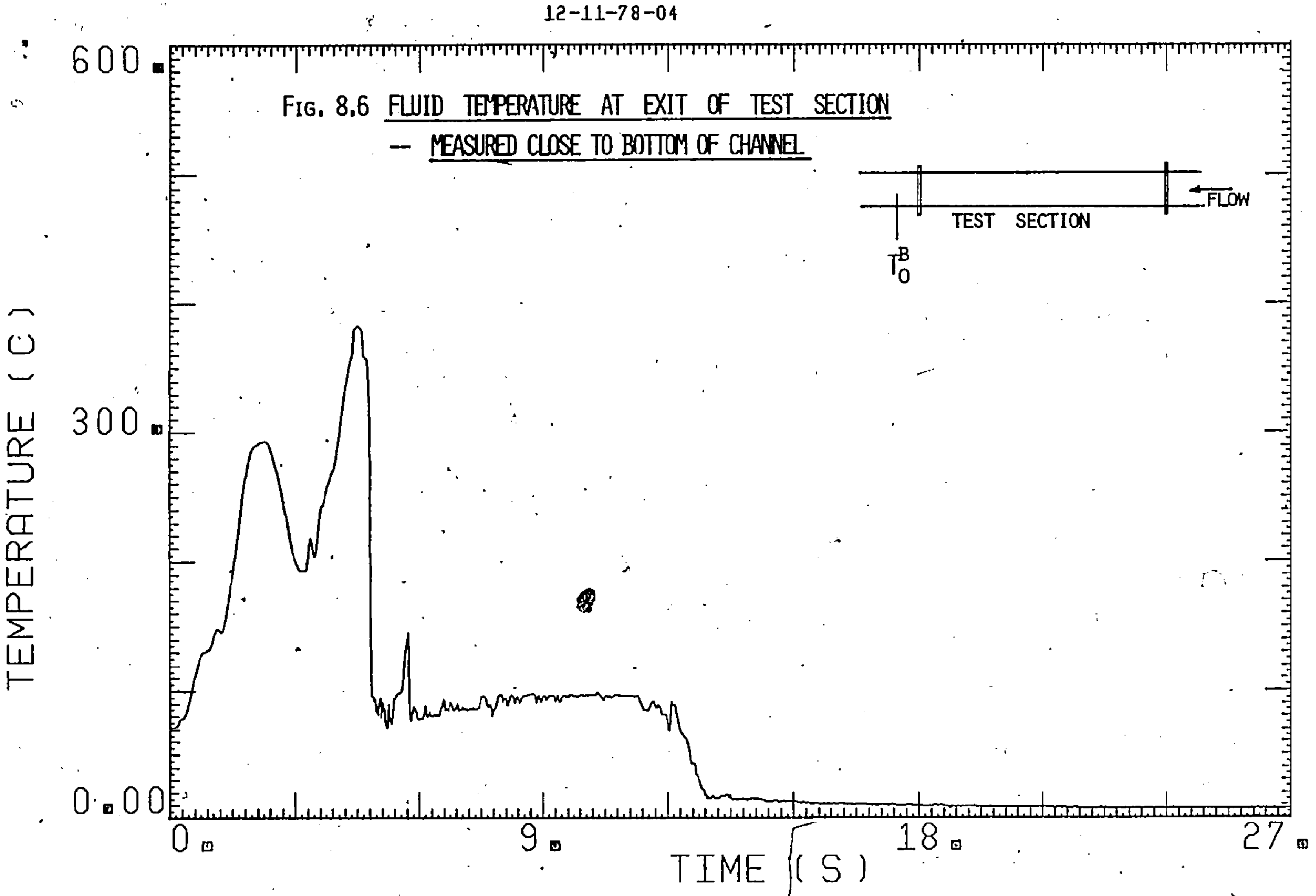

FIG. 8.6 FLUID TEMPERATURE AT EXIT OF TEST SECTION — MEASURED CLOSE TO BOTTOM OF CHANNEL

12-11-78-04

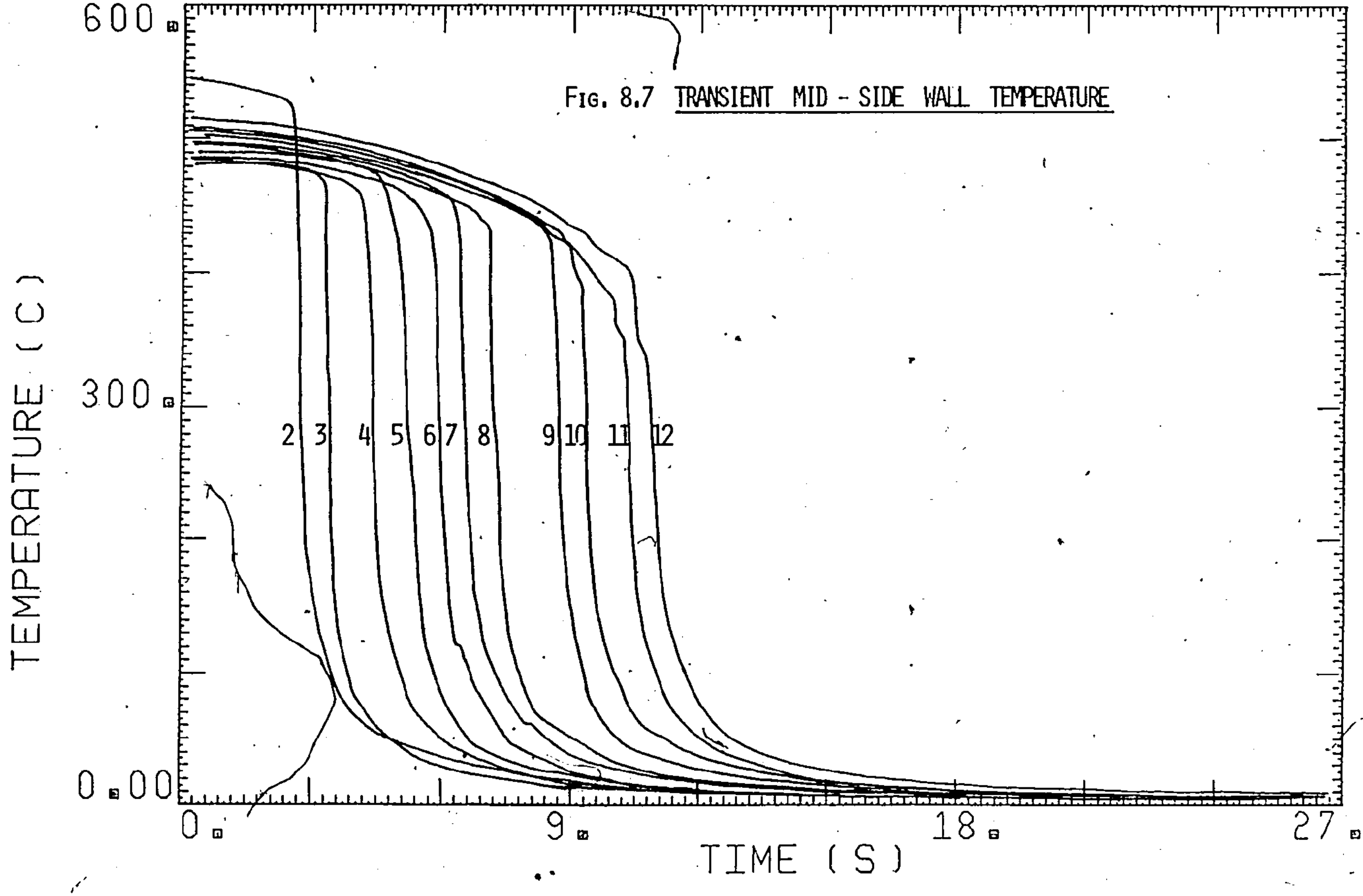

FIG. 8.7 TRANSIENT MID - SIDE WALL TEMPERATURE

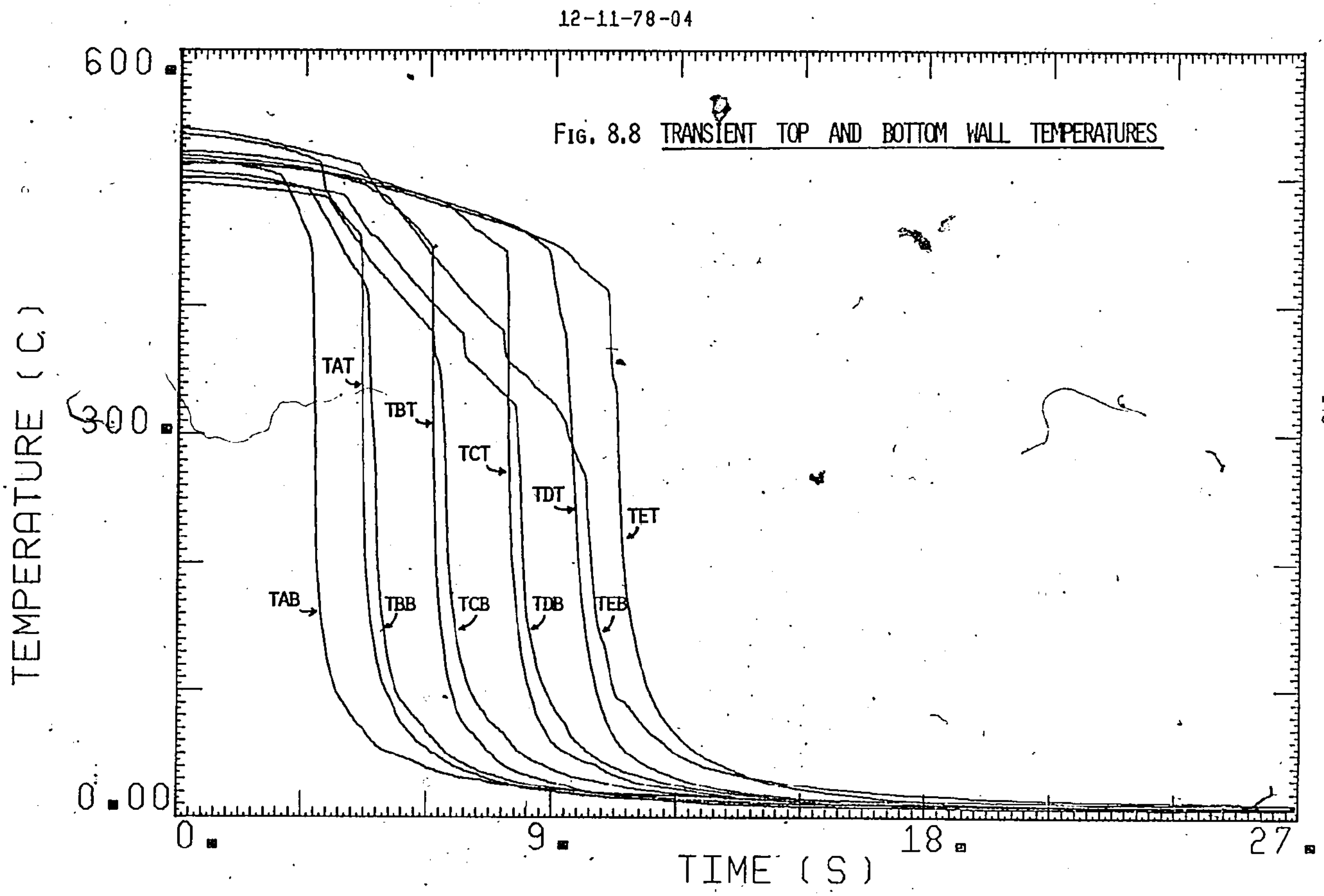

FIG. 8.8 TRANSIENT TOP AND BOTTOM WALL TEMPERATURES

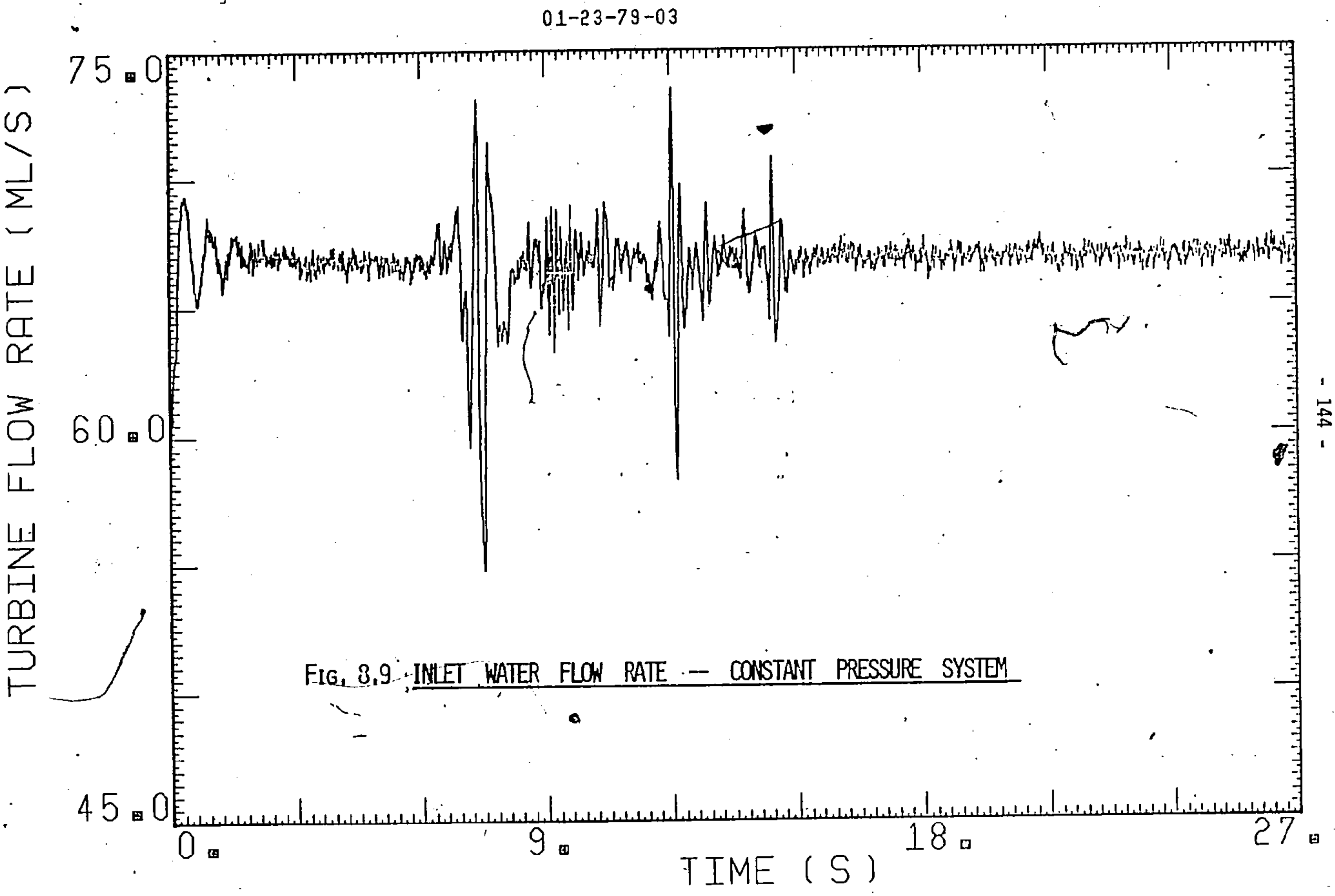

FIG. 3.9 INLET WATER FLOW RATE — CONSTANT PRESSURE SYSTEM

Therefore, the results will be quite similar if other flow and boundary conditions are held identical in our experiments.

Figure 8.2 is the input power curve. Since the motor generator was switched off at the start of the transient, the figure shows a decay curve corresponding to the residual power input. If a circuit breaker was used, the power would drop instantaneously to zero.

Figure 8.3 shows the system inlet pressure. Packets of high frequency, but relatively small amplitude pressure fluctuations are observed. At the exit of the test section, the pressure remains at atmospheric throughout the transient.

The transient void fraction measurements are shown in Figure 8.4. The first gamma densitometer (γD1) was located 14.0 centimeters and the second (γD2) 182.0 centimeters downstream of the heated test section inlet. γD2 was close to the end of the channel (Figure 4.3). In some cases, γD1 was moved to the middle of the tube and the distance between the two densitometers was about 80 centimeters. The curves give a good indication of the local void fractions during a transient. However, it should be noted that only some form of volume averaged void fractions were obtained. The phase distribution cannot be deduced from these measurements. By cross correlating the two void fraction measurements, some additional information of interest can be deduced. For example, the average quench velocity and entrained liquid velocity may be calculated as discussed later. The existence of water that does not wet the walls is evident from the γD2 curve. It can be seen that a substantial amount of water is detected, well before the arrival of the quench front, which corresponds to the rapid drop in measured void fraction.

Figures 8.5 and 8.6 are the exit fluid temperature measurements. Two exposed junction microthermocouples were used. They were located about 5.1 centimeters from the end of the heated section, one inserted from the top and the other one from below (Figure 4.3). The junctions were about 0.6 centimeter (one-third of the inner diameter of the tube) from the top and bottom respectively. They were designed to measure the vapour and liquid temperatures. Using Figures 8.5 and 8.6, together with the void fraction measurements (figure 8.4), some qualitative flow information at the exit of the heated section during the transients can be obtained. In general, shortly after the initiation of the transient, very hot air (or air-vapour mixture) is ejected. Hotter fluid is detected by the upper thermocouple (T_0^T). The temperatures then plunge below the saturation temperature when entrained water first appears (Figure 8.4). This suggests that the entrained water is subcooled at the exit. The rise in temperatures immediately afterwards indicates a decrease in entrainment for a short time. This is particularly apparent in the void fraction measurement (γD2), when a lower inlet flow is used (Figure 8.10). Vapor superheating can be seen. As the quench front moves closer to the exit, a mixture of saturated steam and entrained water appears until the channel is totally quenched. The exit temperatures will then drop slowly to the inlet water temperature.

Figure 8.7 summarizes the quenching of the mid-side of the heated section. The location of the thermocouple are as shown in Figure 4.3. It can be seen that the initial dry wall temperature is almost uniform along the test section (500 ± 20°C). This means that the test section is fairly uniformly heated. T2R has a higher initial temperature because it

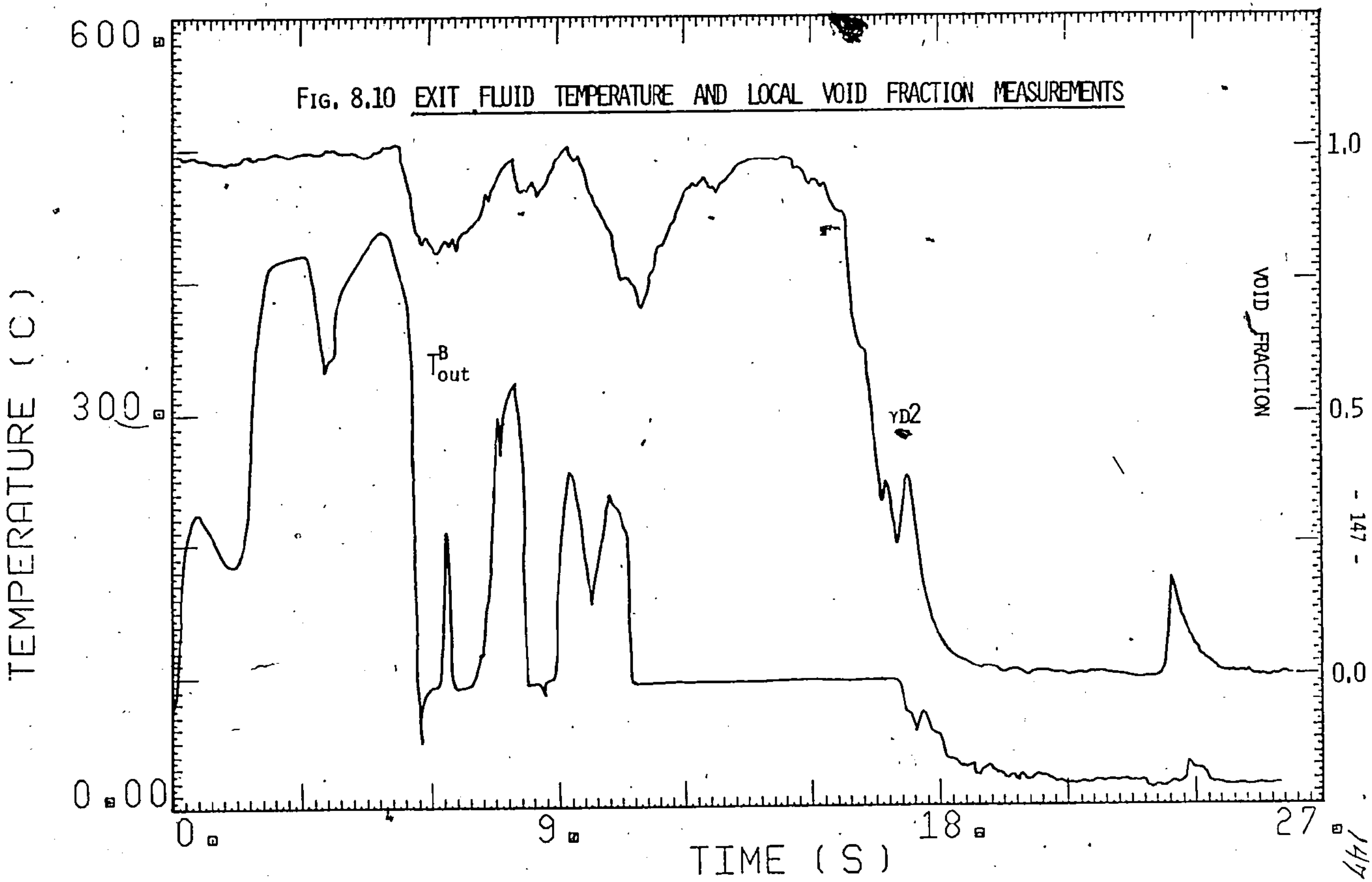

Fig. 8.10 EXIT FLUID TEMPERATURE AND LOCAL VOID FRACTION MEASUREMENTS

is located in the collimation zone for the first gamma densitometer, the collimator cuts down heat losses to the surroundings and thus results in a somewhat higher temperature. Because of the residual power input (Figure 8.2), constant wall temperature is maintained in the first few seconds. The wall temperature then decreases slowly due to free convection and radiation heat losses until it is quenched. Since the thermocouples are spaced an equal distance apart, the rewetting or quenching velocity can be deduced. The rewetting velocity is of particular interest in the recovery phase of reactor LOCA analysis and will be discussed in detail in the next section.

Figure 8.8 shows the quenching of the bottom (B) and top (T) of the channel. Again the locations of the thermocouples are as shown in Figure 4.3. It can be seen that the flow of rewetting water is highly stratified, the top of the channel at different locations rewets later than the bottom. The rewetting velocities for the top and bottom of the channel can also be obtained. In general, they are not equal and are different from the rewetting velocity defined at the mid plane of the channel in Figure 8.7. The bottom of the tube is cooled significantly before being quenched by the "water tongue" as discussed in Section 7.3.2.

Similar rewetting results were obtained when different boundary conditions were used. Figures 8.11 and 8.12 show a set of Group III results. The situation was very close to that given in Figure 8.7 and 8.8. A circuit breaker was used to cut the power input to zero instantaneously at the start of the transient. An apparent difference is that the wall temperature drops steadily from the very beginning until it is quenched because there is no residual power input. The steady drop in temperature is mainly due to natural convection and radiation heat losses. Figures

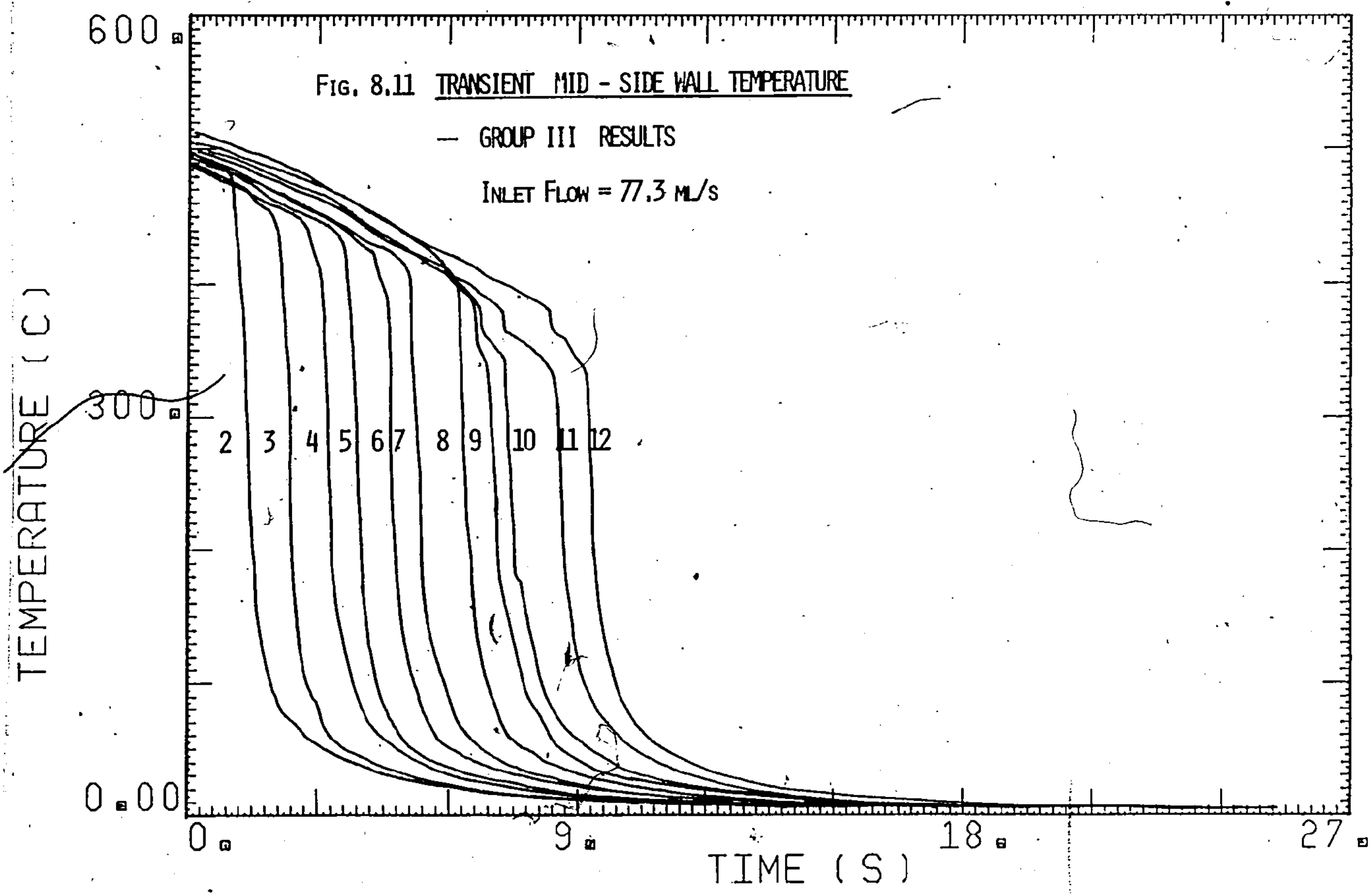

01-15-79-02

Fig. 8.11 TRANSIENT MID - SIDE WALL TEMPERATURE

— GROUP III RESULTS

Inlet Flow = 77.3 mL/s

01-15-79-02

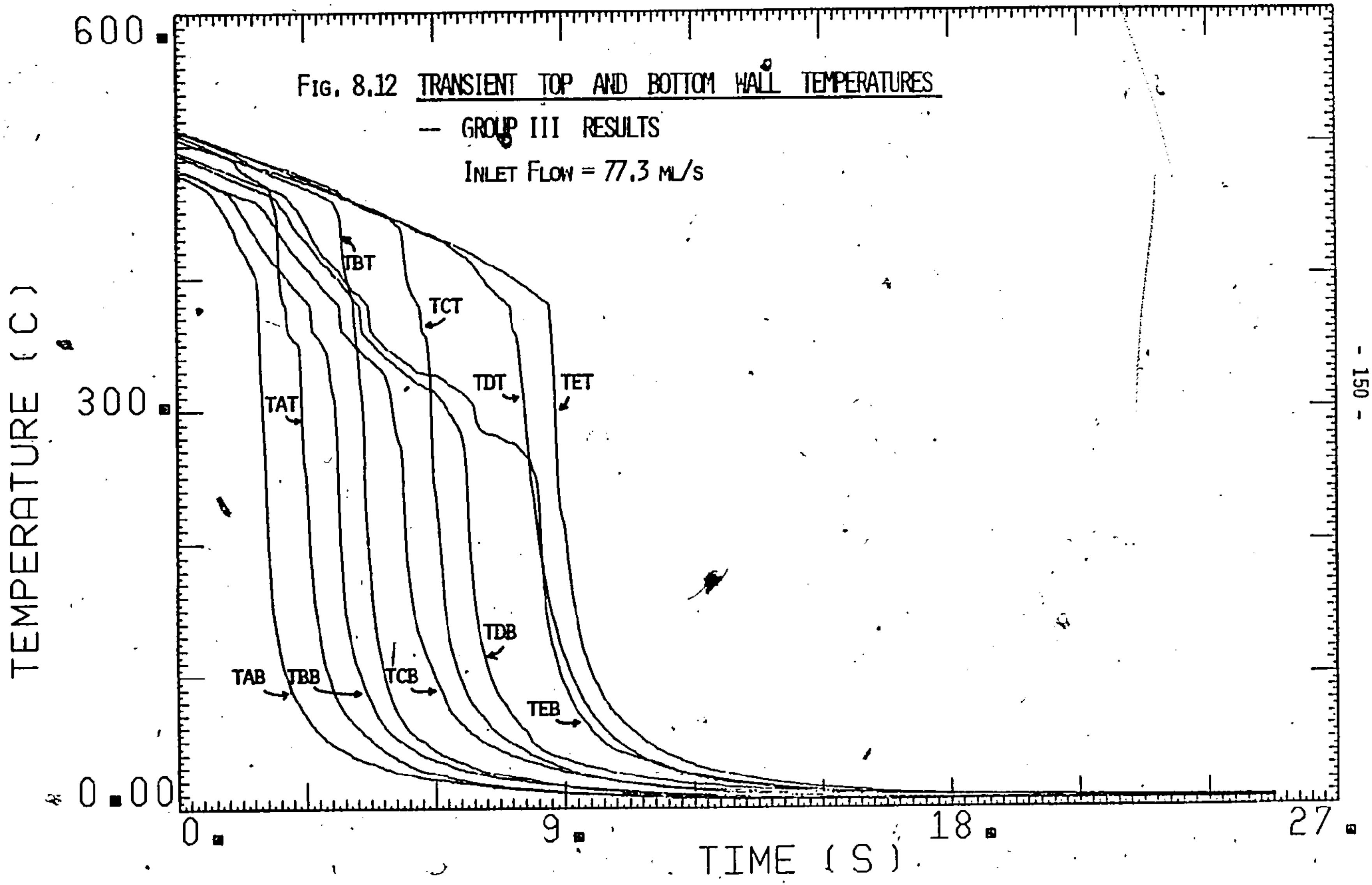

Fig. 8.12 TRANSIENT TOP AND BOTTOM WALL TEMPERATURES

— GROUP III RESULTS

Inlet Flow = 77.3 ml/s

8.13 and 8.14 give the results for a similar case with the heated section well-insulated (Group VI data). Compared to cases with no insulation, less than 25% of the required power input was needed to maintain the same initial wall temperature. The lower initial temperatures for T2R and T12R was probably due to axial conduction heat loss to the unheated flanges and feeders. Since heat losses to the surrounding was negligible, the near constant wall temperature in the dry region before quench indicates that heat transfer to the vapor flow in the channel is small.

Comparing these three different cases, it can be seen that the quenching characteristics are slightly different. The rewetting velocities are not the same. The quench front appears more stratified in the insulated case (Figure 8.14). In general, the time required to quench the channel is shortest for the second case when the power is cut off and the channel is not insulated. Effects of different initial and boundary conditions on the rewetting velocities will be discussed in Section 8.3. The general quenching characteristics will now be described.

8.2 The Rewetting Model

A physical model for the refilling and rewetting processes in horizontal channels was given in Section 7.3.2. We can picture the quench front moving smoothly down the channel, quenching the bottom, mid-side and the top of the channel on its way. A "liquid tongue" stretching out from the quench front (Figure 7.2) cools the bottom portion of the dry surface in front. The model assumes a stratified interface and the level of water at any location is well defined. This is an important assumption for the model developed later because quenching is possible only when the level of water (h_L) is higher than the quench level, for example, the

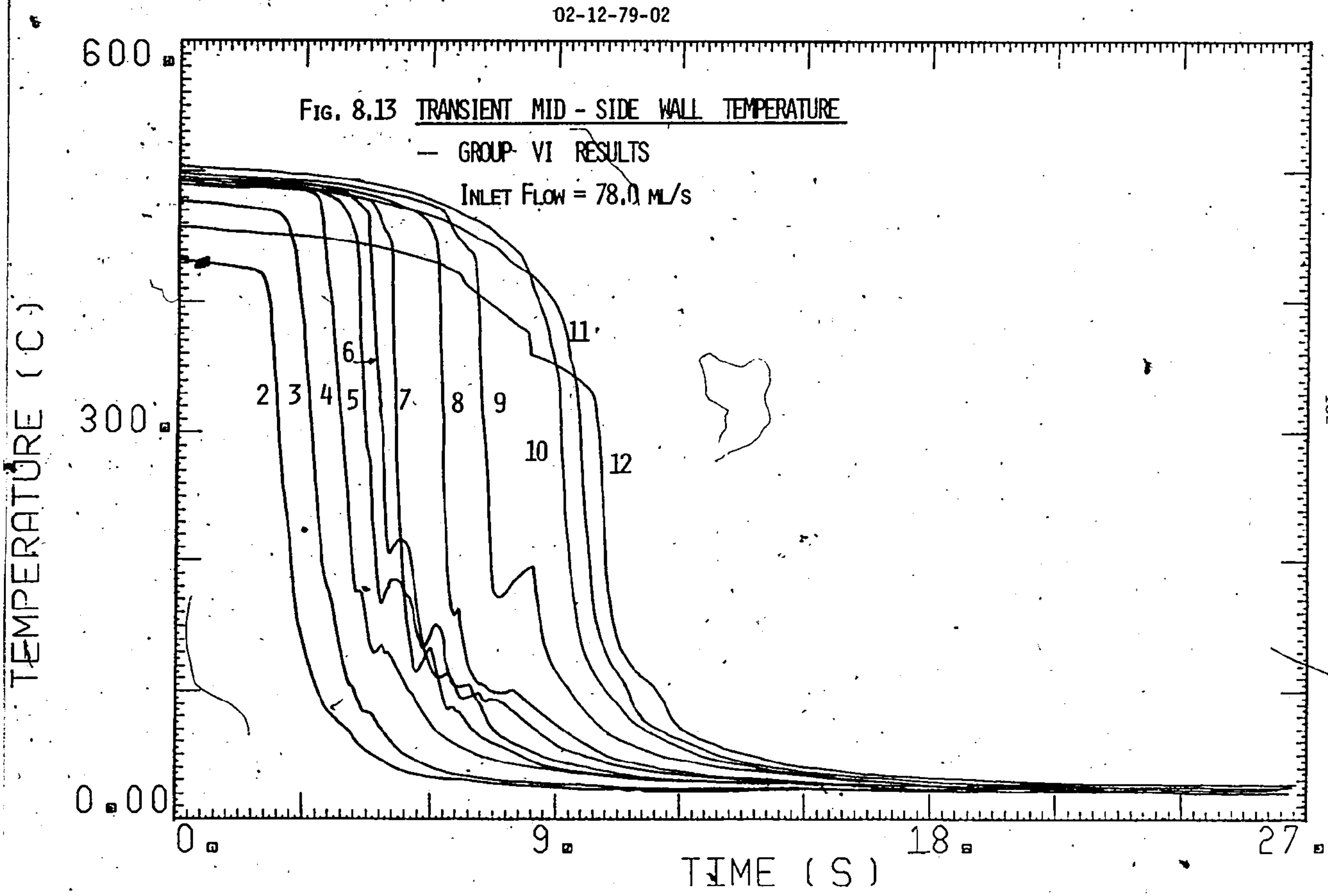

Fig. 8.13 TRANSIENT MID - SIDE WALL TEMPERATURE — GROUP VI RESULTS

Inlet Flow = 78.0 ml/s

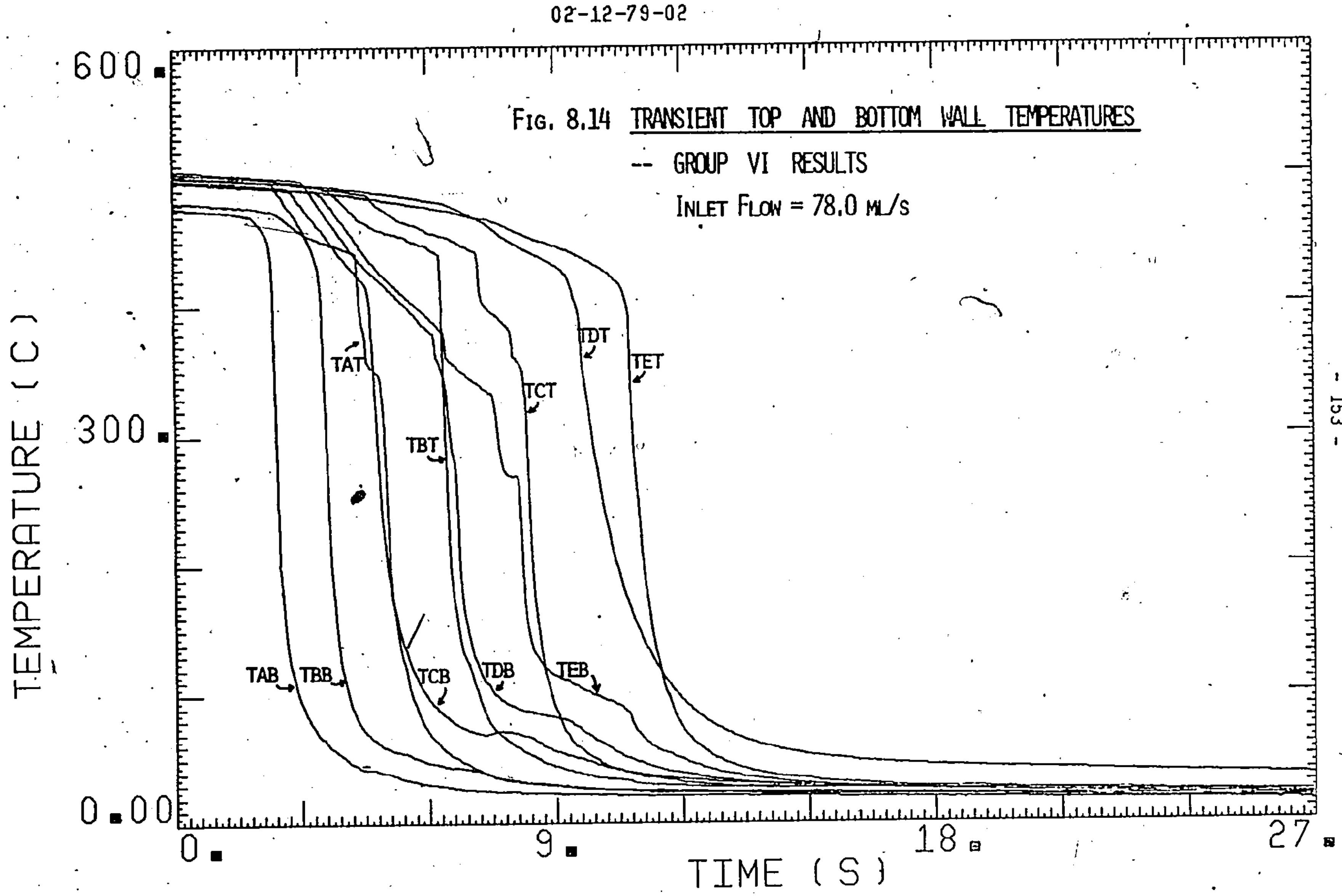

Fig. 8.14 TRANSIENT TOP AND BOTTOM WALL TEMPERATURES
-- GROUP VI RESULTS
Inlet Flow = 78.0 ml/s

mid-side of the channel cannot be quenched if h_L at that location is less than the radius (R) of the channel. This is indeed the case for high initial wall temperatures and/or high flow rates. An example is given in Figure 8.15. Figure 8.15 superimposes the mid-side quenching sequence with a void fraction profile. The void profile was obtained using a gamma densitometer located between the T7 and T8 thermocouples. It can be seen that γD1 drops below 0.5 (or $h_L > R$) after the quenching of T7R and before the quenching of T8R. This means that between T7 and T8, the mid-side of the channel is quenched when $h_L > R$. Since the location between T7 and T8 is no different from any other point along the channel, the same result will hold everywhere. That is what the simple model used later also implies.

When the flow rate is low, however, this model does not describe the processes well. The water level in the quench front is no longer well defined. An example is shown in Figure 8.16. The inlet flow rate used was 32 ml/s. Again, γD1 is plotted together with the mid-side quenching sequence. It can be seen that γD1 stays high when T7R and T8R are quenched. This means that the mid-side of the channel is quenched when the water present cannot provide a collapsed water level that half fills the tube. Since the surface must be in "contact" with water before it can be quenched, and because there is not enough water to fill the channel up to the necessary level, a possible explanation for the observed phenomenon is that a semi-annular quench front is formed. This is shown in the insert of Figure 8.16. The formation of a semi-annular quench front is possible if the

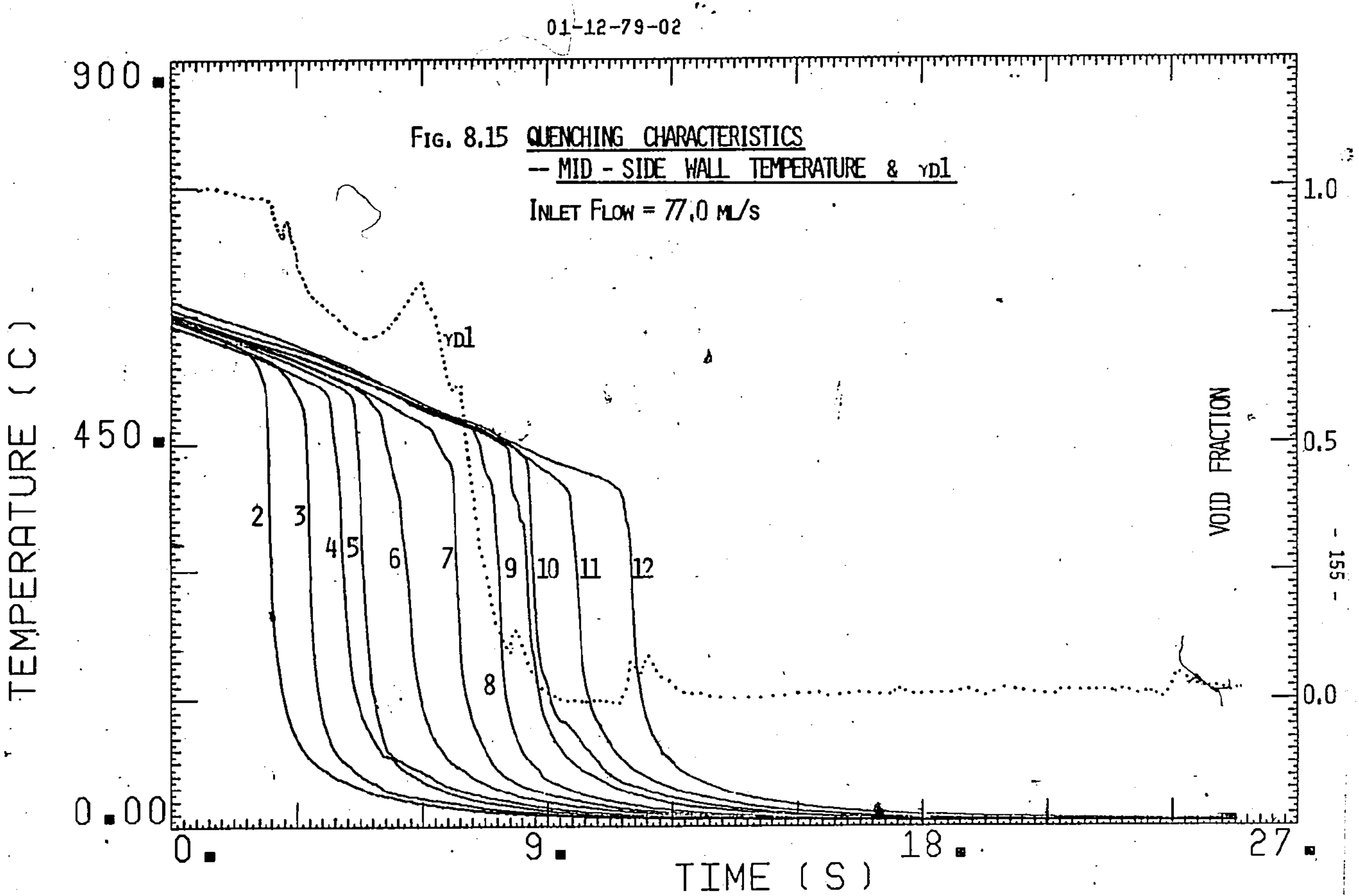

FIG. 8.15 QUENCHING CHARACTERISTICS
-- MID - SIDE WALL TEMPERATURE & YD1
INLET FLOW = 77.0 ML/S

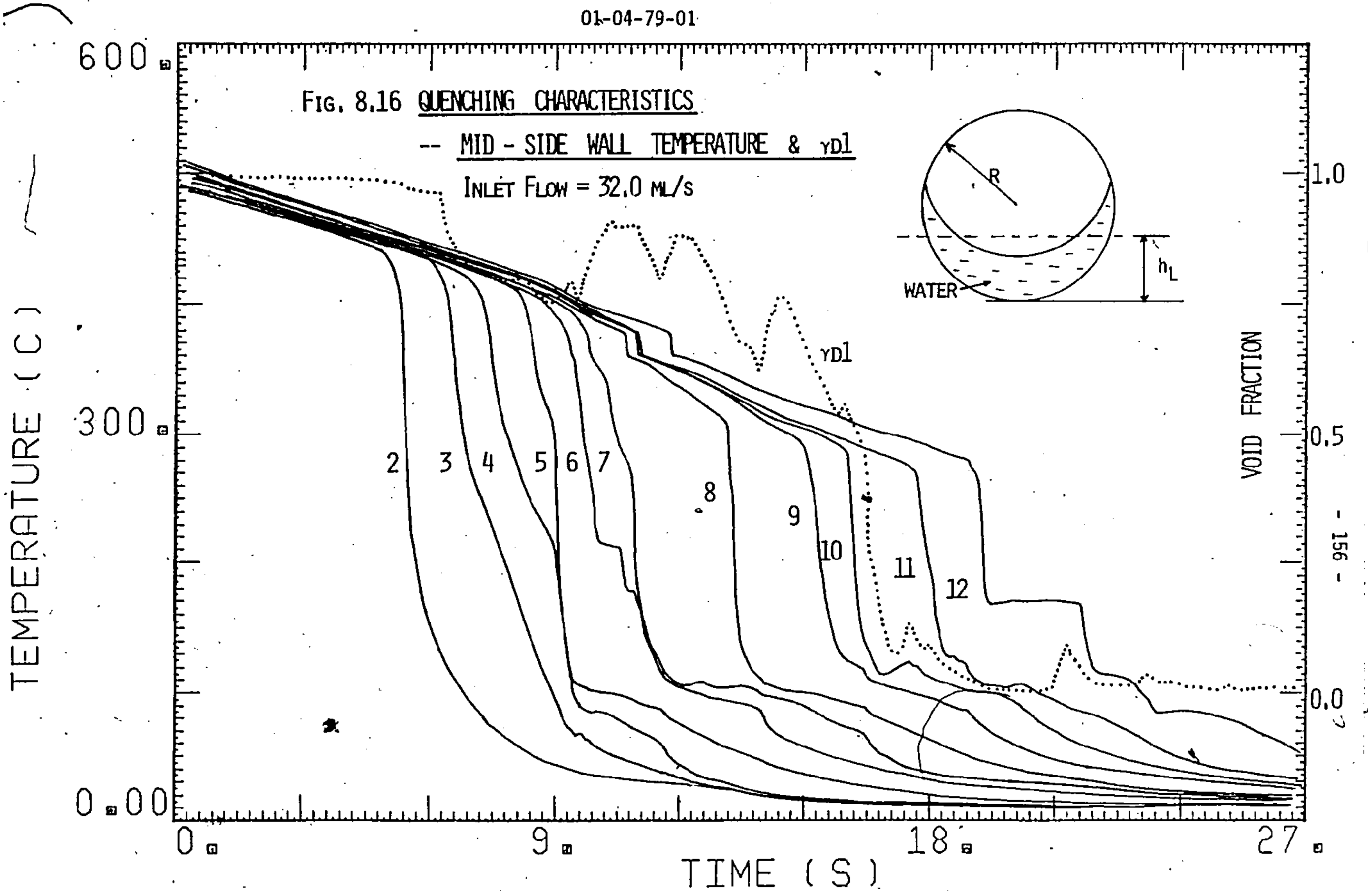

Fig. 8.16 QUENCHING CHARACTERISTICS
-- MID - SIDE WALL TEMPERATURE & YD1
INLET FLOW = 32.0 ML/S

vapour velocity is high. For example, if when the flow rate is low, the water resides in the hot channel for a relatively long time and a large amount of vapour can be produced. A large vapour drag may result from the high vapour flow and form a liquid film around the periphery of the tube. The film may not, of course, be continuous around the entire circumference and will certainly be thicker at the bottom of the channel.

Since the stability and shape of the interface has to be considered, the refilling and rewetting processes will be much more complicated. The simple rewetting model proposed later is no longer really applicable. However, it may still be useful in studying the parametric effects on the rewetting velocities. Because the interfacial instability tends to enhance rewetting of the side and top of the channel, the simple model will tend to under-estimate these rewetting velocities. This will be discussed in Chapter 10.

8.3 Rewetting Velocities

Since the quench front is stratified and the angle of stratification is not constant, the rewetting velocity cannot be defined uniquely. From the experimental results obtained, we can define three rewetting velocities: with respect to the quenching of the top, mid-side and bottom of the channel. In general, they are not equal. The rewetting velocities can be obtained locally or averaged over the length of the test section.

8.3.1 Local Rewetting Velocities

The local rewetting velocities are calculated by measuring the time difference between the quenching of adjacent thermocouples along the channel. The top, mid-side and bottom thermocouples are used to obtain the local rewetting velocities for the top, mid-side and bottom respectively. From Figures 8.7, 8.8 and 8.11 to 8.14, it can be seen that these quench time differences can vary. That is, the local velocities can change significantly along the channel. Some typical results are shown in Figure 8.17. Plotted in the figure are the ratios of the local and the corresponding average velocities along the channel. The mid-side velocities are shown for various initial wall temperatures. The large variations of the local velocities are apparent from the figure.

In general, the local rewetting velocities tend to be more uniform along the channel for high initial wall temperatures and/or high inlet mass flows. Since local rewetting velocities are complicated functions of the local flow situations, local heat transfer coefficients and local heater surface conditions, the results are hard to generalize. In order to compare the results when different initial and boundary conditions are used, average rewetting velocities are more useful. By ignoring the local variations and taking the average rewetting velocities over the whole test section, most of the experimental data can be summarized by the rewetting velocity versus inlet flow curves. This will be discussed below.

8.3.2 Average Rewetting Velocities

Like the local rewetting velocities, three average rewetting velocities can be defined, $\overline{V}_T$, $\overline{V}_S$ and $\overline{V}_B$. They are, in general, quite close to each other. Some typical examples are given in Figure 8.18 to 8.20. Plotted in the Figures are the three average rewetting velocities

Fig. 8.17 <u>LOCAL REWETTING VELOCITY -- MID - SIDE OF TEST SECTION</u>

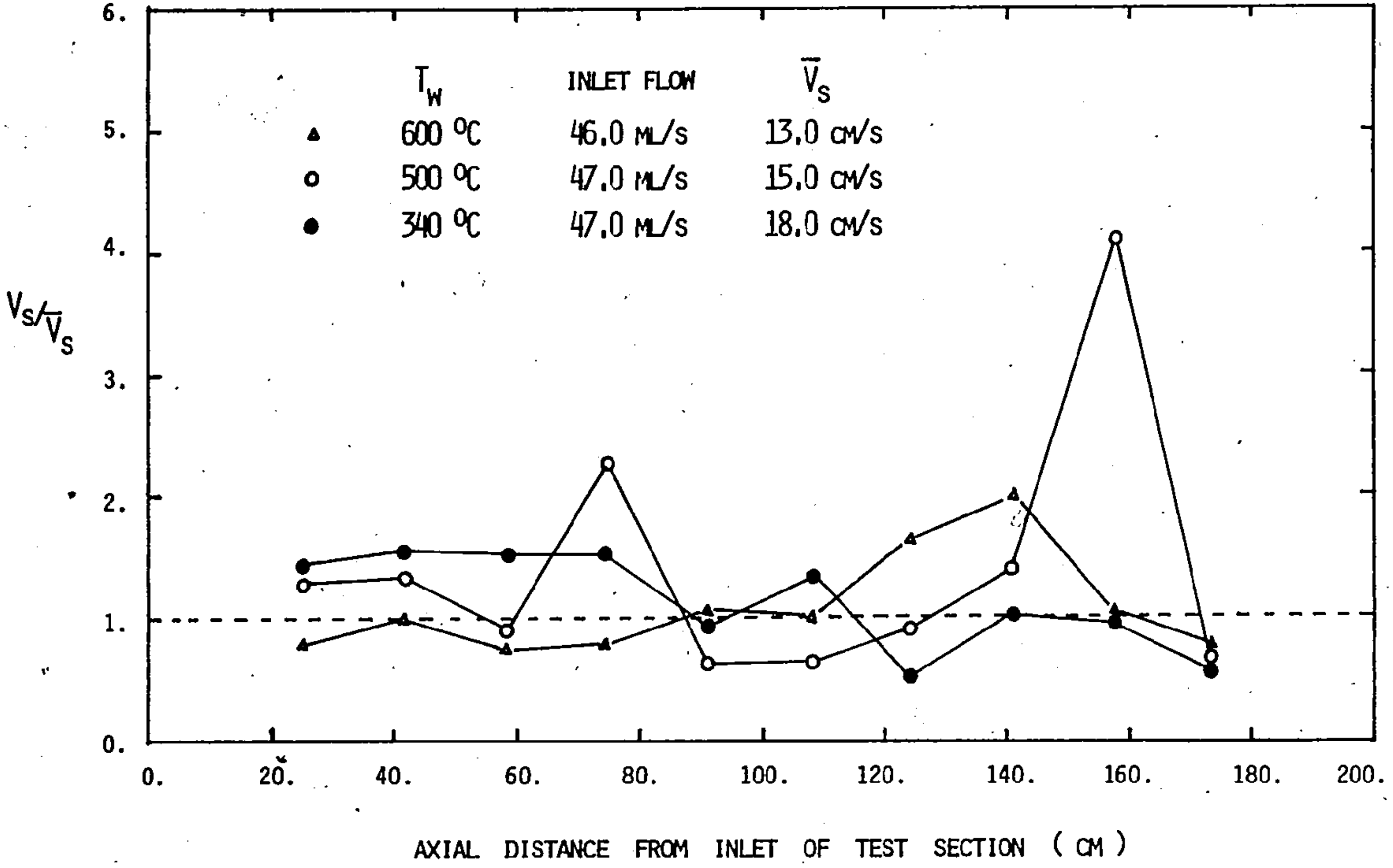

FIG. 8.18 AVERAGE REWETTING VELOCITIES VS INLET FLOW RATES

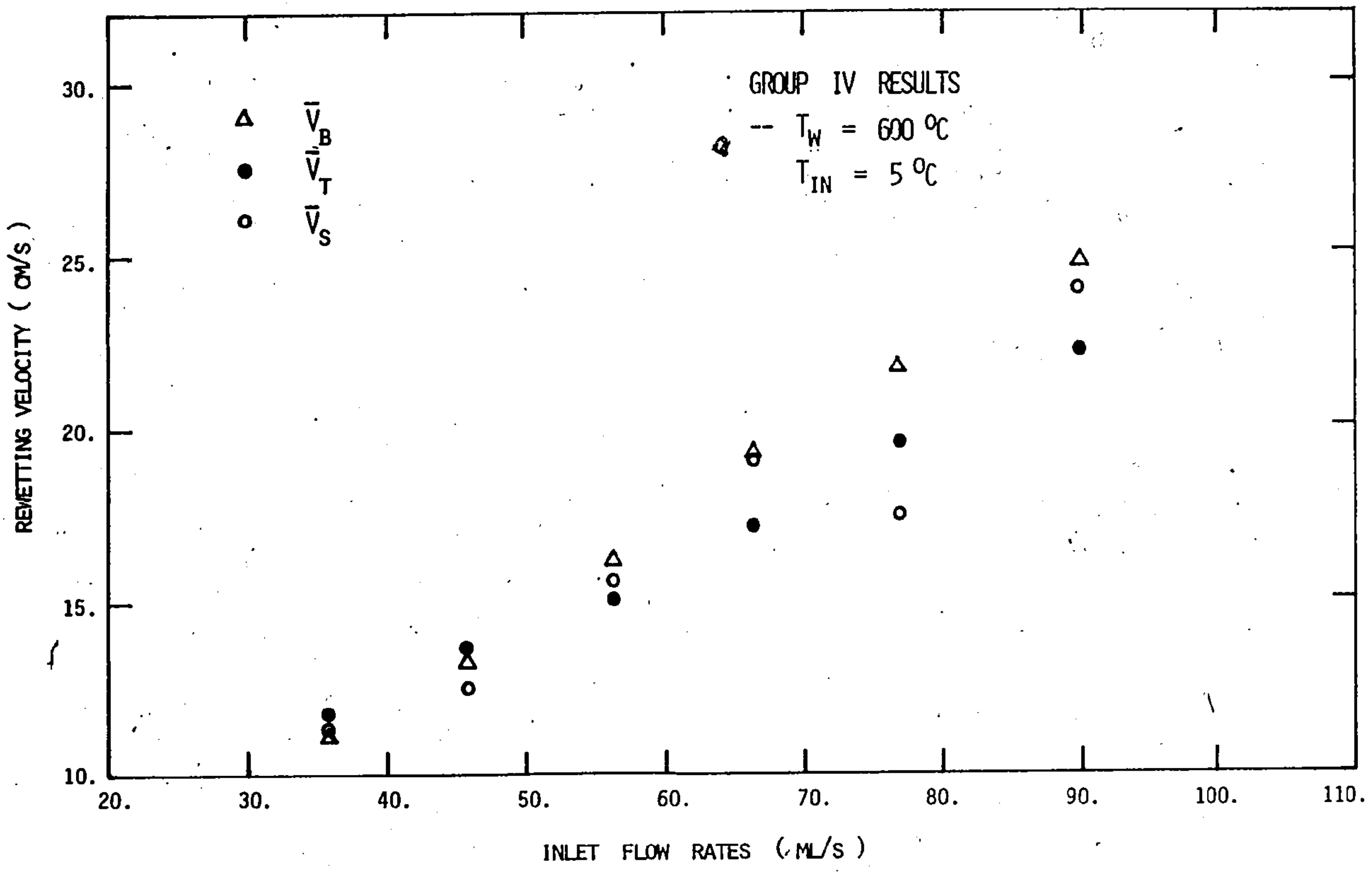

FIG. 8.19 AVERAGE REWETTING VELOCITIES VS INLET FLOW RATES

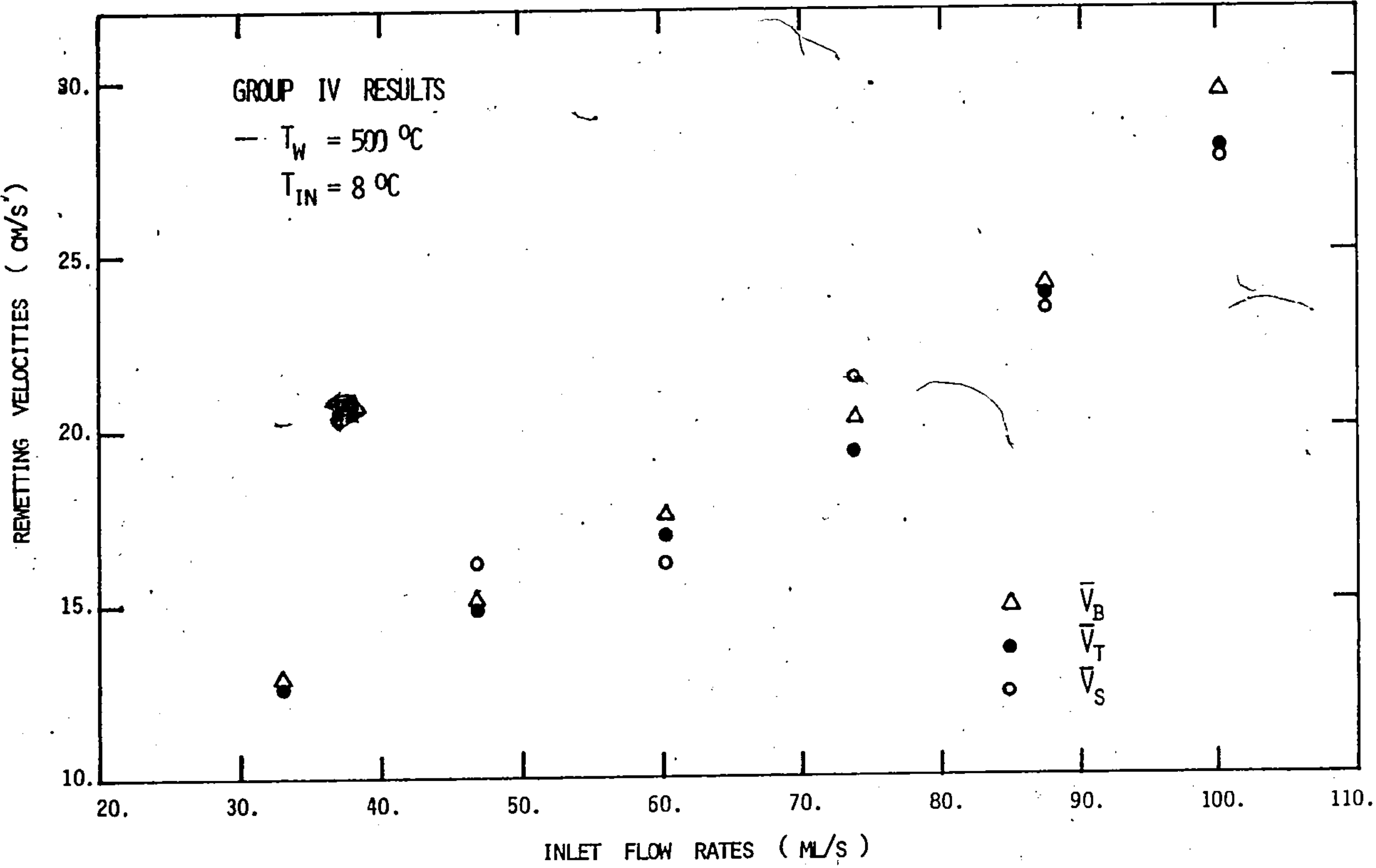

FIG. 8.20 AVERAGE REWETTING VELOCITIES VS INLET FLOW RATES

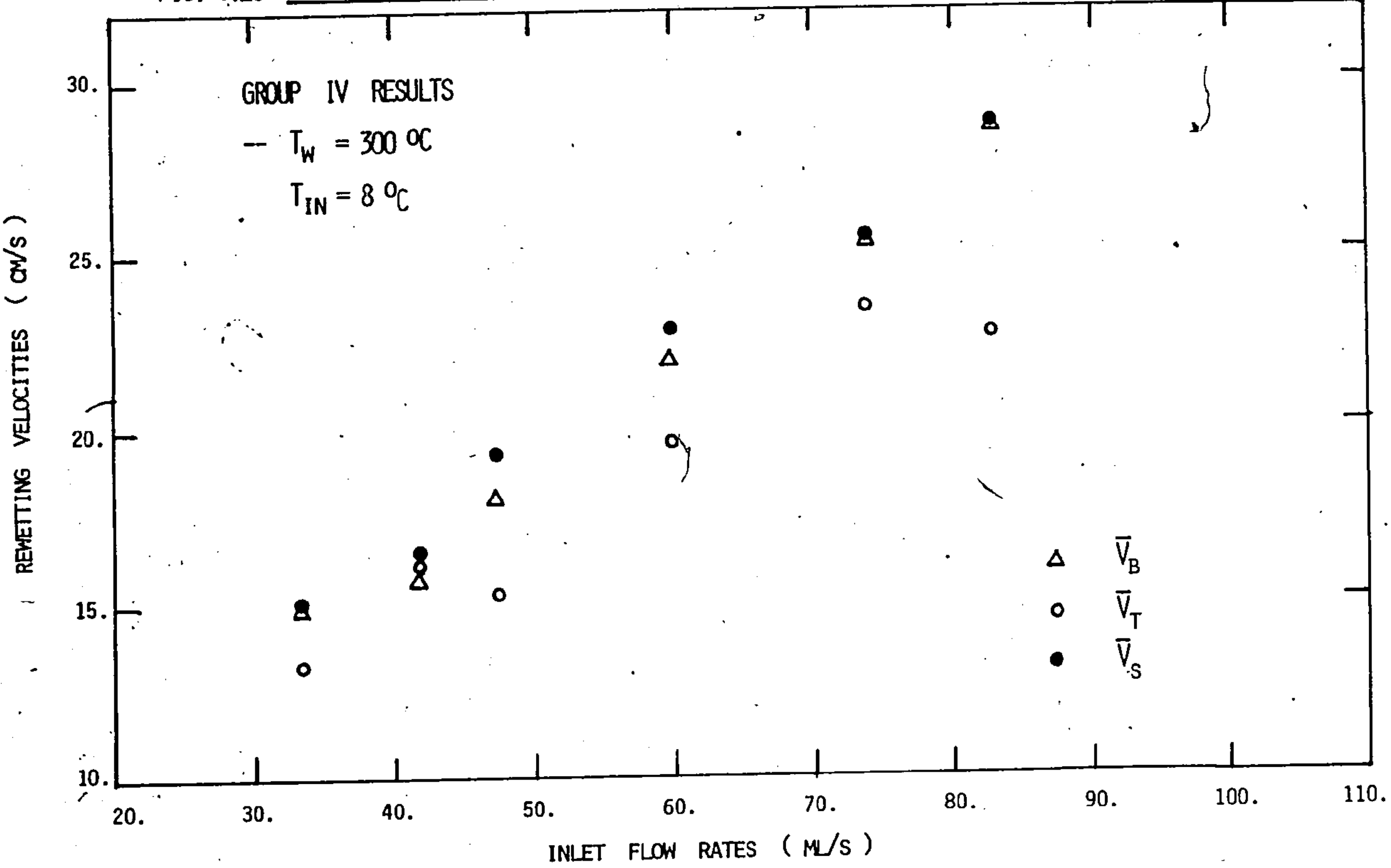

as a function of inlet mass flow for different initial wall temperatures. It can be seen that, the average rewetting velocities tend to deviate more from each other at high inlet flows. $\overline{V}_B$ and $\overline{V}_S$ are very close in most cases. For low initial wall temperatures (Fig. 8.20), $\overline{V}_T$ is consistently lower than $\overline{V}_B$ and $\overline{V}_S$.

The rewetting data are summarized in Figures 8.21 through 8.30. The average rewetting velocities are plotted as a function of inlet flow rates for different initial wall temperatures. Results for the Group I experiments are given in Figures 8.21 to 8.23. $\overline{V}_S$, $\overline{V}_B$ and $\overline{V}_T$ curves are shown respectively. The Group II results are shown in Figures 8.24 to 8.26. Results for the Groups III, IV and VI experiments are shown respectively in Figures 8.27, 8.28 and 8.29. Figure 8.30 compares the Group V results with the corresponding results when building tap water was used instead of deaerated and de-ionized water. Only $\overline{V}_S$ curves are shown in the latter cases, because in general similar trends are observed for $\overline{V}_B$ and $\overline{V}_T$.

From the figures shown, effects of different parameters on the rewetting velocities can be clearly seen. This will be discussed and compared with existing experimental and theoretical results.

8.3.2.1 Effect of Initial Wall Temperature

It was found that the rewetting velocity decreases as the initial dry wall temperature increases. This is in agreement with all existing investigations, both for vertical channel flooding (Thompson [22], Yamanouchi [25], Bennett et al. [28] and Groeneveld and Young [39]) and horizontal channel rewetting (Lee et al. [40]). If the inverse

FIG. 8.21 AVERAGE REWETTING VELOCITY ($\bar{V}_S$) VS INLET FLOW RATES FOR DIFFERENT WALL TEMPERATURES

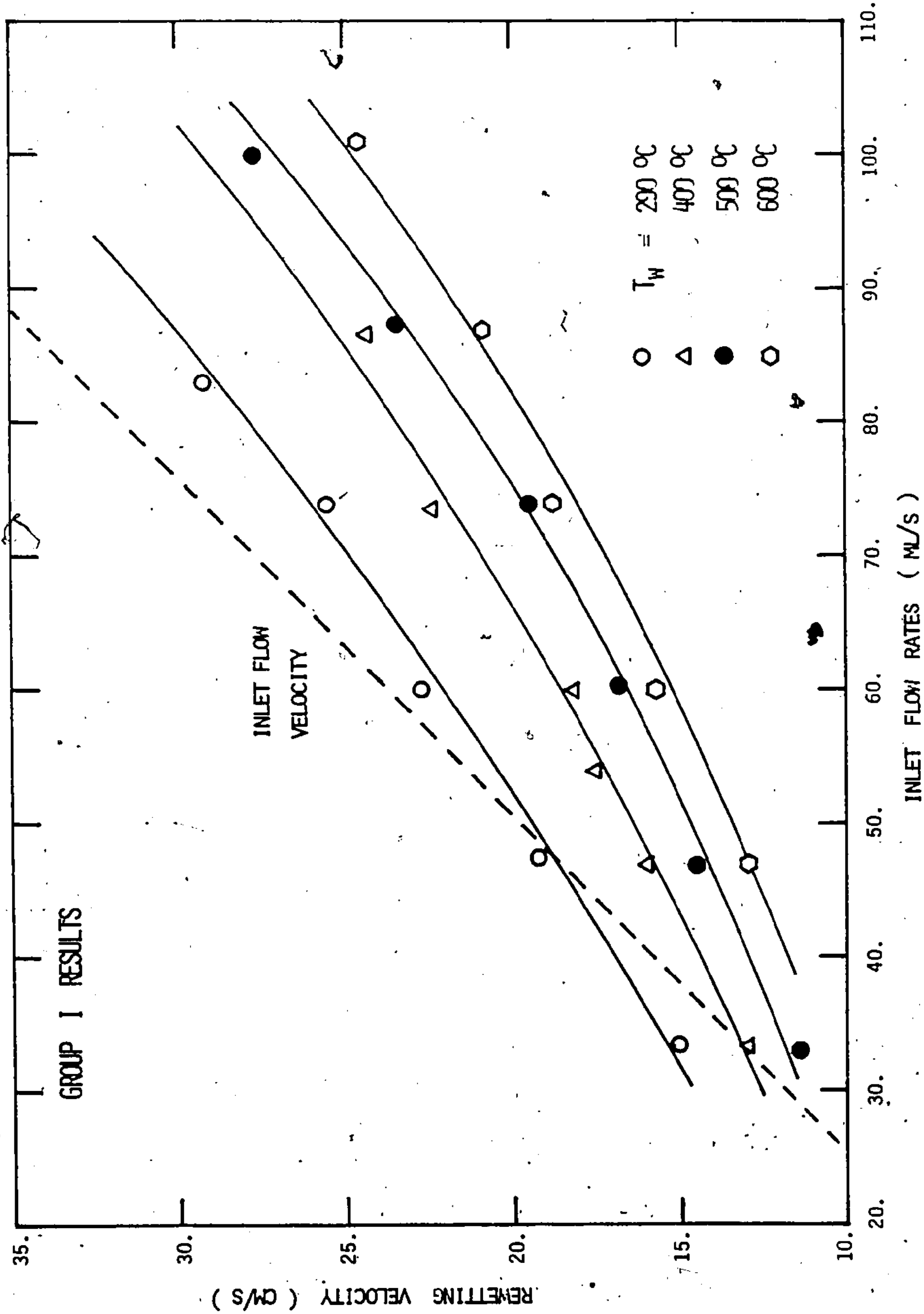

FIG. 8.22 AVERAGE REWETTING VELOCITY ($\bar{V}_B$) VS. INLET FLOW RATES FOR DIFFERENT WALL TEMPERATURES

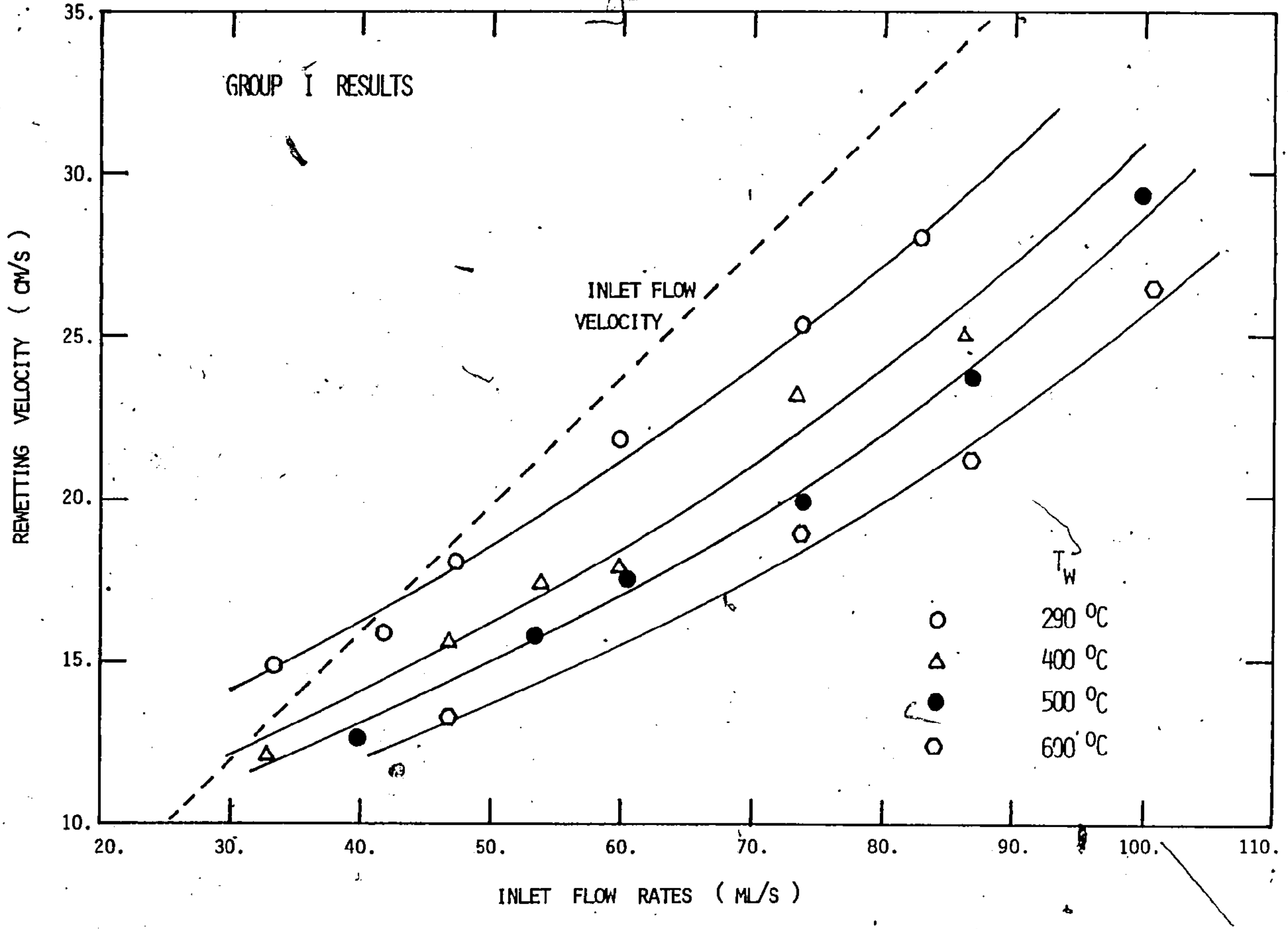

FIG. 8.23 AVERAGE REWETTING VELOCITY ($\bar{V}_T$) VS INLET FLOW RATES FOR DIFFERENT WALL TEMPERATURES

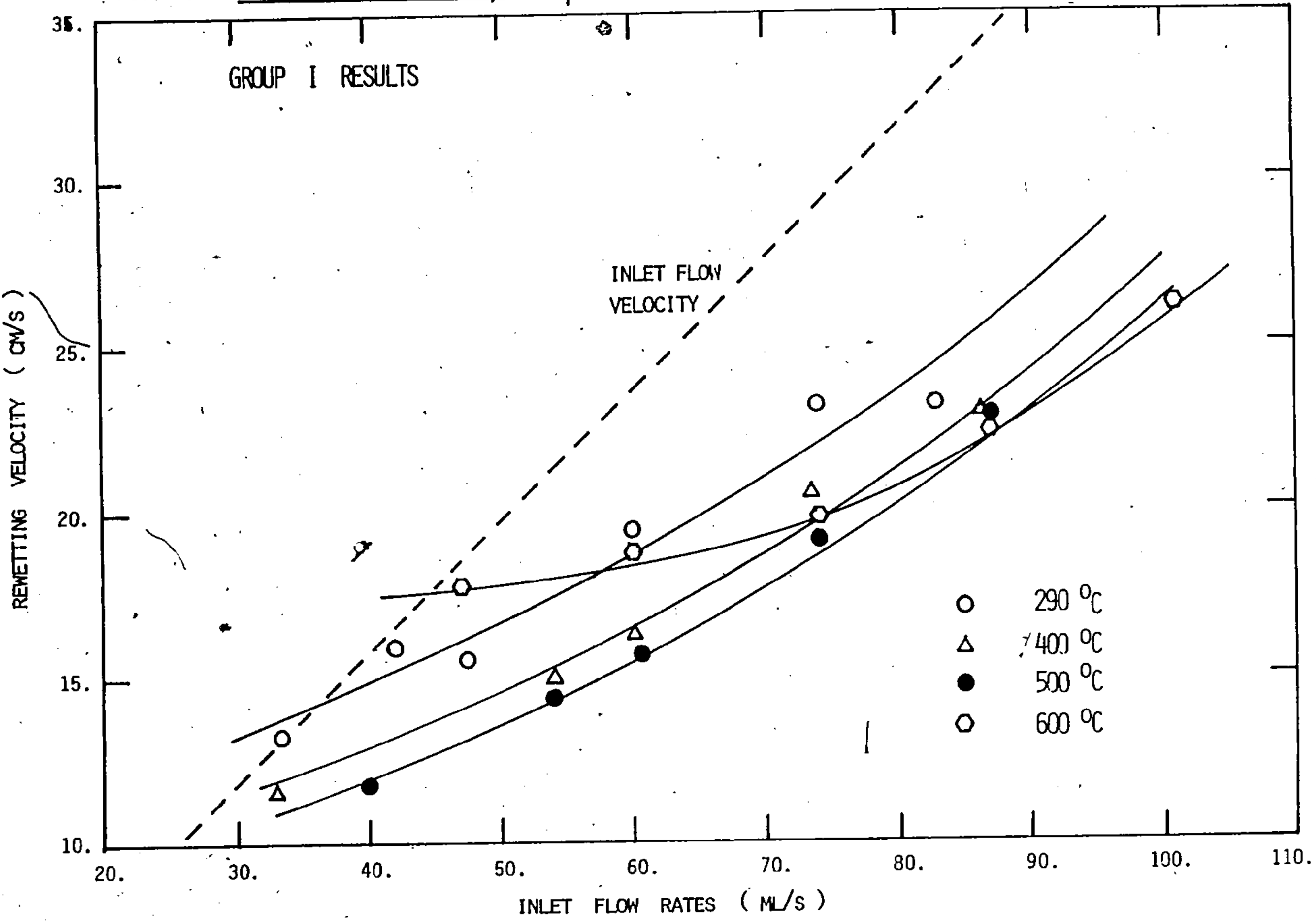

FIG. 8.24 AVERAGE REWETTING VELOCITY ($\bar{V}_S$) VS INLET FLOW RATES FOR DIFFERENT WALL TEMPERATURES

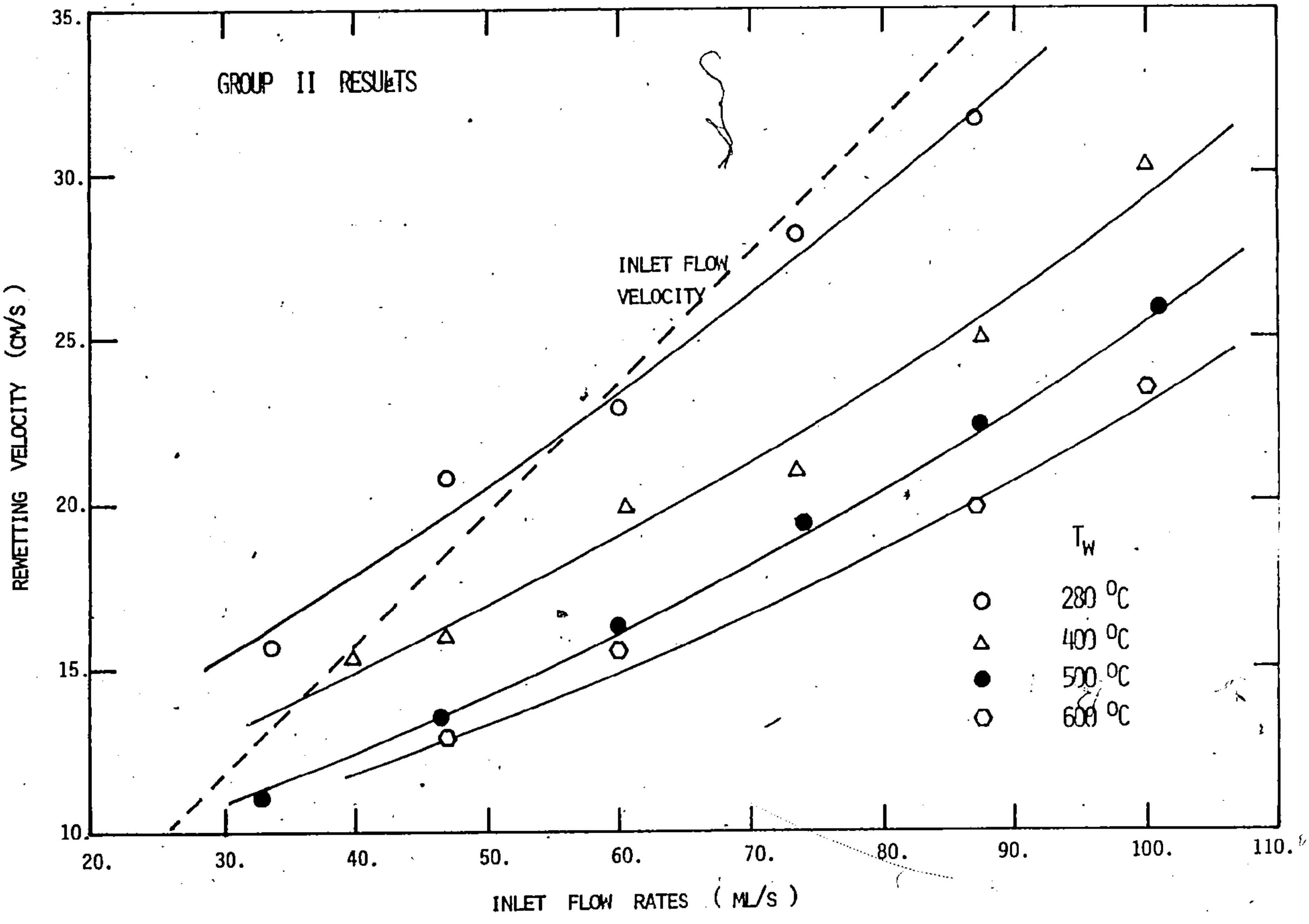

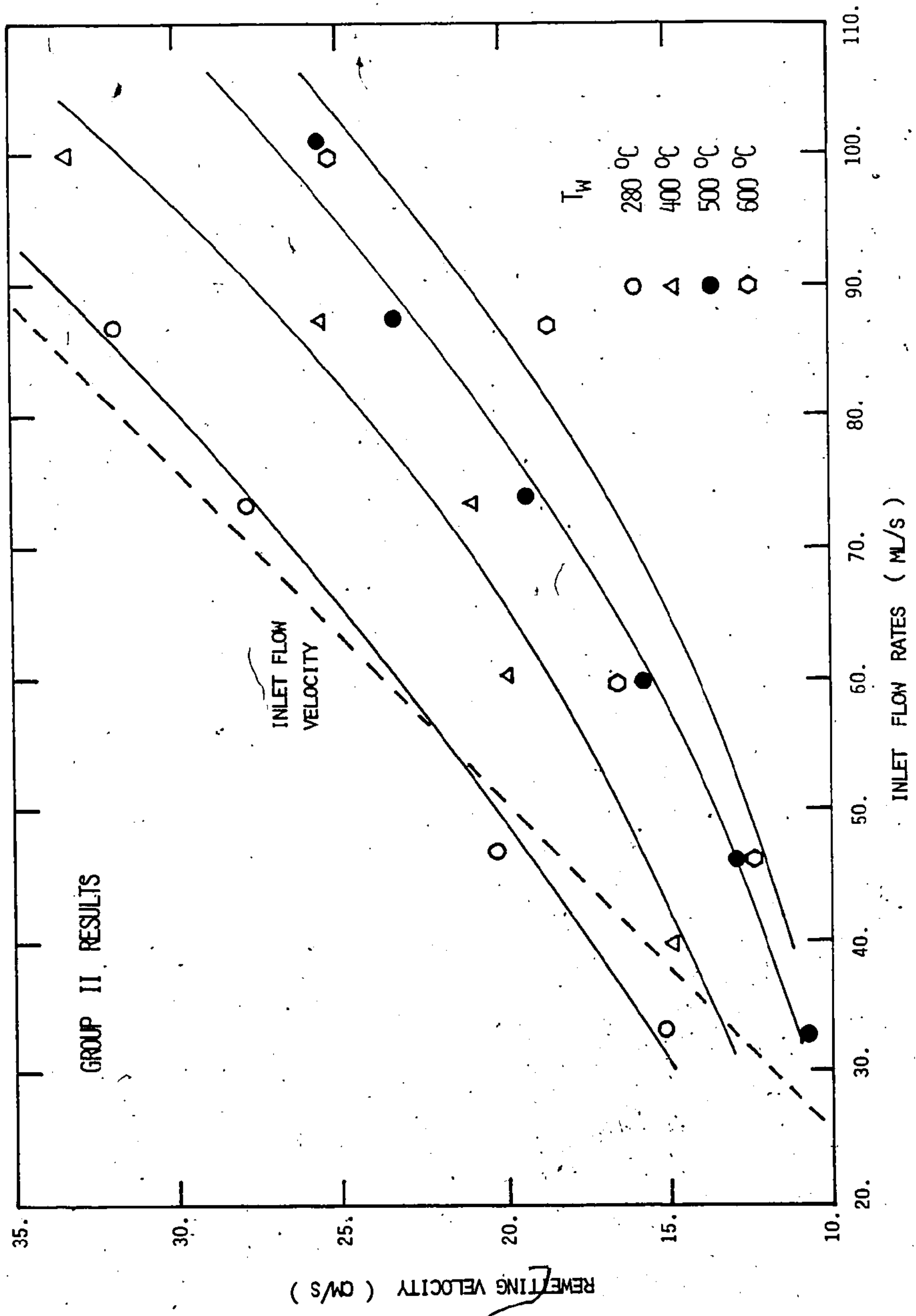

FIG. 8.25 AVERAGE REWETTING VELOCITY ($\overline{V}_B$) VS INLET FLOW RATES FOR DIFFERENT WALL TEMPERATURES

Fig. 8.26 AVERAGE REWETTING VELOCITY ($\bar{V}_T$) VS INLET FLOW RATES FOR DIFFERENT WALL TEMPERATURES

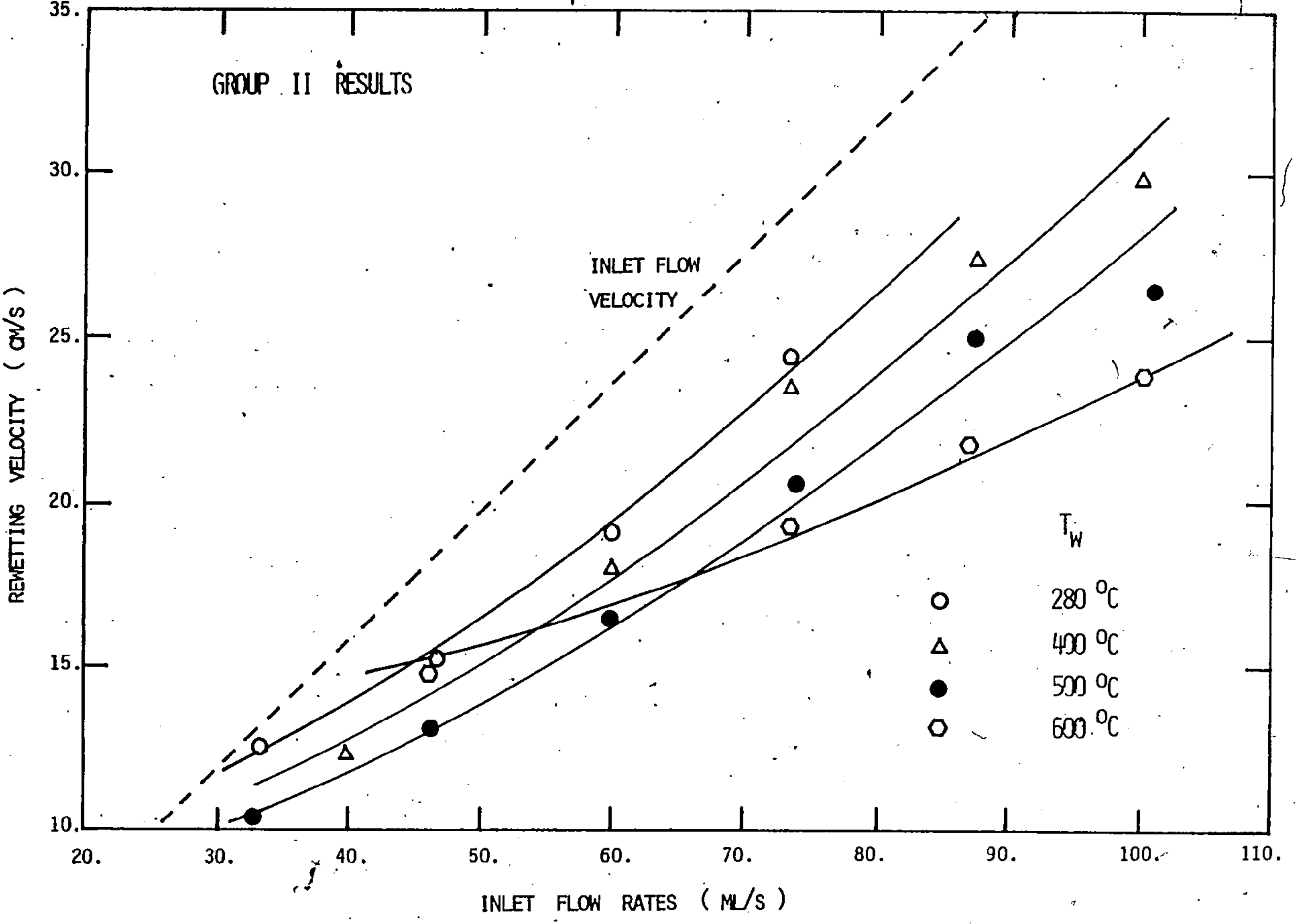

FIG. 8.27 AVERAGE REWETTING VELOCITY ($\bar{V}_S$) VS INLET FLOW RATES FOR DIFFERENT WALL TEMPERATURES

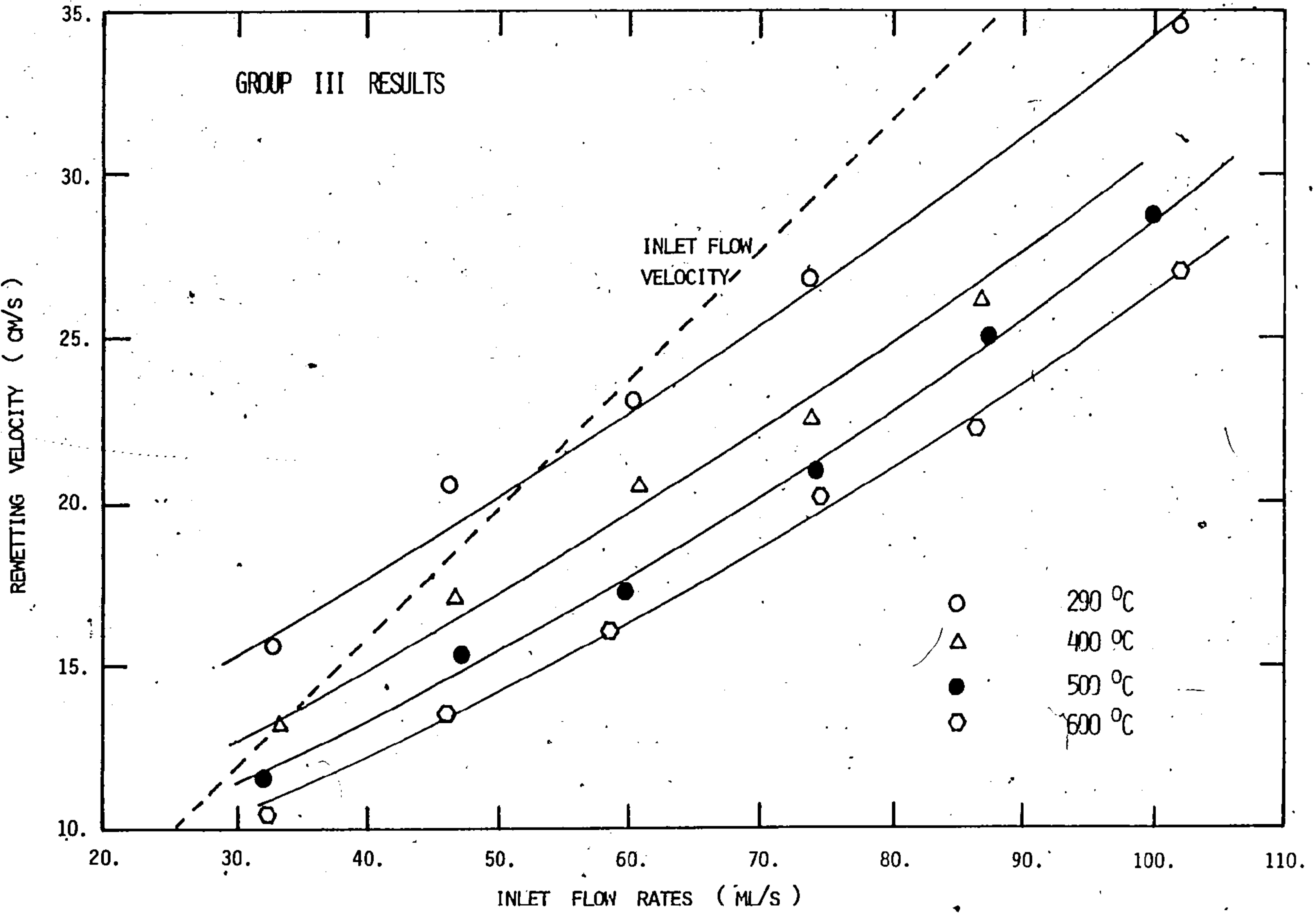

FIG. 8.28 AVERAGE REWETTING VELOCITY ($\overline{V}_S$) VS INLET FLOW RATES FOR DIFFERENT WALL TEMPERATURES

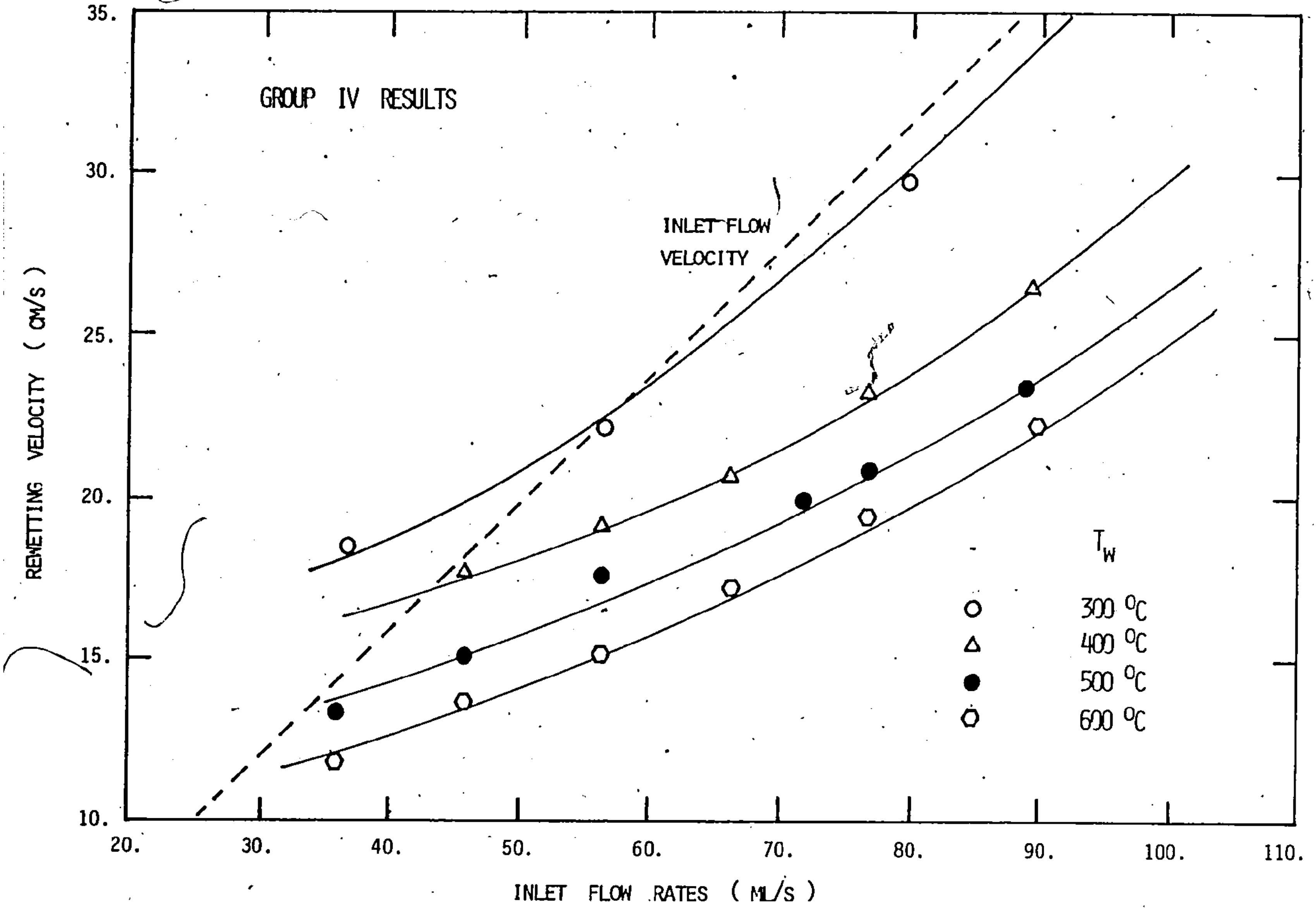

FIG. 8.29 AVERAGE REWETTING VELOCITY ($\bar{V}_S$) VS INLET FLOW RATES FOR DIFFERENT WALL TEMPERATURES

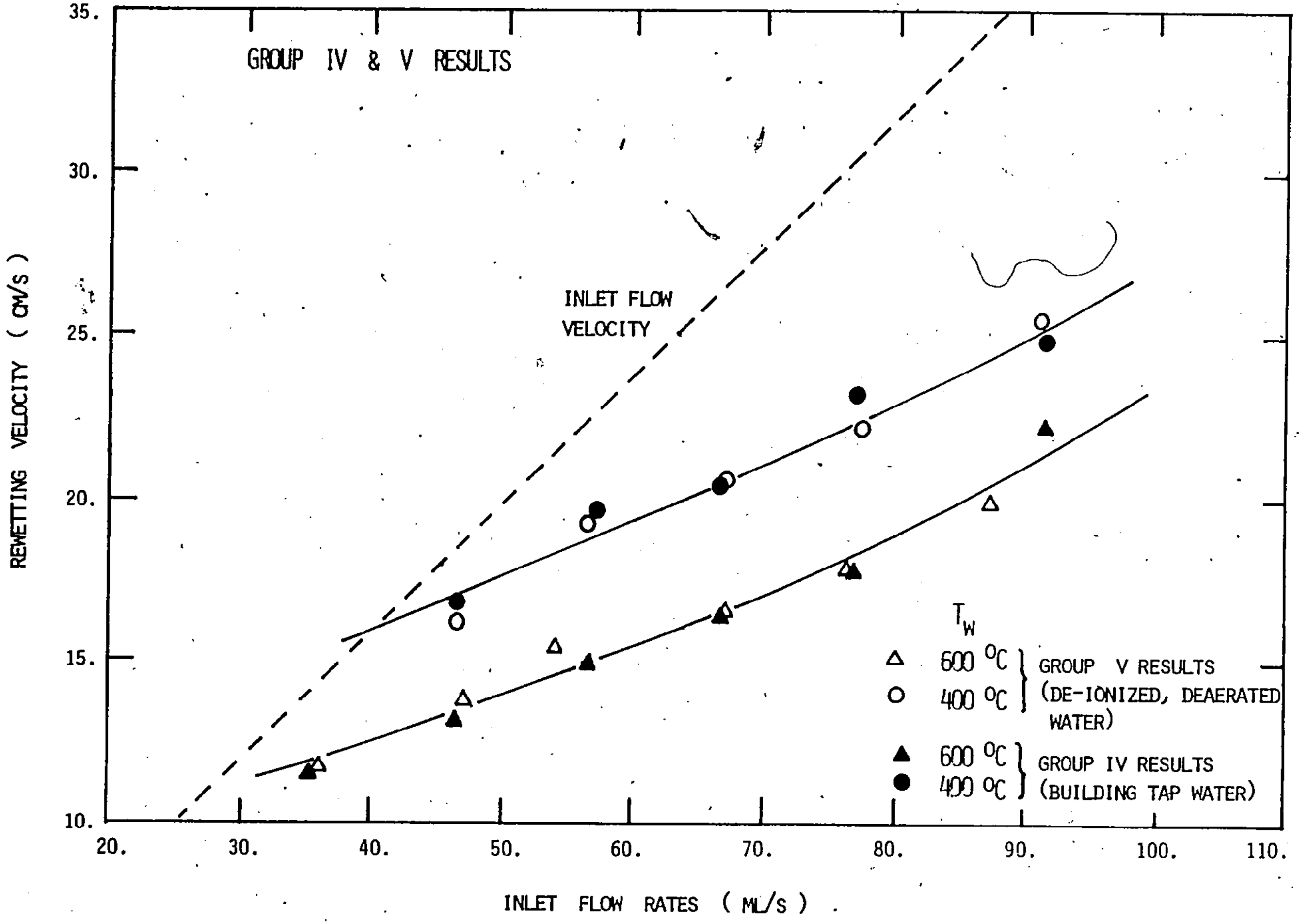

Fig. 8.30 AVERAGE REWETTING VELOCITY ($\overline{V}_S$) VS INLET FLOW RATES FOR DIFFERENT WALL TEMPERATURES

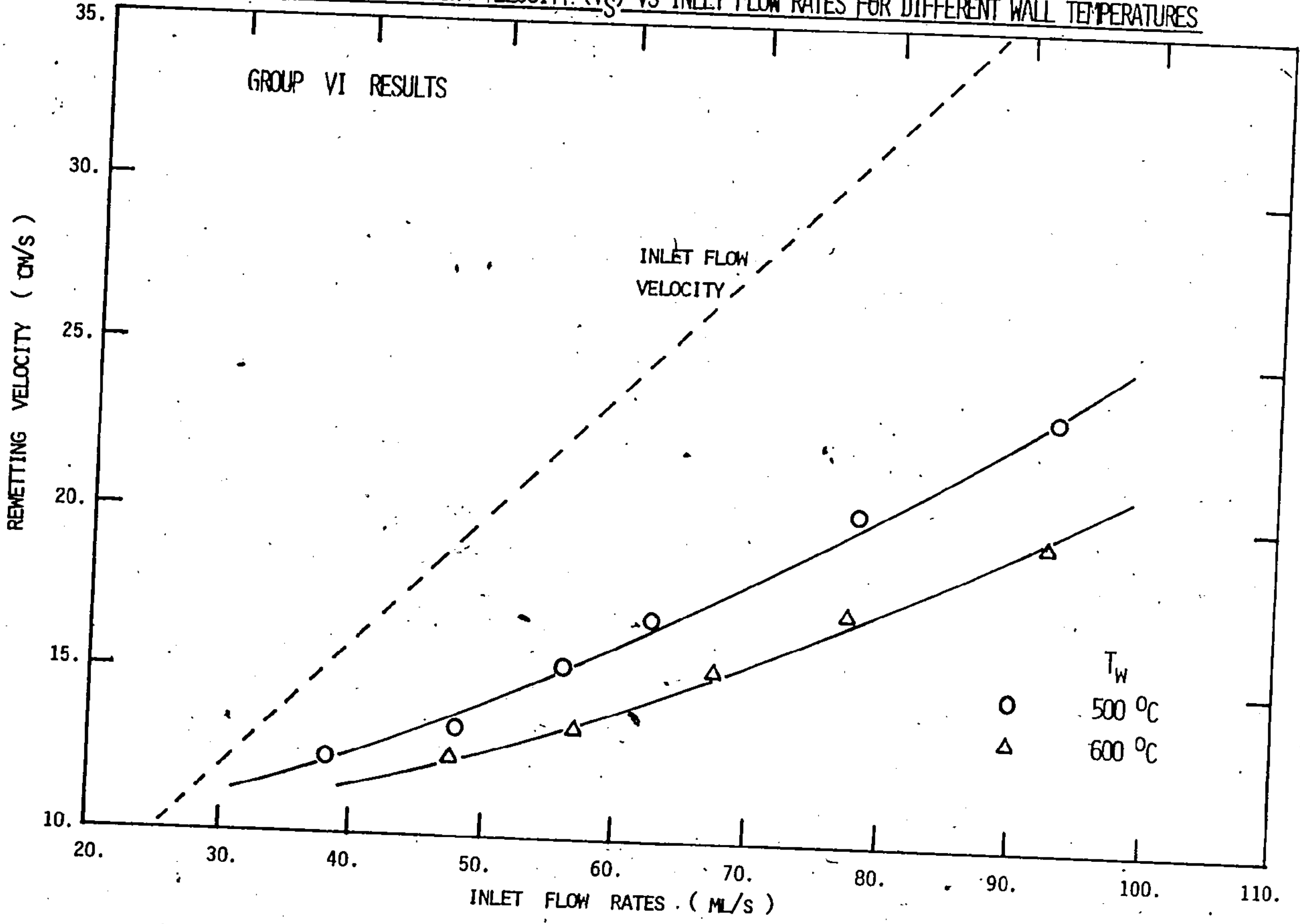

rewetting velocity is plotted against the initial dry wall temperature, a linear relationship is obtained as shown in Figures 8.31 through 8.33. Similar linear relationships are obtained when $\overline{V}_B$ and $\overline{V}_T$ are used. Since such a linear relationship is predicted by using a conduction controlled model as discussed in Section 2.2.4 previously, this suggests that the conduction controlled model which is widely used in correlating data in vertical channel rewetting may also have a role in the phenomena observed in horizontal systems. However, it should be noted that the applicability will be very limited because the conduction controlled model ignores the thermohydraulic aspects of the problem. In horizontal systems, the stratification of the quench front and the hydrodynamics of the flow have a significant effect on quenching behaviour, and cannot be ignored. The limitations of the model are evident when results in Figures 8.31 through 8.33 are studied. First of all, it can be seen that results are strongly dependent on inlet flow rates and to a lesser extent on inlet water subcoolings. These dependences are not expected in the conduction controlled model. Secondly, the sputtering temperature (T_0) cannot be obtained by extrapolating the $1/\overline{V}$ curves to the x-intercept as suggested by the model. Therefore, it may be concluded that the conduction controlled model, when applied to horizontal system only gives the qualitative trends with regard to the wall temperature dependence. It is not capable of predicting the rewetting velocity for different initial and boundary conditions. Hence, a more sophisticated model has to be used. This will be discussed in the next chapter.

FIG. 8.31 INVERSE REWETTING VELOCITY ($1/\bar{V}_S$) VS WALL TEMPERATURE

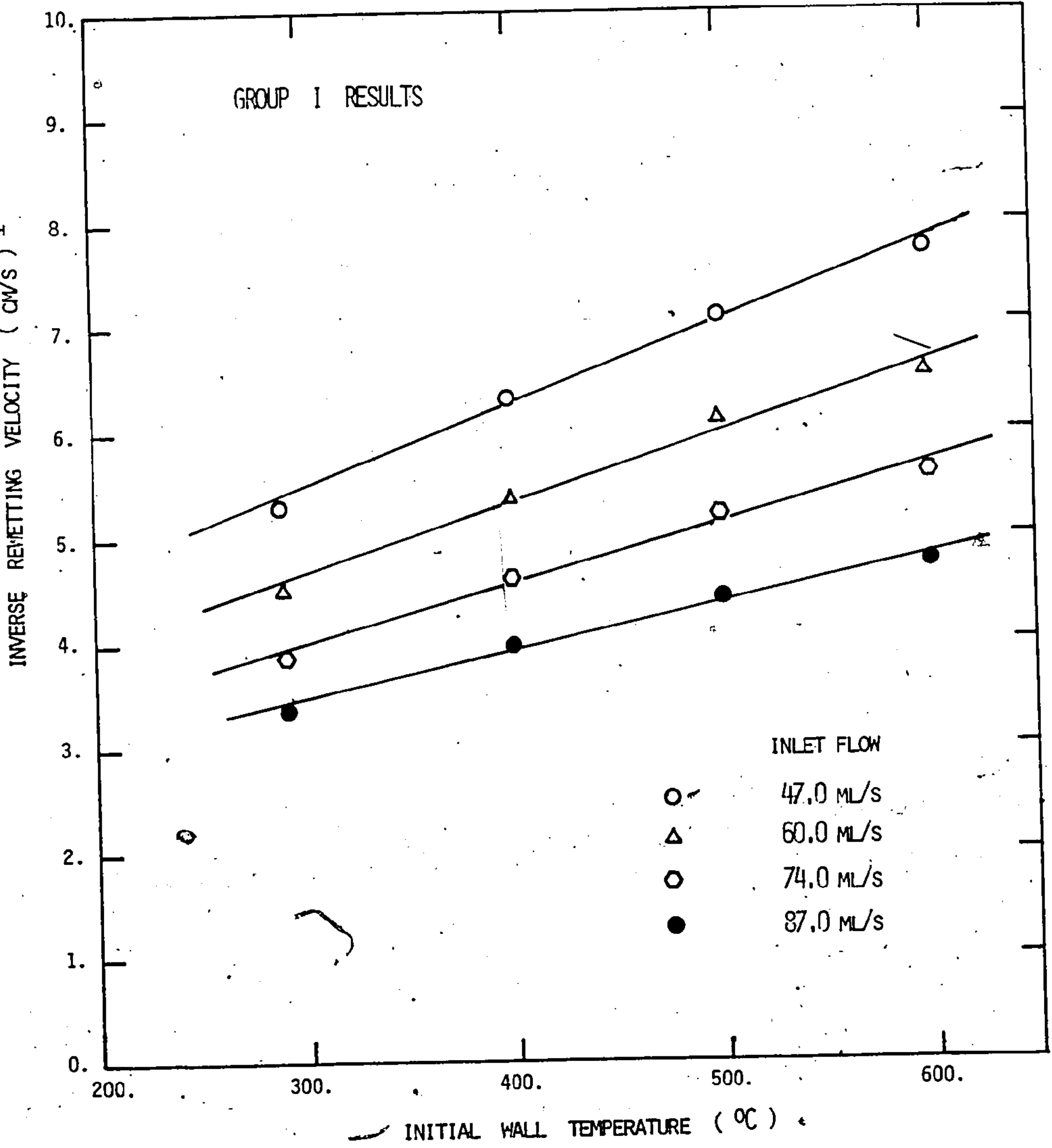

FIG. 8.32 INVERSE REWETTING VELOCITY ($1/\bar{V}_S$) VS WALL TEMPERATURE

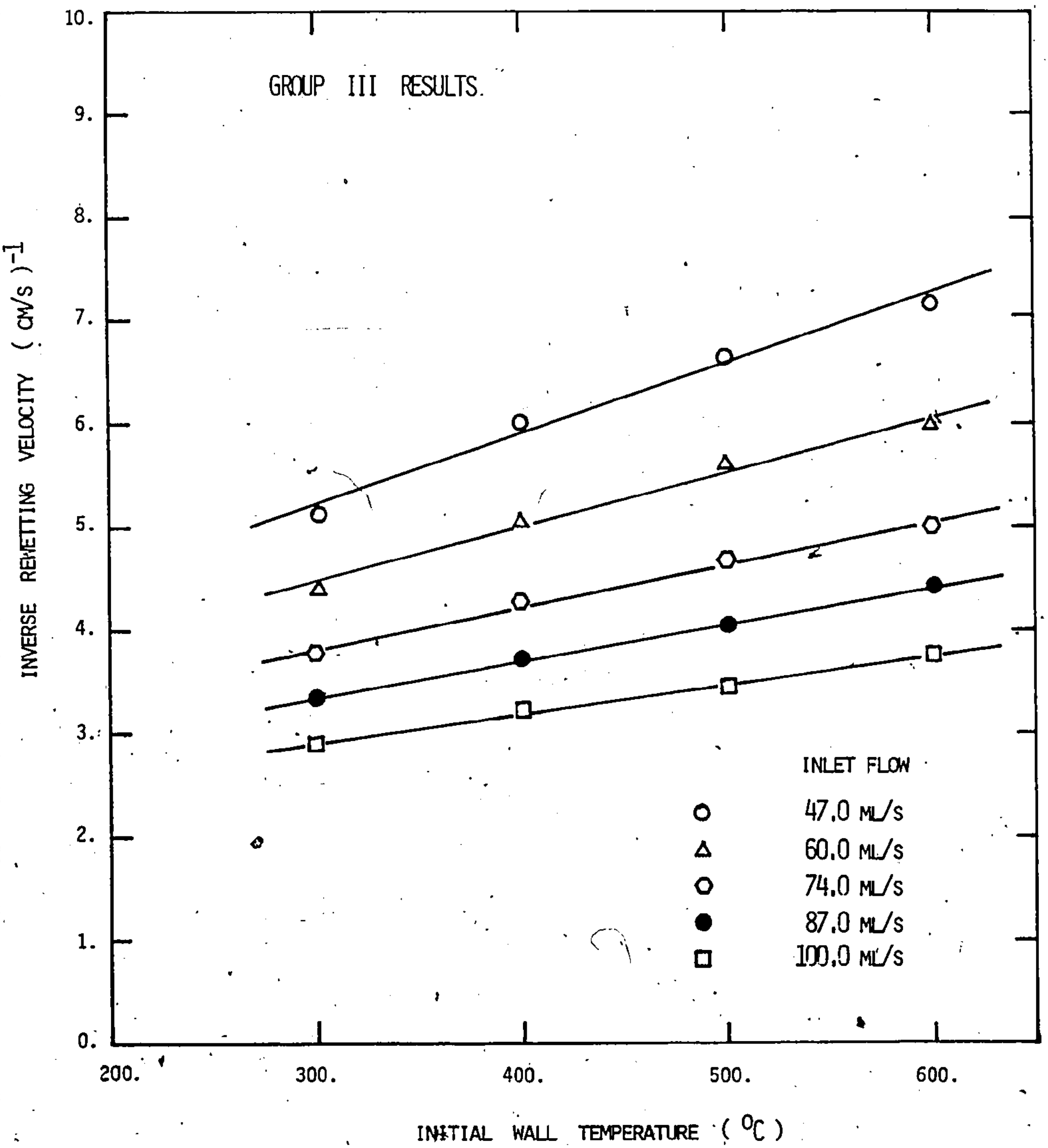

FIG. 8.33 INVERSE REWETTING VELOCITY $(1/\bar{V}_S)$ VS WALL TEMPERATURE

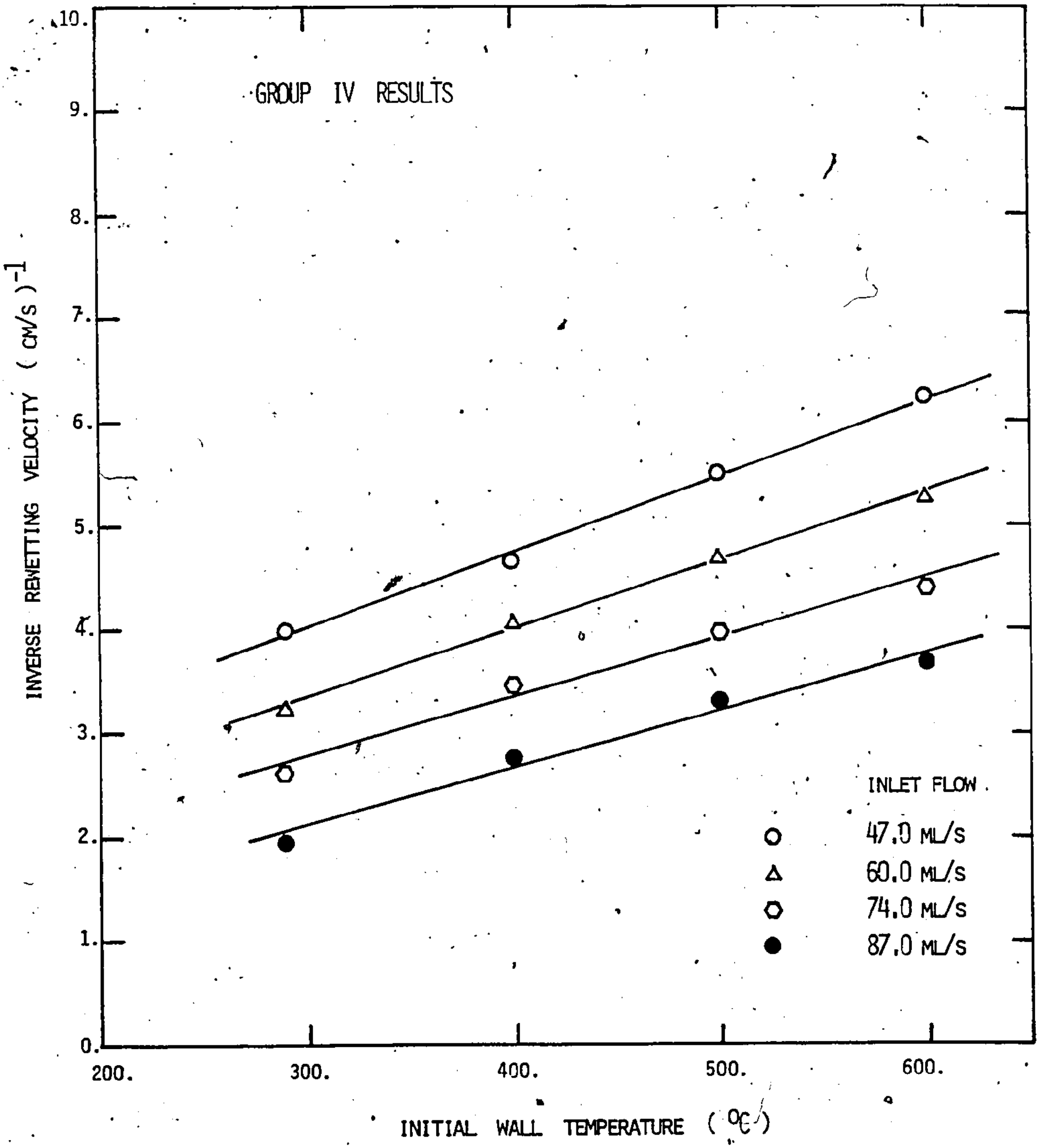

8.3.2.2 Effect of Inlet Flow Rate

For a given initial wall temperature, it can be seen that the rewetting velocity increases as inlet flow increases. This is true for all cases and is in agreement with other experiments (Yamanouchi [25], Shires et al. [27], and Duffey and Porhouse [31]). The reason for the observed effect is not clear in vertical systems. Duffey and Porthouse [31] suggested that the flow rate effect results from increasing the wet side heat transfer coefficient with higher inlet flow. This improves the rate of axial heat conduction and hence leads to a faster rewetting rate. Thompson [105] on the other hand, suggested that the inlet flow rate affects precooling in the dry side rather than heat transfer in the wet side. In the case of horizontal channels, with the rewetting model as described in section 7.3.2, it is obvious that increases in inlet flow rate increases the amount of water entrained in the "liquid tongue" and hence increases the film boiling heat transfer coefficient in the dry region. In other words, precooling may also have a significant role in horizontal systems.

An interesting phenomenon that can be readily seen in Figures 8.21 through 8.30 is that under certain conditions the rewetting velocity can actually be higher than the inlet flow velocity. The inlet flow velocity is shown in broken lines in the figures. This rather surprising result occurs when both inlet flow rate and initial wall temperature have relatively low values, for example, when $Q \leq 40$ ml/s and $T_w \leq 400°C$. The reason is quite simple. At the start of the rewetting and refilling transients, water is directed into the heated section with a constant inlet flow rate. Since the channel is dry, the flow will be stratified and the leading edge can acquire a velocity which is considerably higher than the inlet flow velocity. The process in many ways is analogous to the idealized dam break problem (Streeter [106]). This problem will be discussed in detail in the next chapter. It will suffice here to say that the velocity of the leading edge can be much higher than the inlet flow velocity for low inlet flow rates. This high leading edge velocity, together with low initial wall temperature can result in rewetting velocity higher than the inlet flow velocity. On the other hand if the wall temperature is high, the quenching process will be retarded and a "normal" rewetting velocity lower than the inlet flow velocity will be obtained. Therefore, the phenomenon is directly related to the thermohydraulic behaviour of the refilling and rewetting processes in horizontal channels.

Since the trailing edge of the refilling water always travels at the same velocity as the inlet flow in a cold, dry channel, in principle, $\bar{V}_T$, the rewetting velocity defined with respect to the quenching of the top of the channel, cannot have values higher than the inlet flow velocity from a strictly hydrodynamic point of view. This is certainly not true from the results shown in Figures 8.23 and 8.26. The same phenomenon as for $\bar{V}_B$ and $\bar{V}_S$ can be seen, although at lower inlet flow rates. This is probably because of circumferential conduction.

More interestingly, at high initial wall temperatures (e.g. T_W = 600°C), $\bar{V}_T$ behaves quite differently. It cuts through the curves of lower initial wall temperatures. In other words, it can have values higher than the corresponding cases with lower initial wall temperatures. The reason for the observed behaviour is not clear. A possible explanation is that the channel can be filled up to a level close to the top for a certain length, it is prevented from being totally quenched because the temperature at the top is still high. Since regions below the top have been quenched, when quenching begins at the top, it will move downstream rapidly and quench the length which has been held up from quenching by the high wall temperature. This will give a high rewetting velocity for the top.

In fact, the higher top rewetting velocity does not mean that the trailing edge of the quench front can travel faster than the leading edge, what it means is the trailing edge cannot propagate when the wall temperature is too high, it can be held up momentarily at the inlet region of the heated section. It tends to match up the time lag later on when conditions become favourable due to circumferential conduction as the level rises and an apparently high rewetting velocity results.

8.3.2.3 Effect of Inlet Water Subcooling

In all the vertical channel rewetting experiments, it was observed that the quench rate increases as the inlet water subcooling increases. It was suggested by Piggot and Porthouse [32] that the observed effect results from an increase in heat transfer coefficient with subcooling behind the quench front. Thompson [105] however, argued that the effect is due to an increase in the sputtering temperature with water subcooling at the rewetting front.

In the present experiment, using horizontal channels, somewhat different effects of inlet water subcooling were found. This is shown in Figures 8.34 and 8.35 which compares the average rewetting velocities for two different inlet water temperatures. It can be seen that the effect of the inlet water subcooling is not the same depending on the initial wall temperature.

FIG. 8.34 INVERSE REWETTING VELOCITY ($1/\overline{V}_B$) VS WALL TEMPERATURE

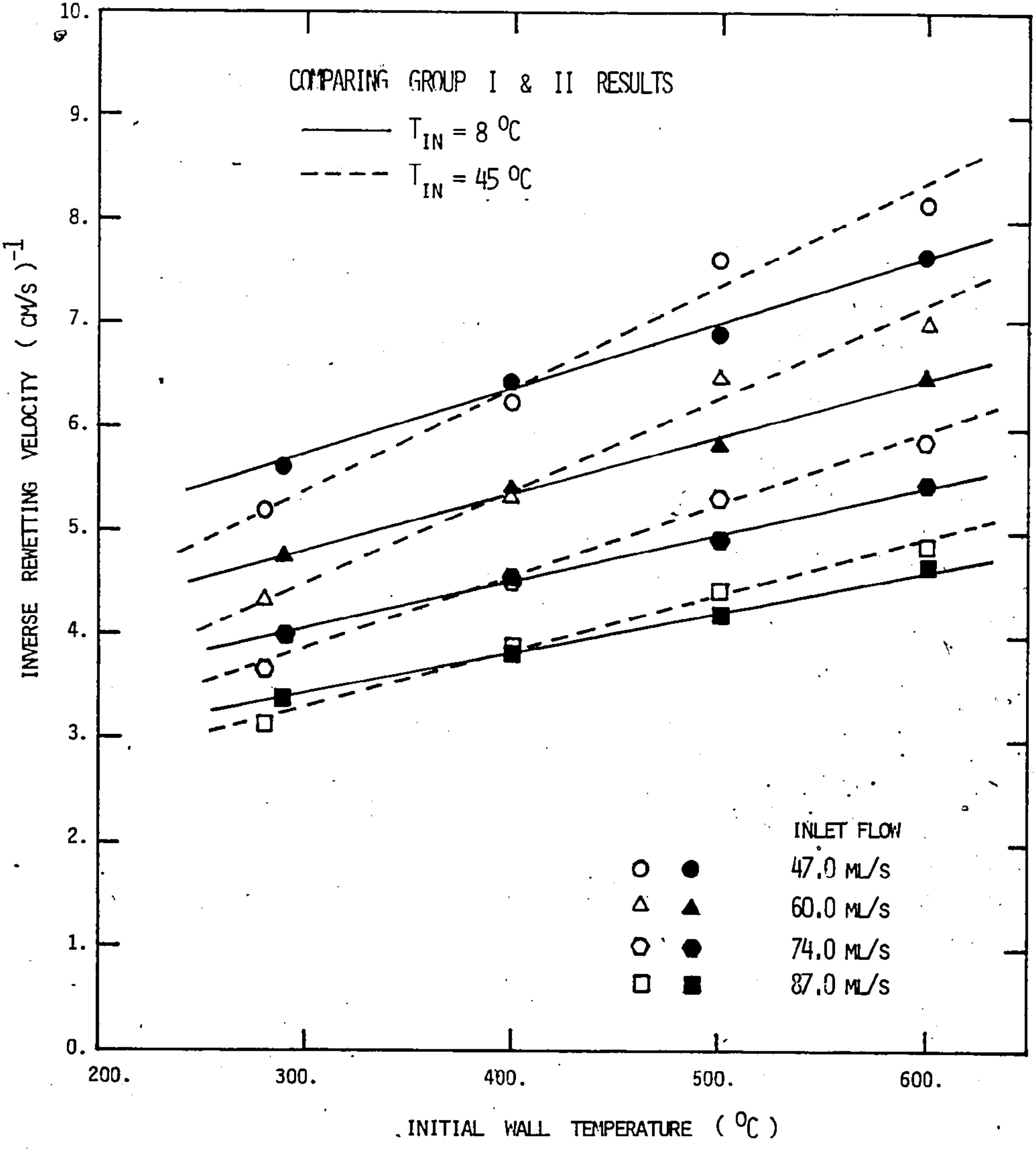

FIG. 8.35 INVERSE REWETTING VELOCITY ($1/\bar{V}_S$) VS WALL TEMPERATURE

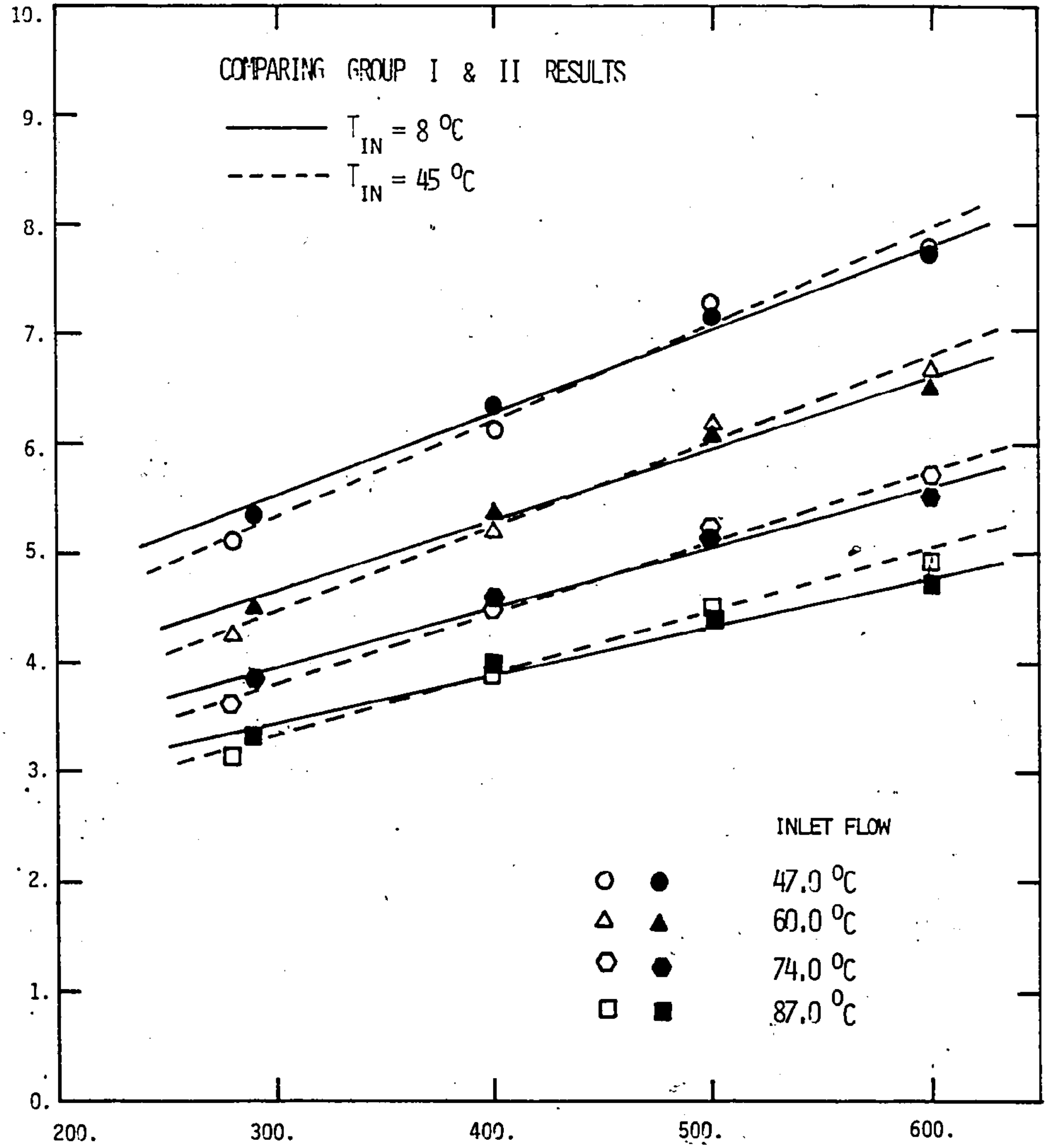

For higher wall temperatures (T_w > 400°C), the average rewetting velocities are lower for lower inlet water subcooling. The opposite is true for lower wall temperatures (T_w < 400°C). The reason for this observed effect is not clear. The stratification of the flow and the existence of an unstable stratified interface may be part of the reason.

8.3.2.4 Effect of Power Input

The effects of the power input during the transients can be seen by comparing the Group I and III results (Figures 8.21 and 8.27 and Figures 8.31 and 8.32). As is expected, with the residual power input (Group I experiments), the rewetting velocities are lower than without power input during the transients (Group III experiments). The reason is obvious, the input power retards the quench front propagation and thus results in lower rewetting velocities.

8.3.2.5 Effect of Flow Boundary Conditions

The effect of constant flow and constant pressure boundary conditions can be seen by comparing Figures 8.27 and 8.28 and Figures 8.32 and 8.33 (Group III and Group IV results respectively). It can be seen that, in general, the effect is not very strong. The average rewetting velocity tends to be slightly higher in constant flow cases.

8.3.2.6 Effect of Insulation

When the test section is insulated, heat losses to the surroundings by natural convection and radiation will be close to zero. More heat has to be removed by the quench front before it can advance. Therefore, a lower rewetting velocity is expected. This is indeed the case as can be seen by comparing the Group VI results (Figure 8.30) with Groups IV and I data (Figures 8.28 and 8.23).

8.3.2.7 Effect of Inlet Water

Building tap water was used in most of the experiments. Effect of dissolved air and minerals in tap water was investigated by using de-ionized and deaerated water in some cases. Results are shown in Figure 8.29. No difference in the average rewetting velocity was observed.

8.4 Void Fraction Profiles

The transient volume averaged void fraction measurements have proved to be extremely valuable in understanding the refilling and rewetting processes both qualitatively and quantitatively. Qualitatively, the void profiles show strong support for the simple rewetting model proposed as discussed in section 8.2. They are also very helpful in identifying flow regimes and heat transfer mechanisms involved. This will be discussed later. Quantitatively, the average rewetting velocity and entrained liquid velocity can be deduced by correlating the two void profiles obtained.

8.4.1 Average Rewetting Velocity

The rewetting velocities, as discussed in the previous section are normally calculated by noting the time delay in quenching different thermocouples along the channel. These rewetting velocities can be defined with respect to the top, mid-side and bottom of the channel respectively. In section 8.2, it was found that when the flow is high, the quench of the mid-side of the channel corresponds closely to the drop of the void fraction at that location to below 0.5. Therefore, by correlating the void profiles, and measuring the time difference between them, the average rewetting velocity can also be obtained. This is possible because the void profiles drop to zero void with a similar shape (or slopes) along the channel when it rewets. An example is shown in Figure 8.36. The time difference is defined with respect to 0.5 void. However, in general, different void fraction can be used without significant effect.

Some results are given in Figure 8.37 which compares the average rewetting velocities obtained by the two different methods. It can be seen that very good agreement results. They compare very well even at low flow rates. Since it was discussed in section 8.2 that when the flow rate is low, there is a long time delay between the quenching of the mid-side of the channel and the drop of the void fraction to below 0.5 at a given location, the good agreement of $\overline{V}_{\gamma}$ and $\overline{V}_S$ suggests that the same time delay appears in both void profiles.

From figure 8.37, it is evident that the volume averaged void fraction profiles can be used as a practical alternate way of determining the average rewetting velocity in horizontal channels. More gamma densitometers can be used if velocity variations along the channel are required.

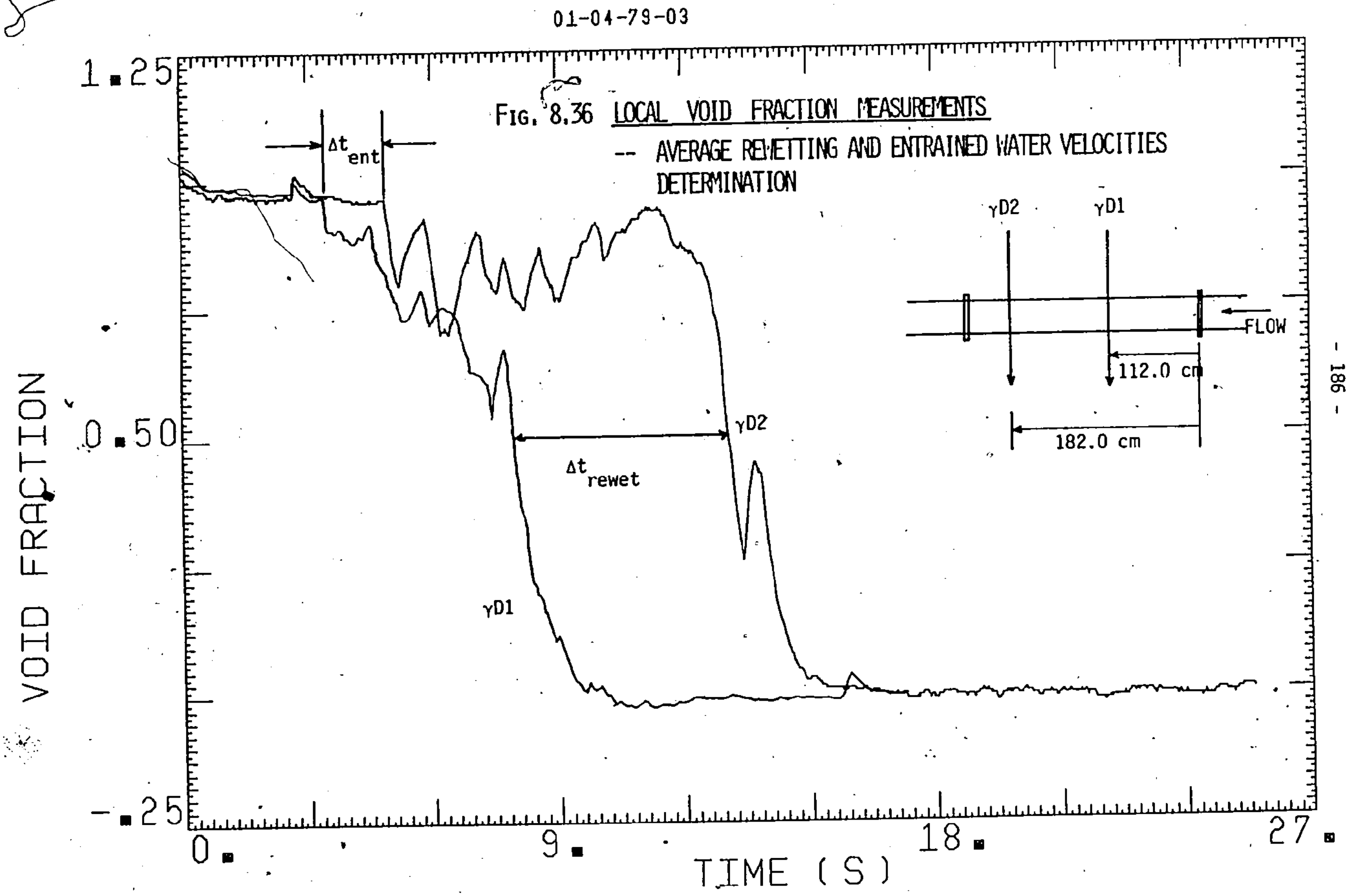

Fig. 8.36 LOCAL VOID FRACTION MEASUREMENTS
-- AVERAGE REWETTING AND ENTRAINED WATER VELOCITIES DETERMINATION

FIG. 8.37 AVERAGE REWETTING VELOCITY VS INLET FLOW RATES FOR DIFFERENT WALL TEMPERATURES

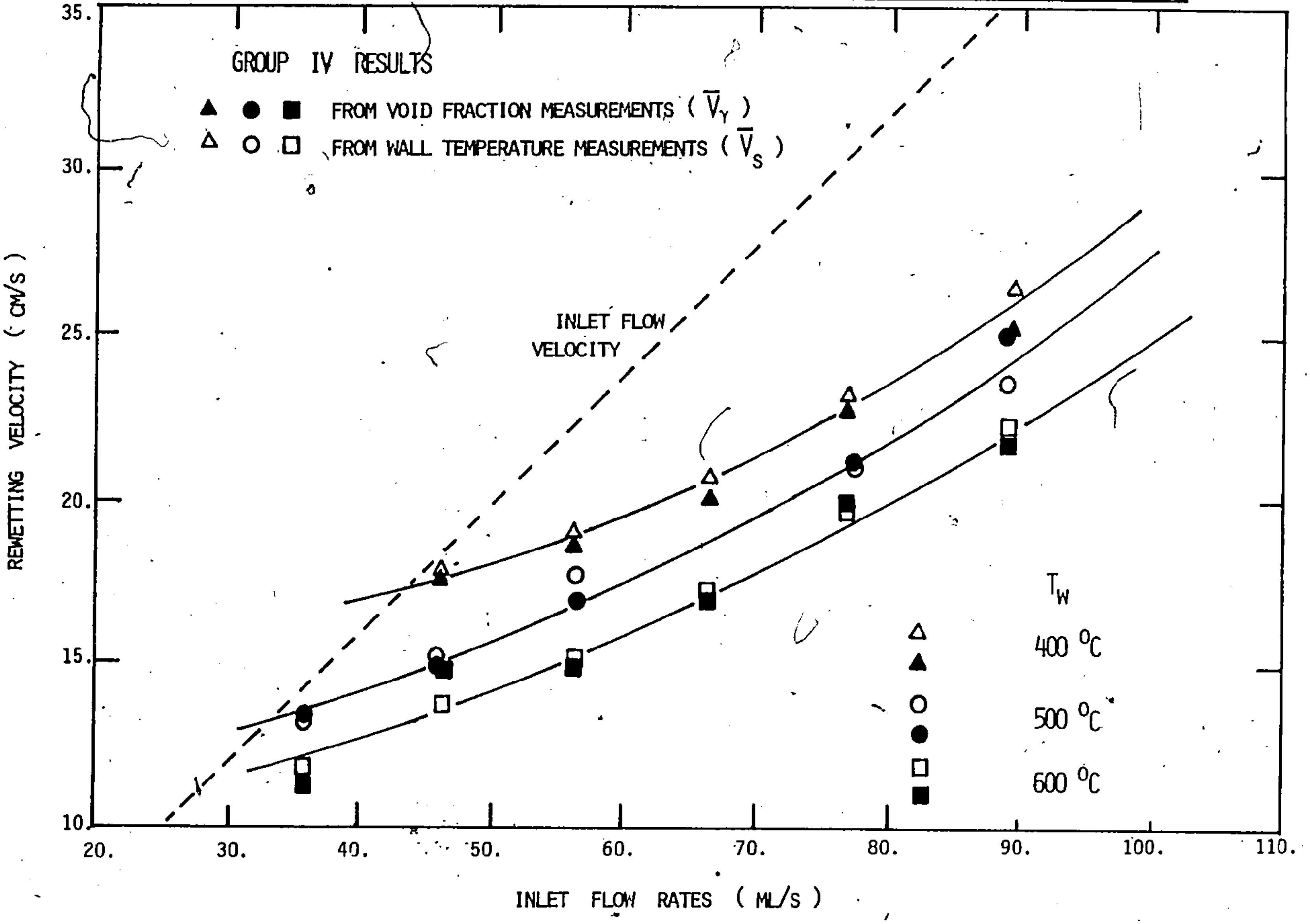

8.4.2 Average Entrained Water Velocity

At the start of the transients, when the refilling water first comes into contact with the heated channel, it cannot wet the wall because the surface temperature is much higher than the sputtering temperature. Instead, it will travel down the channel on a steam cushion and form a "liquid tongue". The velocity of the tip of this liquid tongue is defined here as the entrained water velocity. This velocity is of interest because it affects the heat transfer mechanisms downstream of the quench front. It should be noted that, before the arrival of the "liquid tongue", the channel loses heat only by natural convection, radiation and forced convection vapor flow. With the presence of the "liquid tongue" film boiling exists in the lower portion of the channel. Since film boiling is a more efficient heat transfer process in our experiments, the bottom of the channel will be precooled significantly. Therefore, the entrained liquid velocity can affect the precooling characteristics of the bottom.

The entrained water velocity can be obtained by correlating the void fraction profiles; by measuring the transit time of the water front between the two densitometers. An example is shown in Figure 8.36. The time difference (Δt_{ent}) can be obtained as shown.

Some typical results are given in Figure 8.38. It can be seen that the average entrained water velocity ($\overline{V}_{ent}$) increases with T_w, the initial wall temperature as opposed to the average rewetting velocity which decreases with T_w. $\overline{V}_{ent}$ also increases with inlet flow rate and tends to level off for high inlet flows ($Q \geq 90$ ml/s).

FIG. 8.38 AVERAGE ENTRAINED WATER VELOCITY ($\bar{V}_{ent}$) VS INLET FLOW

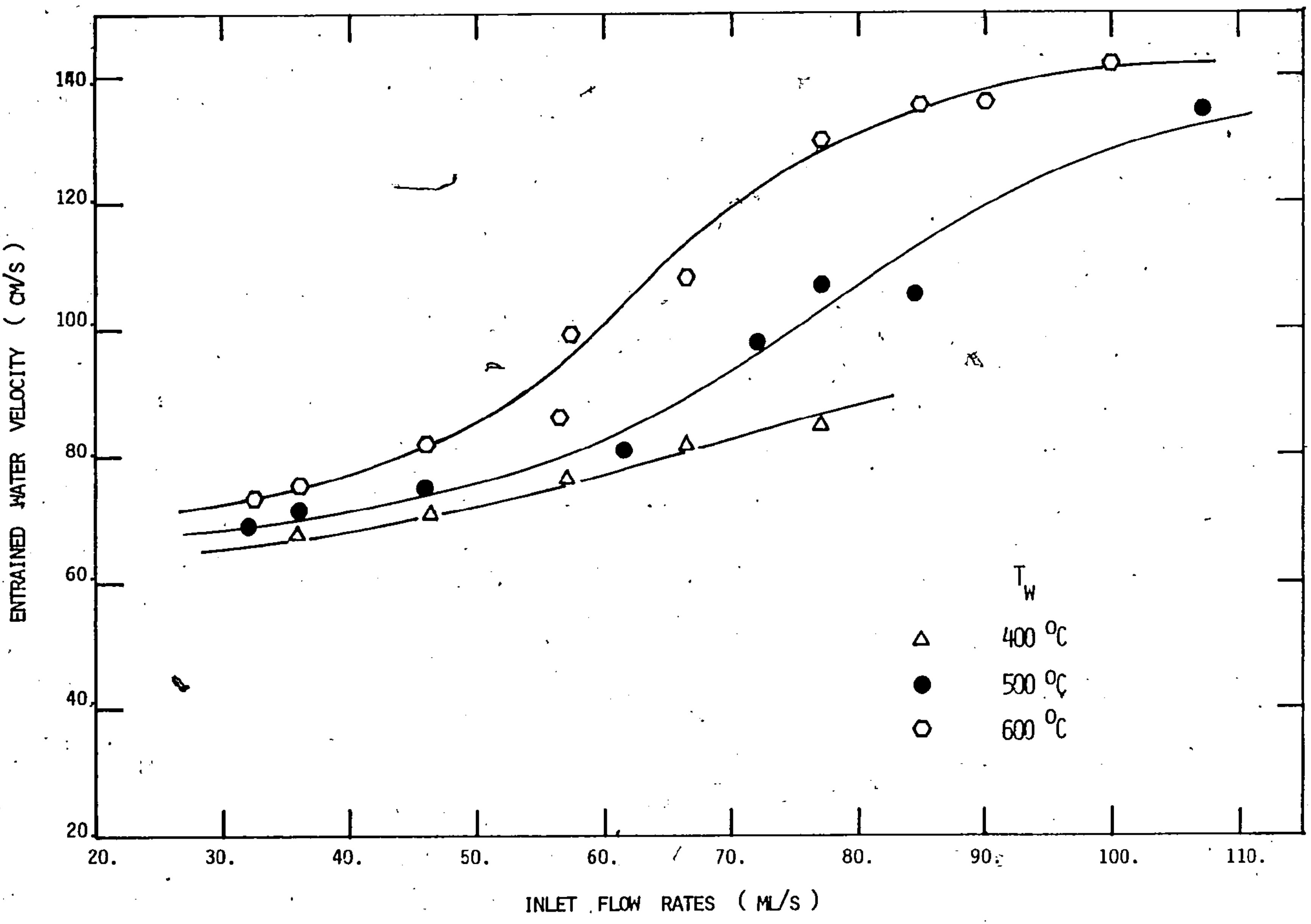

Comparing with the average rewetting velocity, the average entrained liquid velocity is much higher. This is not surprising because the "liquid tongue" moves down the channel on a vapour cushion which is practically frictionless whereas, the quench front has to cool the surface in front of it before it can propagate. When the ratios of the two velocities are taken, roughly constant values are obtained for different initial wall temperatures. This is shown in Figure 8.39.

8.5 Stratified Length of the Quench Front

The stratified length ($\bar{\ell}_s$) is the axial distance between the points where the bottom and top of the channel are quenched at a given time. It can be deduced from the surface temperature measurements. Consider the temperature traces as shown in Figure 8.40, an expression for the stratified length will be derived. We want to locate the position of the leading edge of the quench front when the top is quenched at a given location. For example, if T5T (with axial location x_5) quenches at time, t_A as shown in Figure 8.40, T5B (axial location x_5) quenches at t_B and T7B (axial location x_7) at t_c, and $t_B < t_A < t_c$, it is obvious that the leading edge is somewhere between x_5 and x_7 when T5T quenches. The position of the leading edge can be shown to be

$$x_{LE} = x_5 + \frac{x_7 - x_5}{t_c - t_B} (t_A - t_B) \tag{8-1}$$

where $(x_7-x_5)/(t_c-t_B)$ is the local rewetting velocity with respect to the quenching of the bottom. The stratified length is then given by

$$\bar{\ell}_s = x_{LE} - x_5 \tag{8-2}$$

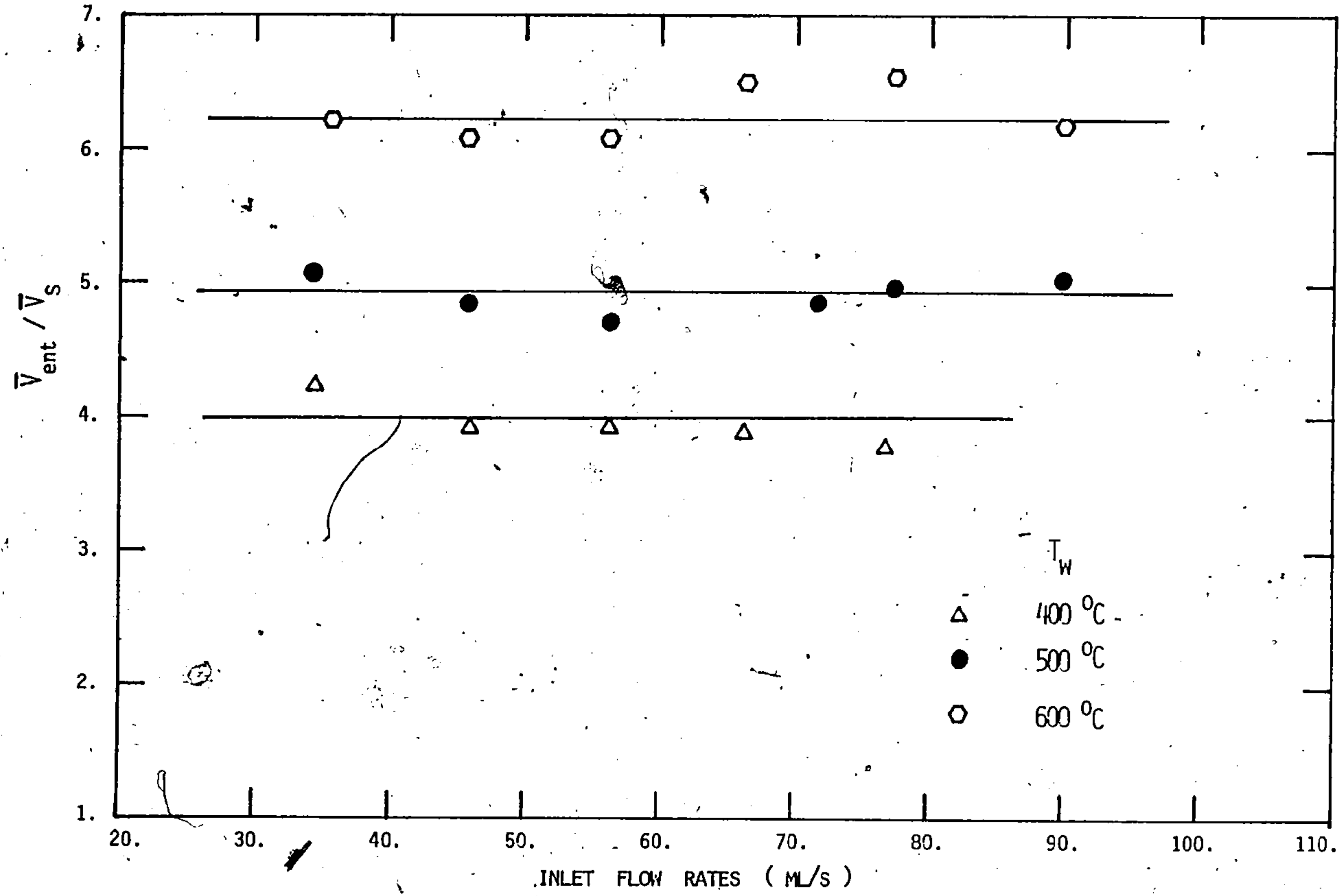

FIG. 8.39 $\overline{V}_{ent} / \overline{V}_s$ RATIO VS INLET FLOW RATES

Fig. 8.40 DETERMINATION OF STRATIFIED LENGTH (ℓ_s) OF THE QUENCH FRONT

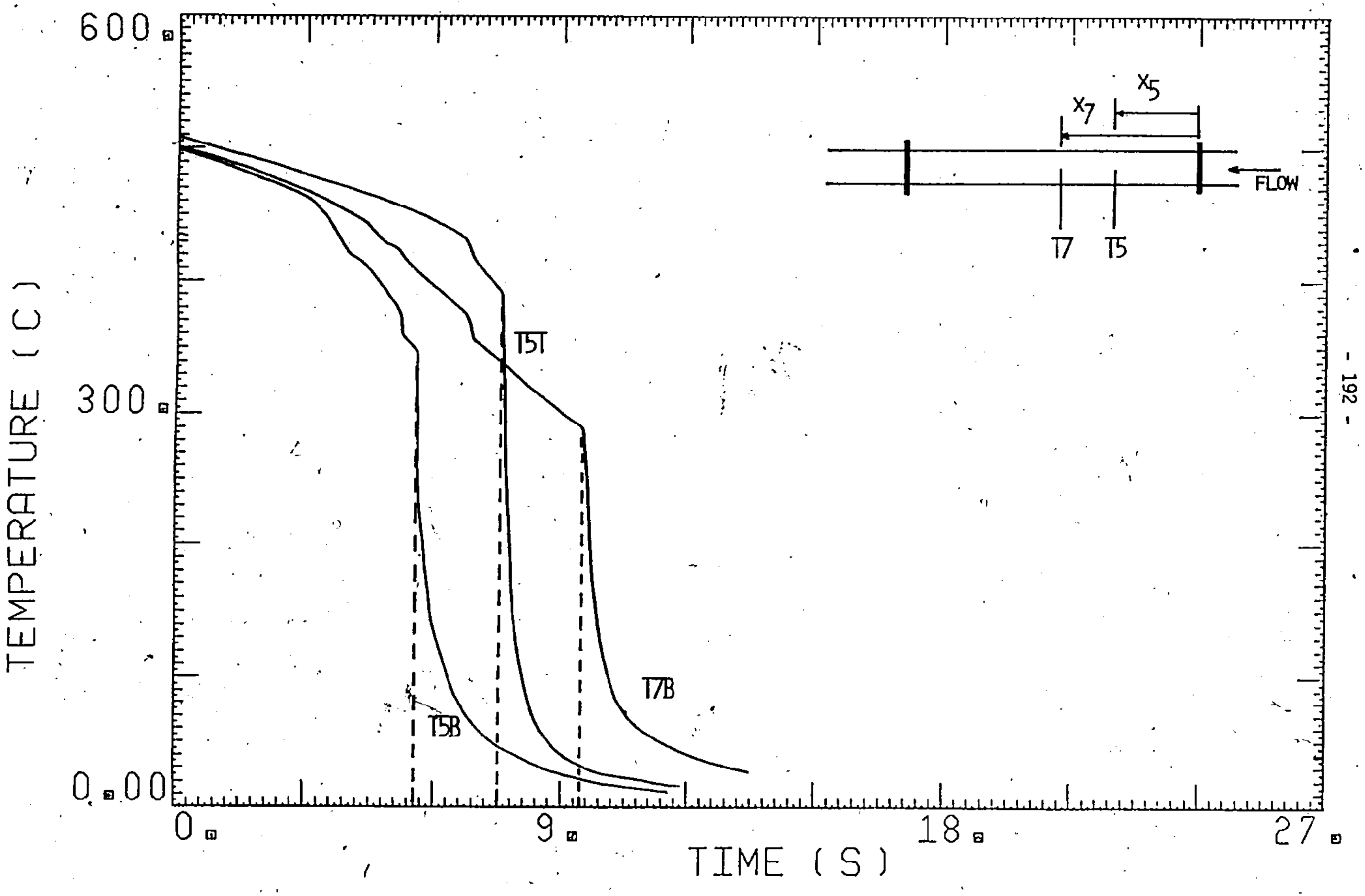

Some results are shown in Figure 8.41. The stratified length is plotted as a function of the axial distance from the inlet of the heated channel. An initial wall temperature of 500°C is used. Results for different inlet flow rates are given. In general, $\bar{\ell}_s$ is not uniform along the channel, it changes as the channel refills and rewets. There is no definite trend of variation, since $\bar{\ell}_s$ is a complicated function of local heat transfer coefficient, wall and liquid temperatures, surface condition, void fraction and other parameters. However, it tends to be more uniform along the channel for high inlet flows, for example when $Q \geq 74$ ml/s.

8.6 Heat Transfer Mechanisms and Coefficients

During the refilling and rewetting transients, heat transfer mechanisms vary along the channel, axially as well as circumferentially. In rough terms, the channel can be in one of the following stages: the pre-quench stage, the quenching stage or the quenched stage. Since the effective heat transfer coefficients are different in these stages, the rate of temperature drop in the wall will be different. This is shown explicitly in Figure 8.42. Taking for example, the temperature traces TCB and TCT, region (a)-(b) is in the pre-quench stage. (b)-(c) is in the quenching stage and (c)-(d) in the quenched stage. It can be seen that the wall temperature drops steadily in the pre-quench state (a)-(b). The steady drop in temperature is usually called "pre-cooling" or "precursory cooling". For the bottom thermocouples the pre-quench stage can be sub-divided into two stages (a)-(a') and (a')-(b). These two stages have distinctly different slopes and are associated with different heat transfer mechanisms. This will be discussed in detail later.

Fig. 8.41 STRATIFIED LENGTH OF QUENCH FRONT AT DIFFERENT AXIAL LOCATIONS

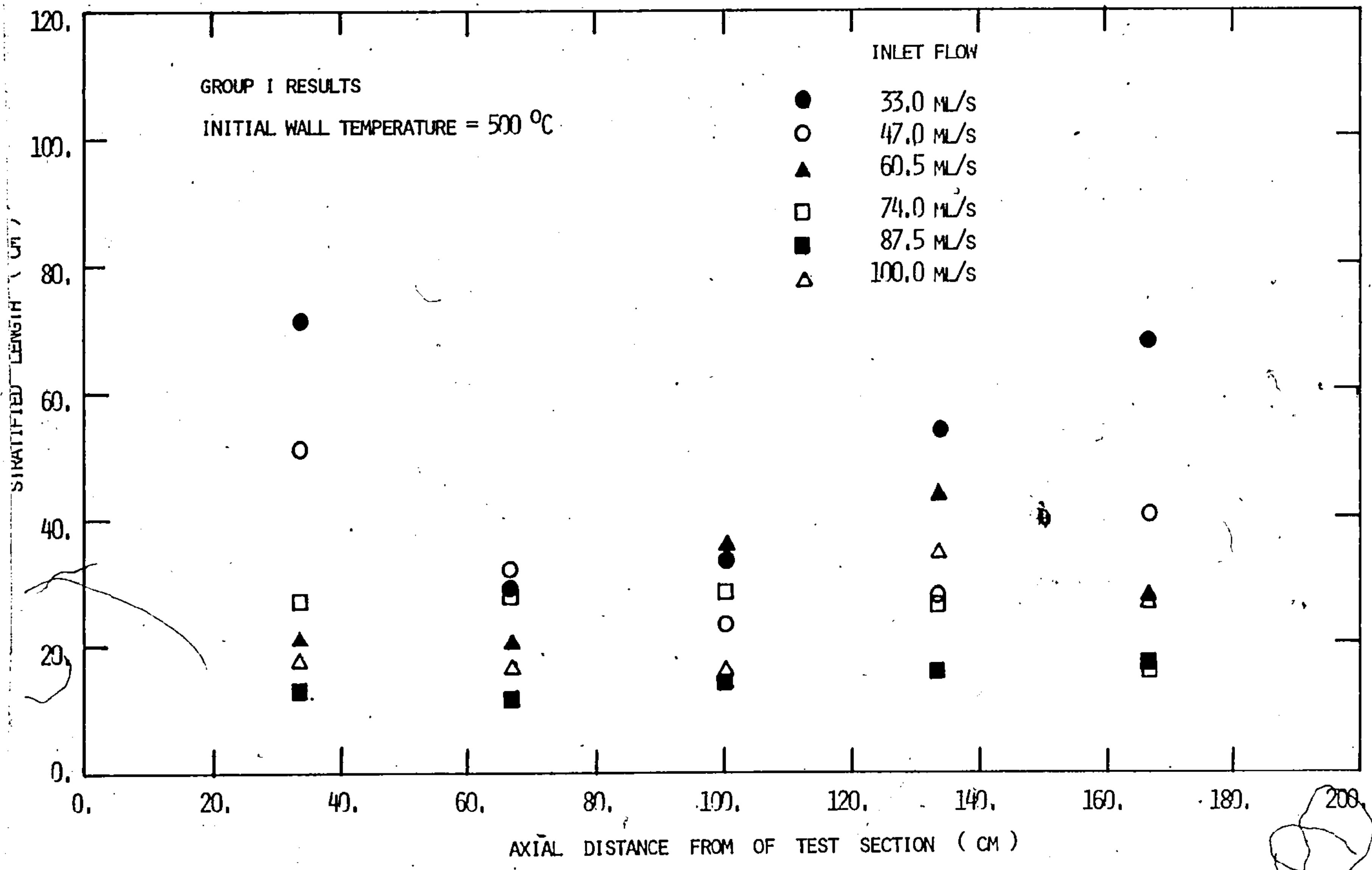

01-04-79-03

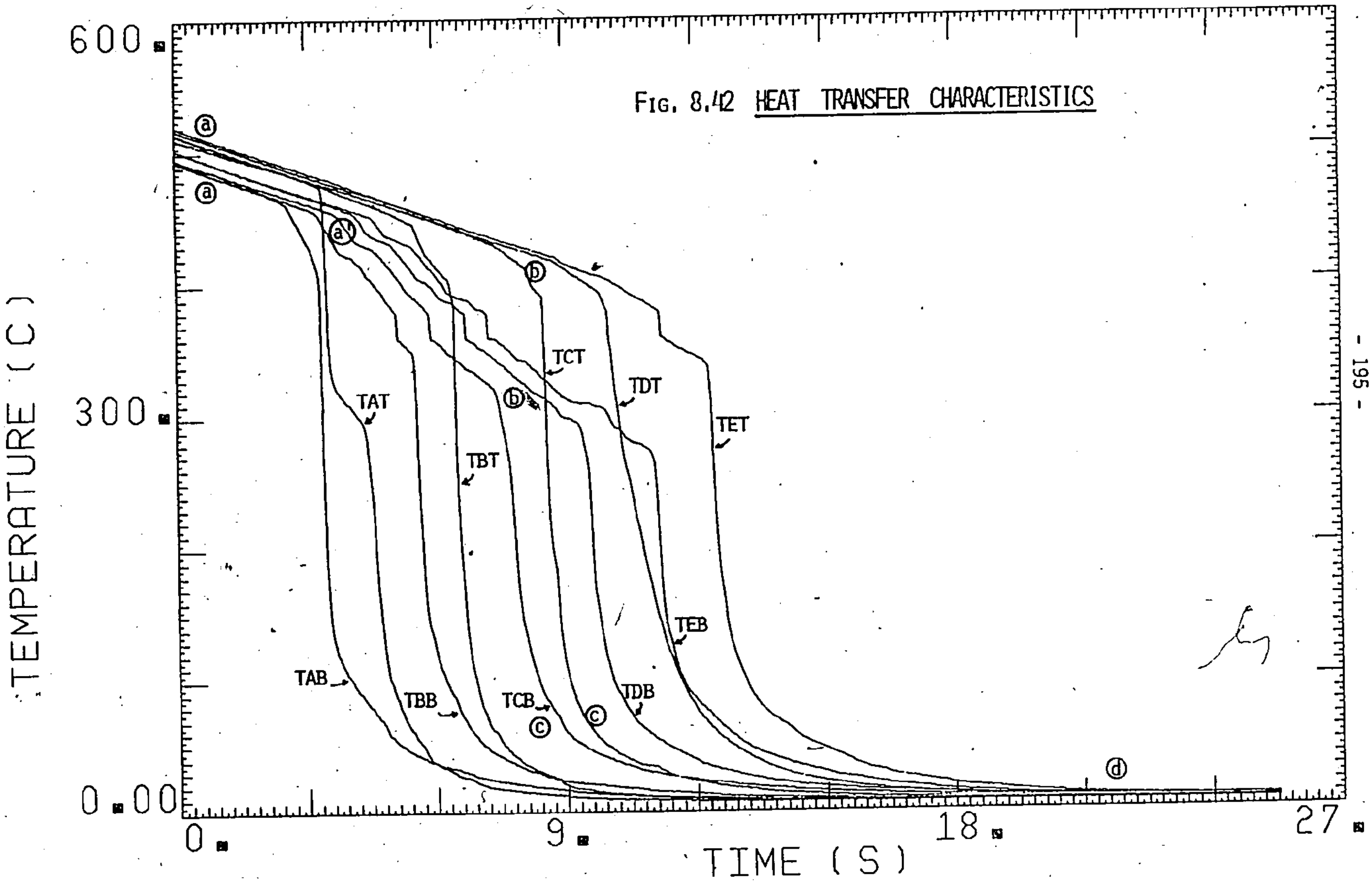

FIG. 8.42 HEAT TRANSFER CHARACTERISTICS

In the quenching stage, the wall temperature drops rapidly ~~to~~ below the liquid saturation temperature. Here an "apparent rewetting temperature" (T_A) can be defined. It is defined as the temperature below which rapid drop in wall temperature begins, i.e. the wall temperature at point (b). This same definition was also used by other workers, for example, by Groeneveld and Young [39], Lee et al. [40], and Yu et al. [51]. It should be noted that T_A is not the true rewetting (or sputtering) temperature which cannot be measured from the present experiments, rather it is the surface temperature when the heat transfer mechanism changes, resulting in a dramatic increase in the effective heat transfer coefficient. This will be discussed in Chapter 10 when a heat transfer model is proposed.

In the quenched stage, the wall temperature is below the water saturation temperature, no boiling exists and water is in contact with the surface. The heat transfer mechanism is essentially single phase forced convection. The heat transfer coefficient may then be obtained from the Dittus Boelter type of correlations.

In the pre-quench stage, the channel loses energy through a number of heat transfer mechanisms. They are (a) natural convection; (b) radiation to the surroundings (c) radiation to the steam or steam-water mixture inside the tube; (d) forced convection to steam or steam-water mixture inside the channel and (e) film boiling. The first four heat transfer processes ((a) to (d)) are fairly uniform circumferentially whereas, film boiling only affects the portion of the channel that is covered by the "liquid tongue" extending downstream from the quench front. This is precisely the reason why two regions exist in the bottom thermocouples. Region (a')-(b) is associated with film boiling. Since film boiling is a more efficient heat transfer process, a steeper slope is obtained. The point (a') marks the arrival of the "liquid tongue", therefore the entrained water velocity as defined in section 8.4.2 can be deduced from the temperature curves as well. It can be obtained by measuring the time differences between the (a') points for different bottom thermocouples. It was found that the entrained water velocity so obtained compared very well with that deduced from the void fraction profile (Figure 8.38).

It should also be noted that when the test section is well insulated, the first two heat transfer processes ((a) and (b)) will be negligible and the wall temperature will be constant in the early stage of the transients as shown in Figure 8.14.

The heat transfer coefficient in each stage can be evaluated from the transient temperature traces. In order to do that, it is necessary to know both the heat flux and the inside wall temperature. Since only the outside wall temperature is obtained experimentally, in principle, the inverse heat conduction problem has to be solved to get the inner wall temperature. The problem is very complicated and may be ill-posed. Fortunately, for thin walled tubes, the temperature difference in the radial direction across the tube wall is always negligible except at the quench front where the heat transfer coefficient is high and the temperature changes rapidly. Therefore, a uniform wall temperature can be assumed in the radial direction everywhere except in the immediate vicinity of the quench front. The local heat transfer coefficient can be evaluated as described below.

Consider the transient one-dimensional heat conduction equation in the radial direction

$$\frac{1}{\alpha}\frac{\partial T}{\partial t} = \frac{\partial^2 T}{\partial r^2} \tag{8.3}$$

where $\alpha = k/\rho C_p$ is the thermal diffusivity of the wall.

For thin walls and relatively slow transients, the radial distribution of wall temperature can be assumed to be uniform and we can approximate

$$\frac{\partial^2 T}{\partial r^2} = \lim_{\Delta r \to o} \frac{\left.\frac{\partial T}{\partial r}\right|_{r=o} - \left.\frac{\partial T}{\partial r}\right|_{r=\varepsilon}}{\Delta r} \tag{8.4}$$

where the coordinates are defined in Figure 8.43 and ε is the wall thickness. If $(\partial T/\partial r)_{r=o}$ is assumed to be zero and $\Delta r = \varepsilon$, Eq. (8.4) becomes

$$\frac{\partial^2 T}{\partial r^2} = -\frac{h}{k\varepsilon}\,(T - T_f) \tag{8.5}$$

Where h is the local heat transfer coefficient, k is the wall thermal conductivity, ε is the wall thickness and T_f is the fluid temperature.

Using Eqn. (8.5), (8.3) can be written as

$$\frac{\partial T}{\partial t} = -\frac{h}{\rho C_{p\varepsilon}}\,(T - T_f) \tag{8.6}$$

with ρ and C_p as the density and heat capacity of the wall respectively.

Assuming a constant T_f and a constant average heat transfer coefficient $(\bar{h})$ over a certain region in the temperature curve, and assuming the physical properties of the wall are constant, Eqn. (8.6) can be integrated

$$T - T_f = (T - T_f)_0\; e^{-\lambda(t-t_o)} \tag{8.7}$$

where $\lambda = \bar{h}/\rho C_{p\varepsilon}$

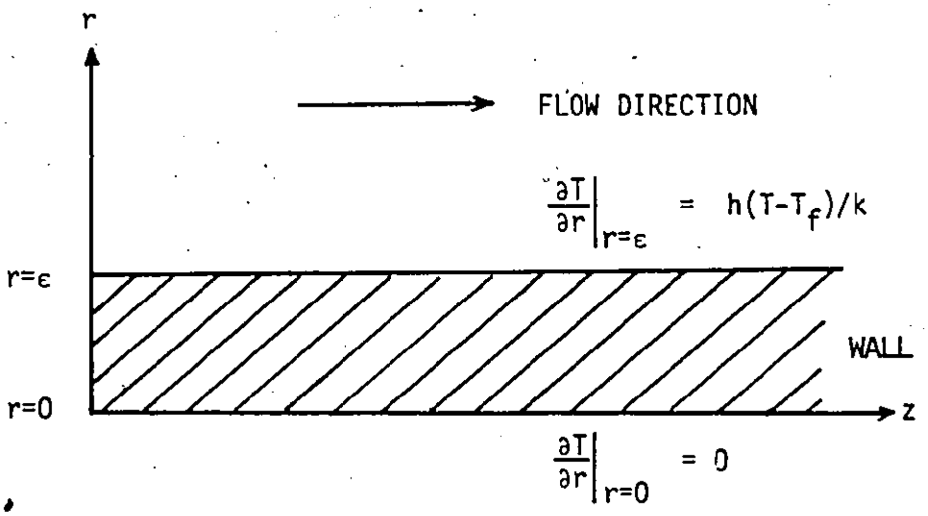

FIG. 8.43 COORDINATE SYSTEM FOR TRANSIENT RADIAL HEAT CONDUCTION CALCULATION

Taking the derivative of Eqn. (8.7), we have

$$\frac{dT}{dt} = - \lambda(T - T_f)_o \, e^{-\lambda(t-t_o)} \qquad (8.8)$$

It can be seen that Eqns. (8.6) and (8.8) are not the same. (8.6) applies locally whereas (8.8) applies over a certain region such that $\bar{h}$ is constant. When $t \to t_o$, (8.8) reduces to (8.6). Both equations can be used to evaluate the heat transfer coefficient. If (8.6) is used, $\bar{h}$ can be obtained by averaging the local heat transfer coefficients (h) over the given region in the temperature curve.

In both cases, h depends on T_f. In general h increases as T_f increases. Since T_f is not known explicitly when heat is transferred to the fluid inside the channel, some degree of uncertainty exists. In Figure 8.44, h is plotted against T_f for a given $(\partial T/\partial t)$ and T. It can be seen that the difference between the two extremes (T_f=0 and 100 ^oC) is not too large, less than 18%. Therefore, by using appropriate values for T_f under different conditions, the uncertainty resulting from the uncertainty in T_f can be relatively small.

The effective heat transfer coefficient in the pre-quench stage is shown in Figure 8.45. Two sets of data are shown. The lower one is for the stage (a)-(b) for the top thermocouples and stage (a)-(a') for the bottom thermocouples. The upper set is for the stage (a')-(b) (Figure 8.42).

Fig. 8.44 AVERAGE HEAT TRANSFER COEFFICIENT VS BULK LIQUID TEMPERATURE

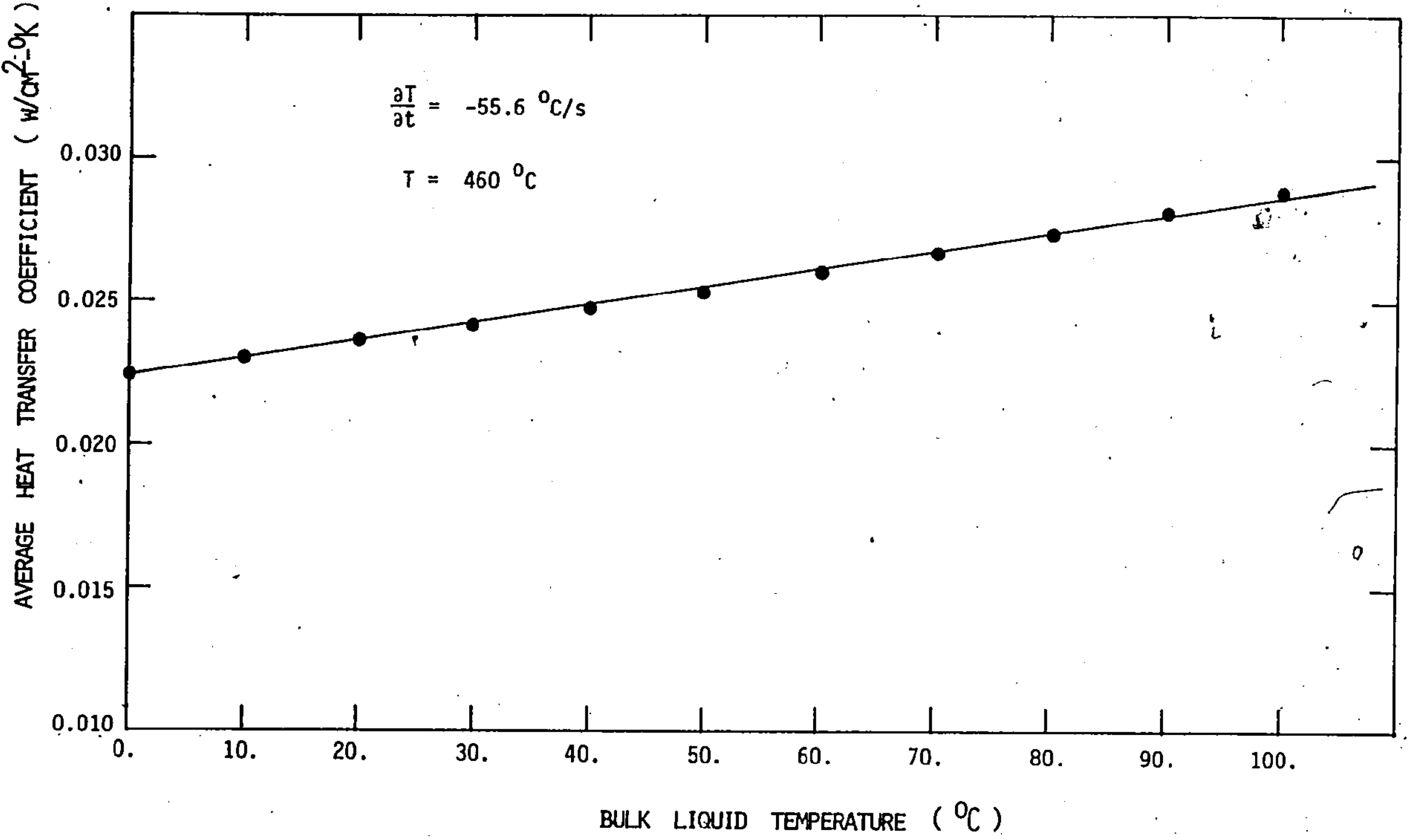

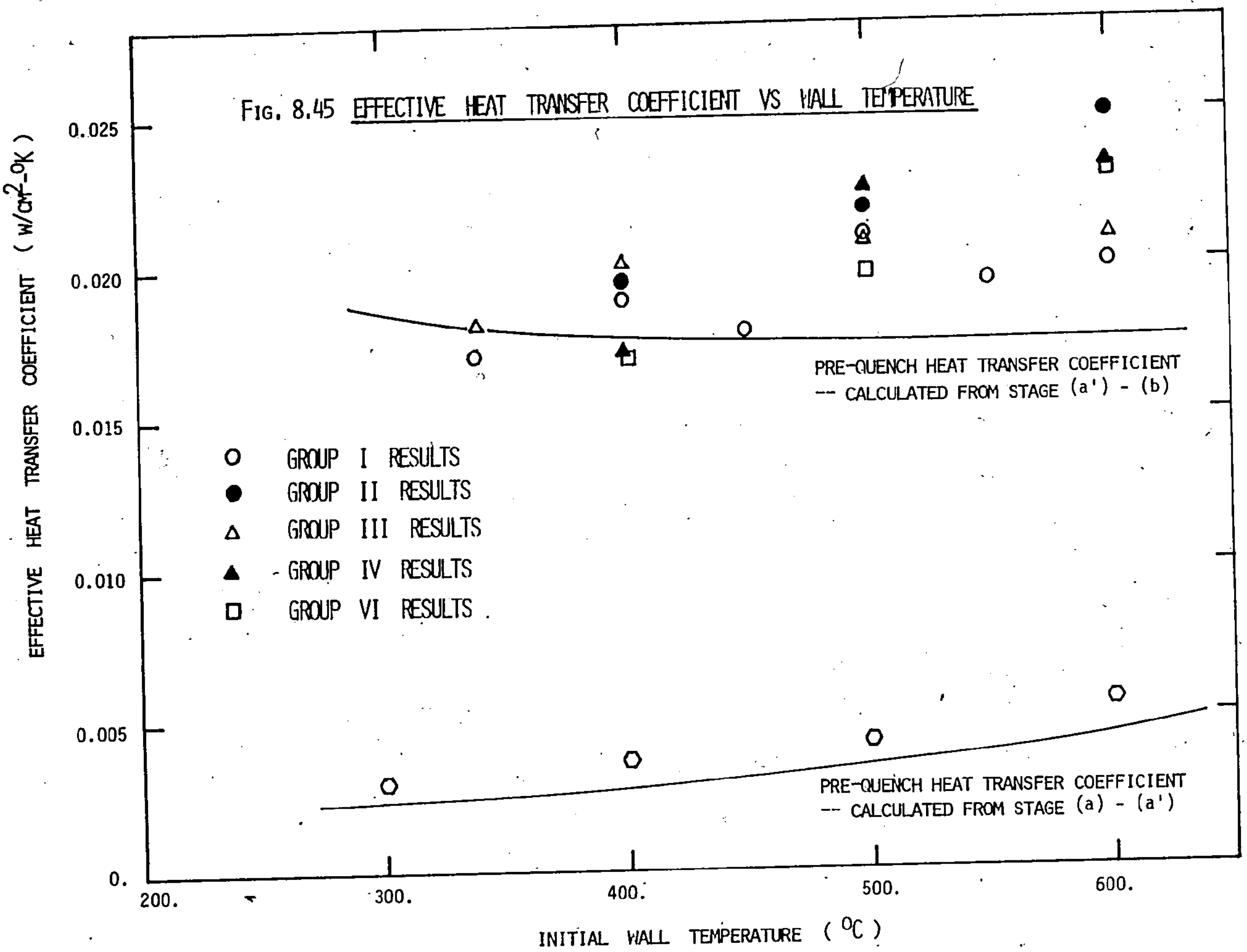

Fig. 8.45 EFFECTIVE HEAT TRANSFER COEFFICIENT VS WALL TEMPERATURE

The lower set is the effective heat transfer coefficient due to natural convection and radiation. Since a uniform wall temperature is maintained before the transients, the total heat loss by natural convection and radiation must be equal to the total power input. They are compared in Figure 8.46. The total energy loss is computed using the equation

$$Q = \bar{h} A (T - T_a), \qquad (8.9)$$

where the lower set of data in Figure 8.45 is used to obtain the effective heat transfer coefficients. A is the outside surface area of the channel. T_a is the ambient temperature.

From Figure 8.46, it can be seen that the power input and total heat loss agree very well. Therefore, we can conclude that the way in which the effective heat transfer coefficients are evaluated is adequate and gives good results.

The upper set of data shown in Figure 8.45 is the effective heat transfer coefficient resulting from the five heat transfer mechanisms mentioned previously. Film boiling is the most important mechanism. It can be seen that $\bar{h}$ increases slightly with T_w and it is not a strong function of the flow conditions.

The experimental $\bar{h}$ curves can be compared with existing results. Well known correlations are used for the different heat transfer mechanisms. They are listed below.

Fig. 8.46 TOTAL POWER INPUT AND HEAT LOSS

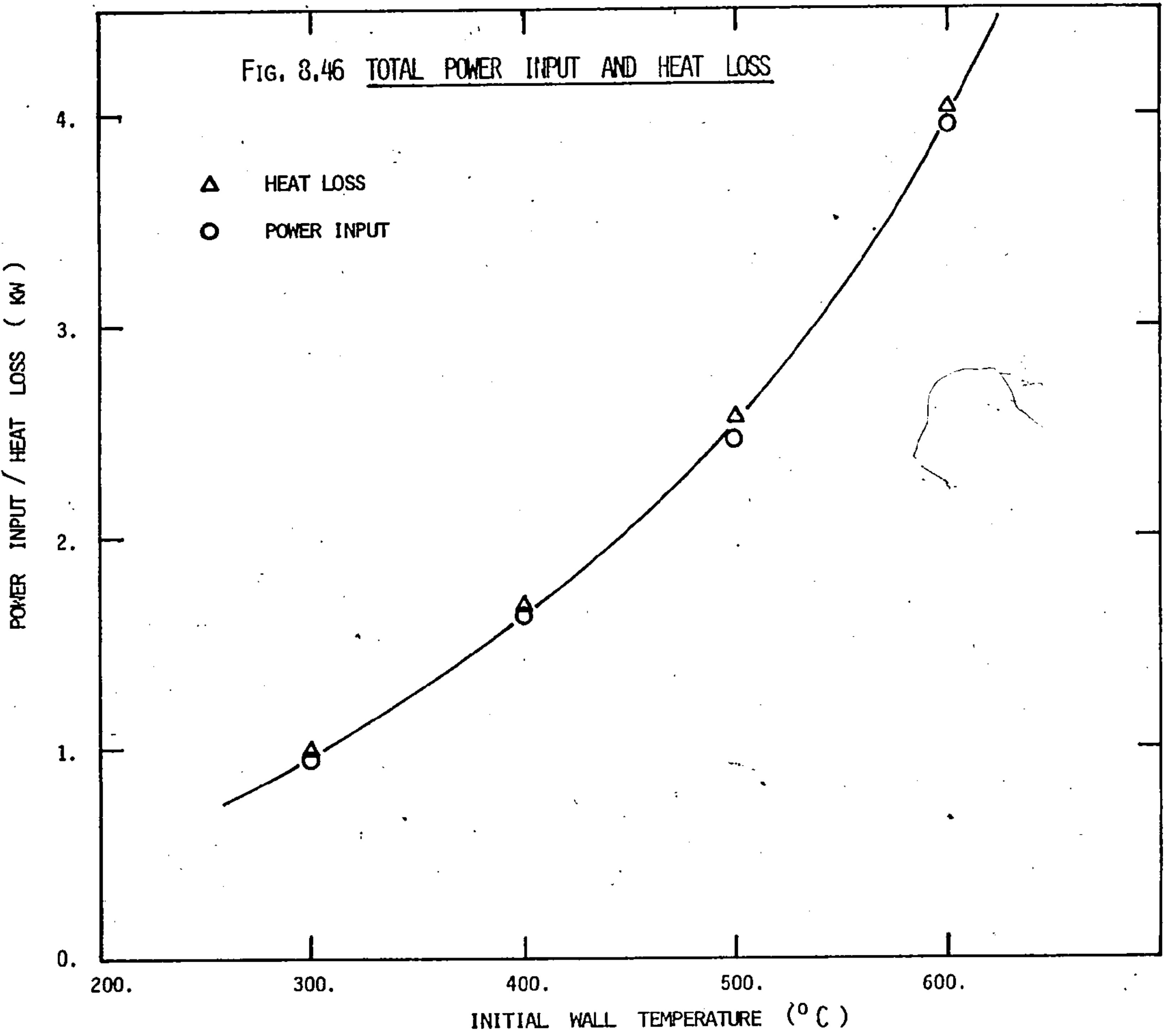

Natural Convection Heat Transfer (McAdams [107])

For a long horizontal pipe in an infinite fluid and $GrPr > 10^4$

$$h = 0.525\ (Gr\ Pr)^{0.25}\ \frac{k_f}{D} \qquad (8.10)$$

where

$$Gr\ Pr = \left(\frac{D^3 \rho_f^{\ 3}\ g\ \beta_f\ \Delta T}{\mu_f^{\ 2}}\right)\left(\frac{C_p\ \mu_f}{k_f}\right)$$

Radiation Heat Transfer (Bird et al [108])

The radiation heat transfer coefficient is calculated by assuming radiation between infinite parallel planar surface with the fluid or surrounding object acting as a perfect black body

$$h = \sigma\ e\ \left[\frac{T_w^{\ 4} - T_f^{\ 4}}{T_w - T_f}\right] \qquad (8.11)$$

where σ is the Stefan-Boltzman constant and e is the emissivity of the heating surface. $\sigma = 1.355 \times .0^{-12}$ cal/sec - cm^2 - $^{o}K^4$ and e = 0.05 - 0.7 depending on the condition of the tube surface.

Forced Convection Heat Transfer to Vapor Flow (Sissom and Pitts [109])

The Dittus Boelter equation can be used

$$h = 0.023\ \left(\frac{\rho_g\ u_g\ D_h}{\mu_g}\right)^{0.8} \frac{kg}{D_h} \qquad (8.12)$$

where the Prandlt number for steam has been taken as unity.

Film Boiling Heat Transfer (Berenson [98])

For film boiling on horizontal surfaces

$$h = 0.425\ \left[\frac{k_g^{\ 3}\ h_{fg}\ \rho_g\ g\ (\rho_f - \rho_g)}{u_g\ \Delta T\ \sqrt{\sigma / g(\rho_f - \rho_g)}}\right]^{0.25} \qquad (8.13)$$

Using the correlations given in Eqns. (8.10) through (8.13), the effective heat transfer coefficients for stages ((a)-(a') and (a')-(b)) can be calculated. They are compared with the experimentally obtained data in Figure 8.45. For the stage (a)-(a'), only natural convection and radiation heat transfer are considered in the calculations. For the stage (a')-(b), the forced convection heat transfer to the vapor flow inside the channel is not included in the calculated curve, because forced convection heat transfer depends on the vapor flow velocity which in this simplified analysis is not explicitly known. It should be noted that for high wall temperatures, this mode of heat transfer can be important and this will account for the higher heat transfer coefficient obtained experimentally. In general, the agreement between the calculated and experimental values is good for both stages. This suggests that the heat transfer mechanisms assumed are correct.

9. SIMPLIFIED TWO FLUID MODEL

(I) REFILLING OF DRY HORIZONTAL CHANNEL WITH NO HEAT TRANSFER

9.1 Simplified Two Fluid Model

From a macroscopic point of view, there are basically two mechanisms involved in the rewetting process. The first mechanism is the conduction controlled advance of the quench front. The second mechanism involves the thermohydraulic aspects of the process which can determine the quench front propagation as well. For vertical channel rewetting, the first mechanism may dominate. Thus the conduction controlled model (Section 2.2.4) has been used with some success in correlating experimental data and predicting parametric trends. However, percursor cooling effects can be very important. For horizontal channels, the thermohydraulic aspects of the process are also very important, especially the gravitational effects leading to flow stratification. These thermohydraulic aspects may be incorporated by using a simplified two fluid model. The wall effects and transient wall temperature distribution will appear as boundary conditions and through the use of appropriate heat transfer coefficients. This approach is necessary because most of the important physical mechanisms can be included in a simple model.

9.2 Mathematical Formulation

Starting with the general one-dimensional two fluid model as derived in Chapter 3, a simplified model can be obtained by making appropriate assumptions. It should be stressed again that the assumptions made must be consistent with the physical process. The set of generalized space/time averaged conservation equations is reproduced below.

Mass Conservation

$$\frac{\partial}{\partial t}\overline{\alpha_k<\rho_k>} + \frac{\partial}{\partial z}\overline{\alpha_k<\rho_k u_k>} = -\overline{<\dot{m}_k>_i} \tag{3.18}$$

Momentum Conservation

$$\begin{aligned}
&\frac{\partial}{\partial t}\overline{\alpha_k<\rho_k u_k>} + \frac{\partial}{\partial z}\overline{\alpha_k<\rho_k u_k^2>} + \overline{\alpha_k\frac{\partial<P_k>}{\partial z}} - \frac{\partial}{\partial z}\overline{\alpha_k<\tau_{zz,k}>} \\
&- \overline{\Delta P_{ki}\frac{\partial\alpha_k}{\partial z}} = \overline{\alpha_k<\rho_k F_{z,k}>} - \overline{<\dot{m}_k u_k>_i} - \overline{<\Delta P'_{ki}>_i} \\
&+ \overline{<(\hat{n}_k\cdot\overline{\tau}_z)>_i} + \overline{<(\hat{n}_{kw}\cdot\overline{\tau}_z)>_w}
\end{aligned} \tag{3.21}$$

Energy Conservation

$$\begin{aligned}
&\frac{\partial}{\partial t}\overline{\alpha_k<\rho_k(h_k + \frac{u_k^2}{2})>} + \frac{\partial}{\partial z}\overline{\alpha_k<\rho_k u_k(h_k + \frac{u_k^2}{2})>} - \overline{\alpha_k\frac{\partial<P_k>}{\partial t}} \\
&+ \overline{\Delta P_{ki}\frac{\partial\alpha_k}{\partial t}} + \frac{\partial}{\partial z}\overline{\alpha_k<q_{z,k}>} - \frac{\partial}{\partial z}\overline{\alpha_k<\hat{n}_z\cdot(\overline{\overline{\tau}}_k\cdot\vec{v}_k)>} \\
&= \overline{-<[\dot{m}_k(h_k + \frac{u_k^2}{2}) + \hat{n}_k\cdot\vec{v}_i\,\Delta P'_{ki} + \hat{n}_k\cdot\vec{q}_k - \hat{n}_k\cdot\vec{v}_k\cdot\overline{\overline{\tau}}_k]>_i} \\
&\overline{- <(\hat{n}_{kw}\cdot\vec{q}_k)>_w + \alpha_k<(\rho_k\vec{v}_k\cdot\vec{F}_k + Q_k)>}
\end{aligned} \tag{3.25}$$

where the overbar denotes time or ensemble averaging.

The equations can be simplified if the following assumptions are made:

(1) The distribution coefficients equal unity. For example

$$\langle u_k^2\rangle = \langle u_k\rangle_k^2$$

and

(2) The time average of a product equals the product of the time averaged variables, that is

$$\overline{\alpha_k\langle u_k\rangle} = \overline{\alpha}_k\overline{\langle u_k\rangle}_k$$

With these assumptions and further assuming constant liquid and vapor densities, the simplified phase conservation equations can be written as shown below. It should be noted that the constant vapor density assumption implies that the vapor is treated as essentially incompressible. This is true when the vapor velocity is much less than the sonic velocity.

Liquid Phase

$$\rho_L \frac{\partial \alpha_L}{\partial t} + \rho_L \frac{\partial(\alpha_L u_L)}{\partial z} = -\dot{m}_L \qquad (9.1)$$

$$\rho_L \frac{\partial(\alpha_L u_L)}{\partial t} + \rho_L \frac{\partial(\alpha_L u_L^2)}{\partial z}$$

$$= -\tau_L a_L + \tau_i a_i - \alpha_L \frac{\partial P_L}{\partial z} + \Delta P_{Li} \frac{\partial \alpha_L}{\partial z}$$

$$-\dot{m}_L u_i \qquad (9.2)$$

where the symbols have their usual meanings, the subscripts L and i denote the liquid phase and interface respectively. The variables are as defined in Figure 9.1 for a horizontal circular channel. P_L is the bulk liquid

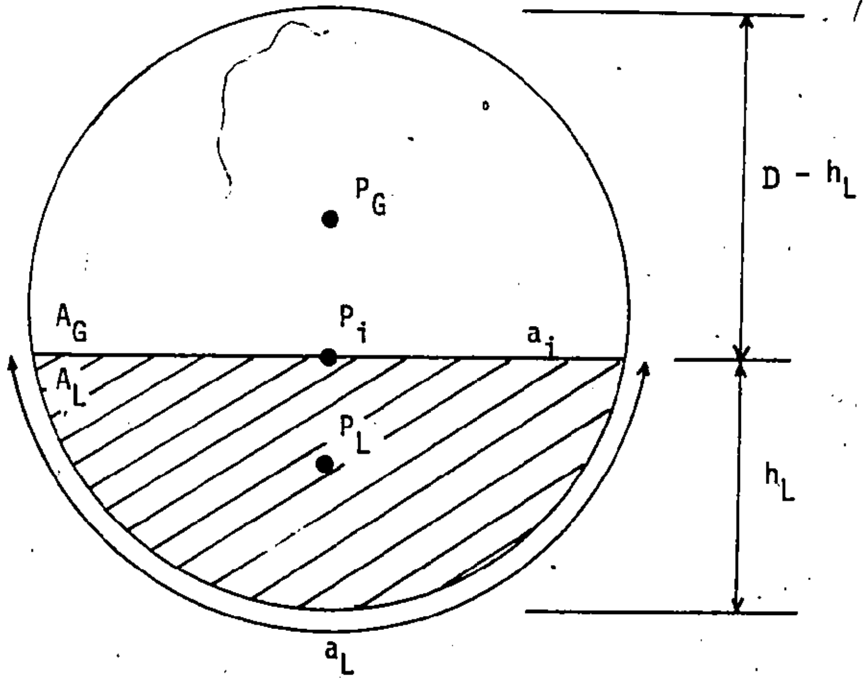

FIG. 9.1 DEFINITION OF VARIABLES IN THE SIMPLIFIED TWO FLUID MODEL FORMULATION

pressure,

$$P_L = \frac{1}{A_L} \int_{A_L} p_L \, dA \tag{9.3}$$

$$p_L = \rho_L g(h_L - y) \tag{9.4}$$

$$\Delta P_{Li} = P_L - P_i \tag{9.5}$$

In Eq. (9.2), the fluctuating part of the pressure term, $<\Delta P'_{ki}>_i$ is assumed to be zero. This is true only in stratified flow with no waves. The space and time averaging symbols for the dependent variable are omitted in the equations for simplicity. However, they should be understood to be space and time or ensemble averaged.

Since the liquid fraction (α_L) and ΔP_{Li} are functions of h_L, the liquid level, we will have

$$\partial \alpha_L = \alpha'_L \, \partial h_L \tag{9.6}$$

$$\partial \Delta P_{Li} = (\Delta P_{Li})' \, \partial h_L \tag{9.7}$$

where α_L, ΔP_{Li} and their derivatives are given below for a circular channel with a given h_L.

For $h_L \leq R$, the radius of the channel

$$\alpha_L = \frac{1}{\pi R^2} [R^2 \cos^{-1} (\frac{R-h_L}{R}) - (R-h_L)(2Rh_L - h_L^2)^{1/2}] \tag{9.8}$$

$$\alpha'_L = \frac{2}{\pi R^2} (2Rh_L - h_L^2)^{1/2} \tag{9.9}$$

$$\Delta P_{Li} = \frac{2\rho_L g}{A_L} [\frac{1}{2} (R-h_L)^2 (2Rh_L - h_L^2)^{1/2} + \frac{1}{2} R^2 (R-h_L) \sin^{-1}(\frac{R-h_L}{R})$$

$$- \frac{1}{4}\pi R^2 (R-h_L) + \frac{1}{3} (2Rh_L - h_L^2)^{3/2}] \qquad (9.10)$$

where A_L is the cross-sectional liquid flow area

$$A_L = R^2 \cos^{-1} (\frac{R-h_L}{R}) - (R-h_L)(2Rh_L - h_L^2)^{1/2} \qquad (9.11)$$

$$\Delta P'_{Li} = \frac{2 \rho_L g}{A_L^2} \{A_L . [\frac{1}{2}(3Rh_L^2 - 2R^2 h_L - h_L^3).(2Rh_L - h_L^2)^{-1/2}$$

$$- \frac{1}{2} R^2 \sin^{-1} (\frac{R-h_L}{R}) + \frac{1}{4}\pi R^2] - 2(2Rh_L - h_L^2)^{1/2} [\frac{1}{2}(R-h_L)^2 (2Rh_L - h_L^2)^{1/2}$$

$$+ \frac{1}{2} R^2 (R-h_L) \sin^{-1} (\frac{R-h_L}{R}) - \frac{1}{4}\pi R^2 (R-h_L) + \frac{1}{3}(2Rh_L - h_L^2)^{3/2}]\} \qquad (9.12)$$

For $h_L \geq R$

$$\alpha_L = 1 - \frac{1}{\pi R^2} [R^2 \cos^{-1}(\frac{h_L-R}{R}) - (h_L-R)(2Rh_L - h_L^2)^{1/2}] \qquad (9.13)$$

$$\alpha'_L = \frac{2}{\pi R^2} (2Rh_L - h_L^2)^{1/2} \qquad (9.14)$$

ΔP_{Li} and $\Delta P'_{Li}$ are identical to Eqs. (9.10) and (9.12) with

$$A_L = \pi R^2 - R^2 \cos^{-1}(\frac{h_L-R}{R}) + (h_L-R)(2Rh_L - h_L^2)^{1/2} \qquad (9.15)$$

Using (9.6) and (9.7), Eqs. (9.1) and (9.2) can be expressed in terms of h_L

$$\frac{\partial h_L}{\partial t} + u_L \frac{\partial h_L}{\partial z} + \frac{\alpha_L}{\alpha_L'} \frac{\partial u_L}{\partial z} = - \frac{\dot{m}_L}{\rho_L \alpha_L'} \tag{9.16}$$

and

$$\frac{\partial u_L}{\partial t} + u_L \frac{\partial u_L}{\partial z} + \frac{1}{\rho_L \alpha_L} [\alpha_L (\Delta P_{Li})' + \Delta P_{Li} \alpha_L'] \frac{\partial h_L}{\partial z}$$

$$= - \frac{\tau_L a_L}{\rho_L \alpha_L} + \frac{\tau_i a_i}{\rho_L \alpha_L} - \frac{1}{\rho_L} \frac{\partial P_i}{\partial z} + \frac{\dot{m}_L}{\rho_L \alpha_L} (u_L - u_i) \tag{9.17}$$

Vapor Phase

$$\rho_G \frac{\partial \alpha_G}{\partial t} + \rho_G \frac{\partial (\alpha_G u_G)}{\partial z} = \dot{m}_L \tag{9.18}$$

$$\rho_G \frac{\partial (\alpha_G u_G)}{\partial t} + \rho_G \frac{\partial (\alpha_G u_G^2)}{\partial z}$$

$$= -\tau_G a_G - \tau_i a_i - \alpha_G \frac{\partial P_G}{\partial z} + \Delta P_{Gi} \frac{\partial \alpha_G}{\partial z} + \dot{m}_L u_i \tag{9.19}$$

where subscript G denotes vapor phase and

$$\Delta P_{Gi} = P_G - P_i \tag{9.20}$$

Assuming $P_G = P_i$, that is the vapor phase density does not contribute to gravity head terms, Eq. (9.19) can be reduced to

$$- \alpha_G \frac{\partial P_i}{\partial z} = \rho_G \alpha_G \left[\frac{\partial u_G}{\partial t} + u_G \frac{\partial u_G}{\partial z}\right] + \tau_G a_G + \tau_i a_i + \dot{m}_L (u_G - u_i) \tag{9.21}$$

where Eq. (9.18) has been used in obtaining (9.21).

It should be noted that the energy equations are left out in both phases. The reason is to decouple them from the momentum and mass conservation equation in our numerical solutions. The energy equations will be solved after the hydraulic equations. The procedure is acceptable if kinetic energy terms are relatively small in the energy equation.

Substituting Eq. (9.21) into (9.17), we obtain

$$\frac{\partial u_L}{\partial t} + u_L \frac{\partial u_L}{\partial z} + \frac{1}{\rho_L \alpha_L} [\alpha_L (\Delta P_{Li})' + \Delta P_{Li} \alpha_L'] \frac{\partial h_L}{\partial z}$$

$$= - \frac{\tau_L a_L}{\rho_L \alpha_L} + \frac{\tau_i a_i}{\rho_L} [\frac{1}{\alpha_L} + \frac{1}{\alpha_G}] + \frac{\dot{m}_L}{\rho_L} [\frac{u_L - u_i}{\alpha_L} + \frac{u_G - u_i}{\alpha_G}]$$

$$+ \frac{\rho_G}{\rho_L} [\frac{\partial u_G}{\partial t} + u_G \frac{\partial u_G}{\partial z}] + \frac{\tau_G a_G}{\rho_L \alpha_G} \tag{9.22}$$

Equations (9.16), (9.18) and (9.22) can be used to obtain u_L and h_L values along the channel. These values are directly comparable to the experimental data. Hence, the validity of the model or individual assumptions can be checked in a straight forward manner.

To solve the set of equations ((9.16), (9.18) and (9.22)), the vapor generation term, $\dot{m}_L$ has to be supplied externally. This requires a knowledge of heat flux into the system and the temperature of the liquid. This in turn requires that the wall temperature be known, assuming the heat transfer coefficients can be supplied separately. The liquid and wall temperatures are obtained by solving the energy equations independent of the hydraulic equations as discussed in next chapter.

9.3 Refilling of a Dry Horizontal Channel with No Heat Transfer

Before applying the two-fluid model approach to the very complicated refilling and rewetting situation, it will be useful to first consider a relatively simple problem: the refilling of a dry horizontal channel with no heat transfer. This case highlights the hydraulic aspects of the problem.

In this simple case, we do not have to consider the vapor phase. We need only solve the liquid phase equations ((9.16) and (9.17)) which can be written as

$$\frac{\partial h_L}{\partial t} + u_L \frac{\partial h_L}{\partial z} + A \frac{\partial u_L}{\partial z} = 0 \tag{9.23}$$

and

$$\frac{\partial u_L}{\partial t} + u_L \frac{\partial u_L}{\partial z} + B \frac{\partial h_L}{\partial z} = E \tag{9.24}$$

where

$$A = \alpha_L / \alpha_L' = y_h$$

$$B = \frac{1}{\rho_L \alpha_L} \left[\Delta P_{Li} \frac{\partial \alpha_L}{\partial h_L} + \alpha_L \frac{\partial \Delta P_{Li}}{\partial h_L} \right] = g$$

$$E = \frac{\tau_L a_L}{\rho_L \alpha_L}$$

It is interesting to note that B can be simplified and reduces to the gravitational constant g for both rectangular and circular ducts. A is the ratio of flow area and free surface width. It is commonly defined as the hydraulic depth (y_h) in the open channel flows (Sissom and Pitts [110]). The set of equation is identical to the well known unsteady open channel flow equations as given by Chow [111], Henderson [112] and Liggett [113].

Equations (9.23) and (9.24) can be written in the characteristic form (Street [114] and Courant and Friedrichs [115]).

$$\frac{\partial \tilde{U}}{\partial t} + \tilde{A} \frac{\partial \tilde{U}}{\partial z} = \tilde{E} \tag{9.25}$$

with

$$\tilde{U} = \begin{bmatrix} h_L \\ u_L \end{bmatrix}; \quad \tilde{A} = \begin{bmatrix} u_L & y_h \\ g & u_L \end{bmatrix}; \quad \tilde{E} = \begin{bmatrix} 0 \\ E \end{bmatrix} \tag{9.26}$$

The characteristic directions are given by

$$\frac{dz}{dt} = u_L \pm \sqrt{g\ y_h} \tag{9.27}$$

They are the slopes of the forward and backward characteristics respectively.

The characteristic equations are obtained by multiplying Eq. (9.23) by $\sqrt{g/y_h}$ and adding and subtracting the resulting equation from Eq. (9.24),

$$[\frac{\partial u_L}{\partial t} + (u_L + \sqrt{g\ y_h})\frac{\partial u_L}{\partial z}] + \sqrt{g/y_h}\ [\frac{\partial h_L}{\partial t} + (u_L + \sqrt{g\ y_h})\frac{\partial h_L}{\partial z}] = E \tag{9.28}$$

$$[\frac{\partial u_L}{\partial t} + (u_L - \sqrt{g\ y_h})\frac{\partial u_L}{\partial z}] - \sqrt{g/y_h}\ [\frac{\partial h_L}{\partial t} + (u_L - \sqrt{g\ y_h})\frac{\partial h_L}{\partial z}] = E \tag{9.29}$$

The equations can be simplified if we introduce the Escoffier stage variable, ω, defined as (Henderson [112])

$$\omega = \int_{h_L^\circ}^{h_L} \sqrt{g/y_h}\ dh \tag{9.30}$$

where $h_L^\circ = 0$ for rectangular channels. However, for circular ducts, $y_h \rightarrow 0$ as $h_L \rightarrow 0$, therefore, a small but non-zero h_L° value should be used to prevent the integrand from going to infinity in numerical calculations. This is done for mathematical convenience and will not affect the calculated results.

From the definition of Eq. (9.30), it follows immediately that

$$d\omega = \sqrt{g/y_h}\, dh_L \tag{9.31}$$

Thus, Eqs. (9.28) and (9.29) can be written in terms of ω, the stage variable

$$\left[\frac{\partial u_L}{\partial t} + (u_L+c)\frac{\partial u_L}{\partial z}\right] + \left[\frac{\partial \omega}{\partial t} + (u_L+c)\frac{\partial \omega}{\partial z}\right] = E \tag{9.32}$$

$$\left[\frac{\partial u_L}{\partial t} + (u_L-c)\frac{\partial u_L}{\partial z}\right] - \left[\frac{\partial \omega}{\partial t} + (u_L-c)\frac{\partial \omega}{\partial z}\right] = E \tag{9.33}$$

where $c = \sqrt{g\, y_h}$ or $\sqrt{g\, \alpha_L/\alpha_L'}$ is the gravity wave velocity. This is the velocity with which a disturbance in open channel flow will move over the water surface. c is sometimes called the critical velocity. When u_L, the flow velocity is less than c, the wave from a disturbance can move upstream. When u_L is greater than c, the wave will be swept downstream and no distrubance can propagate its influence in the upstream direction. The flows are said to be subcritical ($u_L < c$) and supercritical ($u_L > c$) respectively. When u_L equals c, it is called critical flow.

9.4 Numerical Solution - The Method of Characteristics

The set of equations ((9.32) and (9.33)) is solved numerically using an explicit finite difference characteristics method. The method of characteristics (Abbot [116,117]) is chosen because it has less numerical diffusion. An explicit scheme is used because it is easier to program and because implicit schemes usually fail to represent supercritical flow so that when u_L becomes greater than c during computations, the results may be unstable unless special arrangements are made in the formulation and programming of the solution (Liggett and Cunge [118]). The other reason for choosing an explicit scheme is because the pressure wave is not considered in the present situation, the time step size is not limited by the very high sonic speed. Therefore, there is no real advantage in having an implicit scheme.

The time step size will, of course, be still limited by the gravity wave speed,

$$\Delta t \leq \min\left\{\frac{\Delta z}{|u_L+c|}, \frac{\Delta z}{|u_L-c|}\right\} \tag{9.34}$$

which is the Courant consideration as given by Isaacson and Keller [119] and Δz is the mesh size.

Since c can be large in closed conduit flows, small time steps may have to be used when the conduit is nearly full. Typical time step sizes used in the present case is about 0.005 second. This value is acceptable because the experiments last less than 20 seconds in general.

The method of characteristics is a semigraphical method. Its basic principle is to fill the (z,t)-plane with characteristics so that the dependent variables are defined at the intersections. The method is accurate but formulation and programming can be difficult and tedious. Simpler methods have thus been developed, notably the Hartree method (Fox [120]) and the method used by Stoker [121]. Stoker's method is particularly simple, the characteristic equations are solved explicitly using a fixed grid. The explicit finite difference characteristic method used here is based on the Stoker's method, though some modifications had to be made. The formulation is extended to include supercritical flows.

The fixed finite difference grid used in the computation is shown in Figure 9.2. The time step size, Δt, must be chosen small enough in relation to Δz (Eq. (9.34)) so that the points such as P will fall within the appropriate domains of determinacy relative to the points used (L,M,R) in calculating the solution at P (Stoker [121]). The domain of determinacy is the region included within the forward characteristic from L and the backward characteristics from R. That is, points outside the range L-R (the domain of dependency of P) will have no influence on the solution at P.

With the dependent variables known at points L, M and R, values at point P can be calculated by replacing the time and space derivatives in Eqs. (9.32) and (9.33) by the following difference quotients

$$\frac{\partial u_L}{\partial t} = \frac{U_P - U_M}{\Delta t} \; ; \quad \frac{\partial \omega}{\partial t} = \frac{\omega_P - \omega_M}{\Delta t} \tag{9.35}$$

$$\frac{\partial u_L}{\partial z} = \frac{U_M - U_L}{\partial z} \; ; \quad \frac{\partial \omega}{\partial z} = \frac{\omega_M - \omega_L}{\Delta z} \tag{9.36}$$

in Eq. (9.32) and

$$\frac{\partial u_L}{\partial z} = \frac{U_R - U_M}{\Delta z} \; ; \quad \frac{\partial \omega}{\partial z} = \frac{\omega_R - \omega_M}{\partial z} \tag{9.37}$$

in Eq. (9.33). The reason for using different difference quotients for Eqs. (9.32) and (9.33) is because (9.32) is associated with the forward characteristic whereas (9.33) with the backward characteristic. The coefficients of the derivatives, $(u_L \pm c)$ and the function E are evaluated at the point M by Stoker. However, it was found that very poor mass

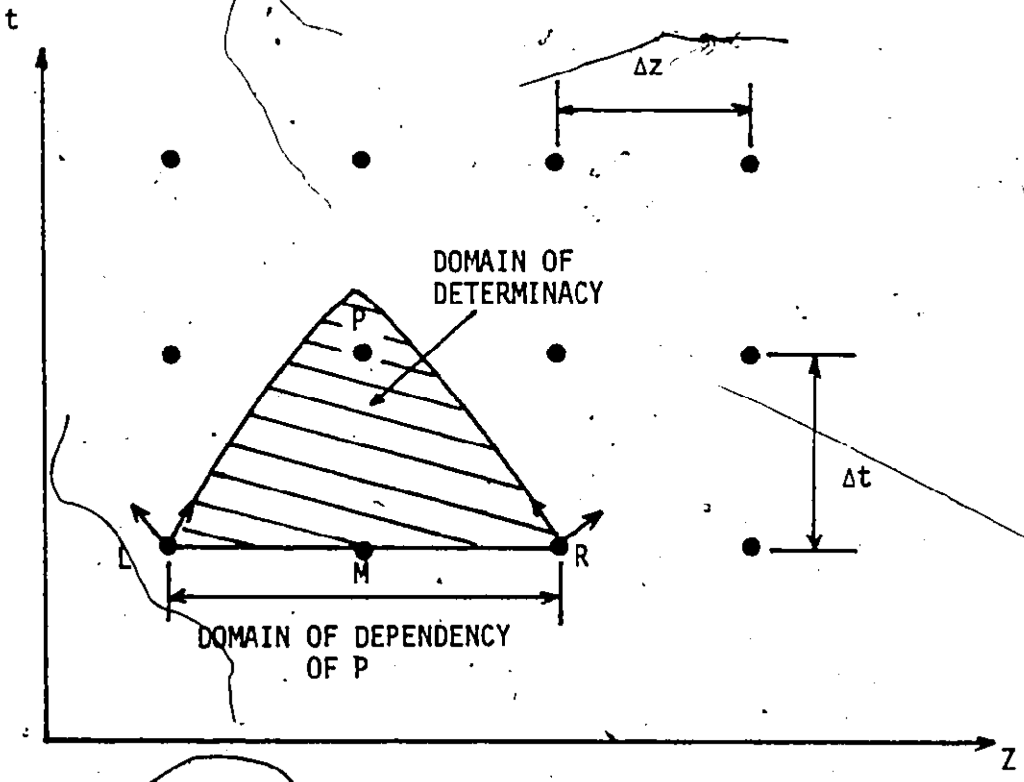

FIG. 9.2 FINITE DIFFERENCE GRID USED

conservation results. In the present numerical scheme, $(u_L \pm c)$ are evaluated at the points where the characteristics originate, i.e. an upwind characteristic finite difference scheme. For example, $(U + c)_L$ is used in Eq. (9.32) and $(U - c)_R$ in Eq. (9.33) for subcritical flows. E is always evaluated at point M. With this modification, mass can be conserved to within 3% using 30 nodes. The convergence of the numerical scheme will be discussed later.

Substituting Eqs. (9.35) to (9.37) into (9.32) and (9.33), and solving for U_p and ω_p, we have for subcritical flows, i.e. $(U + c)_L > 0$ and $(U - c)_R < 0$.

$$\omega_p = -\frac{\Delta t}{\Delta z}[(U + c)_L(U_M - U_L) - (U - c)_R(U_R - U_M)$$

$$+ (U + c)_L(\omega_M - \omega_L) + (U - c)_R(\omega_R - \omega_M)] + \omega_M$$

and

$$U_p = -\frac{\Delta t}{\Delta z}[-E_M\,\Delta z + (U + c)_L(\omega_M - \omega_L) - (U - c)_R(\omega_R - \omega_M)$$

$$+ (U + c)_L(U_M - U_L) + (U - c)_R(U_R - U_M)] + U_M \qquad (9.39)$$

For supercritical flows, i.e. $(U - c)_R > 0$, no backward characteristic exists at point R, the other characteristic will have to come from M or M'. Two cases have to be distinguished as shown in Figure 9.3.

(a) If flow at M is subcritical, i.e. $(U - c)_M < 0$, a point M' $(z_M < z_M' < z_R)$ will be chosen such that $(U - c)_{M'} < 0$ constitutes the backward characteristic and P is included in the domain of determinacy defined by the range L-M'. The dependent variables at M' can be obtained

FIG. 9.3 FORWARD AND BACKWARD CHARACTERISTICS

(A) SUBCRITICAL FLOW

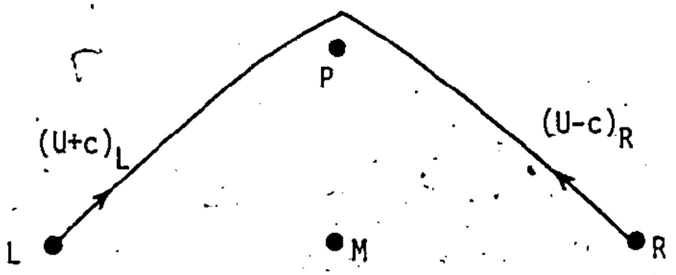

(B) SUPERCRITICAL FLOW

(1) SUBCRITICAL AT M

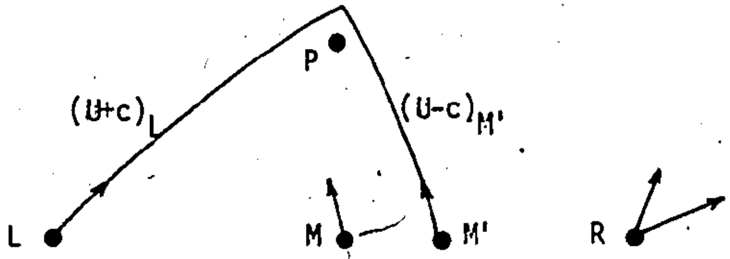

(2) SUPERCRITICAL AT M

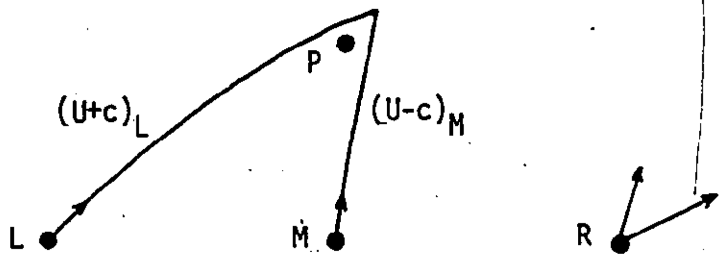

by interpolation between M and R. We define

$$D\omega = (U - c)_{M'} (\omega_R - \omega_{M'})$$

$$DU = (U - c)_{M'} (U_R - U_{M'}) \qquad (9.40)$$

(b) If flow at M is supercritical, $(U - c)_M > 0$ constitutes the other characteristic and we define

$$D\omega = (U - c)_M (\omega_M - \omega_L)$$

$$DU = (U - c)_M (U_M - U_L) \qquad (9.41)$$

ω_P and U_P will then be given by

$$\omega_P = - \frac{\Delta t}{\Delta z} [(U+c)_L (U_M-U_L) - DU + (U+c)_L(\omega_M-\omega_L) + D\omega] + \omega_M \qquad (9.42)$$

$$U_P = - \frac{\Delta t}{\Delta z} [-E_M \Delta x + (U + c)_L (\omega_M - \omega_L) - D\omega$$

$$+ (U + c)_L(U_M - U_L) + DU] + U_M \qquad (9.43)$$

It should be noted that the technique is about first order accurate (Liggett and Cunge [118]), and care must be taken to make sure that P always lies within the domain of determinacy for a given range L-R so that the convergence condition is satisfied.

In general, the technique works as follows. Starting at $t = 0$ with the dependent variables U, ω and c defined at all the grid points, U and ω at the next time step can be calculated using Eqs. (9.38) and (9.39) or Eqs. (9.42) and (9.43). The c values at each grid points are then obtained using the equation $c = \sqrt{g\, y_h}$ where y_h is related to

ω through Eq. (9.30). The new U, ω and c values are then used as starting values for the next time step computation.

The treatment of boundary conditions will now be described (Liggett and Cunge [118]). The number of conditions specified on a boundary must equal the number of characteristics originating at that boundary. The possible boundaries are shown in Figure 9.4. In cases (a) and (b), one boundary condition is required. In the upstream boundary (Case (a)), the condition is used with the equation along the backward characteristic (R-Q) to obtain the other dependent variable at Q. At the downstream boundary, (Case (b)), it is used with the equation along the forward characteristic (L-Q). In case (c), both dependent variables must be specified at the boundary and in case (d), no boundary condition is needed. The dependent variables at Q' for case (d) are given by Eqs. (9.42), (9.43) and (9.41). That is, Q' can be treated as an interior point. The dependent variables at the boundary can be obtained by interpolating between L-Q'. In case (a), the equation along the backward characteristic is used (Eq. (9.33)) that is

$$\left[\frac{U_Q - U_M}{t} + (U - c)_R \frac{U_R - U_M}{\Delta z}\right] - \left[\frac{\omega_Q - \omega_M}{\Delta t} + (U - c)_R \frac{\omega_R - \omega_M}{\Delta z}\right] = E_M \quad (9.44)$$

If ω_Q is specified, U_Q will be given by

$$U_Q = \Delta t \left[E_M + \frac{\omega_Q - \omega_M}{\Delta t} + (U - c)_R \frac{\omega_R - \omega_M}{\Delta z} - (U - c)_R \frac{U_R - U_M}{\Delta x}\right] + U_M \quad (9.45)$$

FIG. 9.4 POSSIBLE BOUNDARIES

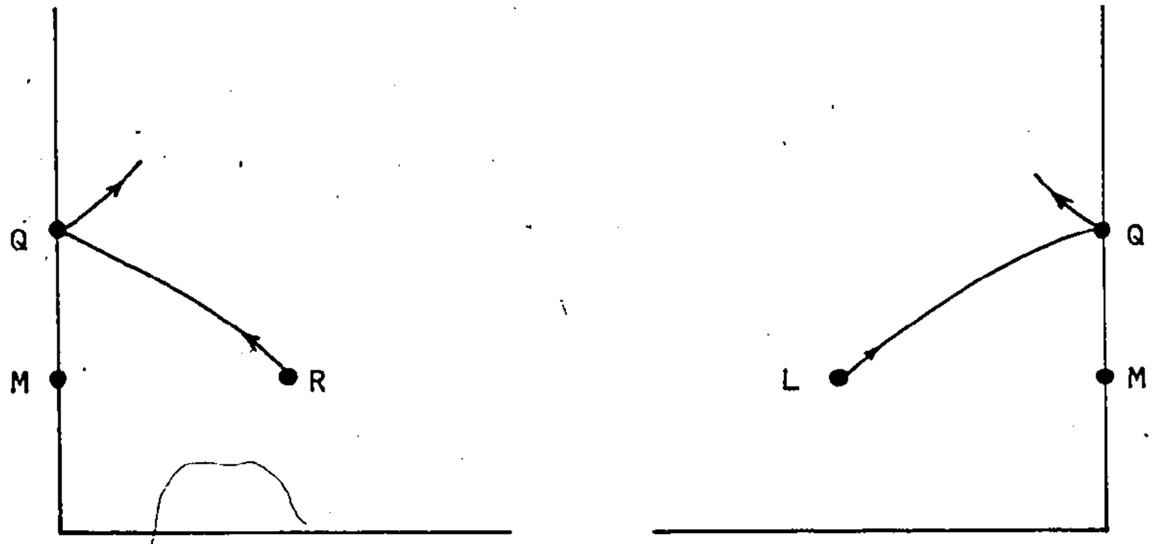

(A) INLET BOUNDARY
— SUBCRITICAL FLOW

(B) EXIT BOUNDARY
— SUBCRITICAL FLOW

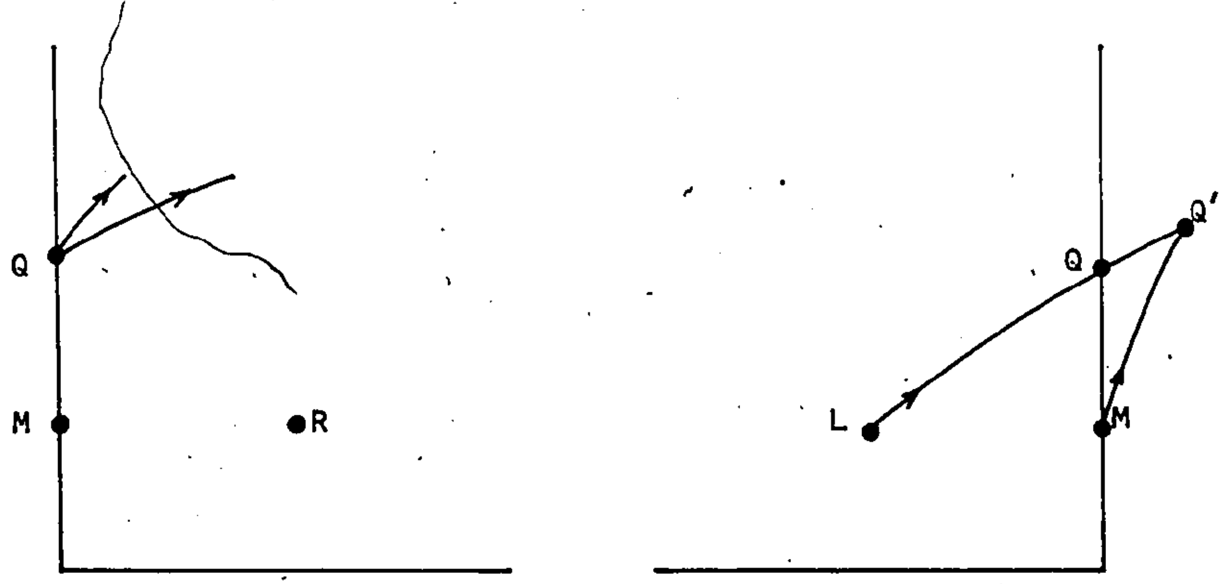

(C) INLET BOUNDARY
— SUPERCRITICAL FLOW

(D) EXIT BOUNDARY
— SUPERCRITICAL FLOW

Likewise, if U_Q is given as the boundary condition, ω_Q can be obtained from Eq. (9.44). Other boundary conditions can also be applied, for example, given inlet flow rates.

In case (b), the equation along the forward characteristic will be used (Eqs. (9.32)),

$$\left[\frac{U_Q - U_M}{\Delta t} + (U + c)_L \frac{U_M - U_L}{\Delta z}\right] + \left[\frac{\omega_Q - \omega_M}{\Delta t} + (U + c)_L \frac{\omega_M - \omega_L}{\Delta z}\right] = E_M \quad (9.46)$$

Again, ω_Q (or U_Q) can be obtained if U_Q (or ω_Q) is given as a boundary condition.

A computer code called WAVEST has been developed. It solves numerically the relatively simple problem of refilling with no heat transfer using the explicit finite difference characteristic method described above. Results will be discussed and compared with experiments in Section 9.6.

9.5 Frictional Resistance in Developing Open Channel Flow

In order to solve Eqs. (9.32) and (9.33), the functional dependence of the right hand side of the equations must be known. In the present case

$$E = \frac{\tau_L \, a_L}{\rho_L \, \alpha_L} \quad (9.47)$$

where τ_L is the shear stress, a_L is the liquid contact surface area per unit volume and α_L is the liquid fraction. Both a_L and α_L are functions of h_L, the water level. For a circular channel, expressions for α_L are given by Eqs. (9.8) and (9.13) in Section 9.3. a_L can be shown to be

$$a_L = \frac{2R\cos^{-1}((R-h_L)/R)}{R^2\cos^{-1}((R-h_L)/R) - (R-h_L)(2Rh_L-h_L^2)^{1/2}} \tag{9.48}$$

for $h_L \leq R$ and

$$a_L = \frac{2\pi R - 2R\cos^{-1}((h_L-R)/R)}{\pi R^2 - [R^2\cos^{-1}((h_L-R)/R) - (h_L-R)(2Rh_L-h_L^2)^{1/2}]} \tag{9.49}$$

for $h_L \geq R$.

Expression for τ_L in developing open channel flow will now be derived.

The form of τ_L in developing or unsteady flow is not well understood. However, for steady, non-uniform flow in open channels, τ_L can be shown to have the following form (Henderson [122])

$$\tau_L = \rho_L\, g\, R_h\, S_f \tag{9.50}$$

where R_h is the hydraulic mean radius which is the ratio of the flow area to the wetted perimeter. S_f is the friction or energy slope.

In order to interpret Eq. (9.50), we need information on τ_L. By analogy with pipe flow, dimensional analysis leads to the result

$$\tau_L = k\, \rho_L\, u_L^2 \tag{9.51}$$

where k is a dimensionless constant.

Substituting Eq. (9.51) into (9.50), we obtain the Chezy equation for open channel flows

$$u_L = C\sqrt{R_h S_f} \tag{9.52}$$

where $C = \sqrt{g/k}$ is called the Chezy coefficient.

The Chezy coefficient may be expected to depend, like the Fanning coefficient, on the surface roughness, Reynolds number and the shape of the channel. By inference from pipe flow friction factor, C can be written as

$$C = \sqrt{2g/f} \tag{9.53}$$

where f is the Fanning friction factor. This inference is allowable provided that the channel parameters are in the same range normally found in pipe work and covered in pipe experiments.

Substituting C into Eq. (9.52) and then into (9.51), we obtain

$$\tau_L = \frac{1}{2} \rho_L \ f \ u_L^2 \tag{9.54}$$

This is identical to the shear stress given in pipe flows. For smooth channels, f may be given by the Blasius equation

$$f = 0.0791/Re^{0.25} \tag{9.55}$$

The shear stress has been derived for steady, non-uniform flow in open channels (Eq. (9.54)). However, for developing flows, for example, the refilling of a dry horizontal channel, the result may not be applicable. Physically, one would expect that τ_L be larger when filling a dry duct, because the refilling front has to set up the boundary layer as it advances. A simple mechanistic model which is capable of estimating τ_L during the refilling process will be desribed below.

Let us consider the filling of a dry horizontal channel as shown in Figure 9.5. Because of the transverse gravitational effect, the refilling

FIG. 9.5 FILLING OF A DRY HORIZONTAL TUBE

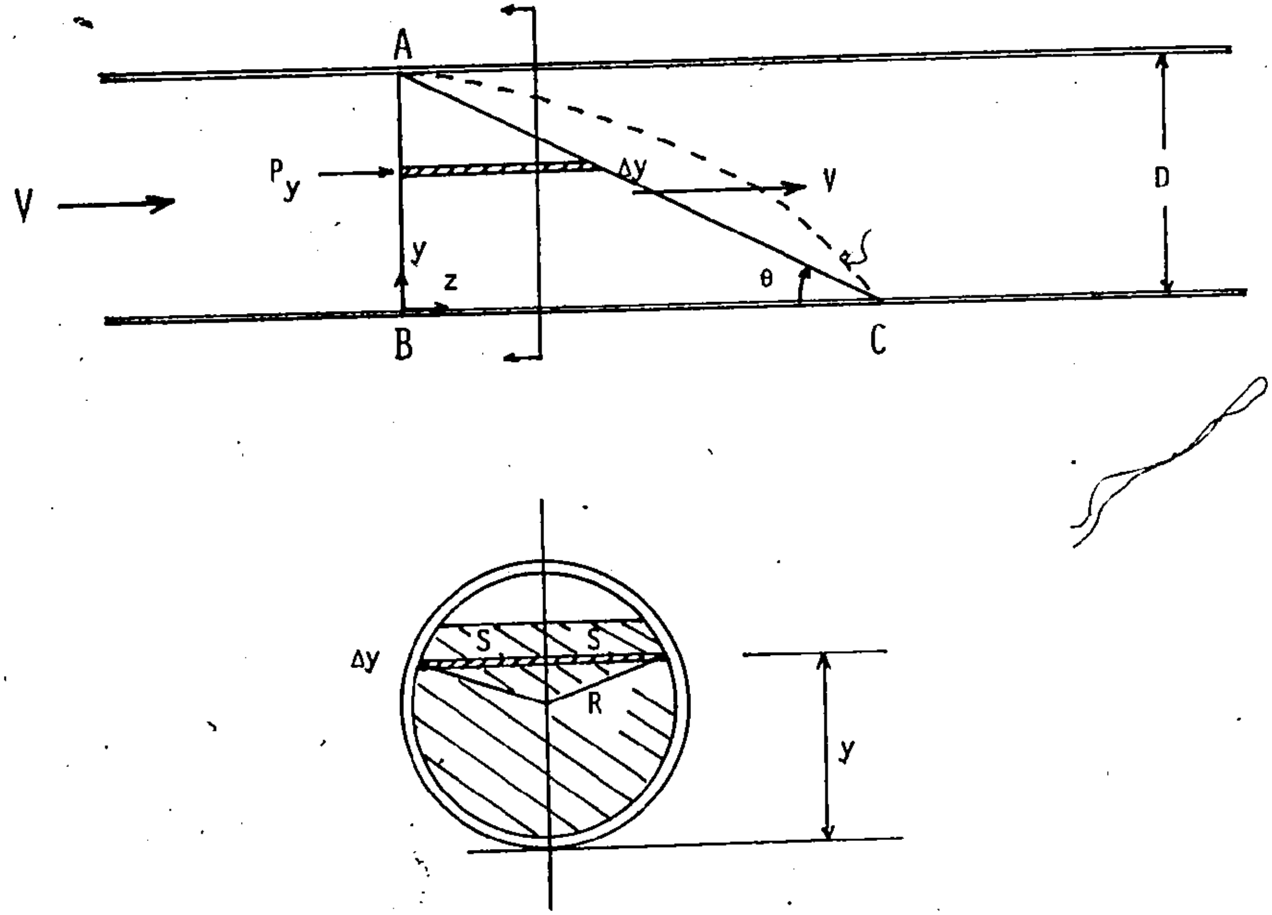

front that travels down the tube will be inclined at an angle θ to the axis as shown. It should be noted that the actual shape of the front will be better represented by the dotted line because of wall friction. However, for simplicity, a straight line AC is assumed. The angle of inclination (θ) can be calculated by a simple force balance taking the region ABC as the control volume. Using the symbols as defined in Figure 9.5, the hydrostatic pressure at a point along AB with a distance y from the bottom of the channel is given by

$$P_y = \rho_L g \, (D-y) \tag{9.56}$$

The corresponding force term in the flow direction, taking an elementary volume of width 2S and thickness Δy is

$$|dF_y| = \rho_L \, g \, (D-y) \, 2 \, S \, \Delta y \tag{9.57}$$

where 2 S is the chordal length in the x-direction.

Equation (9.57) can be integrated across the cross-section BA and the total horizontal hydrostatic thrust on the volume ABC can be shown to be

$$|F_y| = \rho_L \, g \, \pi R^3 \tag{9.58}$$

Assuming the flow is "well developed" in the sense that θ remains constant as the refilling front travels downstream, the hydrostatic thrust will be balanced by the shear force, that is

$$F_y = \tau_L \, A \tag{9.59}$$

where A is the contact surface area. A can be expressed as a function of θ and it can be shown for a circular channel to have the form

$$A = 2\pi R^2 \cot\theta \tag{9.60}$$

Substituting A into Eq. (9.59), we will have

$$\tan\theta = \frac{2\tau_L}{\rho_L g R} \tag{9.61}$$

Using Eq. (9.54), (9.61) becomes

$$\tan\theta = \frac{f\, u_L^2}{g\, R} \tag{9.62}$$

Therefore, θ can thus be calculated if the appropriate f is given. Or conversely, f can be determined if θ is known provided that u_L is given. It should be noted that the θ values can be obtained readily from simple experiments. A simple experiment will be described below. The experiment is also used to obtain data to verify the numerical technique described in the previous section. The validity of the simplified two-fluid model approach can also be tested by comparing the experimental and numerical results.

9.6 Verification of the Simplified Two-Fluid Model Approach - A Simple Experiment

A simple experiment was used to study the refilling characteristic of a dry horizontal duct. The experimental setup and dimensions are shown schematically in Figure 9.6. A pyrex tube with about the same inner diameter of the heated section used in the refilling and rewetting experiments is used. The movement of the refilling front can thus be observed visually. The water injection system is the same as in the other set of experiments. We have two quick acting valves. QAV1 is closed and QAV2 opened when the duct is being blown dry by compressed air. To initiate the transients, QAV1 will be opened and QAV2 closed at the same time,

FIG. 9.6 SCHEMATIC OF REFILLING SETUP WITH NO HEAT TRANSFER

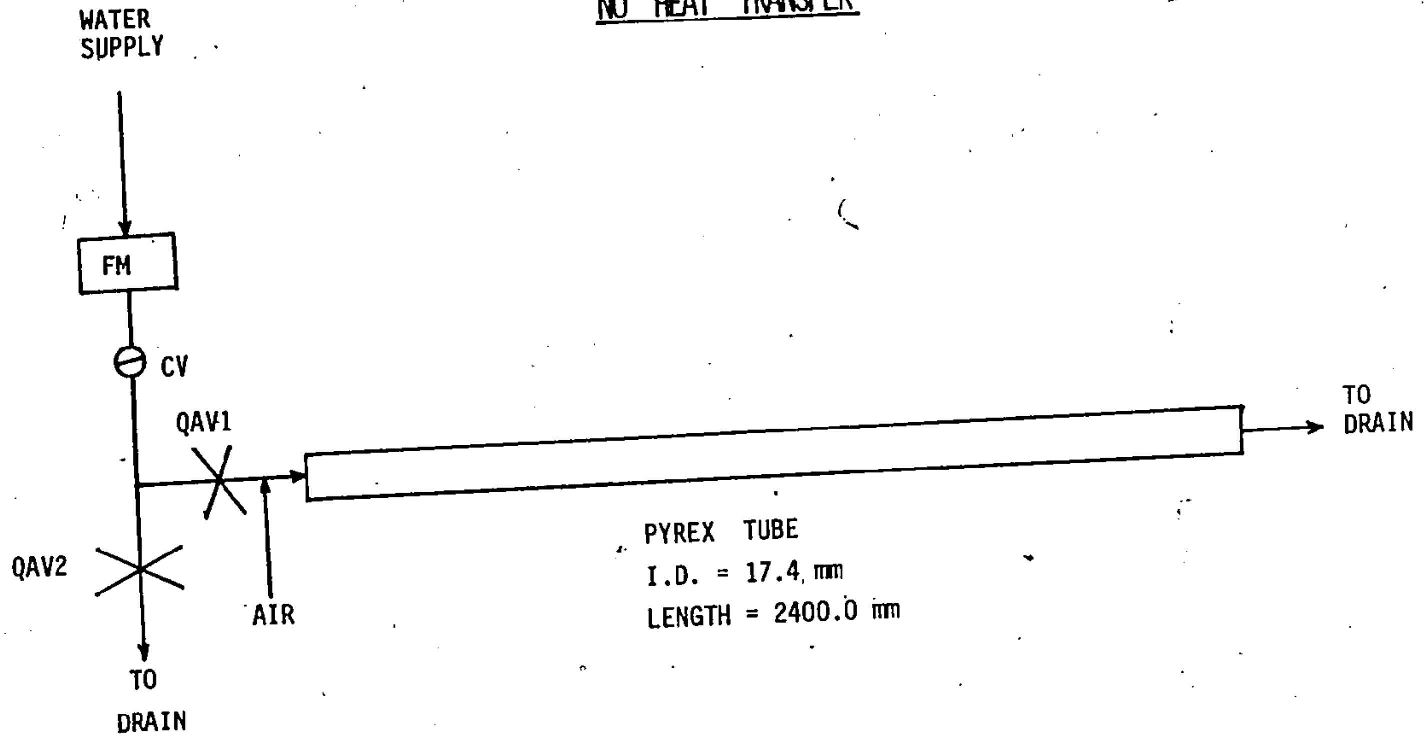

FM = FLOW METER
QAV = QUICK ACTING VALVE
CV = CONTROL VALVE

injecting water into the channel.

In this set of experiments, the average velocities of the leading and trailing edges of the refilling front were measured along the channel. The stratified length, ℓ_s (distance BC in Figure 9.5) or the angle of inclination, θ was also measured for different inlet flows.

When a dry horizontal duct is being filled, say by a constant water supply by the removal of a vertical dividing wall, the refilling characteristic can be summarized as shown in Figure 9.7. Again, the refilling fronts are assumed to be straight lines for simplicity. As soon as the dividing wall is removed, water level behind the wall collapses and water rushes out at relatively high speed because of the hydrostatic thurst. Flow stratification develops under the influence of the gravitational effect. The leading edge of the front will have an initial velocity of $(V_o + 2\ C_o)$, where V_o is the inlet flow velocity and $C_o = \sqrt{gD}$ is the gravity wave velocity (Henderson [112]). A flow reversal may occur at the top at the start of the transient. The top or trailing edge of the filling front will then move downstream if there is a constant supply of water at the inlet. Its velocity will be roughly the same as the inlet velocity. Therefore, it is clear that the velocities of the leading and trailing edges are quite different at the initial stage. The leading edge velocity (V_B) will be slowed down by viscous forces as the water front moves out. The angle of inclination (θ) decreases as the flow develops. At "steady state", the two edges will move with the same velocity which is equal to the inlet flow velocity. The angle of inclination will be constant and is given by Eq. (9.62).

FIG. 9.7 REFILLING CHARACTERISTIC OF A DRY HORIZONTAL TUBE WITH NO HEAT TRANSFER

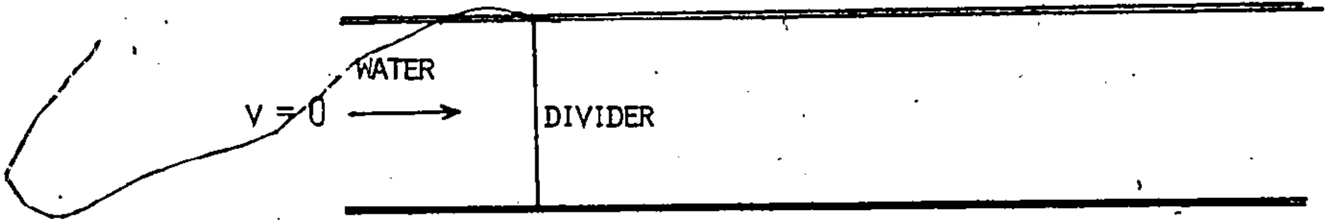

(A) BEFORE REMOVAL OF DIVIDER

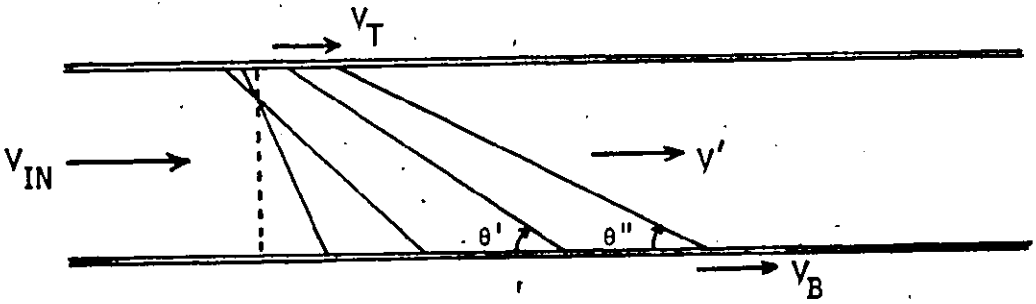

(B) AFTER REMOVAL OF DIVIDER

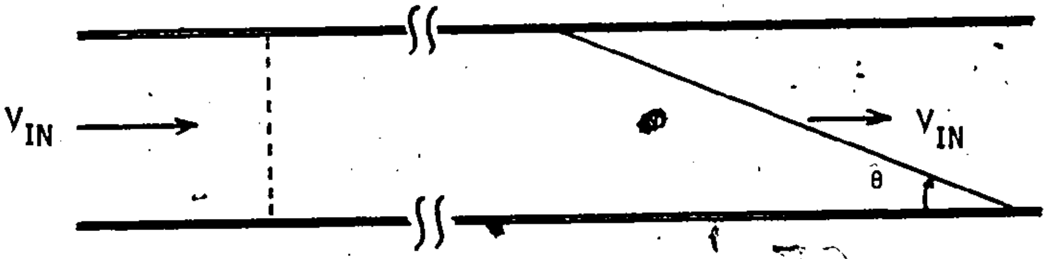

(C) STEADY STATE

The stratified length as a function of the location of the leading edge along the tube is shown in Figure 9.8. It can be seen that it takes a shorter distance for the flow to develop and achieve "steady state" for high inlet flows. For low inlet flows, ℓ_s can be very long, greater than 150 cm for $Q \leq 35$ ml/s. The stratified length approaches the steady state value as the flow develops. Since ℓ_s is directly related to θ ($\tan \theta = D/\ell_s$), therefore the friction factor can be calculated using Eq. (9.62). Assuming it can be written as

$$f_s = mf \tag{9.63}$$

where f is friction factor in pipe flow and may be given by the Blasius equation (Eq. (9.55)). m is a multiplier to account for the increase in friction force in the filling of a dry channel. The values of m at steady state can be estimated. It is shown in Figure 9.9 for different constant inlet flow rates. It can be seen that m has higher values for low inlet flows and approaches a constant value of about 2.5 at higher flows ($Q \geq 70$ ml/s).

The velocities of the leading and trailing edges as a function of the axial position are shown in Figures 9.10 to 9.12 for different inlet flow rates. The numerical results obtained using the computer code WAVEST are also shown. It can be seen that the initial velocity of the leading edge (V_B) is very high and it approaches the steady inlet flow velocity (V) as the leading edge moves down stream. The axial distance (or time) required for V_B to approach V is shorter for higher inlet flows as expected. The velocity of the trailing edge (V_T) is about the same as V.

FIG. 9.8 TRANSIENT STRATIFIED LENGTH — REFILLING WITH NO HEAT TRANSFER

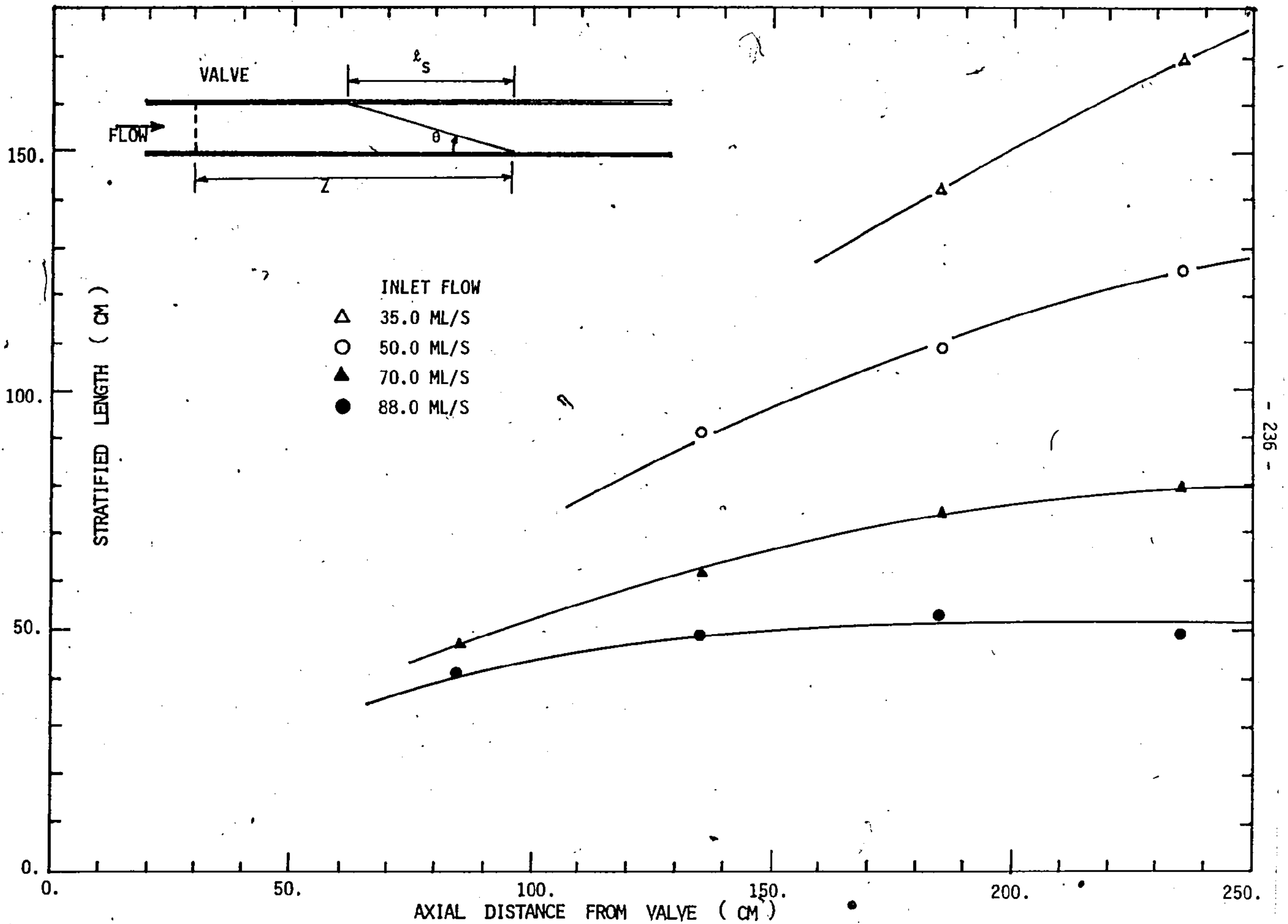

FIG. 9.9 STEADY STATE FRICTION FACTOR MULTIPLIER

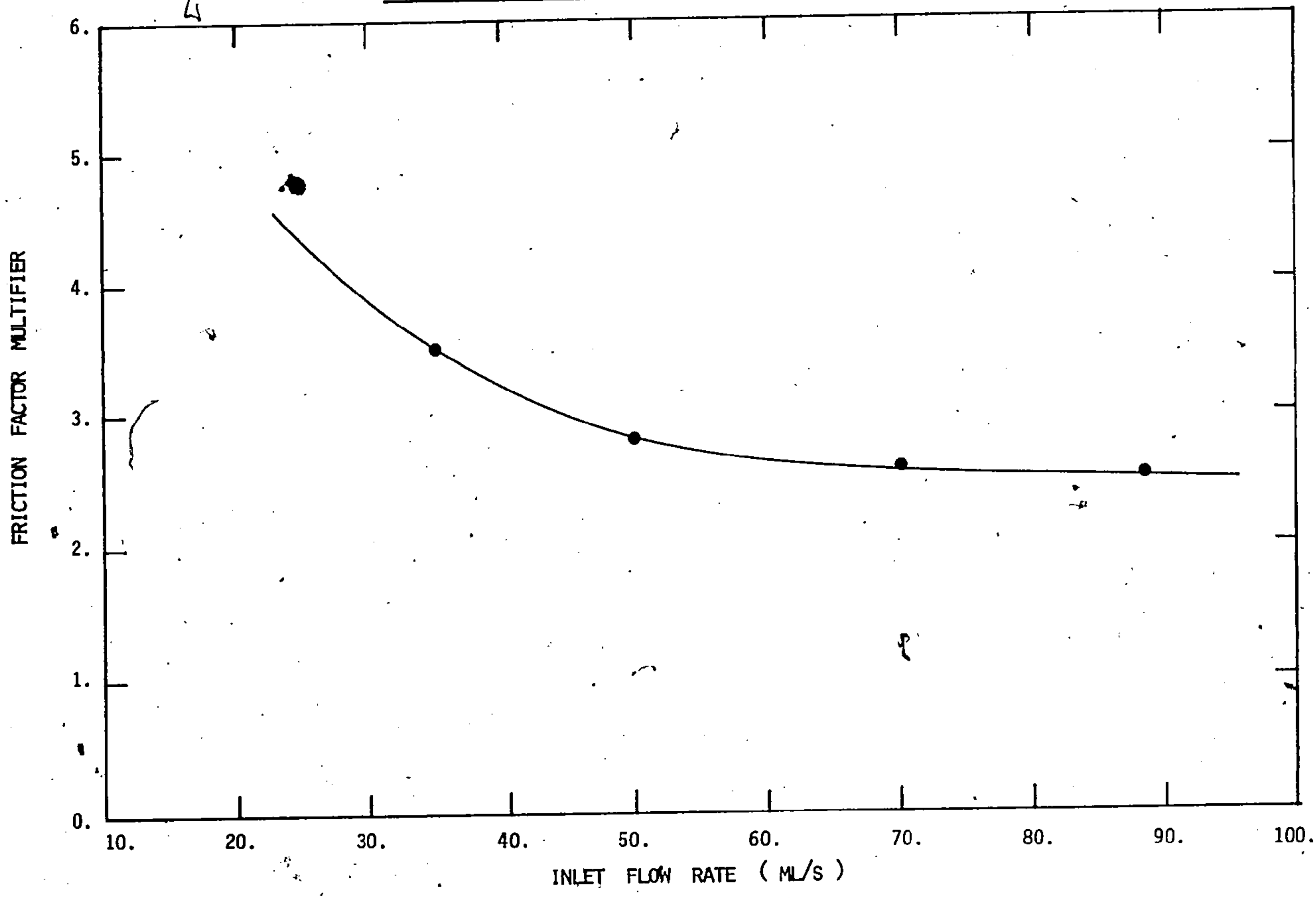

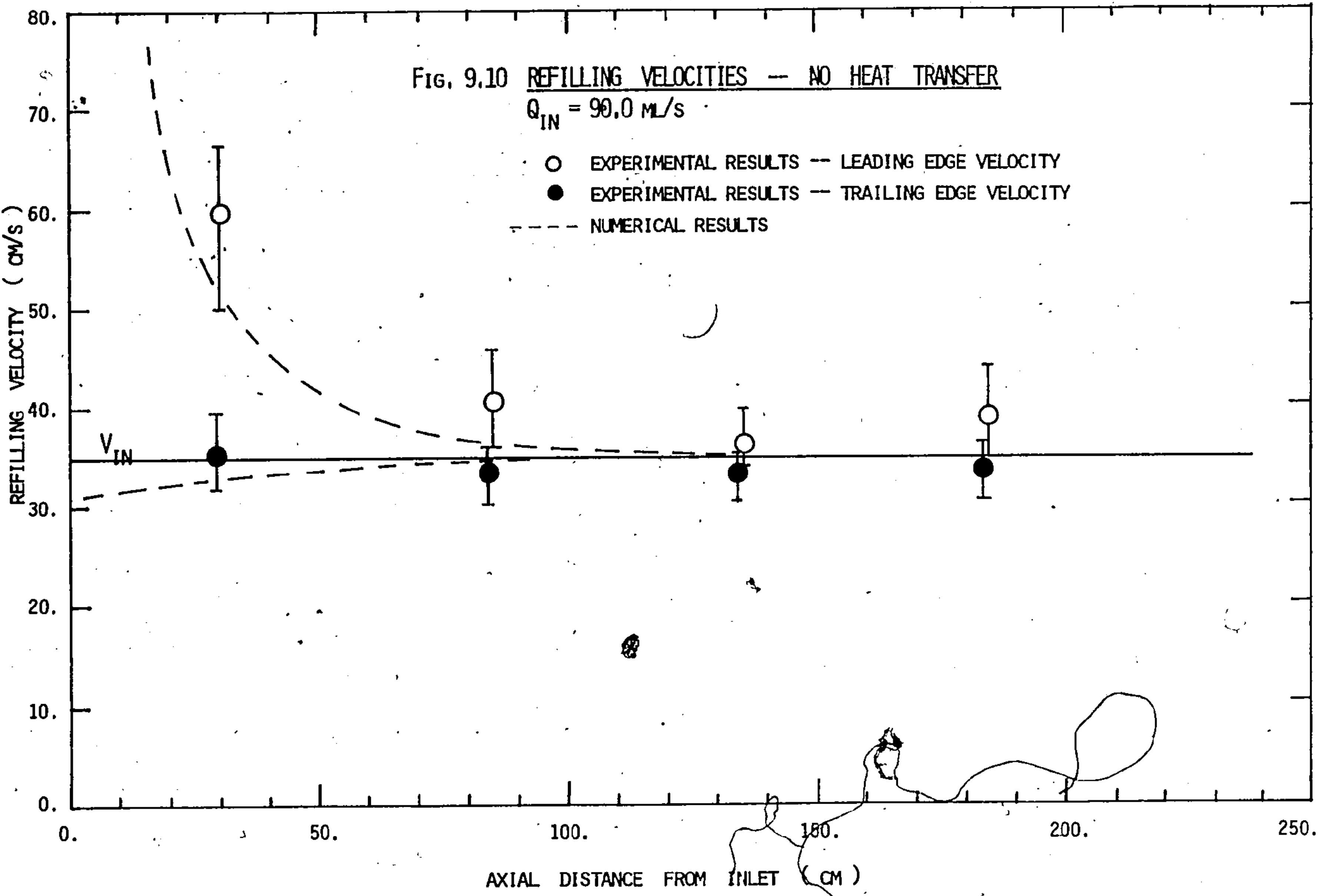

Fig. 9.10 REFILLING VELOCITIES — NO HEAT TRANSFER

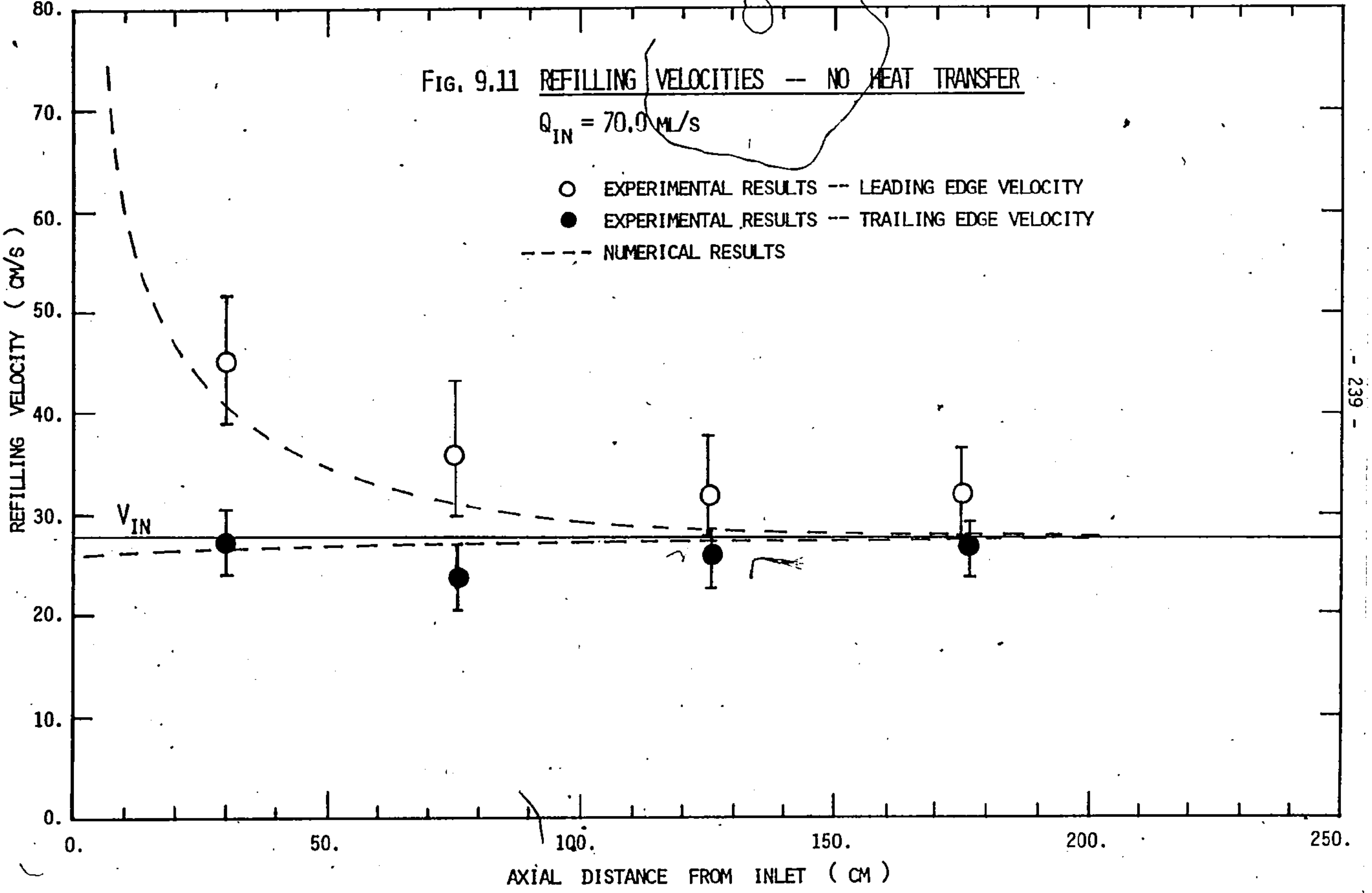

Fig. 9.11 REFILLING VELOCITIES — NO HEAT TRANSFER

$Q_{IN} = 70.0$ ML/S

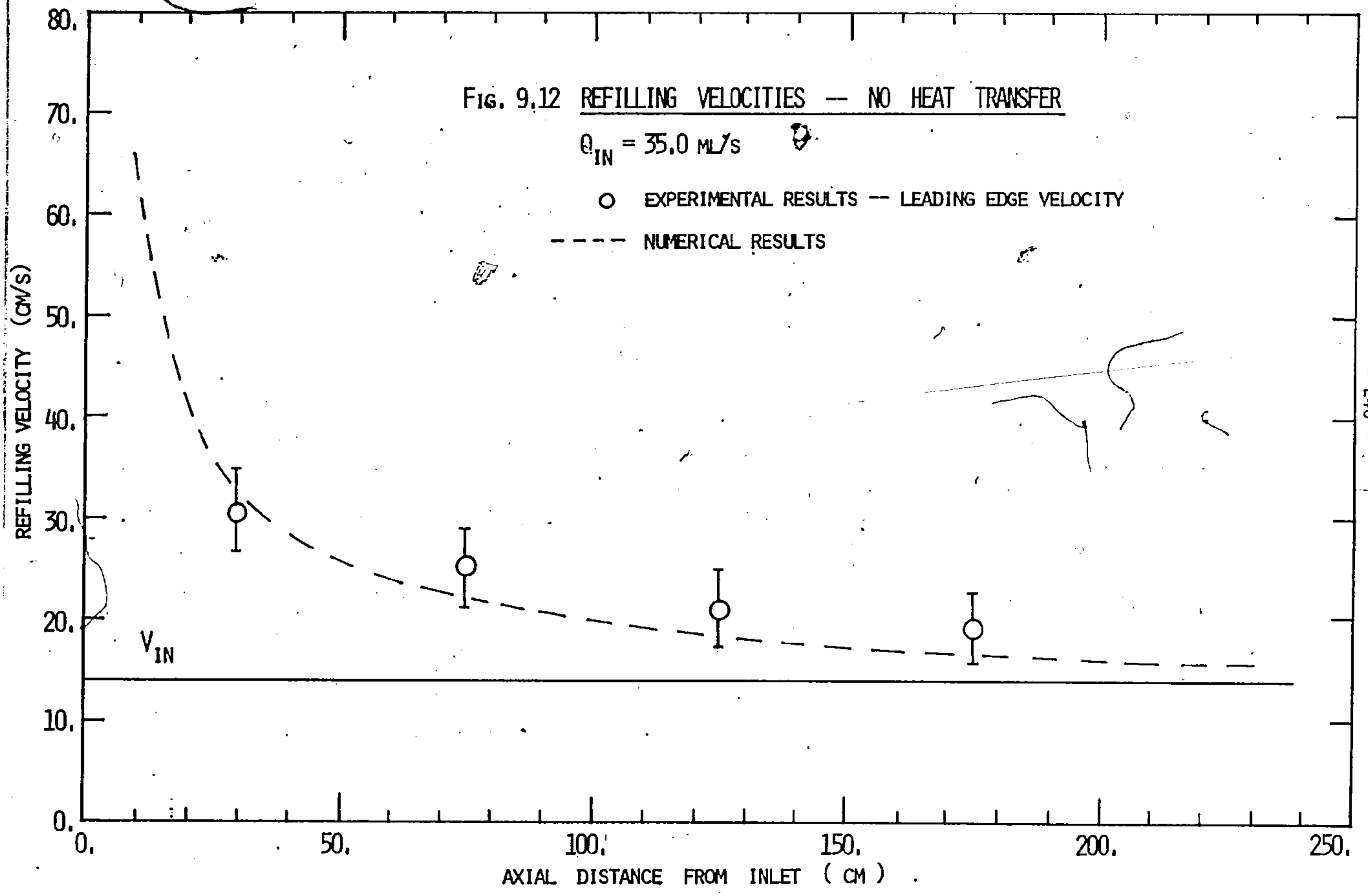

FIG. 9.12 REFILLING VELOCITIES -- NO HEAT TRANSFER

The numerical results are obtained using friction multipliers given in Figure 9.9. It should be noted that the multipliers are obtained for "steady state" situations, when the shape of the water front does not change, they may not be applicable in the rapid developing flow region (i.e. at the inlet end of the tube). Another source of error lies in the large vertical accelerations arising from the steep water surface slopes immediately after the dam breaks or valve opens. These accelerations invalidate the assumption of hydrostatic pressure distribution (Eq. (9.4)) on which the mathematical formulation is based. However, the overall effect may not be serious as the errors apply only to the initial stage of the transient. Once this initial period of high vertical acceleration and rapid flow development has passed, the mathematical formulation and the frictional multipliers as given in Figure 9.9 should be applicable. In fact, the numerical results do compare very well with the experimental data (Figures 9.11 to 9.12). Thus, we may conclude that the simplified two-fluid model approach is adequate and the numerical technique used gives good results.

The convergence of the solutions has been tested with respect to mesh size or nodalization. The results are listed in Table 9.1. 30, 60 and 100 nodes were used. ΔM is the difference of the liquid inventory in the system and the total mass of liquid inflow from the inlet. M is the total mass of liquid inflow. ΔM/M is a measure of how well the numerical scheme conserves mass. It can be seen that, in general, the scheme conserves mass pretty well and is not affected by the mesh sizes used. The average refilling velocities are also shown in the Table. They do not differ much for the different mesh sizes used. Therefore, we may conclude that the numerical results are converged if the number

Table 9.1

CONVERGENCE STUDIES FOR THE CASE OF REFILLING WITH NO HEAT TRANSFER

	No. of Nodes Used					
	Q_{in} = 70 mℓ/s			Q_{in} = 90 mℓ/s		
	30	60	100	30	60	100
$\frac{\lvert \Delta M \rvert}{M}$	2.3%	2.5%	2.1%	4.5%	4.4%	-
$\overline{V}$ (cm/s)	28.3	28.0	28.5	35.1	34.7	-

of nodes used is 30 or more.

The time step used is determined by Eq. (9.34). However, reducing Δt to half of that given by Eq. (9.34) does not affect the refilling results to any significant extent.

Figure 9.13 shows the propagation of the refilling front in a dry horizontal channel with no heat transfer. Results are obtained using the computer code WAVEST. Plotted in the figure is the level of refilling water along the channel at different times. The shape of the refilling front is similar to the wave profile following a dam-break as reported by Dressler [123]. It can be seen that the flow is highly stratified and because the movement of the leading edge is strongly impeded by the viscous forces, a steep front is formed behind the leading edge. The shape of the refilling front is quite different from the idealized smooth surface shown in Figures 9.5 and 9.7. This can partly explain the high friction factors we obtained (Figure 9.9). With the idealized surface shape, the surface contact area of the filling front is smaller, thus to balance the hydrstatic thrust (Eq. (9.59)), a higher friction factor is required. It can also be seen that before steady state is achieved, the leading edge moves much faster than the trailing edge and the stratified length increases as the filling front travels downstream.

FIG. 9.13 PROPAGATION OF REFILLING FRONT -- REFILLING OF A DRY HORIZONTAL CHANNEL

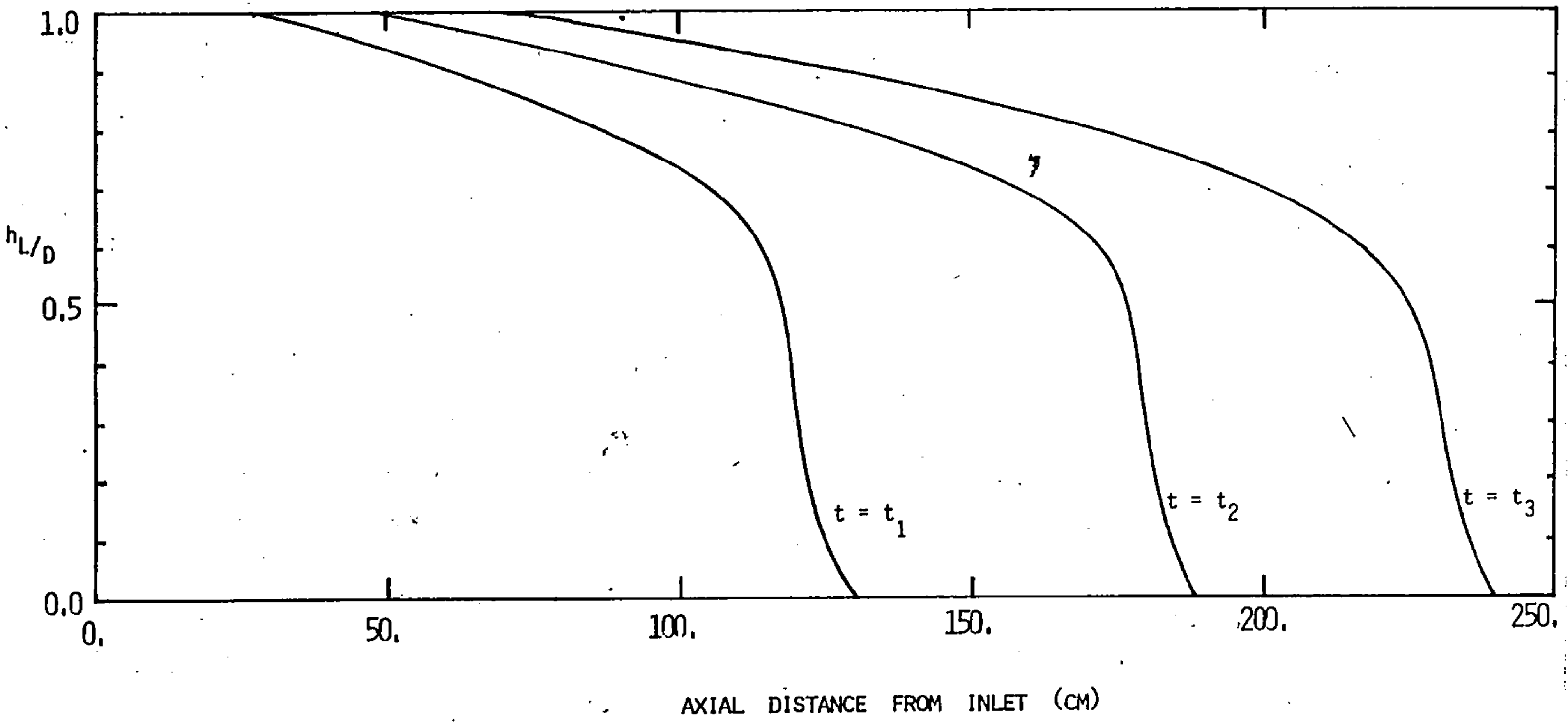

10. SIMPLIFIED TWO FLUID MODEL

II. REFILLING AND REWETTING OF HOT HORIZONTAL CHANNEL

10.1 General

The simplified two fluid model approach to the refilling and rewetting problem has been described in detail in Chapter 9. The model and numerical technique have been checked experimentally for the simple case of refilling a horizontal tube with no heat transfer. The model is then used to interpret the refilling and rewetting experiments. The computer code, REWET, which is an extension of WAVEST has been developed. Details of the code will now be described. The mathematical formulation, interfacial transfer terms and numerical results will also be discussed.

10.2 Mathematical Formulation

10.2.1 Hydraulic Equations

The simplified two-fluid model has been derived in general form in Section 9.2. The resulting hydraulic equations are reproduced here

$$\frac{\partial h_L}{\partial t} + u_L \frac{\partial h_L}{\partial z} + \frac{\alpha_L}{\alpha_L'} \frac{\partial u_L}{\partial z} = -\frac{\dot{m}_L}{\rho_L \alpha_L'} = E_1 \qquad (9.16)$$

$$\frac{\partial \alpha_G}{\partial t} + \frac{\partial(\alpha_G u_G)}{\partial z} = \frac{\dot{m}_L}{\rho_G} \qquad (9.18)$$

and

$$\frac{\partial u_L}{\partial t} + u_L \frac{\partial u_L}{\partial z} + g \frac{\partial h_L}{\partial z}$$

$$= -\frac{\tau_L a_L}{\rho_L \alpha_L} + \frac{\tau_i a_i}{\rho_L} \left[\frac{1}{\alpha_L} + \frac{1}{\alpha_G}\right] + \frac{\tau_G a_G}{\rho_L \alpha_G}$$

$$+ \frac{\dot{m}_L}{\rho_L}\left[\frac{u_L-u_i}{\alpha_L} + \frac{u_G-u_i}{\alpha_G}\right] + \frac{\rho_G}{\rho_L}\left[\frac{\partial u_G}{\partial t} + u_G \frac{\partial u_G}{\partial z}\right] = E_2 \qquad (9.22)$$

Since $\alpha_G = (1-\alpha_L)$, therefore, if $\dot{m}_L$ is known, the set of equations can be solved numerically. However, the solution scheme can be complicated. The equations can be greatly simplified if we make a physically realistic assumption: that the time derivative in Eq. (9.18) is small comparing to the other terms in the equation. This is true for "slow" transients when the water level at a given location does not change rapidly. For the case of refilling and rewetting in hot horizontal channels, this assumption can be shown to hold well in general. The $\partial u_G/\partial t$ term in the right hand side of Eq. (9.22) can likewise be ignored.

With this assumption, Eq. (9.18) can be integrated to give u_G. Equations (9.16) and (9.22) can thus be solved for u_L and h_L. Following the same procedure as given in Section 9.3, the set of equations ((9.16) and (9.22)) can be written in characteristic form in terms of the stage variable, ω as defined in Eq. (9.30)

$$\left[\frac{\partial u_L}{\partial t} + (u_L+c)\frac{\partial u_L}{\partial z}\right] + \left[\frac{\partial \omega}{\partial t} + (u_L+c)\frac{\partial \omega}{\partial z}\right] = E_2 + \sqrt{g\alpha_L'/\alpha_L}\; E_1 \qquad (10.1)$$

and

$$\left[\frac{\partial u_L}{\partial t} + (u_L-c)\frac{\partial u_L}{\partial z}\right] - \left[\frac{\partial \omega}{\partial t} + (u_L-c)\frac{\partial \omega}{\partial z}\right] = E_2 - \sqrt{g\,\alpha_L'/\alpha_L}\,.\,E_1 \qquad (10.2)$$

Equations (10.1) and (10.2) are identical to (9.32) and (9.33) except for the terms on the right hand side. Therefore, the same numerical scheme that was used to solve Eqs. (9.32) and (9.33) (Section 9.4) can be used here. It should be noted that the terms on the right hand side are quite complicated in the present case. E1 and E2 involve the interfacial mass and momentum transfer, vapor inertia as well as phase to wall viscous terms. These terms have to be known explicitly before equations ((10.1) and (10.2)) can be solved.

10.2.2 Thermal Equations

The channel wall and fluid temperatures are required in order that the heat flux into the system can be calculated using appropriate heat transfer coefficients. Knowing the heat flux and the fluid temperature, the interfacial mass transfer ($\dot{m}_L$) and momentum transfer ($\dot{m}_L\ u_i$) terms can be estimated. The temperature of the wall (T_w) can be obtained using the three-dimensional transient heat conduction equation in cylindrical co-ordinates

$$\frac{1}{\alpha_w}\frac{\partial T_w}{\partial t} = \frac{1}{r}\frac{\partial T_w}{\partial r} + \frac{\partial^2 T_w}{\partial r^2} + \frac{\partial^2 T_w}{\partial z^2} + \frac{1}{r^2}\frac{\partial^2 T_w}{\partial \theta^2} + \frac{Q'}{k} \tag{10.3}$$

with convective thermal boundary condition at the inner surface

$$k_w \frac{\partial T_w}{\partial r}\bigg|_{r_i} = \bar{h}\ (T_w - T_F) \tag{10.4}$$

where $\alpha_w = (k/\rho C_p)_w$ is the thermal diffusivity of the wall. Q' is the rate of heat generation in the wall per unit volume. $\bar{h}$ is an appropriate effective heat transfer coefficient, it can be a function of T_w, θ and z. T_F is the temperature of the fluid in contact with the surface. The contacting fluid can be liquid, vapor, or air. The thermal boundary condition at the outer surface can be adiabatic or convective depending on whether the test section is insulated or not.

The bulk liquid temperature (T_L) is given by the one-dimensional space/time average energy equation derived in Chapter 3 (Eq. (3.25)). The equation can be simplified to

$$\frac{\partial}{\partial t}(\alpha_L T_L) + \frac{\partial}{\partial z}(\alpha_L u_L T_L) = \left(\frac{k}{\rho C_p}\right)_L \frac{\partial}{\partial z}\left(\alpha_L \frac{\partial T_L}{\partial z}\right) + \left(\frac{1}{\rho C_p}\right)_L (1-\beta)q''' \qquad (10.5)$$

where q''' is the heat flux per unit volume and is given by

$$q''' = \frac{1}{V}\int_0^{2\pi} \bar{h}(\theta,z)\, A(\theta)(T_W(\theta,z) - T_F(\theta,z))\, d\theta \qquad (10.6)$$

The vapour temperature (T_G) is taken as the saturation temperature. That is, no vapor superheating is assumed. (1 - β) is the fraction of energy input that goes into the liquid phase.

It should be noted that the thermal equations (10.3 and 10.5) are coupled to the hydraulic equations ((10.1) and (10.2)). In principle, the two sets of equations have to be solved simultaneously. However, in order to simplify the problem and to reduce the complexity of the solution scheme, the two sets of equations will be solved numerically assuming explicit coupling, i.e. one set of equations (hydraulic or thermal) are solved first using previous time step values for the coupling terms. The coupling terms that appear in the other set are then evaluated from these solutions. Solutions to the second set of equations are then obtained. The procedure is then repeated for another time step.

The numerical scheme and solution procedures will now be outlined.

10.3 Numerical Procedures

The governing equations for the refilling and rewetting problem in a hot horizontal duct are solved numerically using the computer code REWET. REWET is an extension of WAVEST which solves the hydraulic equations using the explicit finite difference characteristic method (Section 9.4). The thermal equations are included in REWET and are solved with an explicit finite difference technique. A flow diagram of the code is shown in Figure 10.1. The computation steps can be summarized:

1. Specify initial and boundary conditions.
2. Evaluate the effective local heat transfer coefficient, $\bar{h}(z,\theta,T_W)$ based on the local flow conditions and empirical correlations (Subroutine HTRAN).
3. Calculate $T_W(z,\theta,t)$ using Eq. (10.3). (Subroutine WTEMP).
4. Calculate $T_L(z,t)$ using Eq. (10.5). (Subroutine FTEMP).
5. Output the dependent variables, this includes $T_W(z,\theta,t)$, $T_L(z,t)$, $u_L(z,t)$ and $u_G(z,t)$. (Subroutine OUTPUT)
6. Determine the time step size used with respect to given Δz.
7. Evaluate the right hand side terms in the hydraulic equations ((10.1) and (10.2)), that is E_1 and E_2 which are given in Eqs. (9.16) and (9.22). (Subroutines FRICT and VAPOR).
8. Solve the hydraulic equations ((10.1) and (10.2)) for $u_L(z,t)$ and $\omega(z,t)$ or $h_L(z,t)$ at the advanced time step.

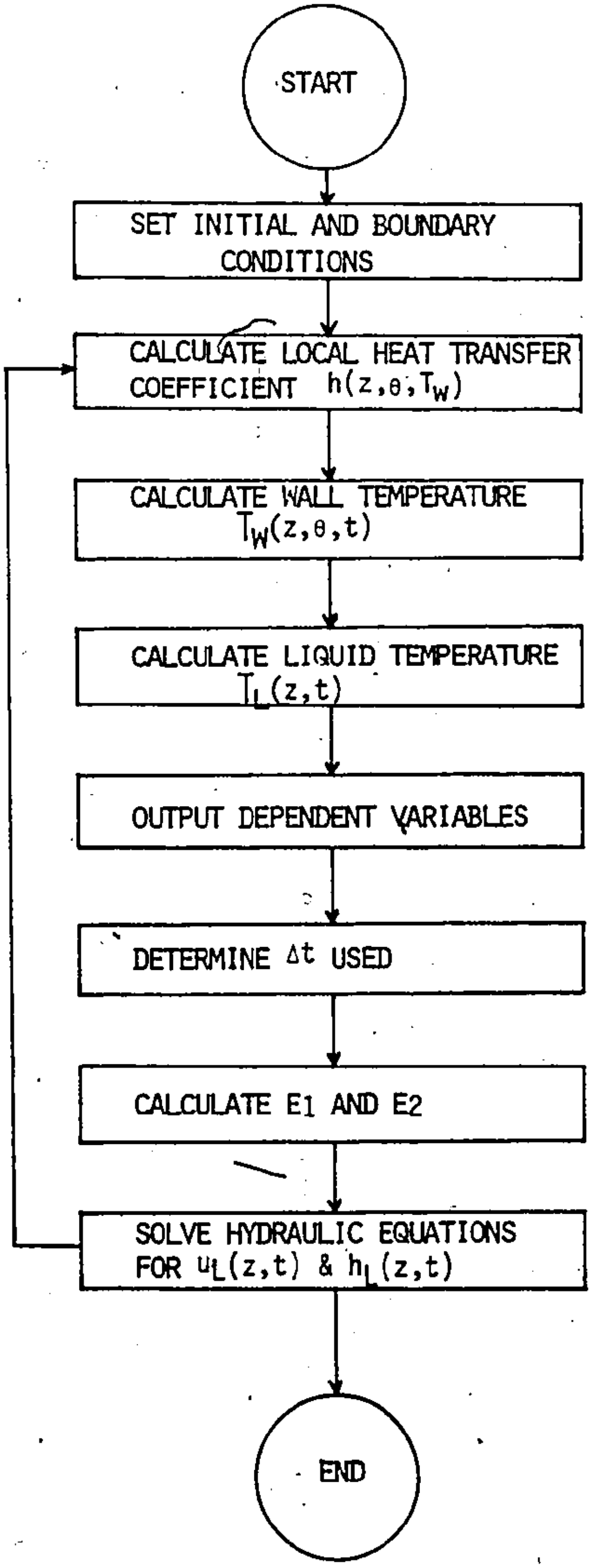

FIG. 10.1 FLOW DIAGRAM OF COMPUTER CODE REWET

9. Steps 2 to 8 are repeated until the channel is totally quenched.

A listing of the computer code REWET can be found in Appendix IV.

10.3.1 System and Nodalization

A schematic of the system and nodalization used is shown in Figure 10.2. Twenty-four cells are used to represent the heated test section. Six cells are used to simulate the inlet and outlet feeders respectively. The locations of the wall thermocouples are also shown. It should be noted that more cells can be used for higher accuracy and computation costs. Uniform mesh sizes are used in the present case, however, non-uniform meshes can be incorporated into the computer code with minor modifications.

In a given cell, the dependent variables are defined as shown in the insert of Figure 10.2. The flow parameters (u_L, h_L, c, u_G) are defined at the cell boundary whereas the temperatures (T_W,T_L) and heat transfer coefficient (h) are defined at the cell center.

10.3.2 Initial and Boundary Conditions

The initial and boundary conditions are defined as follows.

Initial Conditions

At $t \leq 0$, we have a dry channel. There is no water and no flow in the system. That is

$$(u_L)_j = (u_G)_j = (h_L)_j = c_j = 0 \qquad 2 \leq j \leq 38 \qquad (10.7)$$

FIG. 10.2 SCHEMATIC OF SYSTEM AND NODALIZATION

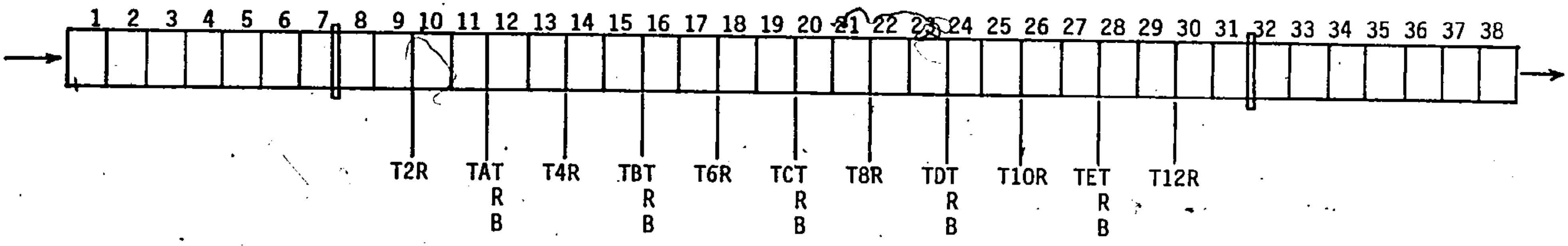

NODES 1 & 38 -- BOUNDARY NODES
NODES 2 - 7 -- INLET FEEDER
NODES 8 - 31 -- TEST SECTION
NODES 32 - 37 -- OUTLET FEEDER

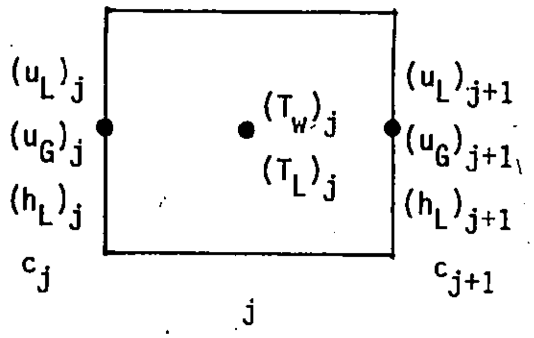

at the inlet

$$(u_L)_1 = 0$$

$$(h_L)_1 = D \qquad (10.8)$$

The wall temperatures are given by

$$(T_w)_j = T_w^\circ \qquad 8 \le j \le 31$$

$$(T_w)_j = T_{room} \qquad 8 > j > 31 \qquad (10.9)$$

Boundary Conditions

(i) Flow Boundary Conditions:

Constant flow boundary is used at the inlet, or

$$(u_L)_1 = u_L^\circ$$

$$(h_L)_1 = D \qquad (10.10)$$

At the exit,

$$\frac{\partial h_L}{\partial z} = 0 \qquad (10.11)$$

(ii) Thermal Boundary Conditions:

Liquid temperature at the inlet,

$$T_L = T_L^\circ \qquad (10.12)$$

Wall temperature along the channel,

$$k_w \left.\frac{\partial T_w}{\partial r}\right|_{\text{inner surface}} = \bar{h}(T_w - T_F) \qquad (10.13)$$

$$k_w \frac{\partial T_w}{\partial r}\bigg|_{\text{outer surface}} = \begin{cases} 0 & \text{channel insulated} \\ \bar{h}(T_w - T_{room}) & \text{not insulated} \end{cases} \quad (10.14)$$

10.3.3 Local Heat Transfer Coefficients

The heat transfer mechanisms during the refilling and rewetting transients are very complicated (Section 8.6). Different modes of heat transfer exist along the channel depending on the water level and wall temperature. The effective heat transfer coefficient ($\bar{h}$) is in most cases the sum of the coefficients of a number of heat transfer processes. Since $\bar{h}$ is a function of z and θ, in order to estimate $\bar{h}$, the local flow and thermal conditions have to be known. In general, the effective heat transfer coefficients can be evaluated in different axial regions as shown in Figure 10.3.

(i) "Dry" Region ($h_L = 0$)

This is the region downstream of the "liquid tongue". Vapor flow with entrained water droplets may exist.

$$\bar{h} = h_{\text{vapor flow}} + h_{\text{free convection}} + h_{\text{radiation}}$$

$$0 \leq y \leq D \quad (10.15)$$

where y is the vertical projection of the angular position θ.

(ii) Film Boiling Region

This is the region with the "liquid tongue". The wall temperature is high, thus stable film boiling exists in areas covered by the "liquid tongue".

FIG. 10.3 AXIAL HEAT TRANSFER REGIONS

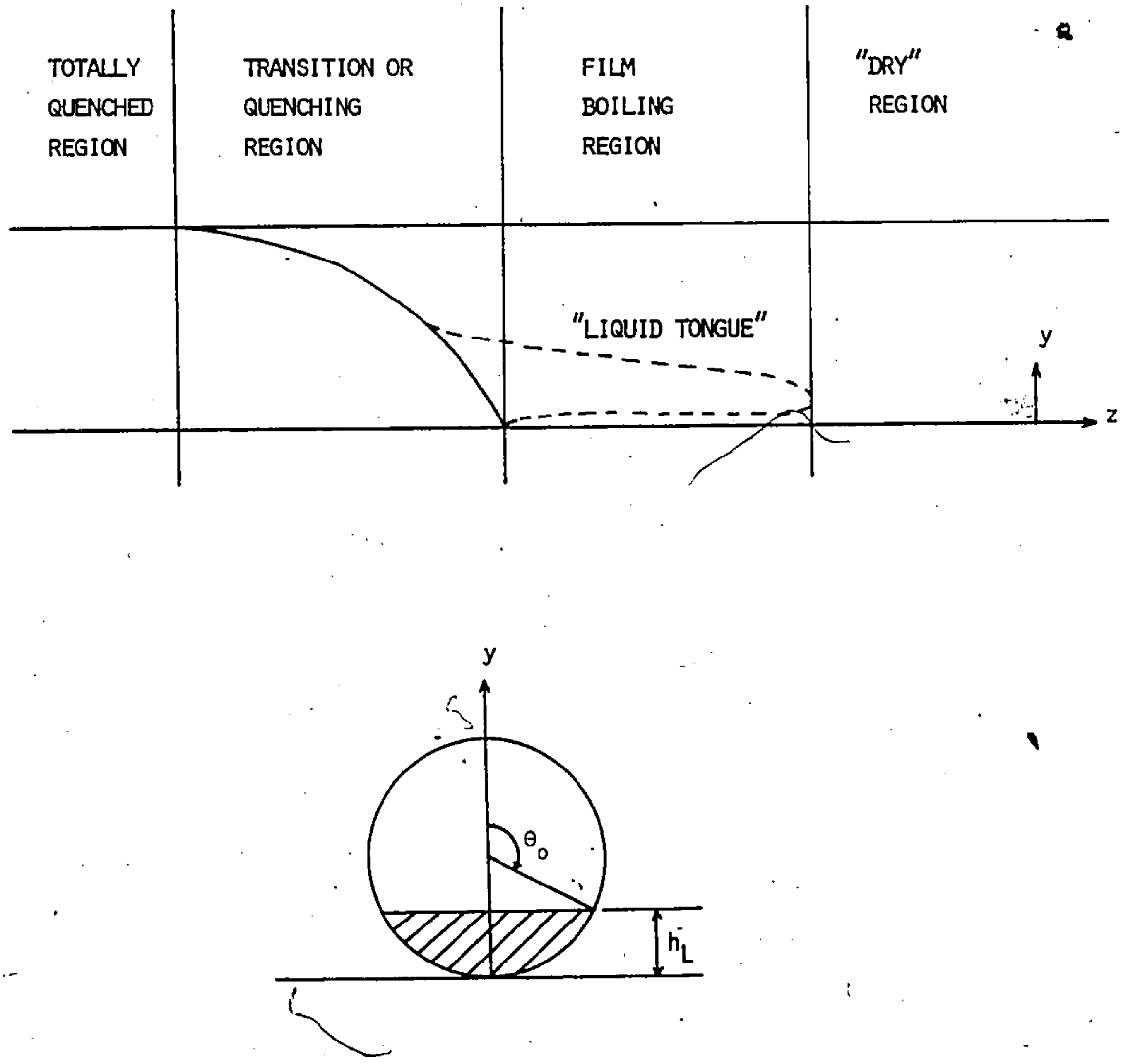

$$\theta > \pi/2 \qquad y = R - R\cos(\pi-\theta)$$

$$\theta < \pi/2 \qquad y = R + R\cos\theta$$

$$\bar{h} = h_{\text{film boiling}} + h_{\text{free convection}} + h_{\text{radiation}}$$

$$0 \leq y < h_L \qquad (10.16)$$

For the remaining area, i.e. $h_L \leq y \leq D$, the heat transfer mechanisms can be assumed to be the same is in the "dry" region, and $\bar{h}$ is given by Eq. (10.15).

(iii) Transition or Quenching Region

This is the region that quenching of the channel surface occurs. The heat transfer mechanisms during quenching are not well understood. Macroscopically, quenching is associated with very high heat transfer coefficients (h_{quench}). Therefore, a high h_{quench} can be assumed when quenching begins at a location. Since the heat transfer mechanisms are not well known, therefore, the conditions under which quenching first begins are likewise not well defined. A semi-empirical model will be discussed later in the chapter. Assuming there exists a critical water level, $(h_L)_{\text{crit}}$ and an effective quench water level, h_q which can be defined in terms of $(h_L)_{\text{crit}}$ such that

$$\bar{h} = h_{\text{quench}} + h_{\text{free convection}} + h_{\text{radiation}} \text{ for } y \leq h_q \qquad (10.17)$$

where

$$\begin{aligned} h_{\text{quench}} &= h_{\text{transition boiling}} \quad \text{if} \quad T_w \geq T_{CHF} \\ &= h_{\text{nucleate boiling}} \quad \text{if} \quad T_{sat} < T_w < T_{CHF} \\ &= h_{\text{liquid flow}} \quad \text{if } T_w \leq T_{sat} \end{aligned}$$

T_{CHF} and T_{sat} are the critical heat flux and saturation temperatures respectively. h_q equals zero when h_L is smaller than $(h_L)_{crit}$ (Section 10.5).

For the areas not covered by h_q,

$$\bar{h} = h_{film\ boiling} + h_{free\ convection} + h_{radiation}$$

$$h_q < h \leq h_L$$

$$\bar{h} = h_{vapor\ flow} + h_{free\ convection} + h_{radiation}$$

$$h_L < y \leq D$$

(iv) Totally Quenched Region

This is the region that the channel has been rewetted and refilled. T_w is less than T_{sat}. No boiling exists.

$$\bar{h} = h_{liquid\ flow} + h_{free\ convection} + h_{radiation}$$

$$0 \leq y \leq D \tag{10.18}$$

The heat transfer coefficients for a number of heat transfer modes have been discussed in Section 8.6. The correlations used are given by Eqns. (8.10) through (8.13) for $h_{free\ convection}$, $h_{radiation}$, $h_{vapor\ flow}$ and $h_{film\ boiling}$ respectively. The heat transfer coefficient for forced convection liquid flow is given by

$$h_{liquid\ flow} = 0.023 \left(\frac{\rho_f u_L D_h}{\mu_f}\right)^{0.8} \left(\frac{C_p \mu}{k}\right)_f \frac{k_f}{D_h} \tag{10.19}$$

For transition boiling heat transfer, the PWR-FLECHT data at low pressure can be used as suggested by Tong [124].

$$h_{transition\ boiling} = 9 \times 10^3 \exp(-0.0054\ \Delta T_w) \tag{10.20}$$

where $\Delta T_w = T_w - T_{sat}$ is in °F and h in Btu/hr-ft^2-°F.

For nucleate boiling heat transfer, Thom's correlation is recommended by Tong [124]

$$h_{\text{nucleate boiling}} = \frac{\exp(P/630)}{(0.072)^2} \Delta T_w \tag{10.21}$$

where P is in psia, $T_w = T_w - T_{sat}$ in $^{\circ}$F and h is in Btu/hr-ft^2-°F. It should be noted that Thom's correlation is for high pressure systems (750 to 1000 psia), it may not work well for low pressures. In fact, Thom's correlation was found to give a higher $h_{\text{nucleate boiling}}$ than was observed from the rewetting and refilling data.

The change in the dominant heat transfer mechanisms for a given location can be depicted using a boiling curve as shown in Figure 10.4. The surface is in stable film boiling until the arrival of the quench front. The quench front is defined by h_q, the effective quench water level. At this point (point C), the surface enters into transition boiling and the surface temperature is T_q, the "apparent" quench temperature. It should be noted that T_q is not constant, it depends on the local thermal and hydraulic conditions. The surface is partially wetted when in transition boiling. This mode of heat transfer, however, rapidly gives way to nucleate boiling as the surface is rapidly quenched for a thin walled tube and the maximum heat flux point (point B) is reached. When the surface drops below T_{sat}, single phase liquid flow is assumed.

FIG. 10.4 BOILING CURVE

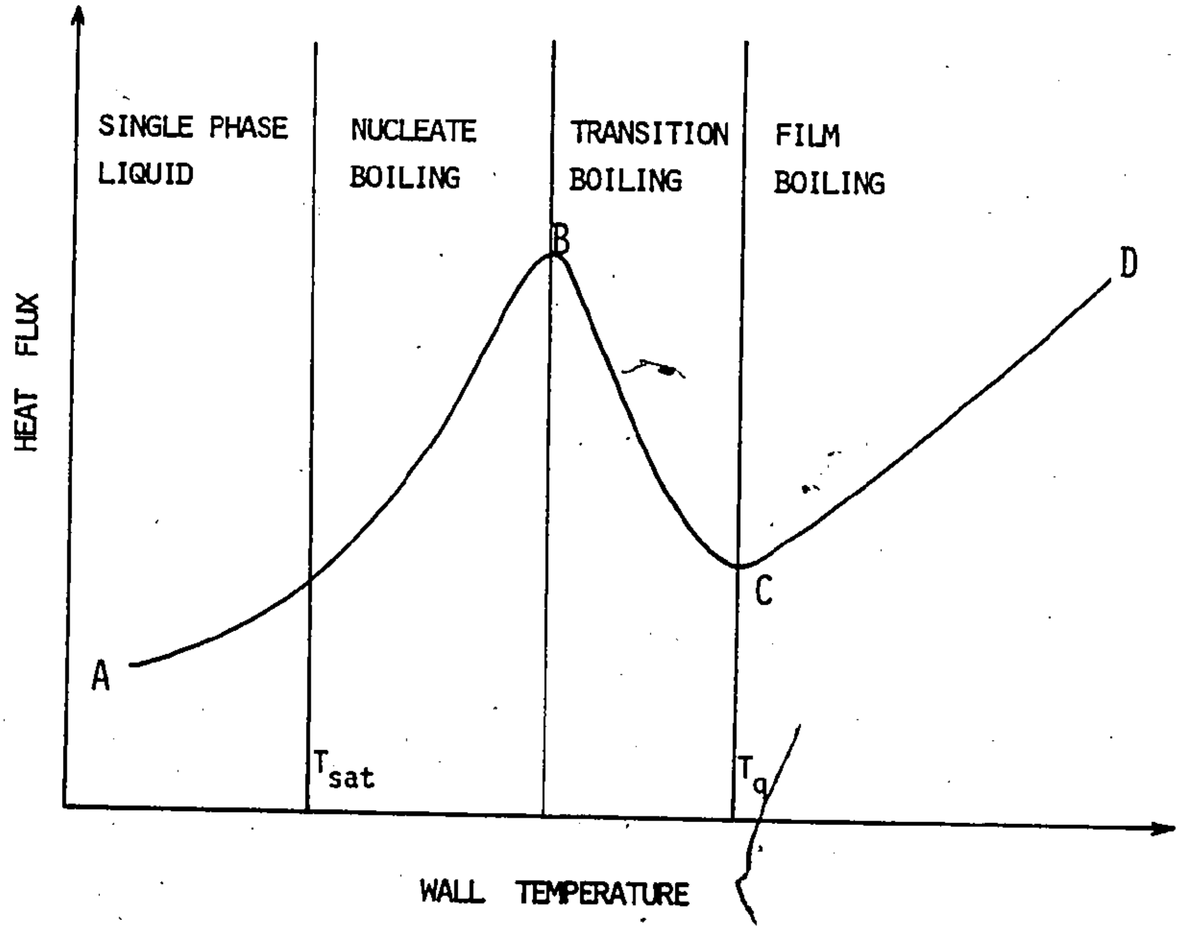

0.3.4 Wall Temperature

The transient heat conduction equation (Eq. (10.3)) is solved numerically using an explicit finite difference method. The finite difference grid used is as shown in Figure 10.5. The channel is divided into twelve cells azimuthally. Since the solution is expected to be symmetric with respect to the vertical diameter, the energy equation is solved only for half of the channel. Temperatures at the other half are just mirror images of the first half.

The channel wall is divided into three parts in the radial direction. A boundary cell is used on the outer surface to impose the adiabatic boundary condition if the channel is insulated, i.e.

$$T_w(z,\theta,r_5) = T_w(z,\theta,r_4) \tag{10.20}$$

For the interior nodes, i.e. $i = 2,4$ ($i \equiv r$); $j = 2$, $JZ-1$ ($j \equiv z$) and $k = 2,8$ ($k \equiv \theta$), the energy equation can be written in finite difference form

$$\begin{aligned}\frac{1}{\alpha^n_{i,j,k}}\,\frac{T^{n+1}_{i,j,k} - T^n_{i,j,k}}{\Delta t} = {} & \frac{1}{R_i}\,\frac{T^n_{i+1,j,k} - T^n_{i-1,j,k}}{2\Delta r} \\ & + \frac{T^n_{i+1,j,k} + T^n_{i-1,j,k} - 2\,T^n_{i,j,k}}{(\Delta r)^2} \\ & + \frac{T^n_{i,j,k+1} + T^n_{i,j,k-1} - 2T^n_{i,j,k}}{(R_i\ \Delta\theta)^2} \\ & + \frac{T^n_{i,j+1,k} + T^n_{i,j-1,k} - 2\,T^n_{i,j,k}}{(\Delta z)^2} + \frac{Q'^n_{i,j,k}}{k^n_{i,j,k}}\end{aligned} \tag{10.21}$$

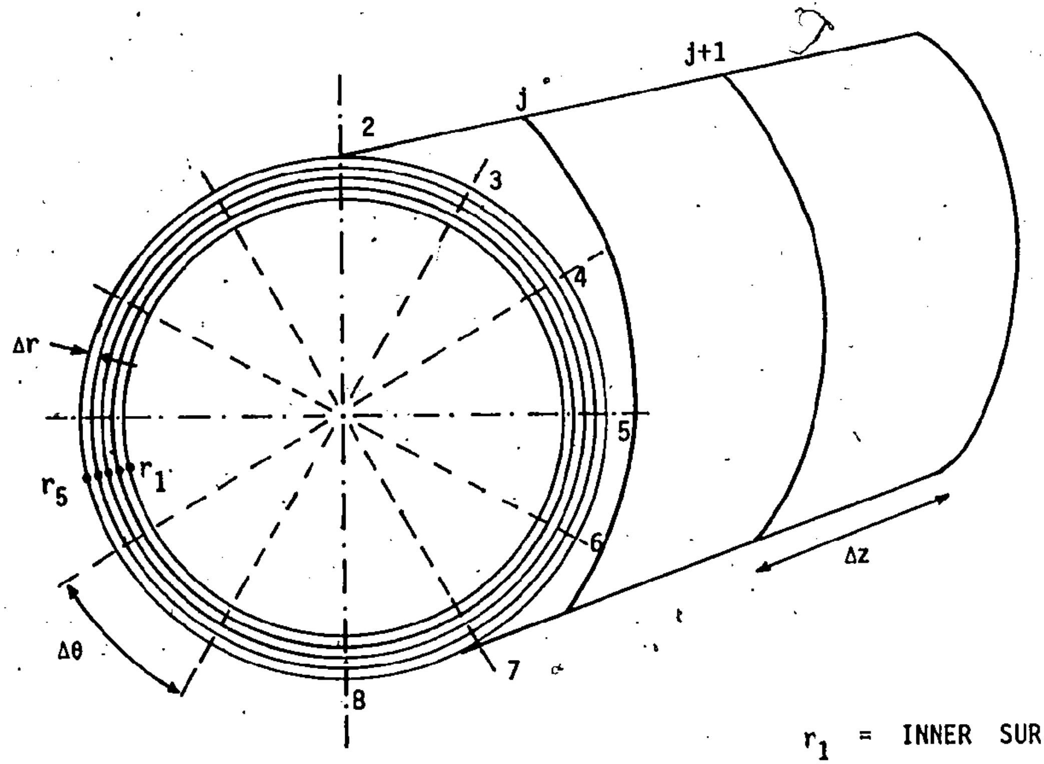

r_1 = INNER SURFACE
r_4 = OUTER SURFACE
r_5 = BOUNDARY CELL

FIG. 10.5 FINITE DIFFERENCE GRID FOR T_W COMPUTATION

It can be seen that the terms on the right hand side are known explicitly and the equation can be solved for $T^{n+1}_{i,j,k}$.

Boundary Conditions

The boundary conditions used are as follows:

(i) z-direction

$$T_{i,1,k} = T_{i,2,k}$$

$$T_{i,JZ,k} = T_{i,JZ-1,k}$$

(ii) θ-direction

$$T_{i,j,1} = T_{i,j,3}$$

$$T_{i,j,9} = T_{i,j,7}$$

(iii) r-direction:

Adiabatic boundary condition:

Taking for example, the outer surface to be insulated

$$T_{5,j,k} = T_{4,j,k}$$

Convective boundary condition:

Taking the inner surface as an example, consider the finite difference grid shown in Figure 10.6(a), a control volume ABCD which is defined by the surface temperature $T_{1,j,k}$ is used. Where

$AB = CD = \Delta r/2$

$BC = AD = R\Delta\theta$

FIG. 10.6 FINITE DIFFERENCE GRID FOR CONVECTIVE BOUNDARY CONDITION

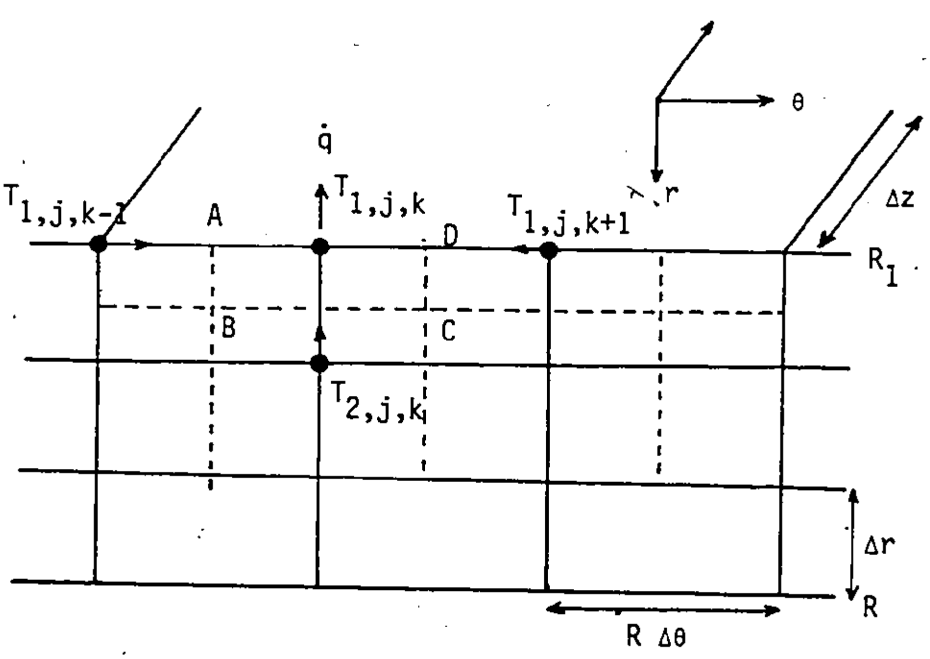

(A) THREE DIMENSIONAL FORMULATION

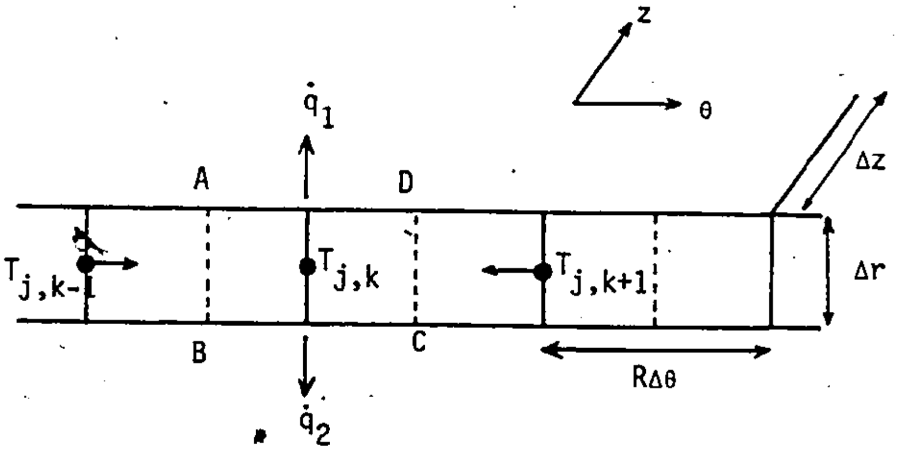

(B) TWO DIMENSIONAL FORMULATION

An energy balance on the control volume results in the following equation

$$\frac{1}{\alpha^n_{1,j,k}}(R_1\Delta\theta)(\frac{\Delta r}{2})(\Delta z)\ \frac{T^{n+1}_{1,j,k} - T^n_{1,j,k}}{\Delta t} - (R_1\Delta\theta)(\frac{\Delta r}{2})\ \frac{Q'^n_{1,j,k}}{k^n_{1,j,k}}\ (\Delta z)$$

$$= (\frac{\Delta r}{2})(\Delta z)[\frac{T^n_{1,j,k+1} - T^n_{1,j,k}}{R_1\Delta\theta} + \frac{T^n_{1,j,k-1} - T^n_{1,j,k}}{R_1\Delta\theta}]$$

$$+ (\frac{\Delta r}{2})(R_1\Delta\theta)[\frac{T^n_{1,j+1,k} - T^n_{1,j,k}}{\Delta z} + \frac{T^n_{1,j-1,k} - T^n_{1,j,k}}{\Delta z}]$$

$$+ (R_1\Delta\theta)(\Delta z)\ \frac{T^n_{2,j,k} - T^n_{1,j,k}}{\Delta r} - \frac{\bar{h}}{k^n_{1,j,k}}\ (R_1\Delta\theta)(\Delta z)(T^n_{1,k,j} - T^n_{Fj}) \qquad (10.22)$$

It can be seen that the first three terms on the right hand side are the heat conduction terms from the surrounding into the control volume, the last term is the heat loss from the surface by convection.

Dividing Eq. (10.22) by the volume of the control volume, we have

$$\frac{1}{\alpha^n_{1,j,k}}\ \frac{T^{n+1}_{1,j,k} - T^n_{1,j,k}}{\Delta t} = \frac{T^n_{1,j,k+1} + T^n_{1,j,k-1} - 2T^n_{1,j,k}}{(R_1\Delta\theta)^2}$$

$$+ \frac{T^n_{1,j+1,k} + T^n_{1,j-1,k} - 2T^n_{1,j,k}}{(\Delta z)^2} + \frac{2(T^n_{2,j,k} - T^n_{1,j,k})}{(\Delta r)^2}$$

$$- \frac{2\bar{h}}{\Delta r\ k^n_{1,j,k}}\ (T^n_{1,j,k} - T^n_{Fj}) + \frac{Q'^n_{1,j,k}}{k^n_{1,j,k}} \qquad (10.23)$$

Equation (10.23) gives the surface temperature in three dimensional formulation with a convective boundary. This equation, together with Eq. (10.21) can be used to give detailed temperature variations along the channel.

Stability Considerations

When the transient heat conduction equation (Eq. (10.3)) is solved using the forward-difference explicit method shown in Eq. (10.21), care must be taken in choosing the time step size (Δt) so that numerical stability can be assured. Detailed discussion on the stability problem can be found in Eckert and Drake [125], here it will be suffice to state the stability requirement,

$$\Delta t \leq \min\left\{ \frac{(\Delta r)^2}{6\alpha}, \frac{(r\Delta\theta)^2}{6\alpha}, \frac{(\Delta z)^2}{6\alpha} \right\} \tag{10.24}$$

where α is the thermal diffusivity.

From Equation (10.24), it is obvious that the size of Δt is severely limited by Δr when a thin walled tube is used. Since the channel wall is very thin in the rewetting and refilling experiments (δ = 0.08636 cm), Δt used must be less than 0.001 second to ensure stability. This time step size is less than one fifth of that used in solving the hydraulic equations (Section 9.4).

Because a small step means longer computation time and higher computation costs, in order to reduce costs, a possible way is to assume a uniform temperature across the channel wall. This is a very good assumption for thin walls. In fact, the temperature difference across the wall is found to be small in general in the present experiment (less than 5°C except near the quench front where a difference of 20 to 30°C is possible) when the three dimensional equation is solved.

If the assumption that the temperature be uniform across the wall is made, the finite difference equation can be derived using the grid shown in Figure 10.6 (b).

$$\frac{1}{\alpha^n_{j,k}} \frac{T^{n+1}_{j,k} - T^n_{j,k}}{\Delta t} = \frac{T^n_{j,k+1} + T^n_{j,k-1} - 2T^n_{j,k}}{(R\Delta\theta)^2}$$

$$+ \frac{T^n_{j+1,k} + T^n_{j-1,k} - 2T^n_{j,k}}{(\Delta z)^2} - \frac{h^n_{1,j,k}}{k^n_{j,k}\,\delta} (T^n_{j,k} - T^n_{F_1})$$

$$- \frac{h^n_{2,j,k}}{k^n_{j,k}\,\delta} (T^n_{j,k} - T^n_{F_2}) \qquad (10.25)$$

The second last and the last term on the right hand side are the convective heat losses from the inner and outer surfaces respectively. h_2 will be zero when the outer surface is insulated. Since there is no interior point in the two-dimensional formulation, Eq. (10.21) does not apply and the temperature variations are given by Eq. (10.25). The stability requirement becomes

$$\Delta t \leq \min\left\{\frac{(R\Delta\theta)^2}{4\alpha}, \frac{(\Delta z)^2}{4\alpha}\right\} \qquad (10.26)$$

10.3.5 Liquid Temperature

The bulk liquid temperature is given by Eq. (10.5) which again can be solved numerically using an explicit finite difference technique. The finite difference grid used is shown in Figure 10.7. If we ignore the conduction term which is normally small compared to the other terms, the equation can be written in finite difference form

$$\frac{(\alpha_L T_L)^{n+1}_j - (\alpha_L T_L)^n_j}{\Delta t} = - \frac{\alpha^n_{j+1/2}(u_L)^n_{j+1}(T_L)^n_j - \alpha^n_{j-1/2}(u_L)^n_j(T_L)^n_{j-1}}{\Delta z}$$

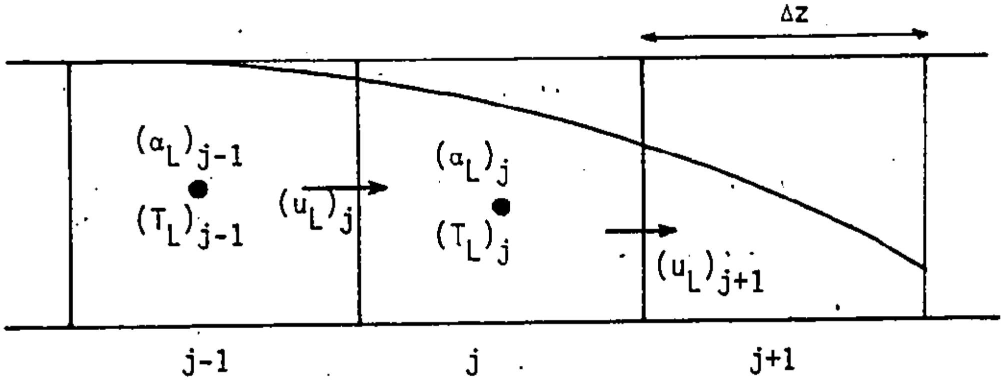

FIG. 10.7 FINITE DIFFERENCE GRID USED FOR BULK LIQUID TEMPERATURE CALCULATION

$$+ \left(\frac{1}{\rho C_p}\right)_j^n q_j^n \tag{10.27}$$

where q_j^n is obtained by numerically integrating Eq. (10.6) and $(\alpha_L)_j^{n+1}$ can be estimated using the expression

$$(\alpha_L)_j^{n+1} = (\alpha_L)_j^n + \frac{\Delta t}{\Delta z}\left[\alpha_{j-1/2}(u_L)_j - \alpha_{j+1/2}(u_L)_{j+1}\right]^n \tag{10.28}$$

To solve the finite difference equation (10.27), a constant inlet liquid temperature is assumed, i.e.

$$(T_L)_1 = T_L^\circ .$$

The stability requirement for the solution scheme is

$$\Delta t \le \frac{\Delta z}{u_L} \tag{10.29}$$

10.3.6 Output of the Dependent Variables

In the computer code REWET, the dependent variables are output at every time step for all nodes (Figure 10.2). The variables shown include h_L, u_L, u_G, c, T_L and T_W. The wall temperatures are output at three locations, bottom (T_W^B), mid-side (T_W^R) and top (T_W^T). Since T_L and T_W are defined at the cell centers in the cell arrangements shown in Figure 10.2, the temperatures at the cell boundary (which are output) are obtained by taking the mean temperatures between the two adjacent cells.

10.3.7 Time Step Size

The time step size (Δt) must be chosen such that stability conditions are satisfied. In the computer code REWET, the hydraulic equations (Eq. (10.1) and (10.2)), the wall temperature (Eq. (10.3)) and the bulk liquid temperature (Eq. (10.5)) are solved numerically "independent" of each other. Therefore, there are three stability conditions. They are

$$\Delta t \leq \min \{ \frac{\Delta z}{|u_L + c|} , \frac{\Delta z}{|u_L - c|} \} \tag{9.34}$$

$$\Delta t \leq \min \{ \frac{(R\Delta\theta)^2}{4\alpha} , \frac{(\Delta z)^2}{4\alpha} \} \tag{10.26}$$

$$\Delta t \leq \frac{\Delta z}{u_L} \tag{10.29}$$

It can be shown that in general, Eq. (9.34) tends to limit Δt the most because of the large gravity wave velocity (c) when the tube is nearly filled. Equation (9.34) can also be written in a slightly different form numerically

$$\Delta t \leq \{ \frac{2\ \Delta z}{|(U+c)_L| + |(U-c)_R|} \}_j \quad j = 1, \ldots JZ \tag{10.30}$$

This is used to determine Δt at each time step.

10.3.8 Interfacial Transfer Terms

The interfacial transfer terms include interphase mass and momentum transfer, vapor inertia and phase to wall viscous terms. These terms appear on the right hand side of the hydraulic equations (E_1 and E_2) and have to be known before equations (10.1) and (10.2) can be solved.

Constitutive models are required to obtain these transfer terms and they are, in general, flow regime dependent. Constitutive models for one-dimensional two-phase flows are given by Hughes et al [58] for different flow regimes. Here, a brief description of the interfacial transfer terms used in the REWET code will be given. Stratified flow is assumed.

In the REWET code, the hydraulic equations of the liquid phase are solved. However, the vapour phase equations are not solved in detail. This is necessary in order to simplify the model as well as the solution scheme (Section 10.2.1). Instead, the vapor phase is assumed to be in quasi-static state and the vapor phase velocity is obtained by integrating the steady state vapor continuity equation

$$u_G = \frac{1}{\rho_G \alpha_G} \int \dot{m}_L \, dz$$

or in finite difference form

$$(u_G)_j = \frac{1}{\rho_G} \sum_{\lambda=1}^{j} (\dot{m}_L \, \Delta z) \, / (\alpha_G)_j \qquad (10.31)$$

It should be noted that ρ_G is assumed to be constant (incompressible) and since u_G is obtained only by mass conservation considerations, u_G as given in Eq. (10.31) is expected to be higher than the actual value. This is because wall and interfacial shears as well as vapor inertia which are not included in the equation will tend to retard the vapor flow in the real situation. This will lead to an increase in ρ_G and decrease in u_G.

The over-prediction of u_G in REWET will mean a stronger coupling between the vapor and liquid phases. The effects on the refilling and rewetting results, however, are expected to be relatively small. This is because the liquid flow which dominates the refilling and rewetting characteristics is determined primarily by the inlet flow rate and the hydrostatic pressure head behind the stratified quench front. The good agreements between the numerical and experimental results and the relatively insensitivity of the numerical results to interfacial transfer terms (Section 10.6 and 10.7) strongly support the above argument. However, the high vapor velocity may induce surface wave on the interface and may cause stability concerns.

10.3.8.1 Interfacial Mass Transfer

The net interfacial mass transfer is given by

$$\dot{m}_L = \frac{\beta Q}{h_{fg}} \tag{10.32}$$

where Q is the total energy input, h_{fg} is the heat of vaporization and β is the fraction of total energy input for evaporation. β is unknown except under some special situations and assumptions have to be made regarding to the values used. This will be discussed later when numerical results are presented. It should be noted that $(1-\beta)$ will be the fraction of energy input used to reduce the liquid subcooling.

10.3.8.2 Wall Shear -- Liquid Phase

The liquid to wall viscous force per unit volume can be written in the form

$$F_{WL} = \frac{1}{2} f_L \, u_L \, |u_L| \rho_L a_L / \alpha_L A_0 \tag{10.33}$$

where a_L is the liquid to wall contact perimeter as defined by Eqs. (9.48) for $h_L \le R$ and (9.49) for $h_L \ge R$. α_L is the liquid fraction. A_0 is the cross-sectional channel area. f_L is the liquid friction factor.

In general, f_L is not constant. It assumes different values in different flow regions. The values used in REWET are as follows:

(a) $f_L = mf$ in the inlet feeder region
(b) $f_L = f$ in the totally quenched or filled region (h_L=D)
(c) $f_L = \phi f$ in the quenching region
(e) $f_L = 0$ in the film boiling region

where f is given by the Blasius equation (Eq. (9.55)). m is the friction factor multiplier for the refilling of a dry channel (Figure 9.9). ϕ is the two phase frictional multiplier. ϕ can be large because of the voilent boiling in the quenching region. For homogeneous steam-water system, it has been found (Wallis [126]) that ϕ can have values from 16 to 120 for steam qualities of 1 to 10% at atmospheric pressure. Values of 25 to 200 have been used in REWET. It was found that the results are not sensitive to the range of ϕ values used.

10.3.8.3 Wall Shear -- Vapor Phase

Analogous to the liquid phase, the vapor to wall viscous force per unit volume is given by

$$F_{WG} = \frac{1}{2} f_G \, u_G |u_G| \rho_G \, a_G/\alpha_G A_o \tag{10.34}$$

where $a_G = (2\pi R - a_L)$ and $\alpha_G = 1 - \alpha_L$.

The vapor friction factor (f_G) is, in principle, a function of the vapor Reynolds number. However, for simplicity, a constant value of 0.005 (Wallis [126]) is used in REWET. A value of 0.001 has also been used in an effort to compensate for the possible over-prediction in vapor velocity.

The results show no significant difference in rewetting rates.

10.3.8.4 Interfacial Shear

The interfacial viscous force per unit volume acting on the vapor-liquid interface because of the relative motions of the two phases is given by

$$F_{GL} = \frac{1}{2} f_i \; u_r \; |u_r| \rho_G a_i / A_0 \qquad (10.35)$$

where $u_r = u_G - u_L$ and a_i is the interfacial surface area per unit length. Assuming a stratified interface

$$a_i = 2 \sqrt{2Rh_L - h_L^2}$$

where h_L is the water level.

f_i is the interfacial friction factor and is a function of the interface Reynold's number. Again, for simplicity, $f_i = 0.005$ (Wallis [126]) is used. $f_i = 0.001$ has also been used as in the vapor to wall shear. Again, no significant difference in the rewetting results is observed.

10.3.8.5 Vapor Inertia

The vapor inertia term can be written as

$$V_{int} = \rho_G \; u_G \frac{\Delta u_G}{\Delta z} \qquad (10.36)$$

It should be noted that since u_G is not solved properly in REWET and over-prediction in u_G is expected, vapor inertia can act as a strong de-stabilizing term in the liquid hydraulic equations. It has been found that in some cases the contribution of vapor inertia has to be reduced in order to stabilize the numerical scheme.

10.3.8.6 Momentum Transfer due to Mass Transfer

The effect of mass transfer on the momentum of a phase is given by

$$T_m = \dot{m}_L \, u_i \tag{10.37}$$

where $\dot{m}_L$ is the net mass transfer across the interface and is given by Eq. (10.32). u_i is the interface velocity. In general, u_i is different from the velocity of either phase.

Physically, we would expect u_i to be bounded by the phase velocities and we may assume

$$u_i = u_G + (1-\gamma)\, u_L \tag{10.38}$$

where γ is a weighting factor ($0 \leq \gamma \leq 1$). $\gamma = 0.5$ is used in REWET.

10.3.9 Hydraulic Equations

The hydraulic equations are solved using the explicit finite difference characteristic method. The numerical procedure has been discussed in detail in Section 9.4. With the terms on the right hand side evaluated using previous time step values, the flow parameters (u_L, u_G, h_L and c) can be obtained at the advanced time step.

The procedure can then be repeated until the channel is totally quenched.

10.4 Surface Rewetting

In order that the REWET code can predict the right quenching behaviour, the appropriate local heat transfer coefficients have to be supplied. As discussed in Section 10.3.3, quenching is associated with high heat transfer and since it is always preceded by stable film boiling except may be in the region closed to the top in a horizontal channel, it is clear that the high heat transfer results from the transition from stable film to transition or nucleate boiling. The conditons under which such transition takes place are not well understood. However, they are of paramount importance in the understanding of the rewetting processes. A transition model based on stability consideration will be described. The model is capable of predicting the right quenching conditions for our experiments and results compare very well with experimental data.

10.4.1. Necessary and Sufficient Conditions for Surface Rewetting

When in film boiling, the heating surface is blanketed by a thin film of vapor. Surface rewetting suggests break up of the liquid-vapor interface. It should be emphasized here that the break up of the interface does not automatically lead to surface rewetting. A good example will be the break up of an extended liquid mass boiling over a very hot surface into a number of smaller masses when disturbed. No surface rewetting results. When the interface breaks up, regions of enhanced heat transfer (rewet spots) may form on the heating surface. This provides the necessary conditions for surface rewetting. However, if the surface is highly conductive and has a high heat capacity, these rewet spots will dry up rapidly and film boiling is restored. Therefore, the sufficient conditions for surface rewetting would require that the rewet spots could grow or spread.

A process which has been widely observed experimentally leading to surface rewetting is the so called Leidenfrost transition. Leidenfrost transition is described by Hsu [127] as the transition from a dry heating surface (Leidenfrost state) to a partially wetted heating surface. It also means the end of stable film boiling. Physically, when a hot surface is in stable film boiling, the surface temperature drops slowly if more heat is lost from the surface by film boiling than is supplied externally, the vapor generation rate will also decrease. Eventually, a point will be reached at which the vapor thrust due to vapor generation can no longer support a continuous liquid-vapor interface. The liquid thus collapses onto and wets the surface. The surface temperature at this transition point is known as the "Leidenfrost" or "rewetting temperature" (see Section 7.1 and 7.2). It is believed that the thermal capacity of the surface at the rewetting temperature is low enough for the rewet spots to spread when they are formed, therefore, the decrease of the surface temperature to the rewetting temperature provides, in general, the necessary and sufficient conditions for surface rewetting. Since the spread or decay of the rewet spots is expected to be locally conduction controlled, this will explain why the rewetting temperatures have been found to depend on the physical properties of the surface as well as the surface finish.

It should be noted here that the concept of a "Leidenfrost" or "rewetting temperature" is not always tenable. Wachters et al. [99] has shown that under carefully designed experimental conditions, liquid drops can exist without wetting the heated surface even when the surface is below the saturation temperature of the liquid. This can happen when an intact vapor layer can be maintained.

The existence of intermittent solid-liquid contacts or rewet spots in stable film boiling has been detected by Bradfield [100] and Kovalev [128]. Their results give strong experimental support to the fact that interface break up or the formation of rewet spots on the heating surface does not, in general, provide sufficient conditions for surface rewetting if the surface temperature is above the rewetting temperature.

However, if the thermal capacity of the hot surface is low, e.g. a thin walled tube, rewet spots can spread once formed even if the surface temperature is high. Thus, the break up of the liquid-vapor interface will provide both necessary and sufficient conditions for surface rewetting. In other words, rewetting can occur independent of the surface temperature.

This has been found to be the case for our refilling and rewetting experiments which used a thin walled test section (δ = 0.00898 m). It was found that rewetting can occur at wall temperatures much higher than the corresponding "Leidenfrost temperature" and the "apparent" quench temperatures are quite different at different axial locations. Some typical experimental results have been shown in Figures 8.8 and 8.12. At atmospheric pressure, the Leidenfrost temperature of water has been found to be about 160-260°C (Table 7.1). However, from the Figures, it can be seen that the apparent quench temperature can be as high as 450°C for an initial wall temperature of 500°C. More important is that the bottom of the channel quenches at wall temperatures which can differ by more than 100°C. Since quenching can take place at relatively high, and also over a wide range of temperatures, instability of the liquid-vapor interface in film boiling is thus believed to be the dominant mechanism that results in surface quenching in our experiments. The mechanism that, in turn, leads to instability of the liquid-vapor interface will now be examined.

10.4.2 Instability in Film Boiling

The mechanism is based on the instability of a wave at the liquid-vapor interface. The instability is hydrodynamic in nature, the wall temperature affects it indirectly through the velocity and the thermophysical properties of the vapor. The use of wave stability in analyzing transition from film boiling was first proposed by Chang [129] and later formulated by Zuber [130]. The existence of capillary waves (or ripples) on the interface in film boiling has been observed experimentally, for example, by Bromley [131] and by Westwater and Santangelo [132], therefore, they are worth examining for an explanation for interface break up.

Hydrodynamically, when two fluids which are in contact with each other are in relative motion, then if the relative velocity is high enough, a Kelvin-Helmholtz instability (Lamb [133]) would set in. The amplitude of the capillary wave on the interface would grow under favourable conditions.

For a flat interface which oscillates under the influence of surface tension, the propagation equations of a small disturbance as derived by Lamb [133] and adopted by Zuber [130] is given by

$$c^2 = \frac{\sigma m}{\rho_L + \rho_G} - \frac{\rho_L \rho_G}{(\rho_L + \rho_G)^2} (u_G - u_L)^2 \qquad (10.39)$$

where σ is the water surface tension, u_G and u_L are the vapor and liquid velocities, m is the wave number and is given by

$$m = \frac{2\pi}{\lambda} , \qquad (10.40)$$

where λ is the wavelength.

The condition for instability is that the disturbance or wave can grow. That is, c should have an imaginary part. The stability criterion can be obtained for c to be wholly real as

$$u_{rel} = u_G - u_L \leq [\frac{\sigma m}{\rho_L \rho_G} (\rho_L + \rho_G)]^{1/2} \qquad (10.41)$$

When Eq. (10.41) is not satisfied, the interface becomes unstable and the necessary conditions for a transition from film boiling and subsequent surface rewet are present. It should be emphasized again that these may not be sufficient conditions except for very thin walled tubes. Sufficient conditions would require that the localized high heat transfer regions (rewet spot) could grow.

In the remainder of this section, a model based on an instability mechanism will be described. The vapor velocity in the vapor film will be evaluated. The stability criterion (Eq. (10.41)) will be studied under different hydraulic and thermal conditions and results compared with the quench data obtained from the experiments.

10.4.3 Vapor Flow in Film Boiling

Film boiling occurs when a continuous layer of vapor is generated at the liquid-vapor interface due to the heat conducted through the vapor film from the heating surface. Considerable experimental and analytical work has been done on film boiling under different physical situations. For example, film boiling on vertical surfaces was studied by Bromley [131] and Chang [134]. On horizontal surfaces it was analyzed by Chang [134], Berenson [98] and Hamill and Baumeister [135]. The analysis of film boiling on a horizontal cylinder was given by Bromley [131] and Breen and Westwater [136]. Film boiling for stratified flow in horizontal tubes was investigated by Kruger and Rohsenow [137]. In all these investigations, the primary objective was to obtain heat transfer coefficients. The vapor flow in the vapor film has not received much attention. Since the vapor velocity in the vapor film may determine the stability of the film if Kelvin Helmholtz instabilities are considered, it is one of the most important parameters in predicting the boiling transition and subsequent quenching of the surface in thin walled test sections. A detailed analysis of the vapor flow in the vapor film for stratified flow in horizontal tubes is given below.

The flow model used is as shown in Figure 10.8. It is a cross-section taken in the film boiling region in Figure 7.2. The liquid is separated from the tube wall by a thin vapor film. The thickness of the vapor film (δ) can vary under the influence of hydrostatic pressure, vapor thrust and pressure drop due to vapor flow. The flow of vapor in the film is assumed to be one dimensional as shown. Vapor is produced at the interface by boiling and it flows upward and vents to a vapor layer at the top of the tube.

Considering the vapor channel, we can write down the mass and momentum conservation equations for the vapor phase:

Mass Conservation

Assuming constant vapor density, the continuity equation can be written as

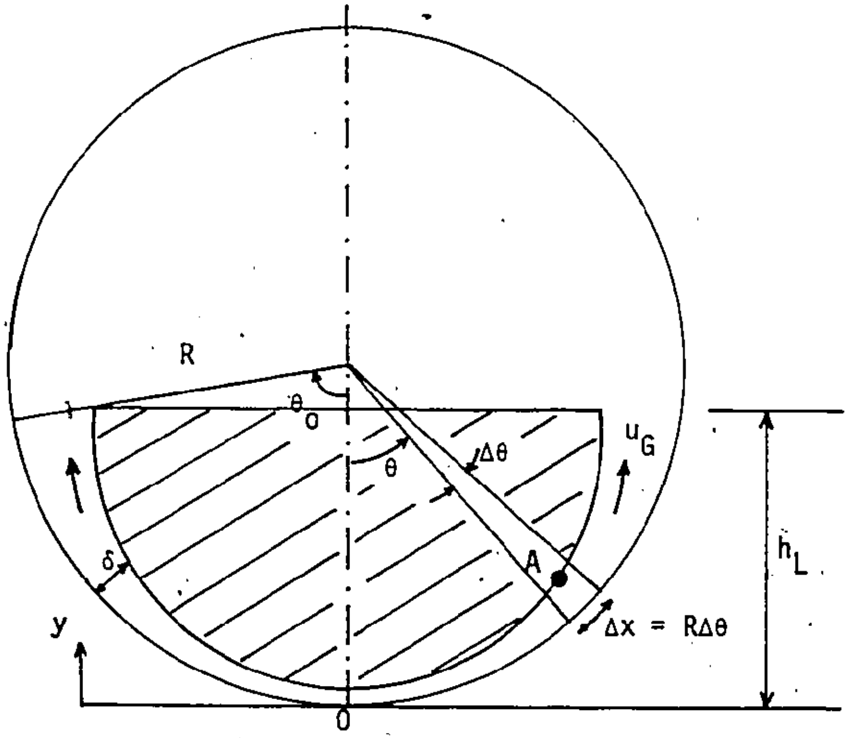

FIG. 10.8 FILM BOILING MODEL

$$\rho_G \frac{\partial \delta}{\partial t} + \rho_G \frac{\partial}{\partial x} (\delta . u_G) = \frac{h \Delta T}{h_{fg}} \tag{10.42}$$

where δ is the film thickness and u_G is the vapor velocity. The term on the right hand side is the vapor generation term. ΔT is the wall superheat ($\Delta T = T_w - T_{sat}$), h_{fg} is the heat of vaporization and h is the heat transfer coefficient. If heat transport was assumed to be by molecular conduction across the vapor film, h would be given by

$$h = \frac{k}{\delta} \tag{10.43}$$

where k is the vapor thermal conductivity.

Substituting Eq. (10.43) into (10.42), we have

$$\rho_G \frac{\partial \delta}{\partial t} + \rho_G \frac{\partial}{\partial x} (\delta . u_G) = \frac{k \Delta T}{h_{fg}} \frac{1}{\delta} \tag{10.44}$$

Momentum Conservation

The momentum conservation equation can be written as

$$\frac{\partial}{\partial t}(\delta . u_G) + \frac{\partial}{\partial x}(\delta . u_G^2) = - \frac{1}{\rho_G} \frac{\partial}{\partial x} (\delta . p) - \frac{1}{\rho_G} (\tau_G + \tau_i) + \frac{k \Delta T}{\rho_G h_{fg}} \frac{u_i}{\delta} \tag{10.45}$$

where P is the local pressure, τ_G and τ_i are shear stresses on the wall and vapor-liquid interface respectively, and u_i is the interfacial velocity. The last term on the right hand side is the momentum transfer due to phase changes. Considering a point A in the vapor film (Figure 10.8), the local pressure can be shown given by

$$P = \underbrace{\rho_L g(h_L - y)}_{P_{HH}} - \underbrace{\frac{1}{\rho_G}\left(\frac{k\Delta T}{h_{fg}}\frac{1}{\delta}\right)^2}_{P_{VT}} - \underbrace{\sigma\frac{\partial^2\delta}{\partial x^2}/\left[1 + \left(\frac{\partial\delta}{\partial x}\right)^2\right]^{3/2}}_{P_{ST}} \tag{10.46}$$

The terms are hydrostatic head (P_{HH}), vapor thrust (P_{VT}), and surface tension (P_{ST}). P_{HH} is maximum at $y = 0$ and equals zero at $y = h_L$. P_{VT} results from mass transfer. When there is mass transfer by evaporation, the evaporating vapor undergoes a change in normal velocity when crossing the interface. According to continuity across the interface, a pressure exists and exerts a force from vapor to liquid. Its magnitude is given by the second term in Eq. (10.46) (Wallis [138]). The contribution from P_{ST} is usually small except near $\theta = 0$ and can be ignored.

Substituting for P, Eq. (10.45) becomes

$$\begin{aligned}\frac{\partial}{\partial t}(\delta . u_G) + \frac{\partial}{\partial x}(\delta . u_G^2) &= -\frac{1}{\rho_G}\left[\rho_L g(h_L - y) - \frac{1}{\rho_G}\left(\frac{k\Delta T}{h_{fg}}\frac{1}{\delta}\right)^2\right]\frac{\partial\delta}{\partial x} \\ &- \frac{\delta}{\rho_G}\left[-\rho_L g\frac{\partial y}{\partial x} + \frac{2}{\rho_G}\left(\frac{k\Delta T}{h_{fg}}\right)^2\frac{1}{\delta^3}\frac{\partial\delta}{\delta x}\right] \\ &- \frac{1}{\rho_G}(\tau_G + \tau_i) + \frac{k\Delta T}{\rho_G h_{fg}}\frac{u_i}{\delta}\end{aligned} \tag{10.47}$$

Equations (10.44) and (10.47) can be simplified if the time derivatives are assumed to be small. The equations thus become

$$\delta\frac{\partial u_G}{\partial x} + u_G\frac{\partial\delta}{\partial x} = \frac{k\Delta T}{\rho_G h_{fg}}\frac{1}{\delta} \tag{10.48}$$

and

$$\delta . u_G \frac{\partial u_G}{\partial x} + A \frac{\partial \delta}{\partial x} = \frac{\rho_L}{\rho_G} g\,\delta \sin\theta - \frac{1}{\rho_G}(\tau_G + \tau_i) - \frac{k\Delta T}{\rho_G h_{fg}} \frac{u_G - u_i}{\delta} \qquad (10.49)$$

where

$$A = \frac{\rho_L}{\rho_G} g(h_L - R + R\cos\theta) + \left(\frac{k\Delta T}{\rho_G h_{fg}} \frac{1}{\delta}\right)^2 \qquad (10.50)$$

and Eq. (10.49) is obtained using (10.48) and $y = R - R\cos\theta$. It can be further simplified if we assume

$$\tau_G = \tau_i = \frac{1}{2} \rho_G \bar{f} u_G^2$$

and

$$u_G = u_i$$

where $\bar{f}$ is an average friction factor. We have

$$\delta . u_G \frac{\partial u_G}{\partial x} + A \frac{\partial \delta}{\partial x} = \frac{\rho_L}{\rho_G} g\delta\sin\theta - \bar{f} u_G^2 \qquad (10.51)$$

The set of equations ((10.48) and (10.51)) can be solved for δ and u_G. Since the equations are non-linear, numerical solutions are required.

The derivatives, $\partial u_G/\partial x$ and $\partial\delta/\partial x$ in Eq. (10.51) can be eliminated one at a time using Eq. (10.48) and the resulting equations are

$$(A - u_G^2) \frac{\partial \delta}{\partial x} = \frac{\rho_L}{\rho_G} g\,\delta \sin\theta - \bar{f} u_G^2 - \frac{k\Delta T}{\rho_G h_{fg}} \frac{u_G}{\delta} \qquad (10.52)$$

$$\delta(A - u_G^2) \frac{\delta u_G}{\partial x} = \frac{k\Delta T}{\rho_G h_{fg}} \frac{A}{\delta} - \left(\frac{\rho_L}{\rho_G} g\,\delta \sin\theta - \bar{f} u_G^2\right) . u_G \qquad (10.53)$$

An explicit finite difference technique is used to solve the set of equations which can be written as

$$\delta_{j+1} = R\Delta\theta\left[\frac{\rho_L}{\rho_G} g\,\delta\sin\theta - \bar{f}\,u_G^2 - \frac{k\Delta T}{\rho_G h_{fg}}\frac{u_G}{\delta}\right]_j / (A-u_G^2)_j + \delta_j \tag{10.54}$$

and

$$(u_G)_{j+1} = R\Delta\theta\left[\frac{k\Delta T}{\rho_G h_{fg}}\;\frac{A}{\delta} - \left(\frac{\rho_L}{\rho_G} g\,\delta\sin\theta - \bar{f}\,u_G^2\right)u_G^2\right]_j / \delta_j(A-u_G^2)_j + (u_G)_j \tag{10.55}$$

In order to start off the computation of δ_{j+1} and $(u_G)_{j+1}$, boundary conditions at $x = 0$ (or $\theta = 0$) have to be specified. By symmetry considerations,

$$(u_G)_o = 0 \quad\text{and}\quad \left.\frac{\partial\delta}{\partial x}\right|_o = 0 \tag{10.56}$$

It should be noted that the boundary conditions needed for the numerical scheme proposed are δ_o and $(u_G)_o$. δ_o is not known. However, Eqn. (10.56) can be used to evaluate $(u_G)_1$ and δ_1 at a small distance $R\Delta\theta$ from $x = 0$. For $\Delta\theta \rightarrow 0$, $\delta_1 \rightarrow \delta_o$ which gives the required boundary condition.

Applying the boundary conditions (Eq. (10.56)) to Eq. (10.48) and (10.51) and finite differencing the resulting equations, we have

$$\delta_1(u_G)_1 = R\Delta\theta\frac{k\Delta T}{\rho_G h_{fg}}\cancel{\frac{1}{\delta_1}} \tag{10.57}$$

and

$$\delta_1(u_G)_1^2 = R\Delta\theta\left[\frac{\rho_L}{\rho_G} g\;\delta_1\;\sin(\Delta\theta) - \bar{f}(u_G)_1^2\right] \tag{10.58}$$

These equations hold only for small $\Delta\theta$ and can be rewritten in the following form

$$\delta_1^2 = \frac{R\Delta\theta\;k\Delta T}{\rho_G\;h_{fg}}\frac{1}{(u_G)_1} \tag{10.59}$$

and

$$(u_G)_1^2 = \frac{\rho_L}{\rho_G} g\;\delta_1\;\sin(\Delta\theta)[\delta_1/R\Delta\theta + \bar{f}]^{-1} \tag{10.60}$$

For a given $\Delta\theta \to 0$, δ_1 and $(u_G)_1$ can be solved by iteration. The solutions are shown in Figure 10.9, where δ_0 (or δ_1) is plotted as a function of wall superheat (ΔT). It can be seen that δ_0 increases at ΔT increases. This is because for higher ΔT, the vaporization rate is higher, resulting in higher vapor thrust and larger δ_0. An interesting observation that can be made from this simple analysis is that δ_0 is independent of h_L. This means that the local heat transfer coefficient for stable film boiling is independent of h_L. The result is in agreement with other film boiling studies.

With the appropriate boundary conditions known, that is δ_0 and $(u_G)_0$ or δ_1 and $(u_G)_1$, Eqs. (10.54) and (10.55) can be used to compute δ and u_G along the vapor film channel. Some typical results are shown in Figure 10.10. It can be seen that δ is nearly constant in the first half of the vapor channel and opens up rapidly after that. u_G rises linearly from zero at the origin, gets to a maximum at the point when δ starting to increase rapidly. u_G then decreases due to an increase in flow area as δ increases.

10.4.4 Onset of Instability

The instability criterion for boiling transition as given by Eq. (10.41) can be reduced to

$$u_G \geq \left[\frac{2\pi\sigma}{\rho_G\lambda}\right]^{1/2} \qquad (10.61)$$

because in our experiments U_L is practically zero in the direction of the vapor flow in the vapor film and $\rho_L \gg \rho_G$.

FIG. 10.9 VAPOR FILM THICKNESS AT ORIGIN (δ_o) VS WALL SUPERHEAT (ΔT_W)

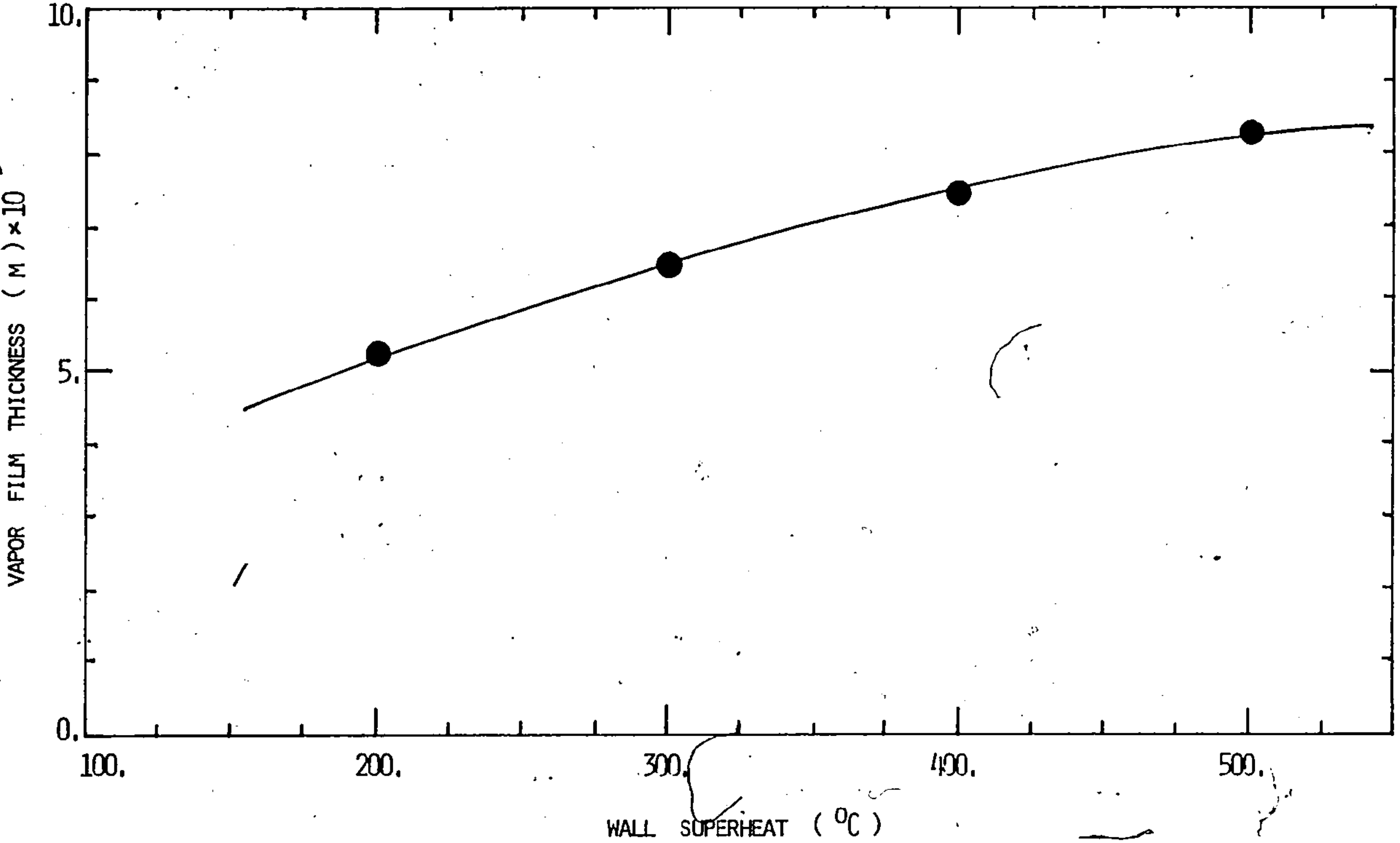

Fig. 10.10 VAPOR VELOCITY AND VAPOR FILM THICKNESS

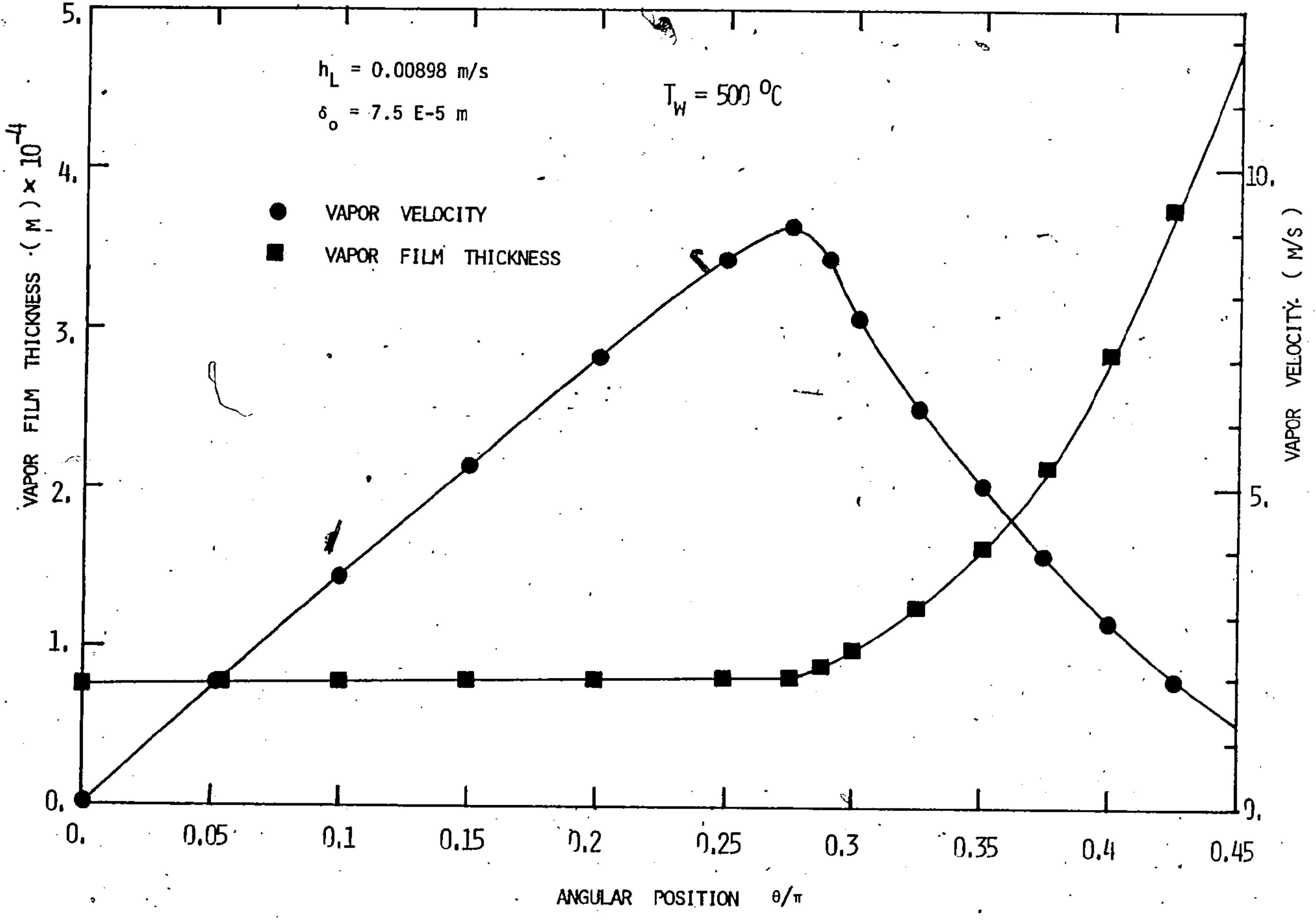

In order to study the stability of the vapor film, we need to know λ and u_G. λ is the wavelength of the Kelvin-Helmholtz instability and is dependent on the system geometry. For the flow situation shown in Figure 10.8, the two lowest possible modes of oscillation are given in Figure 10.11. Higher order harmonics can be excited at the later stage of the boiling transition when u_G can become large locally. However, at the onset of instability, only the fundamental mode and its first harmonic need be considered. It is not clear which of the two lowest possible modes will be excited because it is not clear whether the vapor channel length should be taken as the entire liquid-vapor interface length or just half of that due to symmetry.

Assuming the wavelength, λ equals the vapor channel length, the critical vapor velocity (u_{crit}) for the onset of the Kelvin-Helmholtz instability can thus be calculated using Eq. (10.61). Results for the fundamental mode and its first harmonic are plotted in Figure 10.12 for different water levels (h_L). It can be seen that u_{crit} is always higher for the first harmonic. This means that the first harmonic will be harder to excite.

The averaged vapor flow velocities in the vapor channel are also plotted in Figure 10.12. Results for different wall superheats (ΔT) are shown. Averaged vapor velocities are used here instead of the local vapor velocities because the growth of the interfacial wave is believed to be effected by the vapor flow over a certain distance, possibly over half of the wavelength (0-0' in Figure 10.11). Since it is not quite clear over what distance u_G should be averaged, a certain degree of uncertainty is involved in $\overline{u}_G$. Results shown in the Figure are averaged over a distance

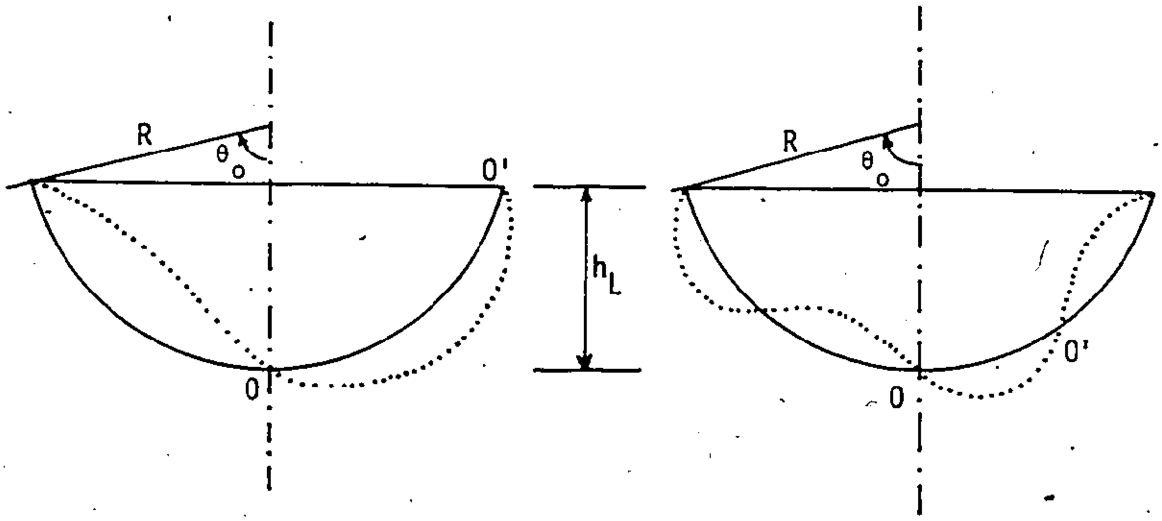

(a) $n = 0$
$\lambda = 2R\theta_o$

(b) $n = 1$
$\lambda = R\theta_o$

FIG. 10.11 POSSIBLE MODES OF OSCILLATION

FIG. 10.12 CRITICAL AND AVERAGE VAPOR VELOCITIES VS WATER LEVEL

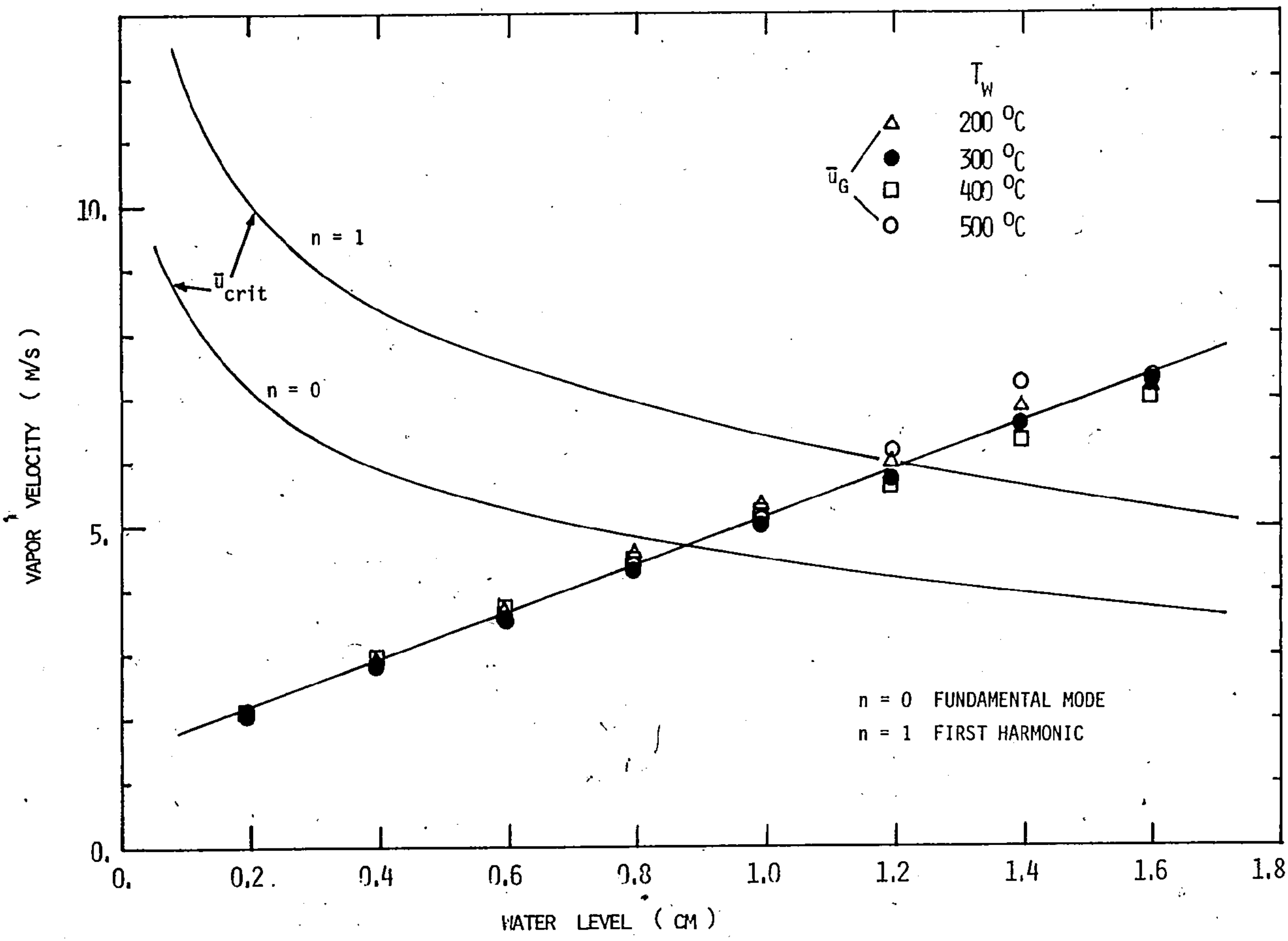

of 1/2 $R\theta_o$ from the origin. However, they do not differ significantly when a distance of $R\theta_o$ is used instead. This is because u_G is almost symmetric with respect to $\theta = \theta_o/2$ (Figure 10.9).

The critical water level for the onset of instability can be readily obtained from Figure 10.12. This is the water level at which $\bar{u}_G$ equals u_{crit}. Since $\bar{u}_G$ is essentially independent of ΔT, the wall superheat, $(h_L)_{crit}$ is also independent of ΔT. This result is expected as discussed in Section 10.4.1. It should also be noted that $(h_L)_{crit}$ is higher for the first harmonic.

From the above analysis, it is obvious that the $(h_L)_{crit}$ values so deduced are only good to a first approximation because λ and $\bar{u}_G$ are not known explicitly. Also the initiation of an interfacial instability may not always lead to rewetting as mentioned previously, though for very thin walled systems, it might provide both necessary and sufficient conditions. Empirically, $(h_L)_{crit}$ is adjusted until the rewetting velocities are in close agreement with experiments. This procedure will be described in the next section. The results are compared in Figure 10.13 for different initial wall temperatures. The agreement between the theoretically and empirically deduced values are surprisingly good. It may of course be fortuitous. The empirical curve lies between the corresponding curves for the fundamental mode and its first harmonics. A weak wall temperature dependence is observed for the empirical curve. $(h_L)_{crit}$ is found to increase slightly with T_W. This means that the wall temperature can have some effect on the boiling transition, which is expected physically. This is because an instability may result in conditions necessary for an instantaneous local rewetting, however, it is not sufficient for a rewet

FIG. 10.13 COMPARISON OF THEORETICAL AND EMPIRICAL CRITICAL WATER LEVEL FOR VAPOR FILM INSTABILITY

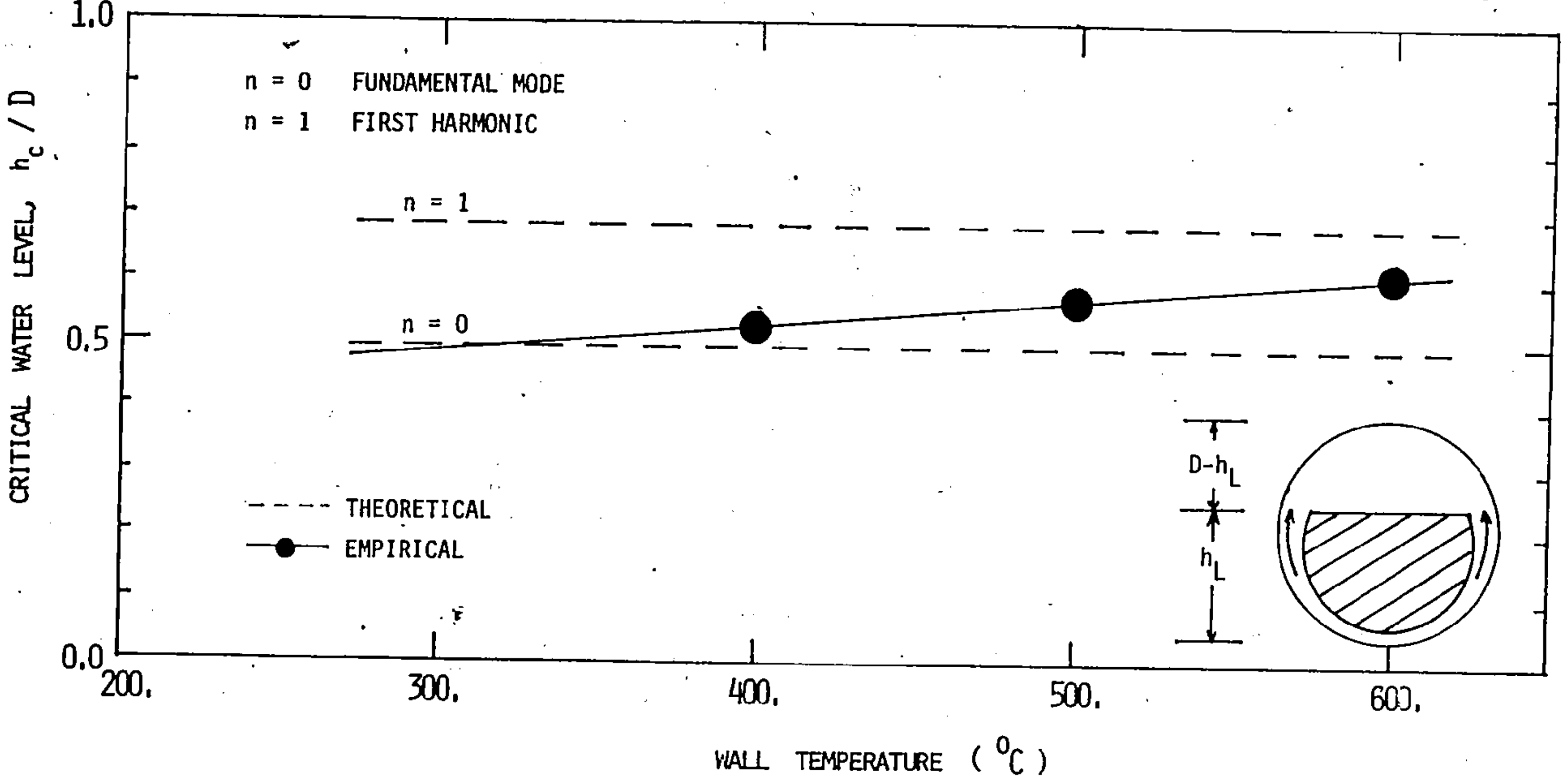

spot to grow except in the case of very thin walled tubes. Otherwise, the wall temperature and conductivity will also be important. However, the tube used in these experiments was thin, so the effect of wall temperature is weak.

10.5 The Quench Model

REWET requires the use of a quench model which can predict boiling transitions under different hydraulic and thermal conditions. As discussed in Section 10.4, the mechanism suggested for boiling transition in the present situation (refilling and rewetting of horizontal channels) is a Kelvin-Helmholtz type of hydrodynamic instability. A critical water level, $(h_L)_{crit}$ can then be defined. A simple quench model based on $(h_L)_{crit}$ is shown in Figure 10.14. In the Figure, the tube wall level (h_q) at which boiling transition occurs, is plotted against h_L, the water level. It can be seen that no transition takes place at the lower portion of the tube covered by water until $(h_L)_{crit}$ is reached. At this point, the vapor film becomes unstable, and boiling transition is postulated to occur. It is not clear how h_q changes with h_L. However, it is certain that h_q rises as h_L increases. At $h_L = D$, i.e. when the tube is filled to the top, boiling transition at the top is assumed or $h_q = D$. This assumption can be justified as follows.

When the tube is being filled up, that is h_L approaches D, the vapor flow area at the top rapidly decreases. A vapor film may form separating the wall from the liquid. However, because the vapor flow velocity in the axial direction will be high, the film will be very unstable and stable film boiling cannot exit. In addition, circumferential heat conduction is very effective in cooling the top of the tube if the tube has been quenched to a level close to the top. An example is given in Figure 10.15. The transient circumferential heat conduction problem is solved as discussed in Section 7.3.2. It can be seen that for $h_q >$ 0.975 D, the temperature at the top of the tube drops rapidly by circumferential heat conduction as shown in Figure 10.15. Less than 0.7 second is needed to reduce the temperature from 500°C to 250°C.

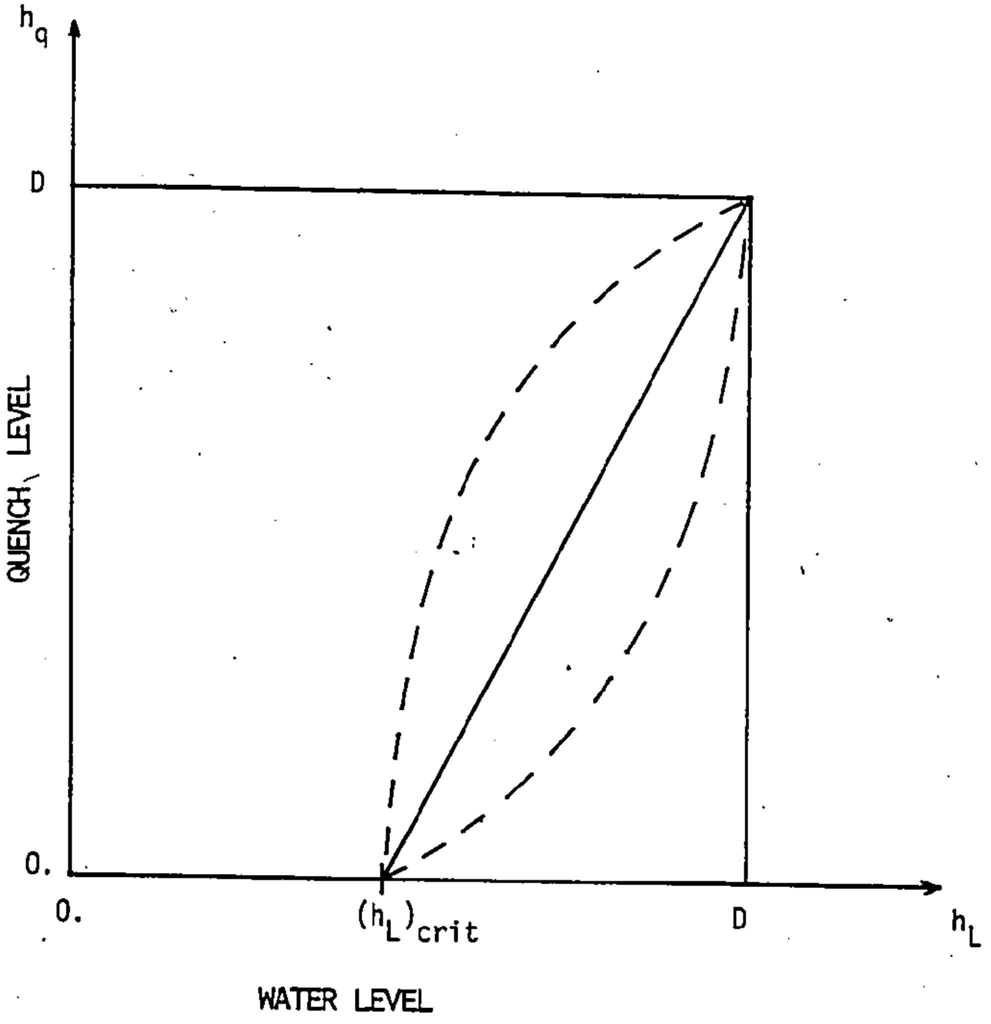

FIG. 10.14 QUENCH MODEL

FIG. 10.15 TRANSIENT CIRCUMFERENTIAL HEAT CONDUCTION

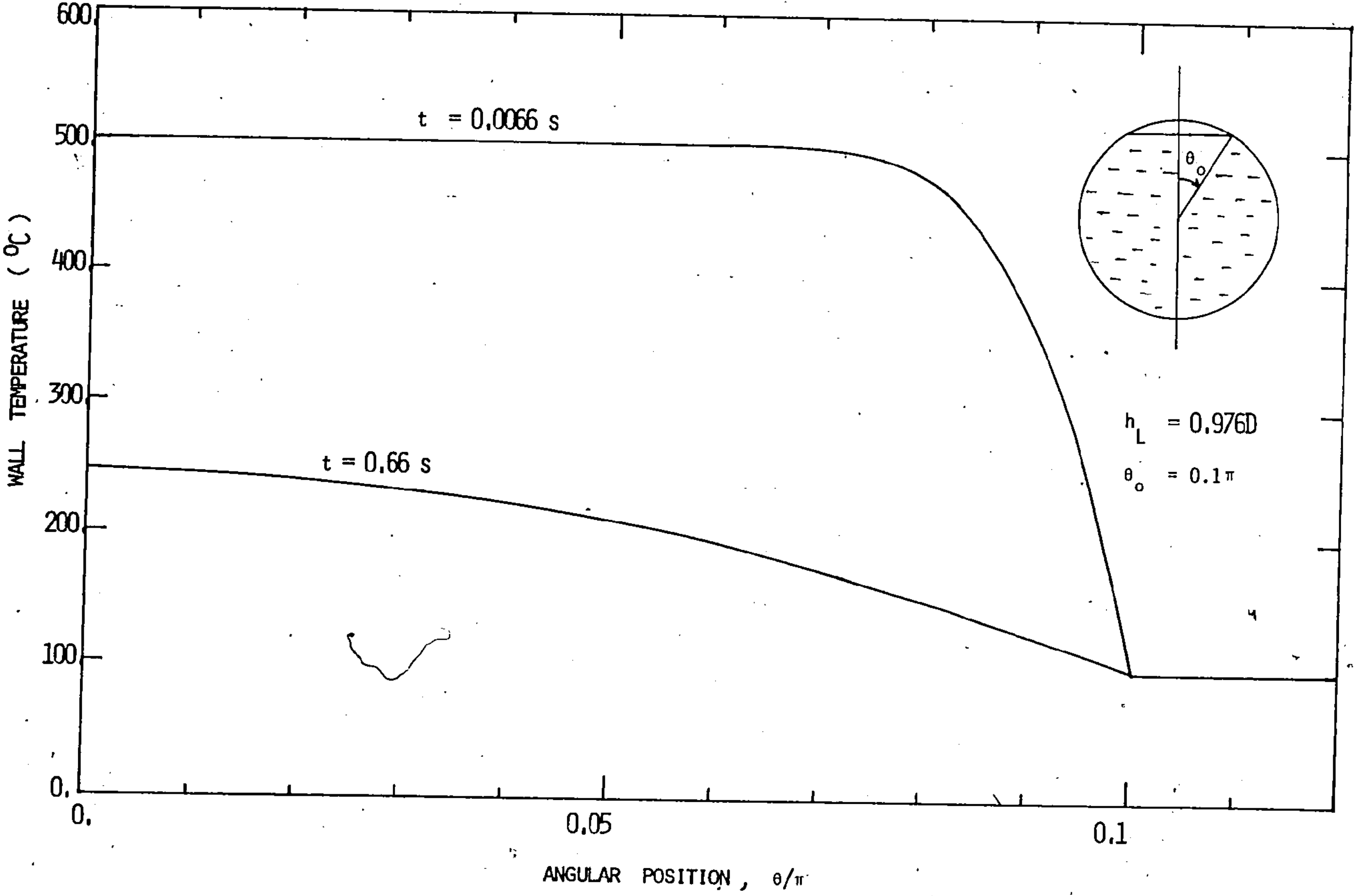

In Figure 10.14, h_q is assumed to be linearly dependent on h_L between $(h_L)_{crit}$ and D. However, this need not be the case. Other functions can be used. Examples are shown by broken lines in the Figure. Since the way the surface is quenched with respect to h_L is not known in detail, a straight line is drawn between the two known points given by h_{Lcrit} and D on the abscissa.

This straight line quench model is used in REWET. $(h_L)_{crit}$ can be obtained as discussed in Section 10.4. Details of the adjusting procedure for $(h_L)_{crit}$ is given below. Numerical results obtained will also be presented and compared with experiments in the following sections.

10.5.1 Critical Water Level

In the modelling of the refilling and rewetting processes using the simplified two-fluid model and the computer code REWET, the critical water level for the onset of vapor film instability is the only important parameter that needs to be adjusted. Theoretically, $(h_L)_{crit}$ is obtainable using the hydrodynamic instability model (Section 10.4.4). However, since the transition process is not well understood, $(h_L)_{crit}$ cannot be determined precisely. Depending on the wavelength and to a lesser degree, the distance over which the vapor velocity is averaged, the results can be somewhat different as shown in Figure 10.13. Therefore, more precise values of $(h_L)_{crit}$ may be obtained from the experimental data as discussed now.

Since $(h_L)_{crit}$ determines the onset of surface quenching for the bottom or lower portion of the tube, it will have a first order effect on the advancement of the leading edge of the quench front. Hence it can be adjusted numerically with regard to the experimentally measured $\overline{V}_B$. The code REWET is used to accomplish the adjustment. For given identical initial and boundary conditions, REWET is run for different $(h_L)_{crit}$ values. Results are then compared with the corresponding experiments. The $(h_L)_{crit}$ value that give the closest agreement is chosen.

The adjusted results are shown in Figure 10.16. The average rewetting velocities defined with respect to the bottom of the tube ($\overline{V}_B$) are plotted against $(h_L)_{crit}$ for different initial wall temperatures. A constant inlet flow rate of 85.0 ml/s is used. The experimentally obtained data points are also shown in bands. It can be seen that $\overline{V}_B$ decreases as $(h_L)_{crit}$ increases and intercepts the data bands. The $(h_L)_{crit}$ values that give $\overline{V}_B$ which are within the data bands are obtained. It should be noted that the $(h_L)_{crit}$ so deduced are highly empirical. Their accuracy depends on the accuracy of the experimental data (data band) used. In general, $(h_L)_{crit}$ can be determined to within 0.025D as can be seen in Figure 10.16. The empirical curve for $(h_L)_{crit}$ has been shown in Figure 10.13. As mentioned previously, they are reasonably well predicted by our instability theory. These values are used in the numerical calculations which will be presented below.

Fig. 10.16 REWETTING VELOCITY ($\overline{V}_B$) VS CRITICAL WATER LEVEL $(h_L)_{crit}$

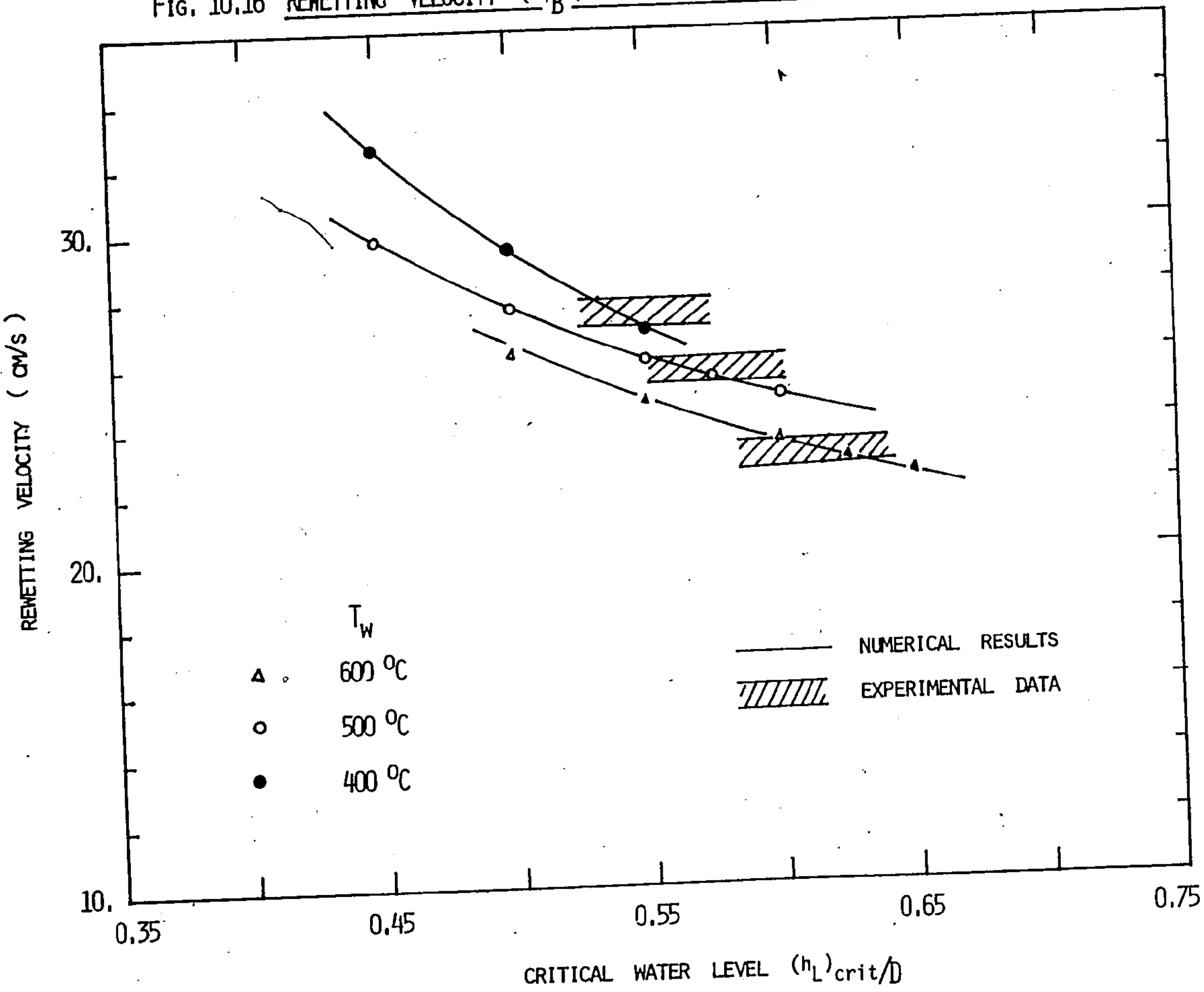

10.6 Numerical Results

Numerical results on the refilling and rewetting of hot horizontal channels are presented in this section. Transient behaviour was analysed using the computer code REWET. Results are compared with experimental data.

10.6.1 Constitutive Models

The constitutive relations or transfer terms required for the thermohydraulic calculations have been discussed in Sections 10.3.3 and 10.3.8. They are summarized here in Table 10.1. These relations were used in the REWET code.

It should be noted that the constitutive models used have been kept as simple as possible. For example, the friction factors, f_G and f_i assume constant values of 0.005 in the wall and interfacial shear terms. β assumes constant values of unity and zero in the film boiling and quenching regions respectively in the interfacial mass transfer model. Changes in these and other assumptions may change the numerical results. This will be discussed later in the chapter.

One of the most important parameters assumed in the constitutive models is β, the fraction of total energy input used for evaporation. This is because β determines the local net mass transfer across the interface and hence the vapor phase velocity. Consequently, all the interfacial transfer terms will be affected. In view of its importance, therefore, some justifications regarding to the β values used seem appropriate. It is fortunate that in our experiments, the results are believed to be only weakly dependent on the vapor velocity (Section 10.3.8). In other words, the numerical results are not going to be very sensitive to β, as shown later.

From the physical processes involved in the refilling and rewetting of a hot horizontal channel, it is obvious that β will depend on the local thermal and hydraulic conditions. However, for simplicity, a simple two-region model as shown in Figure 10.17 is used. β assumes constant values in the two regions separated by the leading edge of the quench front (JQ). JQ is defined at the point where $h_L = (h_L)_{crit}$. In the quenching region, because of the violent boiling and sputtering, the flow can be assumed to be well mixed. And because the quenching water is subcooled in general except may be in the leading edge of the quench front, $\beta_2 = 0$ is normally used. That is, all the heat input is assumed to be used to reduce the water subcooling. It should be noted that when the local water temperature reaches saturation, $\beta_2 = 1$ will be used. In fact, some form of subcooled boiling formulation can also be included.

In region 1, because of the existence of stable film boiling, part of the energy input will have to be used to generate the vapor film separating the wall and liquid. The energy required to sustain stable film boiling can be estimated as described below.

Using the film boiling model as shown in Figure 10.8, it can be seen that the rate of vapor vented from the vapor channel is given by

$$\dot{m}_v = 2\rho_G u_{vg} \delta_v \Delta z \tag{10.62}$$

where u_{vg} and δ_v are the vapor velocity and film thickness at the exit of the vapor channel respectively.

The rate of vapor generation by evaporation is given by

$$\dot{m}_e = \frac{\bar{h}A\,(T_w - T_{sat})}{h_{fg}} \tag{10.63}$$

where $\bar{h}$ is an average heat transfer coefficient, $A = 2R\theta_0\Delta z$ is the contact surface area.

To sustain the vapor film, we require $\dot{m}_v = \dot{m}_e$

or $$\bar{h} = \frac{\rho_g u_{vg} \delta_v h_{fg}}{R\theta_0 (T_w - T_{sat})} \tag{10.64}$$

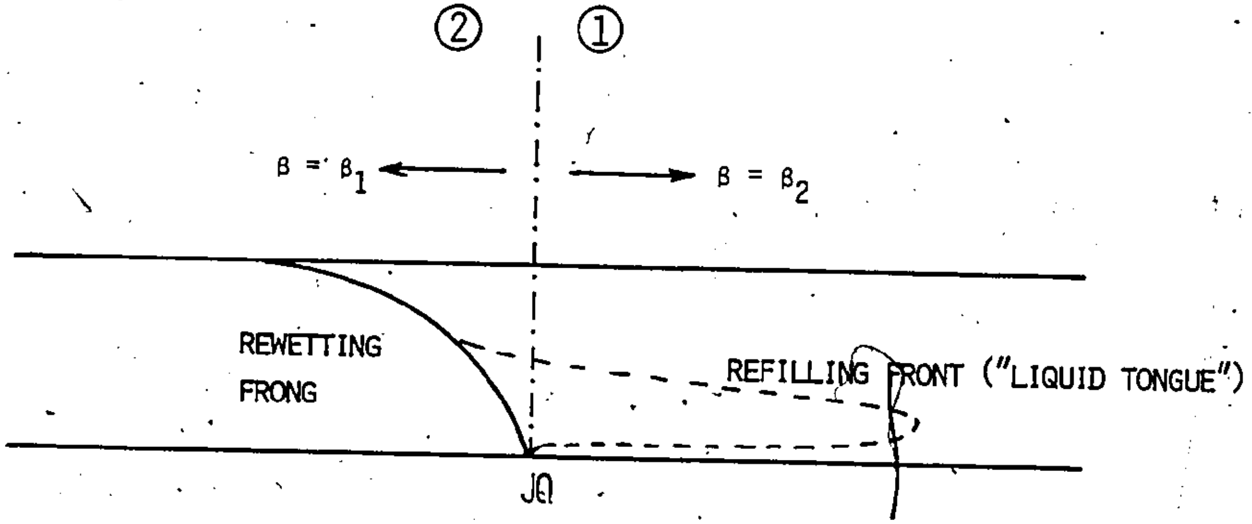

FIG. 10.17 A SIMPLE MODEL TO DETERMINE β

Since u_{vg} and δ_v can be obtained for given T_w and θ_o (Section 10.4.3), therefore, $\overline{h}$ can also be calculated. Using the typical results as shown in Figure 10.10, $\overline{h}$ is found to be ~0.019 W/cm^2-°C. This compares closely with the film boiling heat transfer coefficients obtained under similar conditions; $\overline{h}_{expt} \simeq 0.021$ W/cm^2-°C and $h_{calc} \simeq 0.018$ W/cm^2-°C for $T_w = 500$ °C (Figure 8.45).

Since nearly all the energy input will be used to sustain the vapor film in this region (i.e. $\overline{h}/h_{expt} \simeq 1$), therefore, $\beta_1 = 1$ is normally used in this region.

Table 10.1

Constitutive Relations Used in REWET

Constitutive Relations	Equations Used	Reference
Interfacial Mass Transfer	$\dot{m}_L = \frac{\beta Q}{h_{fg}}$ where $\beta = 1$ Film Boiling Region $= 0$ Quenching Region	Eq. (10.32) Section (10.6.1)
Wall Shear -Liquid Phase	$F_{WL} = \frac{1}{2} f_L u_L \lvert u_L \rvert \rho_L a_L / \alpha_L A_o$ where $f_L = mf$ Inlet Feeder Region $= f$ $h_L = D$ $= \phi f$ Quenching Region $= 0$ Film Boiling Region and $f = 0.0791/Re^{0.25}$ $m = F(u_L^o)$ $\phi = 60$	Eq. (10.33) Section (10.3.8.2) Eq. (9.55) Eq. (9.9)

Constitutive Relations	Equations Used	Reference
Wall Shear - Vapor Phase	$F_{WG} = \frac{1}{2} f_G u_G \lvert u_G \rvert \rho_G a_G / \alpha_G A_o$ where $f_G = 0.005$	Eq. (10.34)
Interfacial Shear	$F_{GL} = \frac{1}{2} f_i u_r \lvert u_r \rvert \rho_G a_i / A_o$ where $u_r = u_G - u_L$ $f_i = 0.005$	Eq. (10.35)
Momentum Transfer	$T_m = \dot{m}_L u_i$ where $u_i = \gamma u_G + (1-\gamma) u_L$ and $\gamma = 0.5$	Eq. (10.37)
Local Heat Transfer Model	(i) $h_L = 0$ $\overline{h} = h_{VF} + h_{FC} + h_{RAD}$ $0 \leq y \leq D$	Eq. (10.15)
	(ii) $0 < h_L < (h_L)_{crit}$ $\overline{h} = h_{FB} + h_{FC} + h_{RAD}$ $0 < y < h_L$ $\overline{h} = h_{VF} + h_{FC} - h_{RAD}$ $h_L \leq y \leq D$	Eq. (10.16)
	(iii) $(h_L)_{crit} \leq h_L < D$ $\overline{h} = h_{VF} + h_{FC} + h_{RAD}$ $h_L < y < D$ $\overline{h} = h_{FB} + h_{FC} + h_{RAD}$ $h_q < y \leq h_L$ $\overline{h} = h_Q + h_{FC} + h_{RAD}$ $0 \leq y \leq h_q$ where $h_Q = h_{TB}$ $T_w \geq T_{CHF}$ $= h_{NB}$ $T_{sat} < T_w < T_{CHF}$ $= h_{LF}$ $T_w \leq T_{sat}$	Eq. (10.17)

Constitutive Relations	Equations Used	Reference
	(iv) $h_L = D$ and $T_w < T_{sat}$ $\overline{h} = h_{LF} + h_{FC} + h_{RAD} \quad 0 \le y \le D$	Eq. (10.18)
Free Convection Heat Transfer Coefficient	$h_{FC} = 0.525(G_r P_r)^{0.25}\ k_f/D_h$	Eq. (8.10)
Radiation Heat Transfer Coefficient	$h_{RAD} = \sigma e(T_w^4 - T_f^4)/(T_w - T_f)$	Eq. (8.11)
Vapor Phase Heat Transfer Coefficient	$h_{VF} = 0.023\left(\frac{\rho_g u_G D_h}{\mu_g}\right)^{0.8} \frac{k_g}{D_h}$	Eq. (8.12)
Liquid Phase Heat Transfer Coefficient	$h_{LF} = 0.023\left(\frac{\rho_f u_L D_h}{\mu_f}\right)^{0.8} \left(\frac{C_p \mu}{k}\right)_f \frac{k_f}{D_h}$	Eq. (10.19)
Film Boiling Heat Transfer Coefficient	$h_{FB} = 0.425\left\{\frac{k_g^3 h_{fg} \rho_g g(\rho_f - \rho_g)}{\mu_g \Delta T \sqrt{\sigma / g(\rho_f - \rho_g)}}\right\}^{0.25}$	Eq. (8.13)
Transition Boiling Heat Transfer Coefficient	$h_{TB} = 9 \times 10^3 \exp(-0.0054\ \Delta T_w)$	Eq. (10.20)
Nucleate Boiling Heat Transfer Coefficient	$h_{NB} = \frac{\exp(P/630)}{(0.072)^2} \Delta T_w$	Eq. (10.21)

10.6.2 Quenching Characteristics

The characteristics of refilling and rewetting of hot horizontal channels are studied numerically using the computer code REWET. Results are compared with experiments. Depending on how well the experimental and numerical results compare, the applicability and usefulness of the simplified two-fluid model approach to the refilling and rewetting problem can be evaluated.

10.6.2.1 Transient Wall Temperatures

The wall temperatures are calculated in REWET by solving the transient heat conduction equation under given thermohydraulic conditions. The transient temperatures can be plotted as a function of time. An example is shown in Figure 10.18 where the temperatures at the top and bottom of the tube are plotted at different axial locations.

The corresponding experimental results are shown in Figure 10.19. The numerical and experimental results are superimposed in Figure 10.20 for direct comparison. Only temperatures at three locations (A,C,E) are shown for simplicity. It can be seen that the agreement between the numer~~ical~~ and experimental results is very good. The code REWET can predict the quench of the tube in reasonable detail, especially for the bottom of the tube. The "apparent" quench temperatures correspond very well. Different modes of heat transfer can also be easily identified. The slopes of the temperature curves in different regions are close to those observed in the experiments. This means that the heat transfer coefficients used in REWET are close to the actual values during the transient.

The results shown in Figures 10.18 and 10.19 are true only for relatively high inlet flows and initial wall temperatures. Different locations along the channel can be seen to be quenched in the proper order, i.e. the bottom and top of

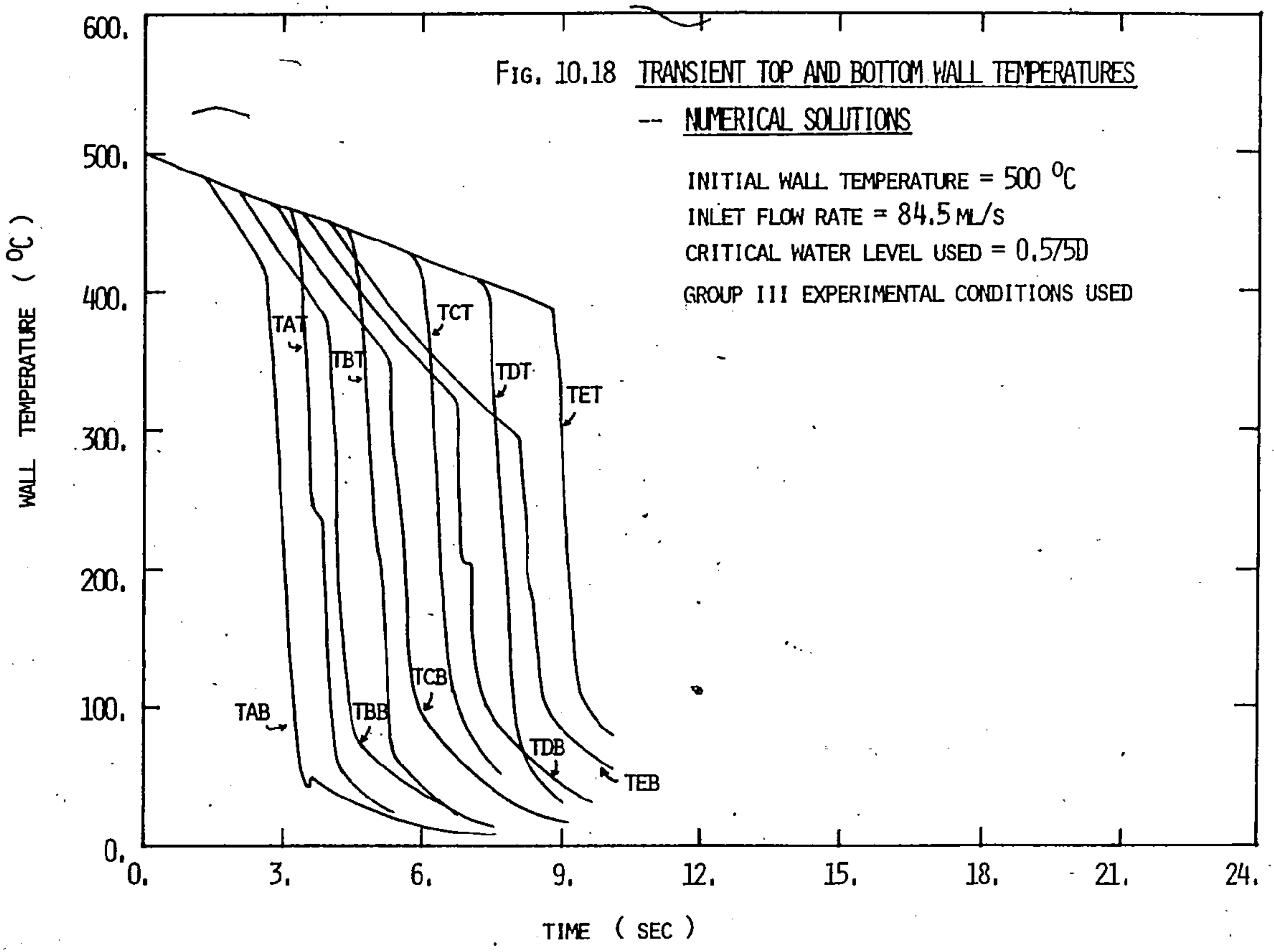

FIG. 10.18 TRANSIENT TOP AND BOTTOM WALL TEMPERATURES -- NUMERICAL SOLUTIONS

INITIAL WALL TEMPERATURE = 500 °C
INLET FLOW RATE = 84.5 ML/S
CRITICAL WATER LEVEL USED = 0.575D
GROUP III EXPERIMENTAL CONDITIONS USED

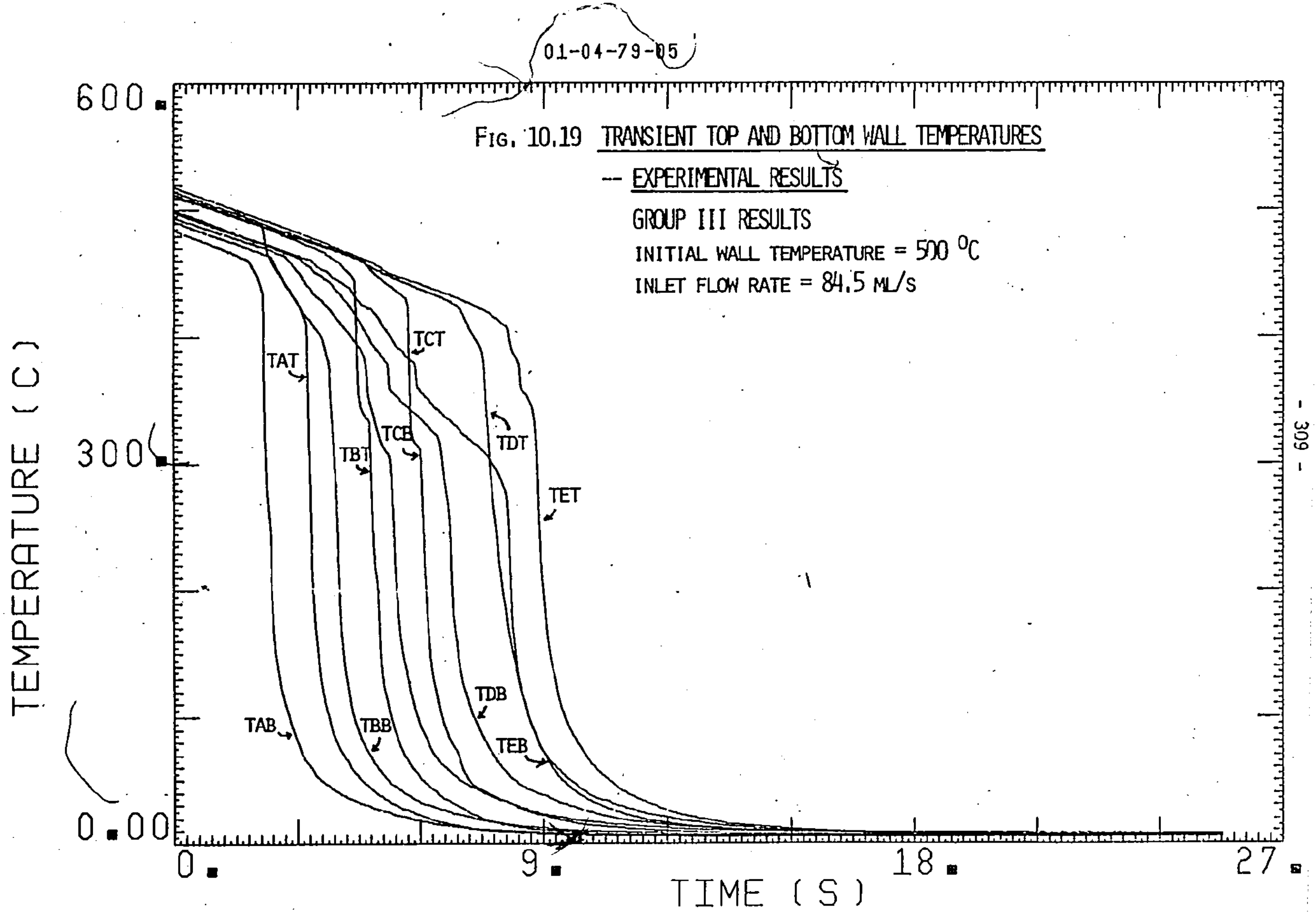

Fig. 10.19 TRANSIENT TOP AND BOTTOM WALL TEMPERATURES

-- EXPERIMENTAL RESULTS

GROUP III RESULTS

INITIAL WALL TEMPERATURE = 500 °C

INLET FLOW RATE = 84.5 ML/S

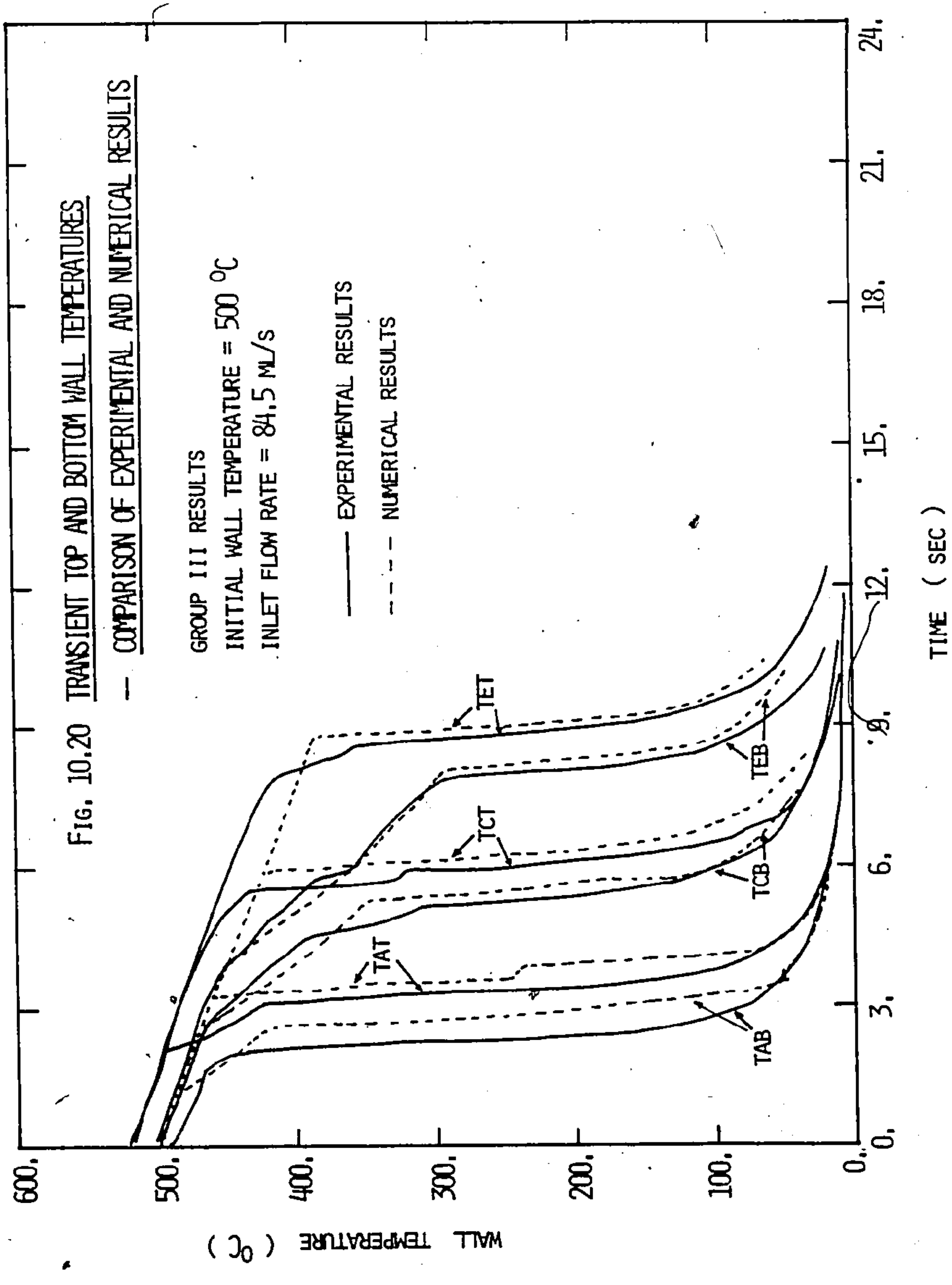

Fig. 10.20 TRANSIENT TOP AND BOTTOM WALL TEMPERATURES — COMPARISON OF EXPERIMENTAL AND NUMERICAL RESULTS

location A, then bottom and top of location B and so on. The local rewetting rates are quite uniform along the channel.

For low inlet flows ($\lesssim$ 60 ml/s) or low initial wall temperatures (< 400°C), the quenching characteristics have been found to be more complicated due to possible flow regime transitions (section 8.2). An example is given in Figure 10.21. The corresponding numerical results are shown in Figure 10.22. It can be seen that, the experimental and numerical results do not compare well in general. Experimentally, the bottom of the tube at locations B and C can be quenched before the top at location A (Figure 10.21). Whereas, numerical results predict the same orderly quenching of the channel as in the higher inlet flow cases (Figure 10.22). A more important difference is the 'apparent' quench temperatures of the bottom of the channel. Numerical results show significantly lower "apparent" quench temperatures than are observed experimentally. The pre-quenching characteristics of the bottom of the tube are also quite different. In Figure 10.22, the bottom is pre-cooled uniformly by stable film boiling until it is quenched. In Figure 10.21, the pre-cooling of the bottom appears to be quite complicated as is evident from the shape of the temperature traces (e.g. TDB and TEB).

The reasons for the poor agreement between experimental and numerical results for the low inlet flow cases are believed lying in the formulation of the simplfied two fluid model used in REWET. The model used assumes a flat stratified interface with a well defined water level. This assumption is also used in the determination of $(h_L)_{crit}$. Physically, the assumption may not be valid if there is vapor flow above, and mass transfer across, the interface. These effects will tend to create waves on the interface and if the vapor flow is high enough, the interface will be depressed in the middle and the edges will climb higher up the wall, resulting in semi-annular flows (see Taitel and Dukler

12-21-78-02

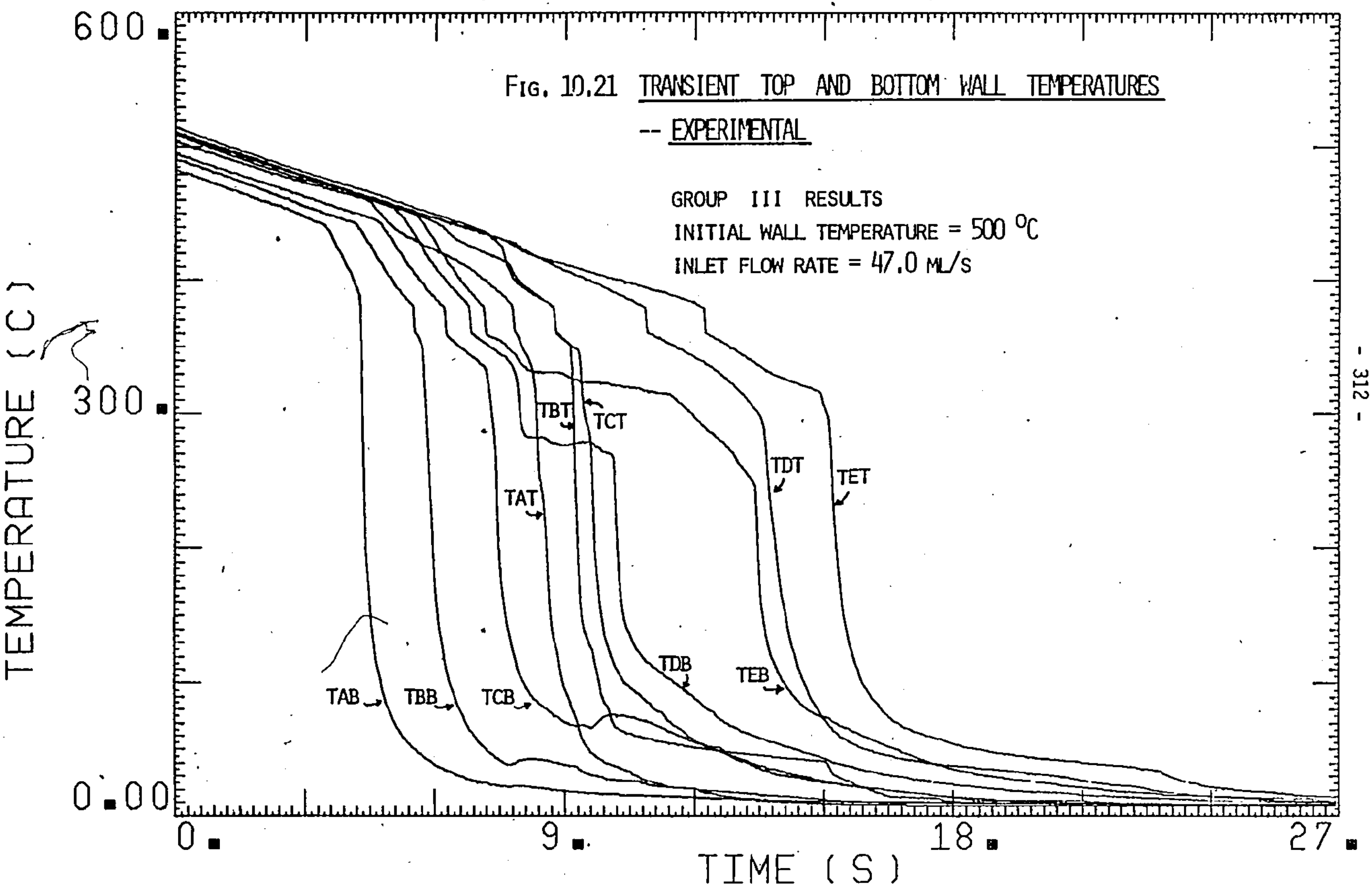

Fig. 10.21 TRANSIENT TOP AND BOTTOM WALL TEMPERATURES -- EXPERIMENTAL

GROUP III RESULTS
INITIAL WALL TEMPERATURE = 500 °C
INLET FLOW RATE = 47.0 ML/S

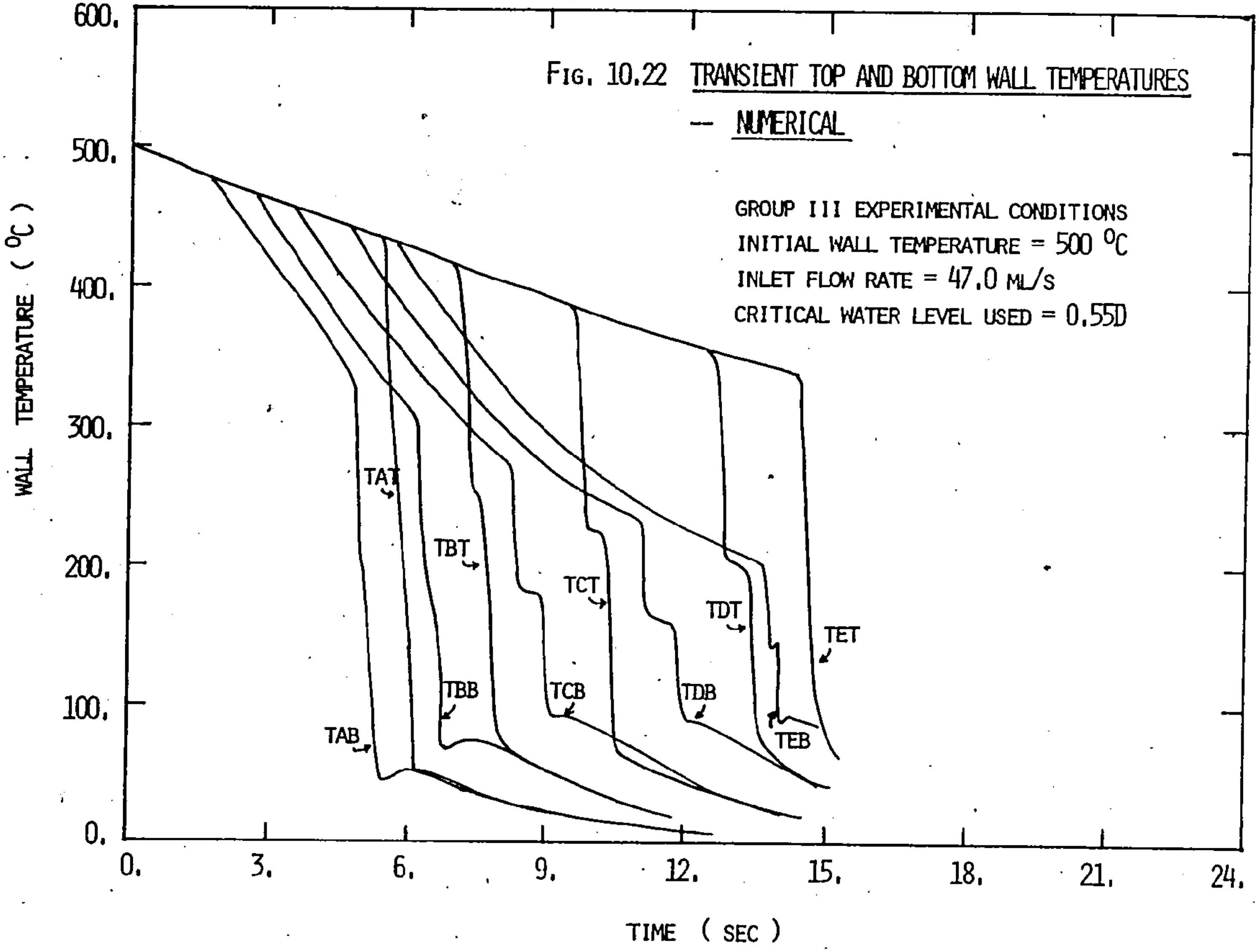

FIG. 10.22 TRANSIENT TOP AND BOTTOM WALL TEMPERATURES — NUMERICAL

[139]). When this happens, h_L is no longer well defined and the formulation will have to be modified to account for interface deformation. This will be discussed further in Section 10.8. It should be noted here that the problem of interface deformation or possible flow regime transition is particularly serious when the liquid flow is low. This limits the applicability of the REWET code.

The rewetting velocities can be obtained from the numerical results the same way as they are deduced using experimental data -- by measuring the time delay between the quenching of different axial locations. The average rewetting velocities obtained from numerical results are compared with experimental values below. A surprising result is, despite the apparent differences in quenching characteristics, the average rewetting rates of the bottom of the channel ($\overline{V}_B$) obtained from Figures 10.21 and 10.22 compare well with each other. However, since the applicability of REWET to this case is doubtful, the good agreement could be just accidental. In fact, the average rewetting rates of the top are found to be quite different (0.20 m/s experimentally as compared to 0.15 m/s numerically). Therefore, the low inlet flow cases will not be included in the results presented below.

10.6.2.2 Average Rewetting Velocities

The REWET code has been used to study the refilling and rewetting experiments under different initial and boundary conditions. The average rewetting velocities deduced are compared with experimental results.

The conditions for the Group III experiments (Section 6.3) are used in the present study. The conditions are: (i) constant inlet flows; (ii) input power cut off at the start of the transient; (iii) no insulation and (iv) T_{in} = 8°C. Different initial wall temperatures are used over a range of inlet flow rates.

The results are shown in Figure 10.23. Only the average rewetting velocities defined with respect to the midside of the tube ($\overline{V}_S$) are plotted. Results for $\overline{V}_B$ and $\overline{V}_T$ are quite similar. Three initial wall temperatures (400°C, 500°C and 600°C) are used. The corresponding experimental results are also shown in broken lines in Figure 10.23. It can be seen that the agreement is very good.

The good agreement is obtained by adjusting $(h_L)_{crit}$ slightly for different inlet flow rates. The ranges of $(h_L)_{crit}$ used for different wall temperatures are given in Figure 10.23. It should be noted that the ranges of $(h_L)_{crit}$ used are within the accuracies of $(h_L)_{crit}$ as deduced from Figure 10.16 (Section 10.5.1). In general, slightly lower $(h_L)_{crit}$ values are used for lower inlet flow rates.

Effects of other parameters on the average rewetting velocity can also be studied systematically using the REWET Code. An example is shown in Figure 10.24. The effect of inlet water subcooling is investigated. An initial wall temperature of 500°C and two different inlet water temperatures are used. It can be seen that the rewetting velocities are higher for lower inlet water temperature. That is, colder water is more effective in quenching the tube. This is consistent with other existing experimental results (Section 2.2.3) as well as the present experimental investigation (Section 8.3.2.3).

Effects of residual power input and insulation on the quench velocities can also be studied using REWET. The two cases correspond to the groups I and VI experiments respectively (Section 8.1). The latter case can be realized by making the heat transfer coefficients for the free convection and radiation to the surroundings equal to zero in REWET. The first case involves heat generation in the tube wall. This heat source function has to be supplied externally.

FIG. 10.23 AVERAGE REWETTING VELOCITY ($\bar{V}_S$) VS INLET FLOW RATE

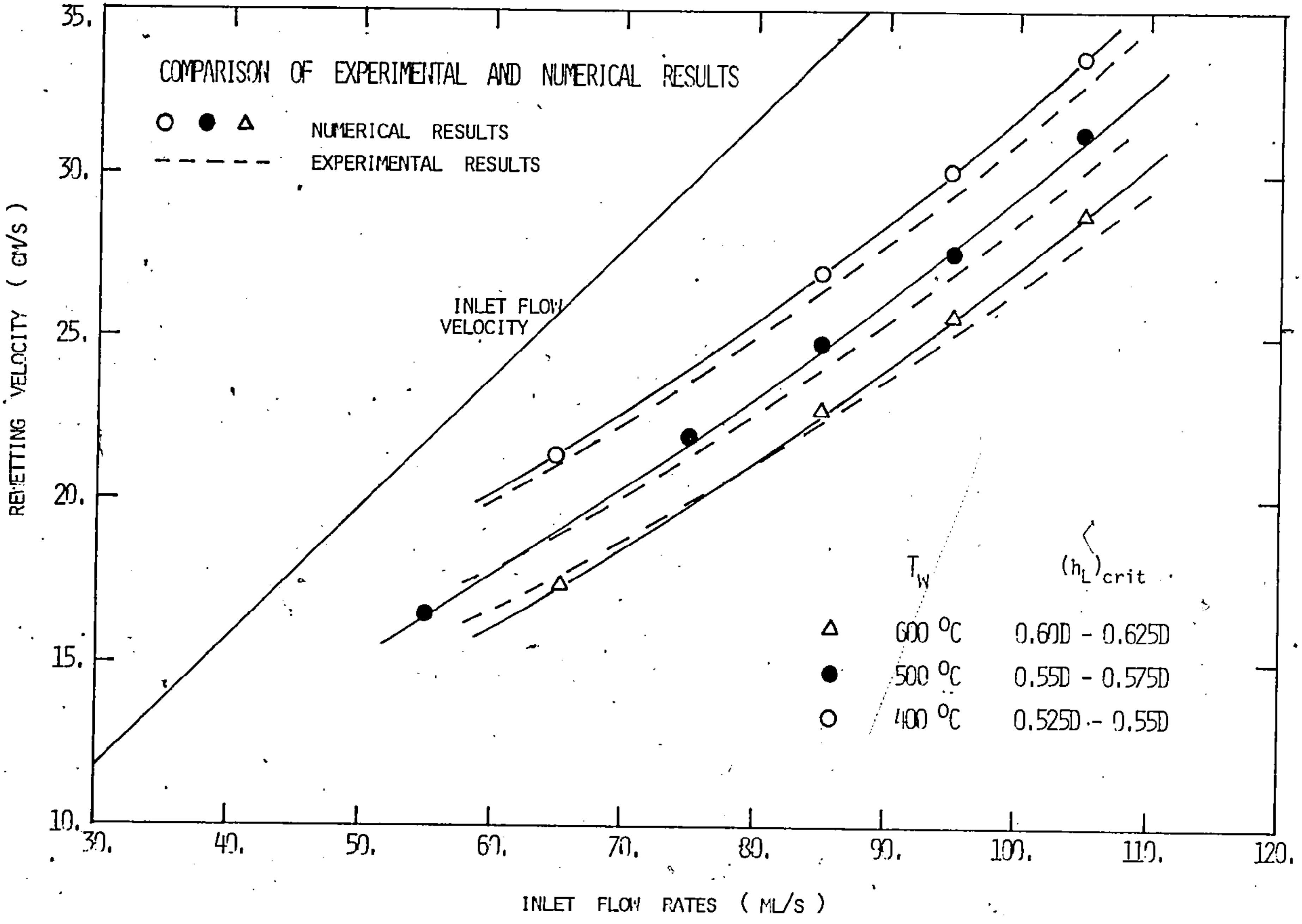

Fig. 10.24 AVERAGE REWETTING VELOCITY ($\overline{V}_S$) FOR DIFFERENT INLET WATER SUBCOOLINGS

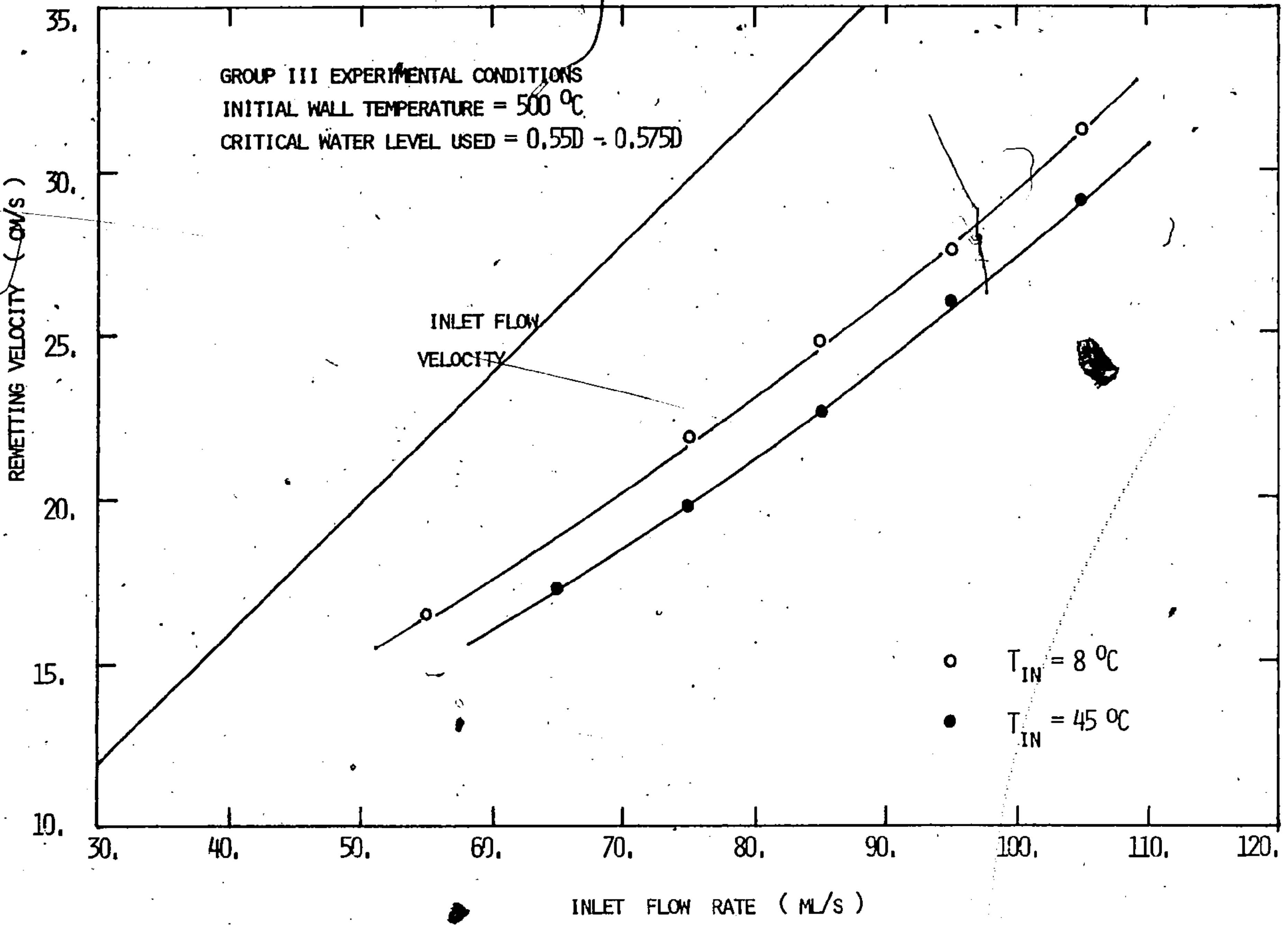

In the experiments, the heat source function was not uniform along the tube, this is because the tube wall temperature was non-uniform and thus the resistivity was different. In Principle, a temperature dependent resistivity function can be used. However, since the local current is not known (only the total current passing through the tube was measured), the heat source function is thus not known explicitly. Therefore, no attempt has been made to study its effects numerically.

10.6.2.3 Refilling and Rewetting Fronts

In the refilling and rewetting processes, we can define two moving fronts: one with respect to the quenching of the tube, the rewetting front, and the other with respect to the filling of the tube, the refilling front. In general, the refilling front always precedes the rewetting front, because quenching can occur only under given hydraulic conditions when there is liquid present.

The movement of these fronts during a transient is of practical interest, because they affect the mode of heat transfer and consequently the tube wall temperatures. In principle, their movements can be deduced experimentally from wall temperature measurements. However, this would require many wall temperature measurements, along and around the tube so that the detailed motion of the front may be tracked.

The locations of the refilling and rewetting fronts at any distant are however, readily obtainable from the numerical calculations. By following the motion of these fronts along the tube, a clear picture of the refilling and rewetting process can be obtained. Examples are shown in Figure 10.25 to 10.27.

In these figures, the liquid level, h_L is plotted along the tube at different times after the initiation of the transients. The refilling front

FIG. 10.25 PROPAGATION OF REFILLING AND REWETTING FRONTS — NUMERICAL RESULTS

INITIAL WALL TEMPERATURE = 400 °C INLET FLOW RATE = 85.0 ML/S

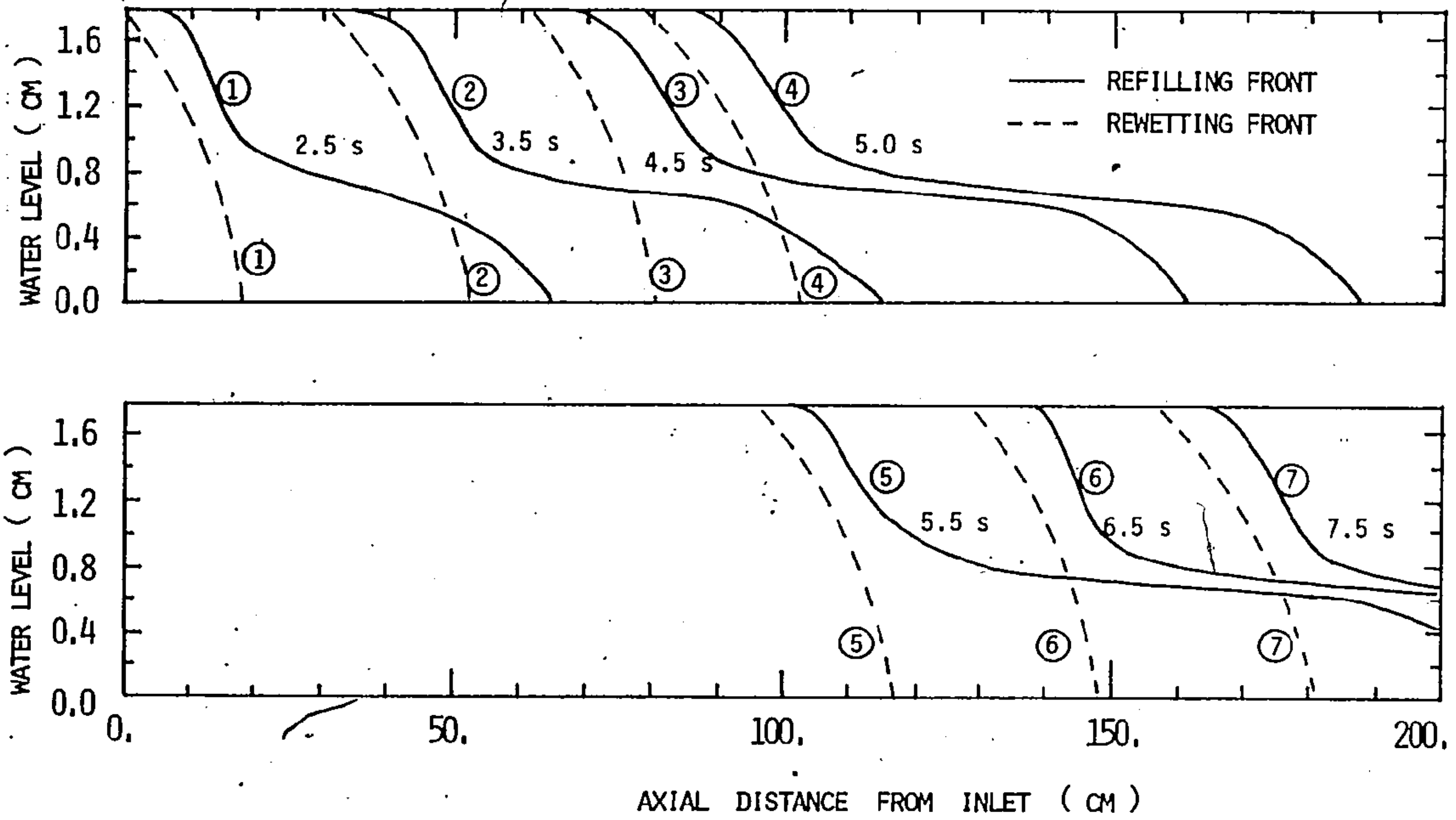

Fig. 10.26 <u>PROPAGATION OF REFILLING AND REWETTING FRONTS -- NUMERICAL RESULTS</u>

INITIAL WALL TEMPERATURE = 500 °C INLET FLOW RATE = 85.0 mL/s

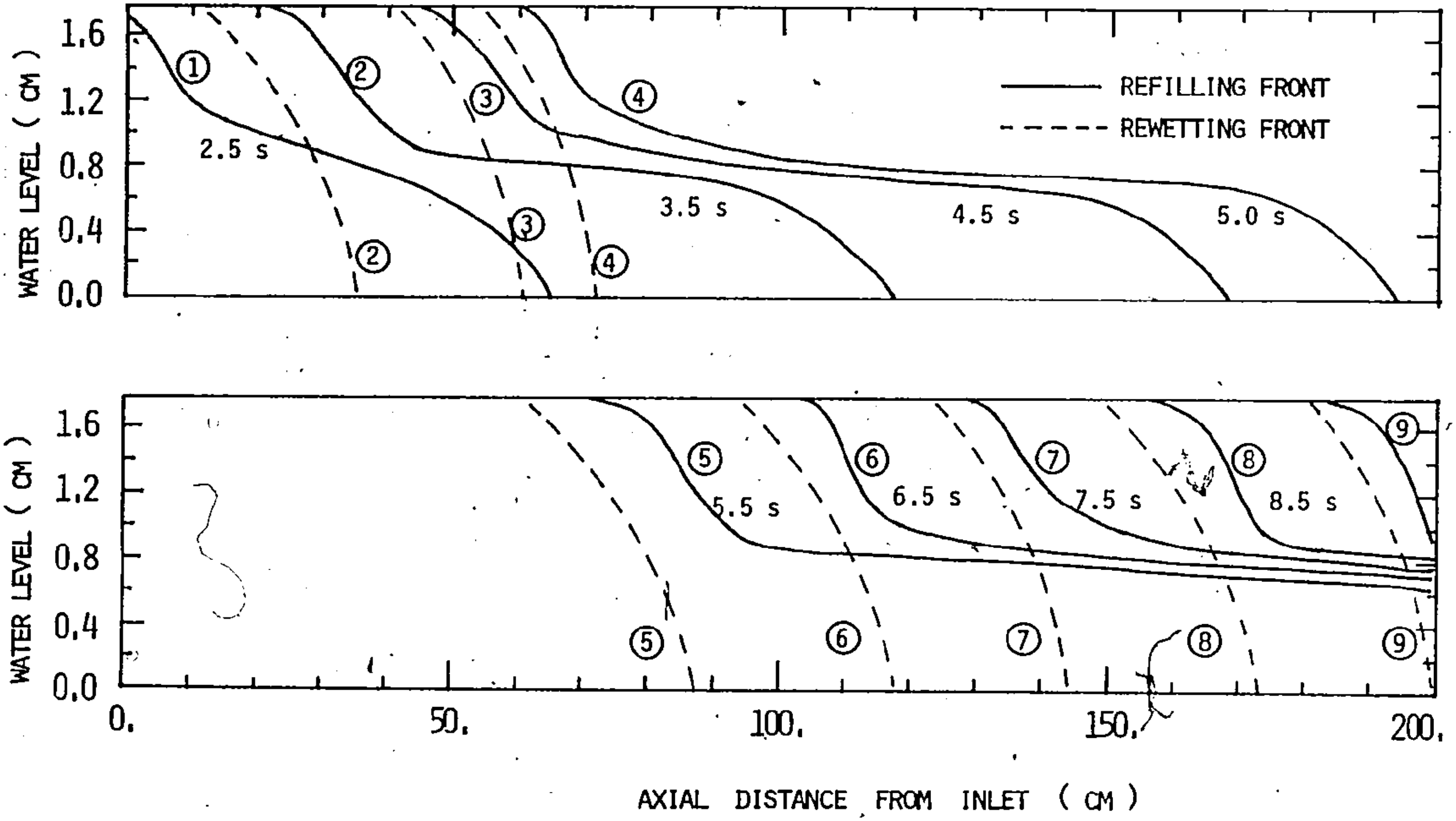

FIG. 10.27 PROPAGATION OF REFILLING AND REWETTING FRONTS -- NUMERICAL RESULTS

INITIAL WALL TEMPERATURE = 600 °C INLET FLOW RATE = 85.0 ML/S

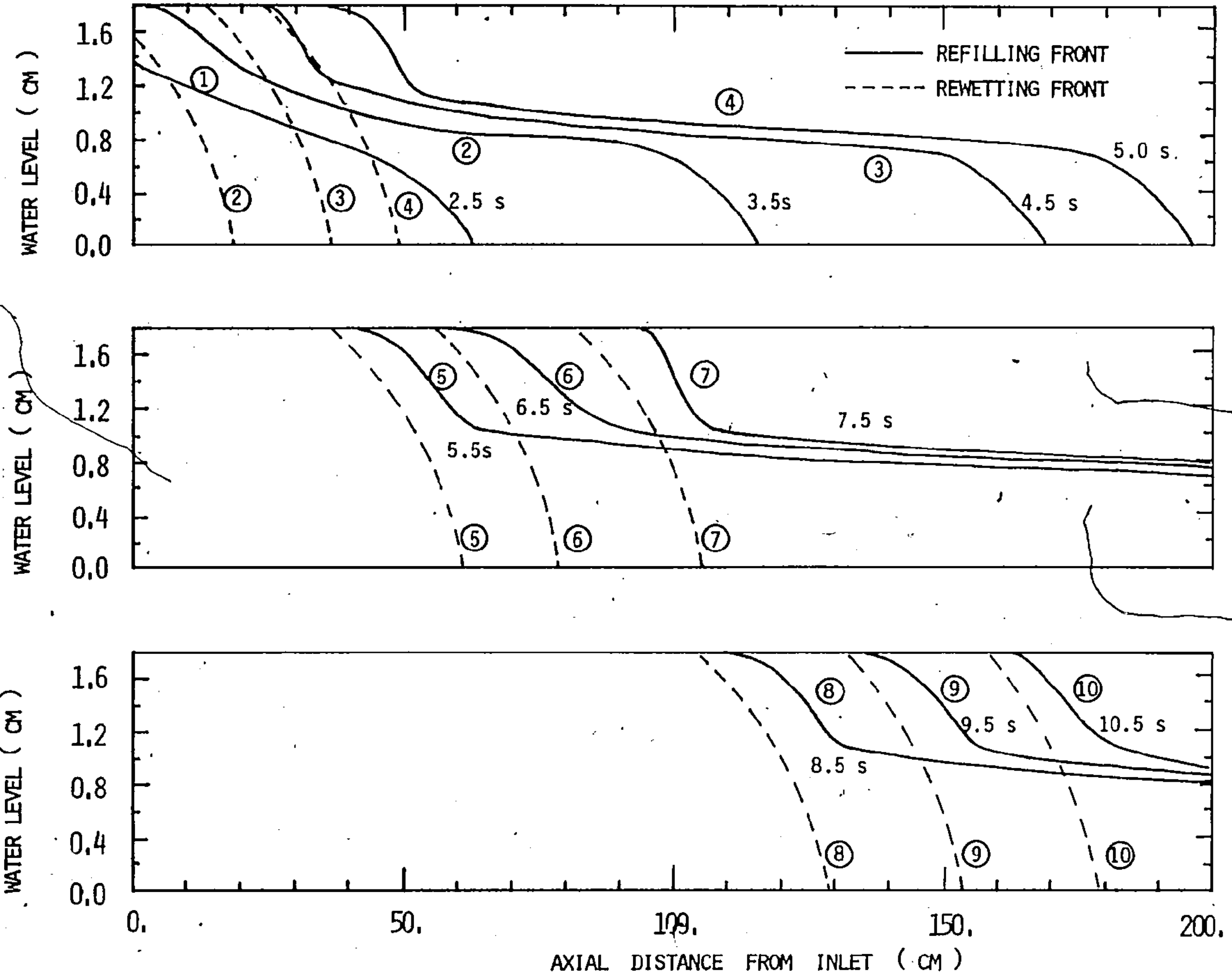

is defined by the solid line in the figures whereas the broken line define the rewetting fronts. Refilling water in the form of a liquid "tongue" is observed numerically extending far downstream. This is in agreement with photographic studies (Section 7.3.1) as well as our simple physical model (Section 7.3.2).

Different initial wall temperatures are used in Figures 10.25 to 10.27. It can be seen that the refilling and rewetting characteristics are basically the same. However the advancement of the refilling and rewetting fronts is different. The fronts tend to advance faster and quench the entire tube in a shorter time with lower initial wall temperatures. This is again consistent with experimental data.

10.7 Numerical Tests

In order to assess its performance, the REWET code has been subjected to a series of numerical tests. The tests are for: (i) spatial and temporal convergence and (ii) sensitivity to constitutive relations. The tests in the second category are useful in assessing the relative importance of the constitutive models used. They also provide information on how the code can be improved by adopting more accurate constitutive relations.

The test results are described below.

10.7.1 Convergence Studies

The spatial and temporal convergence of the numerical scheme has been tested. The case chosen for these studies has an initial wall temperature of 500°C and a constant inlet flow of 95 ml/s. Other conditions used are the same as in the Group III experiments (Section 6.3). The constitutive relations used are as listed in Table 10.1.

The heated test section is divided into 24 and 35 nodes respectively in the spatial convergence tests. The time step (Δt) used is determined by Eq. (10.30). Numerical solutions are also obtained for the 24-node case with Δt reduced to half of that given by Eq. (10.30) in order to test for temporal convergence.

The average rewetting velocities, $\Delta M/M$ and Q_{in}/Q_{out} ratios are compared in these tests. $\Delta M/M$ is defined the same way as in Table 9.1. It is a measure of how well the code conserves mass. Q_{in} is the total energy transferred. It is obtained by summing the local heat transfer from both the inside and outside tube walls at every time step. Q_{out} is the energy lost by the test section in the form of decrease in thermal capacity due to the decrease in wall temperature. Q_{in}/Q_{out} is a measure of energy conservation. The results are given in Table 10.2. $\overline{V}_B$, $\overline{V}_s$ and $\overline{V}_T$ are the average rewetting velocities defined with respect to the quench of the bottom, mid-side and top of the tube respectively.

Table 10.2

Convergence Tests - Computer Code REWET

	$\Delta t = \Delta t$		$\Delta t = \Delta t/2$
	24 Nodes	35 Nodes	24 Nodes
$\overline{V}_B$ (cm/s)	27.1	27.0	28.7
$\overline{V}_s$ (cm/s)	28.0	27.6	28.1
$\overline{V}_T$ (cm/s)	27.6	27.4	28.0
$\|\Delta M\|/M$	1.2%	1.8%	2.0%
Q_{in}/Q_{out}	0.97	0.97	0.96%

In Table 10.2, it can be seen that the results compare well for the three different cases. Therefore, we may conclude that converged results are obtained when 24 nodes and Δt as given by Eqn. (10.30) are used. It can also be seen that the code conserved mass and energy well for all cases.

10.7.2 Sensitivity to constitutive models

The sensitivity of the numerical results to the constitutive relations used has been investigated. A case with an initial wall temperature of 500°C and a constant inlet flow of 85 ml/s is used as a reference against which results obtained by using different constitutive relations can be compared. The conditions used are the same as in the Group III experiments (Section 6.3). The constitutive relations in Table 10.1 are used in the reference case. m = 2.5 is used in the liquid to wall friction factor in the inlet feeder region.

Changes to the liquid to wall, vapor to wall and interfacial shear as well as interfacial mass transfer relations are made. Results are summarized in Table 10.3. The specific changes are given in each case. Other consitutive relations are kept the same as in the reference case. The average rewetting velocities are listed for comparison. No significant changes in the rewetting rates are observed in all cases. This means that the numerical results are relatively insensitive to the interfacial transfer terms.

This conclusion is very important. Because of the simplified two fluid model used, the vapor phase velocity is not solved in detail in REWET (Section 10.3.8). Had the numerical results been more sensitive to the interfacial transfer terms, a more accurate vapor velocity would have been needed. Thus, the simplified model would no longer apply in this hypothetical situation.

10.8 Usefulness and Limitations of the Simplified Two Fluid Model Approach

Some numerical results obtained using the simplified two fluid model formulation have been presented. They were found to agree very well with experiments for relatively high inlet flow (≥60 ml/s). The model was also found to predict the effects of the inlet water subcooling on the rewetting velocities correctly. The predicted shape of the interface and the advancement of the refilling and rewetting fronts were also consistent with experiments. Therefore, the simplified two fluid model appears to be applicable to some aspects of the refilling and rewetting problem. Such models may be useful in the study of parametric effects on the quenching process under similar flow

Table 10.3

Sensitivity Studies

Changes in Constitutive Relations	$\overline{V}_B$ (cm/s)	$\overline{V}_s$ (cm/s)	$\overline{V}_T$ (cm/s)
Reference Case (constitutive relations in Table 10.1 are used)	25.4	24.9	25.0
Liquid to wall shear			
(i) $m = 5.0$; $\phi = 50.$	24.8	25.0	25.5
(ii) $m = 1.0$; $\phi = 10.$	25.1	24.7	25.2
(iii) $m = 3.0$; $\phi = 210.$	24.4	24.6	25.1
Vapor to wall and Interfacial shear (i) $f_i = 0.001$; $f_G = 0.001$	26.0	26.5	26.2
Interfacial mass transfer (i) $\beta = 0$ for both film boiling and quenching region	25.7	25.5	25.9

conditions, e.g. the quenching of a reactor fuel channel in a CANDU system.

The major limitation of the model is the assumption of a stratified interface with a well defined water level. Possible flow regime transitions and interface deformation are not taken into account. This leads to unacceptable results predicted by the REWET code for low inlet flow rate as discussed in Section 10.6.2.1.

As pointed out previously, this flat stratified interface assumption may not be valid physically, especially when the vapor velocity is high. In the numerical calculations, vapor velocities as high as 10 to 20 m/s are obtained in many situations. For lower inlet flows, it can even be higher because the local subcooling of the refilling water decreases rapidly along the tube due to the longer residence time. This results in higher vaporization rates and hence higher vapor velocities.

To investigate the possibility of flow regime transition under given flow situations, a flow regime map is normally used. A recent flow regime map for air-water system in horizontal pipes was proposed by Mandhane et al. [140] and is reproduced here in Figure 10.28. It should be noted that the map is not strictly applicable to the present flow situations because it is for air-water systems. However, some qualitative observations can be made. From Figure 10.28 it can be seen that for high gas flow velocities (greater than about 5 m/s), stratified flow is not possible. Depending on the liquid velocity, it can be slug flow, wavy flow or annular flow.

From the experiments, as discussed in Section 8.2, it appears that the stratified interface assumption is valid in general for high inlet flows. However, it does not hold for low inlet flow situations. By comparing the local void fraction measurements and the quenching results, there is evidence that semi-annular flow pattern, or patterns other than stratified, may indeed exist

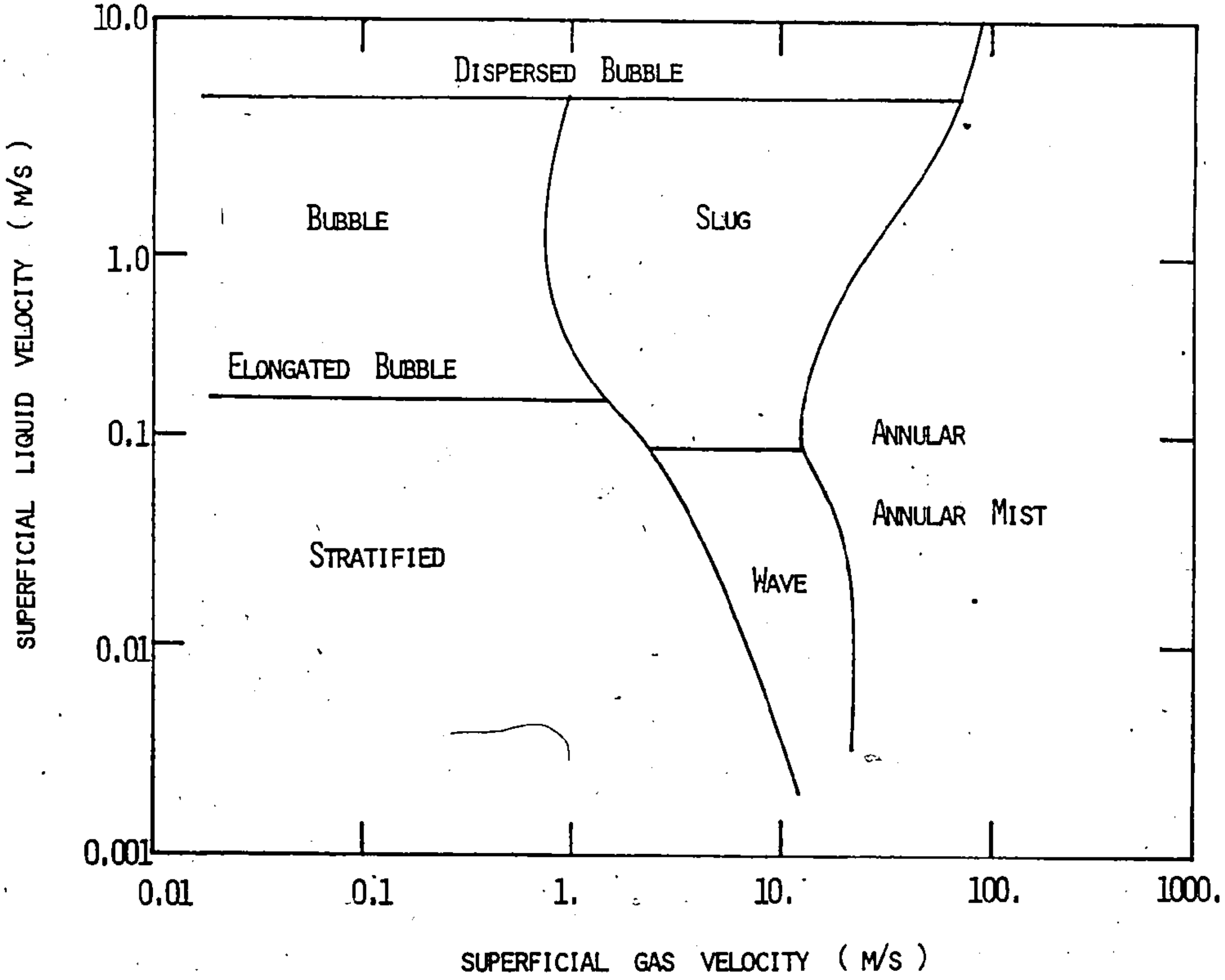

FIG. 10.28 <u>FLOW - PATTERN MAP FOR HORIZONTAL FLOW.</u>
(AFTER MANDHANE ET AL. (140))

for low inlet flow cases.

When the interface is not stratified, the well defined water level, h_L is no longer applicable. The quench model as shown in Figure 10.14 can no longer be used. Simple modification to the quench model, however, is possible so that this kind of flow situations can still be handled.

To modify the existing quench model, we can define a different water level, h_L^m as shown in the insert of Figure 10.29. h_L^m is defined with respect to the highest point the interface can reach up the tube wall. It should be noted that h_L^m so defined is always greater than h_L for semi-annular flows. h_L^m can reach the top of the tube when h_L is substantially below the top. In the extreme case of annular flow, h_L^m will equal D, the diameter of the tube regardless of the value of h_L. Since the vapor film instability model only depends on the vapor channel length and the vapor velocity in the vapor film, a modified quench model can be proposed as shown in Figure 10.29.

This model is similar to the previous one, but another parameter $(h_L)'$ is introduced. $(h_L)'$ is the well defined water level which corresponds to $h_L^m = D$. For stratified flows, $(h_L)'$ equals D. In principle, $(h_L)_{crit}$ and $(h_L)'$ can be adjusted with respect to experimental data. However, there are some difficulties involved.

In the refilling and rewetting processes, the vapor and liquid velocities change along the tube and flow regimes may change accordingly. It can be stratified, slug, wavy, semi-annular and annular depending on the local flow condition. On the other hand, $(h_L)_{crit}$ and $(h_L)'$ may be expected to be strongly dependent on the flow regime involved. Therefore, unless the local flow regime is known, the modified quench model, although it has some physical basis, is difficult to use.

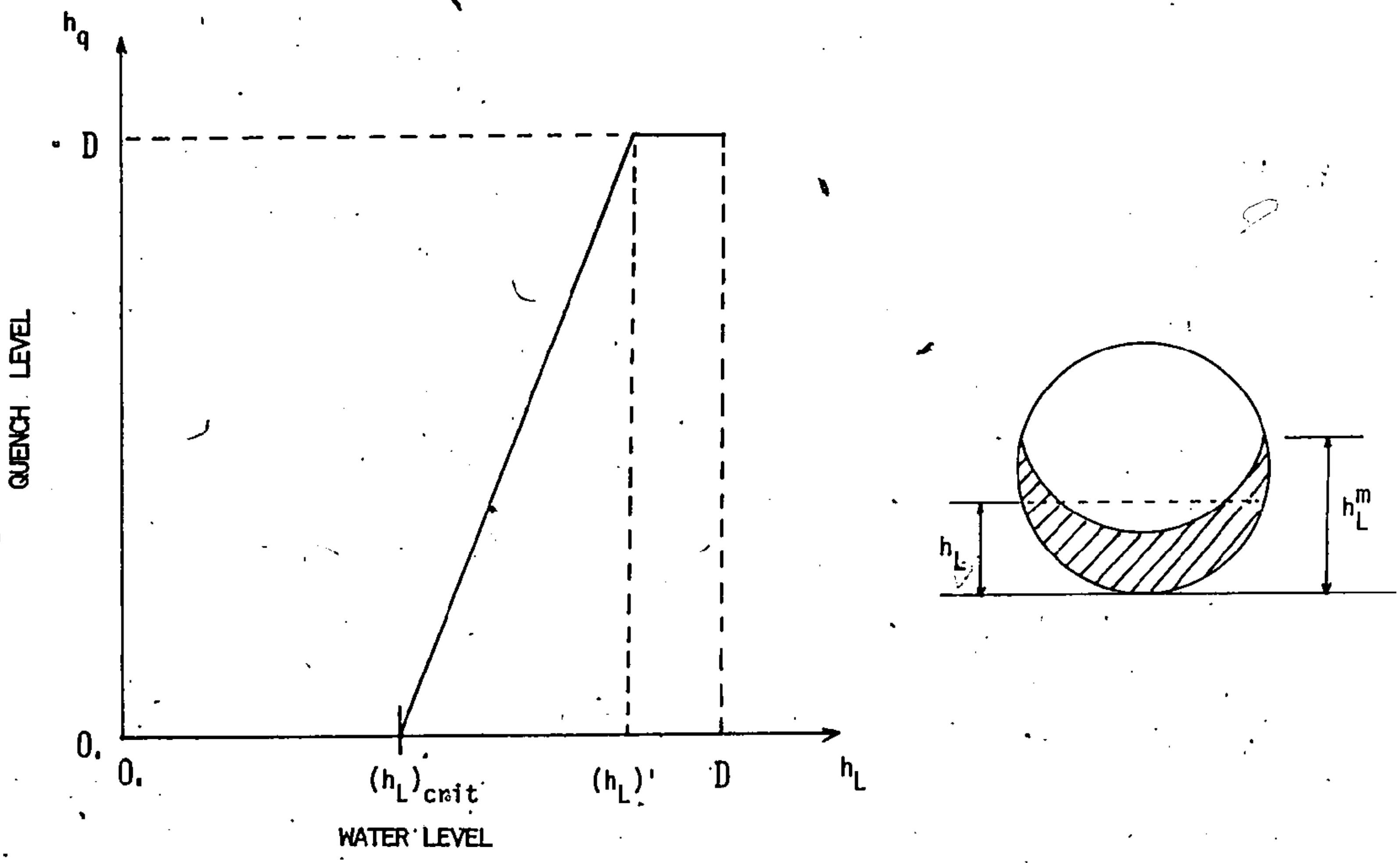

FIG. 10.29 A MODIFIED QUENCH MODEL

An extensive development of flow regime transitions is not the main objective of this thesis, therefore further development of the model has not been pursued for low inlet flow rates. Furthermore, in the practical situation of interest, rewetting of rod bundles, the stratified model may be expected to work reasonably well even at low flow rates. This is because the presence of rods reduce the interfacial area in a channel and increase the wall frictional forces in each phase. Therefore, the next phase of development will be to, apply the stratified flow model to predicting rewetting and refilling of full size rod bundles which have been studied in a separate investigation.

11. CONCLUSIONS AND RECOMMENDATIONS

11.1 Concluding Remarks

The work presented in this report can be divided into two parts: experimental and theoretical. The concluding remarks will mainly be divided into these categories. Some aspects of the instrumentation developed will also be discussed.

11.1.1 Experimental Work

The refilling and rewetting of a directly heated horizontal channel has been investigated experimentally. considerable data have been taken for tests under different initial and boundary conditions. The data obtained are of interest in developing models for reactor LOCA analysis. They are of particular interest to the Canadian nuclear industry because the system used was horizontal, as in CANDU reactor fuel channels.

The experiments were done with well defined initial and boundary conditions. Although they were performed in a simply geometry - a thin walled horizontal tube, they contained many of the phenomena important in thermal and hydraulic aspects of the emergency cooling phase of LOCA in CANDU reactors. The experiments thus provide data for benchmark problems against which existing thermohydraulics codes can be compared and assessed. The data and physical insight gained in doing these experiments are also valuable in testing and further developing thermohydraulic analysis based on more advanced fluid flow models.

Some of the more important results obtained or observed under the experimental program can be summarized below:

1. Transverse gravity forces significantly affect the hydraulic, and consequently thermal, behavior of the system during the refilling and rewetting process for a horizontal tube. Because of gravity, the flow is stratified. Thus the tube is refilled and rewetted in the sequence of bottom, mid-side and top for any given location along the tube.

2. The heat transfer mechanisms vary along the channel during transients, both axially and circumferentially. The heat transfer coefficients appear to be functions of the local thermal and hydraulic conditions. The two most important parameters affecting the local heat transfer coefficients are the local wall temperature and void fraction or liquid level.

3. The pre-quenching characteristics are quite different with regard to the bottom and top of the tube. This results from different heat transfer mechanisms before quenching. Because of the presence of a "liquid tongue", the bottom region of the tube is precooled significantly due to stable film boilding, whereas the top is not (Figure 7.3). The heat transfer from the top is quite small, and is due mainly to forced convection to the vapor flow.

4. The existence of the "liquid tongue" which extends downstream from the quench front and is prevented from wetting the wall by a vapor film (stable film boiling), is evident from the experiment data. Its presence was deduced originally from temperature measurements and later supported by observations in a transparent test section.

5. The propagation of the quench or rewetting front is largely controlled by hydrodynamic mechanisms. The effects of heat conduction in the wall (conduction controlled model) are not apparent. This is again evident from experimental data. It has been found that surface quenching can occur at very different wall temperatures along the tube (see Figure 8.8).

In other words, there is no well defined rewetting temperature. This is contrary to the predictions of the conduction controlled model. To account for the observed phenomenon, hydrodynamic instability of the liquid-vapor film interface underneath the "liquid tongue" is suggested as a possible mechanism that initiates the quenching.

6. In horizontal channel refilling and rewetting, the rewetting velocity is not uniquely defined. We define it with respect to the quenching of positions up the tube, e.g. bottom, mid-side, top etc. This is because the quench front is stratified and the angle of inclination or shape of the front changes as it moves downstream. As mentioned, we measured rewetting velocities defined with respect to the quenching of the bottom, mid-side and top of the tube. These velocities were somewhat different.

7. In general, the rewetting velocities are not uniform along the tube, especially when the initial wall temperature and/or inlet flow rates are low.

8. To summarize the experimental results and to determine the effects of different initial and boundary conditions, averaged rewetting velocities were obtained over the length of the whole test section. The following parametric effects were observed.

(i) The average rewetting velocities are higher for lower initial wall temperatures (Figures 8.21-8.28).

(ii) The average rewetting velocities are higher for higher inlet flows (Figures 8.21-8.28).

(iii) Cooler water is more effective in quenching the channel for high wall temperatures ($T_W > 400\ ^{\circ}C$). The average rewetting velocities increase with inlet water subcooling for $T_W > 400\ ^{\circ}C$. The opposite is true for lower wall temperatures (Figures 8.34 and 8.35).

(iv) When the inverse of the average rewetting velocites are plotted against the initial wall temperatures, straight lines are obtained for different inlet flow rates. (Figures 8.31-8.35).

(v) Internal heat generation (in the form of residual power input) retards the quenching process (Figures 8.22 and 8.27).

(vi) The rewetting rate is also retarded if the tube is insulated. This reduces the heat losses by free convection and radiation from the outside tube surface (Figure 8.30).

(vii) No significant difference in the quenching rate is observed when deaerated and de-ionized water is used instead of building tap water (Figure 8.29).

9. The average entrained liquid velocity or the average velocity of the leading edge of the "liquid tongue" can be obtained from the void fraction measurements. They were found to be four to six times higher than the corresponding average rewetting velocities (Figures 8.38 and 8.39).

11.1.2 Theoretical Work

The complicated thermohydraulic processes of refilling and rewetting of a hot horizontal channel have been analyzed using the generalized one-dimensional two-fluid model. It has been demonstrated that the two-fluid model approach is very powerful in analyzing such flow systems and the formulation used can still be relatively simple and close to the real physics of the situation.

The general model is simplified to reduce computational effort. The governing equations are the hydraulic equations for the liquid phase and the thermal equations for the liquid phase and the channel wall. The vapor phase is assumed to be at saturation temperature. The transient terms in the vapor phase mass and momentum equations are neglected.

The governing equations are solved numerically. Results obtained compare well with experimental data, both for refilling with no heat transfer and the more complicated refilling and rewetting case.

For the latter case, a quench model based on a critical water level, $(h_L)_{crit}$ which determines the transition of heat transfer mode from film boiling or the occurrence of quenching at the bottom of the tube is used. $(h_L)_{crit}$ is obtained using a model based on initiation of an Kelvin-Helmholtz instability at the vapor film - liquid interface in the film boiling region.

The initiation of the interfacial instability is believed to be the governing mechanism that leads to surface rewetting. However, this is only a necessary condition. The sufficient condition will be the rapid growth of the rewet spots on the surface. For thin walled tubes, because of the low heat capacity, rewet spots can always grow once they are formed. Therefore, interfacial instability appears to be both necessary and sufficient to quench the wall.

The simple quench model was found to be quite successful in predicting the rewetting rates for relatively high inlet flow rates. However, for low inlet flows (e.g. less than 55 ml/s), the quenching characteristics obtained can be quite different from the corresponding experimental results (cf. Figures 10.21 and 10.22). The reason for this discrepancy is believed to result from deformation of the refilling front and possible break up of the stratified "liquid tongue" in the film boiling region. The flow in this region may thus be semi-annular or even dispersed. A modified quench model has been proposed.[6] The modified model is, in principle, capable of handling the effects of flow regime transitions. However, more work is necessary before the low inlet flow experiments can be interpreted.

The REWET code has been found to give converged solutions with respect to mesh and time step sizes when the heated section is simulated by 24 nodes and Δt as given by eqn. (10.30) is used. Effects of the interface transfer terms (interfacial shear, mass transfer etc.) on the rewetting rates are found to be relatively small. This is because the refilling and rewetting characteristics are dominated by the liquid flow which is in turn affected primarily by the inlet flow rate and the hydrostatic pressure head behind the stratified quench front.

11.1.3 Two Phase Flow Instrumentation

Under the experimental program, in order to measure the local volume averaged void fractions during transients, non-intruding void measuring techniques were studied.

The possibility of building a neutron voidmeter based on fast neutron scattering was investigated. Since neutrons are very sensitive to the water content in a two phase mixture, accurate results are expected, especially in the high void region where photon attenuation technique are not usually sensitive. Indeed, in a series of simulated static and air-water flow quasi-static experiments using the McMaster Nuclear Reactor as the neutron source, it was found that the fast neutron scattering technique gives accurate average void measurements and the results are relatively insensitive to flow distribution. The use of this technique in the refilling and rewetting experiments, however, was not realized. This is because the scattered neutron flux is usually low and long counting periods are needed in order to get good statistics. Therefore, it was concluded that the fast neutron scattering technique was not applicable to fast transients such as the refilling and rewetting experiments unless an intense neutron source (> 10^9 neutrons/s) is available. Such sources are now being acquired for use in our laboratory.

Because of the practical limitation of fast neutron scattering to slow transients, gamma (photon) attenuation technique was used. Fast response single-beam gamma densitometers were designed using Co-57 sources and 10% lead loaded plastic scintillators. The densitometers were calibrated with test sections using Lucite to simulate various water distributions. The results obtained were generally satisfactory, though somewhat dependent on flow regimes. The best results were obtained for stratified flows with the gamma beam directed normal to the interface. This was the flow regime of most interest for the experiments.

Since relatively low energy gamma rays (∿ 122 keV) are used, a very compact voidmeter design with little shielding was possible. The densitometers built are thus easy to handle and easy to operate. They can be used with good accuracy in rapid transients. Though not necessary in our experiments, it appears possible to make them less sensitive to flow regimes by shaping the gamma beam.

11.2 Recommendations for Future Work

The recommendations for future work are based on the experimental and theoretical results obtained as well as the experience gained in the present investigation.

11.2.1 Experimental Work

1. It appears from the present investigation that rewetting of a hot surface can occur due to hydrodynamic instability of the vapor film underneath

an extended liquid mass. It has been pointed out that instability of the vapor film may only be a necessary but not sufficient condition for surface quenching. That is, if the wall has a very low heat capacity, then it would probably rewet once the instability sets in. Otherwise the rewet spots would have to be able to grow; therefore, the process may become locally conduction controlled. Thus for conductive walls of high heat capacity the growth of the rewet spot may be the sufficient condition for rewetting. Experiments are therefore needed to systematically study the effect of wall heat capacity and conductivity on surface quenching.

A relatively simple experiment in this direction would be to refill and rewet a uniformly heated horizontal tube with high heat capacity patches. Copper blocks can be used to produce the patches. It is expected that surface quenching will occur downstream of a high heat capacity patch when the patch is still dry. Detailed temperature measurements in the block and other locations would be used to determine the correctness of our postulate that instability of the vapor film is a necessary but not sufficient condition for surface rewetting. The most interesting phenomenon would be if the high heat capacity patch was actually colder than the upstream and downstream sections, but did not rewet. This would support our model strongly.

Experiments can also be performed to investigate the more fundamental aspects of surface rewetting. They can be designed to look at the rewet spots and their subsequent growth or decay. Several experiments related to this have been conceived and will be the subject of subsequent theses. These experiments will enhance understanding of the basic mechanisms that lead to surface quenching.

2. A hydrodynamic instability model has been used to determine the conditions under which a change in the mode of heat transfer (from stable film boiling to transition boiling) may take place. It was proposed that this change in heat transfer mode is responsible for the initiation of tube rewetting. Although, numerical results suggest that the model works well, more direct experimental support is needed. In particular, experiments are needed to determine $(h_L)_{crit}$ explicitly under different thermohydraulic conditions. This will remove the empiricism from the quench model.

11.2.2 Code Development

1. The REWET code can be made more general by extending it to include fuel bundles in the channel. The geometry of a CANDU fuel channel can be used. Results can be compared with some experiments that have already been completed (see Banerjee and Hancox [54]).

2. The boundary conditions in REWET can be easily modified to study the ECC injection phase in LOCA analysis for CANDU reactors.

REFERENCES

1. S. Banerjee, W. T. Hancox, R.B. Jeffries and M.T. Sulatisky, "Transient Two-Phase Flow and Heat Transfer During Blowdown from Subcooled Conditions with Heat Addition", AIChE Symposium Series, No. 174, Vol. 74 (1978), pp 141-148.

2. G. Yadigaroglu, K.P. Yu, L. A. Arrieta and R. Greif, "Heat Transfer During the Reflooding Phase of the LOCA - State of the Art", EPRI 248-1 Topical Report, September 1975.

3. M. E. Swan and M.W. Carbon, "A Review of Spray-Cooling and Bottom-Flooding Work for LWR Cores", Nuclear Eng. and Design, Vol. 32, 1975. pp 191-207.

4. D. Butterworth and R. G. Owen, "The Quenching of Hot Surfaces by Top and Bottom Flooding - A Review:, AERE-R7992, 1975.

5. J. D. Duncan and J. E. Leonard, "BWR Standby Cooling Heat Transfer Performance Under Simulated Loss-of-Coolant Conditions between 15 and 300 psia", GEAP-13190 (May, 1971).

6. J. D. Duncan and J. E. Leonard, "Emergency Cooling in BWR's Under Simulated Loss-of-Coolant Conditions (BWR-FLECHT Final Report)", GEAP-13197 (June 1971).

7. J. C. Haire and G. F. Brockett, "Pressurized Water Reactor - Full Length Emergency Cooling Heat Transfer (PWR-FLECHT) Tests Project", IN-1386 (April 1970).

8. J. L. O'Brien, Jr. (ed), "Full-Length Emergency Cooling Heat Transfer Test (FLECHT) Conceptual Design", WCAP-7200 (May 1968).

9. J. O. Cermak, et al, "PWR FLECHT Final Test Plan", WCAP-7228 (January 1969).

10. F. F. Cadek, D.P. Dominicio and R.H. Leyse," PWR FLECHT (Full Length Emergency Cooling Heat Transfer) - Final Report", WCAP-7665 (April 1971).

11. F. F. Cadek, et al, "PWR FLECHT Final Report Supplement", WCAP-7931 (October 1972).

12. F. F. Cadek, et al, "PWR FLECHT System Effects Tests - Program Plan", WCAP-7906 (April 1972).

13. J. A. Blaisdell, L.E. Hochreiter and J. P. Waring, "PWR FLECHT-SET Phase A Report", WCAP-8238 (December 1973).

14. W. F. Cleary, et al., "FLECHT-SET Phase B System Design Description", WCAP-8410.

15. J. P. Waring, et al., "PWR FLECHT-SET Phase B1 Data Report", WCAP-8431 (Dec. 1974).

16. S. G. Forbes, et al., "Scoping Emergency Cooling Heat Transfer (SECHT) Test Project", IDO-17258D (April 1969).

17. L. D. Schlenker, et al., "Interim Report on SECHT Series I and II Tests and Analysis", IDO-17278 (August 1968).

18. C. M. Moser and R.W. Griebe, "SECHT III - An Experimental Investigation of Top and Bottom Flooding of a Nuclear Bundle Simulator", IN-1355 (Feb. 1970).

19. J. L. Plum, "SECHT-IV Performance Evaluation of Stainless Steel and Zircaloy-Clad Electrically Powered Heaters", IN-1378 (June 1970).

20. H. D. Curet, et al., "Fuel Heatup Simulation Tests - FHUST", IDO-17258F (April 1969).

21. R. T. Jensen, "Experimental Results of the Fuel Heatup Simulation Tests (FHUST) - Emergency Core Cooling Test Series", IN - 1390 (Sept. 1970).

22. T. S. Thompson, "Simulated Bottom-Flooding Emergency Cooling of a Close-Spaced Rod Bundle", European Two-Phase Flow Group Meeting, Casaceia (June, 1972).

23. A Campanile and G.P. Pozzi, "Low Rate Emergency Reflooding Heat Transfer Tests in Rod Bundle", Proceedings of the CREST Specialist Meeting on Emergency Core Cooling for Light Water Reactors, Garching/Munchen, October 18-20, 1972, MRR115, Volume 1.

24 H. Ogasawara, S. Kashiwai and Y. Takashima, "Cooling Mechanism of the Low Pressure Coolant Injection System of Boiling Water Reactors and Other Studies on the Loss-of-Coolant Accident Phenomena", Topical Meeting on Water Reactor Safety, Salt Lake City, Utah , March 26-28, 1973, CONF-730304, pp. 351-370.

25. A. Yamanouchi, "Effect of Core Spray Cooling in Transient State after Loss of Coolant Accident", J. Nucl. Sci. Tech., Vol. 5, 1968 pp. 547-558.

26. K. Riedle and F. Winkler, "ECC-Reflooding Experiments with a 340-Rod Bundle", Proceedings of the CREST Specialist Meeting on Emergency Cooling for Light Water Reactors, Garching/Munchen, October 18-20, 1972, MRR 115, Volume 1.

27. G. L. Shires, A. R. Pickering and P.T. Blacker, "Film Cooling of Vertical Fuel Rods", UKAEA Report, AEEW-R343 (1964).

28. A. W. Bennett, G. F. Hewitt, H.A. Kearsey and R.K. F. Keeys, "The Wetting of Hot Surfaces by Water in a Steam Environment at High Pressures", UKAEA Report, AERE-5146 (1966).

29. D. F. Elliot and P. W. Rose, "The Quenching of a Heated Surface by a Film of Water in a Steam Environment at Pressures up to 53 Bar", UKAEA Report, AEEW-M976 (1970).

30. D. F. Elliot and P. W. Rose, "The Quenching of a Heated Zircaloy Surface By a Film of Water in a Steam Environment at Pressures up to 53 Bar", UKAEA Report, AEEW-M1027 (1971).

31. R. B. Duffey and D.T.C. Porthouse, "Experiments on the Cooling of High Temperature Surfaces by Water Jets and Drops", Proceedings of the CREST Specialist Meeting on Emergency Cooling for Light Water Reactors, Garching/Munchen, October 18-20, 1972, Paper II2.

32. B.D.G. Piggott and D.T.C. Porthouse, "Water Reactor Emergency Core Cooling: The Effect of Pressure, Subcooling and Surface Condition of the Rewetting of Hot Surfaces", Central Electricity Generating Board Report RD/B/N2692 (June 1973).

33. E. P. White and R. B. Duffey, "A Study of the Unsteady Flow and Heat Transfer in the Reflooding of Water Reactor Cores", Central Electricity Generating Board Report RD/B/N3134 (Sept. 1974).

34. B. D. G. Piggott and R. B. Duffey, "The Quenching of Irradiated Fuel Pins", Nucl. Eng. and Design, Vol. 32 (1975) pp. 182-190.

35. D. Andreoni and M. Courtand, "Study of Heat Transfer During the Reflooding of a Single Rod Test Section", Proceedings of the CREST Specialist Meeting on Emergency Core Cooling for Light Water Reactors, Garching/Munchen, October 18-20, 1972, MRR 115, Volume 1.

36. D. Andreoni, M. Courtand and R. Deruaz, "Heat Transfer during the Reflooding of a Tubular Test Section", European Two-Phase Flow Meeting, Harwell, 3-7 June 1974.

37. Schneider and Thomas. "Further Development of the Technology of Light Water-Cooled Reactors - Project 2b - Cooling Conditions of the Reactor Core in the Case of the Maximum Credible Accident During Refilling by the Safety Feed System - Final Report", AEC-tr-7396 (Feb. 1973).

38. R. Martini and A. Premoli, "Bottom Flooding Experiments with Simple Geometries under Different ECC Conditions", Energia Nucleare, Vol. 20, 1973, p. 540.

39. D. C. Groeneveld and J. M. Young, "Film Boiling and Rewetting Heat Transfer During Bottom Flooding of a Hot Tube", 6th International Heat Transfer Conference, Toronto, 1978, Vol. 5, pp. 89-94.

40. Y. Lee, W. J. Chen and D.C. Groeneveld, "Rewetting of Very Hot Vertical and Horizontal Channels by Flooding", 6th Interational Heat Transfer Conference, Toronto, 1978, Vol. 5, pp. 95-100.

41. R. B. Duffey and D.T.C. Porthouse, "The Physics of Rewetting in Water Reactor Emergency Core Cooling", Nucl. Eng. & Design, vol. 25 (1973) pp. 379-394.

42. R. Semeria and B. Martinet, "Calefaction Spots on a Heating Wall: Temperature Distribution and Resorption", Proc. Inst. Mech. Eng., vol. 180 (1965) pp. 192-205.

43. T. S. Thompson, "An Analysis of the Wet-Side Heat Transfer Coefficient During Rewetting of a Hot Dry Patch", Nucl. Eng. & Design, vol. 22 (1972), pp. 212-224.

44. K. H. Sun, G.E. Dix and C.L. Tien, "Cooling of a Very Hot Vertical Surface by a Falling Liquid Film", J. of Heat Transfer, Vol. 96, 1974, pp. 126-131.

45. K. Yoshioka and S. Hasegawa, "A Correlation in Displacement Velocity of Liquid Film Boundary formed on a Heated Vertical Surface in Emergency Cooling", J. Nucl. Sci. & Tech. Vol. 7, 1970, pp. 418-425.

46. A. R. Ewards and D. J. Mather, "Some U.K. Studies Related to the Loss-of-Coolant Accident", *Proceedings of the Topical Meeting on Water Reactor Safety*, Salt Lake City, March 26-28, 1973, pp. 720-739.

47. J. M. Blair, "An Analytical Solution to a Two-Dimensional Model of the Rewetting of a Hot Dry Rod", Nucl. Eng. & Design, Vol. 32, 1975, pp. 159-170.

48. C. L. Tien and L. S. Yao, "Analysis of Conduction-Controlled Rewetting of a Vertical Surface", J. of Heat Transfer, Vol. 97, 1975, pp. 161-165.

49. J. G. M. Anderson and P. Hansen, "Two-Dimensional Heat Conduction in Rewetting Phenomena", Report No. NORHAV-D-6, DAECRER, Denmark, June 1974.

50. M. W. E. Coney, "Calculations on the Rewetting of Hot Surfaces", Nucl. Eng. and Design, Vol. 31, 1974, pp. 246-259.

51. S.K.W. Yu, P. R. Farmer and M.W.E. Coney, "Methods and Correlations for the Prediction of Quenching Rates on Hot Surfaces", Int. J. Multiphase Flow, Vol. 3, 1977, pp. 415-443.

52. K. H. Sun, G. E. Dix and C. L. Tien, "Effect of Precursory Cooling on Falling-Film Rewetting", J. of Heat Transfer, Vol. 97, 1975, pp. 360-365.

53. S. S. Dua and C. L. Tien, "Two-Dimensional Analysis of Conduction-Controlled Rewetting with Precursory Cooling", J. of Heat Transfer, Vol. 98, 1976, pp. 407-413.

54. S. Banerjee and W. T. Hancox, "On the Development of Methods for Analysing Transient Two-Phase Flow", Int. J. Multiphase Flow, Vol. 4, pp. 437-460, 1978.

55. L. J. Agee, R.B. Duffey and S. Banerjee, "Multi-Fluid Models for Transient Two-Phase Flow Analysis", EPRI NP-618-SR, Nov. 1977.

56. S. Banerjee and A.M.C. Chan, "Separated Flow Models: Part I, Analysis of the Averaged and Local Instantaneous Formulation", Int. J. of Multiphase Flow (in press).

57. M. Ishii, "Thermo-Fluid Dynamic Theory of Two-Phase Flow"; Eryolles, Paris, 1975.

58. E. D. Hughes, R. W. Lyczkowski and J. H. McFadden, "An Evaluation of State-of-the-Art Two-Velocity Two-Phase Flow Models and Their Applicability to Nuclear Reactor Transiet Analysis", EPRI Report NP-143, 1976.

59. J. M. Delhaye and J. L. Achard, "On the Averaging Operators Introduced in Two-Phase Flow Modelling", paper presented at First OECD/NEA Specialists' Meeting on Transient Two-Phase Flow, Toronto, August, 1976.

60. L. J. Agee, S. Banerjee, R. B. Duffey, and E.D. Hughes, "Some Aspects of Two-Fluid Models and their Numerical Solution", paper presented at Second OECD/NEA Specialists' Meeting on Transient Two-Phase Flow, Paris, 1978.

61. P. Vernier and J. M. Delhaye, "General Two-Phase Flow Equations Applied to the Thermodynamics of Boiling Nuclear Reactors", Energie Primaire, Vol. 4, No. 1, 1968.

62. R. I. Nigmatulin, "Averaging in Mathematical Modelling of Heterogeneous and Dispersed Mixtures", paper presented at International Center of Heat and Mass Transfer Symposium, Yugoslavia, 1978.

63. S. Banerjee, P.S. L. Yuen and M. Vandenbroek, "Calibration of a Fast Neutron Scattering Technique for Measurement of Void Fraction in Rod Bundles", J. of Heat Transfer, Vol. 101, 1979, pp. 295-299.

64. R. B. Brid, W. E. Stewart and E. N. Lightfoot, "Transport Phenomena, Wiley, 1960.

65. S. G. Bankoff, "A Variable Density Single-Fluid Model for Two-Phase Flow With Particular Reference to Steam-Water Flow", J. of Heat Transfer, Vol. 82, pp. 265-272, 1960.

66. T. Saito, "Multi-Fluid Modelling of Two-Phase Flow and Heat Transfer: Application to CHF prediction for BWR Conditions", Ph.D. thesis, Nuclear Engineering, University of Wisconsin, 1977.

67. S. Banerjee, "Separated Flow Models: Part II, Higher Order Dispersion Effects in the Averaged Formulation:, Int. J. of Multiphase Flow (in press).

68. J. A. Boure, "On A Unified Presentation of the Non-Equilibrium Two-Phase Flow Models", Non-Equilibrium Two-Phase Flows, Winter Annual Meeting of ASME, Nov. 30-Dec. 5, 1975.

69. K. P. Yu, E. Elias, D. Abdollahian, G. Yadigaroglu, W. T. Peake, and R. Greif, "UC-B Reflood Experimental Plan", EPRI NP-457, April 1977.

70. W. H. Cook, "Boiling Density in Vertical Rectangular Multi-Channel Sections With Natural Circulation", ANL-5621, 1956.

71. M. Petrick and B. S. Swanson, "Radiation Attenuation Method of Measuring Density of a Two-Phase Fluid", Review of Scientific Instruments, Vol. 29, 1958, pp. 1079-1085.

72. R. T. Lahey, Jr., "A Review of Selected Void Fraction and Phase Velocity Measurement Technique", Fluid Dynamics Institute Short Course on Two-Phase Flow Measurements, Dartmouth College, Aug. 1978.

73. "7471 Series Low-Level Analog Input Systems", Technical Manual, Computer Products, March, 1977.

74. G. Hewitt and P.C. Lovegrove, "Experimental Methods in Two-Phase Flow Studies", EPRI NP-118, 1976.

75 J. C. Rousseau, J. Czerny and B. Riegel, "Void Fraction Measurements During Blowdown by Neutron Absorption or Scattering Methods", Invited paper presented at OECD/NEA Specialist Meeting on Transient Two-Phase Flow, Toronto, August, 1976.

76. S. Banerjee, "Radiation Methods For Two-Phase Flow Measurements", Invited lecture at USNRC Two-Phase Instrumentation Review Meeting, Washington, January 1977.

77. P. S. L. Yuen, "Fast Neutron Scattering and Attenuation Technique for Measurement of Void Fraction and Phase Distribution in Transient Flow Boiling", Masters Thesis, Dept. of Engineering Physics, McMaster University, 1978.

78. S. Banerjee, A.M.C. Chan, N. Ramanathan and P.S.L. Yuen, "Fast Neutron Scattering and Attenuation Technique for Measurement of Void Fractions and Phase Distribution in Transient Flow Boiling", Sixth International Heat Transfer Conference, Aug. 1978, Toronto, Vol. 1, pp. 351-355, (Hemisphere Press).

79. H. A. Enge, "Introduction to Nuclear Physics", Addison Wesley, 1966.

80. G. D. Lassahn, "LOFT Three-Beam Densitometer Data Interpretation", TREE-NUREG-1111, 1977.

81. T. R. Heidrick, J. R. Saltvold and S. Banerjee, "Application of a 3-Beam Gamma Densitometer to Two-Phase Flow Design and Density Measurements", AICHE Symposium Series - Nuclear, Solar and Process Heat Transfer, Vol. 73, 1977.

82. B. A. Piggott, "Evaluation of Densitometer Performance", Technical Memorandum CWTM-057-FD, Atomic Power Division, Westinghouse Canada Ltd., August 1977.

83. "Radioactive Low Energy Photon Sources", Technical Bulletin 75/6, Amersham/Searle Corp.

84. "Cesium Fluoride Scintillation Crystals", Harshaw Chemical Co.

85. L. A. Eriksson, C.M. Tsai and Z.H. Cleo, "Comparative Studies on Plastic Scintillators - Applications to Low Energy High Rate Photon Detection", Nuclear Inst. Methods, Vol. 122, 1974, pp. 373-376.

86. Z. H. Cho and C.M. Tsai, "Tin and Lead loaded Plastic Scintillators for Low Energy Gamma-Ray Detection with Particular Application to High Rate Detection", IEEE Trans. on Nucl. Science, Vol. NS-22, 1975, pp. 72-80.

87. "Health Physics Manual", McMaster University, Hamilton, Ontario. 1971.

88. R. G. Jaeger ed., "Engineering Compendium on Radiation Shielding", Vol. I - Shielding Fundamentals and Methods, Springer-Verlag, 1968.

89. "Versatec-1200A Printer-Plotter Programmers Guide", (Old Reference no. 96).

90. E. S. Godleski and K. J. Bell, "The Leidenfoot Phenomenon for Binary Liquid Solutions", Proc. of 3rd International Heat Transfer Conference, Chicago, 1966, Vol. IV, pp. 51-58.

91. K. J. Bell, "Heat Transfer With Phase Change", Chem. Engrg. Prog. Symp. Series, Vol. 63, 1967, pp. 73-82.

92. B. S. Gottfried,C. J. Lee and K. J. Bell, "The Leidenfrost Phenomenon: Film Boiling of Liquid Droplets on a Flat Plate", Paper presented at A.I. Ch. E. National Meeting, Minneapolis, 1965.

93. F. Tamura and Y. Tanasawa, "Evaporation and Combustion of a Drop Contacting with a Hot Surface", Seventh Symposium (International) on Combustion, London, 1958, pp. 509-522.

94. F. B. Kenrick, C. S. Gilbert and K. L. Wismer, "The Superheating of Liquids", J. of Phys. Chem., vol. 28, 1924, pp. 1297-1307.

95. D. C. Groeneveld, "The Thermal Behaviour of a Heated Surface at and Beyond Dryout", AECL-4309, 1972.

96. B. M. Patel and K. J. Bell, "The Leidenfrost Phenomenon for Extended Liquid Masses", Paper presented at the Eighth National Heat Transfer Conference, Los Angeles, Cal. 1965.

97. E. R. Hosler and J. W. Westwater, "Film Boiling on a Horizontal Plate", ARS Journal, Vol. 32, 1962, pp. 553-558.

98. P. J. Berenson, "Film Boiling Heat Transfer from a Horizontal Surface", J. Heat Transfer, Vol. 83, 1961, pp. 351-358.

99. L.H.J. Watchers, H. Bonne, H.J. Van Nouhius, "The Heat Transfer from a Hot Horizontal Plate to Sessile Water Drops in Spheroidal State", Chem. Engrg. Sci., Vol. 21, 1966, pp. 923-926.

100. W. S. Bradfield, "Liquid Solid Contact in Stable Film Boiling", Ind. & Engrg. Chemistry Fundamentals, Vol. 5, 1966, pp. 200-204.

101. K. J. Baumeister and F. F. Simon, "Leidenfroot Temperature - Its Correlation for Liquid Metals, Cryogens, Hydrocarbons, and Water", J. of Heat Transfer, Vol. 95, 1973, pp. 166-173.

102. G. Kendall, "Heat Transfer to Impacting Drops and Post-Critical Heat Flux Dispersed Flow", Ph.D. Thesis, MIT, 1978.

103. L.H.J. Wachters and N.A.J. Westerling, "The Heat Transfer from a Hot Wall to Impinging Water Drops in the Spheroidal State", Chem. Engrg. Sci., Vol. 21, 1966, pp. 1047-1056.

104. M. Cumo and D. Pitimada, "On the Determination of the Leidenfrost Point With Sprays of Water and Low-Boiling Organics", ASME paper 73-HT-19 (1973).

105. T. S. Thompson, "Rewetting of a Hot Surface", AECL-5060, 1975.

106. V. L. Streeter, "Fluid Mechanics", 2nd Edition, McGraw Hill (1958), pp. 408-409.

107. W. H. McAdams, "Heat Transmission", McGraw-Hill, New York (1954), Third Edition, pp. 172-176.

108. R. B. Bird, W. E. Stewart and E.N. Lightfoot, "Transport Phenomena", John Wiley, New York (1960), pp. 429-433.

109. L. E. Sissom and D. R. Pitts, "Elements of Transport Phenomena", McGraw-Hill, 1972, pp. 491-492.

110. L. E. Sissom and D. R. Pitts, "Elements of Transport Phenomena", McGraw-Hill, 1972, p. 697.

111. V. T. Chow, "Open Channel Hydraulics", McGraw Hill (1959), Chapter 18.

112. F. M. Henderson, "Open Channel Flow", MacMillan Co. ([illegible]966), Chapter 8.

113. J. A. Liggett, "Basic Equations of Unsteady Flow", Unsteady Flow in Open Channels, Edited by K. Mahmood and V. Yevjevich, Water Resources Publications (1975), Vol. 1, pp. 29-62.

114. R. L. Street, "The Analysis and Solution of Partial Differential Equations", Brooks/Cole Publishing Co. (1973), Chapter 9.

115. R. Courant and K.O.Friedrichs, "Supersonic Flow and Shock Waves", Interscience Publishers (1948), Chapter 2.

116. M. B. Abbott, "An Introduction to the Method of Characteristics", American Elsevier Publishing Co., (1966).

117. M. B. Abbott, "Method of Characteristics", Unsteady Flow in Open Channels, Edited by K. Mahmood and V. Yevjevich , Water Resource Publications (1975), Vol. 1, pp. 63-88.

118. J. A. Liggett and J. A. Cunge, "Numerical Methods of Solution of the Unsteady Flow Equations", Unsteady Flow in Open Channels, Edited by K. Mahmood and V. Yevjevich, Water Resources Publications (1975), Vol. 1, pp 89-179.

119. E. Isaacson and H. B. Keller, "Analysis of Numerical Methods", John Wiley and Sons, Inc., (1966), pp. 485-487.

120. L. Fox, "Numerical Solution of Ordinary and Differential Equations", Pergamon Press (1962).

121. J. J. Stoker, "Water Waves - The Mathematical Theory and Applications", Interscience Publishers (1957), Chapters 10 and 11.

122. F. M. Henderson, "Open Channel Flow", MacMillan Co. (1966), pp. 90-101.

123. R. F. Dressler, "Comparison of Theories and Experiments for the Hydraulic Dam-Break Wave", International Assoc. of Hydrology, Assemblee generale de Rome, Vol. III (1954). p. 319.

124. L. S. Tong, "Heat Transfer Mechanisms in Nucleate and Film Boiling", Nuclear Engr. & Design, Vol. 21 (1972), pp. 1-25.

125. E. R. G. Eckert and R.M. Drake, Jr., "Analysis of Heat and Mass Transfer", McGraw Hill (1972), Chapter 4.

126. G. B. Wallis, "One Dimensional Two-Phase Flow", McGraw Hill, 1969, Chapter 2.

127. Y. Y. Hsu and R. W. Graham, "Transport Processes in Boiling and Two-Phase Systems", Hemisphere Publishing (1976), Chapter 4.

128. S. A. Kovalev, "An Investigation of Minimum Heat Fluxes in Pool Boiling of Water", Int. J. Heat Mass Transfer, Vol. 9, 1966, pp. 1219-1226.

129. Y. P. Chang, "A Theoretical Analysis of Heat Transfer in Natural Convection and in Boiling", Trans. ASME, Vol. 79, 1957, pp. 1501-1513.

130. N. Zuber, "Stability of Boiling Heat Transfer", Trans. ASME, Vol. 80, 1958, pp. 711-720.

131. L. A. Bromley, "Heat Transfer in Stable Film Boiling", Chemical Engineering Progress, Vol. 46, 1950, pp. 221-227.

132. J. Westwater and J. G. Santangelo, "Photographic Study of Boiling", Ind. Engr. Chem., Vol. 47, 1955, pp. 1605 - 16

133. H. Lamb, "Hydrodynamics", Dover Publications, New York, Sixth Edition, 1955, p. 445.

134. Y. P. Chang, "Wave Theory of Heat Transfer in Film Boiling", J. Heat Transfer, Vol. 81, 1959, pp. 1-12.

135. T. D. Hamill and K. J. Baumeister, "Film Boiling Heat Transfer from a Horizontal Surface as an Optimal Boundary Value Process", Proc. 3rd Int. Heat Trans. Conf., Vol. 4, 1966, pp. 59-64.

136. B. P. Breen and J. W. Westwater, "Effect of Diameter of Horizontal Tubes on Film Boiling Heat Transfer", Chem. Engr. Prog. Symp. Series, 58, 1962, pp. 67-72.

137. R. A. Kruger and W.M. Rohsenow, "Film Boiling Inside Horizontal Tubes", Proc. 3rd Int. Heat Trans. Conf., Vol. 5, 1966, pp. 60-68.

138. G. B. Wallis, "One Dimensional Two-Phase Flow", McGraw Hill, 1969, Chapter 7.

139. Y. Taitel and A. F. Dukler, "A Model for Predicting Flow Regime Transitions in Horizontal Gas-Liquid Flow", A.I.Ch.E.J., Vol. 22, 1976, pp. 47-55.

140. J. M. Mandhane, G. A. Gregory and K. Aziz, "A Flow Pattern Map for Gas-Liquid Flow in Horizontal Pipes", Int. J. Multiphase Flow, vol. 1, 1974, pp. 537-553.

APPENDIX I

(A) Numerical Calculation of Average Void Fraction in a Circular Duct Using a Single-Beam Gamma-Densitometer

The average void is calculated by dividing the beam into thin slits and summing the transmitted photon for each slit numerically. A circular mono-energetic beam with a diameter the same as the duct is used. A uniform beam intensity (I_o) is assumed.

A.1 Stratified Flow

This is applicable to horizontal ducts only. The beam can be either parallel (horizontal system) or perpendicular (vertical system) to the interface.

Figure A.1 shows a schematic view of a horizontal beam system. For a given slit (Δy), if $y \lesssim h_L$, the gamma flux in the slit will be attenuated by a water path length of $\ell(\ell=2S_t)$. The attenuated flux is thus given by

$$\Delta N_R = KI_o \, e^{-\mu\ell} \, \Delta y \int_{-S_b}^{S_b} dS_b \tag{I.1}$$

where μ is the absorption coefficient of water for the particular photon energy, K is a constant of proportionality, R is the beam or duct radius and $2S_t$ (or $2S_b$) is the chordal length.

$$S_t = S_b = \sqrt{2Ry - y^2} = S$$

If $y > h_L$, the beam slit sees no water and is not attenuated. The flux will be given by

$$\Delta N_R = KI_o \, \Delta y \int_{-S_b}^{S_b} dS_b \tag{I.2}$$

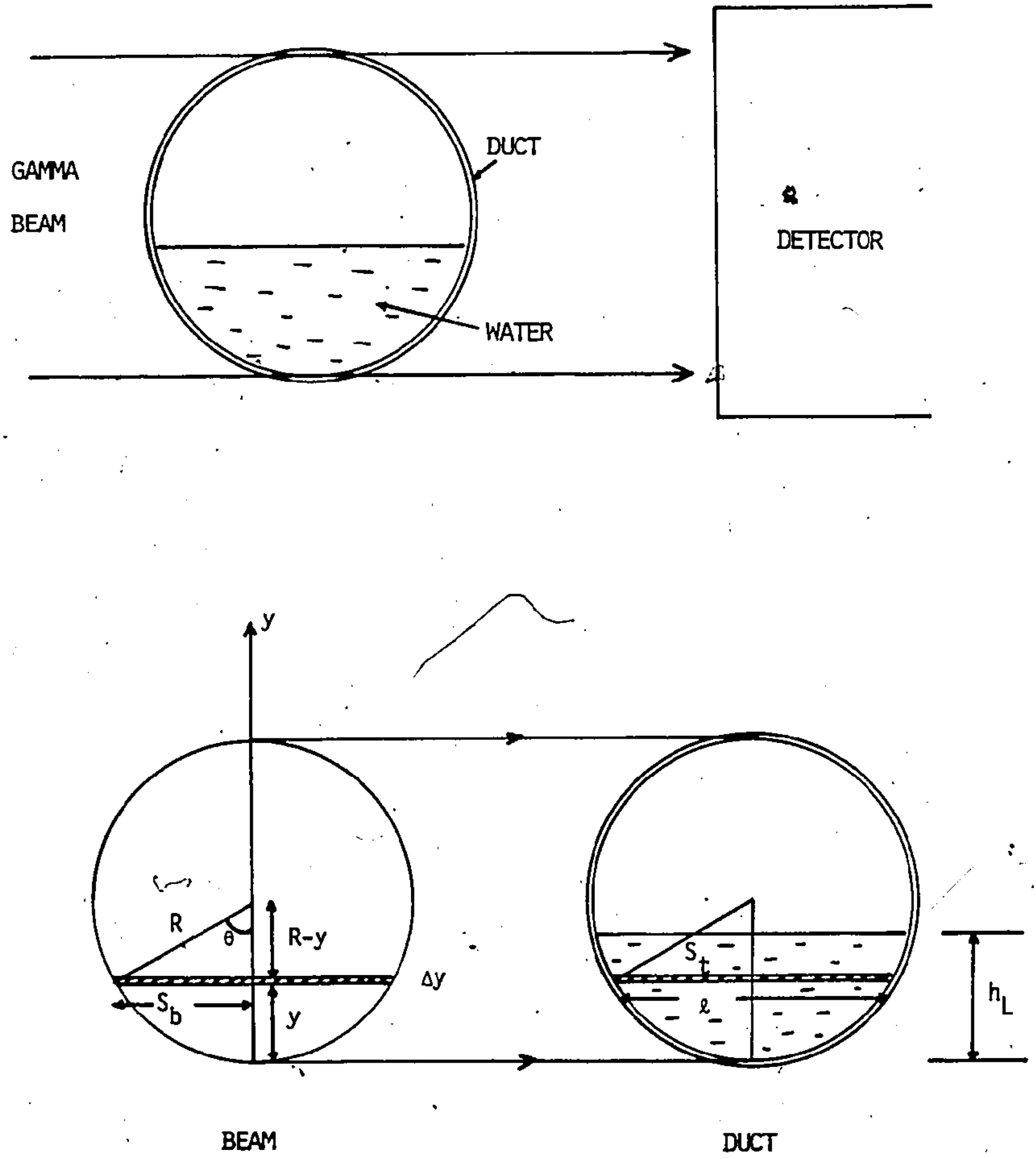

FIG. A.1 GAMMA DENSITOMETER CALIBRATION
— HORIZONTAL BEAM AND STRATIFIED FLOW

It should be mentioned here that there is always attenuation due to the tube walls, however, this is constant for a given photon energy and is absorbed into the constant of proportionality, K.

For a given water level (h_L), the total transmitted flux can be obtained by integrating

$$N_R(\alpha) = KI_o \int_0^{h_L} \int_{-S}^{S} e^{-2\mu S}\, dSdy + KI_o \int_{h_L}^{D} \int_{-S}^{S} dSdy \qquad (I.3)$$

and the average void fraction can be deduced by linear interpolation

$$\alpha_n = \frac{N_R(\alpha) - N(\alpha=0)}{N(\alpha=1) - N(\alpha=0)} \qquad (I.4)$$

where

$$N(\alpha=0) = KI_o \int_0^{D} \int_{-S}^{S} e^{-2\mu S} dS\, d\, y$$

and

$$N(\alpha=1) = KI_o \int_0^{D} \int_{-S}^{S} dS\, dy$$

Equation (I.4) can be compared with the actual void fraction

$$\alpha_a = \frac{\pi R^2 L - V}{\pi R^2 L} \qquad (I.5)$$

where L is the length of the duct and V is the water volume in the duct for the same length.

For a given water level (h_L) in the duct, the volume of water can be shown to be

$$V(h_L) = [R^2\theta - S(R-h_L)]L \qquad \text{for } h_L \leq R$$

$$\theta = \cos^{-1}((R-h_L)/R)$$

α

$$V(h_L) = \{\pi R^2 - [R^2\theta - S(h_L-R)]\}L \quad \text{for } h_L \geq R$$

$$\theta = \cos^{-1}((h_L-R)/R) \tag{I.6}$$

Conversely, if V is given, h_L can be obtained from Eqn. (I.6) by iteration. The bisection method is used. Thus, α_a and α_n can be readily compared.

For the vertical beam system (Figure A.2), the calculation procedures are essentially the same. h_L is found first for a given V and the other parameters are given by

$$\theta = \begin{cases} \sin^{-1}\left(\frac{R-h_L}{R}\right) & h_L \leq R \\ \sin^{-1}\left(\frac{h_L-R}{R}\right) & h_L \geq R \end{cases} \tag{I.7}$$

$$S = S_b = S_t = \sqrt{2Rx-x^2}$$

$$x_o = R(1-\cos\theta)$$

The water path lengths are

$$\ell = \begin{cases} S - (R-h_L) & h_L \leq R \\ S + (h_L-R) & h_L \geq R \end{cases} \tag{I.8}$$

Again, the total transmitted flux is obtained by integrating

$$N_R(\alpha) = 2KI_o\int_o^{x_o}\int_{-S}^{S} dSdx + 2KI_o\int_{x_o}^{R}\int_{-S}^{S} e^{-\mu\ell}dSdx \quad h_L \leq R$$

$$N_R(\alpha) = 2KI_o\int_o^{x_o}\int_{-S}^{S} e^{-2\mu S}dSdx + 2KI_o\int_{x_o}^{R}\int_{-S}^{S} e^{-\mu\ell}dSdx \quad h_L \geq R \tag{I.9}$$

A.2 Annular Flow

For annular flow, the total transmitted flux is given by

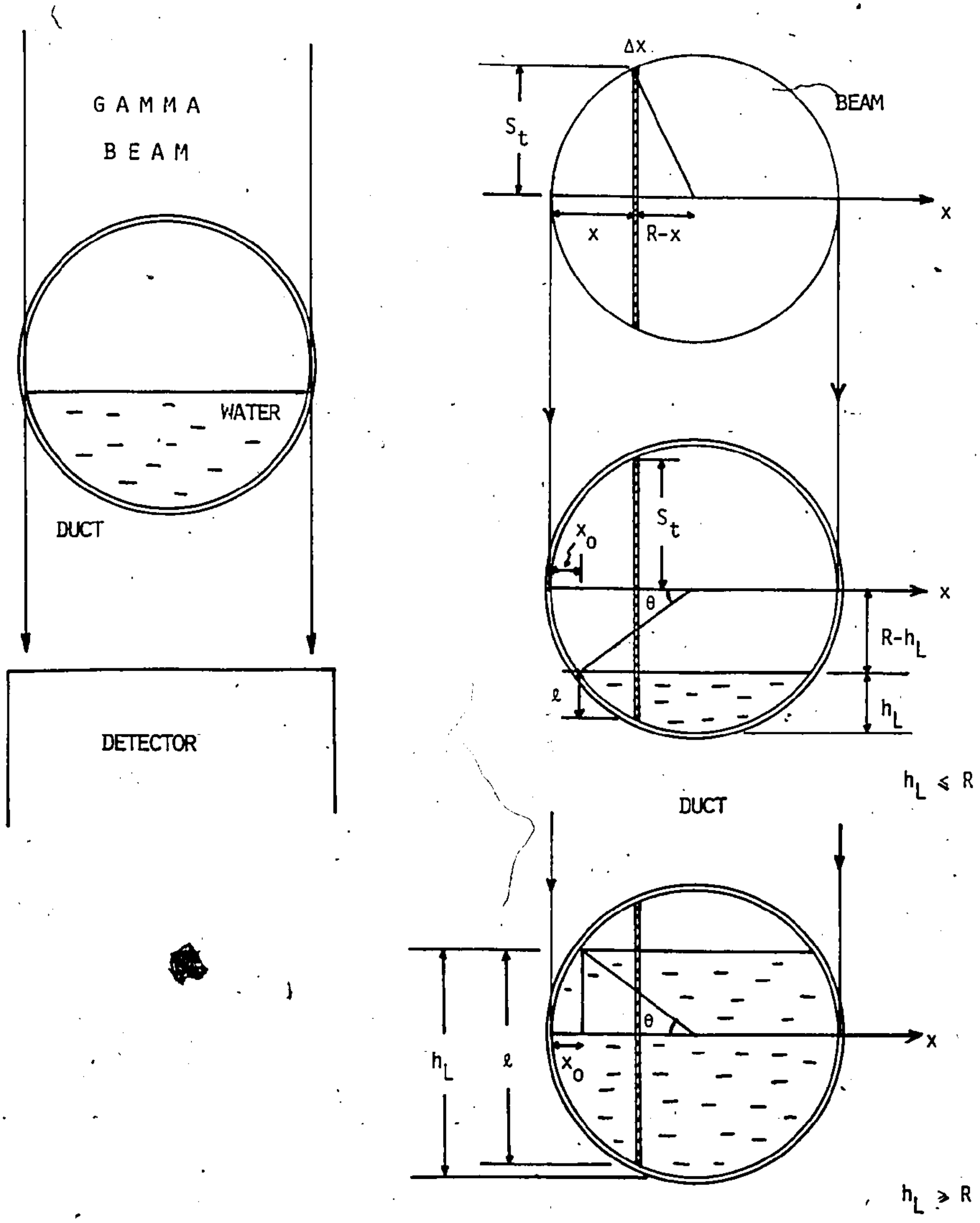

FIG. A.2 GAMMA DENSITOMETER CALIBRATION
— VERTICAL BEAM AND STRATIFIED FLOW

$$N_R(\alpha) = 2KI_o \int_{o}^{R-r}\int_{-S_R}^{S_R} e^{-2\mu S_R} dy dS_R + 2KI_o \int_{R-r}^{R}\int_{-S_R}^{S_R} e^{-2\mu\ell} dy dS_R \qquad (I.10)$$

where the variables are as defined in Figure A.3.

The average void is given by Eqn. (I.4) and the actual void for a given volume of water is given by Eqn. (I.5).

A.3 Core Flow

For core flow, it can be shown that

$$N_R(\alpha) = 2KI_o \int_{o}^{R-r}\int_{-S_R}^{S_R} dS_R dy + 2KI_o \int_{R-r}^{R}\int_{-S_R}^{S_R} e^{-2\mu S_r} dS_R dy \qquad (I.11)$$

The variables are defined in Figure A.4 and α_n and α_a are given by Eqns. (I.4) and (I.5) respectively.

A.4 Transmission of a Circular Beam Through an Empty Duct with Wall Thickness t

This can be treated the same as in the annular flow situation (Section A.2). The volume occupied by water is repalced by the metal wall. The absorption coefficient of the metal wall is used instead of water. The outer and inner radii, R_o and R_i are equivalent respectively to R and r in the annular flow case. The transmitted flux is given by Eqn. (I.10). The transmission ratio is the ratio of the transmitted fluxes with and without the duct. The latter case can be simulated by assuming $R_i = R_o$.

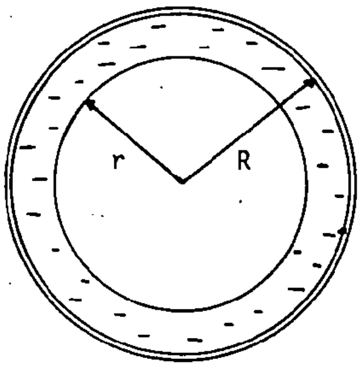

$$\alpha_a = r^2/R^2$$

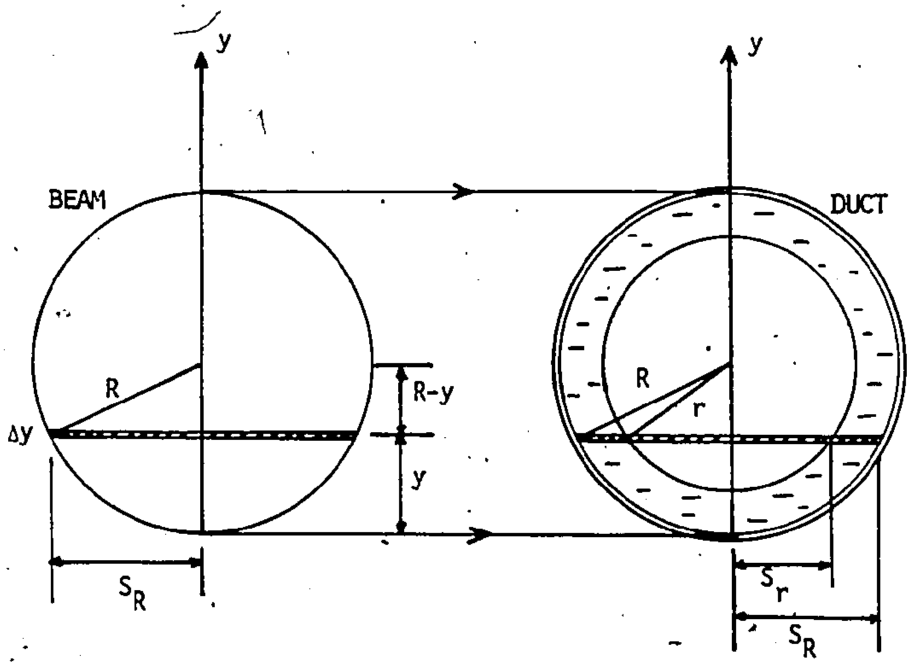

$$S_R = \sqrt{R^2 - (R-y)^2}$$

$$S_r = \sqrt{r^2 - (R-y)^2}$$

$$\ell = S_R - S_r$$

FIG. A.3 GAMMA DENSITOMETER CALIBRATION — ANNULAR FLOW

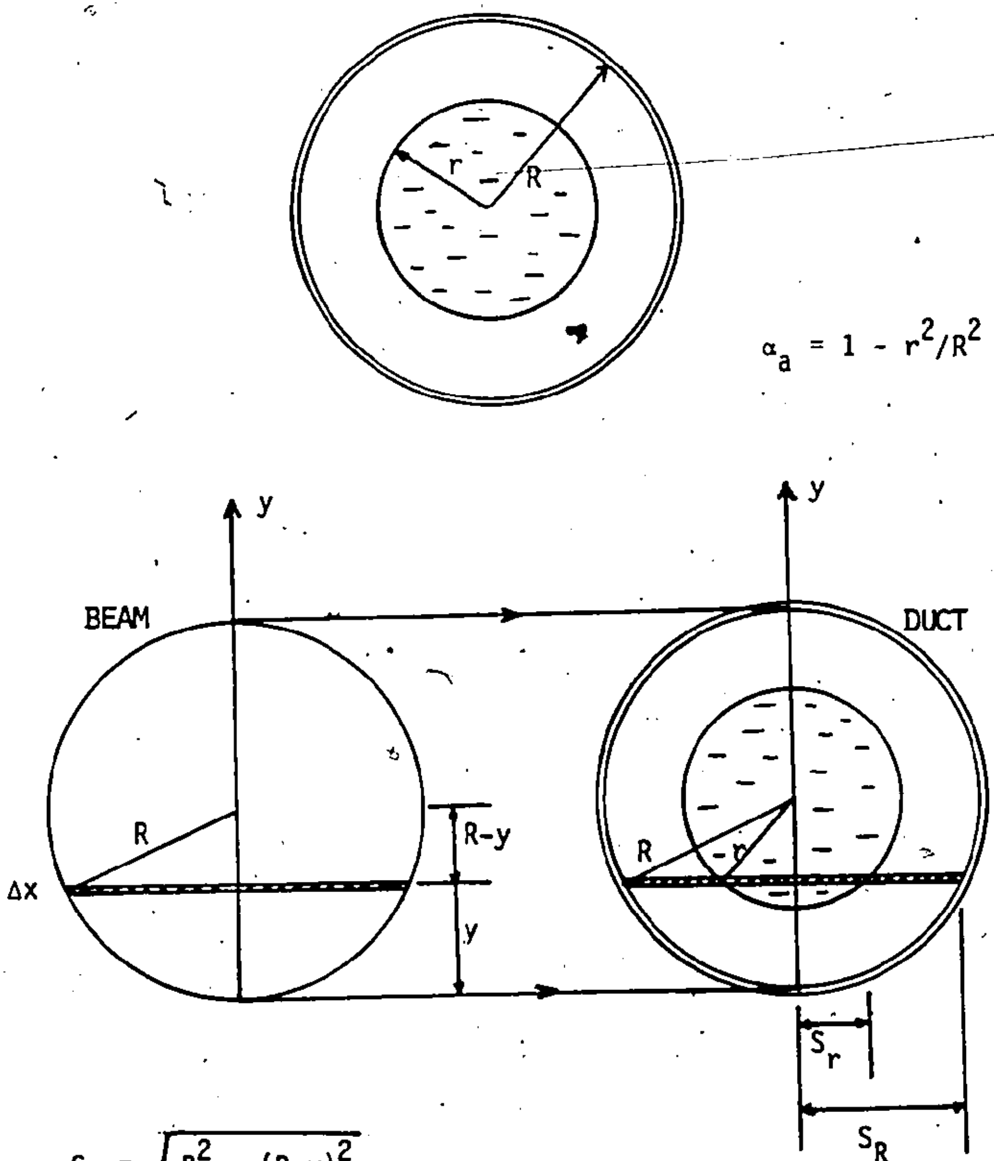

$$\alpha_a = 1 - r^2/R^2$$

$$S_R = \sqrt{R^2 - (R-y)^2}$$

$$S_r = \sqrt{r^2 - (R-y)^2}$$

$$\ell = 2S_r$$

FIG. A.4 GAMMA DENSITOMETER CALIBRATION — CORE FLOW

(B) Calculation of Dose Rate for a 50 mCi Sealed Co-57 Source with Shielding Container

Assumptions:

1. Isotropic source
2. Negligible self attenuation by source
3. Negligible attenuation by source capsule
4. Steel shielding container thickness - 1 1/2" (38.1 mm)
5. Exposure:
   - (i) On contact with the shielding container for fifteen minutes per day to set up the densitometers.
   - (ii) At one meter away for four hours a day attending the experiment
6. Experiments last for six months.

Dose Rate

The dose rate can be estimated using the following equation

$$D = \frac{\mu_m}{\rho_m} T\phi\Omega EQC \qquad (I.12)$$

The variables are given below

T is the transmission ratio through the shielding container. This is the ratio of the transmitted gamma flux over the incident flux

$$T = \exp(-\frac{\mu_s}{\rho_s} \rho_s x) \qquad (I.13)$$

where μ_s/ρ_s is the specific mass attenuation coefficient of the shielding material (steel in the present case), ρ_s is the density of steel and x is the shielding thickness (1 1/2").

$$\phi = S \eta \qquad (I.14)$$

where S is the source strength, η is the photon abundance or conversion ratio.

Ω is a geometric factor

$$\Omega = \frac{1}{4\pi L^2} \tag{I.15}$$

where L is the distance from source to experimeter. L = 38.1 mm on contact with shielding container and 100 cm at normal working distance.

μ_m/ρ_m is the specific mass-energy absorption coefficient of body (cm^2/gm). E is the photon energy (keV). Q is the quality factor of radiation which equals to unity for gamma radiation. C is a conversion factor

$$C = \frac{1000 \text{ mRem}}{\text{Rem}} \frac{1.6021 \times 10^{-9} \text{ erg}}{\text{keV}} \frac{\text{gm - rad}}{1000 \text{ erg}} \frac{3600 \text{ s}}{\text{hr}} \tag{I.16}$$

Co-57 gives gammas at four energies as listed below together with their abundance:

Energy (keV)	Abundance (%)
14.4	95
122	85.6
136	10.6
692	0.16

For practical purposes, the 14.4 keV photons can be ignored, the 122 keV and 136 keV radiations can be grouped together with a mean energy of 123.5 keV and abundance of 92.6%. The mean (μ_s/ρ_s) and (μ_m/ρ_m) values for the different photon energies are given below

Energy (keV)	μ_s/ρ_s (cm^2/gm)	μ_m/ρ_m (cm^2/gm)
123.5	0.268	0.0264
692	0.07	0.032

The dose rates can thus be calculated from Eqn. (I.12)

Energy (keV)	D on contact (mR/hr)	D at 1 meter (mR/hr)
123.5	0.6	9×10^{-4}
692	2.6	3.7×10^{-3}

The total expected exposure for six months will be given by

$$D^T = [(0.6+2.6)(0.25) + (9\times10^{-4}+3.7\times10^{-3})(0.4)](30\times6)$$

$$= 0.147 \text{ R}$$

Assuming a maximum permissible annual exposure (whole body) of 5R, the safety factor is

$$SF = \frac{5}{0.147} = 34$$

Since 90% of the total dose exposed to comes from contact with shielding container, care should be taken to minimize this time of contact.

APPENDIX II

Transient Circumferential Heat Conduction

The transient circumferential heat conduction problem in a thin walled tube is analysed. The system is shown in Figure II.1. The tube wall has a high initial temperature. At $t = 0$, the tube is filled with water to a level h_L. The subsequent changes in wall temperatures as a function of angular position (θ) are obtained.

The problem is solved with the following assumptions:

1. No heat loss from the tube to the surrounding, i.e. $h_0 = 0$
2. Heat transfer to air or vapor in the tube is negligible, i.e. $h_g = 0$
3. Heat transfer to liquid from the wall in contact with the liquid is large, i.e. $h_f \to \infty$ or $T_W = T_L$ for $\theta_0 \leq \theta \leq \pi$
4. Negligible axial conduction
5. Temperature gradient across the tube wall negligible
6. Physical properties of the wall are constant

With the above mentioned assumptions, the transient heat conduction equation becomes

$$\frac{\partial T_W}{\partial t} = \alpha \frac{\partial^2 T_W}{\partial \theta^2} \qquad \text{(II.1)}$$

where $\alpha = k/\rho C_p R^2$ is the thermal diffusivity of the wall material. The initial and boundary conditions are:

I.C. at $t \leq 0$, $T_W = T_W^0$ for $0 \leq \theta \leq \pi$

B.C.1 at $\theta = \theta_0$, $T_W = T_L$ for all $t > 0$

B.C.2 at $\theta = 0$, $\partial T_W/\partial t = 0$ for all $t > 0$

If we define the new variables

$$\phi = \frac{T_W - T_L}{T_W^0 - T_L}$$

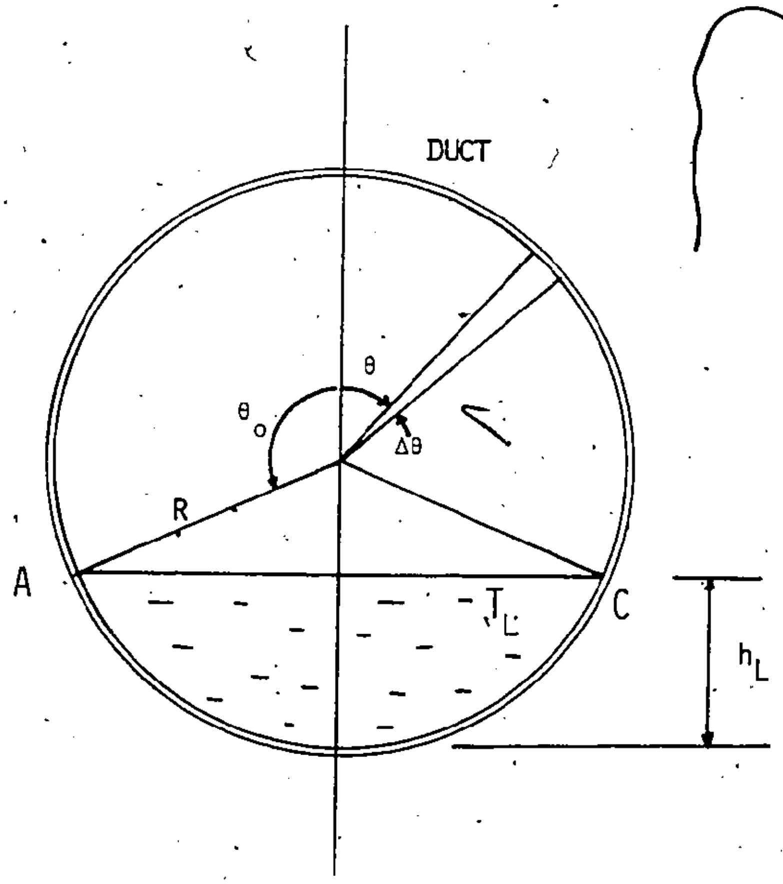

FIG. II.1 TRANSIENT CIRCUMFERENTIAL HEAT CONDUCTION and $\tau = \alpha t$

Eqn. (II.1) can be non-dimensionalized,

$$\frac{\partial\phi}{\partial\tau} = \frac{\partial^2\phi}{\partial\theta^2} \qquad \text{(II.2)}$$

with

I.C. at $\tau \leq 0$ $\quad \phi = 1$ $\quad$ for $0 \leq \theta \leq \pi$

B.C.1 at $\theta = \theta_0$ $\quad \phi = 0$ $\quad$ for all $\tau > 0$

B.C.2 at $\theta = 0$ $\quad \partial\phi/\partial\theta = 0$ $\quad$ for all $\tau > 0$

Now, assuming a solution of the form

$$\phi(\tau,\theta) = f(\theta)g(\tau) \qquad \text{(II.3)}$$

Substituting into Eqn. (II.2), we have

$$f(\theta)\,\frac{dg}{d\tau} = g(\tau)\,\frac{d^2f}{d\theta^2}$$

or $$\frac{1}{g}\frac{dg}{d\tau} = \frac{1}{f}\frac{d^2f}{d\theta^2} = -\lambda^2 \qquad \text{(II.4)}$$

where λ is a constant.

Eqn. (II.4) can be integrated separately to give

$g(\tau) = C_1e^{-\lambda^2\tau}$

and $\quad f(\theta) = C_2\sin\lambda\theta + C_3\cos\lambda\theta$

or $$\phi(\tau,\theta) = e^{-\lambda^2\tau}[A\sin\lambda\theta + B\cos\lambda\theta] \qquad \text{(II.5)}$$

Applying the boundary conditions:

B.C.2 $\quad \frac{\partial\phi}{\partial\theta}\Big/_{\theta=0} = 0 \rightarrow A = 0$

that is,

$$\phi(\tau,\theta) = B\ e^{-\lambda^2\tau}\cos\lambda\theta \tag{II.6}$$

B.C.1 $\phi/_{\phi=\theta_o} = 0$

$$\rightarrow B\ e^{-\lambda^2\tau}\cos\lambda\theta_o = 0$$

or $\cos\lambda\theta_o = 0$

that is,

$$\lambda_n = (n + \tfrac{1}{2})\ \frac{\pi}{\theta_o} \qquad n = 0, \pm 1, \pm 2 \ldots \tag{II.7}$$

Therefore, the general solution is given by

$$\phi(\tau,\theta) = \sum_{n=0}^{\infty} B_n\ e^{-\lambda_n^2\tau}\ \cos\lambda_n\theta \tag{II.8}$$

Where the set of B_n values are determined using the initial condition

$$1 = \sum_{n=0}^{\infty} B_n\cos\lambda_n\theta \tag{II.9}$$

Multiplying both sides of the equation by $\cos\lambda_m\theta d\theta$ and integrating,

$$\int_0^{\theta_o}\cos\lambda_m\theta d\theta = \sum_{n=0}^{\infty} B_n' \int_0^{\theta_o} \cos\lambda_n\theta\ \cos\lambda_m\theta\ d\theta \tag{II.10}$$

Since $\int \cos\lambda_n\theta\ \cos\lambda_m\theta\ d\theta = 0$ if $m \neq n$

Therefore, Eqn. (II.10) becomes

$$\int_0^{\theta}\cos\lambda_n\theta d\theta = B_n \int_0^{\theta_o} \cos^2\lambda_n\theta d\theta$$

or $\frac{1}{\lambda_n}\sin\lambda_n\theta o = B_n[\frac{\theta_o}{2} + \frac{1}{4\lambda_n}\sin 2\lambda_n\theta o]$

which gives

$$B_n = \frac{2\sin\lambda_n\theta_o}{\lambda_n\theta_o + \sin\lambda_n\theta_o\cos\lambda_n\theta_o} = \frac{2\sin(n+\frac{1}{2})\pi}{(n+\frac{1}{2})\pi + \sin(n+\frac{1}{2})\pi\,\cos(n+\frac{1}{2})\pi}$$

that is,

$$B_n = \frac{2(-1)^n}{(n+\frac{1}{2})\pi} \qquad \text{(II.11)}$$

Substituting back into Eqn. (II.8), we have

$$\phi = 2\sum_{n=0}^{\infty} \frac{(-1)^n}{(n+\frac{1}{2})\pi}\; e^{-\lambda_n^2\tau}\cos\lambda_n\theta$$

or

$$T_w = 2(T_w^o - T_L)\sum_{n=0}^{\infty} \frac{(-1)^n}{(n+\frac{1}{2})\pi}\; e^{-\lambda_n^2\alpha t}\cos\lambda_n\theta \qquad \text{(II.12)}$$

This equation gives the transient circumferential temperature of the tube for given h_L or θ_o.

APPENDIX III

List of Experimental Runs and Data Storage

A total of 200 experimental runs have been done. 191 of them have been stored on magnetic tapes. In the following section, detailed information on the raw data will be given so that it can be retrieved when required. This includes the initial and boundary contions of each run, the calibration curves for the sensors, the channel number to sensor correspondence in the Analog Input System (Section 4.3.1), the format in which the raw data are written on magnetic tape and the specifications of the magnetic tapes used.

III.1 List of Experimental Runs

The Analog Input System used for data acquisition has 32 channels. That is, a maximum of 32 sensor inputs can be logged during the experimental transients. Since the raw data obtained from the automatic data acquisition system (Section 4.3) are in sets of 32 numbers each, it is important to know exactly which sensor a given channel corresponds to. The channel number to sensor correspondence is given in Table III-1. The same correspondence was used in most of the runs. However, changes were made in some cases. These changes will be specified when conditions for each run are listed. Also shown in Table III-1 are the channel gains which specify the full scale voltages of the channel outputs. It should be noted that if the output voltage of a sensor goes above the channel full-scale voltage as specified by the amplifier gain, the channel output will get saturated and a constant digital number of 2047 will be acquired by the data logging system. The number 2047 corresponds to the maximum specified voltage. The locations of the sensors can be found in Table 4.2.

The calibration curves for the sensors are given in Table III-2. The equations for the pressure transducers and the turbine flow meters are obtained from the calibration curves shown in Figures 4.4 and 4.5 respectively.

Table III-1

CHANNEL TO SENSOR CORRESPONDENCE

Channel No.	Sensor	Full-Scale Voltage
1	P_{out}	±1000 mV
2	P_{in}	±1000 mV
3	A (input current)	±50 mV
4	V (input voltage)	±1000 mV
5	FL (flow rate)	±1000 mV
6	$\gamma D1$	±1000 mV
7	$\gamma D2$	±1000 mV
8	T_{in}	±20 mV*
9	T_{out}^{T}	±20 mV*
10	T_{out}^{B}	±20 mV*
11	T_{out}^{2}	±20 mV
12	T13R	±50 mV
13	T2R	
14	TAT	
15	TAR	
16	TAB	
17	T4R	
18	TBT	
19	TBR	
20	TBB	
21	T6R	
22	TCT	
23	TCR	
24	TCB	
25	T8R	
26	TDR	
27	TDB	
28	T10R	
29	TET	
30	TER	
31	TEB	
32	T12R	

* Changed to ±50 mV for runs on and after Dec. 4, 1978.

The temperature equation is obtained from a standard temperature table for chromel-alumel, type K thermocouples. A linear interpolation equation as derived in Section 5.2 (Eqn. (5.10)) is used to obtain the void fractions.

The experimental conditions of all the runs are summarized in Table III-3. The runs are grouped into six groups with different operating conditions as described in Section 6.3. In Table III-3; column 1 is the run identification, Column 2 shows the group that the run belongs to, Column 3 gives the average initial wall temperature, Column 4 gives the inlet flow rate, Column 5 gives the inlet water temperature, Columns 6 and 7 give the empty and full conditions for the two densitometers used, Column 8 shows any comments or remarks regarding to that particular run.

Table III-2

CALIBRATION CURVES FOR THE SENSORS

1. Pressure Transducers

   $P = 12.95\ V - 2.655$ (psig)

   where V is in volts

2. Ammeter (Input Current)

   $A = 12.0\ V$ (amp)

   where V is in milli-volts

3. Voltmeter (Input Voltage)

   $V_{in} = 23.0\ V$ (volt)

   where V is in volts

4. Flow Meter*

   (a) $QV = 133.33\ V$ (mℓ/s)

   (b) $QV = 102.0\ V$ (mℓ/s)

   where V is in volts

5. Thermocouples (chromel-alumel, type K)

$T = 24.45\ V$ (°C) for $V \leq 15.5$ mV

$T = 23.33\ V + 18.3$ (°C) for $V > 15.5$ mV

6. Gamma Densitometer

$$\alpha = \frac{V - V_0}{V_1 - V_0} \qquad (5.10)$$

where V_1 and V_0 are the empty and full conditions respectively. The units for V and V_0 and V_1 are volts.

*First curve (QV = 133.33 V) applies for all runs between 11-13-78-02 and 01-05-78-06 inclusively. The second curve (QV = 102.0 V) applies for all runs after.

III.2 Raw Data Storage and Interpretation

The raw data obtained are stored on magnetic tapes in sets of 32 numbers on a continuous basis. Each set of data takes up two 'lines' on the magnetic tape, i.e. 16 numbers are written on each 'line'. Each number consists of 5 integers. The format of reading the data from a magnetic tape or permanent file is:

```
      READ (1, 10) (INBIN(I), I = 1,16)
   10 FORMAT (16I5)
```

To convert the raw data back to the sensor input voltages, the following relationship is used

$$V = \text{INBIN(I)} \times \frac{G}{2047} \qquad (\text{III.1})$$

where G is the channel gain used. The calibration curves (Table III-2) are used to obtain the physical values from V.

A number of experimental runs can be written on a magnetic tape. Each run is separated by an END OF FILE (EOF) mark. The end of the tape is marked by two

EOF's. The Fortran program used to write the data onto magnetic tapes from permanent files is given in Table III-4. A day file generated by the McMaster Computing System is shown. It should be noted that 9L1317 is the magnetic tape identification. 9L indicates that the tape is nine-track and labelled. CHAN2 is the password.

To read the data from a magnetic tape and copy them into a permanent file, the procedures shown in Table III-5 are followed. The same tape used in Table III-4 is used here for illustrative purpose. We skip five EOF marks. The run NOV163A is obtained and transferred into the permanent file NOV163B.

The 191 experimental runs have been stored on twelve magnetic tapes. The specifications of the magnetic tapes and the runs that individual tape contains are listed in Table III-6. The runs in a magnetic tape are listed in sequence. Thus, any run can be read by skipping the appropriate number of EOF marks.

Table III-3

LIST OF EXPERIMENTAL RUNS

Run I.D.	Group	T_w (°C)	Q_{in} (mℓ/s)	T_{in} (°C)	γD1 (volt)	γD2 (volt)	REMARKS
11-13-78-02	1	500	60.0	45.5	0.502 0.426	0.394 0.347	1. Channel/sensor correspondence shown in Table III-1
11-13-78-03	1	500	47.0	45.5	0.496 0.430	0.396 0.348	-id-
11-13-78-04	1	450	33.3	45.5	0.496 0.431	0.396 0.348	-id-
11-16-78-01	1	350	53.3	8.0	0.428 0.340	0.484 0.387	-id-
11-16-78-02	1	450	53.3	8.0	0.430 0.345	0.484 0.391	-id-
11-16-78-03	1	550	53.3	8.0	0.432 0.346	0.487 0.389	-id-
11-16-78-04	1	500	53.3	8.0	0.429 0.348	0.485 0.390	-id-
11-23-78-01	1	290	33.5	9.0	0.424 0.341	0.480 0.386	1. TDT (gain = ±50 mV) replaces P_{outB} in ch. 1. 2. T_{out} (Ch. 10) is broken
11-23-78-02	1	290	47.5	8.3	0.424 0.341	0.480 0.386	-id-
11-23-78-03	1	290	60.0	8.3	0.423 0.340	0.480 0.387	-id-

Table III-3 (continued)
p. 2

Run I.D.	Group	T_w (°C)	Q_{in} (mℓ/s)	T_{in} (°C)	γD1 (volt)	γD2 (volt)	REMARKS
11-23-78-04	1	290	74.0	8.3	0.424 0.340	0.481 0.387	-id-
11-23-78-05	1	290	83.0	8.3	0.423 0.341	0.480 0.387	-id-
11-23-78-06	1	290	42.0	8.3	0.424 0.341	0.480 0.386	-id-
11-27-78-01	1	400	33.0	10.0	0.408 0.328	0.489 0.390	1. TDT replaces P_{out_B} in Ch. 1 2. T_{out} (Ch. 10) is broken 3. T13R (Ch. 12) is broken
11-27-78-02	1	400	47.0	8.5	0.413 0.332	0.490 0.389	-id-
11-27-78-03	1	400	60.0	8.0	0.416 0.334	0.488 0.390	-id-
11-27-78-04	1	400	73.5	8.0	0.416 0.335	0.489 0.390	-id-
11-27-78-05	1	400	86.5	8.0	0.417 0.335	0.489 0.392	-id-
11-27-78-06	1	400	54.0	8.0	0.419 0.336	0.491 0.391	-id-
11-29-78-01	1	500	46.3	8.3	0.402 0.325	0.493 0.394	1. TDT replaces P_{out_B} in Ch. 1. 2. T_{out} (Ch. 10) is broken.
11-29-78-02	1	500	60.5	7.5	0.403 0.325	0.494 0.393	-id-
11-29-78-03	1	500	74.0	7.5	0.401 0.326	0.493 0.394	-id-

Table III-3 (continued)
p. 3

Run I.D.	Group	T_w (°C)	Q_{in} (mℓ/s)	T_{in} (°C)	γD1 (volt)	γD2 (volt)	REMARKS
11-29-78-04	1	500	87.0	7.5	0.406 0.329	0.493 0.393	-id-
11-29-78-05	1	500	40.0	8.0	0.407 0.329	0.496 0.396	-id-
11-29-78-06	1	500	53.5	7.5	0.409 0.331	0.497 0.395	-id-
11-30-78-01	1	600	47.0	10.0	0.402 0.325	0.472 0.377	1. TDT replaces P_{out} in Ch. 1
11-30-78-02	1	600	60.0	7.0	0.402 0.328	0.471 0.377	-id-
11-30-78-03	1	600	74.5	7.0	0.404 0.330	0.475 0.380	-id-
11-30-78-04	1	600	87.5	7.0	0.404 0.329	0.474 0.381	-id-
11-30-78-05	1	600	100.0	7.0	0.405 0.331	0.476 0.381	-id-
11-30-78-06	1	600	54.0	7.0	0.405 0.331	0.476 0.383	-id-
							Clean the tube with dilute HCl Dec. 1, 1978
12-04-78-01	1	600	47.0	10.0	0.413 0.338	0.477 0.380	1. TDT replaces P_{out} in Ch. 1
12-04-78-02	1	600	60.0	8.3	0.413 0.337	0.416 0.380	-id-

Table III-3 (continued)
p. 4

Run I.D.	Group	T_w (°C)	Q_{in} (mℓ/s)	T_{in} (°C)	γD1 (volt)	γD2 (volt)	REMARKS
12-04-78-03	1	600	74.0	6.5	0.415 0.341	0.475 0.381	-id-
12-04-78-04	1	600	87.0	6.5	0.418 0.340	0.475 0.381	-id-
12-04-78-05	1	600	101.0	7.0	0.417 0.342	0.477 0.381	-id-
12-05-78-01	1	555	46.5	7.5	0.418 0.339	0.476 0.381	1. TDT replaces P_{out} in Ch. 1. 2. Gain for T_{out} (Ch. 11) changes to ±50 mV
12-05-78-02	1	555	60.5	7.5	0.418 0.341	0.482 0.384	-id-
12-05-78-03	1	555	75.0	7.5	0.423 0.343	0.487 0.386	-id-
12-05-78-04	1	555	87.5	8.0	0.421 0.343	0.483 0.385	-id-
12-05-78-05	1	555	101.0	7.0	0.419 0.345	0.485 0.387	-id-
12-05-78-06	1	555	40.5	8.0	0.424 0.345	0.485 0.390	-id-
12-06-78-01	1	450	46.5	6.5	0.422 0.341	0.475 0.383	-id-
12-06-78-02	1	450	60.5	6.0	0.423 0.340	0.472 0.378	-id-
12-06-78-03	1	450	75.0	6.5	0.424 0.342	0.474 0.380	-id-
12-06-78-04	1	450	87.0	6.5	0.426 0.343	0.476 0.381	-id-

Table III-3 (continued)
p. 5

Run I.D.	Group	T_w (°C)	Q_{in} (mℓ/s)	T_{in} (°C)	γD1 (volt)	γD2 (volt)	REMARKS
12-06-78-05	1	450	40.0	6.0	0.427 0.345	0.476 0.383	-id-
06-12-78-06	1	450	53.5	7.5	0.428 0.344	0.477 0.382	-id-
12-11-78-01	1	500	33.0	9.2	0.412 0.332	0.468 0.372	-id-
12-11-78-02	1	500	47.0	8.5	0.410 0.331	0.467 0.372	-id-
12-11-78-03	1	500	60.5	8.3	0.414 0.332	0.467 0.372	-id-
12-11-78-04	1	500	74.0	7.5	0.425 0.334	0.474 0.375	-id-
12-11-78-05	1	500	87.5	9.2	0.422 0.335	0.472 0.375	-id-
12-11-78-06	1	500	100.0	7.5	0.419 0.336	0.471 0.376	-id-
12-12-78-01	1	340	33.0	6.7	0.417 0.331	0.472 0.375	1. TDT replaces P_{out} in ch. 1. 2. Gain: $T2_{out}$ (ch. 11)=±50 mV T_{in} (ch. 8) = ±20 mV
12-12-78-02	1	340	47.0	6.0	0.418 0.332	0.471 0.375	-id-
12-12-78-03	1	340	61.0	6.7	0.418 0.332	0.471 0.374	-id-
12-12-78-04	1	340	74.0	6.7	0.417 0.334	0.471 0.376	-id-
12-12-78-05	1	340	87.0	5.8	0.426 0.339	0.474 0.378	-id-

Table III-3 (continued)
p. 6

Run I.D.	Group	T_w (°C)	Q_{in} (mℓ/s)	T_{in} (°C)	$\gamma D1$ (volt)	$\gamma D2$ (volt)	REMARKS
12-12-78-06	1	340	100.0	5.8	0.429 0.341	0.477 0.380	-id-
12-13-78-01	2	280	33.5	41.0	0.414 0.333	0.469 0.376	-id-
12-13-78-2	2	280	47.0	44.0	0.415 0.333	0.469 0.378	-id-
12-13-78-03	2	280	60.0	43.0	0.418 0.334	0.470 0.377	-id-
12-13-78-04	2	280	73.5	44.0	0.420 0.339	0.473 0.381	-id-
12-13-78-05	2	280	87.0	45.0	0.427 0.340	0.480 0.383	-id-
12-13-78-06	2	280	101.0	45.0	0.424 0.340	0.478 0.383	-id-
12-14-78-01	2	400	47.0	44.0	0.413 0.334	0.474 0.379	1. Remarks 1 and 2 in 12-12-78-01 apply 2. T_{out} (Ch. 9) broken, replaced by TBL
12-14-78-02	2	400	60.5	44.0	0.416 0.334	0.478 0.380	-id-
12-14-78-03	2	400	73.5	44.0	0.419 0.338	0.478 0.382	-id-
12-14-78-04	2	400	87.5	44.0	0.421 0.339	0.480 0.385	-id-
12-14-78-05	2	400	100.0	44.0	0.422 0.340	0.479 0.385	-id-
12-14-78-06	2	400	40.0	44.0	0.422 0.341	0.479 0.386	-id-

Table III-3 (continued)
p. 7

Run I.D.	Group	T_w (°C)	Q_{in} (mℓ/s)	T_{in} (°C)	γD1 (volt)	γD2 (volt)	REMARKS
12-15-78-01	2	500	33.0	43.0	0.413 0.332	0.478 0.374	-id-
12-15-78-02	2	500	46.5	45.0	-id-	-id-	-id-
12-15-78-03	2	500	60.0	46.0	0.414 0.336	0.475 0.378	-id-
12-15-78-04	2	500	74.0	46.0	0.418 0.338	0.476 0.379	-id-
12-15-78-05	2	500	87.5	45.0	0.417 0.339	0.478 0.380	-id-
12-15-78-06	2	500	101.0	45.0	0.418 0.340	0.480 0.381	-id-
12-16-78-01	2	600	46.5	47.0	0.397 0.327	0.464 0.370	1. Remarks 1 & 2 in 12-14-78-01 apply 2. T_{out} (Ch.10) broken
12-16-78-02	2	600	60.0	47.0	0.402 0.330	0.465 0.373	-id-
12-16-78-03	2	600	73.5	48.0	0.407 0.334	0.468 0.374	-id-
12-16-78-04	2	600	87.0	47.0	0.410 0.336	0.475 0.378	-id-
12-16-78-05	2	600	100.0	47.0	0.410 0.336	0.469 0.376	-id-
							Clean tube with dilute HCl - Dec. 18, 1978.
							Install circuit breaker. Disconnect A and V in Ch. 3 and 4.
12-20-78-01	3	290	33.0	9.2	0.381 0.304	0.440 0.352	1. Remarks 1 and 2 in 12-12-78-01 apply. 2. Gain: P_{out}(Ch.3) = ±1000 mV TBL(Ch.4)=±50 mV T_{out}(Ch.9)=±50 mV

Table III-3 (continued)
p. 8

Run I.D.	Group	T_w (°C)	Q_{in} (mℓ/s)	T_{in} (°C)	γD1 (volt)	γD2 (volt)	REMARKS
12-20-78-02	3	290	46.5	8.3	0.382 0.307	0.445 0.354	-id-
12-20-78-03	3	290	60.5	8.3	0.386 0.307	0.440 0.352	-id-
12-20-78-04	3	290	74.0	7.0	0.386 0.307	0.440 0.352	-id-
12-20-78-05	3	290	101.0	8.3	0.387 0.309	0.447 0.367	-id-
12-20-78-06	3	290	102.0	8.7	0.389 0.310	0.447 0.357	-id-
12-20-78-07	3	400	33.5	7.5	0.384 0.310	0.449 0.363	-id-
12-20-78-08	3	400	47.0	7.0	0.387 0.310	0.450 0.363	-id-
12-20-78-09	3	400	61.0	7.0	0.388 0.310	0.454 0.363	-id-
12-20-78-10	3	400	74.0	7.0	0.387 0.310	0.456 0.363	-id-
12-20-78-11	3	400	87.0	7.0	0.387 0.310	0.453 0.363	-id-
12-20-78-12	3	400	101.1	7.0	0.388 0.312	0.452 0.362	-id-
12-21-78-01	3	500	33.0	7.5	0.384 0.306	0.455 0.362	-id-
12-21-78-02	3	500	47.0	7.5	0.386 0.308	0.454 0.362	-id-
12-21-78-03	3	500	60.0	7.5	0.389 0.310	0.454 0.362	-id-
12-21-78-04	3	500	74.5	7.5	0.389 0.310	0.454 0.362	-id-

Table III-3 (continued)
p. 9

Run I.D.	Group	T_w (°C)	Q_{in} (mℓ/s)	T_{in} (°C)	$\gamma D1$ (volt)	$\gamma D2$ (volt)	REMARKS
12-21-78-05	3	500	87.5	7.5	0.392 0.313	0.454 0.363	-id-
12-21-78-06	3	500	100.0	7.0	0.392 0.313	0.451 0.364	-id-
12-22-78-01	3	600	33.0	8.5	0.376 0.303	0.448 0.356	-id-
11-22-78-02	3	600	46.5	8.0	0.378 0.304	0.450 0.355	-id-
11-22-78-03	3	600	60.0	8.0	0.376 0.304	0.450 0.356	-id-
11-22-78-04	3	600	74.0	8.0	0.377 0.305	0.458 0.355	-id-
11-22-78-05	3	600	88.0	8.5	0.380 0.307	0.455 0.353	-id-
11-22-78-06	3	600	102.5	7.5	0.377 0.304	0.448 0.355	-id-
							Move $\gamma D1$ from location 1 (0.145 m from inlet of heated section) to location 2 (1.12 m from inlet section).
							Clean Tube - Jan. 3, 1979.
01-04-79-01	3	500	32.0	10.0	0.412 0.329	0.450 0.359	1. Remarks 1 and 2 in run 12-20-78-01 apply.
01-04-79-02	3	500	47.5	11.7	0.414 0.331	0.453 0.360	-id-
01-04-79-03	3	500	61.5	9.0	0.416 0.333	0.453 0.360	-id-

Table III-3 (continued)
p. 10

Run I.D.	Group	T_w (°C)	Q_{in} (mℓ/s)	T_{in} (°C)	$\gamma D1$ (volt)	$\gamma D2$ (volt)	REMARKS
01-04-79-04	3	500	64.0	10.0	0.418 0.332	9.453 0.361	-id-
01-04-79-05	3	500	84.5	8.3	0.415 0.333	0.454 0.361	-id-
01-04-79-06	3	500	107.0	10.0	0.420 0.355	0.455 0.358	-id-
01-05-79-01	3	600	32.5	10.8	0.410 0.327	0.425 0.340	-id-
01-05-79-02	3	600	46.0	10.2	0.408 0.330	0.424 0.340	-id-
01-05-79-03	3	600	57.5	10.0	0.410 0.330	0.423 0.340	-id-
01-05-79-04	3	600	75.0	10.8	0.413 0.330	0.427 0.341	-id-
01-05-79-05	3	600	85.5	10.0	0.413 0.331	0.426 0.341	-id-
01-05-79-06	3	600	100.0	10.4	0.413 0.332	0.427 0.342	-id-
							1. Install constant water-level head tank. 2. Change turbine flowmeter. A new calibration curve applies.
01-12-79-01	4	600	90.0	5.8	0.402 0.326	0.415 0.333	1. Remarks 1 and 2 in run 12-20-78-01 apply. 2. TIR (±50mV) replaces T^8_{out} in Ch.10. 3. T^2_{out} (Ch.11) is broken.
01-12-79-02	4	600	77.0	5.8	0.407 0.327	0.417 0.335	-id-

Table III-3 (continued)
p. 11

Run I.D.	Group	T_w (°C)	Q_{in} (mℓ/s)	T_{in} (°C)	γD1 (volt)	γD2 (volt)	REMARKS
01-12-79-03	4	600	66.5	5.2	0.410 0.327	0.418 0.335	-id-
01-12-79-04	4	600	56.5	5.2	0.409 0.329	0.418 0.335	-id-
01-12-79-05	4	600	46.0	5.2	0.423 0.333	0.422 0.337	-id-
01-12-79-06	4	600	36.0	6.0	0.410 0.329	0.418 0.337	-id-
01-15-79-01	4	500	89.0	5.2	0.401 0.323	0.420 0.337	-id-
01-15-79-02	4	500	77.3	5.2	0.403 0.325	0.422 0.340	-id-
01-15-79-03	4	500	72.0	5.3	0.403 0.324	0.418 0.341	-id-
01-15-79-04	4	500	56.5	5.2	0.404 0.324	0.424 0.335	-id-
01-15-79-05	4	500	46.0	5.4	0.409 0.330	0.423 0.341	-id-
01-15-79-06	4	500	36.0	6.7	0.410 0.330	0.410 0.331	-id-
01-17-79-01	4	400	89.5	7.7	0.400 0.320	0.418 0.334	1. Remarks 1 and 2 in run 01-12-79-01 apply.
01-12-79-02	4	400	77.0	7.5	0.402 0.322	0.420 0.334	-id-
01-17-79-03	4	400	66.5	5.2	0.406 0.325	0.420 0.335	-id-
01-17-79-04	4	400	56.5	5.2	0.404 0.324	0.420 0.336	-id-
01-17-79-05	4	400	46.0	7.5	0.405 0.327	0.420 0.336	-id-

Table III-3 (continued)
p. 12

Run I.D.	Group	T_w (°C)	Q_{in} (mℓ/s)	T_{in} (°C)	γD1 (volt)	γD2 (volt)	REMARKS
01-17-79-06	4	400	36.0	7.7	0.410 0.328	0.423 0.337	-id-
01-18-79-01	4	290	92.5	6.5	0.401 0.323	0.415 0.333	-id-
01-18-79-02	4	290	80.0	6.7	0.405 0.327	0.418 0.336	-id-
01-18-79-03	4	290	66.5	7.5	0.407 0.328	0.420 0.337	-id-
01-18-79-04	4	290	56.5	7.5	0.406 0.327	0.420 0.337	-id-
01-18-79-05	4	290	46.0	5.8	0.406 0.326	0.420 0.337	-id-
01-18-79-06	4	290	37.0	7.5	0.407 0.327	0.421 0.337	-id-
							Clean tube - Jan. 19, 1979
01-23-79-01	5	600	87.5	23.0	0.401 0.322	0.406 0.325	-id-
01-23-79-02	5	600	76.5	21.0	0.401 0.323	0.406 0.326	-id-
01-23-79-03	5	600	67.0	24.0	0.403 0.323	0.408 0.326	-id-
01-23-79-04	5	600	54.0	22.0	0.406 0.325	0.407 0.326	-id-
01-23-79-05	5	600	47.0	22.0	0.403 0.325	0.408 0.327	-id-
01-23-79-06	5	600	36.0	22.0	0.407 0.326	0.408 0.327	-id-
01-24-79-01	5	400	91.0	25.0	0.398 0.321	0.403 0.323	-id-

Table III-3 (continued)
p. 13

Run I.D.	Group	T_w (°C)	Q_{in} (mℓ/s)	T_{in} (°C)	γD1 (volt)	γD2 (volt)	REMARKS
01-24-79-02	5	400	77.5	22.0	0.401 0.323	0.406 0.327	-id-
01-24-79-03	5	400	67.0	23.3	0.403 0.324	0.404 0.325	-id-
01-24-79-04	5	400	56.6	22.5	0.733 0.608	0.405 0.325	-id-
01-24-79-05	5	400	46.5	21.0	0.403 0.325	0.407 0.326	-id-
01-24-79-06	5	400	36.0	21.7	0.406 0.328	0.407 0.328	-id-
							Clean tube - Jan. 24, 1979.
01-25-79-01	4	600	91.5	22.0	0.399 0.321	0.396 0.318	-id-
01-25-79-02	4	600	77.0	25.0	0.402 0.322	0.396 0.317	-id-
01-25-79-03	4	600	67.0	25.4	0.404 0.323	0.394 0.320	-id-
01-25-79-04	4	600	56.5	21.0	0.408 0.324	0.400 0.322	-id-
01-25-79-05	4	600	46.5	22.0	0.586 0.337	0.403 0.325	-id-
01-25-79-06	4	600	35.5	25.0	0.747 0.601	0.401 0.324	-id-
01-30-79-01	4	400	91.5	21.0	0.393 0.316	0.393 0.315	-id-
01-30-79-02	4	400	77.0	21.0	0.395 0.317	0.397 0.317	-id-
01-30-79-03	4	400	66.5	21.0	0.394 0.317	0.398 0.318	-id-
01-30-79-04	4	400	57.0	21.5	0.397 0.321	0.399 0.319	-id-

Run I.D.	Group	T_w (°C)	Q_{in} (mℓ/s)	T_{in} (°C)	γD1 (volt)	γD2 (volt)	REMARKS
01-30-79-05	4	400	46.5	21.5	0.397 0.319	0.399 0.320	-id-
01-30-79-06	4	400	35.0	22.0	0.398 0.320	0.401 0.319	-id-
							1. Clean tube - Feb. 6, 1979 2. Remove γD1 and γD2, wrap tube with glass wool insulation. 3. Place γD1 downstream of outlet of heated section
02-08-79-01	6	400	90.5	22.0	0.712 0.579	- -	1. Remarks 1 and 2 in run 01-12-79-01 apply. 2. Ch.7 - TDL (±50 mV)
02-08-79-02	6	400	77.0	24.0	0.747 0.607	- -	-id-
02-08-79-03	6	400	66.0	22.0	0.782 0.640	- -	-id-
02-08-79-04	6	400	57.5	22.0	0.783 0.638	- -	-id-
02-08-79-05	6	400	45.0	22.0	0.787 0.640	- -	-id-
02-08-79-06	6	400	36.0	22.5	0.790 0.640	- -	-id-
02-09-79-01	6	290	94.0	17.0	0.770 0.634	- -	-id-
02-09-79-02	6	290	78.0	18.0	0.754 0.621	- -	-id-
02-09-79-03	6	290	67.5	20.0	0.773 0.626	- -	-id-

Table III-3 (continued)
p. 15

Run I.D.	Group	T_w (°C)	Q_{in} (mℓ/s)	T_{in} (°C)	γD1 (volt)	γD2 (volt)	REMARKS
02-09-79-04	6	290	59.0	22.0	0.787 0.647	- -	-id-
02-09-79-05	6	290	45.5	22.0	0.801 0.648	- -	-id-
02-09-79-06	6	290	36.0	22.0	0.804 0.650	- -	-id-
02-12-79-01	6	500	93.0	22.0	0.800 0.645	- -	1. Remark 1 in run 02-08-79-01 applies. 2. Ch.7 = TET (±50 mV) Ch.29 = TDL (±50 mV) 3. TET is broken
02-12-79-02	6	500	78.0	20.0	0.683 0.556	- -	-id-
02-12-79-03	6	500	62.5	20.0	0.776 0.633	- -	-id-
02-12-79-04	6	500	56.0	22.0	0.623 0.508	- -	-id-
02-12-79-05	6	500	48.0	22.0	0.621 0.507	- -	-id-
02-12-79-06	6	500	38.0	24.0	0.689 0.558	- -	-id-
02-14-79-01	6	600	92.5	17.0	0.694 0.563	- -	-id-
02-14-79-02	6	600	77.5	23.0	0.728 0.590	- -	-id-
02-14-79-03	6	600	67.5	22.0	0.733 0.597	- -	-id-
02-14-79-04	6	600	57.0	22.0	0.733 0.597	- -	-id-

Run I.D.	Group	T_w (°C)	Q_{in} (mℓ/s)	T_{in} (°C)	γD1 (volt)	γD2 (volt)	REMARKS
02-14-79-05	6	600	47.5	22.0	0.738 0.599	- -	-id-
02-14-79-06	6	600	37.5	20.0	0.740 0.601	- -	-id-

TABLE III.4

PROCEDURES USED TO WRTIE DATA ONTO MAGNETIC TAPE

```
16.38.25.WRITE.                  -. CHAN
16.38.27.USER(7002893,)
16.38.28.CHARGE(SBANEF)
16.38.37.RESTAPE(NT=1)
16.38.37.*
16.38.37.*
16.38.37.* PROCEDURE TO ENSURE REQUIRED TAPE RESO
16.38.37.URCES ARE AVAILABLE BEFORE THE
16.38.37.* JOB ADVANCES. IF THEY ARE NOT THEN ASK
16.38.37. THE OPERATOR TO MAKE THEM AVAILABLE.
16.38.37.IF (NUM(NT) .AND. .NOT. NUM(1) ) CALL,9Z
16.38.37.ZZZRC(P1=NT,P2=0)
16.38.38.IF (.NOT. NUM(NT) .AND. NUM(1) ) CALL,9Z
16.38.38.ZZZRC(P1=1 ,P2=1)
16.38.38.CALL,9ZZZZRC(P1=0 ,P2=1)
16.38.38.NOEXIT.
16.38.40.SET(EF=0)
16.38.40.RESOURC(NT=0,NI=1)
16.38.41.ONEXIT.
16.38.41.IF (EF .NE. 0 .AND. EF .NE. CPE) CALL,2Z
16.38.41.ABORT
16.38.41.IF (EF .EQ. CPE) CALL,9ZZZASK(Q1=1,Q2=1)
16.38.41.IF (NUM(NT) .AND. NUM(1) )          CALL,9Z
16.38.41.ZZZRC(P1=NT,P2=1)
16.38.41.* END OF RESTAPE PROCEDURE
16.38.41.*
16.38.41.*
16.38.41.LABEL(TAPE,NT,D=PE,L=CHANZ,PO=W,VSN=9L13
16.38.41.17,W)
16.41.39.NT1, ASSIGNED TO TAPE     , VSN=9L1317.
16.41.46.FETCH(I=NOV132A)
16.41.55.FILE(I,BT=C,RT=Z,FL=3200,BFS=650)
16.41.55.FILE(TAPE,BT=C,RT=Z,FL=3200,BFS=650)
16.41.57.FORM.
16.49.15.WRITEF(TAPE)
16.49.17.FETCH(J=NOV133A)
16.49.26.FILE(J,BT=C,RT=Z,FL=3200,BFS=650)
16.49.27.FILE(TAPE,BT=C,RT=Z,FL=3200,BFS=650)
16.49.30.FORM.
17.02.01.WRITEF(TAPE)
17.02.02.FETCH(K=NOV134A)
17.02.11.FILE(K,BT=C,RT=Z,FL=3200,BFS=650)
17.02.13.FILE(TAPE,BT=C,RT=Z,FL=3200,BFS=650)
17.02.59.FORM.
17.07.31.WRITEF(TAPE)
17.07.31.FETCH(L=NOV161A)
17.07.40.FILE(L,BT=C,RT=Z,FL=3200,BFS=650)
17.07.41.FILE(TAPE,BT=C,RT=Z,FL=3200,BFS=650)
17.07.47.FORM.
17.11.24.WRITEF(TAPE)
17.11.25.FETCH(M=NOV162A)
17.11.30.FILE(M,BT=C,RT=Z,FL=3200,BFS=650)
17.11.30.FILE(TAPE,BT=C,RT=Z,FL=3200,BFS=650)
17.11.35.FORM.
17.14.44.WRITEF(TAPE)
17.14.45.FETCH(N=NOV163A)
17.14.47.FILE(N,BT=C,RT=Z,FL=3200,BFS=650)
17.14.48.FILE(TAPE,BT=C,RT=Z,FL=3200,BFS=650)
17.14.51.FORM.
17.19.33.WRITEF(TAPE)
17.19.33.FETCH(O=NOV164A)
17.19.44.FILE(O,BT=C,RT=Z,FL=3200,BFS=650)
17.19.45.FILE(TAPE,BT=C,RT=Z,FL=3200,BFS=650)
```

```
[illegible]
17.21.55.WRITEF(TAPE)
17.21.55.WRITEF(TAPE)
17.21.57.UEAD,         0.004KUNS.
17.21.57.UEPF,         1.228KUNS.
17.21.57.UEMT,         1.765KUNS.
17.21.57.UEMS,        49.753KUNS.
17.21.57.UECP,        21.037SECS.
17.21.57.AESR,        72.288UNTS.
17.22.26.UCLP,  33,       0.723KLNS.
```

TABLE III.5

PROCEDURES USED TO READ DATA FROM MAGNETIC TAPE

```
      AP2IACT.   78/11/23.MCMASTER * SYSTEM B
10.21.07.RTAPE.                A. CHAN
10.21.09.USER(7002893,)
10.21.09.CHARGE(SBANER)
10.21.20.RESTAPE(NT=1)
10.21.20.*
10.21.20.*
10.21.20.* PROCEDURE TO ENSURE REQUIRED TAPE RESO
10.21.20.URCES ARE AVAILABLE BEFORE THE
10.21.20.* JOB ADVANCES. IF THEY ARE NOT THEN ASK
10.21.20. THE OPERATOR TO MAKE THEM AVAILABLE.
10.21.21.IF (NUM(MT) .AND. .NOT. NUM(1T ) CALL,9Z
10.21.21.ZZZRC(P1=MT,P2=0)
10.21.21.IF (.NOT. NUM(MT) .AND. NUM(1) ) CALL,9Z
10.21.21.ZZZRC(P1=0 ,P2=1)
10.21.21.CALL,9ZZZZRC(P1=0 ,P2=1)
10.21.22.NOEXIT.
10.21.22.SET(EF=0)
10.21.22.RESOURC(MT=0,NT=1)
10.21.26.ONEXIT.
10.21.26.IF (EF .NE. 0 .AND. EF .NE. CPE) CALL,2Z
10.21.26.ABORT
10.21.26.IF (EF .EQ. CPE) CALL,9ZZZASK(Q1=0,Q2=1)
10.21.27.IF (NUM(MT) .AND. NUM(1) )        CALL,9Z
10.21.27.ZZZRC(P1=MT,P2=1)
10.21.27.* END OF RESTAPE PROCEDURE
10.21.27.*
10.21.27.*
10.21.27.DEFINE(NOV163B)
10.21.28.LABEL(TAPE,NT,D=PE,R,PO=R,VSN=9L1317,L=C
10.21.28.HA,2)
10.21.28.ST41, ASSIGNED TO TAPE    , VSN=9L1317.
10.54.13.SKIPF(TAPE,5)
10.54.33.COPYBF(TAPE,DUMMY)
10.54.40. COPY COMPLETE.
10.54.47.REWIND(DUMMY)
10.54.47.COPYBF(DUMMY,NOV163B)
10.54.52. COPY COMPLETE.
10.54.53.AUDIT.
10.54.57.REWIND(DUMMY)
10.54.57.COPY(DUMMY,OUTPUT)
10.55.03. EOI ENCOUNTERED.
10.55.06.UEAD,         0.004KUNS.
10.55.06.UEPF,         0.092KUNS.
10.55.06.UEMT,         0.251KUNS.
10.55.06.UEMS,        11.962KUNS.
10.55.06.UECP,         0.414SECS.
10.55.06.AESR,         6.418UNTS.
11.17.51.UCLP, 35,         3.584KLNS.
```

Table III-6

DATA STORAGE

TAPE IDENTIFICATION	PASSWORD	EXPERIMENTAL RUNS STORED	TOTAL NO. OF RUNS STORED
9L1317 (Write 2)	Chan 2	11-13-78-02, 11-13-78-03, 11-13-78-04, 11-16-78-01, 11-16-78-02, 11-16-78-03, 11-16-78-04	7
9L4423 (Write 3)	Chan 3	11-23-78-01, 11-23-78-02, 11-23-78-03, 11-23-78-04, 11-23-78-05, 11-23-78-06, 11-27-78-01, 11-27-78-02, 11-27-78-03, 11-27-78-04, 11-27-78-05, 11-27-78-06, 11-29-78-01, 11-29-78-02, 11-29-78-03, 11-29-78-04, 11-29-78-05, 11-29-78-06	18
9L2537 (Write 4)	Chan 4	11-30-78-01, 11-30-78-02, 11-30-78-03, 11-30-78-04, 11-30-78-05, 11-30-78-06, 12-04078-01, 12-04-78-02, 12-04-78-03, 12-04-78-04, 12-04-78-05, 12-05-78-01, 12-05-78-02, 12-05-78-03, 12-05-78-04, 12-05-78-05, 12-05-78-06	17
9L6101 (Write 5)	Chan 5	12-06-78-01, 12-06-78-02, 12-06-78-03, 12-06-78-04, 12-06-78-05, 12-06-78-06, 12-11-78-01, 12-11-78-02, 12-11-78-03, 12-11-78-04, 12-11-78-05, 12-11-78-06, 12-12-78-01, 12-12-78-02, 12-12-78-03, 12-12-78-04, 12-12-78-05, 12-12-78-06	18
9L6119 (Write 6)	Chan 6	12-13-78-01, 12-12-78-02, 12-13-78-03, 12-13-78-04, 12-13-78-05, 12-13-78-06, 12-14-78-01, 12-14-78-02, 12-14-78-03, 12-14-78-04, 12-14-78-05, 12-14-78-06, 12-15-78-01, 12-15-78-02, 12-15-78-03, 12-15-78-04, 12-15-78-05, 12-15-78-06	18

continued ...

Table III-6 (continued)

TAPE IDENTIFICATION	PASSWORD	EXPERIMENTAL RUNS STORED	TOTAL NO. OF RUNS STORED
9L1427 (Write 7)	Chan 7	12-18-78-01, 12-18-78-02, 12-18-78-03, 12-18-78-04, 12-18-78-05, 12-20-78-01, 12-20-78-02, 12-20-78-03, 12-20-78-04, 12-20-78-05, 12-20-78-06, 12-20-78-07, 12-20-78-08, 12-20-78-09, 12-20-78-10, 12-20-78-11, 12-20-78-12	17
9L1534 (Write 8)	Chan 8	12-21-78-01, 12-21-78-02, 12-21-28-03, 12-21-78-04, 12-21-78-05, 12-21-78-06, 12-22-78-01, 12-22-78-02, 12-22-78-03, 12-22-78-04, 12-22-78-05, 12-22-78-06, 01-04-79-01, 01-04-79-02, 01-04-79-03, 01-04-79-04, 01-04-79-05, 01-04-79-06	18
9L1709 (Write 9)	Chan 9	01-05-79-01, 01-05-79-02, 01-05-79-03, 01-05-79-04, 01-05-79-05, 01-05-79-06, 01-12-79-01, 01-12-79-02, 01-12-79-03, 01-12-79-04, 01-12-79-05, 01-12-79-06, 01-15-79-01, 01-15-79-02, 01-15-79-03, 01-15-79-04, 01-15-79-05, 01-15-79-06	18
9L1712 (Write 10)	Chan 10	01-17-79-01, 01-17-79-02, 01-17-79-03, 01-17-79-04, 01-17-79-05, 01-17-79-06, 01-18-79-01, 01-18-79-02, 01-18-79-03, 01-18-79-04, 01-18-79-05, 01-18-79-06, 01-23-79-01, 01-23-79-02, 01-23-79-03, 01-23-79-04, 01-23-79-05, 01-23-79-06	18
9L7122 (Write 11)	Chan 11	01-24-79-01, 01-24-79-02, 01-24-79-03, 01-24-79-04, 01-24-79-05, 01-24-79-06, 01-25-79-01, 01-25-79-02, 01-25-79-03, 01-25-79-04, 01-25-79-05, 01-25-79-06, 01-30-79-01, 01-30-79-02, 01-30-79-03, 01-30-79-04, 01-30-79-05, 01-30-79-06	18
9L7123 (Write 12)	Chan 12	02-08-79-01, 02-08-79-02, 02-08-79-03, 02-08-79-04, 02-08-79-05, 02-08-79-06, 02-09-79-01, 02-09-79-02, 02-09-79-03, 02-09-79-04, 02-09-79-05, 02-09-79-06, 02-12-79-01, 02-12-79-02, 02-12-79-03, 02-12-79-04, 02-12-79-05, 02-12-79-06	18
9L7130 (Write 13)	Chan 13	02-14-79-01, 02-14-79-02, 02-14-79-03, 02-14-79-04, 02-14-79-05, 02-14-79-06	6

APPENDIX IV

COMPUTER PROGRAM LISTINGS

IV.1 Program STRIP
IV.2 Program RWRFPL
IV.3 Program REWET

```
PROGRAM STRIP.                              A. CHAN
SETTL,150.
VSN(TAPE=9U7120)
LABEL(TAPE,NT,D=800,F=L,LB=KU,PO=RE)
SKIPF(TAPE)
SKIPF(TAPE)
COPY(TAPE,TAPE15,BS=2000B,EL=10)
RETURN(TAPE)
REWIND(TAPE15)
FTN,GO(PL=10000)
REWIND(TAPE11)
COPYBF(TAPE11,FEB146A)
SAVE(FEB146A)
AUDIT.
     6400 END OF RECORD
    PROGRAM STRIP(INPUT,OUTPUT,TAPE5=INPUT,TAPE6=OUTPUT,TAPE15,
   *    TAPE11)
        DIMENSION IRAW(3200)
        IU=15
        READ(5,1) NTIMES,NWORDS,NSKIP
1       FORMAT(4I5)
        IF( NSKIP.LE.0) GO TO 21
        DO 20 I=1,NSKIP
        CALL TAPEIN( NWORDS,IRAW,IU )
20      CONTINUE
21      CONTINUE
        DO 10 I=1,NTIMES
        CALL TAPEIN( NWORDS,IRAW,IU )
        WRITE(6,2) ( IRAW(J),J=1,NWORDS )
2       FORMAT ( 16(2X,I5) )
    WRITE(11,3) (IRAW(J),J=1,NWORDS)
  3 FORMAT(16(I5))
10      CONTINUE
    REWIND 11
        STOP
```

```
      END
      SUBROUTINE TAPEIN(NWORDS,IRAW,IU)
      DIMENSION IDATA(1000),IN(4),IOUT(15),IRAW(3200)
      MAX = 1000
      IP=1
      DO 1 I=1,1000
1     IDATA(I)=0
      DO 2 I=1,NWORDS
2     IRAW(I)=0
100   CONTINUE
      BUFFER IN (IU,IP) (IDATA(1),IDATA(MAX) )
      IF( UNIT(IU) ) 10,11,12
12    WRITE(6,13)
13    FORMAT(20X,*PARITY ERROR *)
      STOP
11    WRITE(6,14)
14    FORMAT(20X,*END OF FILE *)
      STOP
10    CONTINUE
      NW=LENGTH(IU)
      WRITE(6,15) NW
15    FORMAT(/ 10X,*NO. OF WORDS*,I6    )
      X=NW/4.0
      M=X
      IF( X.GT. M) M=M+1
      NRAW=0
      ML=M*4
      DO 20 IL=1,ML,4
      I=IL
      J=IL+3
      L=0
      DO 21 IJ=I,J
      L = L + 1
      IN(L)=IDATA(IJ)
21    CONTINUE
```

```
           DO 22 JJ=1,15
22         IOUT(JJ)=0
           CALL STRIP16(IN,IOUT)
           DO 23 JJ=1,15
           NRAW=NRAW+1
           IF( NRAW.GT.NWORDS) RETURN
           IRAW(NRAW)=IOUT(JJ)
23         CONTINUE
20         CONTINUE
           RETURN
           END
       SUBROUTINE STRIP16 (IN,IOUT)
       DIMENSION IN(4),IOUT(15)
       INTEGER C,OUT,S,D
       D = 0
       C=0
       OUT = 0
       S = 1
       N=1
     2 IF(S-60) 4,4,5
     5 N=N+1
       S = 1
     4 IB=SHIFT(IN(N),-59)
       IB = IB.AND.IB
       IN(N) = SHIFT(IN(N),1)
       S=S+1
       D= SHIFT(D,1)
       D = OR(D,IB)
       C=C+1
       IF(C-16) 2,3,3
     3 OUT=OUT+1
       IOUT(OUT) = D
       D=0
       C=0
       IF(OUT-15) 2,7,7
     7 RETURN
       END
```

```
PROGRAM RWRFPL.                A. CHAN
SETTL,150.
FETCH(TAPE1=DEC135A)
FTN(OPT=1)
GRAB(PLOTVER)
LDSET(LIB=PLOTVER)
LGO.
     6400 END OF RECORD
    PROGRAM RWRFPL(TAPE1,OUTPUT,TAPE6=OUTPUT)
C
C     THIS PROGRAM PLOTS ALL THE 32 CHANNELS OF THE RTP SYSTEM
C
     DIMENSION DATA(32,562),INBIN(32),NCH(2),KPLOT1(12),KPLOT2(10)
    REAL NA1,NAO,NB1,NBO
    INTEGER DATA
    DATA XINCH,YINCH,XO/9.,6.,2./
    DATA NA1,NAO,NB1,NBO/0.405,0.331,0.476,0.383/
    DATA NCH/12,10/
    DATA KPLOT1/12,13,15,17,19,21,23,25,26,28,30,32/
    DATA KPLOT2/1,14,16,18,20,22,24,27,29,31/
    DATA KMAX/562/
    DATA DELT/0.016/
    YO = (10.555-YINCH)/2 + 0.25
    FACT = 2047.
    REWIND 1
    I=0
    J=0
 26 J = J + 1
    IF(J.GT.KMAX) GO TO 20
    READ(1,10) (INBIN(I),I=1,32)
 10 FORMAT(16(I5))
    IF(EOF(1)) 20,79
 79 DO 69 I=1,32
    DATA(I,J) = INBIN(I)
 69 CONTINUE
```

```
   READ(1,10) (INBIN(I),I=1,32)
   IF(EOF(1)) 20,73
73 READ(1,10) (INBIN(I),I=1,32)
   IF(EOF(1)) 20,72
72 GO TO 26
20 JFIN = J-1
   WRITE(6,71) JFIN
71 FORMAT(//5X,7HJFIN = ,I5//)
   DO 90 IM=1,2
   CALL FPLOT(XINCH,YINCH,X0,0.,600.,0.,27.,2)
   NCHAN = NCH(IM)
   DO 50 I=1,NCHAN
   IF(IM.EQ.1) KK=KPLOT1(I)
   IF(IM.EQ.2) KK=KPLOT2(I)
   TIME = 0.
   RESULT = 0.
   JJ = 1
   IF(KK.EQ.1) GO TO 12
   IF(KK.EQ.2) GO TO 11
   IF(KK.EQ.3) GO TO 13
   IF(KK.EQ.4) GO TO 50
   IF(KK.EQ.5) GO TO 14
   IF(KK.EQ.6) GO TO 15
   IF(KK.EQ.7) GO TO 15
   IF(KK.EQ.8) GO TO 12
   IF(KK.EQ.9) GO TO 12
   IF(KK.EQ.10) GO TO 12
   IF(KK.EQ.11) GO TO 12
   IF(KK.EQ.12) GO TO 12
   IF(KK.EQ.13) GO TO 12
   IF(KK.EQ.14) GO TO 12
   IF(KK.EQ.15) GO TO 12
   IF(KK.EQ.16) GO TO 12
   IF(KK.EQ.17) GO TO 12
   IF(KK.EQ.18) GO TO 12
```

```
      IF(KK.EQ.19) GO TO 12
      IF(KK.EQ.20) GO TO 12
      IF(KK.EQ.21) GO TO 12
      IF(KK.EQ.22) GO TO 12
      IF(KK.EQ.23) GO TO 12
      IF(KK.EQ.24) GO TO 12
      IF(KK.EQ.25) GO TO 12
      IF(KK.EQ.26) GO TO 12
      IF(KK.EQ.27) GO TO 12
      IF(KK.EQ.28) GO TO 12
      IF(KK.EQ.29) GO TO 12
      IF(KK.EQ.30) GO TO 12
      IF(KK.EQ.31) GO TO 12
      IF(KK.EQ.32) GO TO 12
      GO TO 1000
 11   CALL FPLOT(XINCH,YINCH,X0,-15., 15.,0.,27.,1)
      CF = 6.673
      A = 0.
      B = 12.7
      C = -2.54
      GAIN = 1.
      GO TO 100
   12 CONTINUE
      IF(KK.EQ.8) GO TO 62
      GO TO 60
   62 CALL FPLOT(XINCH,YINCH,X0,0.,100.,0.,27.,6)
   60 A = 0.
      B1 = 23.33
      B2 = 24.45
      C = 0.
      GAIN = 50.
      GO TO 100
   16 CALL FPLOT(XINCH,YINCH,X0,70.,100.,0.,27.,6)
      B1=23.33
      B2=24.45
```

```
      C = 0.
      GAIN = 20.
      GO TO 100
   13 CALL FPLOT(XINCH,YINCH,XO,0.,6.00,0.,27.,3)
      A = 0.
      B = 12.
      C = 0.
      GAIN = 20.
      BV = 23.
      GV = 1.
      GO TO 100
   14 CALL FPLOT(XINCH,YINCH,XO,30.,60.,0.,27.,4)
      A = 0.
      B = 133.33
      C = 0.
      GAIN = 1.
      GO TO 100
   15 CALL FPLOT(XINCH,YINCH,XO,-.25,1.25,0.,27.,5)
      GAIN = 1.
  100 CONTINUE
      IF(KK.EQ.1) GO TO 27
      IF(KK.EQ.6) GO TO 25
      IF(KK.EQ.7) GO TO 28
      IF(KK.GE.8) GO TO 27
      RV = DATA(KK,JJ)*GAIN/FACT
      RESU = A*(RV**2) + B*RV + C
      IF(KK.NE.3) GO TO 30
      V = DATA(KK+1,JJ)*GV/FACT
      RESV=BV*V
      RESU = RESU*RESV/1000.
      GO TO 30
   25 RV = DATA(KK,JJ)*GAIN/FACT
      RESU = (RV-NAO)/(NA1-NAO)
      GO TO 35
   28 RV = DATA(KK,JJ)*GAIN/FACT
```

```
      RESU = (RV-NBO)/(NB1-NBO)
   35 IF(RESU.LT.-.25) RESU = -.25
      IF(RESU.GT.1.25) RESU=1.25
      GO TO 30
   27 IF(ID.EQ.2) KK=KK-8
      IF(ID.EQ.3) KK=KK-16
      IF(ID.EQ.4) KK=KK-24
      RV = DATA(KK,JJ)*GAIN/FACT
      IF(RV.LE.15.5) B=B1
      IF(RV.GT.15.5) B=B2
      RESU = B*RV + C
   30 CALL UNITTO(TIME,RESU,PTIME,PRESU)
      CALL PLOT(PTIME,PRESU,2)
      TIME = TIME + 3.*DELT
      JJ = JJ + 1
      IF(ID.EQ.2) KK=KK+8
      IF(ID.EQ.3) KK=KK+16
      IF(ID.EQ.4) KK=KK+24
      IF(JJ.LE.JFIN) GO TO 100
      CALL PLOT(XO,YO,3)
   50 CONTINUE
   57 XXO = XO+XINCH+3.
      CALL PLOT(XXO,YO,-3)
   90 CONTINUE
      CALL PLOT(0.0,0.0,999)
 1000 STOP
      END
      SUBROUTINE FPLOT(XINCH,YINCH,XO,DMIN,DMAX,TMIN,TMAX,KO
      COMMON/2/XMIN,YMIN,YMAX,XMAX,YO,XA,YA
      DATA INDEX/32/
      CALL LINEAR(XINCH,YINCH,XO)
      XH = XO + 3.
      YH = YMAX + .2
      CALL LETTER(11,0.1,0.,XH,YH,11H12-13-78-05)
      XA = XO + 4.
```

```
      YB = YO - .5
      CALL LETTER(8,0.2,0.,XA,YB,8HTIME (S))
      YE = YO - .25
      CALL LETTER(2,0.2,0.,XO,YE,2H0.)
      XE = XO + 2.8
      IF(INDEX.EQ.2) GO TO 11
      CALL LETTER(2,0.2,0.,XE,YE,2H9.)
      XE = XO + 5.8
      CALL LETTER(3,0.2,0.,XE,YE,3H18.)
      XE = XO + 8.6
      CALL LETTER(3,0.2,0.,XE,YE,3H27.)
      GO TO 12
11    CALL LETTER(2,0.2,0.,XE,YE,2H2.)
      XE = XO + 5.8
      CALL LETTER(3,0.2,0.,XE,YE,3H 4.)
      XE = XO + 8.6
      CALL LETTER(3,0.2,0.,XE,YE,3H 6.)
12    XC = XO - 1.1
      YC = YO + 1.
      XJ = XO - 0.8
      YR = YO + .05
      YJ = YO + 3.
      YY = YO + 5.8
      IF(K.EQ.1) GO TO 21
      IF(K.EQ.2) GO TO 22
      IF(K.EQ.2) GO TO 32
      IF(K.EQ.3) GO TO 23
      IF(K.EQ.4) GO TO 24
      IF(K.EQ.5) GO TO 25
      IF(K.EQ.6) GO TO 26
 21   CALL LETTER(14,0.2,90.,XC,YC,14HPRESSURE (KPA))
      CALL LETTER(4,0.2,0.,XJ,YR,4H-15.)
      CALL LETTER(4,0.2,0.,XJ,YJ,4H00.0)
      CALL LETTER(4,0.2,0.,XJ,YY,4H15.0)
      GO TO 200
```

```
 22 CALL LETTER(15,0.2,90.,XC,YC,15HTEMPERATURE (C))
    CALL LETTER(4,0.2,0.,XJ,YR,4H0.00)
    CALL LETTER(4,0.2,0.,XJ,YJ,4H300.)
    CALL LETTER(4,0.2,0.,XJ,YY,4H600.)
    GO TO 200
 23 CALL LETTER(16,0.2,90.,XC,YC,16HPOWER INPUT (KW))
    CALL LETTER(4,0.2,0.,XJ,YR,4H0.00)
    CALL LETTER(4,0.2,0.,XJ,YJ,4H3.00)
    CALL LETTER(4,0.2,0.,XJ,YY,4H6.00)
    GO TO 200
 24 CALL LETTER(24,0.2,90.,XC,YC,24HTURBINE FLOW RATE (ML/S))
    CALL LETTER(4,0.2,0.,XJ,YR,4H30.0)
    CALL LETTER(4,0.2,0.,XJ,YJ,4H45.0)
    CALL LETTER(4,0.2,0.,XJ,YY,4H60.0)
    GO TO 200
 25 IF(INDEX.EQ.2) GO TO 26
    CALL LETTER(13,0.2,90.,XC,YC,13HVOID FRACTION)
    CALL LETTER(4,0.2,0.,XJ,YR,4H-.25)
    CALL LETTER(4,0.2,0.,XJ,YJ,4H0.50)
    CALL LETTER(4,0.2,0.,XJ,YY,4H1.25)
    GO TO 200
 32 CALL LETTER(15,0.2,90.,XC,YC,15HTEMPERATURE (C))
    CALL LETTER(4,0.2,0.,XJ,YR,4H40.0)
    CALL LETTER(4,0.2,0.,XJ,YJ,4H80.0)
    CALL LETTER(4,0.2,0.,XJ,YY,4H120.)
    GO TO 200
 26 CALL LETTER(15,0.2,90.,XC,YC,15HTEMPERATURE (C))
    CALL LETTER(4,0.2,0.,XJ,YR,4H00.0)
    CALL LETTER(4,0.2,0.,XJ,YJ,4H50.0)
    CALL LETTER(4,0.2,0.,XJ,YY,4H100.)
200 CALL PLOT(XO,YO,3)
    XSC = (TMAX-TMIN)/XINCH
    V = XO*XSC - TMIN
    YSC = (DMAX-DMIN)/YINCH
    W = YO*YSC - DMIN
```

```
      CALL PLTIN(XSC,YSC,-V,-W,TMIN,TMAX,DMIN,DMAX)
      RETURN
      END
      SUBROUTINE LINEAR ( XINCH , YINCH ,XO)
      COMMON /2/XMIN,YMIN,YMAX,XMAX,YO,XA,YA
      DATA XMIN,YMIN,YMX/0.,0.,10.555/
      YO = (YMX-YINCH)*0.5 + 0.25
      XMAX  =    XINCH    + XO
      YMAX  =    YINCH    + YO
      J = XINCH
      L = YINCH
      CALL PLOT (XO,YO,3)
      CALL PLOT (XO,YMAX,2)
      CALL PLOT (XMAX,YMAX,2)
      CALL PLOT(XMAX,YO,2)
      CALL PLOT(XO,YO,2)
      DO 91  I = 1,J
      XI  = XO + FLOAT(I)
      XX = XI - 1.
      DO 92 K=1,9
      XK = XX + FLOAT(K)*0.1
      CALL PLOT(XK,YO,3)
      CALL PLOT(XK,(YO+0.07),2)
      CALL PLOT(XK,YMAX,3)
      CALL PLOT(XK,(YMAX-0.07),2)
   92 CONTINUE
      DO 93 K=1,19,2
      XK = XX + FLOAT(K)*0.05
      CALL PLOT(XK,YO,3)
      CALL PLOT(XK,(YO+0.03),2)
      CALL PLOT(XK,YMAX,3)
      CALL PLOT(XK,(YMAX-0.03),2)
   93 CONTINUE
      CALL PLOT(XI,YO,3)
      CALL PLOT(XI,(YO+.2),2)
```

```
      CALL PLOT(XI,YO,3)
      CALL PLOT(XI,YMAX,3)
      CALL PLOT(XI,(YMAX-.2),2)
      CALL PLOT(XI,YMAX,3)
   91 CONTINUE
      DO 81  K  = 1,L
      YK  =  YO  + FLOAT(K)
      YY = YK - 1.
      DO 82 I=1,9
      YI = YY + FLOAT(I)*0.1
      CALL PLOT(XO,YI,3)
      CALL PLOT((XO+0.07),YI,2)
      CALL PLOT(XMAX,YI,3)
      CALL PLOT((XMAX-0.07),YI,2)
   82 CONTINUE
      DO 83 I=1,19,2
      YI = YY + FLOAT(I)*0.05
      CALL PLOT(XO,YI,3)
      CALL PLOT((XO+0.03),YI,2)
      CALL PLOT(XMAX,YI,3)
      CALL PLOT((XMAX-0.03),YI,2)
   83 CONTINUE
      CALL PLOT(XO,YK,3)
      CALL PLOT((XO+.2),YK,2)
      CALL PLOT(XO,YK,3)
      CALL PLOT(XMAX,YK,3)
      CALL PLOT((XMAX-.2),YK,2)
      CALL PLOT(XMAX,YK,3)
   81 CONTINUE
      RETURN $ END
```

```
PROGRAM REWET.              A. CHAN
SETTL,500.
FTN,GO(PL=100000)
         6400 END OF RECORD
      PROGRAM REWET (INPUT,OUTPUT,TAPE5=INPUT,TAPE6=OUTPUT)
C
C         THIS PROGRAM PREDICTS THE TRANSIENT THERMAL AND HYDRAULIC
C         BEHAVIORS OF THE REFILLING AND REWETTING PROCESSES IN A HOT
C         HORIZONTAL CHANNEL.
C         THE PROGRAM CALCULATES THE WATER LEVEL, WATER VELOCITY,
C         WATER BULK TEMPERATURE AND LOCAL CHANNEL WALL TEMPERATURE
C         DURING TRANSIENTS
C         THE HYDRAULIC AND THERMAL EQUATIONS ARE ASSUMED EXPLICITLY
C         COUPLED.
C         THE HYDRAULIC EQUATIONS ARE SOLVED USING AN EXPLICIT FINITE
C         DIFFERENCE CHARACTERISTICS TECHNIQUE
C         AN EXPLICIT FINITE DIFFERENCE TECHNIQUE IS USED TO SOLVE
C         THE THERMAL EQUATIONS
C         IMPORTANT VARIABLES USED ARE
C           U = LIQUID VELOCITY
C           UAD = LIQUID VELOCITY AT AN ADVANCE TIME STEP
C           W = STAGE VARIABLE
C          WAD = STAGE VARIABLE AT AN ADVANCE TIME STEP
C          HOUT = WATER LEVEL
C          HAD = WATER LEVEL AT AN ADVANCE TIME STEP
C          TL = LIQUID TEMPERATURE
C          TW = CHANNEL WALL TEMPERATURE
C          C = GRAVITY WAVE VELOCITY
C          UGG = VAPOR VELOCITY
C          HCUT = CRITICAL WATER LEVEL
C          QV = CONSTANT INLET FLOW RATE
C          VOIDL = LIQUID FRACTION
C          TWO = INITIAL WALL TEMPERATURE
C          TLO = INLET LIQUID TEMPERATURE
C          TRM = ROOM TEMPERATURE
```

```
C         TSAT = SATURATION TEMPERATURE
C         TSP = DRYOUT TEMPERATURE
C         Q = HEAT INPUT FROM WALL
C         QIN = HEAT INPUT TO SYSTEM IN A TIME STEP
C         QINT = TOTAL HEAT INPUT
C         QWL = TOTAL HEAT LOSS BY CHANNEL WALL
C         AMASS = TOTAL LIQUID INVENTORY IN THE SYSTEM
C         JZ = TOTAL NUMBER OF NODES USED
C         EFR = WALL FRICTIONAL DRAG
C         E1,E2 = RIGHT HAND SIDE TERMS OF THE HYDRAULIC EQUATIONS
C                 IN CHARACTERISTIC FORM
C         LGTH = LENGTH OF CHANNEL
C         DX = MESH SIZE
C         DTM = TIME STEP SIZE
C         DIA = DIAMETER OF CHANNEL
C
      DIMENSION U(70),UAD(70),W(70),WAD(70),EFR(70),C(70),HAD(70),
     $    HOUT(70),E1(70),E2(70),TW(5,70,9),TL(70),Q(70),UGG(70)
      REAL LGTH
      QV = 45.
      QV = 55.
      QV = 65.
      QV = 75.
      QV = 95.
      QV = 105.
      QV = 85.
      QS = 0.
      QINT = 0.
      G = 981.
      DIA = 1.796
      R = DIA/2.
      PI = 3.141592654
      LGTH = 200.
      TF = 1.
      TF = 0.75
```

```
      TF = 0.5
      HFULL = 0.99
      JF = 3.
      JF = 1
      JIN = JF + 1
      JTS = JIN + 6
      JTE = JTS + 23
      JOUT = JTE + 8
      JZ = JOUT
      JTET = JTS + 20
      JSS = 1
      JAA = JZ - 1
      T = 0.
      DX = LGTH/(JTE-JTS+1)
      AREA = PI*R*R
      HMIN = 0.01*DIA
      HM = HFULL*DIA
      HML= HMIN/10.
C         CRITICAL LEVEL
      HCUT = 0.4*HM
      HCUT = 0.45*HM
      HCUT = .5*HM
      HCUT = 0.55*HM
      HCUT = 0.525*HM
      HCUT = 0.6*HM
      HCUT = 0.65*HM
      HCUT = 0.625*HM
      HCUT = 0.575*HM
      CALL STAGE(HMIN,W,HML,DIA)
      WMIN = W
      JS = JSS + 1
      JD = 1
      KA = 6
      KAA = KA + 3
      II = 3
```

```
      IIA = II + 2
      TWO = 400.
      TWO = 600.
      TWO = 500.
      TLO = 45.
      TLO = 10.
      TSAT = 100.
      TSP = 175.
      TSP = 200.
      TRM = 15.
      DTM = 0.
      JZZ = JZ + 1
      JZZ = JZ
C        SET INITIAL CONDITION
      DO 2 J=1,JZZ
      E1(J) = 0.
      E2(J) = 0.
      U(J) = 0.
      W(J) = 0.
      UAD(J) = 0.
      WAD(J) = 0.
      C(J) = 0.
      HOUT(J) = HML
      HAD(J) = HML
      Q(J) = 0.
      TL(J) = TRM
      UCC(J) = 0.
    2 CONTINUE
      CALL STAGE(HM,W,HML,DIA)
      WM = W
      DO 9 J=JSS,JIN
      UAD(J) = 0.
      WAD(J) = WM
      HOUT(J) = HM
      TL(J) = TLO
```

```
    9 CONTINUE
      TL(JIN) = TRM
      HT = HM
      CALL LIQFR(HT,VOIDL,DIA)
      UAD(JSS) = QV/(VOIDL*PI*R*R)
      UFULL = UAD(JSS)
      I=1
      DO 300 J=1,JOUT
      DO 300 K=1,KAA
  300 TW(I,J,K) = TRM
      DO 301 I=1,IIA
      DO 301 J=JTS,JTE
      DO 301 K=1,KAA
  301 TW(I,J,K) = TWO
      JJ = 100
      JQ = 100
   99 CONTINUE
   51 JB = JF + 1
      JC = JF - 1
      IF(JF.EQ.JAA) JC=JF
      DO 3 J=1,JB
      IF(UAD(J).LT.0.) UAD(J)=0.
      WW = WAD(J)
      IF(WW.EQ.WM) GO TO 7
      CALL BSTAGE(WW,HH,HML,DIA,J)
      HAD(J) = HH
      GO TO 3
    7 HAD(J) = HM
    3 CONTINUE
      CALL WTEMP(HOUT,TW,TL,Q,DTM,DX,JC,KA,JIN,JTS,JTE,JOUT,HM,TSP,HAD,
     $    QIN,QWL,TRM,TWO,UAD,UGG,HCUT)
      CALL FTEMP(U,TL,Q,DTM,JC,DX,QG,UAD,DIA,HAD,HOUT,TLO,KA,TW,
     $    JJ,JQ)
      CALL VAPOR(HOUT,U,Q, E1,E2,JC,DIA,DX,HAD,UGG,DTM,JTE,TL,HCUT)
      DO 6 J=1,JB
```

```
      U(J) = UAD(J)
      W(J) = WAD(J)
      HOUT(J) = HAD(J)
    6 CONTINUE
      IF(INDEX.EQ.1) JF=JF-1
      CALL CONT(HOUT,C,DIA,JF,JSS)
      AMASS = 0.
      JA = JF - 1
      DO 255 J=JSS,JA
      H1 = HOUT(J)
      H2 = HOUT(J+1)
      CALL LIQFR(H1,VOID1,DIA)
      CALL LIQFR(H2,VOID2,DIA)
      AMASS = AMASS + (VOID1+VOID2)*AREA*DX/2.
  255 CONTINUE
      AMASS = AMASS + VOID2*AREA*DX/2.
      CALL OUTPUT(HOUT,U,C,TW,TL,JF,T,DX,JSS,AMASS,JOUT,Q,QS,DTM,
     $     QIN,QINT,QWL,UGG)
      IF(TW(1,JTET,2).LT.TSAT) GO TO 100
      GO TO 201
  200 WRITE(6,250) T,AMASS
  250 FORMAT(/10X,'TIME = ',G14.5,'MASS = ',G14.5)
  201 INDEX = 0
      JF = JF + 1
      IF(JF.EQ.JZZ) JD = JZ
      IF(JF.EQ.JZZ) JF=JF-1
      CALL FRICT(U,HOUT,TW,EFR,JF,DIA,JSS,HM,KA,TSP,JTS,JTE,JJ,JQ,
     $     HCUT,TWO)
      DTM = 9999.
      DO 4 I=JS,JF
      DT = 2.*DX/(U(I-1)+C(I-1) - (U(I+1)-C(I+1)))
      IF(DT.LT.DTM) DTM = DT
    4 CONTINUE
      TTF = TF
      IF(JF.LT.5) TTF = TF/4.
```

```
      DTM = TTF*DTM
      T = T + DTM
      JK = JF - 1
      SQR = 1.
      SQL = 1.
      DO 5 J = JS,JF
      IF(JF.EQ.JZ.AND.J.EQ.JF) GO TO 97
      UCL = U(J-1)+C(J-1)
      UCR = U(J+1)-C(J+1)
      IF(J.GE.JK) GO TO 20
      GO TO 21
   9  IF(J.EQ.JF) GO TO 22
      UCR = U(J) - C(J)
      GO TO 21
   22 UCR = U(J) - C(J)
   21 IF(U(J+1).GT.C(J+1)) GO TO 25
           SUBCRITICAL FLOW
      WAD(J) = SQL*UCL*(W(J)-W(J-1)) + SQR*UCR*(W(J+1)-W(J))
     $     + UCL*(U(J)-U(J-1)) - UCR*(U(J+1)-U(J))
      WAD(J) = DTM*(2.*E1(J)-WAD(J)/DX)/2. + W(J)
      UAD(J) = UCL*(W(J)-W(J-1)) - UCR*(W(J+1)-W(J)) +
     $     UCL*(U(J)-U(J-1))/SQL + UCR*(U(J+1)-U(J))/SQR
      UAD(J) = -E2(J) - UAD(J)/(2.*DX)
      UAD(J) = (DTM*UAD(J) + U(J))/(1. + EFR(J)*U(J)*DTM)
      GO TO 26
           SUPERCRITICAL FLOW
   25 UCR = U(J) - C(J)
      IF(U(J).GT.C(J)) GO TO 27
      UD = U(J+1) - U(J)
      WD = W(J+1) - W(J)
      UCR = (U(J)-C(J) + U(J+1)-C(J+1))/2.
      GO TO 28
   27 UD = U(J) - U(J-1)
      WD = W(J) - W(J-1)
   28 WAD(J) = SQL*UCL*(W(J)-W(J-1)) + SQR*UCR*WD +
```

```
  $     UCL*(U(J)-U(J-1)) - UCR*UD
      WAD(J) = DTM*(2.*E1(J)-WAD(J)/DX)/2. + W(J)
      UAD(J) = UCL*(W(J)-W(J-1)) - UCR*WD + UCL*(U(J)-U(J-1))/SQL +
  $     UCR*UD/SQR
      UAD(J) = -E2(J) - UAD(J)/(2.*DX)
      UAD(J) = (DTM*UAD(J) + U(J))/(1. + EFR(J)*U(J)*DTM)
   26 IF(WAD(J).LT.WM) GO TO 5
      WAD(J) = WM
      IF(UAD(J-1).EQ.UFULL) UAD(J)=UFULL
      IF(J.EQ.JZ)  GO TO 100
    5 CONTINUE
      W(JF) = WAD(JF)
      GO TO 98
C           RIGHT HAND BOUNDARY CONDITION
   97 WEXIT = W(JF-1)
      UCL = U(JF-1) + C(JF-1)
      UEXIT =  U(JZZ) -  (WEXIT-W(JZZ))/DTM- UCL*(W(JZZ)-W(JF-1))/DX
  $      - UCL*(U(JZZ)-U(JF-1))/DX
      UEXIT = UEXIT/(1.+EFR(JZZ)*U(JZZ)*DTM)
      U(JZZ) = UEXIT
      CALL BSTAGE(WEXIT,HH,HML,DIA,J)
      HOUT(JZZ) = HH
      CALL LIQFR(HH,VOID,DIA)
      A = AREA*VOID/(2.*SQRT(2.*R*HH-HH*HH))
      C(JZZ) = SQRT(A*G)
   98 IF(WAD(J).GE.WMIN) GO TO 96
      INDEX = 1
      UAD(JF) = 0.
      GO TO 95
   96 TL(JF) = TL(JF-1)
   95 WAD(JZ) = WAD(JZ-1)
      UAD(JZ) = UAD(JZ-1)
      GO TO 99
  100 STOP
      END
```

```
BROUTINE CONT(H,C,DIA,JF,JS)

 THIS SUBROUTINE CALCULATES THE GRAVITY WAVE VELOCITY,C
 FOR GIVEN LIQUID LEVEL,H.

MENSION  H(70),C(70)
 = 3.141592654
 = DIA/2.
,= 981.
)F = 0.96
1 = JF + 1
) 1  I=1,JA
T = H(I)
CCO = R*R*ACOS((R-HT)/R)
C1 = R*R*ACOS((HT-R)/R)
D = SQRT(2.*R*HT - HT*HT)
1 = (R-HT)*SQRT(2.*R*HT-HT*HT)
2 = ASIN((R-HT)/R)
3 = ASIN((HT-R)/R)
N = 2.*CO/(PI*R*R)
M1 = 0.5*(R-HT)*C1 + 0.5*R*R*(R-HT)*C2 - 0.25*(R-HT)*PI*R*R
   + CO**3/3.
DMO = 0.5*(3.*R*HT*HT - 2.*R*R*HT - HT**3)/CO + PI*R*R/4.
DM1 = DMO - R*R*C2/2.
DM2 = DMO - R*R*C2/2.
IF(HT.GE.R) GO TO 100
VOID = (CCO-C1)/(PI*R*R)
AMM = (2.*ROF*G*AM1)/(CCO-C1)
DMM = (CCO-C1)*DM1 - AM1*2.*CO
DMM = 2.*ROF*G*DMM/((CCO-C1)**2)
GO TO 110
) VOID = 1.-(CC1+C1)/(PI*R*R)
AMM = (2.*ROF*G*AM1)/(PI*R*R-CC1-C1)
DMM = (PI*R*R - CC1 -  C1)*DM2 - AM1*2.*CO
DMM = 2.*ROF*G*DMM/((PI*R*R-CC1-C1)**2)
```

```
  110 SVEL = (AMM*AN + VOID*DMM)/(ROF*AN)
      C(I) = SQRT(SVEL)
    1 CONTINUE
      RETURN
      END
      SUBROUTINE LIQFR(HT,VOIDL,DIA)
C
C        THIS SUBROUTINE CALCULATES THE LIQUID FRACTION, VOIDL, FOR
C        GIVEN LIQUID LEVEL, HT
C
      PI = 3.141592654
      R = DIA/2.
      CCO = R*R*ACOS((R-HT)/R)
      CC1 = R*R*ACOS((HT-R)/R)
      C1 = (R-HT)*SQRT(2.*R*HT-HT*HT)
      IF(HT.LT.R) VOIDL = (CCO-C1)/(PI*R*R)
      IF(HT.GE.R) VOIDL = 1. - (CC1+C1)/(PI*R*R)
      RETURN
      END
      SUBROUTINE OUTPUT(H,U,C,TW,TL,JF,T,DX,JS,AMASS,JZ,Q,QS,DT,
     *     QIN,QINT,QWL,UGG)
C
C         THIS SUBROUTINE OUTPUTS THE DEPENDENT VARIABLES
C         XX = DISTANCE FROM INLET
C         HH = WATER LEVEL
C         UU = WATER VELOCITY
C         CC = GRAVITY WAVE VELOCITY
C         UG = VAPOR VELOCITY
C         QQ = HEAT INPUT
C         TWTI = WALL TEMPERATURE AT TOP OF CHANNEL
C         TWRI = WALL TEMPERATURE AT MID-SIDE OF CHANNEL
C         TWBI = WALL TEMPERATURE AT BOTTOM OF CHANNEL
C         TL = LIQUID BULK TEMPERATURE
C
      DIMENSION H(70),C(70),U(70),TW(5,70,9),TL(70),Q(70),UGG(70)
```

```
      Z = T*8.3333333
      WRITE(6,10)
   10 FORMAT(1H1)
      WRITE(6,11) T,AMASS,Z
   11 FORMAT(///5X,"TIME = ",G13.5,"AMASS = ",G14.5,10X,G14.5//)
      WRITE(6,13)
   13 FORMAT(4X,"J",4X,"DIST",7X,"LEVEL",5X,"SPEED",4X,"WAVE SPEED",
     &     5X,"TL",8X,"TWTI",7X,"TWRI",7X,"TWBI",9X,"QQ",9X,"UG"/)
      JA = JF
      JA = JF + 1
      IF(JF.EQ.JZ) JA = JF + 1
      QT = 0.
      DO 1 J=1,JZ
      XX = DX*(J-1)
      HH = H(J)
      UU = U(J)
      CC = C(J)
      UG = UGC(J)
      IF(J.GT.1) GO TO 20
      TLL = TL(J)
      QQ = Q(J)
      TWTI = TW(1,J,2)
      TWRI = TW(1,J,5)
      TWBI = TW(1,J,8)
      GO TO 21
   20 TLL = (TL(J-1)+TL(J))/2.
      QQ = (Q(J-1)+Q(J))/2.
      TWTI = (TW(1,J-1,2)+TW(1,J,2))/2.
      TWRI = (TW(1,J-1,5)+TW(1,J,5))/2.
      TWBI = (TW(1,J-1,8)+TW(1,J,8))/2.
   21 WRITE(6,12) J,XX,HH,UU,CC,TLL,TWTI,TWRI,TWBI,QQ,UG
   12 FORMAT(2X,I3,2X,10G11.5)
    1 CONTINUE
      QIN = QIN*DT
      QINT = QINT + QIN
```

```
      DO 15 J=1,JF
      IF(Q(J).LT.0.) GO TO 15
      QT = QT + Q(J)
   15 CONTINUE
      AM = QT*DT/2258.
      QS = QS + QT
      AMT = QS*DT/2258.
      WRITE(6,14) AM, AMT,QIN,QINT,QWL
   14 FORMAT(//10X,'DM = ',G14.4,3X,'TM = ',G14.4,3X,'QIN = ',G14.4,
     *    3X,'QINT = ',G14.4,3X,'QWL = ',G14.4//)
      RETURN
      END
      SUBROUTINE FRICT(U,H,TW,E,JF,DIA,JS,HM,KA,TSP,JTS,JTE,JJ,JQ,
     *    ECUT,TWO)
C
C        THIS SUBROUTINE CALCULATES THE WALL SHEAR ALONG THE CHANNEL
C         FMM = STEADY STATE FRICTION MULTIPLIER FOR REFILLING OF
C                A DRY CHANNEL
C         JQ = LOCATION OF LEADING EDGE OF QUENCH FRONT
C         AMU = KINEMATIC VISCOSITY
C         REYND = REYNOLD NUMBER
C         F = FRICTION FACTOR
C
      DIMENSION U(70),H(70),E(70),TW(5,70,9)
      HMM = 0.995*HM
      FMM = 5.
      FMM = 4.
      FMM = 3.
      KAA = KA + 2
      JJ = 100
      JQ = 100
      TSAT = 100.
      AMU = 0.013
      R = DIA/2.
      PI = 3.141592654
```

```
      TCO = TWO - 100.
      TGO = 100.
      TCO = TWO - 150.
      JA = JF + 1
      IF(JF.LE.JTS) GO TO 10
      DO 2 J=2,JA
      IF(J.GT.JTE) GO TO 2
      IF(TW(1,J,2).LT.TSAT) JJ=J
      IF(JJ.LE.JTS) JJ=JTS
      IF(H(J).GT.HCUT) JQ=J
      IF(JQ.LT.JTS) JQ=JTS
    2 CONTINUE
   10 DO 1 J=JS,JA
      FM = FMM
      IF(H(J).GE.HM) FM=1.
      IF(J.LT.JQ.AND.J.GE.JJ) FM=20.*FMM
      IF(J.GT.JQ) FM=0.
      IF(J.GT.JTE) FM=1.
      HT = H(J)
      CC1 = R*ACOS((R-HT)/R)
      CC2 = R*ACOS((HT-R)/R)
      CO = (R-HT)*SQRT(2.*R*HT-HT*HT)
      CALL LIQFR(HT,VOIDL,DIA)
      IF(HT.LT.R) AL = 2.*CC1/(R*CC1 -CO)
      IF(HT.GE.R) AL = (2.*PI*R-2.*CC2)/(PI*R*R-(R*CC2+CO))
      RH = 1./AL
      REYND = 4.*RH*U(J)/AMU
C           BLASIUS EQUATION   F = FRICTION FACTOR
      F = 0.0791/(REYND**0.25)
      IF(REYND.EQ.0.) F = 0.
C           FM = ADJUSTABLE PARAMETER FOR DEVELOPING FLOW IN DRY CHANNEL
      F = FM*F
      E(J) = F*AL/2.
      IF(VOIDL.EQ.0.) E(J)=0.
    1 CONTINUE
```

```
      RETURN
      END
      SUBROUTINE STAGE(HT,WW,HML,DIA)
C
C         THIS SUBROUTINE CALCULATES THE STAGE VARIABLE FOR GIVEN
C              WATER LEVEL
C         INTERPOLATION BETWEEN COMPUTED DATA POINTS IS USED
C
      DIMENSION H(41),W(41)
      DATA H/0.00898,0.0449,0.0898,0.1347,0.1796,0.2245,0.2694,0.3143,
     $        0.3592,0.4041,0.449,0.4939,0.5388,0.5837,0.6286,0.6735,
     $        0.7184,0.7633,0.8082,0.8531,0.898,0.9429,0.9878,
     $        1.0327,1.0776,1.1225,1.1674,1.2123,1.2572,1.3021,
     $        1.347,1.3919,1.4368,1.4817,1.5266,1.5715,1.6164,
     $        1.6613,1.7062,1.7511,1.796/
      DATA W/0.,8.97408,15.6826,20.8165,25.1326,28.9242,32.342,35.4751,
     $        38.382,41.1029,43.6673,46.0973,48.4101,50.6192,
     $        52.7357,54.7686,56.7252,58.6118,60.4337,62.1954,
     $        63.9007,65.5528,67.1545,68.7082,70.2158,71.679,
     $        73.0991,74.477,75.8135,77.109,78.3635,79.5765,
     $        80.7473,81.8745,82.9557,83.9876,84.9653,85.8809,86.7211,
     $        87.4594,87.9701/
      DO 1 K=1,41
      IF(HT.EQ.H(K)) GO TO 2
      IF(HT.GT.H(K).AND.HT.LT.H(K+1)) GO TO 3
    1 CONTINUE
    2 WW = W(K)
      GO TO 4
    3 WW = W(K) + (W(K+1)-W(K))*(HT-H(K))/(H(K+1)-H(K))
    4 RETURN
      END
      SUBROUTINE BSTAGE(WT,HH,HML,DIA,J)
C
C        THIS SUBROUTINE CALCULATES THE WATER LEVEL FOR GIVEN
C           STAGE VARIABLE
```

```
C         INTERPOLATION OF COMPUTED DATA POINTS IS USED
C
      DIMENSION H(41),W(41)
      DATA H/0.00898,0.0449,0.0898,0.1347,0.1796,0.2245,0.2694,0.3143,
     $        0.3592,0.4041,0.449,0.4939,0.5388,0.5837,0.6286,0.6735,
     $        0.7184,0.7633,0.8082,0.8531,0.898,0.9429,0.9878,
     $        1.0327,1.0776,1.1225,1.1674,1.2123,1.2572,1.3021,
     $        1.347,1.3919,1.4368,1.4817,1.5266,1.5715,1.6164,
     $        1.6613,1.7062,1.7511,1.796/
      DATA W/0.,8.97408,15.6826,20.8165,25.1326,28.9242,32.342,35.4751,
     $        38.382,41.1029,43.6673,46.0973,48.4101,50.6192,
     $        52.7357,54.7686,56.7252,58.6118,60.4337,62.1954,
     $        63.9007,65.5528,67.1545,68.7082,70.2158,71.679,
     $        73.0991,74.477,75.8135,77.109,78.3635,79.5765,
     $        80.7473,81.8745,82.9557,83.9876,84.9653,85.8809,86.7211,
     $        87.4594,87.9701/
    4 DO 12 K=1,41
      IF(WT.EQ.W(K)) GO TO 10
      IF(WT.GT.W(K).AND.WT.LT.W(K+1)) GO TO 11
   12 CONTINUE
      WRITE(6,15) WT,J
   15 FORMAT(5X,"VALUE OUT OF RANGE IN BSTAGE",5X,"WT = ",G14.5,
     $    5X,"J = ",I3/)
   10 HH = H(K)
      GO TO 13
   11 HH = H(K) + (H(K+1)-H(K))*(WT-W(K))/(W(K+1)-W(K))
   13 RETURN
      END
      SUBROUTINE WTEMP(H,TW,TL,Q,DT,DZ,JF,KA,JIN,JTS,JTE,JOUT,HM,TSP,
     $    HAD,QIN,QWL,TRM,TWO,UL,UG,HCUT)
C
C          THIS PROGRAM COMPUTES THE WALL TEMPERATURE (TW)
C            DISTRIBUTION AS A FUNCTION OF Z AND THETA
C          VARIABLE HEAT TRANSFER COEFF. (HTC) AND FLUID TEMP. (TL)
C            ARE USED
```

```
C       PHYSICAL PROPERTIES OF CHANNEL WALL ARE TEMP. DEPENDENT
C         TWAD = WALL TEMP. AT ADVANCE TIME STEP
C         ROW = WALL DENSITY
C         CP = WALL HEAT CAPACITY
C         COND = WALL CONDUCTIVITY
C         EPS = WALL THICKNESS
C
      DIMENSION TW(5,70,9),TL(70),HTC(70,9),TWAD(5,70,9),H(70),
     $   Q(70),HAD(70),R(4),UL(70),UG(70),QHT(70,9),QA(70)
      ROW(TT) = 6.573 - 0.0000763*TT
      CP(TT) = 0.285 + 0.0001*TT
      COND(TT) = 0.1 + 0.00016*TT
      ROCP(T1,T2) = 1.8733*(T1-T2) + 0.00032*(T1*T1-T2*T2) -
     $   2.533E-9*(T1**3-T2**3)
      EPS = 0.08636
      PI = 3.141592654
      RR = 0.898
      DIA = 1.796
      HMIN = 0.05*DIA
      EFL = 1.15
      EFL = 1.05
      ELF = 1.025
      HMM = HM/EFL
      HTEST = 0.9*HM
      HA = 0.01*DIA
      DR = EPS/3.
      I = 1
      TSAT = 100.
      KAA = KA + 2
      KAE = KAA + 1
      DA = PI/KA
      JA = JOUT - 1
      TL(JA) = TL(JA-1)
      CALL HTRAN(HTC,HHT,HT,HCUT,HA,HM,DA,KAA,TW,UL,UG,TL,H,HAD,JA,TRM,
     $   QHT)
```

```
      DO 10 J=1,JOUT
      QA(J) = 0.
   10 Q(J) = 0.
      DO 52 J=2,JA
      DO 50 K=2,KAA
      QQ = (HTC(J,K)-QHT(J,K))*(TW(1,J,K)-TL(J))*RR*DA*DZ*DT
      QAA = QQ + QHT(J,K)*(TW(1,J,K)-TRM)*RR*DA*DZ*DT
      IF(K.EQ.2.OR.K.EQ.KAA) GO TO 56
      QAA = 2.*QAA
      QQ = 2.*QQ
   56 Q(J) = Q(J) + QQ
      QA(J) = QA(J) + QAA
      T1 = TW(1,J,K)
      CONDM = COND(T1)
      DIFF = CONDM/(ROW(T1)*CP(T1))
      TWAD(1,J,K) = (TW(1,J,K+1)+TW(1,J,K-1)-2.*TW(1,J,K))/
     $      ((RR*DA)**2) + (TW(1,J+1,K)+TW(1,J-1,K)-2.*TW(1,J,K))/
     $    (DZ*DZ) - (HTC(J,K)-QHT(J,K))*(TW(1,J,K)-TL(J))/
     $    (EPS*CONDM) - QHT(J,K)*(TW(1,J,K)-TRM)/(EPS*CONDM)
      TWAD(1,J,K) = DIFF*DT *TWAD(1,J,K) + TW(1,J,K)
      IF(TWAD(1,J,K).LT.TL(J).AND.J.LT.JTE) TWAD(1,J,K)=TL(J)
      TWAD(5,J,K) = TWAD(4,J,K)
   50 CONTINUE
   52 CONTINUE
      Q(1) = 0.
      DO 65 J=2,JA
      DO 65 K=2,KAA
   65 TW(I,J,K) = TWAD(I,J,K)
      DO 51 I=1,5
      DO 51 J=1,JA
      TW(I,J,1) = TW(I,J,3)
      TW(I,J,KAE) = TW(I,J,KAA-1)
   51 CONTINUE
      DO 54 I=1,5
      DO 54 K=1,KAE
```

```
 54 TW(I,1,K) = TW(I,2,K)
 60 CONTINUE
    QIN = 0.
    DO 61 J=1,JOUT
    IF(DT.EQ.0.) GO TO 61
    Q(J) = Q(J)/DT
    QA(J) = QA(J)/DT
 61 QIN = QA(J) + QIN
    QWL = 0.
    DO 62 J=1,JOUT
    TWA = 0.
    DO 63 K=2,KAA
    TT = TW(1,J,K)
    IF(K.EQ.2.OR.K.EQ.KAA) GO TO 64
    TT = 2.*TT
 64 TWA = TWA + TT
 63 CONTINUE
    TWA = TWA/12.
    TWI = TWO
    IF(J.LT.JTS.OR.J.GT.JTE) TWI=TRM
    QW = ROW(TWI)*CP(TWI)*0.50592*DZ*(TWI-TWA)
    QW = ROCP(TWI,TWA)*0.50592*DZ
    QWL = QWL + QW
 62 CONTINUE
    RETURN
    END
    SUBROUTINE FTEMP(U,TL,Q,DT,JF,DX,QG,UAD,DIA,HAD,H,TLO,KA,TW,JJ,JQ)
C
C        THIS SUBROUTINE CALCULATES THE BULK LIQUID TEMPERATURE
C        CONSTANT PHYSICAL PROPERTIES OF WATER ARE USED
C        TLAD = LIQUID TEMP. AT AN ADVANCE TIME STEP
C        BETA = FRACTION OF ENERGY INPUT USED TO HEAT UP THE LIQUID
C
    DIMENSION U(70),TL(70),Q(70),TLAD(70) ,UAD(70),
   $   HAD(70),H(70),TW(5,70,9)
```

```
    ROW = 1.
    CPW = 4.36
    CONDW = 0.00623
    PI = 3.141592654
    R = DIA/2.
    DEFF = 0.75*DIA
    AREA = PI*R*R
    KAA = KA + 2
    TSAT = 100.
    TLS = 85.
    TLS = 95.
    TSP = 280.
    TSP = 200.
    JA = JF - 1
    JA = JF
    DO 1 J=2,JA
    GO TO 101
    BETA = 0.
    IF(J.LE.JQ) GO TO 101
    GO TO 100
101 BETA = 1.
    IF(TL(J).GT.TLS) BETA=1.-(TL(J)-TLS)/(TSAT-TLS)
    IF(BETA.LT.0.) BETA=0.
100 CONTINUE
    H1 = H(J)
    H2 = H(J+1)
    H3 = HAD(J)
    H4 = HAD(J+1)
    CALL LIQFR(H1,VOID1,DIA)
    CALL LIQFR(H2,VOID2,DIA)
    CALL LIQFR(H3,VOID3,DIA)
    CALL LIQFR(H4,VOID4,DIA)
    UL = (U(J)+UAD(J))/2.
    UR = (U(J+1)+UAD(J+1))/2.
    AL = (VOID1+VOID3)/2.
```

```
      AR = (VOID2+VOID4)/2.
      AVOID = (VOID1+VOID2)/2.
      TLAD(J) = AL*UL*TL(J-1) - AR*UR*TL(J) + BETA*Q(J)/(ROW*CPW*AREA)
      TLAD(J) = DT*TLAD(J) + AVOID*DX*TL(J)
      TLAD(J) = TLAD(J)/(AVOID*DX+(AL*UL-AR*UR)*DT)
      IF(TLAD(J).LT.TSAT) GO TO 4
      BETA = (AVOID*DX+(AL*UL-AR*UR)*DT)*TSAT - AVOID*DX*TL(J)
      BETA = BETA/DT - AL*UL*TL(J-1) + AR*UR*TL(J)
      BETA = BETA*ROW*CPW*AREA/Q(J)
      TLAD(J) = TSAT
    4 QD = Q(J)
      Q(J) = (1.-BETA)*QD
      IF(QD.LT.0.) Q(J) = QD
    1 CONTINUE
      DO 2 J=2,JA
      TL(J) = TLAD(J)
    2 CONTINUE
      RETURN
      END
      SUBROUTINE VAPOR(HOUT,U,Q,E1,E2,JF,DIA,DX,HAD,UGG,DT,JTE,TL,HCUT)
C
C        THIS SUBROUTINE CALCULATES THE VAPOR VELOCITY AND OTHER
C          INTERFACIAL TRANSFER TERMS
C         VG = VAPOUR GENERATION FUNCTION = Q/(HFG*AREA*DX)
C         TM = MOMENTUM TRANSFER TERM
C         SHEARI = INTERFACIAL SHEAR
C         SHEARG = WALL - GAS SHEAR
C         STN = SURFACE TENSION
C         VINT = VAPOR INERTIA TERM
C        ST = SURFACE TENSION OF WATER
C        ROF = DENSITY OF WATER
C        ROG = DENSITY OF VAPOR
C        UGG = VAPOR VELOCITY
C        VOIDG = VOID FRACTION
C
```

```
 DIMENSION HOUT(70),U(70),Q(70),E1(70),E2(70),HAD(70),UGC(70)
$     ,TL(70)
 PI = 3.141592654
 G = 981.
 ST = 58.85
 GAMMA = 0.5
 FI = 0.001
 FG = 0.001
 FI = 0.005
 FG = 0.005
 HFG = 2258.
 ROF = 0.9586
 ROG = 5.903E-4
 EPS = 0.08636
 HMM = 0.99*DIA
 HM = 0.90*DIA
 R = DIA/2.
 AREA = PI*R*R
 JC = 36
 JA = JF - 1
 JA = JF - 2
 QQ = 0.
 UGL = 0.
 VOIDGO = 0.
 DO 1 J=2,JF
 HT = (HOUT(J)+HAD(J))/2.
 IF(HT.GE.HMM) HT = HMM
 IF(HT.LT.R) SL=2.*R*ACOS((R-HT)/R)
 IF(HT.GE.R) SL=2.*PI*R-2.*R*ACOS((HT-R)/R)
 SG = 2.*PI*R - SL
 QQ = QQ + (Q(J-1)+Q(J))/2.
 VG = (Q(J-1)+Q(J))/(2.*HFG*AREA*DX)
 VGV = QQ/(HFG*AREA*DX)
 IF(HT.GT.HM) VGV=0.
 IF(QQ.LT.0.) VGV=0.
```

```
   GG = VGV*DX
   CALL LIQFR(HT,VOIDL,DIA)
   VOIDG = 1.-VOIDL
 5 UG = GG/(ROG*VOIDG)
   IF(HT.GE.HM.AND.J.GT.JTE) UG=U(J)
   SHEARG = 0.5*ROG*UG*UG*SG*FG/(VOIDG*AREA*ROF)
   IF(DT.EQ.0.) GO TO 6
   A = (UG-UGG(J))/DT + (UG-UGL)*(UG+UGL)/(2.*DX)
   A = (UG-UGL)*UGL/DX
   A = (UG-UGL)*(UG+UGL)/(2.*DX)
   GO TO 7
 6 A = 0.
 7 VINT = ROG*A/ROF
   UINF = (UG-U(J))/2.
   UINF = GAMMA*UG + (1.-GAMMA)*U(J)
   DVOIDH = 2.*SQRT(2.*R*HT-HT*HT)/AREA
   SHEARI = SQRT(2.*R*HT-HT*HT)*FI*ROG/AREA
   SHEARI = SHEARI*(UG-U(J))**2
   IF(UG.LT.U(J)) SHEARI=0.
   SHEARI = SHEARI*(1./VOIDL + 1./VOIDG)/ROF
   E1(J) = -VG/(ROF*DVOIDH)
   E1(J) = SQRT(G*DVOIDH/VOIDL)*E1(J)
   IF(J.GE.3.AND.J.LT.JC) GO TO 10
   STN = 0.
   GO TO 11
10 D3H = (HOUT(J+2)-2.*HOUT(J+1)+2.*HOUT(J-1)-HOUT(J-2))/(DX**3)
   STN = ST*D3H/ROF
11 CONTINUE
   TM = VG*((U(J)-UINF)/VOIDL + (UG-UINF)/VOIDG)/ROF
   IF(TM.LT.0.) TM=0.
   IF(J.GT.JTE) VINT=0.
12 E2(J) = - TM - SHEARI - SHEARG - STN  - VINT
   VOIDGO = VOIDG
   UGG(J) = UG
   UGL = UG
```

```
    1 CONTINUE
      RETURN
      END
      SUBROUTINE HTRAN(HTC,HHT,HT,HCUT,HA,HM,DA,KAA,TTW,UL,UG,TL,H,
     $   HAD,JA,TAO,QHT)
C
C          THIS SUBROUTINE COMPUTES THE CIRCUMFERENTIAL HEAT
C            TRANSFER COEFFICIENTS
C          HTFCF = FORCED CONVECTION LIQUID HEAT TRANSFER
C          HTFCG = FORCED CONVECTION VAPOR HEAT TRANSFER
C          HTFILM = FILM BOILING HEAT TRANSFER
C          HTFR = FREE CONVECTION HEAT TRANSFER
C          HTRAD = RADIATION HEAT TRANSFER
C          HTNB = NUCLEATE BOILING HEAT TRANSFER
C          HTTB = TRANSITION BOILING HEAT TRANSFER
C          HAP = QUENCH LEVEL
C
      DIMENSION HTC(70,9),TTW(5,70,9),UL(70),UG(70),TL(70),HPSI(10)
     $    ,H(70),HAB(70),QHT(70,9)
      HAP(HM,HT,HCUT) = HM*(HT-HCUT)/(HM-HCUT)
      ROA(T) = 1.29 - 4.242E-3*T + 8.7873E-6*T*T - 7.4E-9*T*T*T
      VISA(T) = 1.7323E-5 + 4.8162E-8*T - 3.0493E-11*T*T + 1.4888E-14*
     $    T*T*T
      CONDA(T) = 0.0243 + 6.2387E-5*T - 4.7983E-9*T*T - 7.18265E-12*
     $    T*T*T
      PRA(T) = 0.714 + 1.815E-4*T - 2.047E-6*T*T + 3.628E-9*T*T*T
      VISF(T) = 1.76435E-3 - 4.9238E-5*T + 6.4949E-7*T*T -
     $    3.10694E-9*T*T*T
      CONDF(T) = 0.56 + 2.3175E-3*T - 1.0241E-5*T*T - 5.41E-9*T*T*T
      PRF(T) = 13.444 - 0.4224*T + 0.00588*T*T - 2.882E-5*T*T*T
      ROF(T) = 1000. - 3.2875E-3*T - 5.4746E-3*T*T + 1.3386E-5*T*T*T
      DHF(H) = .08516 + 1.91813*H + .51535*H*H - .58172*H*H*H
      DHG(H) = 1.8181 + 1.78*H - 2.429*H*H + 0.498*H*H*H
      HTTBF(T) = 5.11E4*EXP(-0.00972*T)
      VISG = 1.202E-5
```

```
  ROG = 0.5904
  CONDG = 0.024436
  TENS = 0.05885
  HFG = 2.258E6
  SBK = 1.355E-12
  TSAT = 100.
  TSP = 280.
  TSP = 200.
  EMISS = 0.7
  EMISS = 1.
  EMISS = 0.85
  G = 9.81
  DIA = 0.01796
  R = 0.898
  HMM = 0.98*HM
  HPSI(2) = HM
  PSI = 0.
  DO 1 K=3,KAA
  PSI = PSI + DA
  HPSI(K) = R + R*COS(PSI)
1 CONTINUE
  DO 3 J=2,JA
  HT = (H(J)+H(J+1)+HAD(J)+HAD(J+1))/4.
  HHT = HT
  HT = HAP(HM,HT,HCUT)
  TF = TL(J)
  ULL = UL(J)/100.
  UGG = UG(J)/100.
  DFF = DHF(HHT)/100.
  DGG = DHG(HHT)/100.
  HTFCF = 0.023*CONDF(TF)/DFF*(ROF(T[illegible]FF*ULL  /VISF(TF))**0.8*
 $    PRF(TF)**0.4
  HTFCG = 0.023*CONDG/DGG*(ROG*DGG*UGG  /VISG)**0.8
   AFILM = SQRT(TENS/(G*(ROF(TF)-ROG)))
  DO 5 K=2,KAA
```

```
      TW = TTW(1,J,K)
      DTW = TW - TSAT
      HTTB = HTTBF(DTW)
      HTNB = 2.*HTTB
      HTNB = HTTB
      HO = HPSI(K)
      IF(TW.LT.TSP) GO TO 100
      HTFILM = 0.425*(CONDC**3*HFC*ROG*G*(ROF(TF)-ROG)/
     *    (VISG* AFILM*(TW-TSAT)))**0.25
      HTFILM = 1.25*HTFILM
      GO TO 101
  100 HTFILM = 0.
  101 IF(TW.LE.TAO) GO TO 102
      ATW = (TW+TAO)/2.
      TABS = ATW + 273.
      GR = (TW-TAO)*G*(ROA(ATW)**2)*(DIA**3)/((VISA(ATW)**2)*TABS)
      GRPR = GR*PRA(ATW)
      HTFR = 0.525*(GRPR**0.25)*CONDA(ATW)/DIA
      TWABS = TW + 273.
      TAABS = TAO + 273.
      HTRAD = (TWABS**4 - TAABS**4)*SBK*EMISS*4.184/(TW-TAO)
      HTRAD = 10000.*HTRAD
      GO TO 103
  102 HTFR = 0.
      HTRAD = 0.
  103 IF(TW.GE.TSAT.AND.TW.LT.TSP) GO TO 104
      IF(HHT.LT.HA) GO TO 10
      IF(HHT.LT.HCUT) GO TO 11
      IF(HHT.LT.HMM) GO TO 12
      HTC(J,K) = (HTFCF + HTFR + HTRAD)/10000.
      IF(TW.GT.TSAT) HTC(J,K) = (HTNB+HTFR+HTRAD)/10000.
      IF(TW.GT.TSP) HTC(J,K) = (HTTB+HTFR+HTRAD)/10000.
      GO TO 2
   10 HTC(J,K) = (HTFCG + HTFR + HTRAD)/10000.
      GO TO 2
```

```
 11 IF(HO.GT.HHT) GO TO 111
    HTC(J,K) = (HTFILM + HTFR + HTRAD)/10000.
    GO TO 2
111 HTC(J,K) = (HTFCG + HTFR + HTRAD)/10000.
    GO TO 2
 12 IF(HO.LT.HT) GO TO 121
    IF(HO.LT.HHT) GO TO 122
    HTC(J,K) = (HTFCG + HTFR + HTRAD)/10000.
    GO TO 2
121 HTC(J,K) = (HTNB + HTFR + HTRAD)/10000.
    IF(TW.GT.TSP) HTC(J,K) = (HTTB + HTFR + HTRAD)/10000.
    IF(TW.LT.TSAT) HTC(J,K) = (HTFCF + HTFR + HTRAD)/10000.
    GO TO 2
122 HTC(J,K) = (HTFILM + HTFR + HTRAD)/10000.
    GO TO 2
104 HTC(J,K) = (HTTB+HTFR+HTRAD)/10000.
  2 QHT(J,K) = (HTFR + HTRAD)/10000.
    IF(J.NE.12) GO TO 5
    HTT = HTC(J,K)
    WRITE(6,300) HTFCF,HTFCG,HTFILM,HTFR,HTRAD,HTNB,HTTB,HTT
300 FORMAT(8G14.5)
  5 CONTINUE
    HTC(J,KAA+1) = HTC(J,KAA-1)
     QHT(J,KAA+1) = (HTFR+HTRAD)/10000.
  3 CONTINUE
    RETURN
    END
```